# AEROSOL CONTRIBUTIONS TO SPELEOTHEM GEOCHEMISTRY

## Jonathan Dredge

A thesis submitted to the University of Birmingham for the University of Birmingham and University of Melbourne joint degree of DOCTOR OF PHILOSOPHY

School of Geography, Earth and Environmental Sciences

College of Life and Environmental Sciences

University of Birmingham

April 2014

# UNIVERSITY OF BIRMINGHAM

## University of Birmingham Research Archive

### e-theses repository

## Abstract

There is developing interest in cave aerosols due to the increasing awareness of their impacts on the cave environment and speleothems. This study presents the first multidisciplinary investigation into cave aerosols and their potential contribution to speleothem geochemistry.

Aerosols are shown to be sourced from a variety of external emission processes, and transported into cave networks. Both natural (marine sea-spray, terrestrial dust) and anthropogenic (e.g. vehicle emissions) aerosol emissions are detected throughout caves. Internal cave aerosol production by human disruption has also been shown to be of importance in caves open to the public. Aerosols produced from floor sediment suspension and release from clothing causes short term high amplitude aerosol suspension events.

Cave aerosol transport, distribution and deposition are highly variable depending on cave situation. Cave morphology, ventilation, and environmental conditions will influence how aerosols are distributed through cave networks. Aerosol deposition monitoring in Obir Cave, Austria has shown the significance of cave chamber size in aerosol transport, with large open chambers presenting higher levels of deposition.

Modern monitoring of suspended aerosol concentrations, $CO_2$ and temperature in Gough's Cave, Cheddar Gorge have presented a strong relationship with cave ventilation processes. Temporal variations of aerosol levels have demonstrated the ability of aerosol monitoring to record seasonal ventilation shifts, beyond anthropogenic influences. Aerosol minima (based

on 24 hours) provide a representation of natural aerosol baseline conditions without diurnal anthropogenic influences. Aerosols have shown a quicker recovery to natural background levels when compared to $CO_2$ and T, making aerosols a sensitive and effective monitoring tool. When used in combination with more established monitoring methods, suspended aerosol monitoring is a beneficial addition to cave environmental studies.

Theoretical modelling and calculations based on modern aerosol monitoring have established that aerosol contributions are highly variable. In some instances, modern aerosol supply is sufficient to account for speleothem geochemistry concentrations entirely. Aerosol contributions are of greatest significance under slow growth or hiatus scenarios and high aerosol deposition scenarios. Geochemical and stratigraphical analysis of a flowstone core from Gibraltar has highlighted the importance of hiatus events for future aerosol studies. Hiatus events provide a unique opportunity to investigate the type and amount of aerosol deposition and accumulation. Marine aerosol contributions have been quantified in the Gibraltar flowstone core and account for 18.5% of speleothem Sr. Sr isotopic analysis has confirmed the significance of marine aerosol contributions. Flowstone analysis has also demonstrated the ability of speleothems to record shifts in the supply of highly radiogenic terrestrial dust.

Bio-aerosol deposits and bacterial colonisation have been identified as a potential source of trace element bioaccumulation and flowstone coloration in Yarrangobilly Caves, Australia. Bio-aerosols have shown to be deposited throughout cave networks. Inorganic aerosol deposition may provide a nutrient supply to cave surfaces allowing for, and sustaining microbial colonisation.

## Acknowledgments

# Thesis contents

## Chapter 1. Introduction

## Chapter 2. Cave aerosols: distribution and contribution to speleothem geochemistry

**Chapter 5: Black coloration of the Yarrangobilly Flowstones: An investigation into forest fire aerosol and microbiological coloration processes**

# Figure list

# Table list

# Introduction to aerosol contributions to speleothem geochemistry



*Cave decorations in Jersey Cave, Yarrangobilly (Cave location used in Chapter 5).*

## Chapter 1. Introduction

The aim of this thesis is to determine the extent and impact of aerosol deposition contributions to speleothem geochemistry. Aerosol transport, introduction, distribution and influences on the cave environment and speleothem formation are explored. This chapter is used to outline the purpose and content of this investigation. In addition to the material introduced here, each chapter included in this thesis presents a separate investigation with a case specific background. Here, aerosol and speleothem sciences are introduced to provide a background of the main themes used in this multidisciplinary study.

This thesis presents the first combined study of aerosols and speleothem. Therefore, supplementary to the background content presented here a synthesis of aerosol-related literature is included in Chapter 2: aerosol introduction (Section 1), aerosol investigation methodologies (Section 2) and cave aerosol processes (Section 3).

Aerosols are defined as "the suspension of fine solid or liquid particles within a gaseous medium". Aerosols are introduced into the atmosphere through a range of emission processes, both natural and anthropogenic, and form as secondary aerosols. The identification of aerosol sources is critical in reconstructing emission processes.

## 1.1. Aerosol processes

Aerosols, once suspended into the atmosphere through emission processes, will be carried with parcels of air. As these parcels of air travel through the troposphere a multitude of aerosol types are incorporated into the air mass. The distance of aerosol transport is determined by the relationship between aerosol size and mass, and weather systems. Figure 1.1 presents the atmospheric residence times of different aerosols based on their size. By determining aerosol types and their associated geographical sources wind trajectories can be reconstructed. If the source of aerosols preserved in speleothems can be recognised palaeowind directions and source emission processes can be reconstructed (e.g. Goede *et al*., 1998).

| Desig-nation | Aitken nuclei | Large particles | Giant particles |
|---|---|---|---|
| Sources | Combustion → / Gas-to-particle conversions → / Coagulation of Aitken nuclei / Cloud droplet evaporation | Fly ash, sea-salt, pollens | Windblown dusts / Giant particles from industries |
| Sinks | Coagulation → / Capture by cloud particles → | Precipitation scavenging / Dry fallout | |
| Resi-dence time | Less than an hour in polluted air or in clouds | Days to weeks | Hours to days | Minutes to hours |

Figure 1.1: Principal sources and sinks of atmospheric particles and estimates of their mean residence times in the troposphere (Wallace & Hobbs, 2006). Aerosol size distributions for organic and inorganic aerosols are also shown in Figure 2.2.

The removal of aerosols from air masses occurs as a result of either dry deposition or wet deposition. Dry deposition is the process by which atmospheric trace chemicals are transferred by air motions to the surface of the Earth (Wesely & Hicks, 2000) and wet deposition involves aerosol association with precipitation. The main mechanisms of dry depositions are: Brownian diffusion, interception, impaction, sedimentation and rebound (Petroff *et al.,* 2008). Few studies have explored aerosols in cave environments. Further details on atmospheric and intra-cave deposition processes can be found in Chapter 2 where cave aerosol literature is reviewed. This investigation considers aerosol contributions to speleothem geochemistry through direct aerosol deposition and over ground surface aerosol deposition which is subsequently transported and incorporated in speleothem.

### *1.1.1. Aerosol sampling*

Surrogate sampling is utilised in this investigation to measure dry deposition of cave aerosols. There is no generally accepted method to directly measure or estimate dry deposition (Chu, 2008). However, it has been established that a smooth horizontal surrogate surface provides a lower bound estimate of the dry deposition flux onto a horizontal surface (Sehmel, 1978; Holsen *et al*. 1992). Pumped samples through a filter medium are used to determine suspended concentrations of both atmospheric and cave aerosols (e.g. Harrison *et al*., 2003). Further details on the aerosol sampling techniques and methods employed in this investigation are shown in Chapter 2, Section 2.2 and in the supplementary material, Section S.1.

### *1.1.2. Aerosol characterisation*

Aerosols can be characterised and categorised by size, shape and chemistry. Sizes are generally grouped to nucleation ($\sim$<0.1$\mu$m diameter), accumulation (0.1-1$\mu$m) and coarse

modes (~1μm) (Whitby & Cantrell, 1975). However, aerosol chemical signatures offer the best opportunity for the determination of aerosol types and for indentifying their source. Inorganic and organic chemistry is used throughout this investigation to reveal insights into processes involving aerosol transport, distribution, deposition and incorporation into speleothem.

*Inorganic analysis*

Inorganic analysis can provide insights into aerosol types and is a well established and developed method for the characterisation and source identification of atmospheric aerosols (Harrison *et al.*, 2003). Listed below is a summary of an investigation by Viana *et al.* (2008) that showed that studies throughout Europe agree on the identification of four main aerosol source types:

- Vehicular source – C, Fe, Ba, Zn, Cu, Pb

- Crustal Source – Al, Si, Ca, Fe (Lawrence & Neff (2009) also includes Mg and K)

- Marine source – Na, Cl, Mg

- Mixed industrial/ fuel-oil combustion – V, Ni, $SO_4^{2-}$

- Secondary aerosol - $SO_4^{2-}$, $NO_3^-$, $NH_4^+$

Crustal and marine sources and their changes in palaeoenvironments are of primary significance to this investigation. Marine aerosols are produced by the bursting of small air bubbles in the foam of breaking waves or "white caps" (Wedyan, 2008). The quantification of marine aerosols to speleothem geochemistry has not been previously directly investigated. Therefore, Chloride cave drip water concentrations are used in Chapter 3 to determine speleothem marine aerosol concentrations in Gibraltar.

Terrestrial dust aerosols occur when fine material is lifted from the ground when surface wind velocity exceeds a certain threshold wind speed, which is dependent on surface roughness, grain size and moisture levels (Engelstaedter *et al*., 2006). Figure 1.2 presents an example of a terrestrial dust transport event which has the potential to influence speleothem geochemistry in Gibraltar, the site of investigation in Chapter 4.
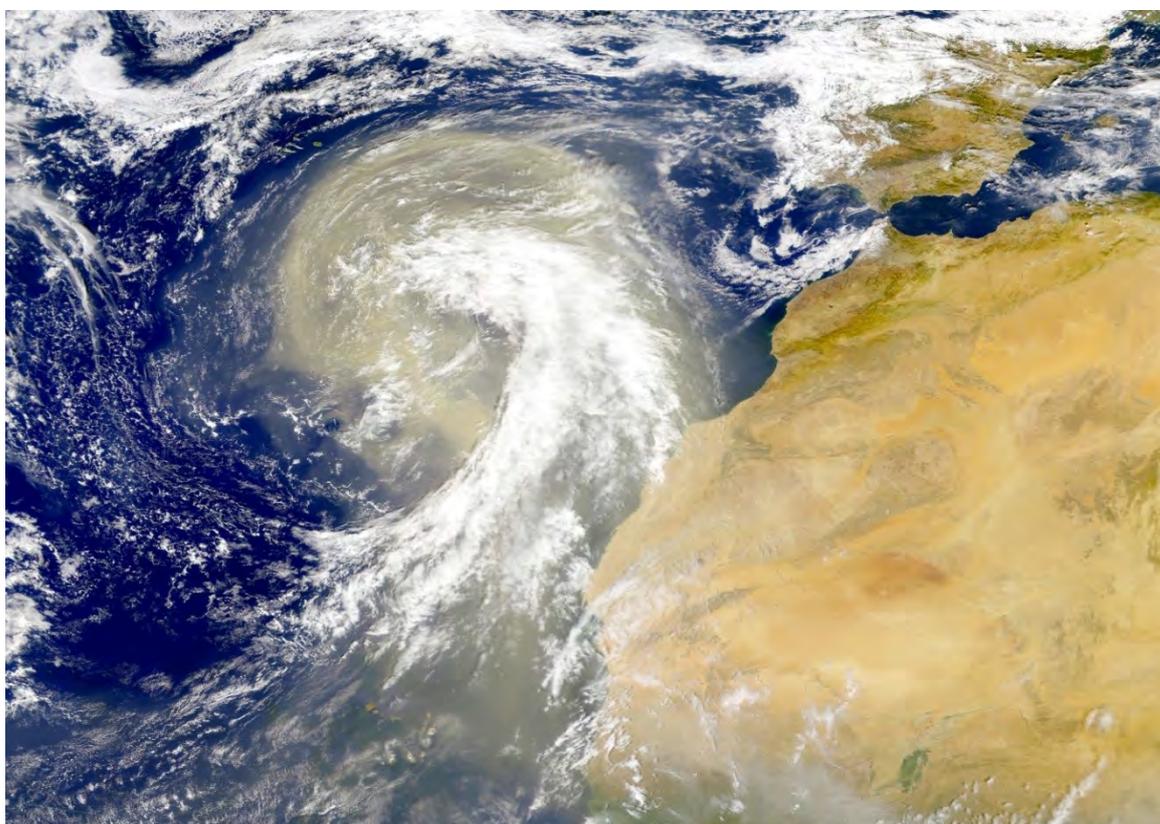


Figure 1.2: Saharan dust plume, wind entrained as a result of the anticyclone system visible. The image was captured by the Sea-Viewing Wide Field-of-View Sensor (SeaWiFS) (SeaWiFS/Ocean Colour Team) (NASA, 2014).

Isotopic measurements can be used to further constrain the source of aerosols to specific continental sources (Chapter 3). Strontium isotope compositions preserve a direct record of the $^{87}Sr/^{86}Sr$ record composition of cave water and therefore reflect the either direct aerosol

deposition to the speleothem or surface deposits. Sr isotope analysis in speleothem studies have been used to reconstruct aerosol source supply to cave locations and changing source region environments (Goede *et al*., 1998; Ayalon *et al*., 1999; Frumkin & Stein, 2004; *Li et al*., 2005; Zhou *et al*., 2009b). The lack of knowledge regarding the extent of terrestrial and marine aerosol incorporation, either through direct aerosol deposition or by external deposition and solution transport led to the theoretical modelling in Chapter 2. Additionally, speleothem marine and terrestrial aerosol incorporation aspects are investigated in Chapter 3.

*Organic analysis*

Polycyclic aromatic hydrocarbons (PAH) are the main component of organic analysis used in aerosol monitoring throughout this investigation. PAHs are widely spread organic compounds generated from the incomplete combustion of organic material (Terzi & Samara, 2005). PAHs are ubiquitous pollutants (Kehrwald *et al*., 2010a) of global significance since they can be transported over global distances by wind systems (Gabrieli *et al.*, 2010). PAHs can therefore provide a record of changing combustion through time. Previous studies have produced PAH records from soils (Zou *et al*., 2010), surface sediments (Perrette *et al.,* 2008), riverine and marine sediments (Boonyatumanonds *et al.,* 2006), snow (Sharma & McBean., 2002), ice cores (Kawamura *et al.,* 1994) and speleothems (Perrette *et al*., 2008). PAH concentrations of speleothem are investigated further in Chapter 5. Additional organic molecular markers can be used for the identification and reconstruction of fire events (reviewed in - Conedera *et al*., 2009). Methoxyphenols and levoglucosan have been suggested as potential forest fire biomarkers identifiers (Simpson *et al*., 2004). Charcoal is a signature of biomass burning worldwide and its presence in the sedimentary record can shed light on both temporal and spatial characteristics of palaeofire regimes (Buckman *et al.,* 2009). Further details of organic

aerosol background and analytical methods are presented in the following chapters. The use of organic aerosol fire proxies in speleothem to investigate forest fire occurrence has not yet been achieved. However, organic analysis of levoglucosan and methoxyphenols is successfully utilised for the detection of palaeofires in flowstone samples in Chapter 5.

## 1.2. Flowstones

Calcareous speleothems are crystalline deposits of calcium carbonate ($CaCO_3$) formed in karstic caves as a result of precipitation from dilute aqueous solutions entering the cave (Schwarcz, 2007). Speleothems are valuable archives of terrestrial climatic conditions, offering numerous advantages over other terrestrial climate proxy recorders such as lake sediments and peat cores (McDermott, 2004). The nomenclatural definition of speleothem includes all cave carbonate forms, including: stalagmites, stalactites and flowstones. In this investigation the analysis of speleothem is limited to selected flowstones. Flowstones are more continuous carbonate deposits that accrete beneath thin sheets of water on cave walls and floors (Fairchild & Baker, 2012). Flowstones were selected for investigation in Chapters 4 and 5 of this thesis as they presented several advantages over stalagmites. Due to the nature of flowstone growth they often form in much greater quantities when compared to stalagmites, offering a far more abundant source for analysis. This is especially of significant importance when large samples are required for destructive analysis, such as the organic analysis used in Chapter 5. Additionally, flowstones often present variable growth rates and complex stratigraphy, this is seen as a disadvantage for palaeoclimate studies. However, changing growth rates and calcite forms offers greater insight into aerosol contribution under different environmental and growth processes, properties considered beneficial to this study.

### *1.2.1. Flowstone formation*

Figure 1.3 presents the chemical processes involved in the precipitation of flowstone calcite. Flowstones generally precipitate at the base of flowing rivulets or streams of water, and therefore represent higher mean discharges (during periods of growth) than dripwater supply to stalagmites (Fairchild & Baker, 2012). Tooth & Fairchild (2003) present models for differing flow pathway types which may control karst water evolution. The models investigate the differing flow rates of conduit, fracture and matrix flows and their palaeohydrological signals at Crag Cave, Ireland.

Speleothems are composed of calcite formed by slow degassing of $CO_2$ from supersaturated groundwater (Richards & Dorale, 2003), the variability of which strongly influences flowstone growth rates (Baker & Smart, 2005). The rate of drip water degassing is often predominantly controlled by cave air $pCO_2$ (Spötl *et al.,* 2005; Johnson *et al*., 2006; Banner *et al*., 2007; Baldini *et al.,* 2008; Mattey *et al*., 2008; 2010). Cave air $pCO_2$ is controlled by the exchange of high $pCO_2$ cave air with 'fresh' low $pCO_2$ external air, known as cave ventilation or cave breathing (Mattey *et al*., 2008; 2010; Kowalczk & Froelich, 2010; Cuezva *et al*., 2011; Frisia *et al*., 2011; Fairchild & Baker 2012). Consequently, an understanding of how caves ventilate with the external atmosphere is critical in reconstructing past environmental scenarios from speleothem. Few studies have been conducted to study the relationship between cave air circulation and cave aerosol transport (Smith *et al.,* 2013, Chapter 2 - Dredge *et al.,* 2013). This research gap is addressed in Chapter 2 and in further detail in Chapter 3, which explores how cave ventilation processes relate to cave aerosols in Gough's Cave, Cheddar Gorge.

Due to the nature of their growth, flowstones can often show small-scale topography reflecting the ponding of surface water (Fairchild & Baker, 2012) consisting of stepped gours bordered by rimstones (Hammer *et al.,* 2010). Flowstone growth morphology controls will influence the collection of aerosol deposits and must be considered when evaluating aerosol contributions. Calcite formation types can offer significant insights into precipitation and environmental processes (Frisia *et al*., 2000; 2010). Changing calcite form and colour are explored in Chapters 4 and 5 respectively. Flowstone growth features result in changing precipitation processes creating a more complex record, both stratigraphically and geochemically. Consequently, flowstones are often viewed as an inferior speleothem source for investigation.

In addition to growth-related processes, pre-precipitation processes can influence flowstone geochemistry. Calcite precipitation may occur before precipitation at the flowstone sampling site; this is known as Prior Calcite Precipitation (PCP). PCP causes changes in flowstone geochemistry separate from external environmental derived change, and often results in enhanced trace element concentrations in calcite (Fairchild *et al*., 2000). Karst dissolution and discharge residence times can also influence the chemistry of cave drip waters and resultant calcite chemistry; further details and example studies are shown in Table 1.1. PCP and dissolution processes are identified and quantified using indices derived from trace element analysis in Chapter 4, section 4.4.2.
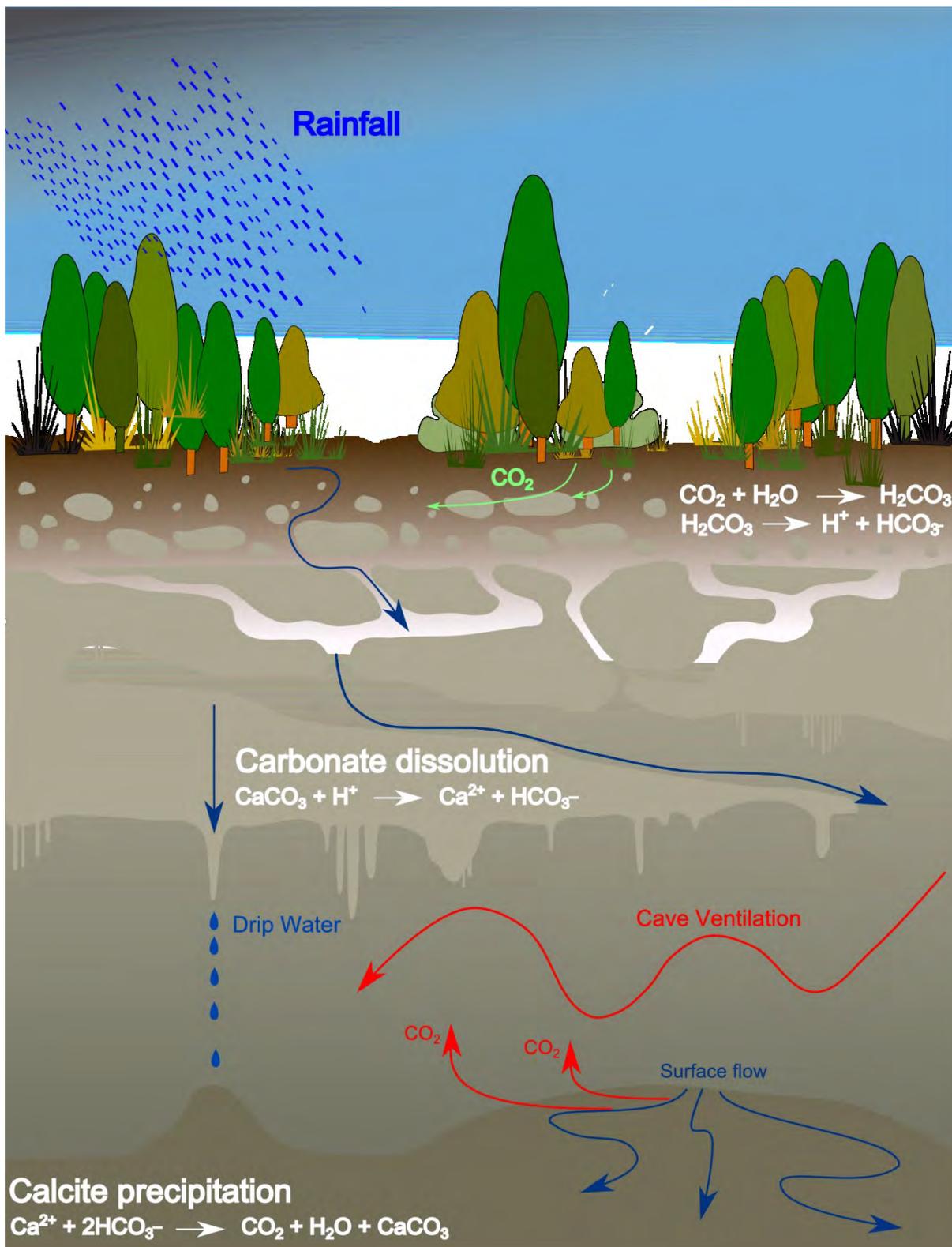
Figure 1.3: Speleothem formation processes. Illustration of processes relating to the formation of speleothem and flowstones: rainfall, percolation, dissolution, degassing and precipitation.

## 1.2.2. Flowstone geochronology

Uranium–thorium ($^{238}$U-$^{230}$Th) is a radiometric dating technique commonly used to determine the age of carbonate materials such as speleothem and coral (Richards & Dorale, 2003; Zhao *et al.*, 2009a). Chapter 2 models the relationship between speleothem growth and aerosol incorporation rates, quantifying potential aerosol contributions to speleothem geochemistry at different growth rates.

Speleothem are ideal materials for precise U-series dating, yielding ages in calendar years, removing radiocarbon calibration problems associated with most other continental records (McDermott, 2004). However, the increased stratigraphic intricacies associated with flowstone growth requires high resolution dating of high precision to identify changing growth rates and constrain hiatus events (which may be short lived). Furthermore, the higher discharge rates associated with flowstone growth often results in increased colloidal material transport and calcite incorporation containing increased levels of detrital Th ($^{230}$Th). U-series dating requires a correction for the initial Th using $^{232}$Th as an indicator for $^{230}$Th content, which introduces increased errors into the dating process (correction methods reviewed in Hellstrom, 2006).

## 1.2.3. Flowstone (speleothem) palaeoenvironmental proxies

It is possible to reconstruct past environments once a sample age model has been established. A range of geochemical palaeoenvironmental proxies are recruited in speleothem studies to provide insights into specific environmental processes. A summary of proxies, associated environmental conditions, method limitations and previous studies are presented in Table 1.1. A range of proxies are used in order to reconstruct past environments in Chapters 4 and 5.

| Proxy | Environmental Condition/ Process | Limitations/Conditions | Studies |
|---|---|---|---|
| $\delta^{18}O$ | $\delta^{18}O$ of rainfall | Carbonate must be precipitated under equilibrium conditions to reconstruct conditions. Resolution dependent on discharge path. Generally mean annual rainfall. | Fleitmann *et al*., 2004; McDermott *et al*., 1999; McDermott *et al*., 2011 |
| | Ventilation controlled isotopic fractionation. | Under low cave $pCO_2$ conditions, rapid degassing can result in fractionation. May present seasonality in $\delta^{18}O$ associated with seasonal ventilation. | Mattey *et al*., 2008; 2010; Johnson *et al*., 2006. |
| | Amount effect | Lower $\delta^{18}O$ values associated with wetter years due to significant precipitation. | Bar–Matthews *et al*. 1996; Treble *et al*., 2005. |
| | Rayleigh fractionation | Fractionation effects occurring as a consequence of increasing latitude, altitude (decreasing temperatures) and distance from source resulting in lowering of $\delta^{18}O$. | McDermott *et al*., 2011 (overlaps with palaeotemperature work) |
| | Palaeo-temperature | There have been several attempts to calibrate speleothem $\delta^{18}O$ to provide a temperature record. However, due to the complexity of the isotopic system this has proved difficult. | Gascoyne *et al*., 1983; Lauritzen & Lundberg, 1999; McDermott *et al*., 1999 |
| | Surface evaporative processes | Evaporation results in $\delta^{18}O$ enrichment through the preferential removal of the light $^{16}O$ isotope. | Bar-Matthews *et al*., 1996; Denniston *et al*., 1999 |
| | Monsoon strength. | Palaeo-precipitation and summer monsoon strength, lighter $\delta^{18}O$ indicating | Fleitmann *et al*., 2003, 2004; Wang |

| | | | |
|---|---|---|---|
| | | stronger summer monsoon and higher rainfall. | *et al.*, 2001; Cheng *et al.*, 2009b; Zhang *et al.*, 2008 |
| | Glacial/inter-glacial transitions. | Millenial scale climatic variation can manifest in a variety of ways, dependent on geographical location. Changing ice volume, thermohaline cycles and atmospheric circulations can all influence the distribution and environmental fractionation of oxygen isotopes. | Bar-Matthews *et al.*, 2000; Genty *et al.*, 2003; 2006; Wainer *et al.*, 2009; Williams *et al.*, 2005; Cheng *et al.*, 2009a. |
| $\delta^{13}C$ | Millennial variations in C3/C4 vegetation. | The distinction could only be made in very slow (completely degassed) drips due to the subtle nature of influence. Local processes tend to dominate. | Dorale *et al.*, 1992; Bar-Matthews *et al.*, 1997; McDermott, 2004 |
| | Microbial activity and vegetation respiration | Changes in biological respiration in the soil profile results in changing soil $CO_2$ and carbon isotopic compositions. | Hodge *et al.*, 2008; Genty *et al.*, 2003 |
| | Drip water degassing | As with $\delta^{18}O$ degassing is controlled by cave $pCO_2$ or drip hydrodynamics (e.g. kinetic, impact and thin film fractionation). Increased degassing rates results in greater fractionation of carbon isotopes through preferential loss of the lighter $^{12}C$ isotope. | Hendy, 1971; Dulinski and Rozanski, 1990; Baker *et al.*, 1997; Spötl *et al.*, 2005; Mühlinghaus *et al.*, 2009; Frisia *et al.*, 2011; Lambert & Aharon, 2011 |
| $^{87}Sr/^{86}Sr$ | Aeolian dust-Seawater-host rock | Aeolian dust, host rock and seawater present differing $^{87}Sr/^{86}Sr$ signatures which must be recorded and demonstrate detectable variation to provide | Bar-Matthews *et al.*, 1999; Frumkin and Stein, 2004; Zhou *et al.*, 2009 |

| | mixing | information on source process variations. | |
|---|---|---|---|
| | Effective rainfall: host rock-aeolian influence | Disparate aeolian and carbonate $^{87}Sr/^{86}Sr$ signatures are required. Complexities arise with carbonate $^{87}Sr/^{86}Sr$ signatures which are similar to other sources e.g. carbonate dust and limestone bedrock. | Ayalon *et al*., 1999 |
| | Ground water modelling | Varying carbonate compositions presenting differing $^{87}Sr/^{86}Sr$ signatures can offer insight into change discharge pathways. | Banner *et al*., 1996 |
| | Palaeowind: Source identification | Changing dust sources can indicate changing palaeowinds. Issues of source identification and distinction are common. | Goede *et al*., 1998 |
| **Trace elements** | Review | A review of trace elements in speleothem. | Fairchild & Treble, 2009 |
| | Residence times - dolomite dissolution | Sufficient separation in Mg compositions between dolomite dissolution and other Mg elevating processes must exist. PCP and changing discharge pathways can also result in elevated Mg; therefore process discrimination analysis is required. | Treble *et al*., 2003; Johnson *et al*., 2006 |
| | Temperature | Partitioning of Mg between water and calcite is temperature dependent. Difficulties in calibration occur due to geochemical, hydrological and crystallographic processes resulting in alterations of trace element concentrations beyond temperature effects. | Oomori *et al*., 1987; Mucci, 1987; Burton & Walter, 1991; Mucci & Morse, 1990; Huang & Fairchild, 2001 |
| | Growth rate | Sr is known to incorporate at greater growth rates as a result of increased crystallographic defect sites for occupancy and substitution with Ca. | Gabitov & Watson, 2006; Gabitov *et al*., 2014 |
| | Seasonal vegetation | P and U may be related because of the stability of uranyl phosphate, and | Treble *et al*., 2003; |

| | | | |
|---|---|---|---|
| | decay | reflect the climatic effects on the rate of bioproduction of P. Relationship is regional and dependent on soil profile conditions. U is known to be strongly associated with organic matter, such as fulvic and humic acids, and inorganic colloids. | Richards & Dorale, 2003 |
| | Detrital influence | Th provides an indication of colloids, humic acid transport. Detrital influences and Th transport have been studied predominantly due to its influence on the U-series dating method. | Richards & Dorale, 2003 |
| | PCP | Prior calcite precipitation removes Ca from the drip water solution resulting in the increase of Tr/Ca in the residual solution. PCP can be used as an indicator for rainfall through the comparison of Mg and $\delta^{13}$C. | Fairchild *et al*., 2000; McMillan *et al*. 2005; Baldini *et al*., 2006; Karmann *et al*., 2007;Treble *et al*., 2008; Mattey *et al*., 2008; Van Beynen *et al*., 2008. Hellstrom & McCulloch, 2000 |
| | Natural organic matter fluxes | Metals are known to bind to organic matter with high fluxes of metals associating with high infiltration flow events. | Borsato *et al*, 2007; Hartland *et al*., 2011;2012 |

Table 1.1: A summary table displaying commonly utilised speleothem geochemical environmental proxies. A range of processes or environmental conditions which are represented by each proxy are listed and selected relevant studies from the literature cited.

## 1.3. Previous flowstone studies

Flowstones have been used in a multitude of palaeoclimatic and archaeological investigations. A range of flowstone studies presented in the literature are outlined within this section.

### *1.3.1. Flowstone palaeoclimate reconstructions*

Flowstones are used for the purpose of palaeoclimatic reconstructions due to their occurrence, age range and growth formation. The widespread distribution and variability in sample types often make flowstones a highly valuable speleothem palaeoclimatic resource.

A 7 cm thick flowstone sequence from Lapphullet Cave, Norway was analysed by Lauritzen et al. (1990) to reconstruct past climate. Dating showed a growth interval of 350 - 730 ka, with stable isotope analysis suggesting deposition during warm periods. Pollen assemblages were also used in this study to reconstruct vegetation changes. Andrews et al. (2007) used flowstone deposits and coralline algae as evidence for the timing of vadose zone ground water deposition and marine conditions respectively. Contaminant Th was an issue with some flowstone samples. However, samples were sufficiently constrained to determine sub-orbital sea-level change in early MIS 5e (Andrews *et al.,* 2007). Meyer et al. (2009) investigated two flowstone samples Wilder Mann Cave and Wildmahd Cave in the northern Austrian Alps. Two samples ~2.0 and ~1.7 Ma in age presented seasonally biased regular lamination. Significantly, flowstone samples were U-rich allowing for U-Pb dating. Wainer et al. (2011; 2013) studied a flowstone core from Villars Cave, France to reconstruct millennial climatic instability. The entire core is 114.2 cm long and 7.5 cm wide and presents varying porosity with columnar fabrics and covers the last 180 ka. Meyer et al. (2012) studied a flowstone

deposit from Entrische Kirche Cave, Austria. Millenial scale temperature fluctuations were identified. Ages were obtained but the detrital content of the flowstone made U-Th dating difficult. Frisia et al. (1993) utilised the variable characteristic of flowstone to investigate the morphology, crystallography and geochemistry of a flowstone calcite in a core from Grotta di Cunturines, Italy. A range of different facies types were identified with layered morphology of varying thicknesses. This study aims to utilise the variable characteristics of flowstones to specifically investigate aerosol chemistry additions and improve the use of palaeoclimate proxies in speleothem. Chapters 4 and 5 explore the palaeoclimatic significance of aerosol contributions from marine and terrestrial, and forest fire sources respectively.

### 1.3.2. Flowstone archaeological importance

Flowstones are often used because of their occurrence in archaeologically significant cave locations. While much work has focused on dating stalagmites, in many archaeological and palaeontological settings flowstones are beneficial as they can provide age constraints for the material associated with them (Pickering, 2012).

A 30 cm thick floor flowstone deposit was dated and combined with sedimentological stratigraphic analysis to determine the ages of archaeological artifacts at Grotte du Lazaret, France by Falguères et al. (1992). The flowstone ages fell between 130 and 70 Ka BP indicating the timing of tool use transition. Hopley et al. (2007a; 2007b) utilise flowstones due to their geographical significance in determining the onset of bipedalism, homo evolution and the appearance of African *Homo erectus*. Flowstone deposits contained within a sedimentary sequence were investigated to reconstruct African palaeoenvironments in Buffalo Cave, South Africa by Hopley et al. (2007a). A large 2.4m thick flowstone deposit was

identified at a depth of 14.09m, with shallower more localised deposits also being detected. Stable isotope results showed a 2.0-1.5 Ma record of continuous climatic and vegetation change. Hopley et al. (2007b) investigated two continuous sequences of flowstone from the Makapansgat Valley, South Africa. The flowstones formed part of a collapsed cone. Stable isotope analysis was combined with a time series to determine two vegetational shifts toward increased savannah grasses between the late Miocene/early Pliocene and at 1.7 Ma. U-Pb dating of a flowstone from South Africa by Pickering et al. (2011) shows ages of 2.3 Ma, 1.8 Ma and 1.7 Ma. The timing of flowstone growth has been used correlate environmental conditions between different caves and develop the understanding of the human evolutionary history.

These studies demonstrate the usefulness of flowstones samples for both palaeoenvironmental and archaeological studies. This study focuses on developing the ability to utilise flowstone speleothems in palaeoenvironmental reconstruction efforts.

## 1.4. Thesis aims and objectives

The aim of this work is to determine the extent and impact of aerosol deposition contributions to speleothem geochemistry. In order to achieve this, several research objectives were formulated.

1. To understand the transport, distribution and deposition within cave networks

2. Define and quantify the contribution of aerosols to speleothem geochemistry

3. Explore and identify aerosol contributions to speleothem samples in different cave environments

## 1.6. Thesis structure

Due to the multidisciplinary nature of this investigation, each chapter is presented as a separate case study. Every chapter has an individual introduction, which outlines the themes of importance for each specific study. The content of each chapter is summarised here:

*Chapter 2: Cave aerosols: distribution and contribution to speleothem geochemistry.*

This chapter provides a synthesis of the impacts of cave aerosols on the cave environment and speleothem. Processes of cave aerosol introduction, transport, deposition, distribution and incorporation are explored and reviewed from existing literature. The contribution of cave aerosol deposition to speleothem geochemistry is modelled and evaluated using a mass balance framework. This collaborative project was published as an invited review in Quaternary Science Review (Dredge *et al*., 2013) and is presented in published form in the supplementary material, section S.18.

*Chapter 3: Processes affecting aerosol concentrations in Gough's Cave, Cheddar Gorge, UK.*

This investigation builds on the findings of Chapter 1 and focuses on the relationship between the cave environment, specifically cave ventilation and suspended cave aerosol loads. Results are presented from seasonal term monitoring of $CO_2$, temperature and suspended aerosols in Gough's Cave, Cheddar Gorge. This chapter has been published in Cave and Karst Sciences (Dredge *et al*., 2014) and the final manuscript is presented in the supplementary material, section S.18.

*Chapter 4: Flowstones as palaeoenvironmental archives: 500 ka flowstone record from New St Michaels Cave, Gibraltar.*

This study focuses on the geochemical analysis of a flowstone core from New St Michaels Cave, Gibraltar. A suite of palaeoclimate proxies are utilised to investigate changing environmental conditions in Gibraltar over the last 500,000 years. The effect of local processes such as prior calcite precipitation and changing hydrology are evaluated and quantified. Seawater contributions are quantified and their changing behaviour studied through time. Additionally, terrestrial aerosol dust signatures are identified. Palaeoenvironmental change is established and qualitatively described by changing hydrological conditions from 'wet' to 'dry'.

*Chapter 5: Speleothem as a recorder of forest fires: Testing Yarrangobilly flowstones for fire aerosol incorporation and preservation.*

The premise that black coloration in Yarrangobilly flowstone samples are a result of forest fire aerosol deposition is investigated in this study. Organic and inorganic geochemistry analysis of two flowstone samples is used to determine environmental and formation conditions which associate with red, black and white flowstone coloration. The likelihood that forest fires aerosols resulting in coloration is evaluated and new theories for coloration are introduced, including alternative aerosol contribution hypotheses.

# Cave aerosols: distribution and contribution to speleothem geochemistry
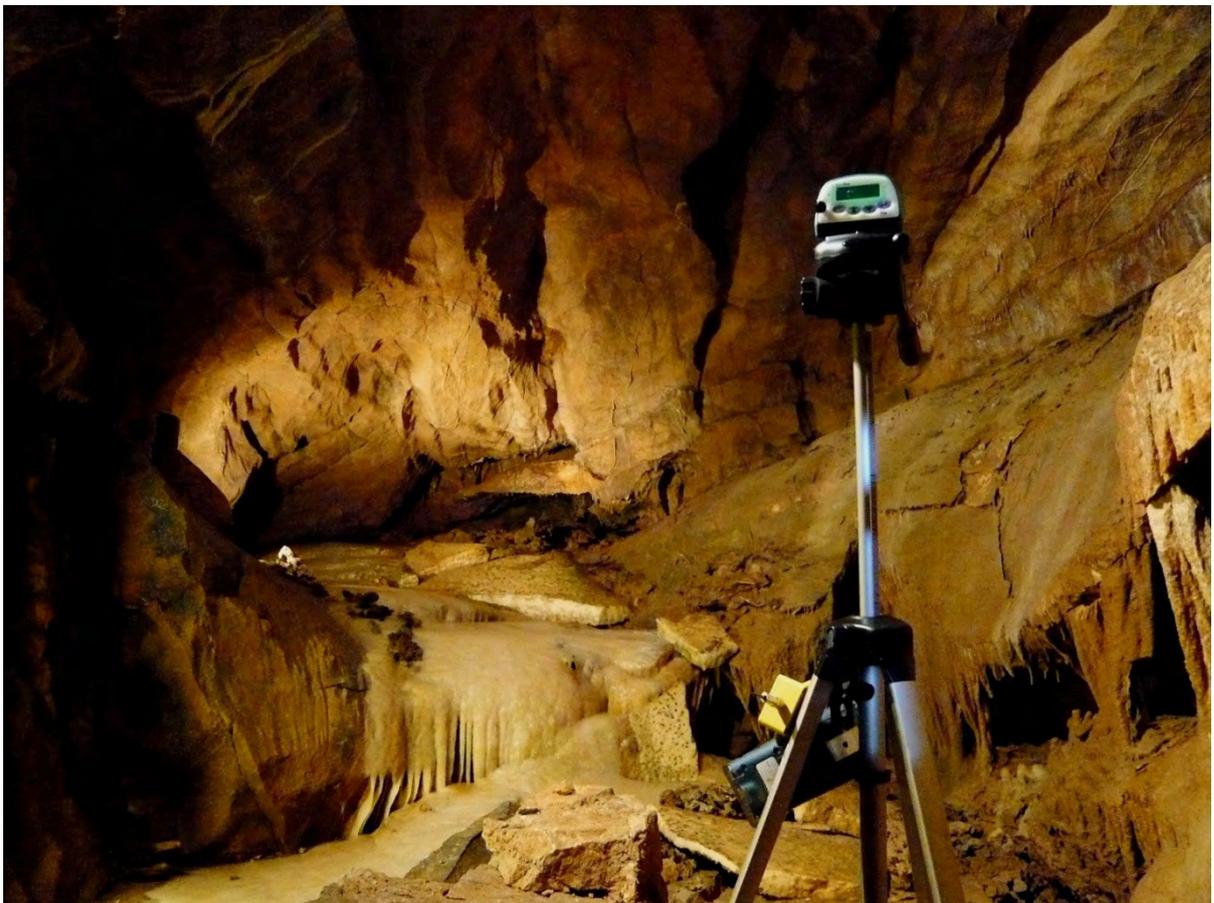


*Aerosol, temperature and CO$_2$ monitoring in Gough's Cave*

# Chapter 2. Cave aerosols: distribution and contribution to speleothem geochemistry

This chapter has been published in the journal of Quaternary Science Reviews (Dredge *et al*., 2013).

## 1. Introduction

A new sector of interest is developing within cave science regarding the influence of aerosols on the cave environment and the potential palaeoenvironmental record, which may be preserved within cave precipitates as a result of aerosol incorporation. This paper provides the first attempt to synthesise the issues concerning cave aerosols, with particular focus on the situations in which aerosols will provide a significant contribution to speleothem chemistry. Examples will be taken from several cave sites including Obir Cave, Austria, where we test the proposition of Fairchild et al. (2010) that aerosols may have contributed significantly to speleothem trace element concentrations. Specific processes affecting the transport and deposition of cave aerosols will be highlighted through the presentation of monitoring data at several sites. Results draw attention to the relative importance of aerosols in different environmental and speleothem growth scenarios, with aerosols generally being of minor influence during normal speleothem growth, but potentially providing a major contribution to bulk chemistry at hiatuses.

Aerosols are generally defined as the suspension of fine solid or liquid particles within a gaseous medium (Hinds, 1999) (often being the earth's atmosphere). Aerosols become suspended into the earth's atmosphere during a multitude of processes both natural (e.g. volcanic eruptions, windblown sands, forest fires) and anthropogenic (e.g. biomass burning, vehicle emissions, constructions); examples of emissions to the external atmosphere are displayed in Figure 2.1. The quantity and type of aerosols emitted are dependent on the process type and intensity. Aerosols can be grouped and identified based on a range of properties, both physical (e.g. colour, morphology, size) and chemical (e.g. inorganic, organic, isotopic).

Atmospheric aerosols enter cave networks due to external transportation processes, travel within caves as a result of cave ventilation, and are either deposited or transported with cave air and eventually removed from the cave system. The removal of aerosols from air occurs as a result of either wet or dry deposition. Dry deposition is the process by which atmospheric trace constituents are transferred by air motions to the surface of the Earth (Wesely & Hicks, 2000). The main processes by which dry deposition occurs are outlined below (Petroff *et al.,* 2008):

- Brownian diffusion – The random movement and collision of particles can cause deposition; this process affects very fine particles typically smaller than $0.1\mu m$

- Interception - Particles entrained in a stream flow are retained by an obstacle when their path passes within one particle radius of the object

- Impaction - An aerosol with significant inertia transported by the flow towards an obstacle cannot follow the flow deviation in the vicinity of the obstacle causing particle collision with the obstacle and remaining on the surface

- Sedimentation – particle fall-out due to gravitation

Wet deposition is the removal of material from the atmosphere by hydrometeors as a result of condensation and precipitation. Wet deposition can also be referred to as precipitation scavenging, rainout (typically used for in-cloud processes), and washout (typically used for below-cloud processes) (Loosmore & Cederwall, 2004).

The dry depositional efficiency is expressed as a deposition velocity, $v_d$, where;

$$v_d = F/C$$

Where, F is the particle flux to the surface, and C the airborne concentration at a reference height. Because deposition involves several mechanisms, as outlined above, $v_d$ is a complex function of particle size, with the highest values for very small (< 0.1 μm diameter) and large (> 1 μm) particles. In the range 0.1-1 μm where much of the mass of atmospheric aerosol resides, values of $v_d$ are very small. For very large particles, typically > 10 μm diameter, $v_d$ becomes almost equal to the gravitational settling velocity, but for smaller particles is substantially greater (Seinfeld & Pandis, 1998).
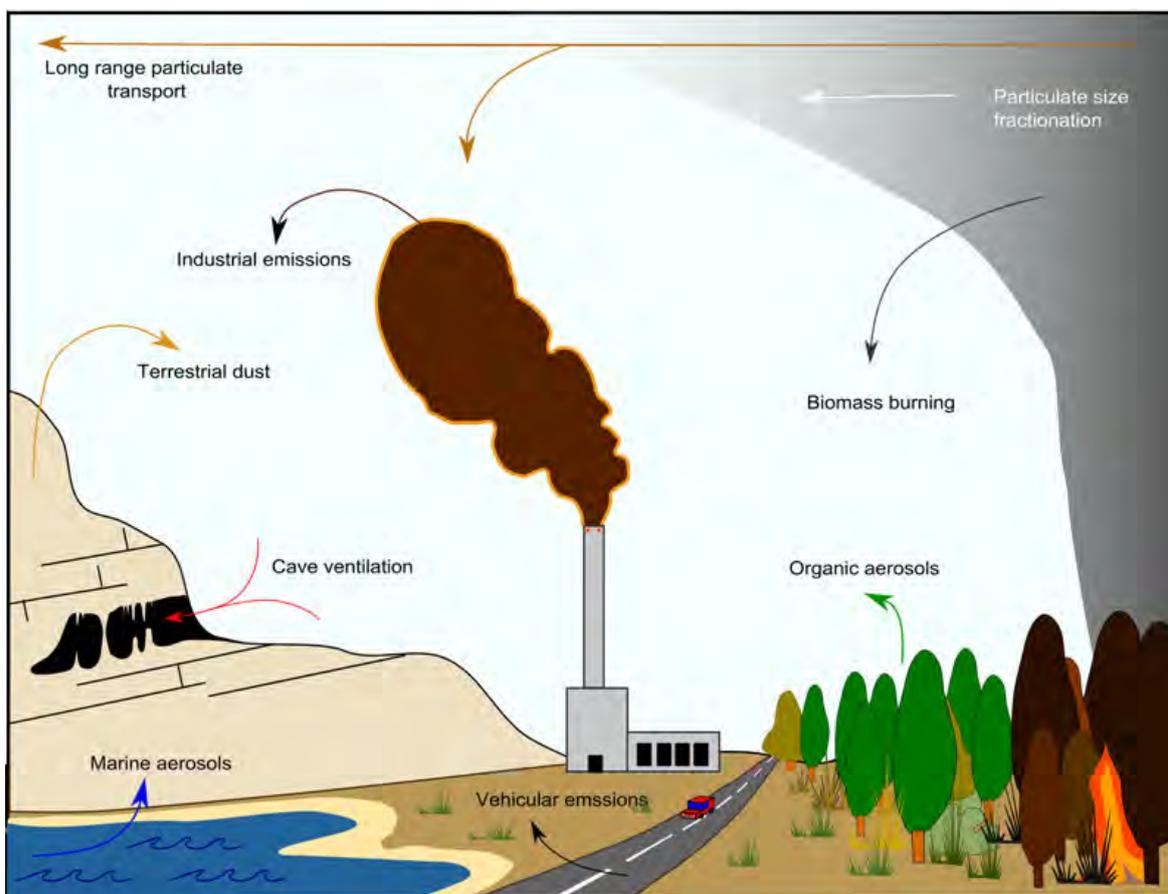
Figure 2.1: Illustration of tropospheric aerosols that are likely to be emitted in large enough quantities to be incorporated and detectable within speleothems. Aerosols produced within the cave environment also have the potential to become incorporated in detectable quantities.

Aerosols, once suspended into the atmosphere through emission processes, will be carried with parcels of air and mixed with other aerosol types, which may have properties characteristic of their emission and geographical source. Hence, it may be possible to determine palaeoenvironmental conditions through the incorporation of aerosols within speleothem. Sr isotope studies have demonstrated the ability to utilise aerosols to identify the geological source region of terrestrial dust by comparing them to the Sr isotopic ratio of dust surface deposits (Li *et al.,* 2005; Yang *et al.,* 2009; Masson *et al.,* 2010), of waters (Jin *et al.,* 2011) and in speleothem (Goede *et al*., 1998; Verheyden *et al.,* 2000; Frumkin *et al*., 2004; Zhou *et al.,* 2009b) although the mode of transmission of the chemical signal is normally

proposed to be via dripwater. Studies have been successful in the identification of fire events and source regions through constraining region-specific vegetation burning events in ice and sediments (Laird *et* al., 2000; Wang *et al.,* 2005; Zhou *et al*., 2007; Kehrwald *et al*., 2010a & 2010b; Wang *et al.,* 2010) with a range of organic proxies (reviewed in - Simoneit, 2002). Different types of vegetation have known associated organic components which are released during burning events; the region of burning and therefore the direction of transport can therefore, in some cases be deciphered. Similar fire-proxy work may be applicable to use with speleothems.

For modern studies, air mass travel paths can be tracked and modelled. Atmospheric transport and dispersion modelling using HYSPLIT and other programs allows air mass trajectory estimation of past air movements, or projections to produce forecast trajectories (http://ready.arl.noaa.gov/HYSPLIT.php). These simulations are based on recorded or predicted meteorological conditions for past and future modelling respectively. Air mass trajectories provide an insight into the likely long-range aerosol source locations and thus aid in the identification of aerosol emission processes.

Interest in cave aerosols has developed due to the increasing awareness of aerosol impacts on the cave environment. Cave preservation and the potential degradation of the cave environment resulting from cave aerosol deposition and associated mitigation practices are growing issues among cave management organisations especially regarding the conservation of show caves (e.g. Ohms, 2003). Degradation can occur from external pollutants or from visitor disturbances to the natural cave environment. The effects of anthropogenic dust on caves may be subtle, but threaten the long term preservation of cave environments.

Christoforou et al. (1996a; 1996b) identified spoiling of statues within Buddist cave temples as a result of aerosol deposits. In some instances aerosol issues are remediated through improved cave conservation practices. For instance, Altamira cave was closed to visitors due to anthropogenic fine particle resuspension from cave floor sediments, provoking microparticle detachment (releasing bacterial and fungal spores), among other factors. Installation of a thermally insulated access door reduced the entry of airborne particles, the condensation rate in the entrance area, and the metabolic activity of the main visible microbial colonies (Saiz-Jimenez et al., 2011). Soiling of the cave environment has occurred as a result of coal industry pollutants and airborne dust from regional dust storms (Christoforou et al., 1994). A similar issue of cave degradation as a result of aerosol deposits from coal mining activities has also been investigated by Salmon et al. (1994; 1995). Black pollutant deposits causing degradation in other caves has been attributed to deposits from vehicle exhaust (Jeong et al., 2003) and a combination of car exhaust and biomass burning emissions (Chang et al., 2008). Michie (1999) partially attributed the slow degradation of cave aesthetic values to cave visitors transporting, releasing and causing re-suspension of aerosols within the cave.

The presence of cave aerosols is controlled by a combination of internal aerosol production and the incorporation of transported externally sourced aerosols. Cave ventilation and morphology will strongly influence how aerosols are transported and deposited within the cave environment. The quantity and effect of cave aerosols on speleothem geochemistry has rarely been explicitly considered so far and is expected to be a combined result of the processes explored. By investigating and gaining an improved understanding of how aerosols are transported, distributed, deposited and ultimately incorporated into forming speleothem we will potentially be able to identify aerosol signatures within the speleothem

palaeoenvironmental record. This investigation will identify the key situations and processes under which aerosol deposition and speleothem incorporation results in significant identifiable contributions to speleothem geochemistry.

This chapter will be structured as follows: Previous aerosol investigations, associated methods and the methods utilised for monitoring work presented in this paper will be discussed (Section 2.2). The latter are divided into sampling, extraction and analytical methods. Next, aerosol sources, processes, distribution and deposition mechanisms are explored (Section 2.3). In the results section (Section 2.4), specific aerosol processes will be highlighted with preliminary data from cave monitoring. Finally, aerosol contributions to speleothem geochemistry will be evaluated through the comparison of known deposition fluxes to drip water and speleothem geochemistry in Obir cave, Austria in section 2.5.

**2.2. Methods**

A plethora of aerosol properties can be analysed to investigate specific processes. Some of the key properties and associated processes are summarised in Table 2.1.

| Cave aerosol property | Reason for investigation |
|---|---|
| Suspended concentration | Aerosol transport and distribution |
| Deposition flux | Aerosol distribution (especially to speleothem surface) |
| Inorganic chemistry | Source identification, potential chemical addition to speleothem, transport. |
| Organic chemistry and /or associated microorgansims | Source identification (especially processes associated with biomass burning), transport, airborne bacteria and fungi identification |
| Aerosol size | Transport, distribution |
| Aerosol morphology | Transport, source identification (lesser extent than chemistry) |

Table 2.1: Aerosol properties and the processes which can be explored as a result of their investigation.

An extensive range of methods exist for the sampling, monitoring and analysis of cave aerosols, each specific to the information required and depending on the application. Due to the logistics of working in the cave environment, cave aerosol investigations will often require passive or self-powered portable equipment for aerosol sampling and in-situ analysis.

### 2.2.1. Sampling

*Dry deposition sampling*

There is no generally accepted method to directly measure or estimate dry deposition (Chu, 2008). However, it has been established that a smooth horizontal surrogate surface provides a lower bound estimate of the dry deposition flux onto a horizontal surface (Sehmel, 1978; Holsen *et al*., 1992). Dry deposition is determined through the capture of aerosol deposition to a known surface area. Surrogate surface sampling does not require power and designs can be portable, making this method highly suitable for cave monitoring studies.

There is a range of apparatus currently being used for surrogate surface sampling. The most basic of surrogate surfaces is often constructed of a smooth plate surface to collect deposition. Flat horizontal surfaces are generally used; however, in locations where there is a high ventilation rate it may be applicable to use an aerodynamic collection surface as in Zuffell et al. (1998). The issue of aerosol retention and aerosols being dislodged in the cave environment is not of critical importance as the high humidity of the cave ensures that strong forces of adhesion retain particulates to the surrogate surface (Michie, 1997). Nevertheless, the shape of the collection surface and factors such as surface roughness will have an impact on the retention of aerosols onto the surface and should therefore be considered. Different surfaces have been used dependent on the aerosol under investigation. Smooth surfaces provide an interface which can be cleaned making it ideal for elemental chemistry analysis: polyvinyl chloride (Lim *et* al., 2006; Chu, 2008, Zhang *et al*., 2011) and glass slides (Salmon *et al*., 1995) have been used. Surfaces can be covered with Apiezon grease (Kim *et al.,* 2000; Lim *et al*., 2006) providing increased collection and retention relative to a smooth surface alone. However, this method is not suitable for elemental analysis due to potential

contamination of the grease, but may be utilised for morphological studies. Specific cation-exchange membranes (Lyman *et al.,* 2007) can be used for element specific studies.

Relative to a smooth surface a filter provides increased surface roughness which improves the aerosol retention of a surrogate surface. As a general observation, an increase of downward aerosol flux is observed with increasing collector surface roughness (Vawda *et al.*, 1990), a property which has been utilised in surrogate sampling studies (Bytnerowicz *et al*., 1987; Zuffel *et al.,* 1998). However, although surface roughness is increased, the extraction efficiency from filter media may be compromised compared to smooth surface collection. Quartz fibre filters provide the advantage to withstand high temperatures and are therefore useful in organic studies (filter combustion cleaning method outlined in following chapter method sections). Membrane filters, made from polycarbonate and PTFE (Teflon), are better suited to trace element analysis studies, but can obtain an electrostatic build-up resulting in altered sample collection, or sample loss (Wieprecht *et al.,* 2004).

In a comparative study, Wai et al. (2010) sampled the dry deposition of crustal particles onto surrogate surfaces of glass and polystyrene as well as Petri dishes filled with de-ionised water. The study demonstrated that in general, the water surface can collect more material (ten times or more of acidic and alkaline species), while glass collects similar or lesser amounts of various species than polystyrene. Water as a collection device in the cave environment has the benefit of being analogous to an actively growing speleothem surface in that both involve aerosol deposition to a wet surface. However, logistically this technique is more complex due to the transportation of the waters to and from the cave site, with much greater risks of sample loss and contamination through handling and spillage.

The positioning of surrogate surfaces within the cave network appears to be relatively robust in its sensitivity. The exposure of the surrogate surface is relatively unimportant: Michie (1997) found that even when sheltered by a covered surface (28 mm above) dust deposition is only reduced by 50%. However, in the external environment, retention has been shown to be influenced by atmospheric precipitation (Lyman *et al.,* 2007). Therefore, care should be taken about the placement of surrogate surfaces in relation to active drip sites.

In this study the surrogate surface method for sampling was selected to provide a sample of aerosols which will most closely represent the quantity and type of aerosols that may become incorporated into speleothem growth. Petri dishes (see supplementary material section S.1, Figure S.1) provide a convenient means as the collection surface can be readily capped and then sealed with parafilm reducing the potential of contamination during transportation once cleaned, and after sampling. Specific preparation and extraction procedures are required for the collection and analysis of the different aerosol species. In this study Polytetrafluoroethylene (PTFE) filters were used as a surrogate surface collection medium in samples where the inorganic aerosol component was to be analysed. PTFE filters provide reduced blank levels in comparison to other filter media available, and provide a rough collection surface. Detailed sampling methods can be found in the supplementary material section S.1.

*Suspended aerosol sampling*

Where access to cave networks and time is available, active sampling provides an alternative to surrogate surfaces. Active sampling is conducted by pumping a known volume of air through a filter medium. The filter medium used will be dependent on the type of aerosol

under investigation. The use of active sampling is advantageous over surrogate surfaces due to its ability to produce quantitative aerosol concentration levels at higher temporal resolution. Total atmospheric aerosol concentrations or specific aerosol species concentrations can be determined. This method of capture offers analytical versatility since post capture aerosols can be weighed, observed and analysed dependent on the investigation type.

Increased pumping rates provide better aerosol collection and shorter durations offer improved temporal resolution. Generally pumped samples are run for 24-48 hours at 1 to 30 L min$^{-1}$ in the cave environment (Sanchez-Moral *et al.,* 1999; Alföldy *et al*., 2000; Alföldy *et al*., 2001; Yang, 2006; Faimon *et al*., 2006) as well as in confined situations (Nava *et al*., 2010) and often in the external environment too (e.g. Allen *et al.,* 2001; Harrison *et al.,* 2003). For this study, pumps were run at 3 L min$^{-1}$ for 24 hours duration. A dual pump setup (see supplementary material section S.1, Figure S.2) was chosen for simultaneous sampling onto two filter media for the collection of both inorganic and organic aerosols. Diffusion driers were tested in order to remove the effects of cave air relative humidity on pumping. However, the pumps reached their targeted pumping volumes successfully without driers and due to the potential aerosol loss, contamination and logistics of working with driers, they were not used beyond testing.

Suspended aerosol particle counters offer essentially instantaneous aerosol concentration values. Particle counters measure directly providing high resolution temporal data. A range of portable battery-powered particle counters exist, which can be used for temporal monitoring of aerosol concentrations in cave systems and are suitable for detailed spatial monitoring. Masses of both suspended and deposited aerosol can also be determined through weighing of

collected aerosols (Harrison *et al*., 2003). Optical measurements can provide an indication of masses, by counting (Christoforou *et al*., 1994; Salmon *et al.,* 1995) or by optical densitometry which measures surface obscuration (Michie, 1999). Condensation particle counters (CPC) can be used for continuous particle concentration data (Harrison *et* al., 2003; Iskra *et al.,* 2010). In addition to total suspended load detection, mass size distributions can be determined using particle sizers (usually impactor-based devices). This has been successful both in the cave environment (Michie, 1999; Sanchez-Moral *et al.,* 1999, Kertész *et al*., 2000; Kertész *et al.,* 2002; Iskra *et al.,* 2010) and in the external atmosphere (Allen *et al.,* 2001; Jones & Harrison, 2005). Particle sizes reflect how aerosols become entrained and transported in the atmosphere; they are therefore a useful tool for the investigation of aerosol transport within the cave environment. Figure 2.2 displays the size ranges for the aerosols types used in this investigation.
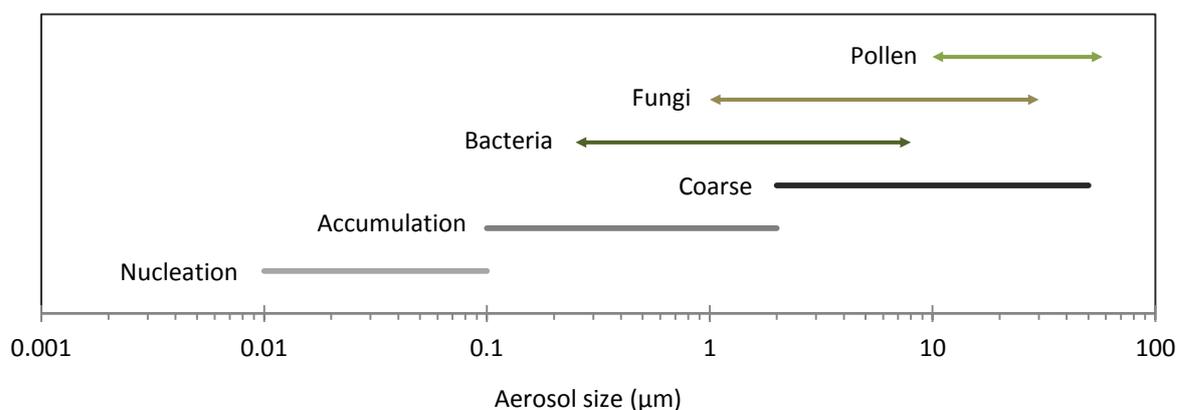


Figure 2.2: Aerosol size distributions, both inorganic (Seinfeld and Pandis, 1998) and organic (Jones & Harrison, 2004) compared with size classes of Whitby & Cantrell (1975).

A TSI SidePak AM510 particle counter for 0.1-10μm diameter particles was used in this investigation to determine suspended aerosol particle mass. Additionally, a TSI Aerotrak™ Model 9306 airborne particle counter was specifically used in the aerosol monitoring carried

out at Altamira Cave (Spain). This device has a 0.1 CFM (2.83 L/min) flow rate and counts up to bin sizes from 0.3 to 25 μm, logging up to 6 particle sizes simultaneously with a minimum sampling interval of one minute.

Filter preparation in this study was the same for both pumped and surrogate surface sampling. PTFE filters and glass Petri dishes were cleaned for a minimum of 24 hours in 2% $HNO_3$ then triple-rinsed with DDIW. The surrogate surface equipment was prepared in a clean laboratory environment to minimise blank values.

### 2.2.2. Extraction and analysis

Protocols for material extraction from filters and chemical analysis of deposited aerosols vary greatly and are dependent on elements under investigation and sampling methods, but all techniques are constructed with the intention of reduced sample contamination throughout the procedure. Extraction methods will only be summarised, detailed methods of extraction and analysis are presented in the supplementary material.

*Inorganic*

One of the most established and widely used methods (Janssen *et al*., 1997; Harrison *et al*., 2003) of air sample extraction from a filter medium is the reverse aqua regia digestion method developed in Harper et al. (1983). Various method combinations exist, but the majority involve ultransonication and acid extraction with nitric acid (or DDIW for ionic species) as key components (Allen *et al.,* 2001; Lim, 2006; Chu, 2008; Wai *et al.,* 2010). More intensive digestion can also be used with a combination of $HNO_3$, HF and $HClO_4$ (e.g. Chang *et al.* 2008). In order to replicate a similar extraction to speleothem analysis a 2% $HNO_3$ and 120

minutes ultrasonication with heat was the chosen extraction method for this investigation. DDIW and 120 mins ultrasonication was used for major ion species extraction (since 98% of sulfate, nitrate, and ammonium can be extracted with 120 minutes of ultrasonication (Chu, 2008)).

A range of techniques can be used for constraining inorganic properties. X-ray diffraction (XRD) can be used to determine the mineralogy of aerosols in confined and cave environments (Sanchez-Moral *et al.,* 1999; Salmon *et al.,* 1995; Nava *et al.*, 2010). Typically inorganic compositions are determined by the following analytical techniques: Inductively Coupled Plasma Atomic Emission Spectrometry (ICP-AES) (Chang *et al.,* 2008), Inductively Coupled Plasma Mass Spectrometry (ICP-MS) (Allen *et al.,* 2001; Harrison *et* al., 2003; Chang *et al.,* 2008), Neutron Activation Analysis (NAA) (Salmon *et al., 1995),* Graphite Furnace Atomic Absorption Spectrometry (GF-AAS) and Ion Chromatography (Harrison *et* al., 2003; Nava *et al.*, 2010). Inorganic aerosol chemistry in this investigation was obtained through ICP-AES analysis at Royal Holloway University of London. A suite of elements were analysed, total deposition in this paper refers to a total deposition of elements: Al, Fe, Mg, Na, K, Ti, P, Mn, Ba, Ni, Sr, V and Zn. Elements that demonstrate key processes will be displayed, as well as elements of importance to speleothems such as Mg and Sr.

Scanning electron microscopy allows for the identification of individual particle morphologies. Additional benefits are offered when microscopy and aerosol morphological identification is often carried out in combination with specific aerosol inorganic analysis. Scanning Electron Microscope (SEM) coupled with Energy Dispersive Spectroscopy (EDS) provides information on aerosol size, morphology and chemistry for individual particles

simultaneously (Sanchez-Moral *et al.,* 1999; Nava *et al.*, 2010). Particle-induced X-ray emission (PIXE) allows for the identification of individual particulate chemistry as well as bulk analysis and has been used in several studies to determine chemistry of a select fraction of cave aerosols (Kertész *et al.,* 2000; Kertész *et al.,* 2002; Alföldy *et al.*, 2001; Nava *et al.*, 2010). Similar results have been achieved with electron probe microanalysis (EPMA) on single cave aerosol particles (Sanchez-Moral *et al.,* 1999; Alföldy *et al.*, 2000).

*Carbon*

Carbon deposits have been established as a significant contributor to cave degradation and therefore the identification of carbon and its types are of increasing importance. Optical and thermal analytical techniques are most frequently used to measure carbon in atmospheric investigations (Ghedini *et al.,* 2000). Studies often aim to investigate carbon types, total carbon (Nava *et al.*, 2010) and differentiate between elemental and organic carbon (Jones & Harrison, 2005). Carbon isotopic composition offers an insight into the carbon mass fraction allowing for improved source identification. Characterization of radiocarbon as well as $^{13}C/^{12}C$ has been utilised by Chang et al. (2008) to distinguish cave carbon deposits and emission sources.

*Organic - bioaerosols*

Methods differ significantly depending on the organic species under investigation. Atmospheric organic aerosol investigations typically involve the emission products of combustion for human health and environment studies. Emission products can be utilised as a tracer for aerosol transportation in suitable case locations. Emission aerosols in speleothem have the potential to be used as a proxy for emission events. PAHs (Polycyclic aromatic

hydrocarbons) are widely investigated as a proxy for hydrocarbon combustion and emission. PAHs are typically analysed by gas chromatography mass spectrometry methods (Bae *et al*., 2002; Harrison *et al*., 2003; Zhang *et al*., 2008b) or high-performance liquid-chromatography (Terzi & Samara, 2005; Perrette *et al*., 2008). Organics are generally extracted from aerosol samples with the use of solvents (solvent extraction) in a combination of solvents and heat (Soxhlet extraction). Extraction methods are refined dependent on the species under investigation. PAHs have also been extracted from soils, sediments (lake and marine), ice cores and speleothem samples. Perrette et al. (2008) used dichloromethane in both Soxhlet and ultrasonication extraction for the extraction of organic species from stalagmites and sediments.

Microbial air sampling was conducted in this investigation to quantify the level of airborne bacteria and fungal spores in the aerosol monitoring survey carried out at Altamira Cave (Spain). A Duo SAS 360 sampler (International PBI, Milan, Italy) containing Petri dishes with Dichloran Rose Bengal Agar was used for the sampling of fungi. The antifungal agent, Dichloran, was added to the medium to reduce colony diameters of spreading fungi. The presence of Rose Bengal in the medium suppresses the growth of bacteria (also the chloramphenicol) and restricts the size and height of colonies of the more rapidly growing fungi (King *et al*., 1979). For bacteria, the medium Tryptone-Soya Agar (TSA) was used. Duplicate samples of 100 L in air volume was selected as the most appropriate method for easy counting in this cave. The dishes were incubated at 25°C, and the fungi were isolated as pure culture in malt extract–agar and kept at 5°C until further study. For bacteria, the dishes were incubated at 28°C and isolated in TSA medium. Some specific applications of these

aerobiological techniques in subterranean environments, including this cave, are described by Fernandez-Cortes et al. (2011) and Porca et al. (2011).

## 2.3. Cave aerosol processes

In this section, aerosol transport, distribution and deposition mechanisms will be highlighted with preliminary data from cave monitoring. Cave locations were chosen to isolate and investigate specific aerosol emitting processes. Data from a range of cave sites throughout Europe will be used to demonstrate the relationship between aerosol deposition flux rates and speleothem growth rates.

### *2.3.1. Cave aerosol sources*

*Externally sourced cave aerosols*

Source areas and long-range transport of external aerosols can be determined to a degree through the utilisation of air mass trajectories, since a body of air will incorporate aerosols released into the atmosphere which will then be transported as the air mass moves (Seinfeld & Pandis, 1998).

*Internally produced cave aerosol*

In addition to the transport of aerosols from external sources, there is the possibility for the addition of suspended aerosols to the cave atmosphere from internal sources. In some cases, the contribution of aerosols from within the cave network will be orders of magnitude greater than that of externally sourced and transported aerosols.

*Anthropogenic (cave visitor) production*

Degradation of the cave environment as a result of aerosol deposits from human or animal visitors is known (Cigna, 1983; 1989; 1993). The disturbed particulate matter can be present

as an existing aerosol deposit and therefore the visitor disruption simply results in the re-suspension of particulates from an aerosol source, or suspension of particulates from subaqueous deposition within the cave. Cave visitors can also act as a carrier of externally sourced aerosol and release them inside the cave (e.g. lint, mud on shoes). The dust released by cave visitors can be considered as having two components: firstly particles large enough to fall straight to the floor and secondly particles small enough to be swept into the plume of warm air rising from the visitors (Michie, 1999).

Measurements in eastern Australia, Western Australia, and England have shown a constant rate of deposition of airborne particulate material from show cave visitors of approximately one microgram per person per second (Michie, 1999). Bartenev and Veselova (1987) carried out measurements of dust sedimentation from aerosols in the Cupp-Coutunn Cave System, noting that the rate of sedimentation raises more than 10 times within 20 m surrounding the main tourist passages, indicating the significant aerosol production from cave visitors.

*Hydrological production*

Aerosols can be generated from water drops falling from a cave ceiling or generated by rapids and waterfalls in cave streams (Maltsev, 1997). Turbulent water can produce aerosols by a similar mechanism to that which occurs in the production of sea spray, with gas scavenging resulting in bubbles which rise to the surface and burst producing hydro-aerosols. 'Splash' aerosols can also be produced as falling drip waters impacting on cave surfaces resulting in small enough liquid aerosols to be transported in suspension. Aerosol deposition to water bodies causes suspension of liquid aerosols in the form of film and jet drops (Bridgman, 1994).

*Bedrock production*

Klimchouk et al. (1994; 1995) proposed that cave aerosols can be generated as a result of radioactivity in the cave environment. It was proposed that alpha decay dislodges the bedrock to form aerosols. This was further investigated by Pashenko & Dublyansky (1997) who suggested that the process of alpha decay dislodging bedrock is a physically plausible but not essential role in the production of cave aerosols. Also sourced from the bedrock, it is possible for particles to become dislodged during erosional processes causing small particles to fall from the ceiling (Pashchenko & Sabelfeld, 1992) and cave walls. Cave wall aerosol generation can be augmented through host-rock alteration and corrosion as a consequence of condensation weathering processes. During further weathering the surface becomes increasingly fragile, from which fine carbonate particles can be derived (Hajna, 2003). Condensation weathering will be controlled by cave humidity and condensation processes as described in section 2.3.3. 'Wet deposition'.

### 2.3.2. Distribution

Once aerosols enter the cave atmosphere they can be removed from suspension through a variety of aerosol deposition processes resulting in the spatial variation of aerosol sedimentation. The mechanisms of aerosol removal will be specific to each cave system and may vary seasonally as the cave environment changes. Cave aerosol distribution processes will be explored in this section.

*Aerosol transport*

In order to be incorporated into a speleothem, aerosols that reach the troposphere region surrounding the cave entrance must be transmitted into the cave air, which occurs via two main routes; direct transport into the cave through air exchange (Pashchenko *et al*., 1993) and dust carried in by visitors (Michie, 1999; Jeong *et al.,* 2003) and animals.

The transport of external and internally sourced aerosols will occur as a result of cave air movements. Air movements in caves occur by convective ventilation and sometimes with short-term local turbulence as a result of anthropogenic influences (Fernandez-Cortes *et al*., 2009). Cave ventilation occurs as a result of several phenomena: cave breathing, wind-induced flow, chimney circulation or stack effect, convection and water-induced flow (Fairchild & Baker, 2012). The vigour of the air circulation affects the removal of internally generated gases such as carbon dioxide, radon (and its particulate daughters) and the introduction of aerosols (Fairchild & Baker, 2012). Christoforou et al. (1996a) determined that cave ventilation and its air flow patterns act as the primary mode of transport for pollutant particles into caves from the outdoors.

The relative influence of cave visitors and natural cave ventilation will be dependent on the cave under investigation and the relative influence of its visitor footfall numbers and ventilation strength on aerosol production. This relationship will often change significantly with seasons i.e. a show cave with strong winter ventilation and fewer aerosols from visitors will be ventilation-dominated in the winter months and then weaker ventilation and substantially increased footfall numbers in the summer will result in the transition to an anthropogenically controlled aerosol atmosphere. The cave ventilation process and hence the degree of mixing between the cave and outside air (and therefore aerosol incorporation into cave air) will vary at each cave site.

*Transport source identification*

Pollen is perhaps the most intensively studied single cave aerosol type due to its significance in speleothem palaeoenvironmental archives as a recorder of terrestrial vegetation. A range of studies exploring the distribution of pollen through caves has been presented in the literature. A comprehensive review of literature regarding their mode of transport and distribution can be found in Caseldine et al. (2008).

Coles *et al*. (1989), proposed three transport mechanisms for pollen: airborne, waterborne and insect-borne. Similarly Lauritzen et al. (1990) emphasized percolating water, floodwaters that submerge speleothems, or airborne transport by cave draughts as predominant pollen transport mechanisms. They noted the importance of understanding transport mechanisms for interpreting pollen assemblages in speleothems. Bastin et al. (1978) attempted the identification and discrimination of pollen transportation modes based on pollen size, with the smallest diameters being indicative of percolation as opposed to airborne transport. However,

results showed a dominance of the largest pollen type across all spectra, demonstrating the difficulty in establishing cave aerosol sources and depositional mechanisms.

Although a method is yet to be established for the source discrimination of pollen, the airborne pollen influx into caves and modern surface pollen deposition has been reported to be similar in several investigations (Burney & Burney, 1993; McGarry & Caseldine, 2004). It is critical for internal cave aerosol composition to be representative of external aerosols for palaeoenvironmental studies. It may be assumed that the behaviour of pollen can be extrapolated to other aerosols of similar size, which are controlled by the same transportation processes.

Distinguishing between aerosols that have been deposited directly to the surface of an actively growing speleothem and consequently incorporated and those which are transported via percolating water poses the next challenge in the ability to utilise aerosols as an environmental proxy. Separation can be achieved through cave monitoring of aerosol deposition and subsequent aerosol chemistry analysis for source identification. Where aerosol deposits are of contrasting composition to that of speleothem growth chemistry, it may be possible to identify periods of significant aerosol deposition. The significance and ability to recognise aerosols in speleothem is discussed later in section 2.5.

### 2.3.3. Aerosol deposition

The fate of aerosols which become incorporated into the cave atmosphere is controlled by the mechanism of aerosol deposition.

*Gravitational sedimentation*

Gravitational sedimentation as a result of reduced airflow rates is thought to be the main mechanism behind aerosol deposition of coarse aerosols in cave networks. Michie (1997) determined the main processes which control the deposition of particles within the cave network: Brownian diffusion and collision for the smaller particles and gravitation for the larger particles. It should be noted that gravitational sedimentation processes will not be of importance for stalactite samples which consequently may receive significantly lower aerosol fluxes than stalagmite surfaces.

The study of pollen and its distribution throughout cave systems provides an insight into cave coarse aerosol transportation mechanisms. Pollen grains which are known to be aerially transported are detected close to the entrance of cave systems (McGarry & Caseldine, 2004; Caseldine *et al.,* 2008) with a reduction towards the cave interior (Burney & Burney, 1993; Cole & Gilbertson, 1994; Navarro *et al.,* 2001). This distribution is expected since pollen as a coarse aerosol requires relatively high energy levels for particle transportation, greater than that which can be sustained by cave ventilation flow. McGarry & Caseldine (2004) suggested that beyond the entrance zone (e.g. Bastin (1978), where pollen was detected 600 m from the cave entrance) one can assume a percolation water transportation source due to the likely airborne transportation distances involved. McGarry & Caseldine (2004) summarised pollen deposition flux rates: entrance zone deposits at approximately 100-700 grains cm$^{-2}$year$^{-1}$; 100-200 grains cm$^{-2}$year$^{-1}$ ~20 m from entrance; and little to no airborne or animal influence in the deep cave.

The pattern of distribution presented by various investigations into pollen, although generally representative, can only be assumed if there is a single known cave entrance. It is also necessary to know that cave air flow rates are high enough to transport coarse aerosols whilst meeting threshold terminal velocity speeds to allow for total gravitational sedimentation of suspended aerosol particulates within the cave. Figure 2.3 displays the relationship between particle size, deposition and air flow rates. Each cave should be monitored (as with other environmental variables) on a case study basis to ensure that an accurate understanding of cave aerosol transportation dynamics has been gained before interpretations are made. It is necessary to understand air flow rates and the factors controlling air flow in order to fully understand aerosol deposition (Christoforou *et al.,* 1996b).
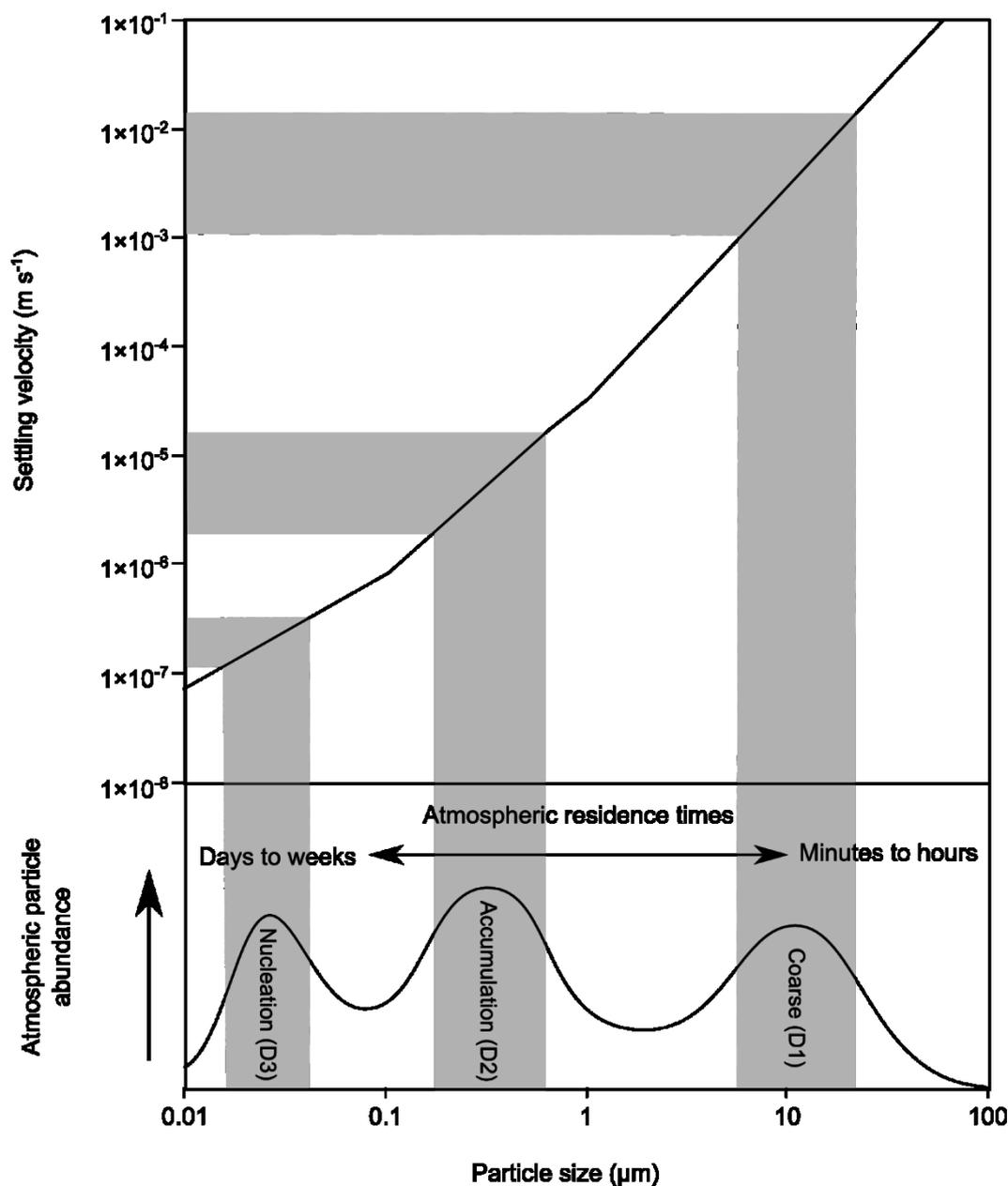
Figure 2.3: Relationship between particle size and settling velocities. Relative atmospheric abundance of aerosols by particle size (Whitby & Cantrell, 1975) and particle size settling velocities (Baron & Willeke, 1999).

Air flow rates in cave locations will vary greatly and are generally too low for the transportation of coarser aerosols. However, it is known in some instances that flow rates are sufficient for the transportation of even very coarse particulates. Flow velocities of 0.5 m sec$^{-1}$ have been reached during winter ventilation in some regions of Obir cave (Fairchild *et al.,*

2010) and exceptionally high air flows (>10 m sec$^{-1}$) are known to be reached in some cave sites (Conn, 1966). During periods of higher ventilation speeds larger suspended aerosol loads and large particles may be transported and deposited within the cave increasing the potential for aerosol contributions to speleothem geochemistry.

It has been demonstrated that there is a significant reduction near the cave entrance zone for specific coarse particle types such as pollen. High ventilation flow velocities are required to transport coarse particles and therefore such particles will be deposited around the entrance zone. The aerosol deposition gradient was noted by Christoforou et al. (1994) with a loss in deposition rates over the entrance region, from 13.4 $\mu$g m$^{-2}$ s$^{-1}$ outdoors to 5.2 $\mu$g m$^{-2}$ s$^{-1}$ inside (over 1 year of monitoring). This indicates either low external aerosol transportation into the cave or significant suspended aerosol loss over the entrance zone.

Figure 2.3 indicates the three dominant aerosol size groups (modes) present in the atmosphere: coarse (D1), accumulation (D2) and nucleation (D3) (Whitby & Cantrell, 1975). Coarse aerosols, sometimes known as mechanical aerosols form when mechanical processes introduce aerosol into the air (e.g. wind blowing over dust or sea spray) (Willeke & Whitby, 1975). Coagulation or condensation of smaller aerosols predominantly accounts for formation of the accumulation mode (Willeke & Whitby, 1975). Nucleation aerosols are formed from emission processes such as combustion (Willeke & Whitby, 1975) and photochemical processes (Seinfeld & Pandis, 1998). Each particle size mode is removed from the atmosphere at its associated deposition velocity. The aerosol contribution to speleothem chemistry will occur as a result of the total deposition to the speleothem surface from all aerosol types and

sizes. Therefore the range and distribution of aerosol particle sizes must be considered when investigating chemistry.

A body of atmospheric air (of average composition) with air velocity greater than or equal to 0.1 m s$^{-1}$ will be have a suspended load (Ls) produced from a combination of groups D1, D2 and D3, therefore Ls= $\Sigma$(D1,D2,D3). Taking the simplified example of a horizontal cave with a single entrance in which air exchange becomes progressively less influential with distance from the entrance (A), air velocity (V) will decrease with distance from the entrance to the back of the cave (A'). At 'A' Ls will be equal to $\Sigma$(D1,D2,D3), as the air progresses towards A' and loses velocity, particle modes D1, D2 and D3 will be progressively depleted by deposition. This progression of loss in suspended load is displayed schematically in Figure 2.4. The flux of aerosols throughout the cave will be a product of the air velocity (driven by ventilation strength), cave cross-section A to A' and cave morphology. Cave ventilation is known to be highly variable displaying strong diurnal and seasonal variations; consequently aerosol transport may display temporal variations. Cave cross-section and morphology will also be highly variable depending on the cave under investigation, altering the distribution of deposition of the particle modes (discussed later in section 2.4.5.).

A cave environment can represent any section of A to A'. For example, a short cave with strong ventilation will display cave entrance depositional characteristics throughout, and deposition will be dominated by coarse fraction aerosols (D1). Conversely, a deep cave with weak ventilation will progress through modes D1-D3 with distance from the entrance with more of the cave's aerosol deposition being composed of aerosols from the nucleation mode

(D3). Figure 2.4 illustrates the process of progressive gravitational sedimentation towards the cave interior.
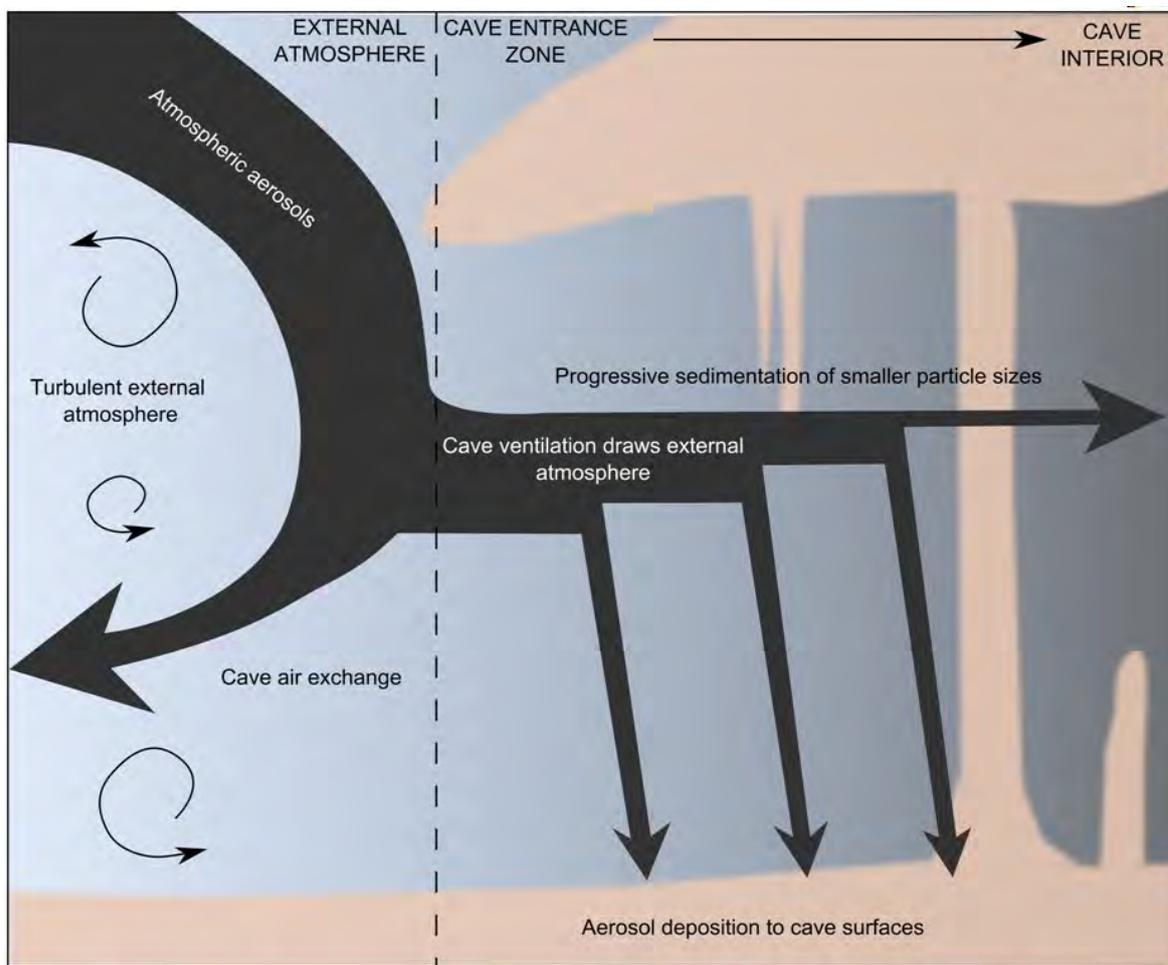


Figure 2.4: Schematic of introduction and gravitational sedimentation of cave aerosols within the cave environment.

*Cave morphology effects on deposition processes*

Cave morphology has been postulated as a control on the distribution of pollen in cave sediments (Burney & Burney, 1993; Navarro *et al*., 2010). Cave morphology will strongly influence the transportation and deposition of aerosols throughout the cave network. Surface irregularity will result in turbulence within the air column. Turbulence will cause increased particle collisions with the walls and consequently greater deposition. Interception of the air

flow streamline by irregularities will also result in impaction onto cave surfaces (as described in section 2.3.3. 'Interception and Impaction'). Aerosols of greater inertia will be removed from the cave ventilation air flow stream. Therefore the 'windward' side of cave features (i.e. stalagmites) will have a greater aerosol impaction flux to the surface.

Cave morphology will also have an effect on the transport of aerosols by altering ventilation forced air flow rates. A flow of air passing through a constriction may pass too rapidly for gravitational sedimentation to occur, but upon reaching an open chamber, air flow rates may reduce sufficiently to reach threshold sedimentation levels. As a result, increased gravitational aerosol depositional flux may be observed in open chambers, with interception and impaction processes being dominant in high flow constriction areas of a cave system. Changes in cave profile (floor elevation) may also induce gravitational processes. A package of cave air that reaches a rise in elevation may stagnate enough to fall below threshold deposition velocities, resulting in zones of increased deposition.

*Interception and Impaction*

Interception and impaction are both the result of an obstacle interrupting the air flow; in the cave environment this is likely to be speleothem formations. In addition to increased interception/impaction processes, the wet surfaces of actively growing speleothems may retain more particles than dry cave surfaces as a consequence of hydraulic retention processes. As a result, speleothem surfaces will potentially have higher depositional flux and aerosol retention rates than other surrounding cave surfaces. This proposed pattern of distribution was noted by Chang et al. (2008) who observed concentrated aerosol deposition to speleothem

surfaces throughout Gosu, Ondal, and Sungryu caves in South Korea of 0.1 mm to several millimetres in thickness.

*Wet deposition*

Wet deposition can occur as dripwater falls through the cave atmosphere. However, this contribution is likely to be negligible.

Badino (2004) considered the processes that could potentially result in the formation of clouds in caves. A key factor in cloud formation is the presence of aerosols which act as nucleation points for vapour condensation. The presence of a stable aerosol forming haze in a cave atmosphere is direct evidence of a supersaturation of moist air (water vapour pressure is above equilibrium), and it leads to thermal imbalances between the aerosols and the air (i.e. clouds are usually found near the cave ceiling and in the highest galleries because a humid air parcel is less dense than the drier air parcel). Aerosols may facilitate the formation of clouds by providing a surface for atmospheric condensate aerosol formation from high humidity cave air.

Condensation from atmospheric humidity can have an important speleogenetic role (Dublyansky & Dublyansky, 2000; Dreybrodt *et al*., 2005). Condensates from cave air will scavenge and deposit aerosol through wet deposition and in specific scenarios may influence speleothem geochemistry. In addition to influencing already precipitating speleothems, aerosols can produce a mineral deposit when it reaches a cave wall or directly from the vapour state (in the same mechanism of sublimation of ice from water vapour) (Cigna & Hill, 1997).

An illustration providing a summary of aerosol processes is displayed in Figure 2.5.
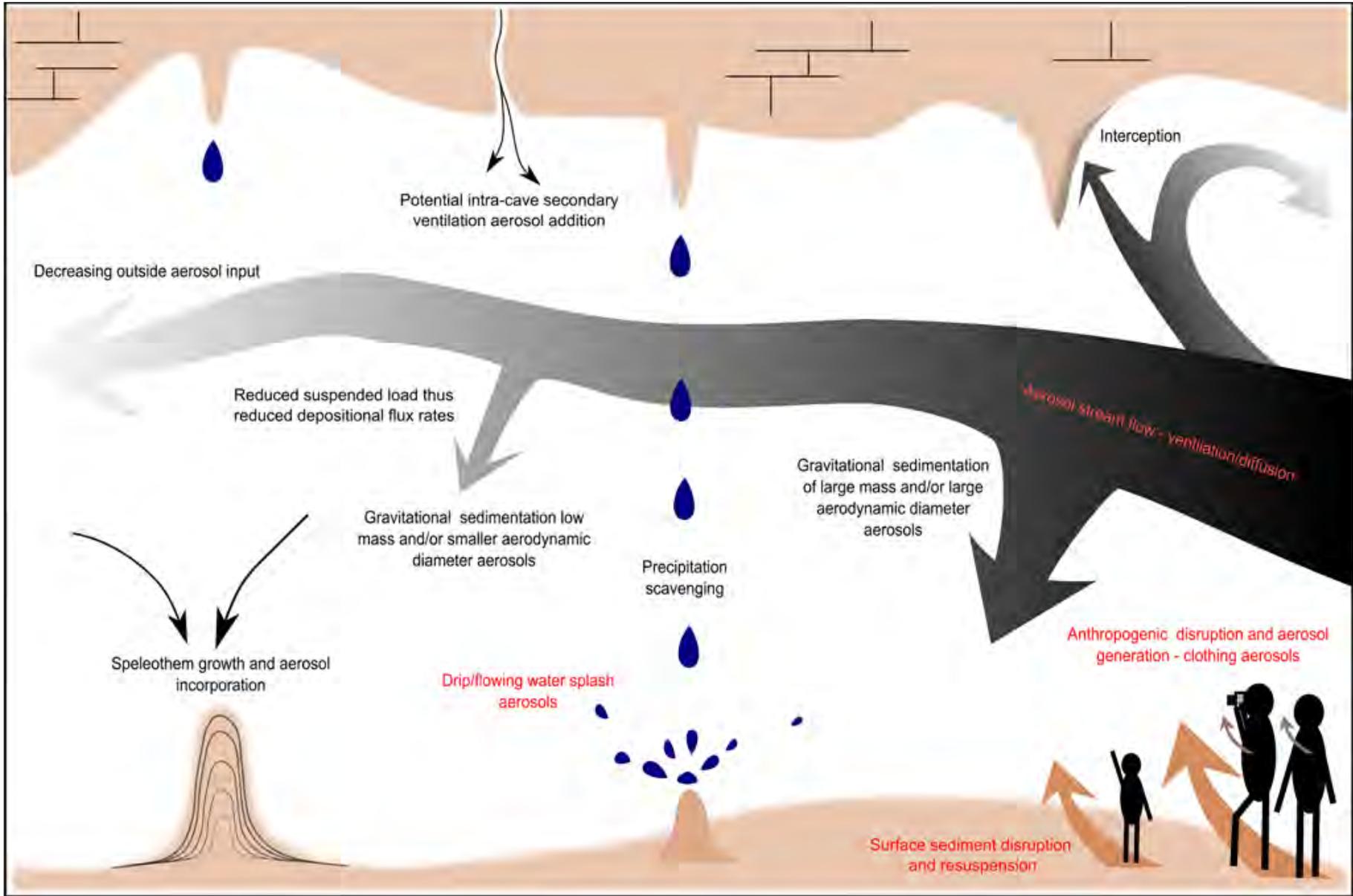
Figure 2.5: An illustration summary of cave processes: aerosol creation (red), and aerosol removal processes (black).

## 2.4. Results

Through cave monitoring, results from this investigation will be displayed to demonstrate some of the key issues discussed in previous sections. This work will provide a contribution to, and further the existing work that has been presented on cave aerosols and discussed previously.

### 2.4.1. Internally sourced aerosols

Internal production of aerosols in some cave locations is likely to be dominated by anthropogenic processes. The magnitude of potential aerosol production relative to show cave background levels is displayed in Figure 2.6. The effect of the disturbance clearly dominates the background levels of aerosols. However, the impact of the disturbance on suspended aerosol loads is short-lived and is dependent on the cave situation and cave ground sediments.
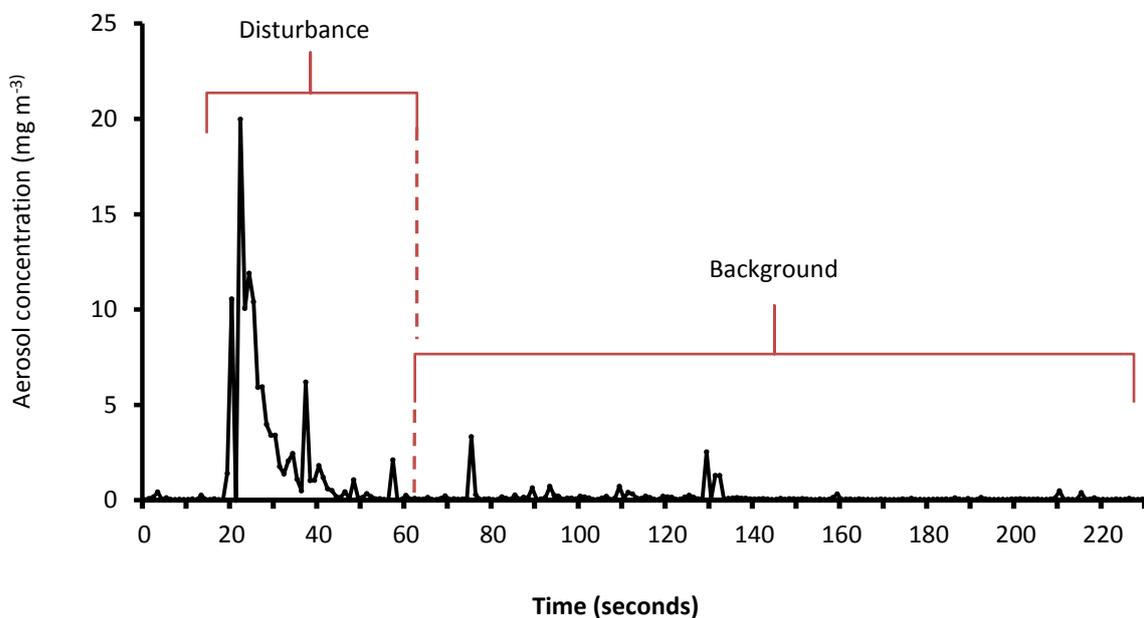


Figure 2.6: Short term anthropogenic cave aerosol production in Gough's cave, Cheddar Gorge Show Cave, UK. Suspended aerosols monitored as a cave visitor passes by with TSI instruments SidePak AM510.

Figure 2.6 displays an example of short term aerosol impacts from a single disruption event by one cave visitor. The data presented in Figure 2.7 displays a much greater duration of cave atmosphere aerosol impact by longer, multiple visitor disturbances.
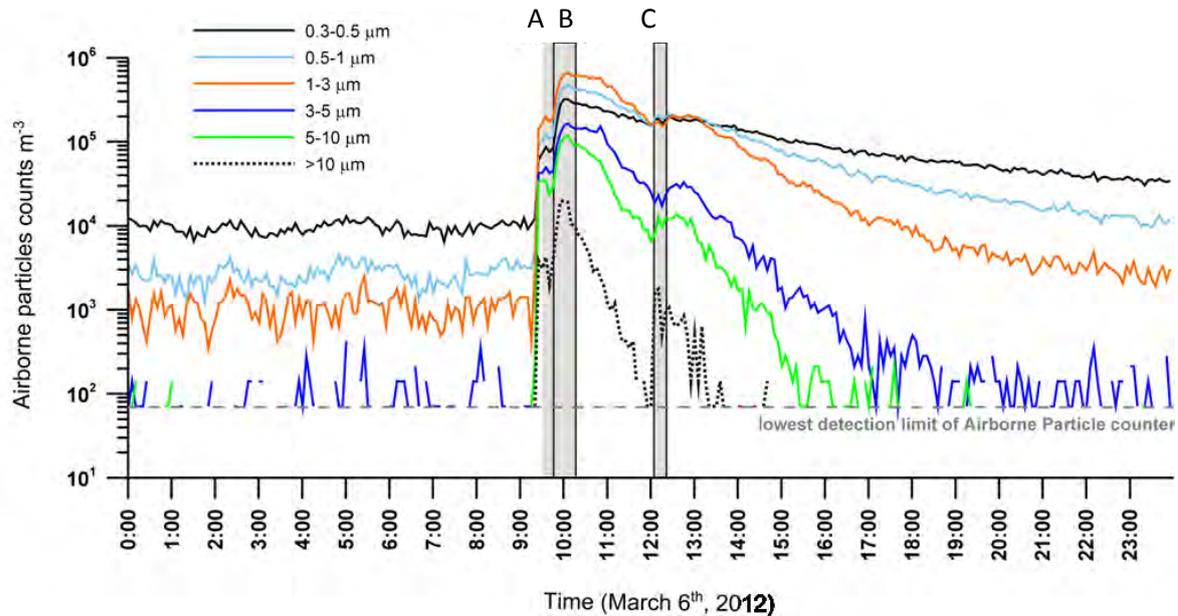


Figure 2.7: Example of aerosol contributions and particle resuspension from ground sediments by short visits to Altamira cave (1-4 people during less than 30 minutes) during maintenance operations of microclimatic monitoring equipments. The size distribution of particles was monitored every 5 minutes during a day cycle (6th March, 2012) by using an airborne particle counter (TSI Aerotrak™ Model 9306). Anthropogenic influence events are shaded in grey with events A, B and C representing visits of 2, 4 and 1 people respectively.

The background level of suspended particles ranged from 70 to $10^4$ particles m$^{-3}$ depending on their size. The coarsest particles (>10 μm) were detected only once the visitors went into cave, provoking the microparticle detachment from soil and their own clothes. Levels of airborne particles rose to more than a thousand times the previous background levels (as in Goughs Cave). Particle detachment affected particles of 0.5-3 μm in size more than the finest particles of 0.3-0.5 μm diameter. Coarsest particles (>10 μm) were removed from suspension three hours after the visit and particles ranging from 3 to 10 μm in size took approximately 9 hours

for removal. The finest particles (<3 μm) remained suspended for longer periods (roughly up to 24 hours). This demonstrates the range of impacts and duration of impact different particle sizes can have on the cave environment.

The production of water aerosols may prove a significant source to the total aerosol budget for specific regions in some cave locations. The impact of hydrologically produced aerosol will only be of notable levels in caves with significant waters flows, which may be seasonally controlled. The formation of drip water aerosols has been postulated to result in trace element enrichments of speleothem at Obir cave through drip water splashing and re-circulating mechanisms by (Fairchild *et al*. 2010). Figure 2.8 displays an example of hydraulic internal aerosol production.
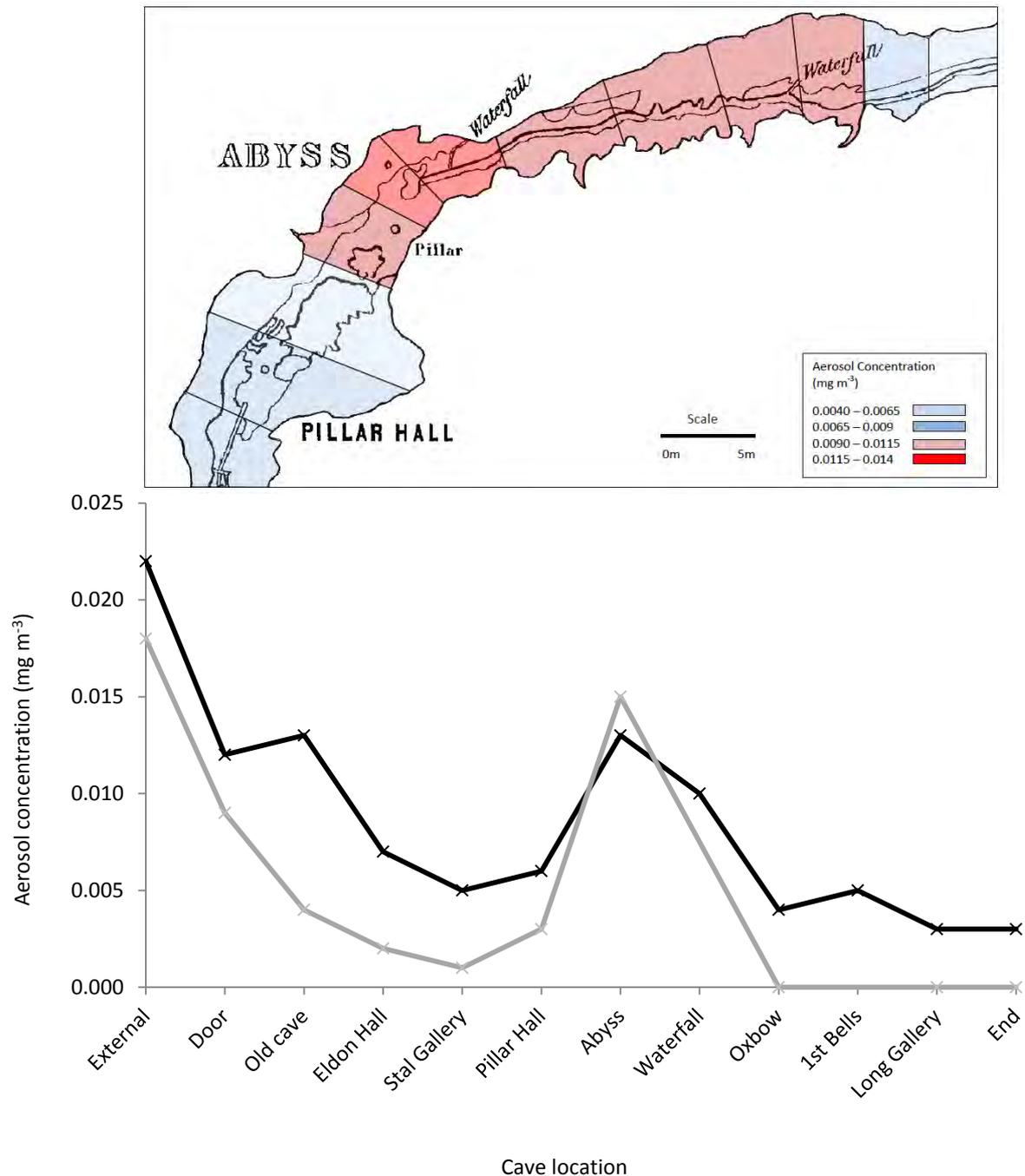
Figure 2.8: Spatial distribution of suspended aerosols from Ingleborough show cave, UK. The 'End' location marks the end of the show cave not the entire system which continues for >100m further. Data collection using TSI AM510 optical aerosol counter during winter (black) on the 28th Feb 2011 and summer sampling (grey) on the 14th July 2009. The insert displays waterfall zone aerosol concentrations (Smith & Wynn, 2010). Hydro-aerosol production remains an apparent feature in both summer and winter monitoring.

The distribution of aerosol concentrations displayed in Figure 2.8 indicates a reduction in suspended aerosols with distance from the cave entrance. However, there is a peak in suspended aerosol concentrations at the Abyss/Waterfall locations which has been attributed to the internal cave production of liquid aerosols, forming as a result of turbulent water from a flowing stream (Smith & Wynn, 2010; Smith *et al*., 2013). The production of aerosols in this specific location is localised but substantial and has the potential to notably alter the geochemistry of proximal speleothem formations.

### 2.4.2. Cave ventilation and aerosol distribution

Cave air $CO_2$ is used as an indicator of cave ventilation as the concentration of $CO_2$ in a cave passage is a function both of production and ventilation processes (Fairchild & Baker, 2012) with increased $CO_2$ concentrations being indicative of reduced air-exchange with the relatively low $CO_2$ concentration external atmospheric air. Figure 2.10 displays data from spot monitoring of Goughs Cave, Cheddar Gorge (sampling locations shown in Figure 2.9).
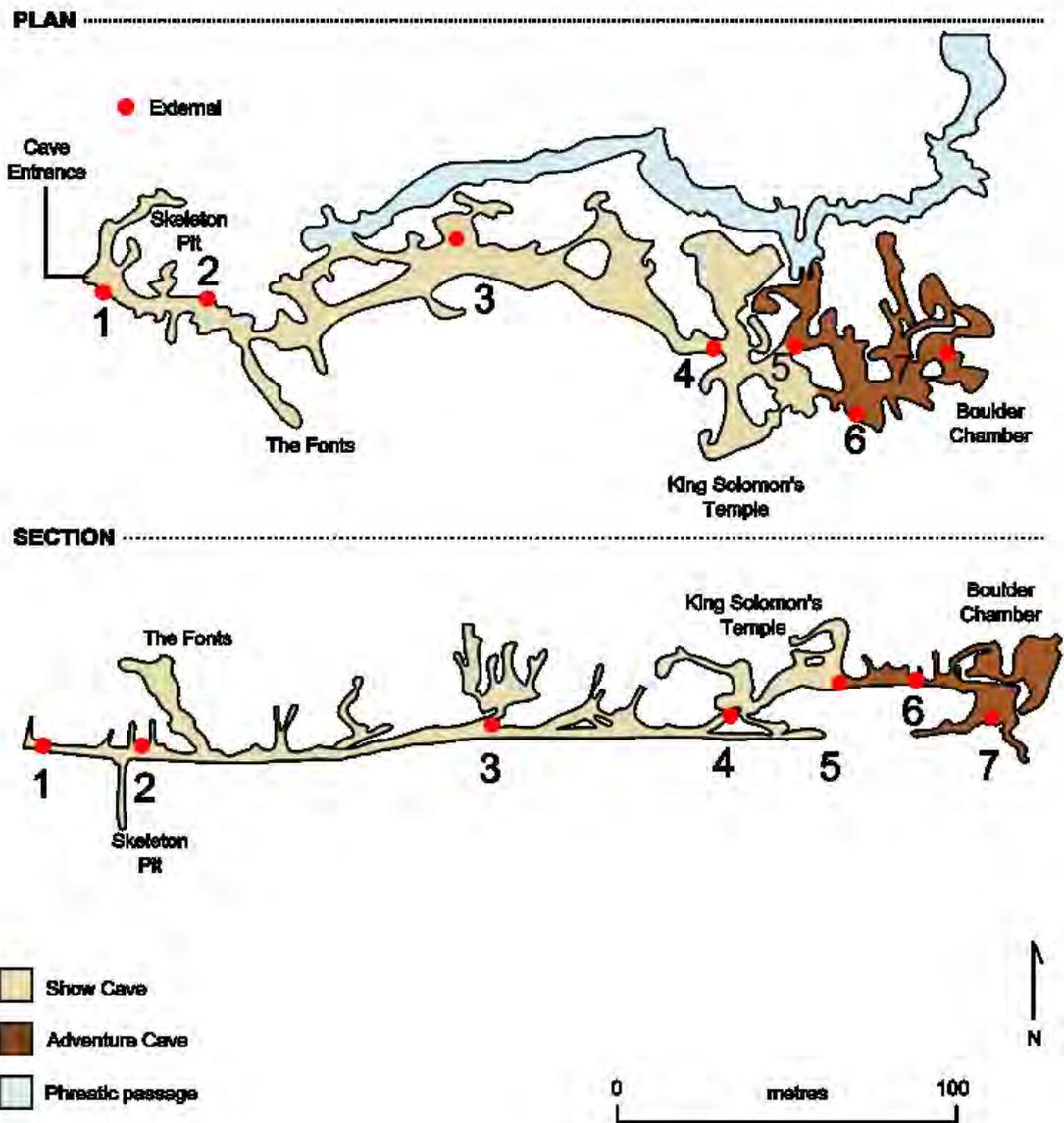
Figure 2.9: Map of Gough's Cave, Cheddar Gorge with aerosol sampling locations. (After Farrant (2010), based on survey data by Stanton (1953).

$CO_2$ rises towards the cave interior which can be interpreted as reducing air exchange and therefore reduced air velocity. Suspended aerosol concentrations demonstrate the opposite of $CO_2$, decreasing towards the cave interior. Temperature demonstrates a similar trend to

aerosols. However, cave interior temperatures are reached closer to the cave entrance (before location 2) and are then maintained relatively constant throughout the cave.
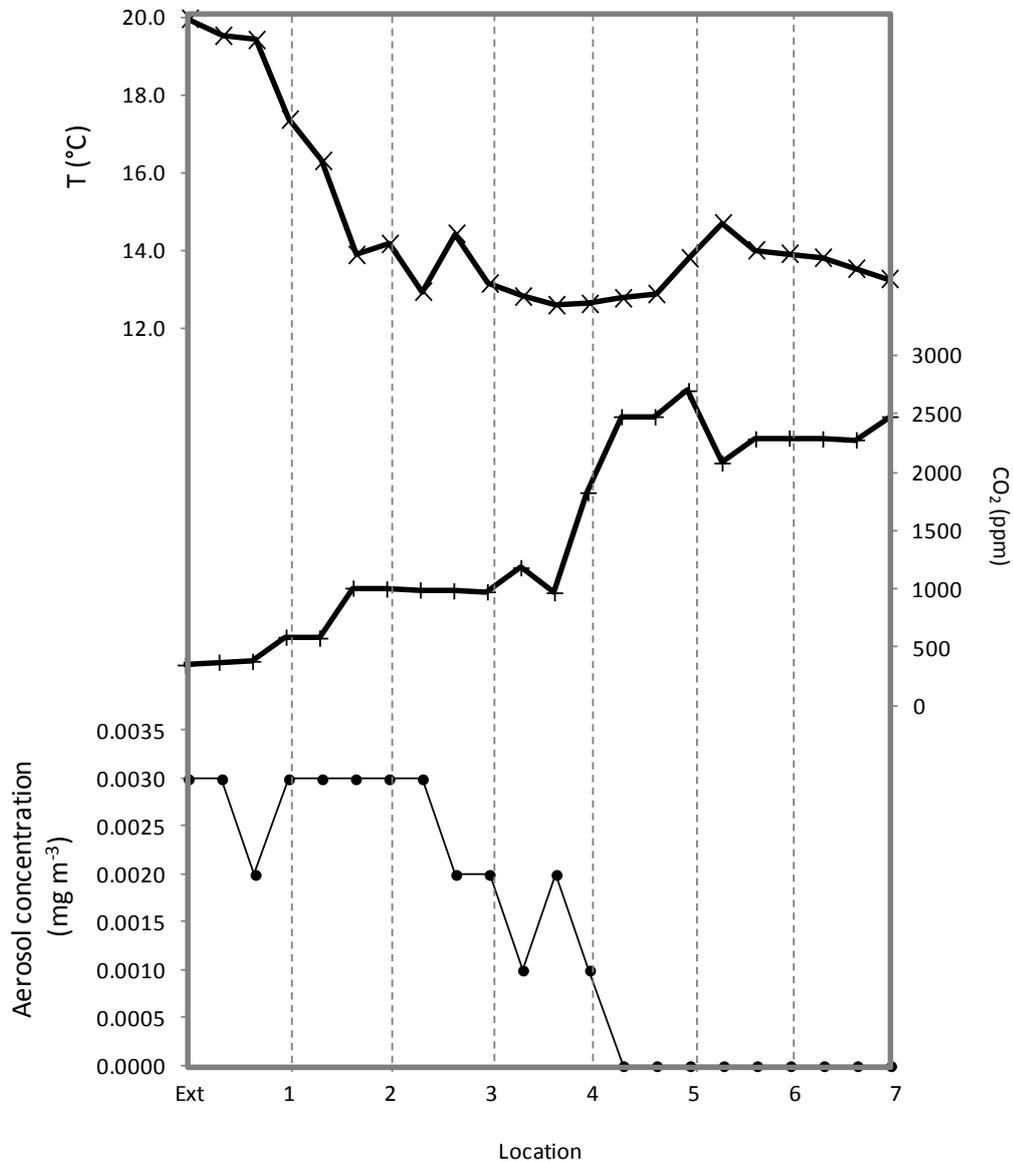


Figure 2.10: Cave air $CO_2$ and suspended aerosol concentrations from spot monitoring throughout the Gough's Cave network on 19th and 20th July 2011. $CO_2$ recorded with a Sperian PHD6 instrument. Aerosol concentrations measured with TSI SidePak AM510 optical counter (data presented are counting duration minima during the 5 minute sampling duration, in order to best achieve background levels). Five minute averages of temperature are displayed, measured with a Tinytag temperature logger. Samples were spread over ~275m from the cave entrance to deepest interior.

The zone of significant change for $CO_2$ and suspended aerosol concentrations occurs between locations 3 and 5. The increase in $CO_2$ and associated reduction in suspended aerosol concentration indicates reduced air exchange. Reduced air exchange will be associated with lower air flow rates allowing for increased settling deposition processes. This is confirmed by an increased aerosol deposition flux being observed between locations 3-5 as shown in Figure 2.11. A rise in cave floor elevation can be observed in Figure 2.9 (in section) between location 2 and 3. This may account for the reduction in air exchange, as discussed in section 2.3.2. and 2.4.5, increased elevation may result in the stagnation of air flow rates resulting in increased aerosol deposition.
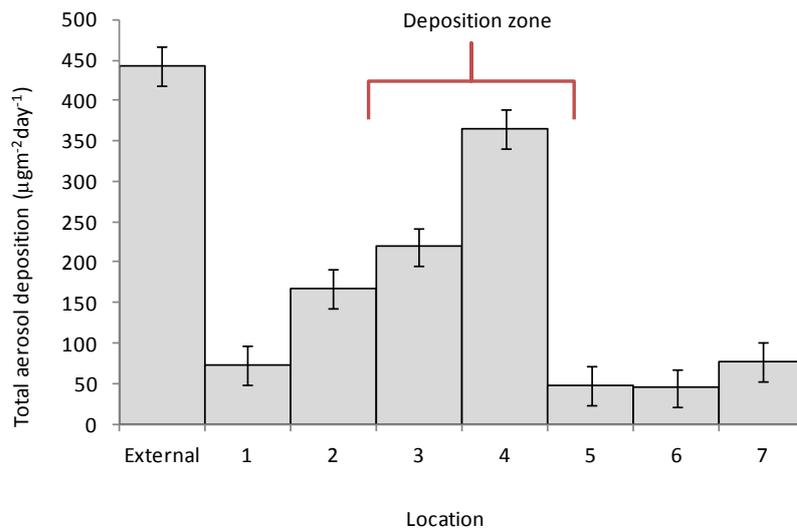


Figure 2.11: Gough's Cave, Cheddar Gorge: the spatial distribution of depositional flux rates based on one month of surrogate surface monitoring over July. Samples collected on the 20th of July. Limit of detection (3σ) displayed with error bars.

The correlation of suspended aerosols, aerosol deposition flux and $CO_2$ demonstrates the relationship between deposition processes and cave ventilation. Cave ventilation has been

confirmed as the one of the key processes controlling cave aerosol introduction, transport and deposition. This relationship is investigated in more detail in Chapter 3.

Based on the observed deposition rates, the rate of aerosol deposition accumulation and vertical accretion rates can be estimated:

Vertical accretion (m/day) = deposition flux ($\mu$g/m$^2$/day)/ aerosol density ($\mu$g/m$^3$)        (1)

Aerosols of lower settling velocities (Figure 2.3) are most likely to be transported throughout cave networks (illustrated in Figure 2.4). Therefore cave aerosols are most likely to be composed of aerosols from nucleation and accumulation particle size modes. Aerosol density is required to calculate accretion rates (see (1)). Hu et al. (2012) estimates mean aerosol material density of 1.62±0.38 ($\mu$g/cm$^3$) for the smallest size fraction in the study of 0-1.8 um diameter. Based on the average cave deposition flux in Gough's cave of 142 $\mu$g/m$^2$/day (Figure 2.11) and average aerosol density of 1.63 $\mu$g/cm$^3$ vertical accretion will equal $8.77\times10^{-08}$ m/day or 32 $\mu$m/year.

This calculation provides an estimation of vertical accretion rates, based on several assumptions and uncertainties. The range in aerosol deposition has shown to be highly variable depending on location (Figure 2.11) and season (explored in Chapter 3). Therefore vertical accretion rates will also be highly variable. The density values proposed by Hu et al. (2012) an estimated value based on assumed composition and size groups. Additionally, further uncertainty occurs as a result of applying the size related density values to the unknown cave aerosol size fractions that are used in determining aerosol flux rates in Gough's

cave. Assuming the chosen density and deposition flux values are accurate, the vertical accretion calculation will provide an upper limit value. It is highly likely that aerosol deposit losses will occur due to disruption and removal by water flow, anthropogenic activity, or resuspension by air flow rather than forming deposits. Furthermore, aerosol deposit compaction processes would result in lower than calculated vertical accretion rates. The ability of aerosols to form accretions will be dependent on their composition. For example, carbonate aerosols may be more likely to form cemented and permanent depositions than silicate particulate deposits.

### 2.4.3. Entrance zone deposition

It has been established that generally the highest concentration of coarse aerosols will be observed in the cave entrance. As investigations of pollen showed, there is a significant loss in suspended coarse aerosols with distance from the cave entrance, with the highest concentrations of palynomorphs in the cave entrance area (Navarro *et al.,* 2001). This will predominantly occur as a result of air flow rate reduction and subsequent gravitational sedimentation of coarse aerosols. There is also the potential for hygroscopic effects due to the high humidity compared to the external atmospheric humidity. Dry aerosols entering the cave environment may absorb water, increase in size, and fall out of the air stream flow. An example of substantial suspended load loss (and therefore deposition) occurring within the entrance zone is displayed in Figure 2.13 presenting aerosol deposition monitoring data from Altamira Cave, Spain.

A detailed survey of suspended aerosol, airborne microorganisms and microclimatic monitoring was carried out at Altamira Cave, a World Heritage UNESCO site, world famous

for its possession of a collection of Palaeolithic rock paintings and engravings that are mainly located in Polychromes Hall (Figure 2.12). The preservation of these paintings is as a result of the cave being characterized by low rates of water infiltration, precipitation of mineral deposits and exchange with the external atmosphere; and the maintenance of very stable microenvironmental conditions because of limited airflow in the Polychrome Hall. However, the opening to the public during previous decades provoked air warming and turbulence caused by visitors causing the increased air exchange between Polychromes Hall and areas closest to the entrance, where there are microbial colonization on walls and ceilings (Cuezva *et al*., 2009). The corrective measures implemented in recent years (since it last closed in 2002) have reduced the exchange between the cave atmosphere and exterior, decreasing the entry of airborne particles, the condensation rate in the entrance area, and the metabolic activity of the main visible microbial colonies (Saiz-Jimenez *et al*., 2011).
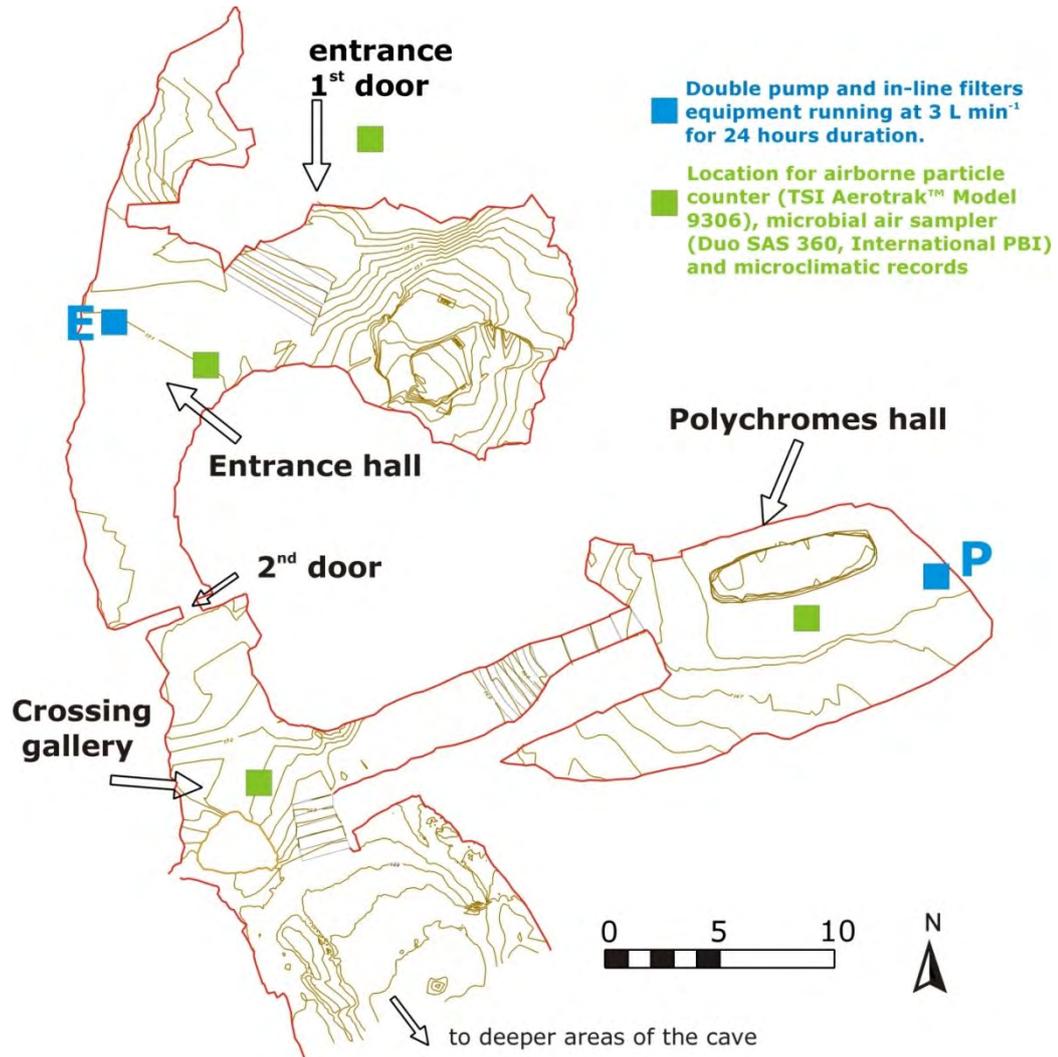
Figure 2.12: Locations at Altamira cave during the aerosols survey by using double pump and in-line filter equipment, running at 3 L min$^{-1}$ for 24 hours duration, airborne particle counter (TSI Aerotrak™ Model 9306), microbial air sampler (Duo SAS 360, International PBI) and microclimatic records.
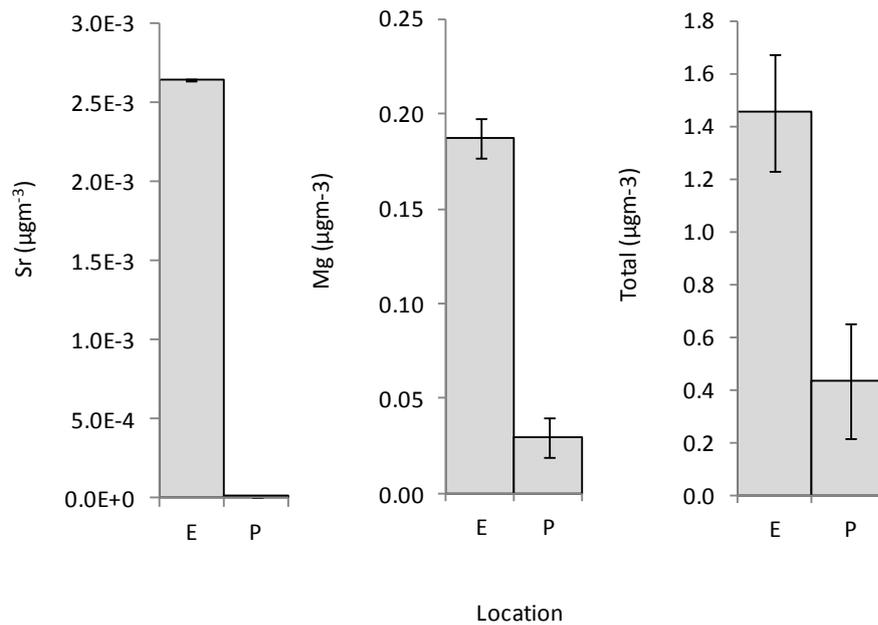
Figure 2.13: Comparison of suspended aerosol concentrations from the cave entrance zone and Polychromes hall, Altamira Cave within the cave interior. Pumped collection of suspended aerosols at 3 L min$^{-1}$ over 24 hours. Limit of detection (3σ) are displayed for each element with error bars.

Figure 2.13 displays a significant reduction in suspended aerosol concentrations from the entrance zone (E) to the Polychromes Hall (P) within the cave interior. This is consistent with the patterns of distribution observed in previous studies involving the transportation of coarse aerosols. However, Location P is a side chamber which may experience reduced ventilation and the lower detected aerosol concentrations can also be attributed to the chamber's location relative to active ventilation streamflow (a bidirectional flux between cave entrance and deeper areas).

This transportation of aerosols will also be hampered by the effect of a double-access door equipped with a thermal insulation system that reduces the entry of airborne particles (Sainz-Jimenez et al., 2011; Garcia-Anton et al., 2012). Therefore suspended load loss is a likely

consequence of deposition occurring as a combined consequence of entrance zone and cave morphology depositional effects.

The same relationship between suspended aerosols, $CO_2$ and temperature as observed in Gough's Cave (Figure 2.10) is apparent in Altamira cave, Spain as shown in Figure 2.14. The loss in suspended aerosols (detected using optical particle counting methods) confirms the results displayed in Figure 2.13 (from pumped sampling and ICP-AES analysis). Smaller particles of less than 1μm demonstrate the strongest relationship with $CO_2$ and the most spatial variance. The spatial distribution effect on aerosols diminishes with increasing aerosol size, as displayed in Figure 2.15. This is likely due to the reduction in the ability of cave ventilation to transport aerosols of increasing size and mass. This is consistent with the idea of entrance zone coarse aerosol deposition and the concept of progressive gravitational sedimentation throughout caves.
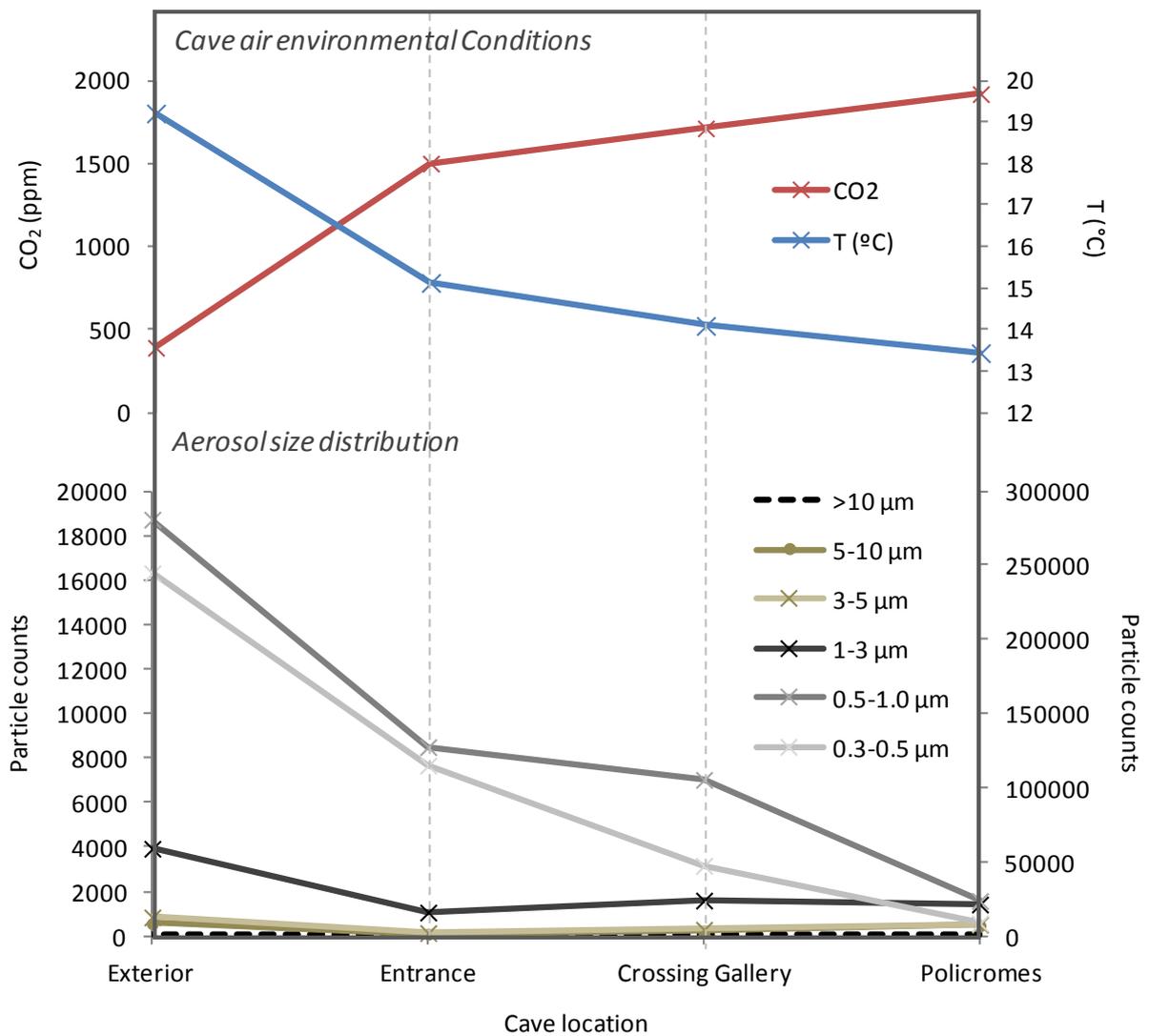
Figure 2.14: Aerosol size distribution: Suspended particle counts of particle size ranges 0.3-0.5µm (secondary axis), 0.5-1µm, 1-3µm and 3-5µm, 5-10 µm, >10 µm. Cave air environmental conditions: $CO_2$ (ppm) and temperature (°C). Data displayed is averaged from four cave visits on the same day 0718hrs-0757hrs, 0929hrs-1005hrs, 1149hrs-1217hrs and 1457hrs-1527hrs. During this time monitoring was only exposed to the influence of the operator.
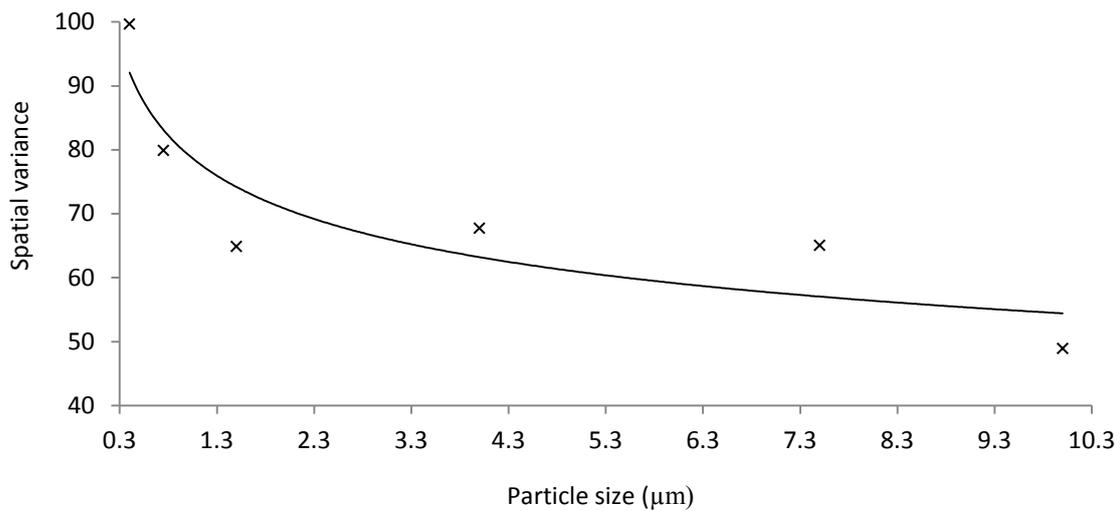
Figure 2.15: Relationship between spatial variance of aerosols and particle size. Spatial variance = [STDEV(aerosol counts)/aerosol counts]×100.

### 2.4.4. Progressive gravitational sedimentation

Under a simplified cave model where gravitational sedimentation is the key process of aerosol deposition, progressive deposition will be observed. Progressive reduction of air ventilation forces and decreasing air flow rates cause progressive aerosol load loss as a result of depositional settling. Evidence of gravitational sedimentation is not observed through all of the case studies used in this investigation. However, Figure 2.17 displays a pattern of aerosol distribution that may represent progressive gravitational deposition in St Michaels Cave, Gibraltar (Figure 2.16) (Mattey *et al.,* 2008; 2010).
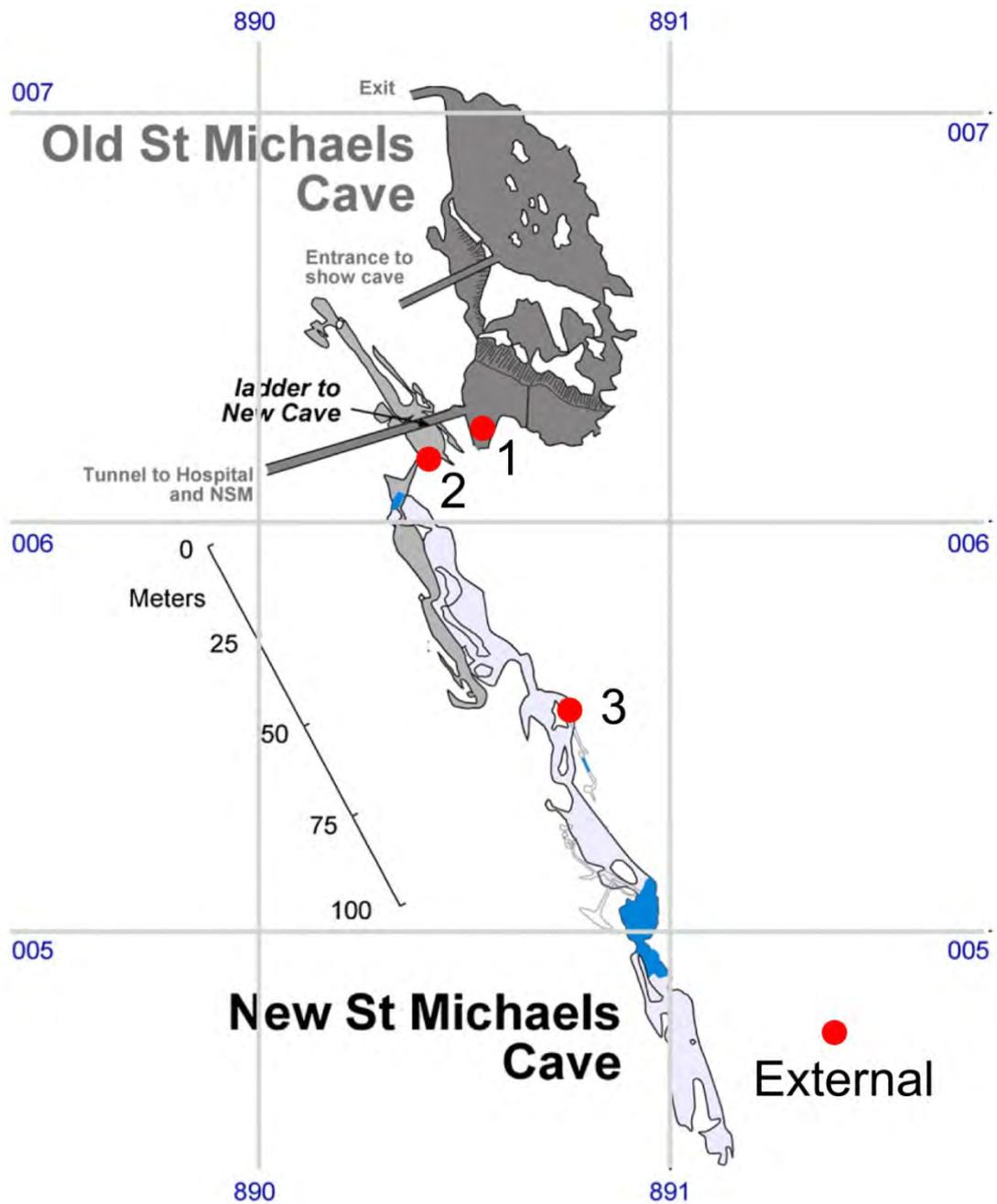
Figure 2.16: Lower New St Michaels Cave network map with cave aerosol sampling locations (after Mattey *et al*., 2008).
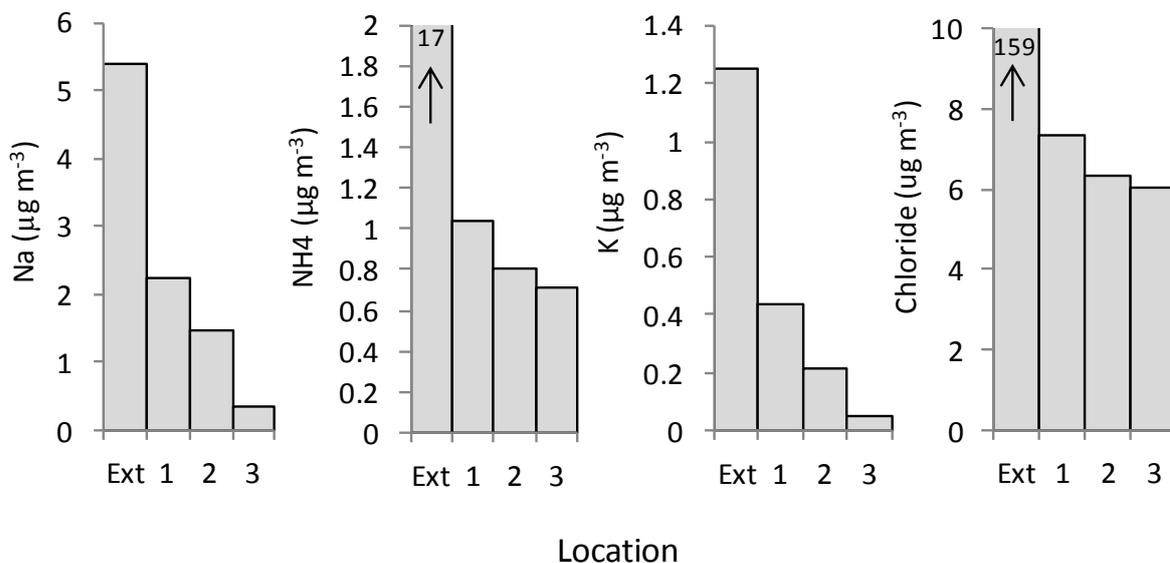
Figure 2.17: Examples of potential evidence for progressive gravitational sedimentation. Suspended aerosol distribution in St Michaels Cave, Gibraltar. Samples spread over approximately 100 m distance from the cave entrance to interior.

Often the relationship between cave ventilation and aerosol processes will be significantly influenced by cave morphology. Caves with an intricate morphology associated with an extensive network of interconnecting fissures will result in a complex distribution of aerosol deposition. Additional processes to gravitational sedimentation may overprint any trends, making deciphering such processes difficult.

***2.4.5. Cave morphology and aerosol deposition***

An example of the control of cave morphology on aerosol deposition rates has been observed at Obir cave, Austria. Surrogate surfaces were deployed in two locations (shown in Figure 2.18) within the cave to determine the deposition rates close to the position of speleothems previously studied by Fairchild et al. (2010). One sample was situated at in Säulenhalle (S), an open chamber with active speleothem formation and a terminal pool (Silbersee) and the other at Düse (D), a nearby constricted passage with air flow sensible by visitors.
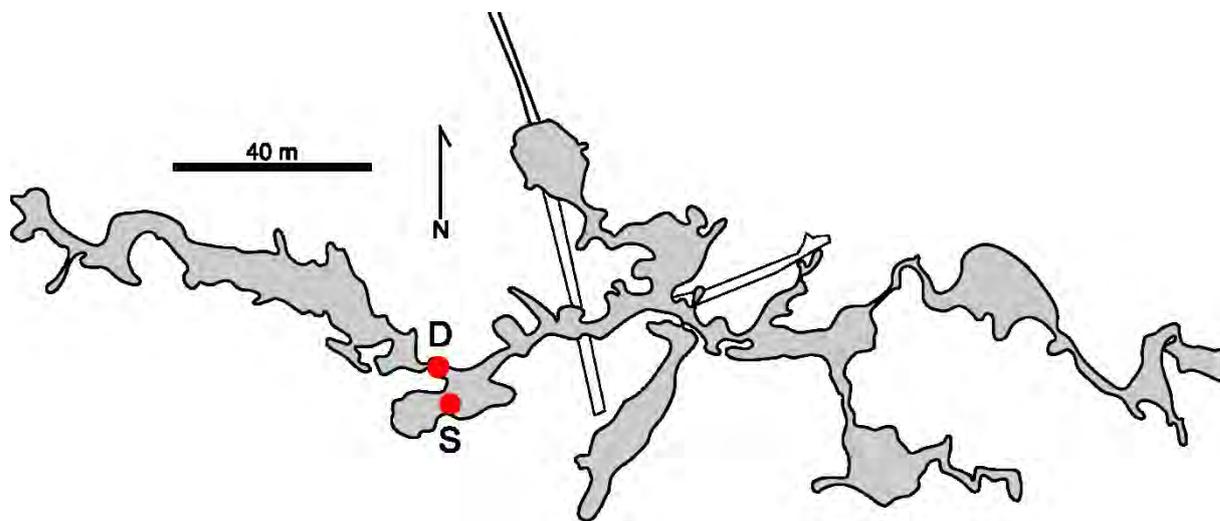


Figure 2.18: Obir Cave map and surrogate surface locations (after Spötl *et al.,* (*2005*)).

Figure 2.19 displays a comparison of depositional flux rates at locations S and D, with location S recording greater levels of total aerosol deposition flux. This can be accounted for simply by gravitational processes. Aerosols remain in suspension as they travel through the constriction due to the higher flow rates, upon entering the larger Säulenhalle chamber where air flow velocities are reduced. The reduction in air flow rates will result in increased gravitational sedimentation and deposition of aerosols to the cave floor. Increased deposition will likely occur near Silbersee pool regardless of the suspended load and ventilation direction

simply as a result of the proposed morphologically controlled reduction in ventilation air flow rates.
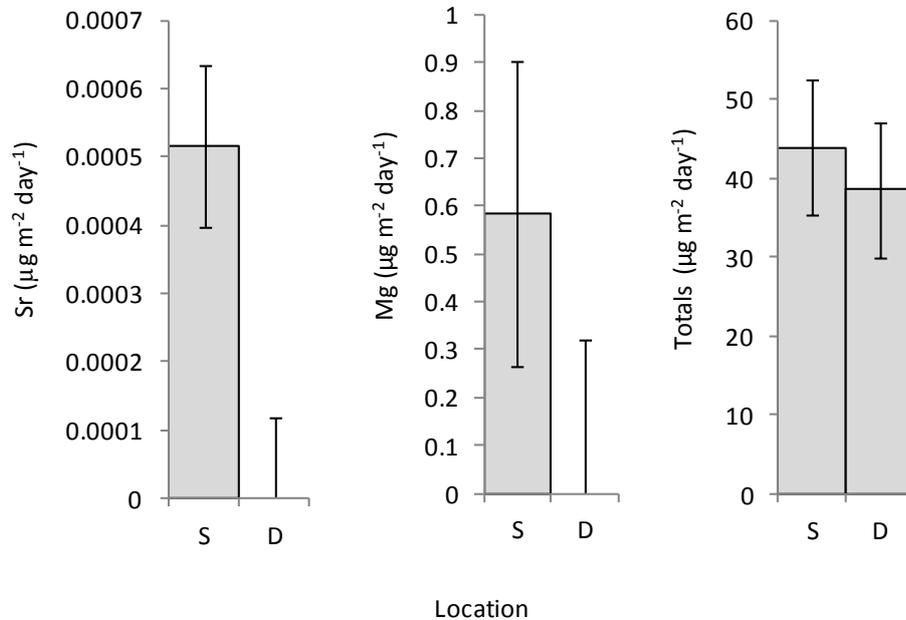


Figure 2.19: Depositional flux rates at two locations: near Silbersee pool (S) and at Düse (D). Results from surrogate surface monitoring from 15th April to 11th July 2012 in Obir Cave, Austria. Error bars display elemental limit of detection (3σ) as errors. Sr and Mg are presented here as element of importance to speleological studies for processes such as PCP. Total deposition refers to the combined deposition of Al, Fe, Mg, Na, K, Ti, P, Mn, Ba, Ni, Sr, V and Zn.

With knowledge of the potential processes affecting aerosol deposition fluxes to speleothem surfaces, it is possible to evaluate the contribution of aerosol deposition to speleothem geochemistry.

### *2.4.6. Results summary*

A range of cave processes can be investigated by measurement of suspended aerosol loads, aerosol deposition and aerosol type. Data has shown that the cave atmosphere aerosols are significantly influenced by cave ventilation and anthropogenic disturbances. Aerosol monitoring is valuable due to its ability to record both anthropogenic and natural ventilation process. The demonstrated sensitivity and recovery of aerosols to anthropogenic and environmental processes offers benefits over other cave environment monitoring tools, which is explored further in Chapter 3. As aerosol monitoring instruments become more widely available, aerosols may become a preferable environmental monitoring indicator providing greater sensitivity over more commonly used indicators such as cave air $CO_2$ and temperature.

## 2.5. Aerosol contributions to speleothem geochemistry

The mode of transport and deposition is expected to have a relationship with the chemistry of aerosols being deposited. For instance, in the case of gravitational sedimentation, the larger and denser particulates will be removed from suspension first and will often be associated with specific sources and chemical composition. In a study by Faimon *et al.* (2006) aerosol compositions were determined to be highly variable with space and time but were broadly composed of Si, Ca, Al and Fe with fine particles formed of S, P, K and Cl. This relationship was not observed with the preliminary spatial deposition monitoring pattern and the chemical composition of aerosol deposition in Obir cave. The lack of a relationship between location and chemistry is likely due to the range of processes effecting the transport and deposition of aerosols, combined with the changing environmental conditions inside the cave and externally.

The comparison of aerosol deposition data from Obir cave demonstrates that elemental deposition flux rates differ between elements and some display trends unlike the overall total depositional flux rate distribution (Figure 2.19). Internally produced aerosols would be expected to be observed at greater concentrations in the cave interior in comparison to the entrance region, but no clear distinction was identifiable.

Based on monitoring data at Obir, it is possible to calculate the aerosol addition to speleothem geochemistry. The following calculations are based on deposition per 1 $mm^2$ of speleothem surface over a period of one year, assuming constant growth (as shown in Figure 2.20).
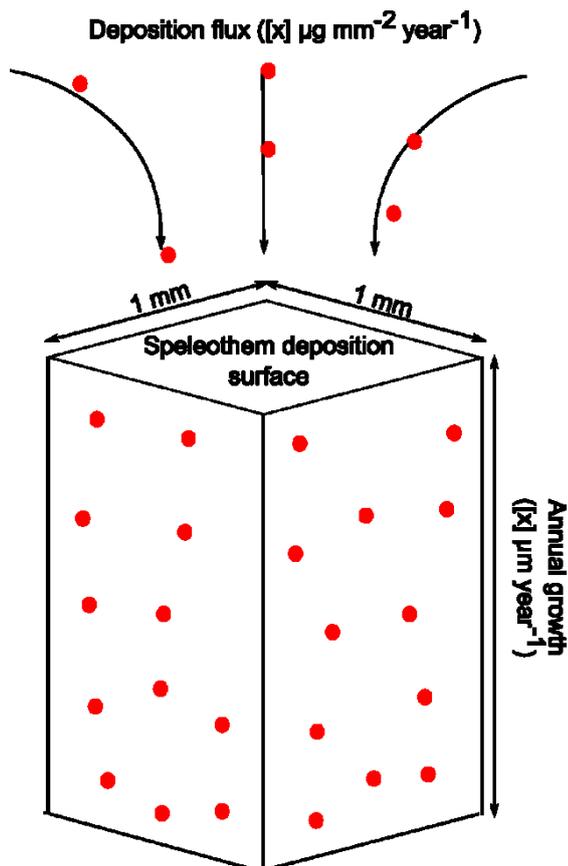
Figure 2.20: Calculation variables: deposition flux and growth rate. Calculations are based on 1 mm$^2$ calcite surface area for one year of speleothem growth.

In order to determine the impact of aerosol deposition upon speleothem composition the rate of deposition and the calcite supply must be known. The potential (maximum) aerosol concentration in calcite (P) is a function of aerosol depositional flux and speleothem growth rate and is related to aerosol deposition and speleothem growth as follows:

P = F/ (R × ρ)

Where    P = Potential aerosol concentration in calcite ($\mu g \ g^{-1}$)

F = aerosol depositional flux ($\mu g \ mm^{-2} \ year^{-1}$)

R = speleothem growth rate ($mm \ year^{-1}$)

$\rho = 0.00271$ = calcite density (g mm$^{-3}$)

The relationship between speleothem calcite concentration and aerosol deposition flux as a function of growth rate is displayed graphically in Figure 2.21.
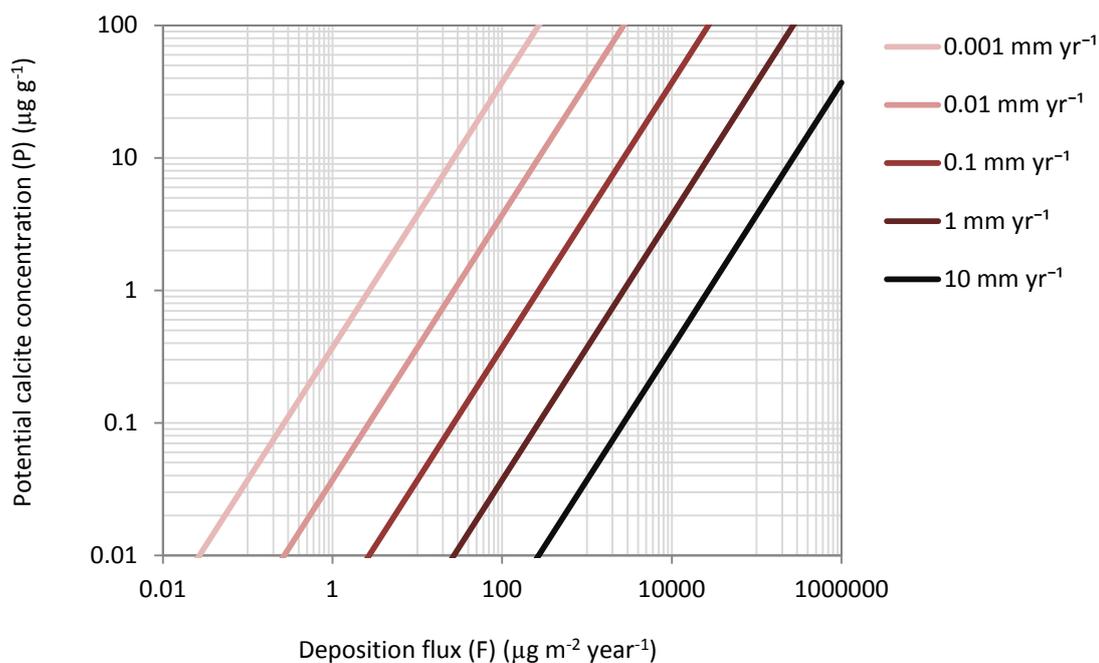


Figure 2.21: Relationship between aerosol deposition flux (F) of a trace species and its potential concentration in calcite (P) as a function of varying growth rates from 0.001 mm yr$^{-1}$ to 10 mm yr$^{-1}$.

By adding known deposition flux rates into the equation the potential calcite contribution can be calculated. Here, data from Obir cave monitoring (Fairchild *et al*., 2010) are presented to demonstrate the maximum possible extent of aerosol contribution to speleothem chemistry. An approximation of calcite concentration contribution is shown in Figure 2.22 based on maximum aerosol deposition flux rates.
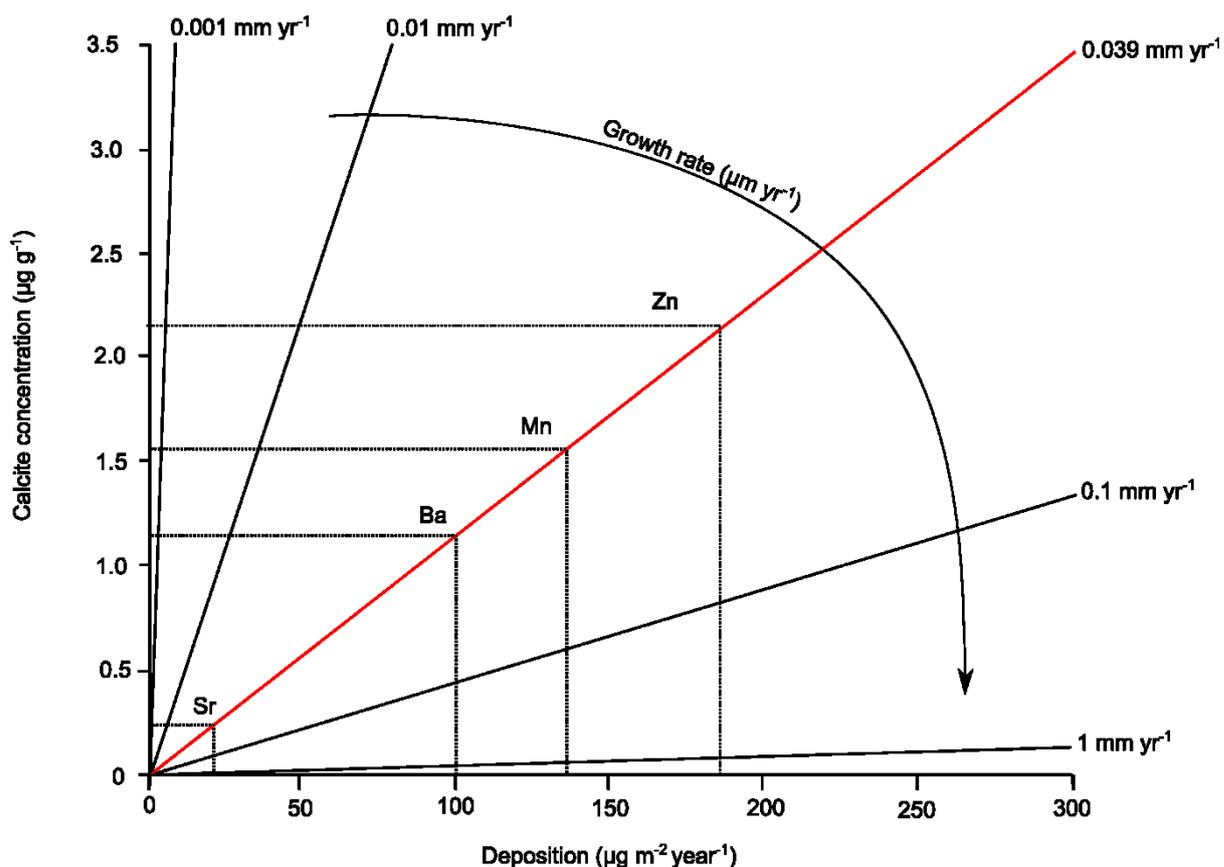
Figure 2.22: The relationship between aerosol deposition flux (F), growth rate (R) and potential calcite concentration (P) for speleothem OBI12 with a recorded growth rate of 0.039 mm yr$^{-1}$. Maximum Sr, Ba, Mn and Zn deposition flux rates are plotted to give their corresponding potential calcite concentration contribution values based on this annual growth rate.

Aerosol contributions can be expressed as a percentage of the speleothem concentration of individual elements:

A (aerosol contribution, %) = (P/C) × 100

Where: C = elemental calcite concentration

The maximum theoretical contribution of aerosols to speleothem chemistry has been shown to vary significantly between different elements as shown in Table 2.2. Values range from

0.002% to 71.8% dependent on the element and speleothem under investigation. This highlights the contribution from drip water on the potential contribution of aerosol deposition on total speleothem geochemistry.

| | Mg | P | Mn | Zn | Sr | Ba |
|---|---|---|---|---|---|---|
| **OBI12** | 1.1 ± 0.31 | 14 ± 5.4 | 72 ± 34 | 0.0068 ± 0.0027 | 0.45 ± 0.11 | 0.20 ± 0.043 |
| **OBI84** | 0.43 ± 0.34 | 5.0 ± 4.0 | 30 ± 32 | 0.0024 ± 0.0015 | 0.13 ± 0.18 | 0.079 ± 0.066 |

Table 2.2: Values of maximum theoretical aerosol contributions (A, %) to concentrations of individual elements for samples taken across the growth range of the Obir speleothems, based on depositional flux at location S. Uncertainties are one standard deviation.

Speleothems with low trace element influx from drip waters will present a greater aerosol contribution relative to those with high trace elements. Aerosols will provide a significant contribution to 'cleaner' speleothem samples and these are therefore more likely to preserve detectable aerosol geochemical signatures representative of environmental conditions. A comparison of drip water to aerosol chemistry supply is shown in Table 2.3.

| | Oversupply (%) | | Limiting drip rate |
|---|---|---|---|
| Element | *Drip water* | *Aerosol flux* | (**L yr$^{-1}$**) |
| Zn | 18 | 0.00014 | 0.0022 |
| Mg | 9583 | 0.00073 | 0.000022 |
| P | 99 | 0.012 | 0.036 |

Table 2.3: Comparison of drip water (at 287 L year$^{-1}$ flow rate) and aerosol flux contributions to speleothem geochemistry. Limiting drip rates are those at which drip water chemistry supply is equal to that of aerosol flux. Drip water oversupply (%) = 1/[ Mg of element per year calcite growth / Mg of drip water supply per year ×100] ×100. Aerosol flux oversupply (%) = 1/[Mg of element per year calcite growth / Mg of aerosol flux to speleothem surface per year) ×100] ×100.

The comparison of drip water supply and aerosol flux supply to modern calcite concentrations (Table 2.3) has shown that at current drip water flow rates the drip water chemistry supply is orders of magnitude greater than that offered by aerosol flux. Limiting drip rates demonstrate that for all elements compared a >99.9% reduction in flow rates is required to reduce the drip water supply to quantities equal to the aerosol supply.

The data and calculations presented here so far are based on several assumptions. The first is that the surrogate surface aerosol deposition provides a suitable replication of the type of aerosol flux that would occur to the speleothem surface. Secondly, and likely to be of greater impact is that the above calculations are based on complete incorporation (i.e. 100% efficiency). There are however several processes that will occur that would result in less than total incorporation of aerosol deposition within growing speleothem.

### 2.5.1. Potential aerosol calcite contribution – incorporation

The aerosol contribution to speleothem geochemistry (P) is in practice an unrealistic maximum since aerosol preservation will be highly dependent on drip water flow rates and the mechanism of deposition. Aerosols deposited to the surface of an actively growing speleothem may be washed away by drip water flowing over the speleothem surface. Conversely, deposition to the surface of a dry speleothem (during a speleothem growth hiatus) could result in the formation of a deposit predominantly composed of aerosol deposits. Any aerosol deposits during a hiatus period would be affected by the possible drip water removal processes upon resumption of drip water flow over the speleothem surface. However, if binding of aerosol deposits occur to produce a consolidated horizon of calcareous or non-calcareous composition, it would be resistant to drip water flow. Since calcite concentration

will be a function of growth rates, it is during hiatus events where aerosol deposition will have the greatest influence on speleothem chemistry. If aerosol deposition in the cave environment has been characterised by monitoring, identification of hiatus horizons in the speleothem chemistry would be possible. This would enable identification of intervals that represent specific environmental conditions.

The type of aerosol will influence the likelihood of preservation. Denser particles will be less likely to be removed by drip water flowing over the speleothem surface relative to low density particles. Soluble components of particles and liquid aerosols deposited to speleothem thin film drip water may become dissolved in the drip water. In evaporative scenarios with low to zero drip rates it may be possible for liquid aerosols to create a defined horizon through precipitation. Aerosol preservation will therefore be a function of: drip water flow rates, speleothem growth rates (also a function of flow rates), aerosol deposition type (wet or dry deposition) and aerosol type.

*Incorporation type*

Deposited aerosols remaining on the surface retain the potential to become incorporated into the speleothem. However, this process will not be 100% efficient in capturing the entire aerosol signature. Solutes will be coprecipitated, providing an addition to drip water chemistry. Particulates are likely to become incorporated through intercrystalline capture. Aerosols which become incorporated into the crystal lattice will be subjected to incorporation factors dependent on the chemistry and type of aerosol deposited. Notably, a number of trace elements are preferentially incorporated in the solid phase as a result of adsorption and complexing processes described in Fairchild and Baker (2012, chapter 8). Here we modelled

potential contributions from aerosols assuming 100% efficiency of incorporation into the solid phase. Whereas ions are removed from dripwater at quite low efficiencies (and this is specifically the case as Obir cave, Fairchild *et al*., 2010), at minimal drip rates, in solid phase accretion, processes will tend to be less discriminatory between elements.

Concentrations in calcite are influenced by a combination of processes each controlled by deposition flux rates and growth rates. The final calcite concentration is controlled by the incorporation efficiency of the deposit aerosols and is also therefore a function of deposition flux rates and growth rates.

Aerosol deposition and incorporation to speleothem is a complex function of a variety of environmental, speleothem and aerosol conditions. Scenarios in which aerosol deposition becomes significant and potentially identifiable in the speleothem record have been observed in both hiatus events, and slow growth – high deposition flux situations. Through monitoring of dry deposition fluxes and comparisons to speleothem geochemistry, aerosol contributions to speleothem geochemistry can be approximated and their significance for further investigation determined. Data demonstrates that aerosol deposition should be considered in speleothem sampling choice. In some scenarios aerosol contributions may contaminate samples for geochemical analysis, such as radiogenic isotope studies, or skew drip water environmental signatures.

### *2.5.2. Cave aerosol, aerobiology and microbial communities*

As with pollen, microbial material is known to be distributed throughout cave networks (Jurado *et al.,* 2009, 2010; Cuezva *et al.,* 2009; Bastian *et al.,* 2009a, 2009b, 2009c, 2010).

The distribution of microorganisms may be influenced by transportation as aerosols. In addition to, or as a separate process, microbiological activity throughout caves is known to occur as a consequence of anthropogenic transportation and is often an issue for cave management practices. Aerosols of fungi (Wang *et al.,* 2011) and bacteria (Wang *et al.*, 2010; Martin-Sanchez *et al.,* 2011) have been shown to be distributed throughout cave networks with visitors having a significant influence of the type and concentration of the biological aerosols. Visitors carry spores, seeds and bacteria on clothing and deposit them within the cave network. In addition to providing an introduction mechanism, visitors result in increased disturbance. A secondary aerosol feedback process may occur as a result of the disturbance where increased suspended aerosol loads and deposition to cave surfaces provide nutrients to sustain biological development resulting in increased communities.

Regarding the contribution of aerosol deposition to speleothem, microbiological processes may provide an additional feedback. Aerosol deposition contributions to speleothem surfaces may not be sufficient to influence speleothem chemistry directly to a significant degree. However, the presence of deposits may facilitate and sustain microbial communities which subsequently, through bio-accumulative processes, result in inorganic concentration horizons of notable levels. Some bacteria are known to be capable of concentrating metals from their environment (Dorn & Oberlander, 1981) and have been known to increase the rate of manganese oxidation by up to five orders of magnitude (Tebo *et al.*, 1997). Microorganisms may contribute to the formation of manganese and iron oxide-rich deposits (Northup *et al.*, 2003). In addition to metals, cave biota have been also shown to accumulate and precipitate calcium phosphate in significant quantities (Jones, 2009). In the particular case study of Altamira cave, the Actinobacteria forming grey spots in the cave surface near the entrance can

use the captured $CO_2$ to dissolve the rock and subsequently generate crystals of $CaCO_3$ in periods of lower humidity and/or $CO_2$ (Cuezva *et al*., 2012). Likewise, bacteria are also involved in the formation of calcitic moonmilk deposits in this cave (Sanchez-Moral *et al*., 2012). In some instances the aerosol contribution to speleothem could be significantly increased as a result of secondary feedback concentrating processes and provide a proxy for emission events, which would not be detectable otherwise. Monitoring of suspended fungi and bacteria was undertaken in Altamira Cave, Spain to determine the spatial distribution of microbial aerosols throughout the cave network, the results of which are displayed in Figure 2.23. Fungi demonstrate the same distribution observed in the suspended aerosol counts carried out during the same fieldwork period indicating the same ventilation driven distribution mechanism as other aerosols. It should be noted that fungi may associate with larger particles which were not detected by the particle counter. However, bacteria demonstrate a pervasive but spatially independent distribution. This is coherent with the distribution of intermediate to coarser aerosols observed from suspended aerosol monitoring, as bacterial aerosols are typically of 0.3-10 μm in size (as shown in Figure 2.2). The aerial distribution of suspended bacteria differs to that of observations of bacterial colonisation, which is dominant nearest the cave entrance. It is plausible that the relationship between bioaerosols and cave surface colonisation is controlled by the distribution of other aerosols, which provide a nutrient flux creating conditions suitable for sustaining microbial production. Therefore entrance zone colonisation occurs as a consequence of relatively high deposition fluxes to the cave surfaces.
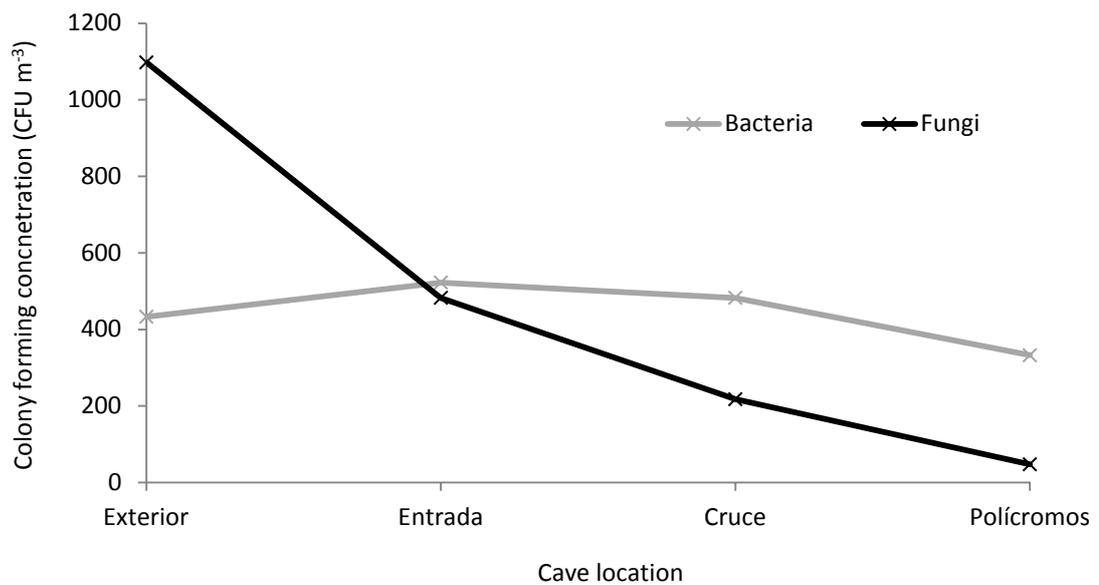
Figure 2.23: Airborne bacteria and fungi aerosol concentrations expressed as colony forming units per $m^3$ of air in Altamira Cave, Spain. Data displayed is averaged from four cave visits on the same day 0718hrs-0757hrs, 0929hrs-1005hrs, 1149hrs-1217hrs and 1457hrs-1527hrs. During this time monitoring was only exposed to the influence of the operator.

## 2.6. Conclusions

Aerosol introduction, distribution, deposition and incorporation are complex and variable processes dictated heavily by the specific cave situation with aerosol spatial distributions having a dominant influence on local deposition. The type of speleothem formation and cave morphology will control deposition through impaction/interception processes and the level of aerosol transport to the surface of the speleothem respectively. Consequently, the within-cave location of speleothem formation and aerosol incorporation will often govern whether deposition flux rates are sufficient to provide a significant contribution to aerosol geochemistry.

Cave aerosols are sensitive to environmental conditions (ventilation, drip water flow rates) and therefore will exhibit temporal and spatial variations. Due to the sensitivity of aerosols to environmental conditions, aerosol monitoring has the potential to be used in cave ventilation studies in place of existing $CO_2$ and temperature work.

Calculations have demonstrated that the ultimate contribution to speleothem geochemistry is predominantly dependent on growth rates, deposition flux, and aerosol incorporation factors. Results have shown that aerosol contributions to speleothem chemistry will commonly be of low significance; but, in certain instances aerosols may provide considerable additions to geochemistry. The elemental deposition and potential contributions of aerosols relative to speleothem geochemistry and drip water chemistry display a large range of influence.

Situations where aerosol deposition may provide noteworthy contributions to speleothem:

- Hiatus events (ceased/very slow speleothem growth)

- Very high deposition flux rates as a result of a combination of efficient aerosol transport and large external suspended loads

- Secondary microbial feedback processes resulting in increased concentrations.

In such instances aerosols through speleothem incorporation may provide a novel environmental indicator not yet constrained by existing proxies.

# Processes Affecting Aerosol concentrations in Gough's Cave, Cheddar Gorge, U.K.
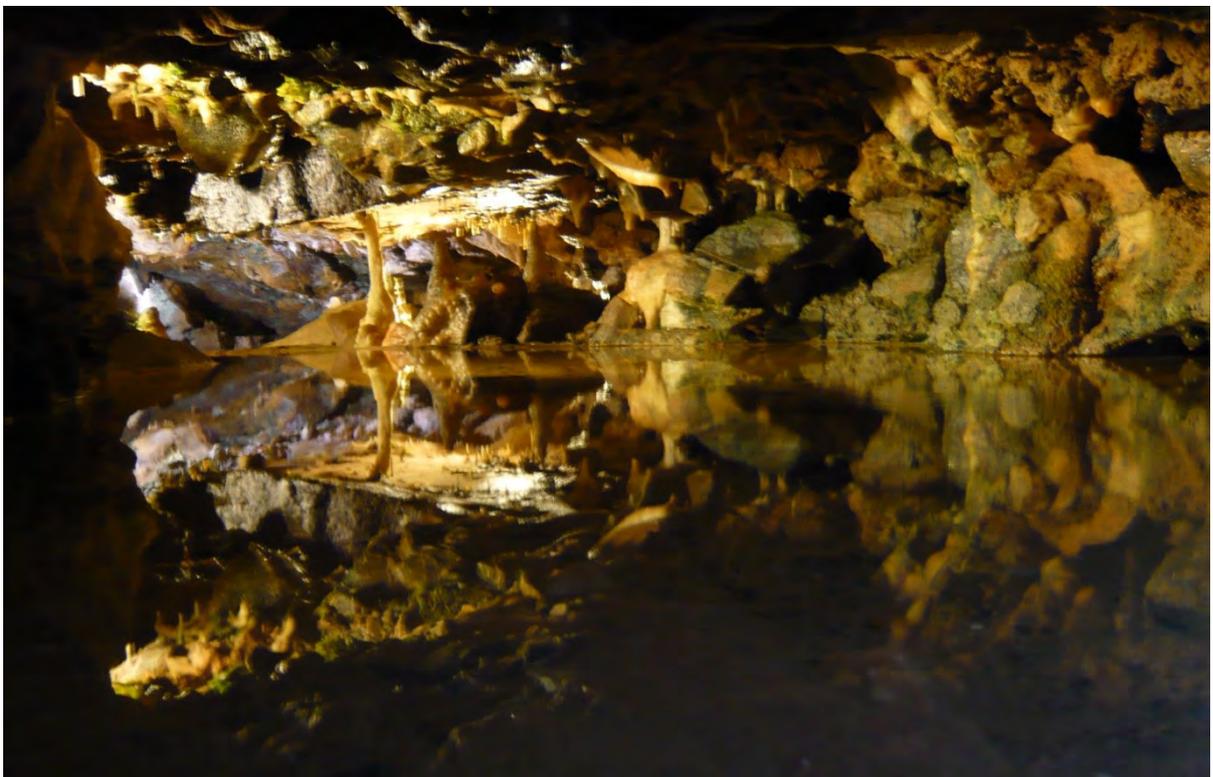


*Decoration and reflection in Alladdin's Chamber, Gough's Cave*

## Chapter 3. Processes Affecting Aerosol Concentrations in Gough's Cave, Cheddar Gorge, U.K.

This chapter has been published in the journal of Cave and Karst Science (Dredge *et al*., 2014).

### 3.1. Introduction

Aerosols are generally defined as the suspension of fine solid or liquid particles within a gaseous medium (Hinds, 1999). Cave aerosols are introduced directly from internal sources or sourced externally and transported by cave ventilation and anthropogenic processes. Cave aerosol monitoring offers an additional environmental proxy to more established methods such as $CO_2$ and temperature. Interest in aerosols is developing due to a combination of their sensitivity as an environmental proxy (Dredge *et al*., 2013; Smith *et al*., 2013), potential contributions to speleothem geochemistry (Dredge *et al*., 2013), cave management (Ohms, 2003) and cave conservation issues (Chang *et al*., 2008).

This paper presents data from a medium-term multi-proxy monitoring programme established in Gough's Cave, Cheddar Gorge (UK) in August 2012 with monitoring continuing through to December 2012. The aim of this study was to identify the effects of seasonal environmental change on suspended aerosol concentrations, cave air carbon dioxide ($pCO_2$) levels and temperature.

This paper explores the benefits of using aerosol monitoring as part of cave environmental studies. Aerosol monitoring is used to identify seasonal changes in cave ventilation, and investigate the processes controlling cave environmental conditions.

### *3.1.1. Location*

Gough's Cave is a show cave with a main entrance opening into the Cheddar Gorge valley, located near the village of Cheddar in the county of Somerset, UK. The cave location within the UK and cave plan is displayed in Figure 3.1.

Gough's Cave is a resurgence cave developed in gently dipping limestone with most of the passages formed by the River Yeo, which resurges just outside the cave entrance in a series of springs known as Cheddar Risings. The Gough's Cave system is developed in the Carboniferous Clifton Down Limestone Formation, part of the Pembroke Limestone Group. The rocks dip to the SSW in the main show-cave at between 20° and 25°, striking at 095° to 115° (Farrant, 2010).

Gough's Cave is a managed show cave that receives tens of thousands of tourist visitors each year, mainly during the summer months (69305 visitors from August to December, 2012). Cheddar gorge is now (and in recent history) dry with a main road running through it and therefore traffic flow provides a potential external source of anthropogenic aerosols in addition to those produced internally by visitors.
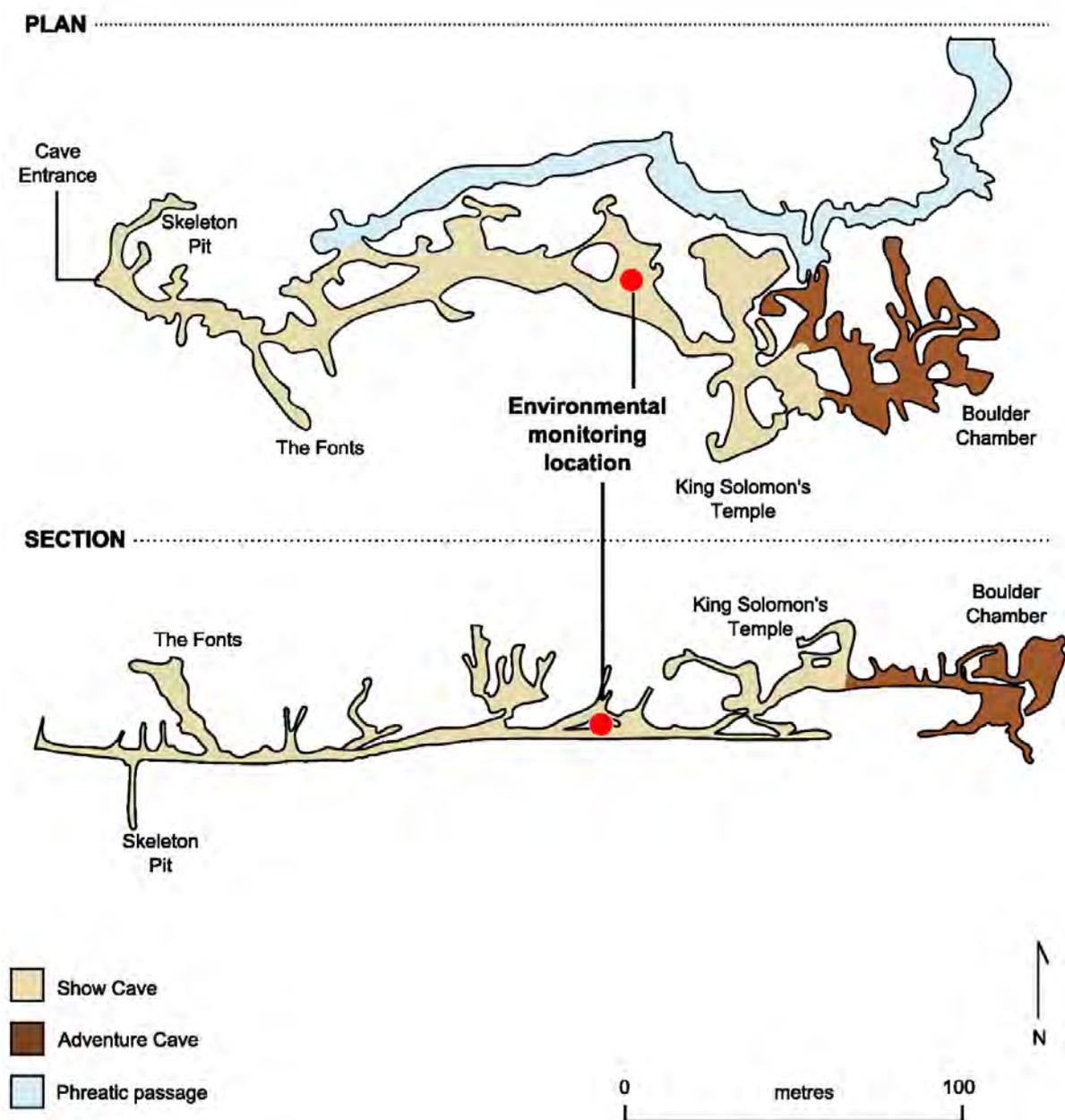
Figure 3.1: Gough's Cave map, in plan (upper illustration) and section (lower illustration). The environmental monitoring station is marked. Image adapted from Farrant (2010), based on survey data by Stanton (1953).

### 3.1.2. Cave ventilation

Cave ventilation is the process by which internal cave air is exchanged with external atmospheric air. It occurs as a result of several phenomena: cave breathing, wind-induced flow, chimney circulation or stack effect, convection and water-induced flow (Fairchild & Baker, 2012). As ventilation is difficult to measure directly, cave environmental conditions are commonly utilised as proxies of cave ventilation processes. The strength and seasonality of cave ventilation has traditionally been determined through the monitoring of $CO_2$, temperature and radon gas. In this investigation, $CO_2$ and temperature are compared to the cave aerosol record in order to better constrain cave environmental processes. It should be noted that this investigation is limited by the length of the monitoring duration and conclusions regarding the winter – spring – summer transition can only be tentative.

It is generally recognized that cave chambers with high cave air $pCO_2$ values (of the order of several thousands of ppm) reflect very poor air circulation (Fairchild & Baker, 2012). The monitoring of $CO_2$ therefore provides a proxy for ventilation intensity (for example Wilkening & Watkins, 1976). Several studies have utilised $CO_2$ monitoring for the determination of ventilation intensity (e.g. Mattey *et al*., 2010; Kowalczk & Froelich, 2010; Cuezva *et al*., 2011; Frisia *et al*., 2011).

Temperature disparities between the external environment, cave interior and bedrock are moderated by heat transfer. Wigley & Brown (1971) calculated the influence of external air and heat transfer into the cave and the influence of temperature disparities, cave humidity, cave size and morphology. Heat flux takes place through conductive and convective processes with the latter resulting in cave ventilation. Only a few studies have utilised cave temperature

monitoring for the investigation of cave process dynamics (e.g. Fernandez-Cortes *et al*., 2006; Stoeva *et al*., 2006; Domínguez-Villar *et al*., 2013) due to the difficulty in conceptualization of the system. However, a range of studies have monitored temperature as a part of a suite of environmental conditions, often to complement the monitoring of $CO_2$ (Spötl *et al*.,  2005; Baldini *et al*., 2008; Mattey *et al.,* 2010).

### 3.1.3. Cave aerosols

An introductory treatment is given here, whereas a more comprehensive review of cave aerosol transportation and distribution processes can be found in Chapter 2 - Dredge et al. (2013).

Figure 3.2 displays the range of aerosol sizes that can be observed in atmospheric air (nucleation, accumulation and coarse modes (Willeke & Whitby, 1975). The group sizes used in this investigation are the total, small and large aerosol groups. The 'small' group (0.5-2.5 µm diameter) includes aerosols such as fine dust, bacteria, mould and smoke particles and corresponds roughly to the upper part of the accumulation mode size group (as presented in Figure 3.2). The 'large' group (>2.5 µm) is composed of aerosols such as: coarse dust, spores and pollen, terrestrial sediment dust, and clothing fibres.
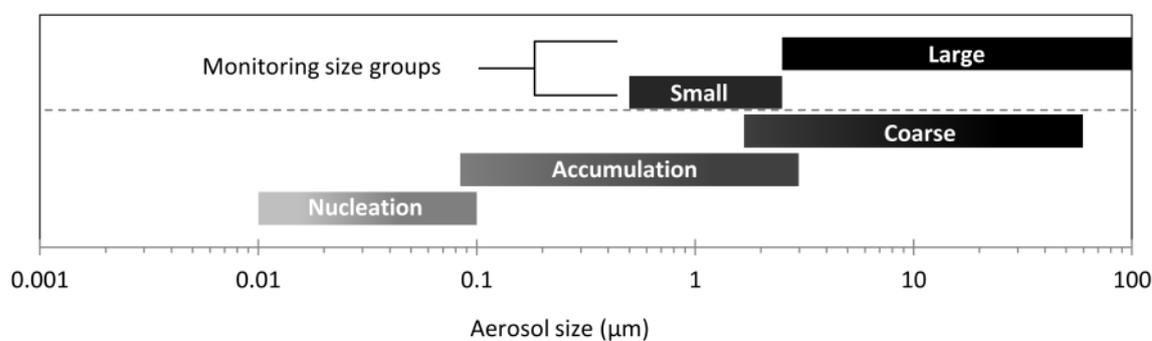


Figure 3.2: Atmospheric aerosol size modes (lower box) and aerosol size modes monitored (upper box). Size mode aerosol ranges taken from Willeke & Whitby (1975).

The investigation of particle size groups can offer further insight into the mechanisms controlling aerosol transport and distribution. Monitored aerosol concentrations represent the net result of aerosol introduction and deposition. The process of aerosol removal from

suspension is known as aerosol deposition, with deposition rate to a surface area expressed as deposition flux. Deposition occurs as a consequence of the following processes: Brownian diffusion, interception, impaction, sedimentation (gravitational fallout) and wet deposition (precipitation scavenging) (Petroff *et al.,* 2008). It should be noted that aerosols may coagulate to form larger particles and in this case suspended aerosol monitoring counts would be reduced and subsequent aerosol mass calculations skewed. However, coagulation effects are likely to be small for the monitored size range due to aerosol static charges (Hinds, 1999). The elevated humidity in the cave environment relative to the exterior may result in aerosols absorbing water and increasing in density. Consequently, aerosols near transport velocity thresholds may increase in density and fall out of suspension. Coagulation, hydroscopic and static charge processes could be investigated through the monitoring of aerosol size fractions, both temporally and spatially throughout the cave environment (explored further in Chapter 6).

Aerosol introduction will occur as a result of transport processes carrying external aerosols into the cave, or by internal cave production by visitor disruption. Aerosol transport into and throughout the cave occurs as a result of air-exchange (Pashchenko *et al*., 1993) and dust carried in by visitors (Michie,1999; Jeong *et al*., 2003) and animals. Air-exchange will carry atmospheric aerosols as part of the package of air into the cave environment. Aerosol monitoring has been carried out to determine anthropogenic influences in caves (Michie, 1999), temporal (Christoforou *et al*., 1996; Kertesz *et al*., 1999; Iskra *et al.,* 2010; Dredge *et al*., 2013; Smith *et al*., 2013) and spatial change (Michie *et al*., 1999 ; Kertesz *et al*., 1999; Genty *et al.,* 2001; Dredge *et al.,* 2013; Smith *et al*., 2013). Studies by Dredge et al. (2013)

(Chapter 2) and Smith et al. (2013) both developed an understanding of aerosol-ventilation relationships through the utilisation of combined $CO_2$, temperature and aerosol monitoring.

Cave ventilation exchanges internal and external aerosols and in principle may have the net effect of either introducing or removing aerosols from the cave environment. External aerosols introduced into the cave environment by active ventilation will tend to be maintained in suspension by air flow rates above threshold values (Kulkarni *et al.,* 2011). Ventilation can act to lower cave atmosphere aerosol levels through air exchange and mixing, in situations where external air has lower aerosol concentrations than the cave interior. Alternatively in exceptionally high air flow rates ventilation can produce aerosols through entrainment processes.

### 3.1.4. Anthropogenic effects on the cave environment

Each of the monitored conditions can be influenced and altered by cave visitor effects. The impact of cave visitors will generally be influenced by visitor numbers and length of visits.

Sanchez-Moral et al. (1999) investigated $CO_2$ and temperature variations associated with cave visitors. The results demonstrated that visitors produce a series of variations in the cave microclimate due to their own metabolism. These alterations are produced by heat emission through radiation via skin, by $CO_2$, and water vapour exhalation, together with the consumption of $O_2$ through respiration. Anthropogenic aerosols can act to alter the cave environment through either transport from external sources (Christoforou *et al*., 1994; Salmon *et al*., 1994; 1995; Jeong *et al*., 2003; Chang *et al*., 2008) or as a result of internal production (Michie, 1999; Ohms, 2003). Cave visitors cause increased suspended aerosol levels through

two mechanisms: 1) transportation into caves on clothes e.g. lint and dust and 2) re-suspension of surface dust and floor sediments (Michie, 2003). Aerosols produced by visitors are principally formed by disturbing surface deposits and previous aerosol deposits; Bartenev & Veselova (1987) recorded a rise in aerosol deposition of more than 10 times within 20 m of the main tourist passages.

Anthropogenic influences and environmental impacts will be cyclic due to the daily show cave opening times. Diurnal anthropogenic cycles will consist of a daytime rising phase, followed by a nightly recovery period to baseline environmental conditions.

This paper seeks to identify the relative significance of anthropogenic influences and natural cave ventilation processes on cave aerosol concentrations. Following a description of the methods employed, short and long-term trends visible in the data will be presented. Relationships between internal cave conditions and external weather conditions will be explored and processes controlling internal environmental conditions identified.

## 3.2. Methodology

### 3.2.1. Environmental monitoring location

The cave environmental monitoring location was chosen to provide sensitivity to changing environmental conditions and ensure equipment security. Key considerations in the choice of site were: availability of mains power, absence of drips and avoidance of vandalism or tampering from cave visitors. Two locations were selected initially, one near the cave entrance and one approximately halfway along the tourist route. However, in December 2012 exceptional flooding (>2 m depth) following prolonged heavy rain destroyed the equipment located at the entrance. The location of the single environmental monitoring site is shown in Figure 3.1.

### 3.2.2. Suspended aerosols

Suspended aerosols were measured using a Dylos air-quality monitor particle counter (DC1700) instrument. The unit uses a laser counter with two size ranges 0.5 μm − 2.5 μm and >2.5 μm to provide aerosol counts for small and large aerosols respectively per volume of air. The suspended aerosol quantities presented in this paper are based on the mean levels during one minute of counting. Recording of counts took place over the first minute of each hour. Data-smoothing and statistics presented were carried out on the minute-mean data.

### 3.2.3. Cave air $CO_2$ and temperature

Cave air $pCO_2$ was recorded using a Tinytag $CO_2$ data logger (TGE-0011). This model offers a 0 to 5000 ppm range with precision stated as being less than 50 ppm plus 3% of the

measured value. Cave temperature was recorded with a Tinytag Plus 2 internal temperature data logger (0.01ºC reading resolution).

### 3.2.4. External environmental conditions

External environmental conditions were taken from the National Oceanic and Atmospheric Administration (NOAA), National Climatic Data Centre database. The nearest location (<16 km away) offers twice-hourly environmental data at the Bristol airport location (Call sign EGGD) latitude 51.383º, longitude -2.717º, and elevation 190 m.

## 3.3. Results

### 3.3.1. Seasonal Environmental change

In this section results will be presented from the environmental monitoring programme. Results will be further explored in the discussion (section 3.4).
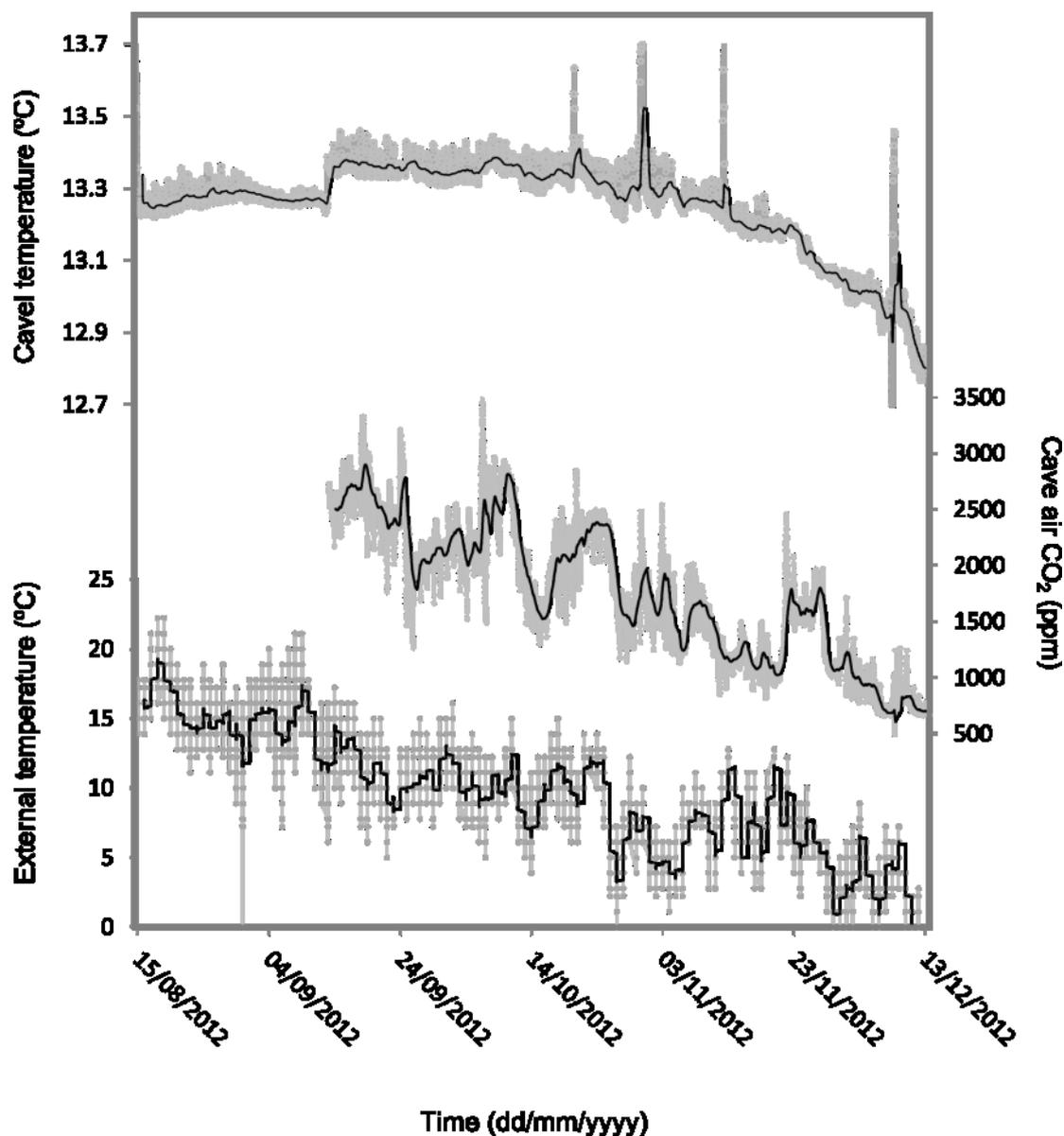


Figure 3.3: Time series of external temperature and cave air $pCO_2$ over the monitoring duration. External temperature from climate data centre observations (see methods) is shown (in grey) as hourly averages from original 30 min observations. Hourly data is presented for cave air $pCO_2$ and temperature in grey. Each condition is presented with a 24 hour running mean (black line).

Seasonal trends presented in Figure 3.3 are most easily discerned with respect to temperature. A trend between cave air $pCO_2$ and cave temperature over the entire monitoring period is observable. The $CO_2$ monitor was placed at a later date than the other monitors; hence data are missing for earlier dates.

### 3.3.2. Seasonal cave environmental change

This section explores long term seasonal environmental change in relation to cave aerosols.

Figure 3.4 displays the entire record of total suspended aerosol concentrations.
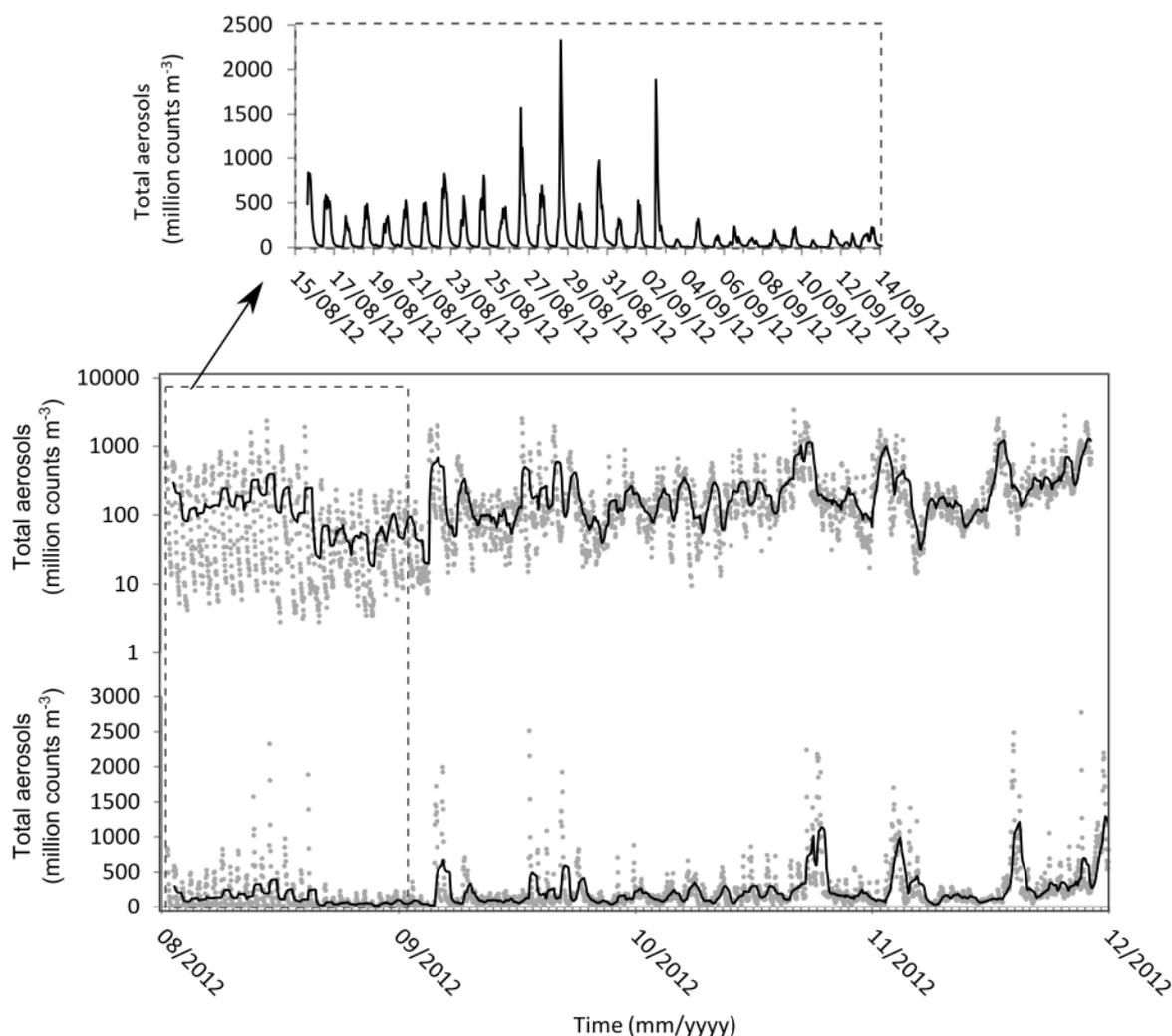


Figure 3.4: Long term trend in aerosols over the summer to winter transition period. Hourly aerosol data with 24 hour moving average trend line. Results are presented with a logarithmic scale used for the y-axis for the upper graph and an arithmetic y-axis for the lower graph (in the lower panel).

The early variability displayed in Figure 3.4 is reflective of diurnal cycles which are observable in all environmental conditions. The predominance of the diurnal pattern

diminishes and is replaced by episodes of high amplitude aerosol concentration excursions as the monitoring progresses into the winter season. The winter diurnal cycle is less pronounced and demonstrates more sporadic change compared to the observed systematic summer cycles.
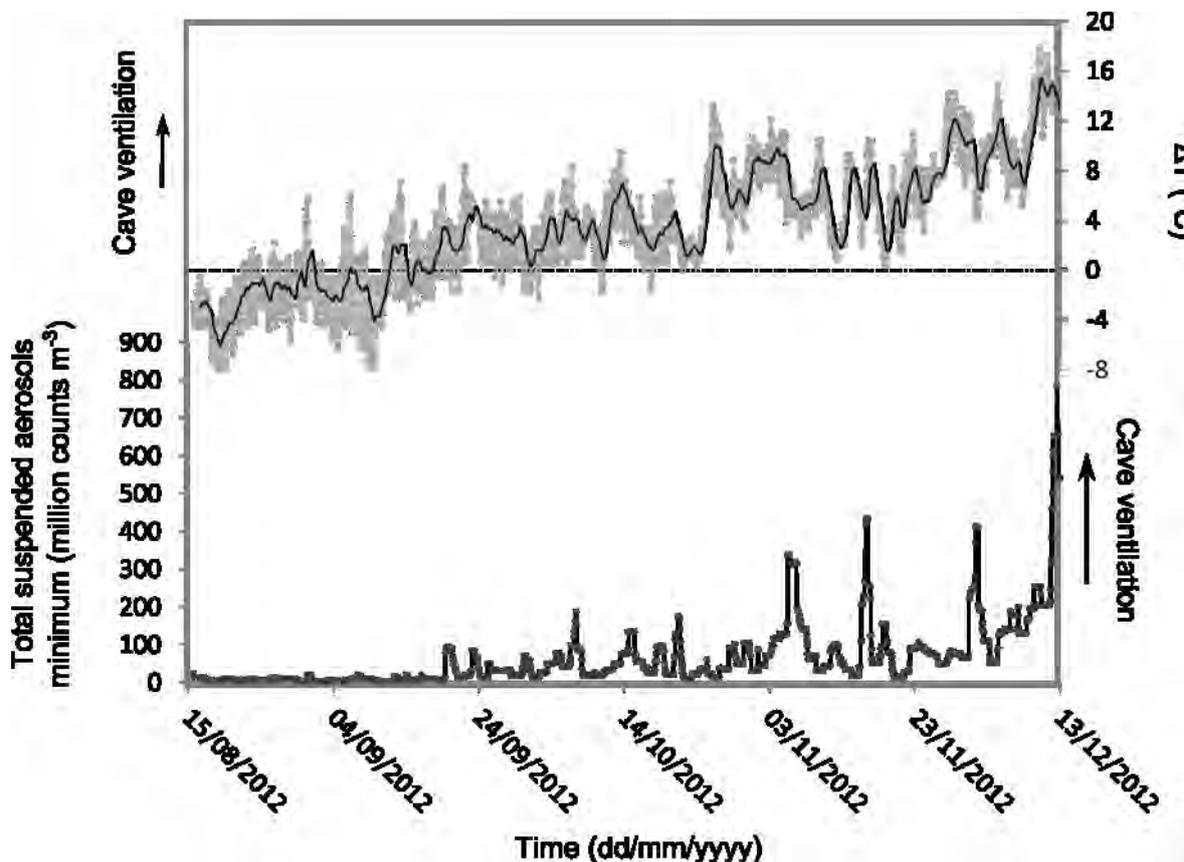


Figure 3.5: Time series of the temperature difference (ΔT) (the internal minus external temperature), with zero value highlighted, based on hourly data (grey) with a 24 hour moving average (black). Suspended aerosol 24 hour minima are displayed based on hourly resolution monitoring (lower panel). Each point represents the lowest hourly value for the preceding 24 hours (referred to as the baseline concentration).

ΔT offers an indication of the changing cave environment relative to the external environment offering a useful comparison to baseline aerosol levels. The long-term increase in the net difference between cave internal and external temperatures demonstrates a relationship to baseline aerosol concentrations. There is a clear distinction between negative and positive ΔT

situations. Highest sustained aerosol concentrations are achieved during periods of positive $\Delta T$, with the baseline aerosol values increasing as $\Delta T$ becomes more positive. $\Delta T$ is a surrogate for ventilation, occurring as a consequence of temperature induced density changes.

### 3.3.3. Anthropogenic and natural process distinctions

In this investigation, visitor footfall levels will be used as an indication of the level of anthropogenic influence occurring on each day. Figure 3.6 shows a comparison of daily recorded cave visitor footfall numbers and cave aerosol baseline levels as represented by daily minimum concentrations. Daily footfall numbers show a broad decrease, which is concurrent with a broad aerosol baseline increase during the progression into the winter season.
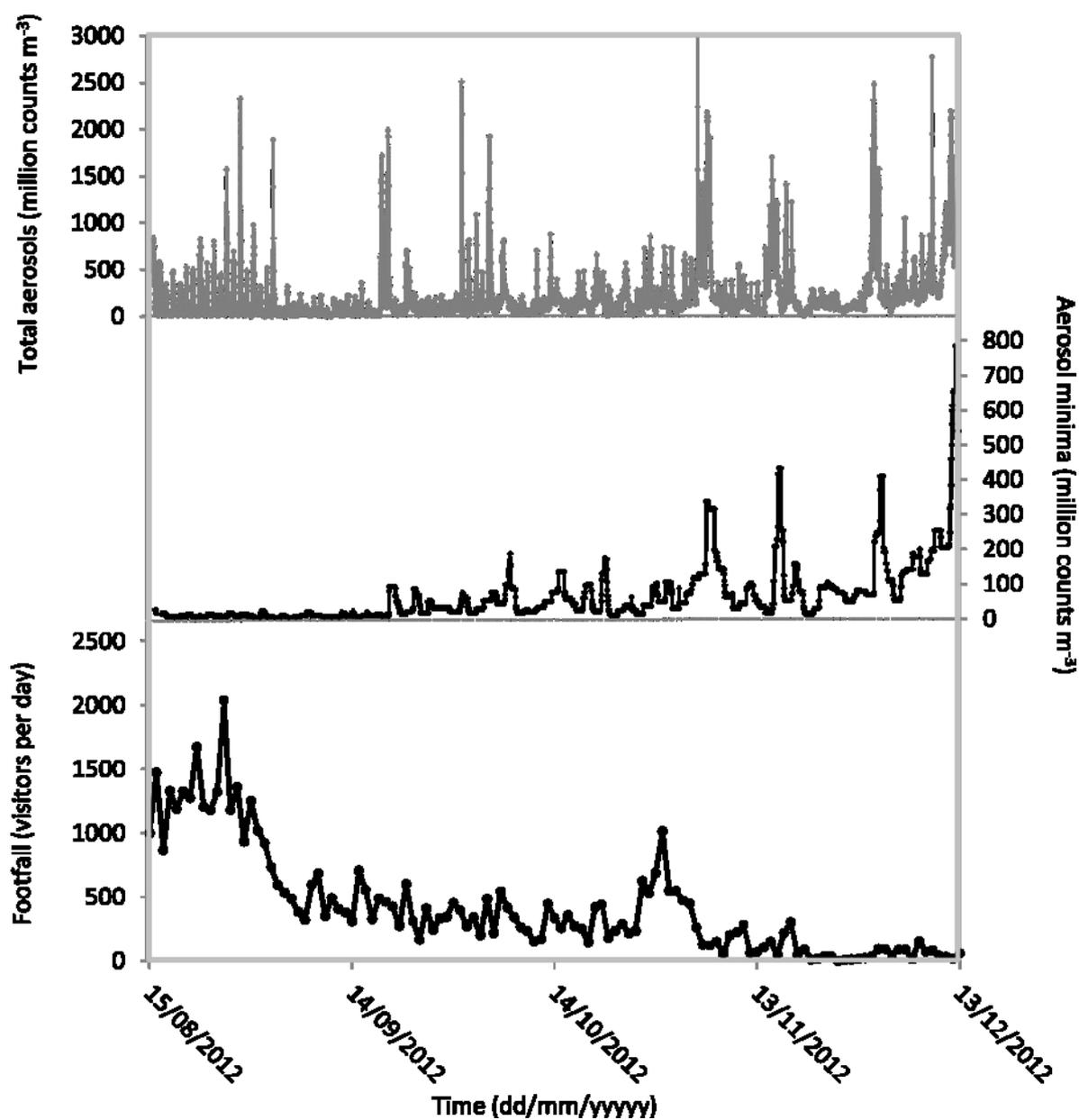
Figure 3.6: Time series of total, daily minimum suspended aerosol levels and daily visitor numbers. Measured total aerosol concentrations are displayed in the upper graph. Daily aerosol minimum values are shown in the centre plot. Daily visitor numbers are presented on the bottom graph.

## 3.4. Discussion

### *3.4.1. Diurnal anthropogenic effects*

Cave air $pCO_2$, temperature and aerosols are sensitive to the disruptions that occur as a consequence of human presence in the cave environment. As outlined in section 3.1, cave aerosol concentrations, $pCO_2$ concentrations and temperature are expected to rise as a result of increasing cave visitor activity. The identified diurnal cycles in the monitoring record have been predominantly assumed to be a result of daily anthropogenic influences.

The daily timings of the diurnal cycle aerosol variability occurring in late summer (presented in Figure 3.4) can be explained by the timing of processes and environmental response sensitivities. The anthropogenic contributions to diurnal cycles will be largely determined by the periods that humans are in the cave. The cave opens at 0900 hrs for maintenance and the first visitors enter around 1000 hrs with last visitors leaving at approximately 1630 hrs and the cave closed by 1700 hrs (however, during the Easter holidays and in July and August last entry is about 1700 hrs with the cave clear by 1730 hrs). The leading phase of the diurnal environmental condition cycle is manifested by an increase in temperature suggesting thermal warming occurring as a result of cave lights being switched on (lights are placed all throughout the cave, including close to the monitor location). The first visitors arrive about an hour after the lights are turned on (apart from the small numbers of maintenance staff) resulting in the later response of aerosols. Cave air $pCO_2$ is the last parameter to rise from background levels, indicating a reduced sensitivity to the anthropogenic disruptions when compared to aerosols.

Recovery of the monitored parameters following the daytime anthropogenic input occurs by ventilation (air-exchange with the exterior) and, only in the case of aerosols, deposition within the cave. Recovery of cave air $p\mathrm{CO_2}$ values is likely attenuated due to natural $\mathrm{CO_2}$ production which continues after the anthropogenic input has stopped in the cave, resulting in the slowest recovery rate out of the monitored conditions. Aerosol recovery occurs in part as a consequence of ventilation. However, ventilation processes also act to maintain aerosols in suspension and limits the minimum levels that aerosols reach diurnally. In the summer months, small aerosols demonstrate a nocturnal return to zero baseline levels during most daily cycles. However, during the winter season the nocturnal aerosol return to zero of small aerosol levels is a rare occurrence. Hence, the higher diurnal-minimum values of aerosols are suggestive of increased winter ventilation rates.

### 3.4.2. Seasonal anthropogenic effects

The decrease in visitor numbers throughout the winter months occurs together with reductions in cave air $p\mathrm{CO_2}$ and temperature reductions. Baseline aerosols provide a representation of natural baseline cave ventilation and indicate increasing ventilation during the progression to winter. Figure 3.6 demonstrates the ability to use baseline aerosol levels to separate natural and anthropogenic influences. This is facilitated by the relatively quick recovery rates of aerosol concentrations after anthropogenic influence. The counter-intuitive medium term relationship between cave aerosols and visitor footfall (Figure 3.6) indicates the reducing influence of anthropogenic effects and the increasing dominance of natural winter cave ventilation on the cave environment over the period studied. This offers the possibility to disaggregate the separate influences of natural ventilation processes and anthropogenic activity upon the cave atmosphere.

### 3.4.3. Seasonal cave environment transition identification

Results from environmental monitoring have identified seasonal environmental modes and demonstrated the strength of aerosol monitoring in recording environmental change on a seasonal timescale. The transition into winter is clearly manifested in cave conditions (Figure 3.3). The decrease in cave temperature and cave air $pCO_2$ suggests increasing cave ventilation and exchange with external air throughout the progression into winter. However, it is not possible to identify seasonal environmental changes in the cave system with a high degree of confidence with these two variables alone.

At $\Delta T = 0$ background levels of aerosols start to increase with this increase continuing into the early winter period (shown in Figure 3.5), indicating increased density driven ventilation. $\Delta T$ switches from positive to negative due to diurnal fluctuation for a period of ~10 days, after which $\Delta T$ stabilises in a positive state. This suggests the development of sustained air movement maintaining greater minimum suspended aerosol loads through increased sustained cave ventilation rates. Aerosol baseline monitoring offers a new environmental indicator of natural cave system seasonality, potentially allowing anthropogenic and natural process to be distinguished when combined with other cave monitoring techniques.

## 3.5. Conclusions

The long-term relationship between $\Delta T$, aerosols and cave air $pCO_2$ indicates $\Delta T$ as the driving influence on cave ventilation processes. Daily aerosol minima provide a unique indicator of natural seasonal ventilation process, little perturbed by anthropogenic influences. This allows for the precise distinction between seasonal cave ventilation modes. The addition of aerosols to an environmental monitoring array improves the investigator's ability to constrain and identify the processes influencing environmental conditions.

Aerosols as a monitoring tool have demonstrated some key advantages over more traditional monitoring tools. Aerosols provide a sensitive ventilation proxy especially with the utilisation of daily minimum values which accurately portray the cave baseline variance. Aerosol recovery rates exceed that of $CO_2$ and temperature allowing for the observation of natural processes beyond diurnal anthropogenic influences.

Cave processes and their operational timescales can be constrained with greater confidence with aerosol monitoring when compared to other monitored metrics. This improved understanding can facilitate the recognition of previously indistinguishable controls. Furthermore the controls on aerosol variability are fewer in comparison to temperature and cave air $pCO_2$, allowing for improved confidence in environmental interpretations and permitting enhanced quantitative understanding of controlling processes such as ventilation.

# Flowstones as palaeoenvironmental archives: A 500 ka flowstone record from New St Michaels Cave, Gibraltar
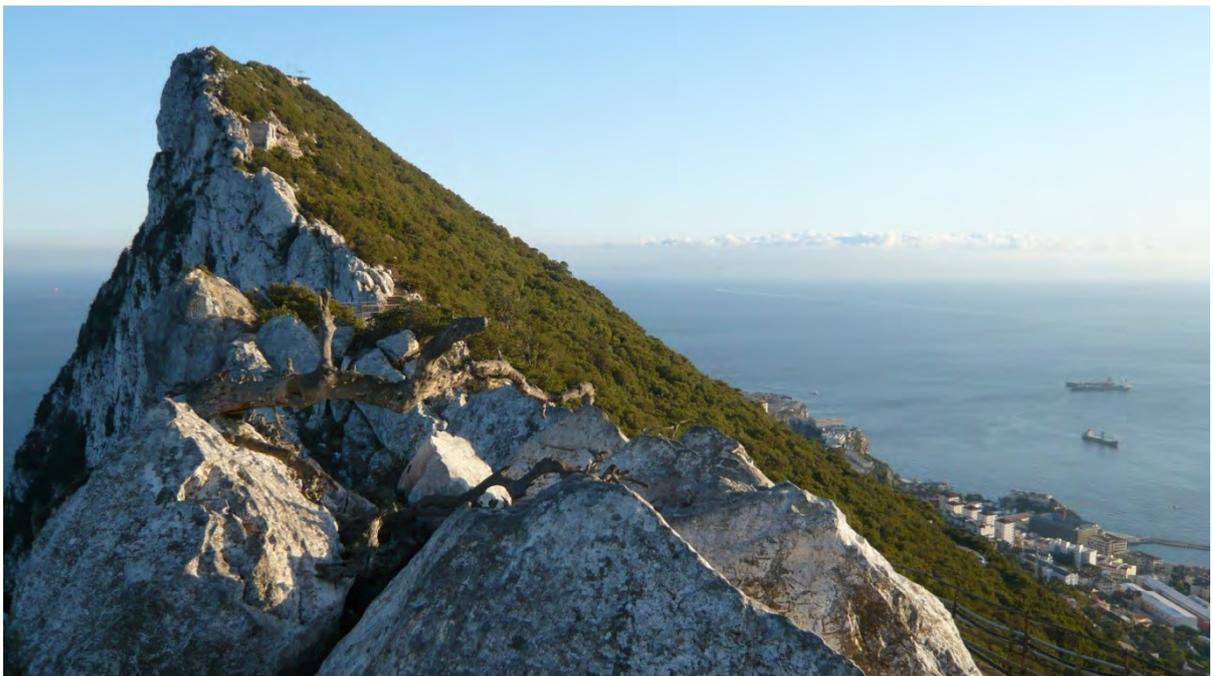


*A view from the ridge of Gibraltar Rock, looking South over the Strait of Gibraltar.*

# Chapter 4. Flowstones as palaeoenvironmental archives: A 500 ka flowstone record from New St Michaels Cave, Gibraltar.

## 4.1. Introduction

This chapter aims to investigate the suitability of flowstones as palaeoenvironmental archives. This will be achieved by careful analysis of drip water chemistry and the flowstone trace element record. Geochemical interpretations will be compared to other palaeoclimate records to determine the extent of environmental influence over local processes.

As outlined in Chapter 1, section 1.3, flowstones are known to demonstrate complex precipitation patterns with punctuated growth. As a consequence of this, they present an opportunity to investigate the changing influence of aerosol contributions. Flowstones are therefore utilised in the following chapters to study the contribution of aerosols to speleothem geochemistry. In this chapter seawater aerosol contributions will be evaluated throughout the growth period of the flowstone and aerosol contributions at hiatus events explored.

This investigation presents results from work undertaken as part of this PhD project combined with past MSci and MSc work. Imaging of the flowstone core, LA-ICP-MS trace element and stable isotope results are taken from previous investigations with all the remaining data being collected as part of this most recent study. All data analysis relating to LA-ICP-MS, drip

water, prior calcite precipitation and precipitation partition coefficients and all relating interpretations are new and do not form part of any previous study.

Speleothems are calcium carbonate cave deposits that take several forms: stalactites growing down from the cave ceiling; stalagmites growing upwards from the cave floor; and flowstones which develop in fan like sheets on the floor or walls of a cave. The study of speleothems for palaeoclimate reconstruction commenced more than three decades ago (e.g. Hendy & Wilson 1968; Thompson *et al*., 1974). Speleothems offer a multiproxy palaeoclimate resource that captures environmental signals at the time of precipitation. They are increasingly recognized as archives of information about past climate, vegetation, hydrology, sea level, nuclide migration, water-rock interaction, landscape evolution tectonics and human action (Richards & Dorale, 2003). A suite of geochemical proxies are utilised in this investigation in order to constrain environmental control dominant throughout the growth period of the flowstone.

### *4.1.1. Location*

Gibraltar offers a unique palaeoclimatic vantage point due to its proximity to the Atlantic Ocean, Mediterranean Sea and Northern African Sahara desert (location shown in Figure 4.1). The North Atlantic Oscillation (NAO) is known to influence the climate of the region (overview in Hurrell et al. (2003)) from the west, and NAO changes through time have been linked to glacial cyclicity and termination events (e.g. Visbeck *et al.,* 2001; McManus *et al*., 2004; Lynch-Stieglitz *et al.,* 2007). Climate at Gibraltar will reflect the proportional influence between Atlantic variability and that of the Mediterranean basin controlled by east (Levante) and westerly winds (Poniente), with the latter being dominant (Rodríguez-Vidal *et al.,* 2013). In addition to east-west interactions Gibraltar climate is also influenced by north-south climate variability controlled by the Bora and Sirocco winds. The Bora is a cold northeasterly wind and the Sirocco blows from the southeast; both are transient phenomena lasting only several days (Orlić *et al.,* 1994).
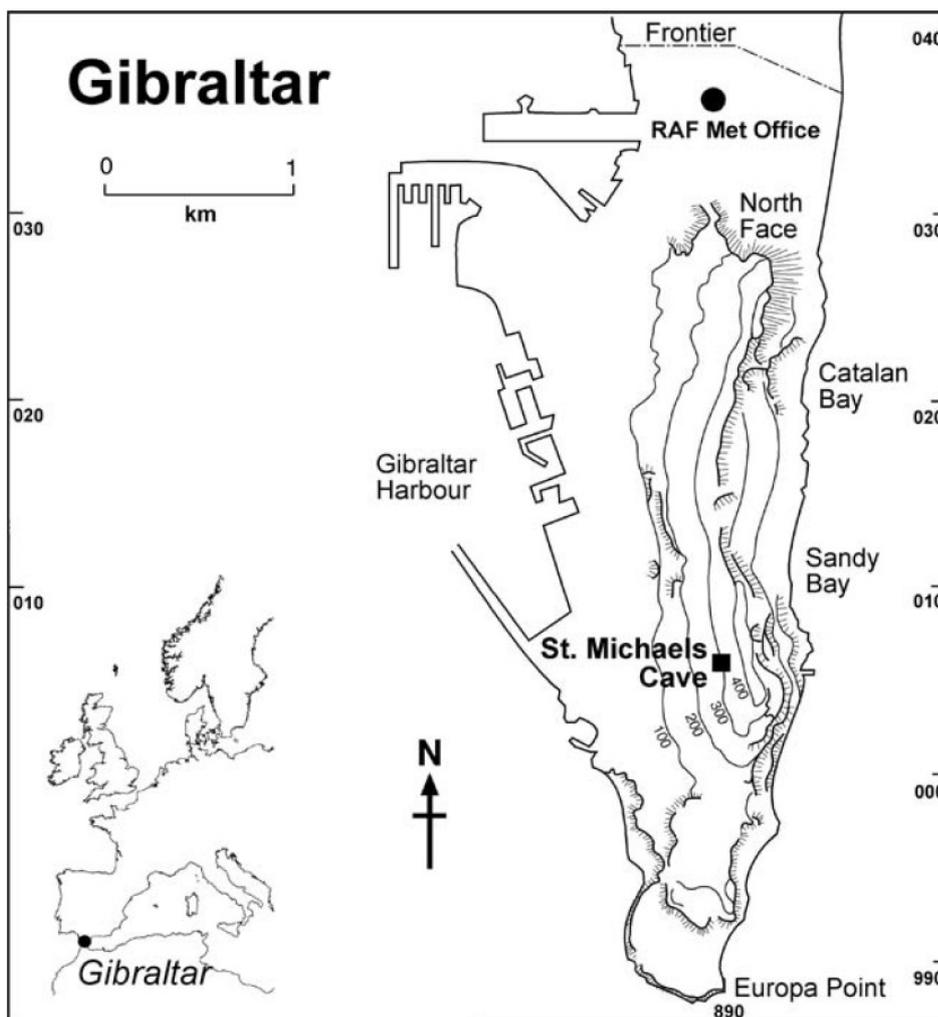
Figure 4.1: Location of Gibraltar, St. Michaels cave and other features described in the text (Mattey et al. (2010) adapted from Mattey et al. (2008)).

The Rock of Gibraltar forms a North–South trending ridge 2.5 km long with a maximum elevation of 423 m. The ridge is asymmetric, having a steep to near-vertical eastern slope against which are banked Pleistocene aeolian dune deposits, and a western slope falling more steadily at 35º towards the town of Gibraltar near sea level (Mattey *et al*., 2010).
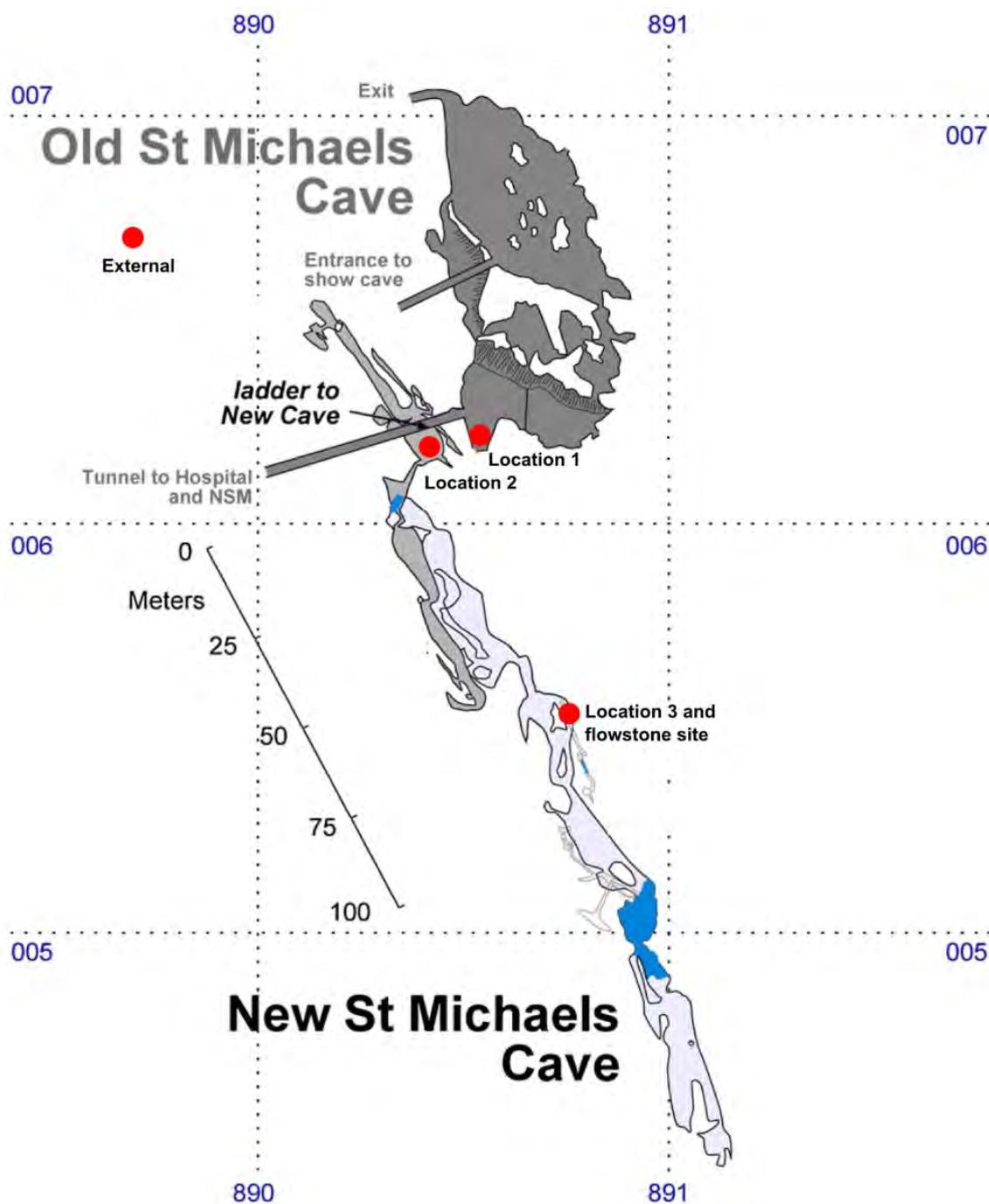
Figure 4.2: Scaled illustration of the St Michaels Cave system. Aerosol and flowstone core sample locations are marked. Positioned relative to 1000 m UTM grid co-ordinates after a new survey carried out in 2007. Plan based on the original cave surveys (see Shaw, 1953a, b; Rose and Rosenbaum, 1991) after Mattey et al. (2008).

### *4.1.2. Flowstones*

This investigation is based on a flowstone core from New St Michaels Cave, Gibraltar. Flowstone deposits are generally larger in surface area in comparison to other cave deposits and form beneath sheet flows of water on cave floors or walls (Fairchild & Baker, 2012). Flowstones offer a substantially large palaeoenvironmental resource, in addition to the more frequently selected stalagmite samples. Further information on speleothem and flowstones are presented in the thesis introduction (Chapter 1).

Stalagmites are more commonly used to generate archives than stalactites because their internal structure is simpler (Fairchild & Baker, 2012); likewise flowstones are utilised less due to the complexity of their stratigraphy. Flowstones often present complex geochemistry, crystallography and stratigraphy, making palaeoenvironmental interpretations difficult and sometimes impossible. Additionally, samples with significant detrital material are usually avoided in speleothem studies because of the need to correct for detrital Th, which results in large age uncertainties (Richards & Dorale, 2003). Flowstones often present increased detrital contents due to higher discharge rates associated with their growth (Fairchild & Baker, 2012), but are still utilised as a palaeoclimate resource since they are abundant in many caves (Meyer *et al*., 2012; Hopley, 2007).

### 4.1.3. Aerosols

Aerosols are generally defined as suspensions of fine solid or liquid particles within a gaseous medium (Hinds, 1999). Atmospheric aerosols are sourced from a range of environmental processes, but sea spray and terrestrial particulates are the main aerosol sources under investigation in this study. Atmospheric aerosols require entrainment and transport and hence their deposition records can provide a proxy record for source atmospheric circulation processes. Aerosols can become incorporated into speleothems either by direct deposition to the forming speleothem surface or through incorporation in the drip water and resultant precipitate.

Aerosol transport to Gibraltar occurs as a consequence of atmospheric circulation that is stable over relatively long time periods, or as a consequence of short term aerosol transportation phenomena, such as Sirocco events which were outlined in the introduction. Climate change and aerosol source location changes cause variations in the intensity and frequency of aerosol transportation events and can be recorded in the speleothem record. Source locations can be identified through geochemical comparisons of signature chemical components of potential source regions and the speleothem sample (e.g. Goede *et al.,* 1998; Frumkin & Stein 2004).

### *4.1.4. Geochemical environmental proxies*

Chapter 1, Table 4.1 presents a summary of each environmental proxy used in this investigation, the processes that they represent, examples of studies which present their use, and the limitations/conditions for each.

*Stable Isotopes*

Oxygen isotope signatures in speleothems are controlled both by temperature and water oxygen isotope composition. The fractionation of water oxygen isotopes through evaporation and condensation processes offers an insight into an array of environmental and climatic conditions. Reviews of stable isotope processes and utilisation for palaeoenvironmental studies can be found in McDermott et al. (2004, 2005), Lachniet (2009) and Fairchild & Baker (2012).

Isotope-controlling processes vary significantly between cave locations and different formations, as well as continuously altering through time. It is therefore important to use a range of different environmental proxies for increased confidence in interpretation.

*Trace elements*

Trace elements have been utilised in a range of speleothem studies for determination of environmental processes (e.g. Verheyden *et al*., 2000; Huang *et al.,* 2001; Mattey *et al.,* 2010; Spötl et al., 2005). A comprehensive review of trace elements in speleothems as recorders of environmental changes can be found in Fairchild & Treble (2009) who identify several different types of controlling processes (e.g. element sources, transport in karst water, and geochemical evolution of waters by prior calcite precipitation). Although the behaviour of

numerous different trace elements can be studied, Borsato et al. (2007) showed that they form groups with coherent responses. Hence, in this study appropriate statistical techniques will be used to establish the main modes of trace element variation. Further details on specific processes for these elements will be provided throughout the discussion.

*Strontium isotopes*

In some cases it may be possible to identify the source of atmospheric aerosols based on chemical signatures; and strontium isotopes are particularly useful for this purpose (Goede *et al*. 1998; Ayalon *et al*., 1999; Frumkin & Stein, 2004; Li *et al*., 2005; Zhou *et al*., 2009.). Generally systems involve mixing between a radiogenic aerosol source such as sea spray or atmospheric dust and less radiogenic carbonate bedrock.

Previous studies have reconstructed dust fluxes to speleothems and identified varying dust sources through Sr isotope analysis. A summary plot of Sr isotope results from the literature is presented in Figure 4.3, demonstrating the general mixing between radiogenic dust, and seawater, and the bedrock. Here Sr isotope signatures are utilised as chemical marker for the input of terrestrial dust to speleothem, both through deposition to the upper soil and direct to the flowstone surface.
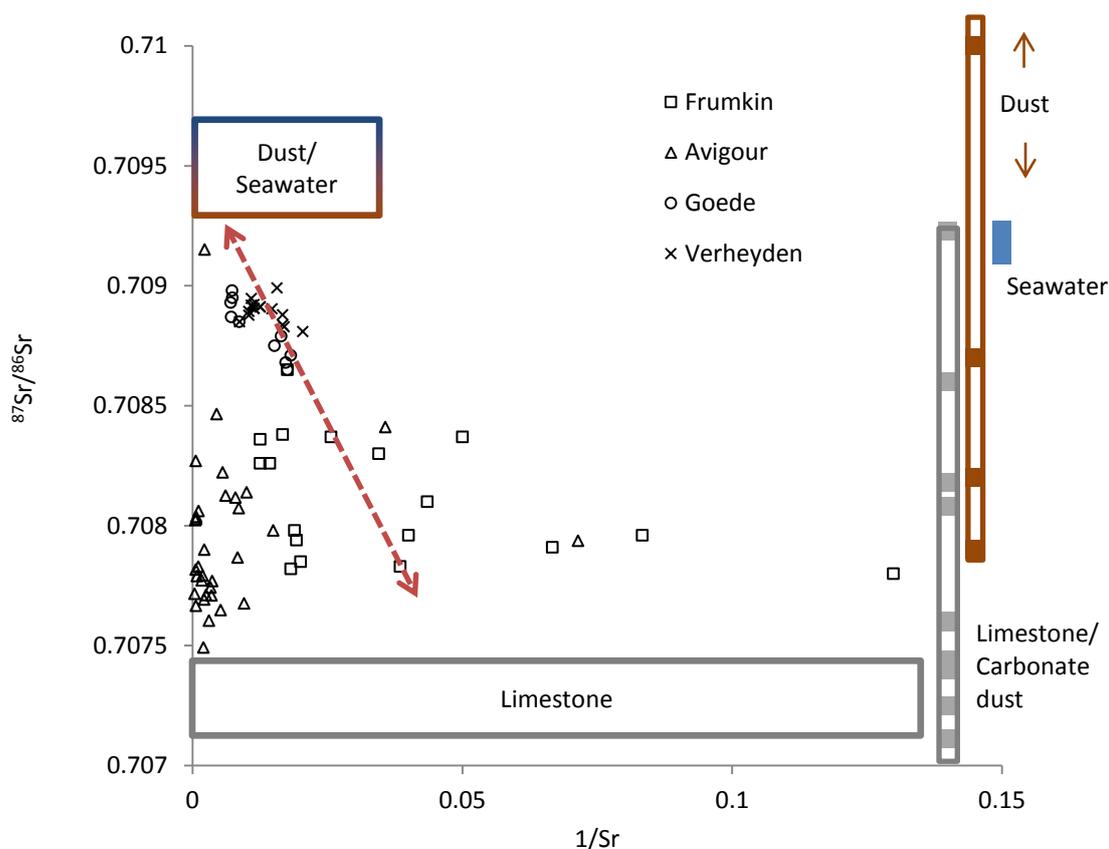
Figure 4.3: Sr isotope against 1/Sr compilation for speleothem studies. Limestone, terrigenous dust and seawater $^{87}$Sr/$^{86}$Sr literature end member values are presented to the right of the diagram (Limestone/carbonate dust in grey, other dust sources in brown, seawater in blue). Speleothem data presented are sourced from: Negev Desert South Israel (Avigour *et al*., 1990); Stalagmite from Frankcombe cave, Tasmania, Australia (Goede *et al*., 1998); Pére Noël Cave, Belgium (Verheyden *et al*., 2000); Jerusalem West Cave, Israel (Frumkin & Stein, 2004) and Maboroshi cave, Hiroshima Prefecture, South West Japan (Hori *et al*., 2013).

Bedrock values for both $^{87}$Sr/$^{86}$Sr and 1/Sr are highly variable between and within studies. The Sr isotope signature of atmospheric dust is highly variable and dependent on geological source, with silicate dust being more radiogenic and carbonate dust being closer or equal to regional limestone values. By contrast, seawater provides a well-constrained end member source due to the well-mixed nature of the oceans.

## 4.2. Methods

Further details of each analytical method can be found in the supplementary material S.1.-S.14.

### *4.2.1. Speleothem sampling and preparation*

The flowstone site was selected as it displays an active drip and modern speleothem growth. The flowstone site was monitored for drip water discharge rates and chemistry (17/06/2008-25/02/2012). The flowstone core was sampled in 2008 to the maximum depth of the drill bit ~30 cm.

### *4.2.2. Flowstone sampling, sectioning and handling*

A section of 1 mm thickness was produced to facilitate the precise mapping of high resolution geochemical analyses to the calcite fabric. It was cut longitudinally from the centre of the core sample in the thin section lab. This section was doubly polished and fixed to glass slides using Crystalbond® mounting adhesive. Initially the polished thick section was mounted in three sections separated by natural core breakages; later in the study the three sections were further separated and mounted on smaller glass plates to meet the spatial requirements of the laser ablation (LA) cell. All high-resolution stable isotope and trace element analyses were carried out on the thick section. The remaining core halves were polished to make a flat surface for recording the sample stratigraphy, microdrilling and sampling for U-series dating and Sr isotope analysis.

Hand drilling using a micro drill with a 1 mm diameter drill bit was used to produce powders for Sr isotope analysis by MC-ICP-MS. Hand drilling was also used for stable isotope sampling at 2 mm resolution.

Automated drilling is superior to hand drilling in terms of control and therefore spatial resolution and was used for U-series sample collection. The flowstone sample was polished flat and mounted in resin in order to attach to the XYZ stage (stage shown in section S.13 and illustrated in Figure S.11).

All surfaces and tools were cleaned with ethanol, removing all powder to ensure no sample cross-contamination.

### *4.2.3. U/Th dating*

Radiometric disequilibrium dating was conducted at the University of Melbourne, Australia. Samples were dissolved and chemically separated to elute non-analyte elements. Isotopic analysis (of $^{229}$Th, $^{230}$Th, $^{232}$Th, $^{233}$U, $^{234}$U, $^{235}$U, $^{236}$U) was performed using a Nu Plasma multi-collector inductively coupled mass spectrometer (MC-ICP-MS) with sample introduction by desolvating nebuliser. Internal reference material (Yarrangobilly flowstone stock, YB-1) was used as a data check and external reference material (Harwell Uraninite, HU-1) was used in calibration. Full details of the analytical procedure can be found in Hellstrom (2003, 2006). Details of chemical separation and sampling can be found in supplementary material section S.11.

### *4.2.4. Strontium isotope analysis*

Four to eight mg of the powdered samples were dissolved in $HNO_3$. An aliquot for trace element ICP-MS analysis was removed at this point. Sr separation and extraction was carried out using Eichrom Sr specific resin in plastic columns. The resin was cleaned and equilibrated before the addition of the samples. Matrix elements were first eluted, and then Sr was collected for analysis. Samples were dried for storage and re-dissolved prior to analysis by Nu Plasma MC-ICP-MS at Melbourne University Earth Sciences. SRM987 and EN1 reference materials were used to establish accuracy and for standardisation (method used in; Maas *et al*., 2005). Further details in supplementary material section S.9.

### *4.2.5. Stable Isotopes*

Microdrilling was chosen for the sample acquisition due to the size of the flowstone core and the length required to be covered in a fairly restricted time period, although micromill

technology would have improved resolution. A study by Spötl & Mattey (2006) demonstrated that both low-resolution microdrill and high-resolution micromill show good correspondence to salient features. Therefore low resolution sampling will be sufficient to identify long term millennial scale features preserved in the geochemical record.

Samples for stable isotopic analysis were obtained using a mounted microdrill at 2 mm intervals for the complete 30 cm length of the core producing 150 samples, each $300\pm50$ μg. The Multiflow system flushed each vial with He for 4 minutes, and then 105% orthophosphoric acid was dispensed for eight minutes into vials heated at 90°C, for sample dissolution. The batch was left to react and equilibrate for 60 minutes. The samples were run in the Royal Holloway stable isotopes laboratory on the GV industries Multiflow-Isoprime IR-MS. Sample batches were performed with 15 samples, Royal Holloway internal carbonate, LSVEC Lithium carbonate and NBS-19 reference materials.

### 4.2.6. Solution trace element analysis

Solution trace element analysis was performed on 20 samples which were also used for Sr isotope analysis. The aliquots for trace element analysis were spiked with an internal standard (containing Rb, Re, Li, Sr, U) and diluted 3000-4000 times with 2% $HNO_3$ as in Eggins et al. (1997) and Zhou (2008). Analysis was carried out using an Agilent Technologies 7700 series Quadrupole Inductively Coupled Mass Spectrometer (Q-ICP-MS) in the University of Melbourne Earth Sciences department. Further details in supplementary material S.10.

### *4.2.7. Laser-ablation trace element analysis*

Laser ablation was chosen as a trace element analytical technique to provide a high-resolution continuous analysis of the flowstone in a relatively short period of time. The custom-built excimer laser-ablation system was used in order to obtain reduced washout times (<1.5s for 99%) and increased sensitivity in comparison to more traditional systems (Müller *et al.,* 2008). Trace element analysis performed using an Agilent 7500 Ce series ICP-MS Octople Reaction System connected to the custom designed ArF excimer (193nm) laser-ablation system (RESOlution M-50, Resonetics LLC, USA) coupled to a two-volume laser-ablation cell (Laurin Technic, Australia) (Müller *et al.*, 2009) in the Earth Sciences Department at Royal Holloway University of London. Ablation was achieved with a 15×311 μm aperture size for the 193 nm laser at a rate of 15 Hz moving across the samples surface at 1mm/minute. The rectangular slit has the benefit of increasing the representative nature of each sample by sampling more calcite for each growth period. Each mounted sample was cleaned with methanol and placed in the sample holder. The cell was then flushed eight times with cell evacuation and helium backfilling cycles to remove all traces of oxygen. Fifteen elements with the isotopes measures as follows were chosen for analysis: $^{31}$P, $^{25}$Mg, $^{88}$Sr, $^{23}$Na, $^{27}$Al, $^{43}$Ca, $^{55}$Mn, $^{57}$Fe, $^{79}$Br, $^{89}$Y, $^{138}$Ba, $^{140}$Ce, $^{208}$Pb, $^{232}$Th and $^{238}$U. Elements were chosen in an attempt to best identify speleothem palaeoenvironmental processes (as summarised in Fairchild & Treble, 2009 and Chapter 1, Table 1.1.). Concentrations were calculated from calibration using the NIST612 reference material. Data calibration and further LA-ICP-MS methods are presented in the supplementary material, section S.15.

### 4.2.8. Suspended aerosols

*Aerosol sampling*

Sampling locations are displayed in Figure 4.2 with 3 internal locations and 1 external location on the north side of Gibraltar rock ~1km from the cave entrance. Filters were placed in the cleaned in-line filter holders connected to air pumps in order to sample suspended aerosol loads (sampling was utilised for personal exposure studies in Harrison et al. (2009), further details and a sampler layout illustration can be found in the supplementary material section S.1). Filter choice was determined by species interest (inorganic or organic). Pumps were calibrated to 3 L min$^{-1}$ and this was verified in the field before the sampling period initiated to ensure that a quantitative calculation of suspended aerosol concentrations could be obtained. A dual pump and filter setup was utilised in order to obtain inorganic and organic samples simultaneously as shown in Figure S.2.

*Inorganic aerosol extraction and analysis*

Glass petri dishes and filters were placed in a 5% $HNO_3$ acid bath for a minimum of 24 hours. The Petri dishes were then triple-rinsed with double de-ionised water (DDIW). PTFE filters were subsequently placed in a DDIW water bath for 24 hours and rinsed again in clean DDIW. Upon completion the cleaned filters were placed in the cleaned Petri dishes and sealed. After the 24 hour collection period, used filters were placed in clean Petri dishes and sealed for transport. All extraction was carried out in high density polypropylene vials with tightly fitting screw caps to avoid losses of volatile species during any heating steps. Filters were cut in half, in order to allow for separate extraction procedures for multiple analytical techniques. A modification of the Harper et al. (1983) technique, using $HNO_3$ extraction method was utilised in order to best replicate that of speleothem analytical techniques.

Submerged samples were shaken for 1 hour and then subjected to a combination of heat (80°C and ultrasonication) for 2 hours. Sample eluents were analysed by Perkin Elmer Optima 3300RL ICP-AES at the Earth Sciences department, Royal Holloway University of London. Chemical concentration data have been converted from mg kg$^{-1}$ in solution to suspended mass concentration ($\mu$g m$^{-3}$) as outlined in the supplementary material section S.3.

*PAH aerosol extraction and analysis*

For PAH collection glass petri dishes and quartz filters were heated at >450°C for a minimum of 5 hours (as of: Leister & Baker, 1994; Odabasi *et al* 1999; Vardar *et al*., 2002; Bozlaker *et al.*, 2008) to ash any potential organic contamination. Data have converted from solution concentrations to pg m$^{-3}$. Filters were placed in cleaned petri dishes and sealed, as with inorganic aerosol methods, for transport. PAHs were removed from the filters using a solvent extraction method and subsequently analysed with GC-MS at the Environmental Health Sciences laboratories, University of Birmingham. Field and laboratory blank analysis was carried out for each batch of GCMS analysis. Further details of PAH extraction methods and GC-MS analysis are presented in the supplementary material sections S.4 and S.5 respectively.

## 4.3. Results

### 4.3.1. Flowstone fabric

| Name | Calcite colour, fabric and habit | Image |
|---|---|---|
| 1) Cave calcareous tufa forms | Light yellow in hand specimen. Porous, macrocrystalline. No morphological orientation of calcite crystals. Some weak and discontinuous layering. |  |
| 2) Micritic-crystalline Fabric | White opaque layering occurs with varying thickness and form. Evidence for dissolution and subsequent precipitation (Shown right). |  1m |
| 3) Columnar Fabric | Relatively homogeneous crystal habit over several layers. Crystallites of each composite crystal have the same morphological orientation. Large calcite crystal habit with elongate columnar crystals. White in younger growth gradational change to light brown |  1m |
| 4) Columnar Fabric/ Elongate or Fibrous Fabric. | Dark and Light brown. Calcite growth normal to layering. Layered with some coupled light and dark layers. Macropores present in sections with larger calcite habit. |  1m |
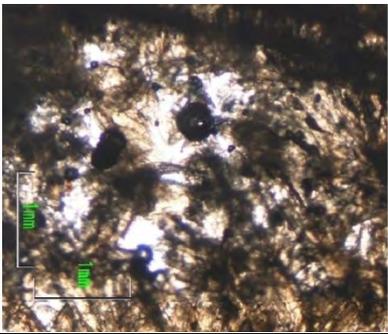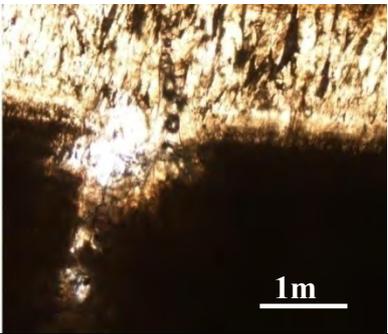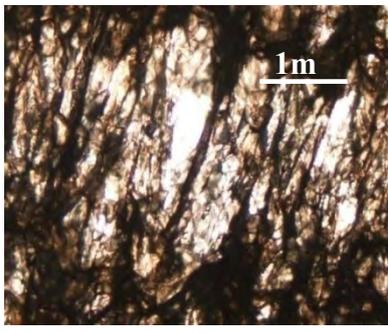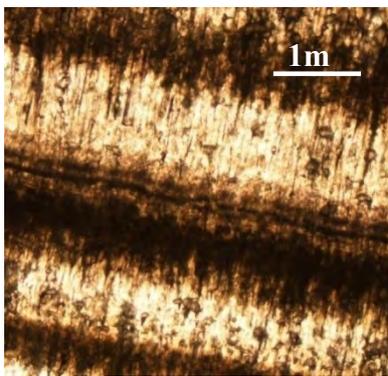
Table 4.1: Calcite fabrics from the Gib08a flowstone core, based on the categorisation established by Frisia et al. (2010). Examples of each main type of growth are displayed and properties outlined in thin section with transmitted light. Microscope images from Dredge (2009) MSci project.
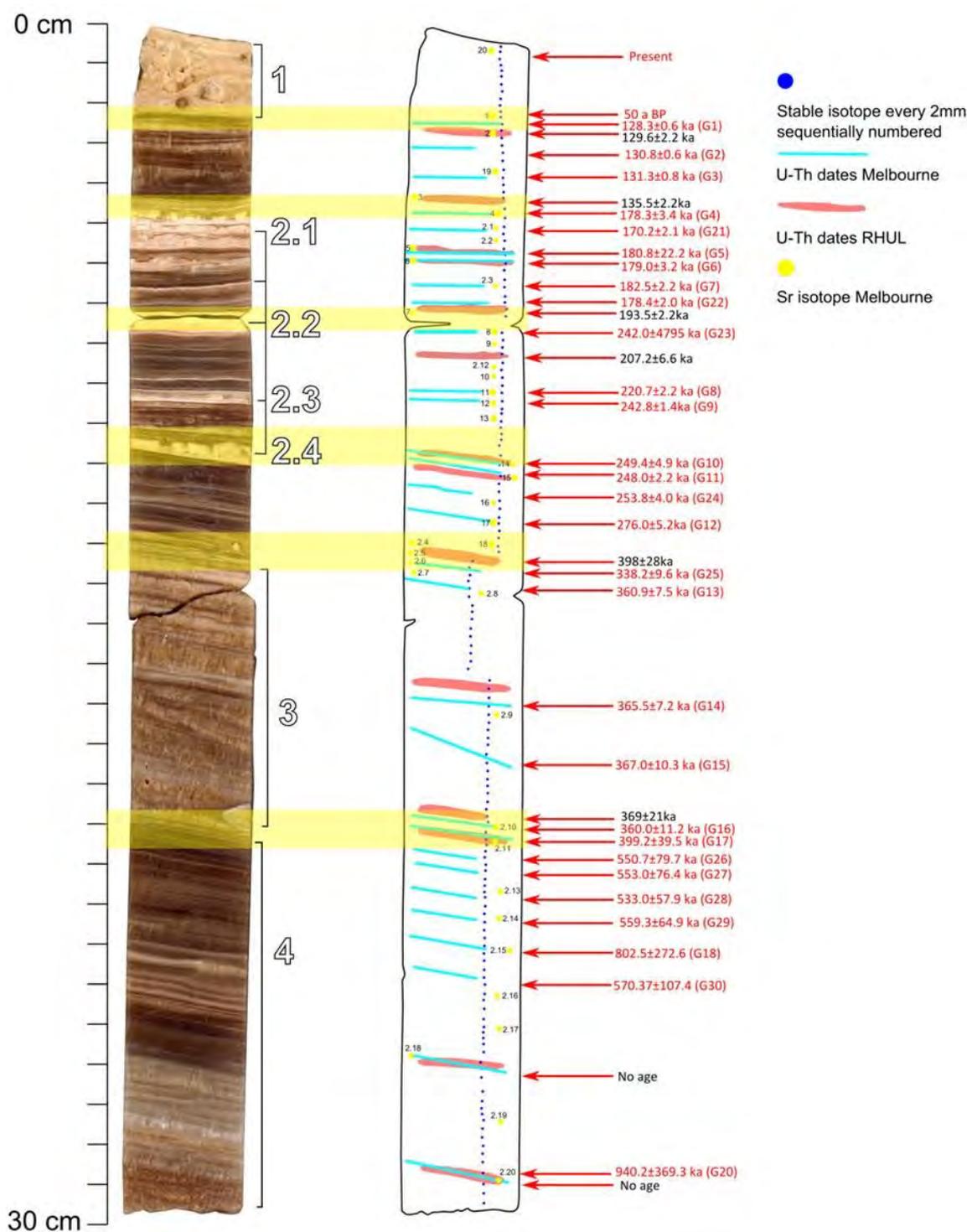
Figure 4.4: Scanned core image of the Gib08a flowstone core (Dredge (2010) MSc images). Sampling locations for stable isotopes (undertaken as part of MSci project) Sr isotope, stable isotope and U/Th geochronology (both carried out at the University of Melbourne as part of this PhD study) are presented. Distance scale presented from 0 = modern growth to 30 cm = oldest growth. Sections marked 1-4 indicate calcite types displayed in Table 4.1. Potential hiatus events are highlighted in yellow.

The flowstone core presents several stages of growth punctuated by hiatuses. Microscopic images of example flowstone fabrics are presented in Table 4.1, and their occurrence in the core displayed in Figure 4.4. The oldest flowstone growth presents layered columnar calcite (4) and is the largest stable section of growth in the core. Changes in colour are observable but the fabric remains relatively constant throughout the section. After a hiatus event the core fabric alters to present larger crystal columnar calcite (3) fabric. Section 3 presents layering which is variable in orientation and thickness. This section transitions into more compact calcite punctuated by micritic calcite (2) events which, in some cases, mark hiatus events. There is no observable trend in the occurrence of micritic calcite events and each event presents different thickness and formation. Sections 2.1 and 2.3 present thin layering within micritic sections, whilst sections 2.2 and 2.4 are composed of homogenous micritic calcite without growth features. The most prominent feature in the flowstone calcite is the contrast between historic and modern growth, marked by a clear hiatus in growth. Modern calcite growth (1) is highly porous and likely represents exceptionally fast growth rates. Some features suggesting layering are observable, but they are not continuous throughout the section. The relationship between calcite fabric types and chemistry will be explored throughout the discussion (section 4.4).

## *4.3.2. Geochronology*

| Sample | Depth (mm) | 238U (ppb) | 2SE | 230/238A | 95% error | 234/238A | 95% Err | 232/238A | 2SE | 230/232A | Age | 95%err | Age cr | 2SE |
|---|---|---|---|---|---|---|---|---|---|---|---|---|---|---|
| G1 | 21 | 183 | 13.70 | 0.86 | 0.00123 | 1.204 | 0.0022 | 0.0038 | 0.000789 | 225 | 129 | 0.53 | 128 | 0.64 |
| G2 | 27 | 204 | 15.27 | 0.82 | 0.00145 | 1.147 | 0.0014 | 0.0033 | 0.000013 | 251 | 131 | 0.49 | 131 | 0.56 |
| G3 | 35 | 223 | 16.75 | 0.84 | 0.00247 | 1.169 | 0.0015 | 0.0043 | 0.000131 | 197 | 132 | 0.74 | 131 | 0.85 |
| G4 | 44 | 166 | 12.45 | 0.96 | 0.00373 | 1.132 | 0.0027 | 0.0448 | 0.000380 | **21** | 188 | 2.06 | 178 | 3.38 |
| G21 | 47 | 278 | 20.83 | 0.96 | 0.00389 | 1.171 | 0.0030 | 0.0095 | 0.000031 | 101 | 172 | 1.79 | 170 | 2.07 |
| G5 | 54 | 182 | 13.67 | 1.11 | 0.01571 | 1.191 | 0.0024 | 0.2279 | 0.000963 | **5** | 240 | 11.07 | 181 | 22.23 |
| G6\ | 56 | 235 | 17.64 | 1.00 | 0.00193 | 1.169 | 0.0016 | 0.0566 | 0.000264 | 18 | 191 | 1.09 | 179 | 3.19 |
| G7 | 62 | 257 | 19.26 | 0.99 | 0.00313 | 1.175 | 0.0020 | 0.0212 | 0.000139 | 47 | 186 | 1.56 | 183 | 2.00 |
| G22 | 66 | 245 | 18.35 | 0.96 | 0.00317 | 1.151 | 0.0027 | 0.0115 | 0.000034 | 83 | 180 | 1.67 | 178 | 1.98 |
| G23 | 74 | 176 | 13.20 | 1.25 | 0.01106 | 1.179 | 0.0027 | 0.4334 | 0.002019 | **3** | 628 | 185.17 | 242 | 4785.33 |
| G8 | 89 | 280 | 21.03 | 1.05 | 0.00208 | 1.164 | 0.0025 | 0.0038 | 0.000015 | 273 | 221 | 1.94 | 221 | 2.20 |
| G9 | 92 | 250 | 18.78 | 1.04 | 0.00115 | 1.128 | 0.0011 | 0.0004 | 0.000001 | 2833 | 242 | 1.22 | 243 | 1.36 |
| G10 | 106 | 222 | 16.67 | 1.02 | 0.00409 | 1.106 | 0.0028 | 0.0184 | 0.000069 | 56 | 253 | 4.24 | 249 | 4.90 |
| G11 | 109 | 217 | 16.26 | 1.04 | 0.00216 | 1.123 | 0.0012 | 0.0063 | 0.000083 | 165 | 248 | 1.96 | 248 | 2.25 |
| G24 | 115 | 199 | 14.93 | 1.18 | 0.00399 | 1.235 | 0.0031 | 0.0028 | 0.000012 | 415 | 253 | 3.59 | 254 | 4.05 |
| G12 | 122 | 234 | 17.56 | 1.12 | 0.00291 | 1.153 | 0.0017 | 0.0006 | 0.000073 | 2019 | 288 | 3.64 | 289 | 4.04 |
| G25 | 135 | 414 | 31.06 | 1.11 | 0.00393 | 1.125 | 0.0028 | 0.0008 | 0.000002 | 1481 | 337 | 8.66 | 338 | 9.60 |
| G13 | 139 | 379 | 28.44 | 1.11 | 0.00231 | 1.114 | 0.0019 | 0.0006 | 0.000002 | 1721 | 360 | 6.82 | 361 | 7.52 |
| G14 | 167 | 377 | 28.27 | 1.12 | 0.00230 | 1.121 | 0.0016 | 0.0026 | 0.000010 | 438 | 365 | 6.50 | 365 | 7.24 |
| G15 | 179 | 409 | 30.66 | 1.12 | 0.00394 | 1.119 | 0.0015 | 0.0025 | 0.000014 | 451 | 366 | 9.49 | 367 | 10.30 |
| G16 | 198 | 154 | 11.53 | 1.10 | 0.00446 | 1.109 | 0.0015 | 0.0042 | 0.000095 | 262 | 359 | 10.22 | 360 | 11.23 |
| G17 | 200 | 84 | 6.29 | 1.16 | 0.01182 | 1.137 | 0.0024 | 0.0343 | 0.000389 | 34 | 403 | 36.01 | 399 | 39.51 |
| G26 | 207 | 255 | 19.13 | 1.08 | 0.00369 | 1.061 | 0.0027 | 0.0004 | 0.000002 | 2971 | 543 | 58.19 | 551 | 79.71 |
| G27 | 210 | 242 | 18.18 | 1.07 | 0.00370 | 1.057 | 0.0024 | 0.0003 | 0.000001 | 3812 | 546 | 57.98 | 553 | 76.40 |
| G28 | 217 | 261 | 19.57 | 1.06 | 0.00310 | 1.050 | 0.0025 | 0.0012 | 0.000004 | 854 | 527 | 46.95 | 533 | 57.89 |
| G29 | 223 | 385 | 28.86 | 1.09 | 0.00321 | 1.068 | 0.0022 | 0.0001 | 0.000000 | 10193 | 554 | 53.10 | 559 | 64.92 |
| G18 | 230 | 83 | 6.22 | 1.05 | 0.00268 | 1.033 | 0.0015 | 0.0013 | 0.000009 | 821 | 1013 | 2341.71 | 803 | 272.55 |
| G30 | 238 | 269 | 20.18 | 1.06 | 0.00412 | 1.049 | 0.0025 | 0.0055 | 0.000019 | 193 | 561 | 74.19 | 570 | 107.37 |
| G20 | 287 | 88 | 6.57 | 1.04 | 0.00329 | 1.024 | 0.0028 | 0.0007 | 0.000004 | 1553 | 0 | 0.00 | 940 | 369.30 |

Table 4.2: U-series isotopic results and ages for flowstone Gib08a from Lower New St Michael's Cave, Gibraltar. $^{238}$U is reported in ng/g. Sample ages and corrected ages (age cr) are reported in ka BP. 230/238A, 234/238A, 232/238A and 230/232A (low ratios indicative of detrital Th contamination are highlighted in bold) refer to the activity ratios. 95% err = 95% confidence interval error. 2SE = 2 standard errors. Age = raw age. Age cr = corrected age for detrital Th contamination.
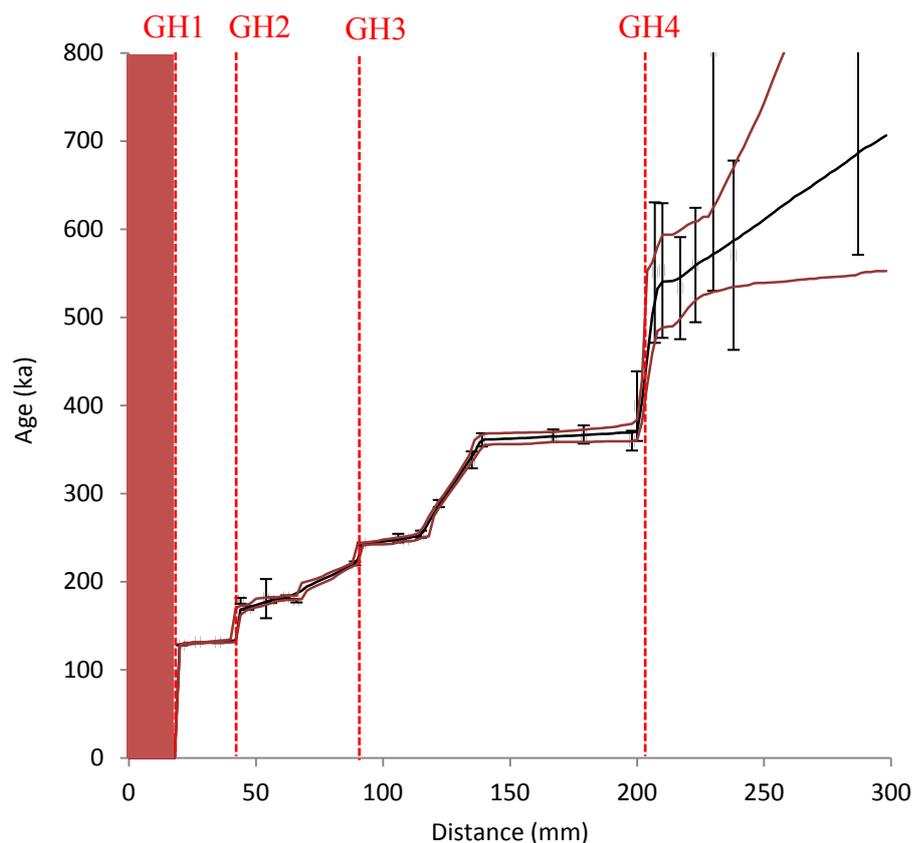
Figure 4.5: The Gibraltar flowstone (Gib08a) core U/Th geochronology age model. Distance (mm) from modern growth shown against U/Th ages in calendar years before present. Age errors (2se) and spatial resolution are presented with error bars for each sample. This age model was produced using the StalAge algorithm produced by Scholz & Hoffmann (2011) in R. Corrected ages, age errors and distances were input from the U-series analysis results presented in Table 4.2. Potential growth hiatuses are marked with red lines; timings of hiatuses are listed in distance (mm)/age (ka): GH1 = 19/0.005-128; GH2 = 35-44/131-178; GH3 = 86-96/218-246-; GH4 = 198-207/360-551. The section of modern growth occurring in the last 50 years is highlighted by the red shading.

The U/Th geochronology of the Gib08a flowstone presents variable growth rates throughout the period of formation. Four notable sections of fast growth are visible within the chronologically well-constrained period of growth. In addition to periods of fast growth, the flowstone demonstrates several punctuations in growth, with 4 highlighted on the age model. Large errors are observed beyond 400 ka and hence this limits the extent of the temporal analysis for palaeoclimatic comparisons. The relationship between growth rate and

palaeoclimate is explored throughout the discussion as shown in Figure 4.18 and fully explored with Figure 4.22.

### *4.3.3. Drip water chemistry*

Modern drip water 1000Sr/Ca and 1000Mg/Ca present a positive relationship. The bedrock 1000Mg/Ca and 1000Sr/Ca reveal a low-Mg limestone group and a dolomite group with similar Sr/Ca ranges and one outlying high Sr value in limestone. The minimum drip water values are close to that of the mean dolomite composition.
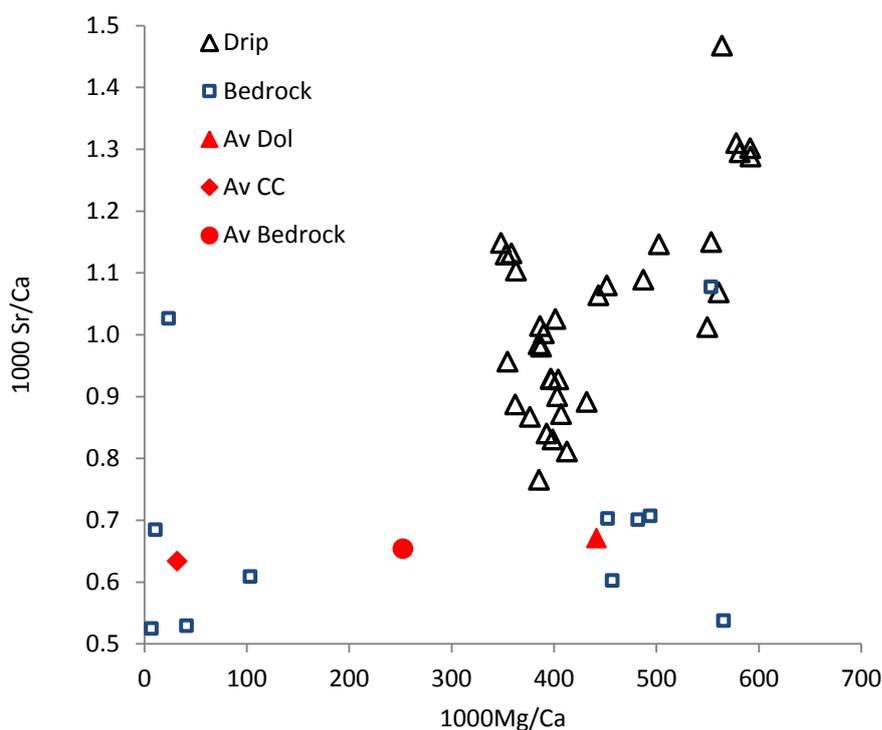


Figure 4.6: 1000Sr/Ca and 1000 Mg/Ca for Gibraltar drip waters and limestone. Legend abbreviations: Drip – Gib08a site drip water chemistry samples; Bedrock – Gibraltar rock analysis samples; Av Dol – Average chemistry for Dolomite bedrock samples; Av CC – Average chemistry for Carbonate bedrock samples; Av Bedrock – Overall average bedrock chemistry. Drip water trace element data are of monthly water samples from between June 2008 and March 2012. Bedrock trace elements are of a range of Gibraltar limestone and dolomite samples (analysis by Bowkett, 2012).

### *4.3.4. Suspended aerosols*

Results are presented from suspended aerosol monitoring, externally and within the cave network. Suspended aerosol monitoring locations (Ext, 1, 2 and 3) are presented in Figure 4.2.
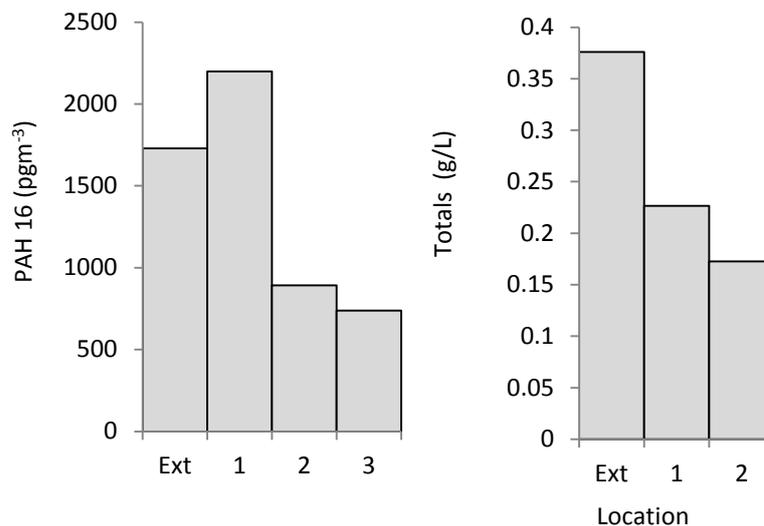


Figure 4.7: PAH (left) and total inorganic (right) suspended cave aerosol distributions throughout New St Michaels Cave.

PAH results present greater levels within the cave entrance when compared to external concentrations. The increased levels at location 1 suggest PAH concentration processes are taking place as suggested in Chapter 2 (Dredge *et al*., 2013). Internally, a progressive loss in suspended loads is observed with distance from the entrance. For inorganic aerosols, increased aerosol loads are observed with proximity to cave entrance, however, greatest levels are observed in the external environment.
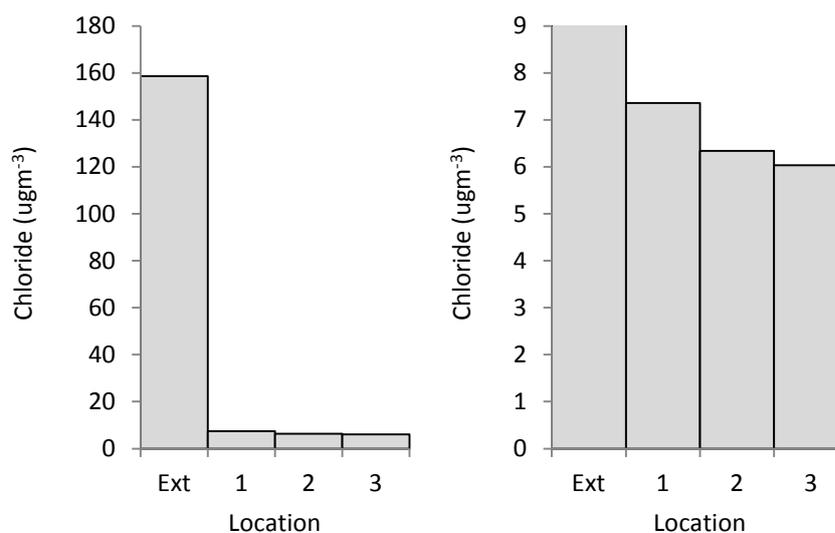
Figure 4.8: Suspended chloride contents in the Gibraltar atmosphere (Ext) and locations 1-3 within the Lower New St. Michaels Cave system. Total y scale (left), low level concentrations (right) to display relative concentrations in locations 1-3.

Chloride concentrations indicate the same transport and distribution as PAH and trace element analysis results. The comparison of internal and external suspended aerosol concentrations offers insight into cave aerosol transport processes and is explored in the discussion.

### 4.3.5. Speleothem trace element chemistry
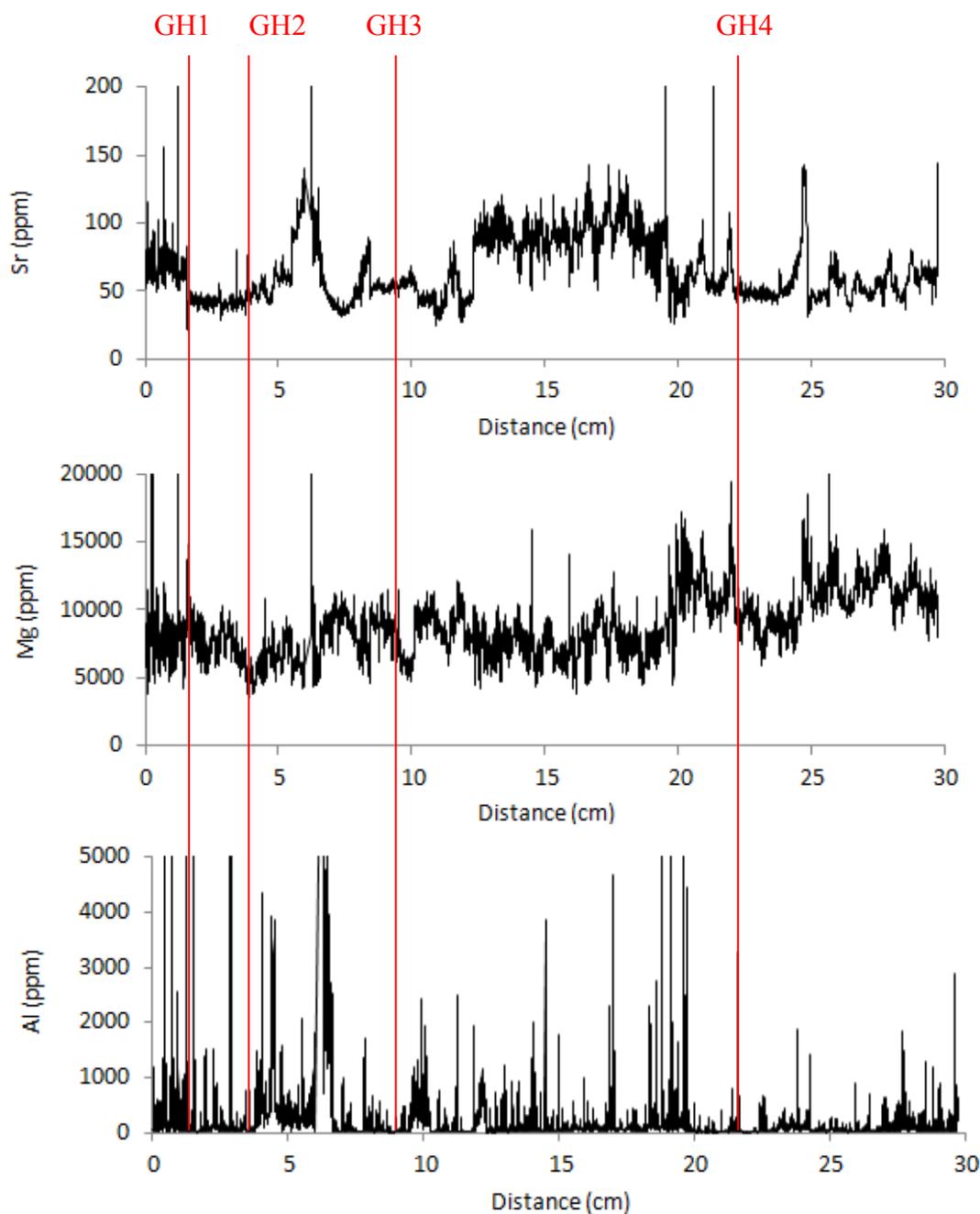


Figure 4.9: LA-ICP-MS data are presented for the length of the flowstone core for Sr, Mg and Al. LA-ICP-MS data for each element analysed are presented in the supplementary material, section S.15, Figure S.19. Hiatus locations established from the Gib08 age model (Figure 4.5) are shown by red lines.

Mg, Al and Sr each show different geochemical records (Figure 4.9). Strong evidence for geochemical recording of hiatuses is not presented. Therefore principal component analysis (PCA) is utilised in the following sections to evaluate the changing relationship and influences of trace elements. Figure 4.10 presents PCA analysis for LA-ICP-MS results.
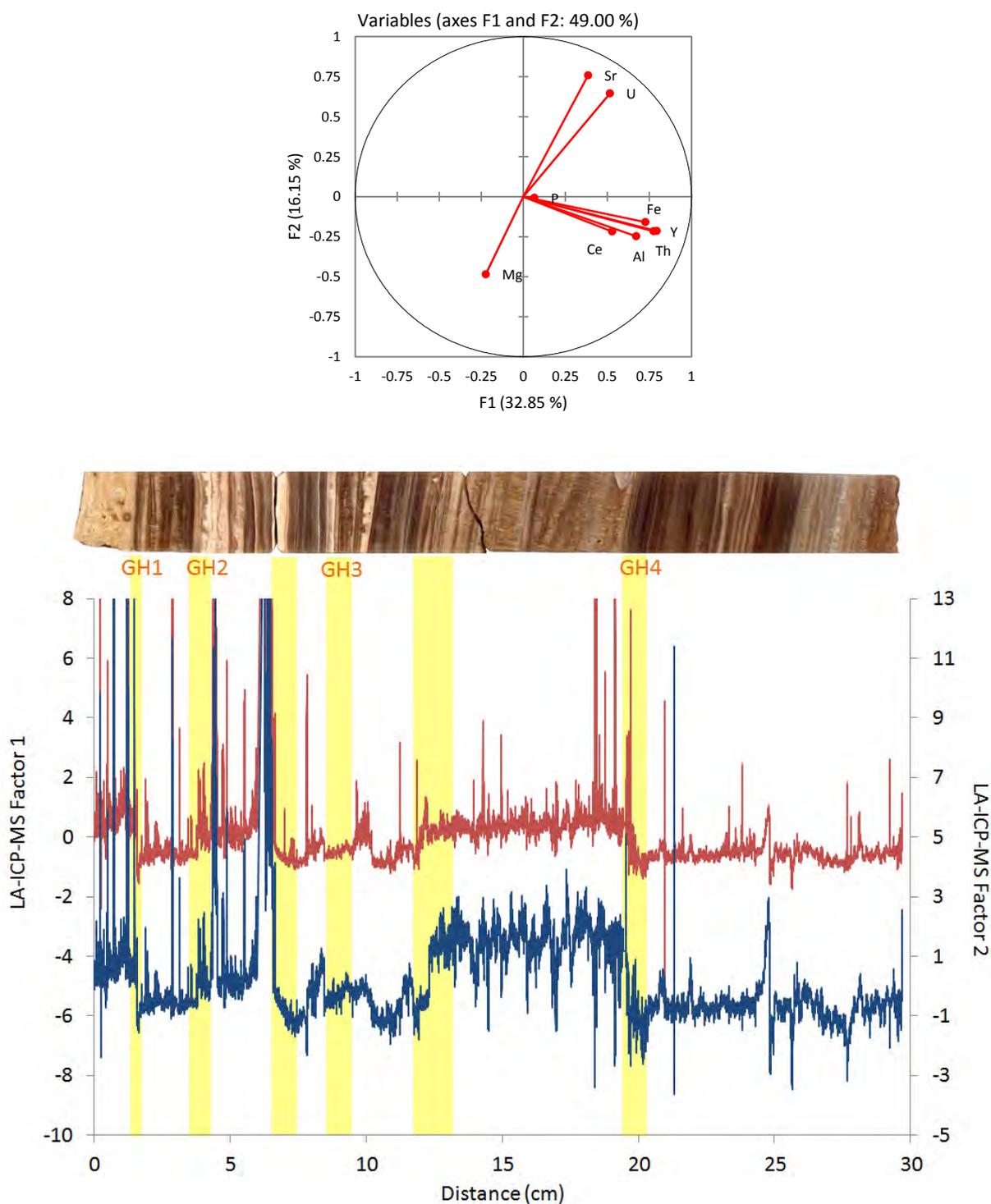
Figure 4.10: PCA analysis of Gib08 LA-ICP-MS analysis results. Factor 1 is presented in red and factor 2 in blue. Growth hiatuses 1-4 are numbered and highlighted in yellow. Sections highlighted in yellow without GH numbering represent potential hiatuses not observed in the Gib08 age model (Figure 4.5).

Results from PCA analysis (Figure 4.10) identifies 3 groups of elements: Mg; Sr and U; Fe, Al, Ce, Y, Th. Each group of elements represents a separate process and geochemical influence. Notable changes are observed in the relative influence of each group throughout the entire growth duration of the flowstone which, is presented in Figure 4.10. Results present clear and sustained geochemical shifts. Hiatus events GH1, GH2 and GH4 correlate with the timing of shifts, GH1 and GH4 mark the point of increase in both factors 1 and 2 (as shown in Figure 4.10). GH3 may be correlated with the increases occurring towards the end of the highlighted section. Two regions where potential hiatuses may occur during slow flowstone growth are highlighted between GH2-GH3 and GH3-GH4. Both potential hiatus events correlate with notable changes in the PCA output record, potentially indicating periods of change. Hiatus events mark changes that may be occurring as a consequence of palaeoenvironmental or flowstone growth processes. The processes controlling flowstone geochemistry are explored further in section 4.4.

## 4.3.6. Isotopic analysis

Isotopic analysis is utilised in this study to investigate changing palaeoclimatic and palaeoeonvironmental influences on the Gib08 flowstone. The significance of each chemical proxy and previous studies in which they have been used are outlined in the introduction Chapter 1, Table 1.1.
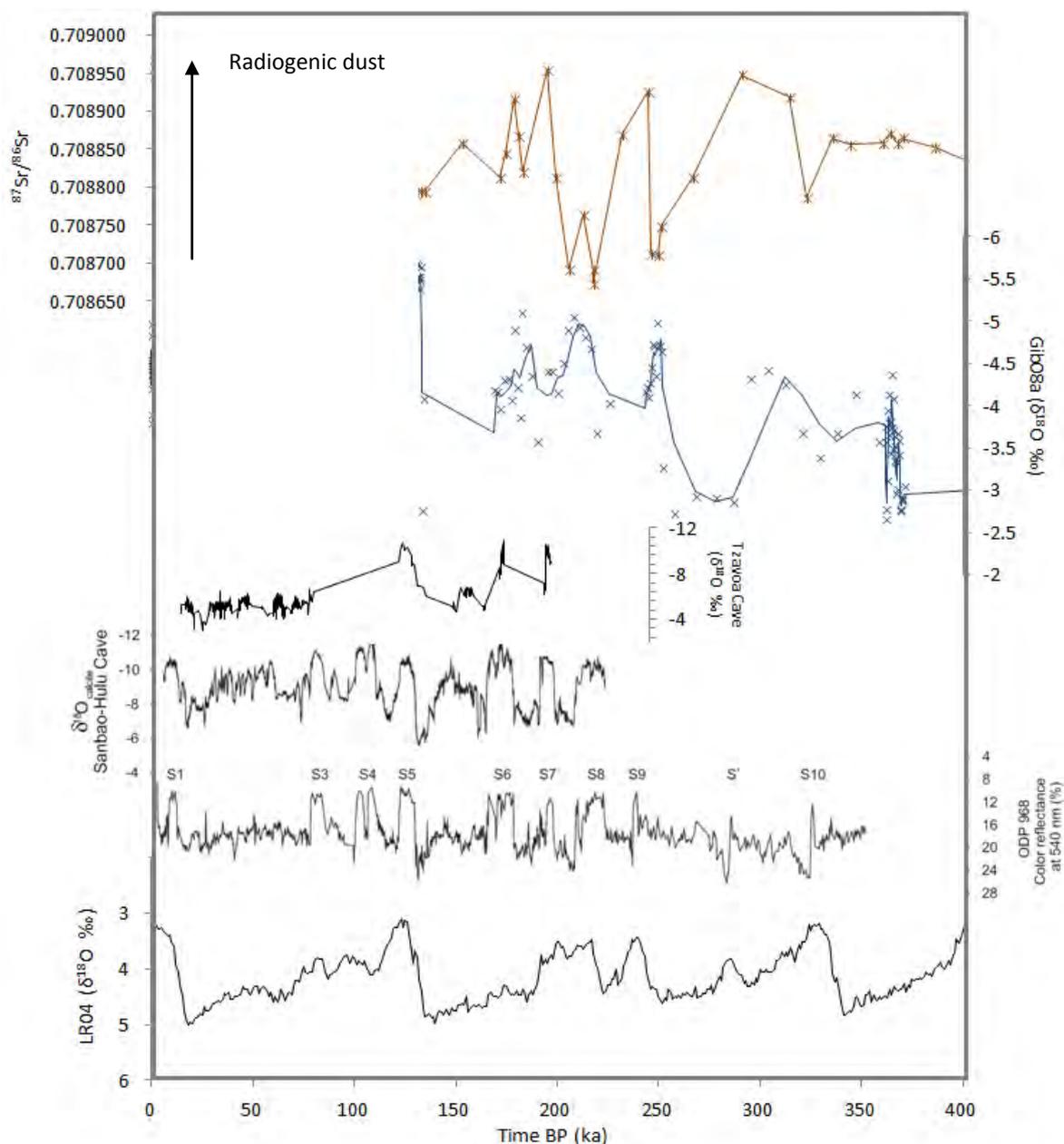


Figure 4.11: Gib08a oxygen and strontium isotope results compared to the glacial-interglacial timings from LR04, ODP 968, Sanbao-Hulu Cave and Tzavoa Cave speleothem records. The Gibraltar $^{87}$Sr/$^{86}$Sr (top, orange) and Gibraltar 2 mm resolution $\delta^{18}$O 3-point average trend line

(middle, blue). Palaeoclimate records for comparison: Tzavoa Cave, Israel speleothem $\delta^{18}O$ record (Vaks *et al*., 2006); Sanbao-Hulu Cave, China speleothem $\delta^{18}O$ record (Wang *et al*., 2008); ODP 968 reflectance record, Eastern Mediterranean marine sediment record − S1 to S10 mark sapropel layers (Ziegler *et al.,* 2010); LR04 $\delta^{18}O$ deep sea sediment stack record (Lisiecki & Raymo, 2005). All records are presented against age, thousand calendar years before present.

$^{87}Sr/^{86}Sr$ and Gib08a $\delta^{18}O$ demonstrate some broad temporal relationships with glacial cycles presented by LR04 $\delta^{18}O$. The pattern presented is suggestive of glacial-interglacial timescale environmental controls on flowstone $\delta^{18}O$ and $^{87}Sr/^{86}Sr$. $\delta^{18}O$ and $^{87}Sr/^{86}Sr$ present a weakly antipathetic relationship ($R^2$ of linear trend line is not considered statistically significant) (Figure 4.12). The Gib08 $\delta^{18}O$ record presents clear shifts with $\delta^{18}O$ becoming more negative during interglacial periods. Due to Gibraltar's location, the $\delta^{18}O$ may be displaying ocean source effects occurring due to varying influences from Mediterranean and Atlantic precipitation sources. Another main feature of the $\delta^{18}O$ record is the progression towards more negative $\delta^{18}O$ values. This may be occurring as a consequence of local processes occurring within the cave. For example, flowstone formation may be progressively changing the flowstone drip water flow system, altering isotopic fractionation processes. Flowstone growth features could extend the flow path or cause drip water reservoiring causing increased and reduced fractionation respectively. Changing cave ventilation processes could also influence fractionation processes. For example, a progressive change in cave ventilation in increased cave $CO_2$, causing reduced drip water degassing and reduced fractionation effects. Long term weathering and uplift of the Gibraltar rock would also influence the isotopic signature through a range of processes e.g. reduced marine influence, changing soil profile dynamics, altering karst-drip interactions etc. There does not appear to be any notable correlation with the Gib08 record and sapropel events (reflected in the Sanbao-Hulu isotopic record) presented in Figure 4.11. However, relationships may not be recorded due to the sampling resolution employed in this investigation.

Figure 4.12: $^{87}Sr/^{86}Sr$ and $\delta^{18}O$ throughout the entire growth period of the flowstone.

## 4.4. Discussion

### *4.4.1. Internal cave aerosols*

Aerosol incorporation from direct aerosol deposition to the flowstone surface has the potential to provide a significant contribution to speleothem geochemistry, especially during growth hiatuses (Chapter 2 - Dredge *et al.,* 2013). Monitoring of suspended aerosols throughout St Michaels cave has shown the distribution of cave aerosols (Figures 4.7 and 4.8).
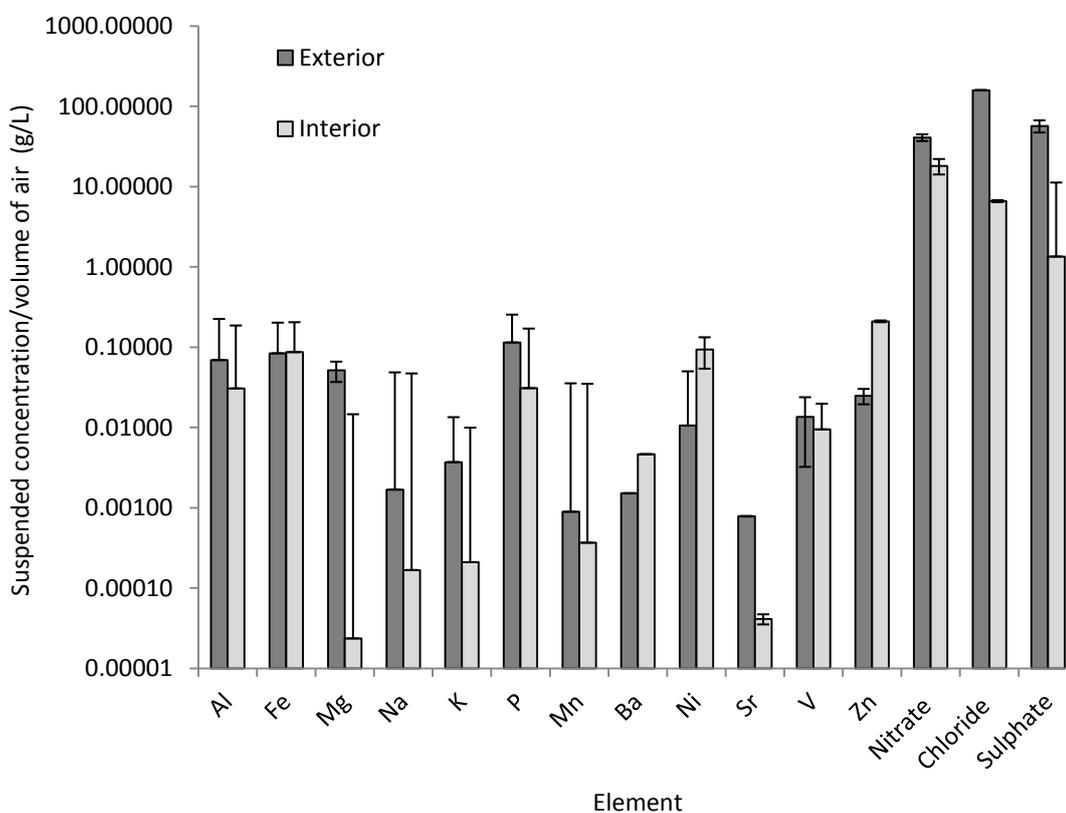


Figure 4.13: Comparison of interior and exterior suspended aerosol elemental concentrations. Interior concentrations presented are the average from the 3 interior monitoring sites.

Na, K, P, Al, Fe, V and Mg are predominantly sourced from the external environment and Ba, Ni and Zn are sourced from the internal environment. Table 4.3 presents the relative proportion of internal aerosols to external concentrations.

| | Al | Fe | Mg | Na | K | P | Mn | Ba | Ni | Sr | V | Zn | N | C | S |
|---|---|---|---|---|---|---|---|---|---|---|---|---|---|---|---|
| E | 0.069 | 0.084 | 0.051 | 0.0017 | 0.0037 | 0.11 | 0.00089 | 0.0015 | 0.011 | 0.00078 | 0.014 | 0.025 | 41 | 159 | 57 |
| I | 0.031 | 0.087 | 0.000024 | 0.00017 | 0.00021 | 0.031 | 0.00037 | 0.0046 | 0.093 | 0.000041 | 0.0094 | 0.21 | 18 | 6.6 | 1.3 |
| I:E | 0.44 | 1.03 | 0.00046 | 0.10 | 0.057 | 0.27 | 0.41 | 3.06 | 8.84 | 0.053 | 0.70 | 8.46 | 0.44 | 0.041 | 0.024 |

Table 4.3: External (E) and internal (I) suspended aerosol elemental concentrations in air (g/L) and the relative levels of internal to external concentrations (concentration ratio). N, C and S are Nitrate, Chloride and Sulphate respectively.

The comparison of internal and external suspended elemental concentrations offers an insight into the source of aerosols. As presented in Table 4.3, internal levels of Sr and Chloride are 4-5% of external levels, indicating significant transport losses occurring throughout the cave network. This suggests that the predominant transport mechanism to the speleothem is through cave drip water from aerosol deposition on the cave surface. However, this also shows that drip water calculations provide a lower bound estimate and that there is potential for additional contributions of seawater from internal and direct aerosol incorporation.

The significant measured components and contributors to the aerosol signature are sourced from Al, Fe, P, Ni, V and Zn. Elements such as Al and Fe are indicative of terrestrial dust and sediment contributions to aerosols. It is possible that elements such as Ni, V and Zn are sourced from modern pollutants and therefore would not contribute to historical flowstone growth geochemistry. Zn is a known to be sourced from vehicles, whilst V and Ni are

indicative of mixed industrial or fuel-oil combustion (Viana *et al.,* 2008). Additionally, V and Ni were not determined in LA-ICP-MS analysis of the flowstone. Al and Fe are commonly associated with colloidal solution transport and incorporation into speleothems (see Chapter 1, Table 1.1). Consequently, solution and aerosol source separation will be difficult based on the chemical signature observed in the modern monitoring.

### 4.4.2. Drip water precipitation processes

In order to properly investigate flowstone chemistry, local processes must be considered and evaluated before external palaeoenvironmental drivers are considered. Drip water chemistry data (Figure 4.6) presents evidence for chemical alteration occurring as a consequence of local processes.

PCP leads to enhanced Mg/Ca and Sr/Ca in the dripwater, as Mg and Sr are excluded relative to Ca during calcite precipitation (Fairchild *et al*., 2000). PCP and changing source dissolution chemistry have been identified as two influencing processes in the flowstone geochemical record. The following section introduces a method which assigns indices to these processes in order to quantify their influence on flowstone geochemistry through time.

By applying partition coefficients to speleothem trace element chemistry, the original dripwater Sr/Ca values can be obtained. A distribution or partition coefficient (Morse & Bender, 1990) can be used to relate solution and mineral compositions, as expressed in equation (1), with equation (2) being used for calculations displayed in Figures 4.14 and 4.15.

$$(Tr/Ca)_{CaCO_3} = K_{Tr}(Tr/Ca)_{solution} \qquad (1)$$

*Tr = trace ion*

$K_{Tr}$ = *partition coefficient*

Therefore:

$$K_{Tr} = (Tr/Ca)_{solution}/(Tr/Ca)_{CaCO_3} \qquad (2)$$

$K_{Tr}$ will vary as a result of changing crystal and environmental conditions (outlined in Fairchild & Treble, 2009 and Fairchild & Baker, 2012). The partition coefficient was calculated by the comparisons of modern flowstone growth (upper most 1.7 cm growth over ~ 50 years) and modern drip water trace resulting in a $K_{Sr}$ of 0.062 ($\sigma = 0.0033$).

|  | Average | Max | Min | Σ |
|---|---|---|---|---|
| **(Mg/Ca)$_{CaCO3}$** | 0.0081 |  |  | 0.0034 |
| **(Mg/Ca)$_{Solution}$** | 0.43 | 1.1 | 0.35 | 0.14 |
| ***K$_{Mg}$*** | *0.019* | *0.007* | *0.023* |  |
| **(Sr/Ca)$_{CaCO3}$** | 0.000065 |  |  | 0.000018 |
| **(Sr/Ca)$_{Solution}$** | 0.0010 | 0.00077 | 0.0025 | 0.0055 |
| ***K$_{Sr}$*** | *0.062* | *0.084* | *0.026* |  |

Table 4.4: Average and standard deviation ($\sigma$) results of Sr/Ca and Mg/Ca for the Gib08a sample and dripwaters, and the calculated $K_{Tr}$. $K_{Tr}$ calculations were carried out using the average $Tr_{CaCO_3}$ and the maximum and minimum $Tr_{solution}$ ratios.

Table 4.4 presents the results of precipitation partition coefficient ($K_{Tr}$) calculations. $K_{Tr}$ results ($K_{Mg} = 0.019$ and $K_{Sr} = 0.062$) are comparable to those found in similar $K_{Tr}$ studies (summarised in Tremaine & Froelich, 2013). $K_{Sr}$ results present a notable range with a maximum of 0.084 and minimum of 0.026 based on calculations using maximum and minimum $(K_{Tr})_{solution}$ values. Values for $K_{Mg}$ are similarly variable. Results demonstrate large variability within the modern growth, and therefore applying the $K_{Tr}$ values to older growth introduces further error.

The comparison of partition coefficients offers an insight into solution composition and evolution of drip waters. This is expressed for Sr and Mg in (3) to (6).

$$(Sr/Ca)_{CaCO_3} = K_{Sr}(Sr/Ca)_{solution} \qquad (3)$$
$$(Mg/Ca)_{CaCO_3} = K_{Mg}(Sr/Ca)_{solution} \qquad (4)$$

*Therefore:*

$$(Sr/Mg)_{CaCO_3} = K_{(Sr/Mg)}(Sr/Mg)_{solution} \qquad (5)$$
$$K_{(Sr/Mg)} = (Sr/Mg)_{solution}/(Sr/Mg)_{CaCaCO_3} \qquad (6)$$

$K_{(Sr/Mg)} = 3.3$, and is similar to the results found in the study by Tremaine & Froelich (2013) indicating that $K_{Tr}$ values are in-line with those found in other studies (e.g. Huang & Fairchild, 2001; Fairchild *et al*, 2010; Karmann *et al*., 2007).

Drip water solutions influenced by prior calcite precipitation (PCP) will evolve to higher Tr/Ca ratios excluding Mg and Sr and enriching the residual solution compared with Ca; this is expressed in (7) to (9) (Fairchild & Baker, 2012).

$$Sr_i = Sr_o - (Ca_i - Ca_o)(K_{Sr}) \qquad (7)$$
$$Mg_i = Mg_o - (Ca_i - Ca_o)(K_{Mg}) \qquad (8)$$
$$\Delta Ca = Ca_i - Ca_o \qquad (9)$$

*$Sr_o$, $Mg_o$, and $Ca_o$ = initial compositions*
*$Sr_i$, $Mg_i$ and $Ca_i$ = residual drip water compositions*

The evolution of PCP influenced water on a (Sr/Ca)/(Mg/Ca) plot can be quantified by PCP vectors. PCP vector calculations can be described by the following equations (10-12) introduced in Tremaine & Froelich (2013):

$$\Delta Sr/\Delta Ca = [Sr_o - \Delta Ca(K_{Sr})]/\Delta Ca \qquad (10)$$

*and,*

$$\Delta Mg/\Delta Ca = [Mg_o - \Delta Ca(K_{Mg})]/\Delta Ca \qquad (11)$$

*therefore,*

$$\Delta Sr/\Delta Mg = [Sr_o - \Delta Ca(K_{Sr})]/[Mg_o - \Delta Ca(K_{Mg})] \qquad (12)$$

The results of these calculations are presented below in Table 4.5.

| Tr | $Tr_0$ (ppm) | $\Delta Ca$ (ppm) | $K_{Tr}$ | $\Delta Tr/\Delta Ca$ | $\Delta Tr$ |
|---|---|---|---|---|---|
| **Sr** | 0.12 | 0.1 | 0.062 | 1.2 | |
| **Mg** | 52 | 0.1 | 0.019 | 516 | |
| **Sr/Mg** | | | | | 0.0023 |

Table 4.5: Results of drip water PCP vector calculations based on Gibraltar drip water data. $Tr_0$ is represented by dripwater values, and therefore calculated PCP vectors indicate PCP occurring before sample precipitation. $\Delta Tr = \Delta Sr/\Delta Mg$.

The PCP vector calculation obtained from the Gib08 data produces a $\Delta Sr/\Delta Mg$ of 0.0023. This is used as an indicator for the evolution vector of speleothem precipitation being influenced by PCP. Figure 4.14 presents the results of the modern Gib08a speleothem data, transformed to represent the original drip water.
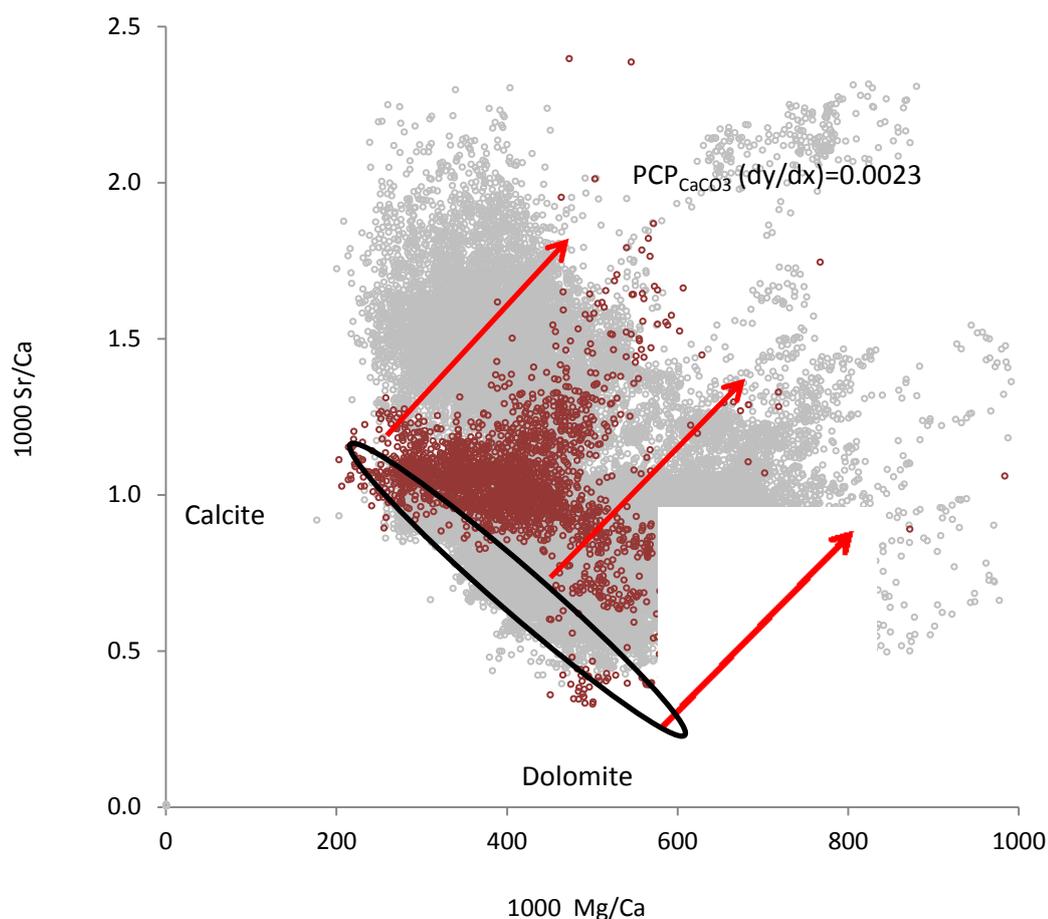
Figure 4.14: Modern data is presented in red (upper 1.8cm of growth until most recent hiatus, ~50 years of growth). All flowstone data shown in grey. Gib08a calcite Sr/Ca and Mg/Ca corrected to represent original solution chemistry using $K_{Tr}$ values from Table 4.4. The calculated PCP vectors from modern drip water samples are displayed with the red arrows. The evolution of each speleothem sample's Mg and Sr due to PCP will have an individual evolution line described by:

$(Sr/Ca)_S = 0.0023(Mg/Ca)_S + C$            (13)

A mixed source between carbonate and dolomite has been identified as shown by the black ellipse. This line can be described by:

$(Sr/Ca)_S = -0.0021(Mg/Ca)_S + 1.5632$        (14)

The terms for each line equation are defined as: $(Tr/Ca)_S$ = Speleothem trace element values corrected to present original drip water values through the application of their respective $K_{Tr}$ values. C = The original source Mg and Sr before the influence of PCP, which is represented by the intercept between the source line and sample PCP vector.

The progression along the PCP vector (red lines in Figure 4.14) away from the original source

line (black ellipse in Figure 4.14) is an indication of each sample's PCP evolution. Figure

4.15 presents the lines, intercepts, intersections and values that are used in the following calculations. Further details of the mathematical methods are explained in the supplementary material, section S.16.
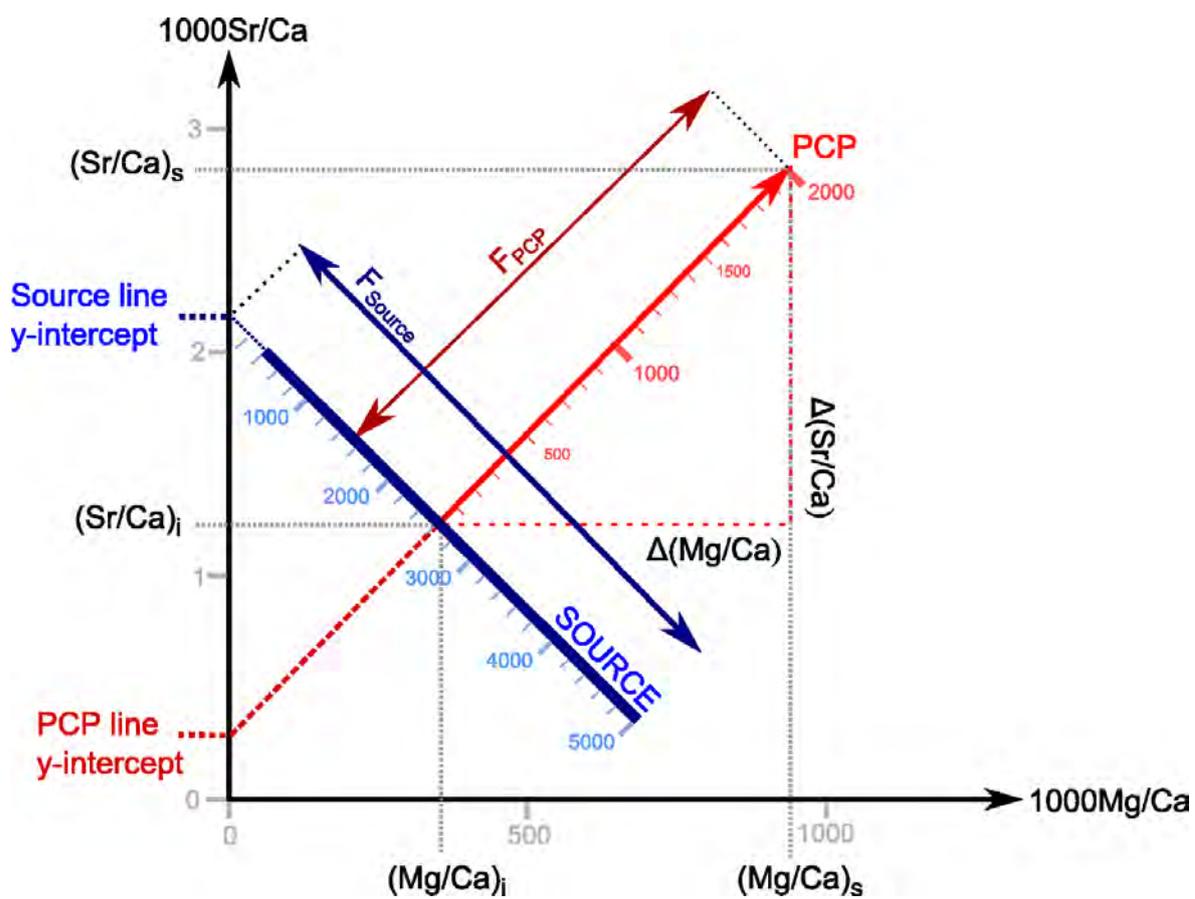


Figure 4.15: Schematic illustration of terms used in expressions 15 and 16 for the determination of $F_{PCP}$ and $F_{SOURCE}$.

In order to determine the extent of progression along the PCP vector for each sample, the original source value must be determined for reference ($(Tr/Ca)_i$). With the original source point determined and the final PCP influenced speleothem chemistry known, the extent of PCP influence can be calculated. This requires calculating the distance of progression along the PCP vector line, which can be expressed by:

$$F_{PCP} = \sqrt{\Delta(Mg/Ca)^2 + \Delta(Sr/Ca)^2} \qquad (15)$$

*Where,*

   *$\Delta(Mg/Ca) = (Mg/Ca)_S - (Mg/Ca)_i$*

   *$\Delta(Sr/Ca) = (Sr/Ca)_S - (Sr/Ca)_i$*

   *$F_{PCP}$ = The extent of PCP influence index.*

In addition to PCP, the correlation between solution Mg/Ca and Sr/Ca in the drip water presents an inclination towards the average bedrock end-member, indicating a mix of dolomite and carbonate along the discharge pathway. Consequently, changing discharge pathways could act to separate Mg and Sr. The changing source between calcite and dolomite can be observed in the modern speleothem data presented in Figure 4.14. Pathway alterations and dissolution source mixing provides the foundation for the calculation of the $F_{SOURCE}$ index.

The type of source can be indexed by determining each sample's origin along the source line. This can be determined by comparing the PCP evolution-source intercept for each sample with the source line y-intercept, as expressed by:

$$F_{source} = \sqrt{((Mg/Ca)_i{}^2 + ((Sr/Ca)_C - (Sr/Ca)_i)^2)} \qquad (16)$$

*Where,*   *$(Tr/Ca)_C$ = the y-intercept value of the source line.*

   *$F_{source}$ = Type of source geochemistry index*

$F_{SOURCE}$ and $F_{PCP}$ outputs are presented against distance for the growth duration of the flowstone in Figure 4.16. Variability is observed in both indices indicating the changeable nature and influence of both processes. The variable relationship between $F_{SOURCE}$ and $F_{PCP}$ indices reveals changing controlling processes, and this is highlighted by PCA analysis in the following sections. GH1, GH3 and GH4 occur at the point of maximum $F_{SOURCE}$, which is not as clearly presented in the $F_{PCP}$ record. Increasing $F_{SOURCE}$ indicates increasing dolomite dissolution occurring under drier conditions leading to complete drying and a growth hiatus. Other known hiatuses (GH2) and potential hiatuses (yellow shading) may be occurring as a result of local processes relating to flowstone formation rather than changing karst dissolution. The data transformation of Sr and Mg presents features that were observed in the original LA-ICP-MS data (Figure 4.9), demonstrating the value of this technique for future investigations.
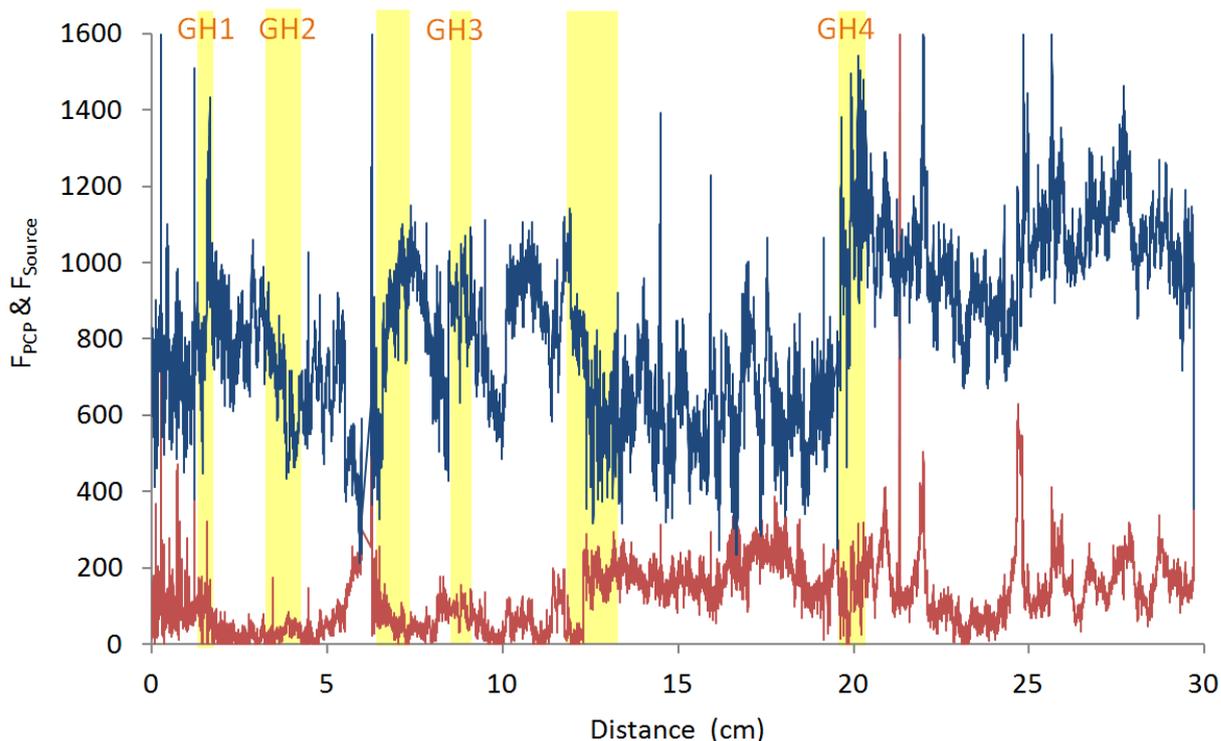
Figure 4.16: $F_{PCP}$ (red) and $F_{Source}$ (blue) against distance along the flowstone core (from youngest growth).

### 4.4.3. Flowstone growth variability

The inclusion of $F_{SOURCE}$ and $F_{PCP}$ indices provides additional insights into processes influencing flowstone chemistry. $F_{SOURCE}$ and $F_{PCP}$ indices will be used in combination with geochemical trace element analysis to study the flowstone sample. The following sections explore geochemical change associated with hiatus and fast growth events.

*Flowstone hiatus/slow growth events*

The Gib08 flowstone growth presents variable growth rates and is punctuated with 4 hiatuses (or slow growth events) named GH1-GH4 as highlighted in the age model in Figure 4.5 (with two addition unconfirmed potential hiatuses). Cessation in drip water flow can occur due to environmental, hydrological or flowstone processes. Drying of the flowstone can also occur

due to hydrological changes in the bedrock flow path resulting in discharge diversion away from the flowstone. Even with continued discharge to the flowstone site, lobe switching on the flowstone surface can result in a hiatus in the sampled core, in the same mechanism as sediment deposition changes in delta environments.
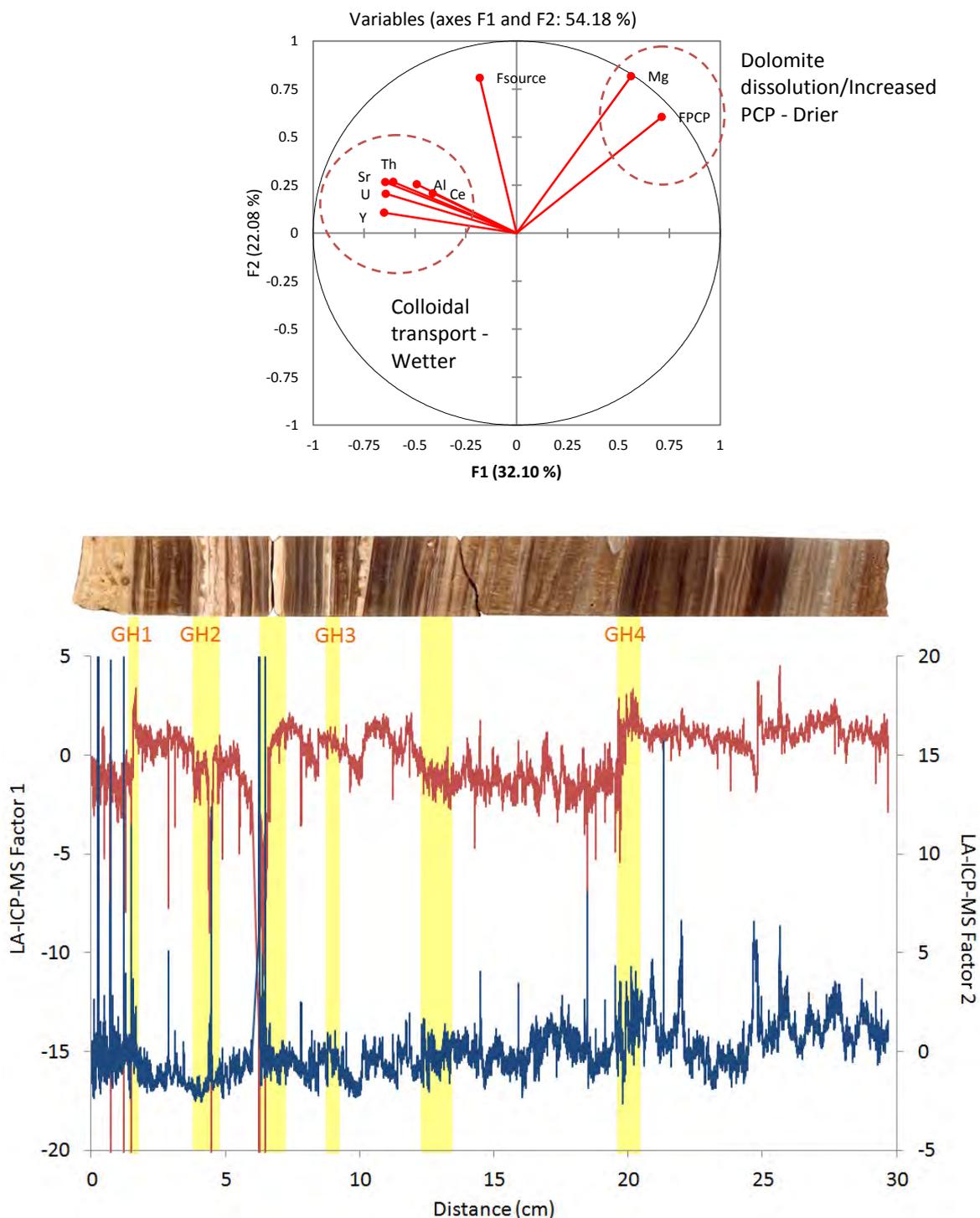
Figure 4.17: PCA analysis presenting trace element results and vector based analysis of PCP and source type $F_{PCP}$ and $F_{SOURCE}$ respectively (Factor 1 in red and Factor 2 in blue). LA-ICP-MS PCA analysis presents results from high resolution trace element analysis. Factor loading results are displayed against distance, with the image of the flowstone core for reference. Hiatus events GH1-GH4 are marked with yellow shading.

In some instances hiatuses are associated with microcrystalline calcite fabric as presented in Figure 4.4 (growth sections 2.1, 2.2 and 2.3). However, the relationship between hiatus events and calcite fabric is not consistent throughout the entire growth period with no micritic calcite being observed at GH1, GH4. GH4 occurs at the end of long term stable growth periods, which likely represent a different calcite precipitation system to the more variable growth occurring after the potential hiatus between GH3 and GH4, in the more modern growth. The introduction of micritic calcite marks a change in the flowstone precipitation from stable periods of calcite formation to shorter term variability marked by numerous small hiatuses. GH1 is the most recent hiatus and marks the separation between historic (>120 ka) and modern (last 50-75 years) growth. The hiatus marks renewed growth probably as a result of exploration activities (Mattey *et al.,* 2008) rather than hydrological or precipitation processes, accounting for the contrast to GH2-GH3. Table 4.6 outlines the characteristics of each hiatus event. There is no light exposure in this part of the cave and therefore has no effect on the type of calcite precipitation that has occurred in the flowstone.

When observing the geochemical record (Figure 4.17) some recurring features are notable. Hiatus events (marked in figures 4, 5, 10, 16 and 17) are clearly marked by shifts in geochemical composition. Each shift represents a "resetting" with an apparent system change after each hiatus. Here we propose that factor 1 in Figure 4.17 presents a record of wetter and drier conditions (as marked on the sample PCA results in Figure 4.17), based on geochemical interpretations summarised in Table 1.1 and observations from modern drip water monitoring outlined in Section 4.4.2. Wetter conditions will result in increased colloidal transport and carbonate dissolution with lower levels of PCP. Drier conditions will cause increased PCP and greater dolomite dissolution processes. GH1, GH3 and GH4 therefore represent the

culmination of periods of drying as suggested by increasing factor 1. Each hiatus event is followed by much wetter conditions with no transition being records. The lack of transition potentially represents that a threshold of water supply is reached before the resumption of speleothem formation.

There is no apparent relationship between climatic change and the timing of hiatus events (as presented in Figure 4.11) suggesting that changes in discharge are occurring as a consequence of local processes rather than a direct consequence of environmental change. Small excursions occur in-between the noted hiatus events, potentially indicating shorter-lived growth hiatus events that are not shown in the sample age model (Figure 4.5). The slight affinity for $F_{SOURCE}$ (increased $F_{SOURCE}$ interpreted as drier conditions) with colloidally derived elements can be accounted for by the elevated contribution of aerosols under slow growth and hiatus conditions. Al and Fe have been identified as an aerosol signature and may cause the observed relationship. $F_{SOURCE}$ (as calculated in Section 4.4.2) may not be a complete indicator of wet and dry conditions (as shown in Figure 4.17), and high flow discharge pathways may preferentially take route through limestone regions of the aquifer resulting in the relationship with colloidally source elements.

| Hiatus Event | Characteristics |
|---|---|
| GH1 | Distinct hiatus marking the change from dark compact calcite formation 128 ka BP and modern porous calcite forming in the last 50 years. An abrupt shift in geochemistry is also observed with the transition to more colloidal influence suggestive of wetter conditions after H1. Leading up to the hiatus a progressive increase in factor 1 observed indicating drying in the lead up to the hiatus. |
| GH2 | A clear transition in calcite fabric is observed from micritic calcite to dark compact calcite. A small shift in geochemistry is displayed from variable conditions to stable drier conditions. |
| Potential hiatus between GH2 and GH3 | A clear change in fabric is displayed from micritic calcite to dark compact calcite. The most prominent micritic features in the sample is observed in the lead up this hiatus. The hiatus event presents the largest geochemical excursion associated with a large increased in colloidally derived elements and increased $F_{SOURCE}$, Mg and $F_{PCP}$. This change is indicative of dry conditions with colloidal influences being attributed to aerosol deposits. |
| GH3 | Fabric presents a transition from dark calcite to micritic white calcite. Geochemistry presents a small but abrupt shift after the timing of the hiatus to lower factor 1 and 2. This indicates a shift toward colloidal influence and increased wetness after which the sample dries until the occurrence of H3. |
| Potential hiatus between GH3 and GH4 | Not observed clearly in the fabric. A clear shift in factor 1 is observed indicating a transition from a long period of stable wet conditions producing large columnar calcite growth to drier conditions. The shift is less apparent in factor two. This suggests that this may be caused by local processes rather than hydrogeological changes, as alterations in $F_{SOURCE}$ and Mg are not recorded. |

| | |
|---|---|
| GH4 | A change from layered dark calcite to large columnar calcite occurs. This hiatus marks a large shift in both factors 1 and 2. Factor 1 presents a period of increase indicating drying, followed by an abrupt shift to low levels representing the onset of wet conditions. This is reflected in factor 2 with a shift from dolomite dissolution and PCP processes to colloidal transport, being indicative of the transition from wet to dry. |

Table 4.6: Hiatus events and their associated geochemical and calcite fabric characteristics.

The key observation in the geochemical record is that most hiatus events mark the shift from progressive increasingly dry conditions to high discharge wet conditions. However, it is possible that the early part of observed shift can partially be attributed to aerosol collection and incorporation of elements such as Al and Fe during hiatus events (cave aerosol results presented in Figure 4.13). As established in Section 4.1, separation of solution and aerosol sources is complicated by multiple transport mechanisms to the flowstone. However, colloidal element excursions over short distances occurring during periods of slow growth or hiatus events most likely indicate the build up of aerosol deposits. Therefore it is tentatively suggested that the excursion observed in factor 1 at GH3 occurs due to aerosol deposition.

*Flowstone fast growth episodes*

Fast growth events offer increased age and analytical resolution owing to the greater temporal sampling resolution and dating accuracy which can be obtained. Flowstone fast growth events are explored to determine the extent of links between precipitation and environmental conditions. Figure 4.18 presents sections of continuous growth; durations of fastest growth are highlighted in blue.
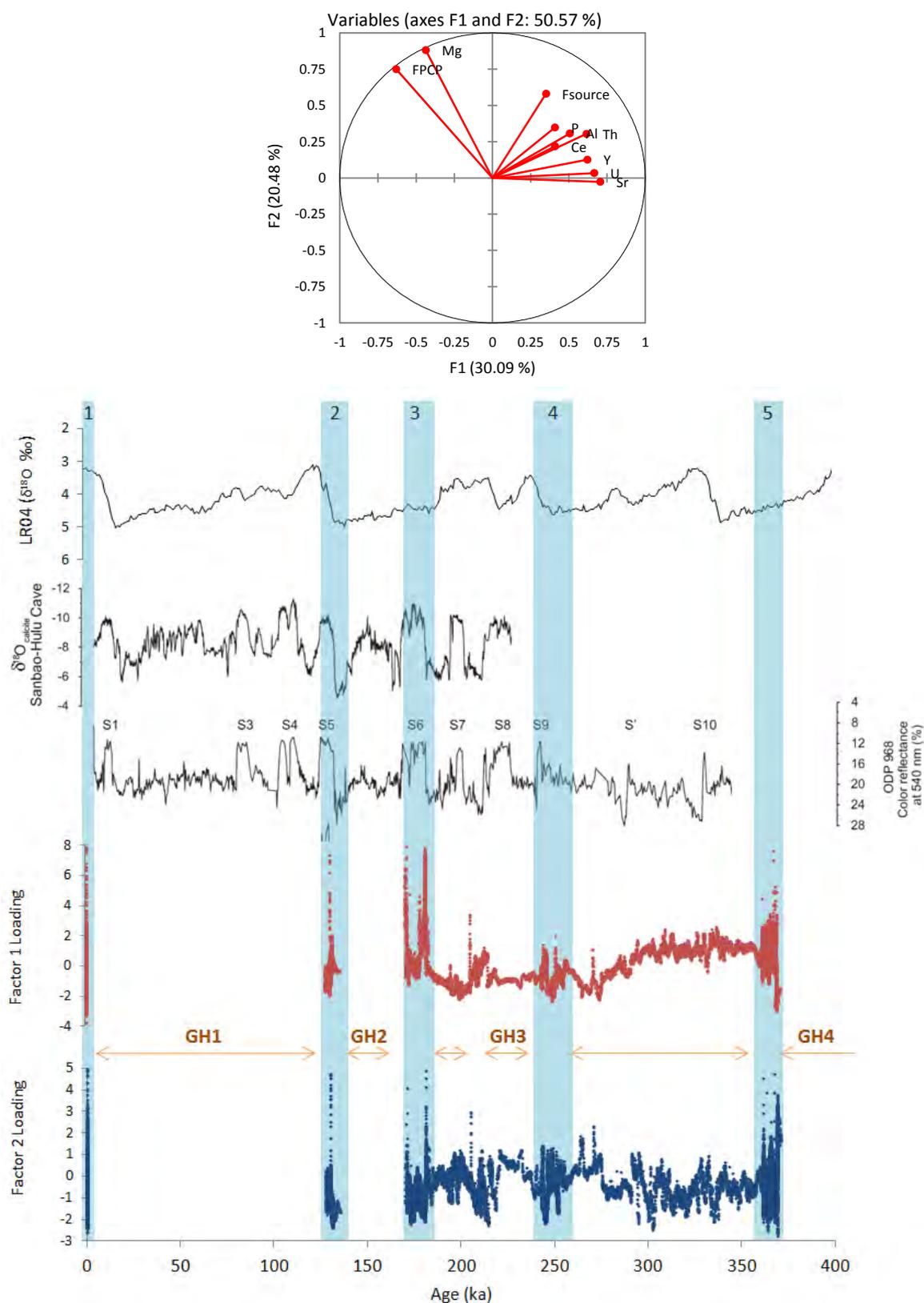
Figure 4.18: PCA analysis of Gib08a LA-ICP-MS data. Data from continuous growth sections based on U/Th geochronology is displayed. Factor 1 (red), factor 2 (blue) and fast growth sections (1-5) are highlighted in blue, GH1-4 locations are marked. Only data from sections of

well constrained growth are presented. Gib08a trace element PCA results are compared to palaeoclimate records: Sanbao-Hulu Cave, China speleothem $\delta^{18}O$ record (Wang *et al.*, 2008); ODP 968 reflectance record, Eastern Mediterranean marine sediment record – S1-10 mark sapropel layers (Ziegler *et al.,* 2010); LR04 $\delta^{18}O$ deep sea sediment stack record (Lisiecki & Raymo, 2005).

Figure 4.18 presents a clear distinction between colloidally derived elements (Ca, Al and Y) and hydrogeologically controlled elements (Mg, Sr and U). Mg strongly opposes Sr and U in its influence. Periods of fast growth correlate with factor loading excursions, with positive shifts observed, indicating increased colloidal flux and incorporation in the flowstone. Fast growth events are therefore suggestive of greater drip water supply. This observation is coherent with those made when observing hiatus events. The 'flashy' nature of geochemical excursions within fast growth sections indicates high-flow scenarios of short duration resulting in episodes of increased colloidal transport are taking place. These episodes potentially indicate exceptional discharge or cave flooding events relating to high precipitation events. High flow events would incorporate colloids from the surface but also incorporate detrital material and aerosol deposits from throughout the cave resulting in the peaks observed peaks in geochemistry. Inorganic surface colloids would be sourced from bedrock erosion and particulate aerosol deposition. Colloidal deposits from within the cave will be composed of sediments from previous high flow/flooding events, cave wall erosion, and internal cave aerosol deposits. Therefore colloidal transport may present a relationship with increased radiogenic Sr supply, occurring as a consequence of surface aerosol deposition transport by drip waters. High flow events may therefore present increased $^{87}Sr/^{86}Sr$ which is not representative of atmospheric transport processes, but the incorporation of previously deposited aerosols (from the surface or from cave surfaces) or from previous high flow event sediments deposited within the cave.

Sapropel events are thin discrete, black, organic-rich layers that were deposited as a marine response to enhanced rainfall and fresh-water runoff from the continents (Bar-Matthews et al., 2000). Sapropel events have been recorded in Eastern Mediterranean speleothem records (Soreq Cave, Israel) by low $\delta^{18}O$ events (Bar-Matthews *et al*., 2000) and correlate with low $\delta^{18}O$ events in the Sanbao-Hulu record (Figure 4.18; Ziegler *et al.,* 2010). The timing of Gib08 fast growth events (2, 3 and 4 in Figure 4.18) present a clear relationship with the timing of sapropel events. This observation indicates that fast growth events occurring in the Gib08 speleothem form as a consequence of enhanced rainfall that occurred on the continent at those times. This is consistent with the geochemical interpretations made based on Figure 4.18, with fast growth periods representing fast flow events. Isotopic shifts are not observed in the Gib08 record (Figure 4.11) in relation to sapropel events observed with other Mediterranean region speleothem records (e.g. Bar-Matthew *et al*., 2000). This may be due to the overriding influence of local isotopic fractionation occurring as a consequence of flowstone formation processes. It is also possible that precipitation $\delta^{18}O$ changes may have been more subtle in the western Mediterranean region due to Atlantic effects mediating isotopic shifts occurring as a consequence of Mediterranean basin process.

By studying each section of growth in detail, it is possible to determine the extent of consistent geochemical features which represent reoccurring environmental processes. Figure 4.19 presents PCA analysis of each growth period identified in Figure 4.18. The PCA analyses for each growth section 1 to 5 presents differing geochemical processes with no singular process explanation for the entire flowstone growth duration. This observation is consistent with the "resetting" observed with hiatus events, where each shift in geochemistry represents a new system. Consequently the variability between growth sections can be

attributed to changing local process such as discharge pathways. Some unifying features are observable: consistent antipathetic relationship between Sr and Mg; and grouping of Al, Fe, Ce, Th, Y elements. Although complex and variable, the flowstone presents a continuous record of changing bedrock and colloidal influence resulting from dissolution and drip water discharge respectively.

As presented in Figure 4.18, fast growth events in Gib08 are significant due to the timing of their occurrence. Each event occurs at the timing of Mediterranean sapropel events. The conclusion is therefore that fast growth episodes occur preferentially during increased continental rainfall.
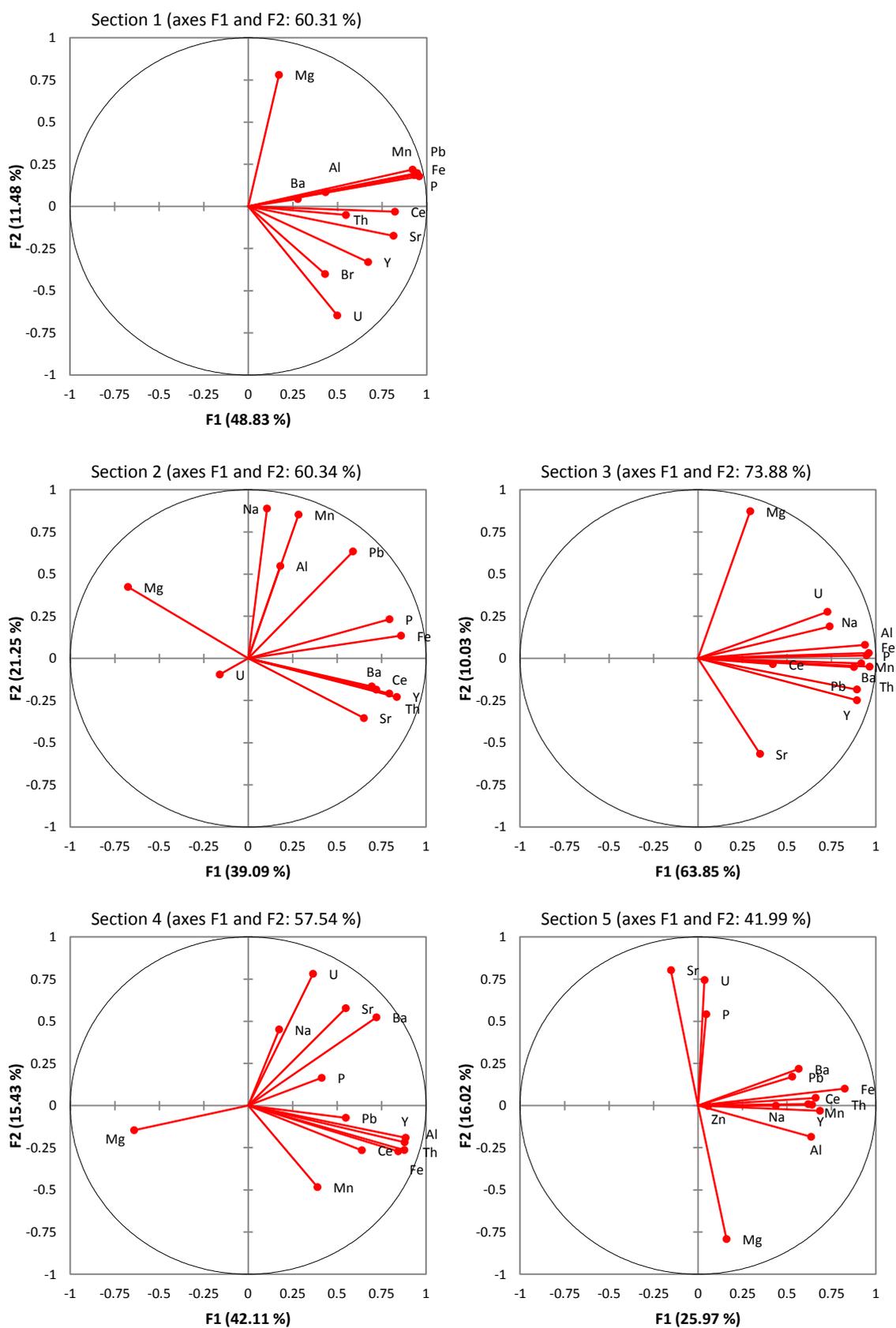
Figure 4.19: PCA models for each of growth section 1-5.

### *4.4.4. Marine aerosol contributions*

Based on the understanding of local process influences on speleothem geochemistry and the changing environmental conditions these represent, it is now possible to explore external aerosol contributions to drip water and speleothem chemistry. When observing the flowstone $^{87}Sr/^{86}Sr$ isotopic composition the same discharge-bedrock mixing system is displayed, as established from the trace element analysis in Section 4.4. Limestone and seawater end members have been identified through the use of Sr isotope source comparison. In this system, discharge and precipitation is represented by seawater influence rather than colloidal transport. End-member mixing and speleothem resultant mixtures are presented in Figure 4.20. Seawater influence from aerosol inclusions into precipitation is identifiable as a significant contributor to speleothem geochemistry and can be quantified by the method described by formulae 1 to 6.
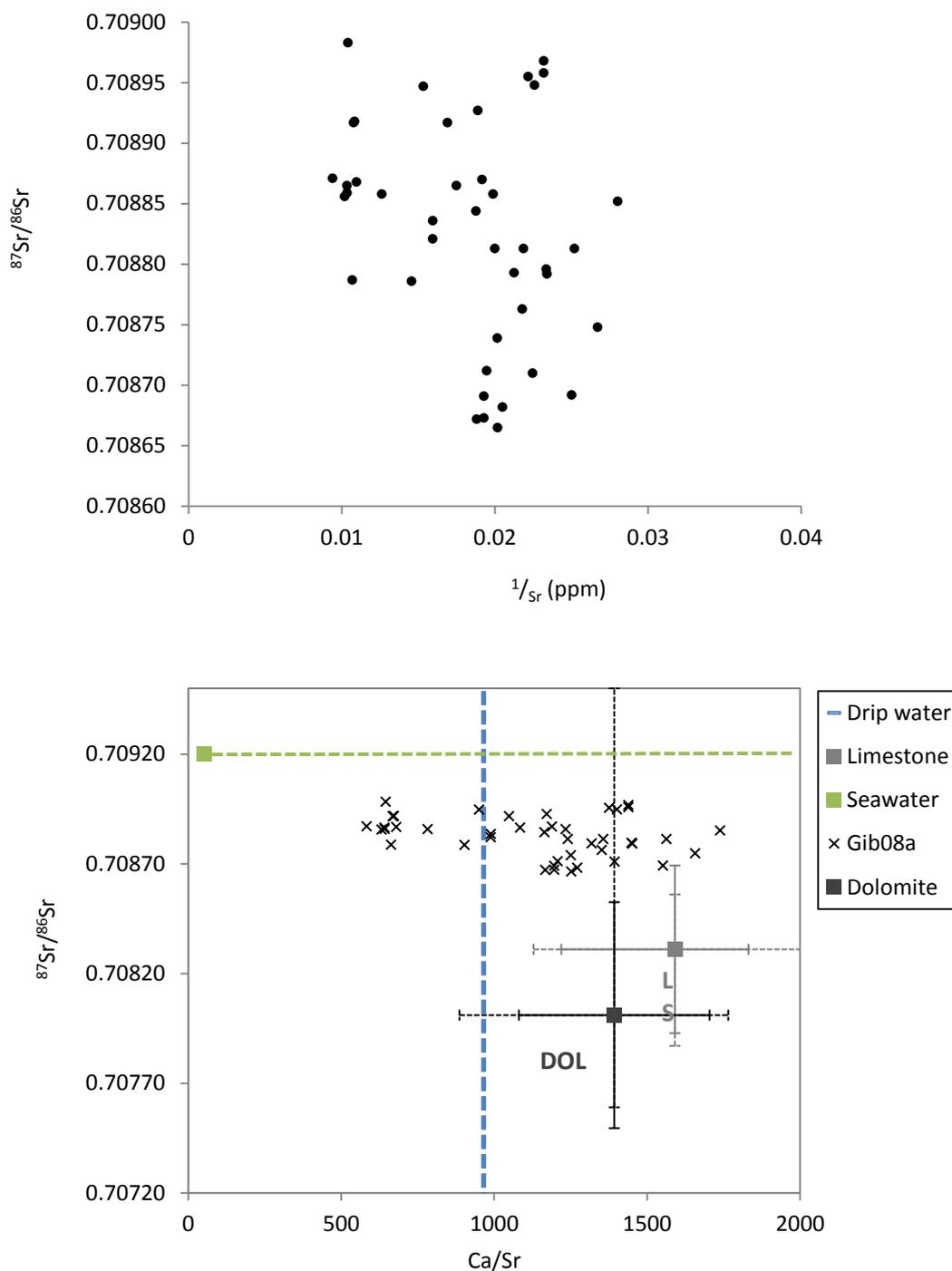
Figure 4.20: Upper: Gibraltar flowstone $^{87}Sr/^{86}Sr$ against 1/Sr trace element concentrations. Lower: Sr isotope aerosol source end members and Gibraltar speleothem source mixing, Ca/Sr against $^{87}Sr/^{86}Sr$ isotopic ratio. *Gib08a (black cross)*: MC-ICP-MS measured $^{87}Sr/^{86}Sr$, Aqueous phase Ca/Sr calculated using a fractionation $K_{Sr} = 0.062$ from measured LA-ICP-MS trace element data. $K_{Sr} = [(Sr/Ca)_{CaCO3}]/[(Sr/Ca)_{Solution}]$ calculated from the comparison of the average modern speleothem growth Sr/Ca to average drip water trace element Sr/Ca geochemistry monitored at the flowstone sample location (defined in equation (1)). *Drip water:* Ca/Sr from measured drip water geochemistry. *Seawater*: Ca/Sr ratio seawater values

taken from Chester (1990), modern seawater $^{87}$Sr/$^{86}$Sr (Fisher *et al.,* 2010). % Seawater additions are calculated from relative Cl$^-$ compositions. *Limestone*: Gibraltar bedrock $^{87}$Sr /$^{86}$Sr from Qing et al. (2001), Ca/Sr from Bowkett (2012). Dotted error bars present the range of limestone chemistry, and solid lines the standard deviation.

Mixing between limestone and seawater aerosol end-members are calculated based on Cl$^-$

concentrations of seawater and limestone end members mixtures. The Cl$^-$ content of the drip

water (Cl$_{mix}$) is equal to the mix of Cl$^-$ from seawater (Cl$_{sw}$) and limestone (Cl$_{lst}$) end member

source components (1). This is based on the principle that all system Cl$^-$ is sourced from

seawater and that limestone does not contain Cl$^-$, an assumption which is validated later.

Consequently, the mixing function can be expressed as in (2). Analogous mixing equations to

(1) can be written to solve for Ca and Sr (3) and (4) respectively. Solving mixing equations

(3) and (4) for the carbonate end-member produces (5) and (6) and the end-member can be

determined.

$$1*Cl_{mix} = f*Cl_{sw} + (1-f)*Cl_{lst} \qquad (1)$$
$$\text{Since } Cl_{lst} = 0, \; f = Cl_{mix}/Cl_{sw} \qquad (2)$$
$$1*Ca_{mix} = f*Ca_{sw} + (1-f)*Ca_{lst} \qquad (3)$$
$$1*Tr_{mix} = f*Tr_{sw} + (1-f)*Tr_{lst} \qquad (4)$$
$$Ca_{lst} = (Ca_{mix} - f*Ca_{sw}) / (1-f) \qquad (5)$$
*where Ca$_{mix}$, Ca$_{sw}$ and f are known*
$$Tr_{lst} = (Tr_{mix} - f*Tr_{sw})/ (1-f) \qquad (6)$$
*where Tr$_{mix}$, Tr$_{sw}$ and f are known*

Results from Cl$^-$ calculations from modern drip water demonstrate that the Sr contribution

from seawater sources ranges from 13-25% (18.5% average) (Results for individual drip

samples and other elements are presented in Table 4.7). Comparisons of results using Cl$^-$ can

be compared to those obtained using Na$^+$ to test the validity of using Cl$^-$ for seawater

contributions, and tests potential Cl- losses occurring as a result of atmospheric H$^+$

interactions. Dripwater Na/Cl values averages 0.51 ($\sigma$ = 0.07) compared to seawater Na/Cl of 0.56 indicating a Na/Cl proportion which is representative of seawater source. Largely elevated Na/Cl ratios would be expected if significant $Cl^-$ losses were occurring. Average seawater contribution calculations based on Na equals 16.8% ($\sigma$ = 2.68) compared to the $Cl^-$ average of 18.5% ($\sigma$ = 2.46). The slightly lower result is likely as a result of Na contributions from bedrock. It can therefore be confirmed that Gib08 Sr isotopes are significantly influenced by the seawater chemistry contributions.

The $^{87}Sr/^{86}Sr$ data do not trend towards the seawater aerosol end-member. When observing the Sr data for drip waters inferred from the flowstone (Figure 4.20), they present a range around the inferred carbonate end-member Ca/Sr. Variable kinetics and trace element incorporation ($K_{Sr}$ 0.084 - 0.026); changing PCP and subsequent Ca/Sr; radiogenic Sr input variability; changing bedrock dissolution source; or a combination of all factors may result in the spread of data presented in Figure 4.20. Bedrock dissolution and PCP have both been recognised as influential processes affecting flowstone precipitation (Section 4.2). Due to the lack of mixing trends it is likely that the seawater influence is stable and that small changes in radiogenic terrestrial dust is resulting in the long term changes observed in Figure 4.11.

| Sample date | Ca | Na | Mg | K | Sr | Cl⁻ | SO4⁻ |
|---|---|---|---|---|---|---|---|
| 22/03/2009 | 0.83 | 101 | 6.55 | 172 | 19.2 | 100 | 13.5 |
| 29/04/2009 | 0.85 | 103 | 6.45 | 215 | 20.0 | 100 | 13.5 |
| 28/05/2009 | 0.78 | 110 | 6.53 | 296 | 17.3 | 100 | 13.6 |
| 28/06/2009 | 0.79 | 107 | 6.31 | 269 | 18.0 | 100 | 13.6 |
| 25/07/2009 | 0.87 | 105 | 6.29 | 228 | 18.6 | 100 | 13.9 |
| 30/08/2009 | 0.76 | 94 | 5.88 | 276 | 16.7 | 100 | 13.9 |
| 27/09/2009 | 1.18 | 83 | 6.55 | 277 | 15.4 | 100 | 14.2 |
| 24/10/2009 | 1.08 | 98 | 6.09 | 115 | 17.9 | 100 | 13.8 |
| 06/02/2010 | 0.85 | 112 | 6.60 | 268 | 18.0 | 100 | 16.7 |
| 06/03/2010 | 0.95 | 141 | 8.30 | 292 | 16.0 | 100 | 16.6 |
| 04/04/2010 | 0.90 | 140 | 8.11 | 214 | 15.0 | 100 | 16.4 |
| 24/04/2010 | 0.84 | 132 | 7.42 | 333 | 14.1 | 100 | 15.9 |
| 23/05/2010 | 0.76 | 111 | 6.57 | 175 | 13.2 | 100 | 15.7 |
| 27/06/2010 | 0.77 | 98 | 6.28 | - | 19.3 | 100 | 15.4 |
| 18/07/2010 | 1.15 | 95 | 6.55 | 559 | 21.7 | 100 | 15.3 |
| 28/08/2010 | 1.18 | 99 | 6.60 | - | 21.1 | 100 | 15.0 |
| 20/09/2010 | 1.36 | 109 | 7.22 | 228 | 20.0 | 100 | 14.9 |
| 22/10/2010 | 1.13 | 106 | 7.05 | 218 | 18.8 | 100 | 14.9 |
| 20/11/2010 | 1.17 | 110 | 7.50 | 208 | 20.4 | 100 | 15.4 |
| 28/12/2010 | 0.90 | 108 | 7.01 | 193 | 18.6 | 100 | 15.4 |
| 14/01/2011 | 0.86 | 99 | 6.82 | 73 | 17.8 | 100 | 15.5 |
| 23/02/2011 | 0.96 | 131 | 8.47 | 301 | 19.1 | 100 | 16.5 |
| 18/03/2011 | 0.94 | 121 | 7.66 | 266 | 17.8 | 100 | 16.3 |
| 22/04/2011 | 0.89 | 113 | 7.18 | 249 | 17.0 | 100 | 15.8 |
| 20/05/2011 | 0.93 | 113 | 7.23 | 234 | 17.2 | 100 | 15.8 |
| 17/06/2011 | 0.89 | 114 | 7.22 | 252 | 17.2 | 100 | 15.7 |
| 23/07/2011 | 1.00 | 110 | 7.10 | 254 | 18.0 | 100 | 15.6 |
| 24/09/2011 | 1.23 | 104 | 6.65 | 229 | 18.2 | 100 | 15.2 |
| 19/10/2011 | 1.29 | 108 | 7.01 | 221 | 18.8 | 100 | 15.5 |
| 25/11/2011 | 1.26 | 105 | 6.67 | 227 | 18.7 | 100 | 15.3 |
| 28/12/2011 | 1.04 | 135 | 8.97 | 286 | 22.3 | 100 | 15.5 |
| 01/02/2012 | 1.12 | 134 | 9.08 | 308 | 21.9 | 100 | 16.7 |
| 25/02/2012 | 0.99 | 119 | 7.78 | 296 | 20.2 | 100 | 14.5 |
| 21/03/2012 | 1.41 | 157 | 10.09 | 309 | 25.9 | 100 | - |
| **Max** | 1.41 | 157 | 10.09 | 559 | 25.9 | 100 | 16.7 |
| **Min** | 0.76 | 83 | 5.88 | 73 | 13.2 | 100 | 13.5 |
| **Average** | 1.00 | 112 | 7.17 | 251 | 18.5 | 100 | 15.2 |

Table 4.7: Seawater aerosol contributions. Percentage of element in drip water sourced from seawater aerosols compared to total drip water abundances.

### *4.4.5. Palaeoenvironmental interpretation*

Finally, by combining the understanding of precipitation, carbonate dissolution and aerosol contribution processes with proxy analysis it is possible to make palaeoenvironmental reconstruction interpretations.
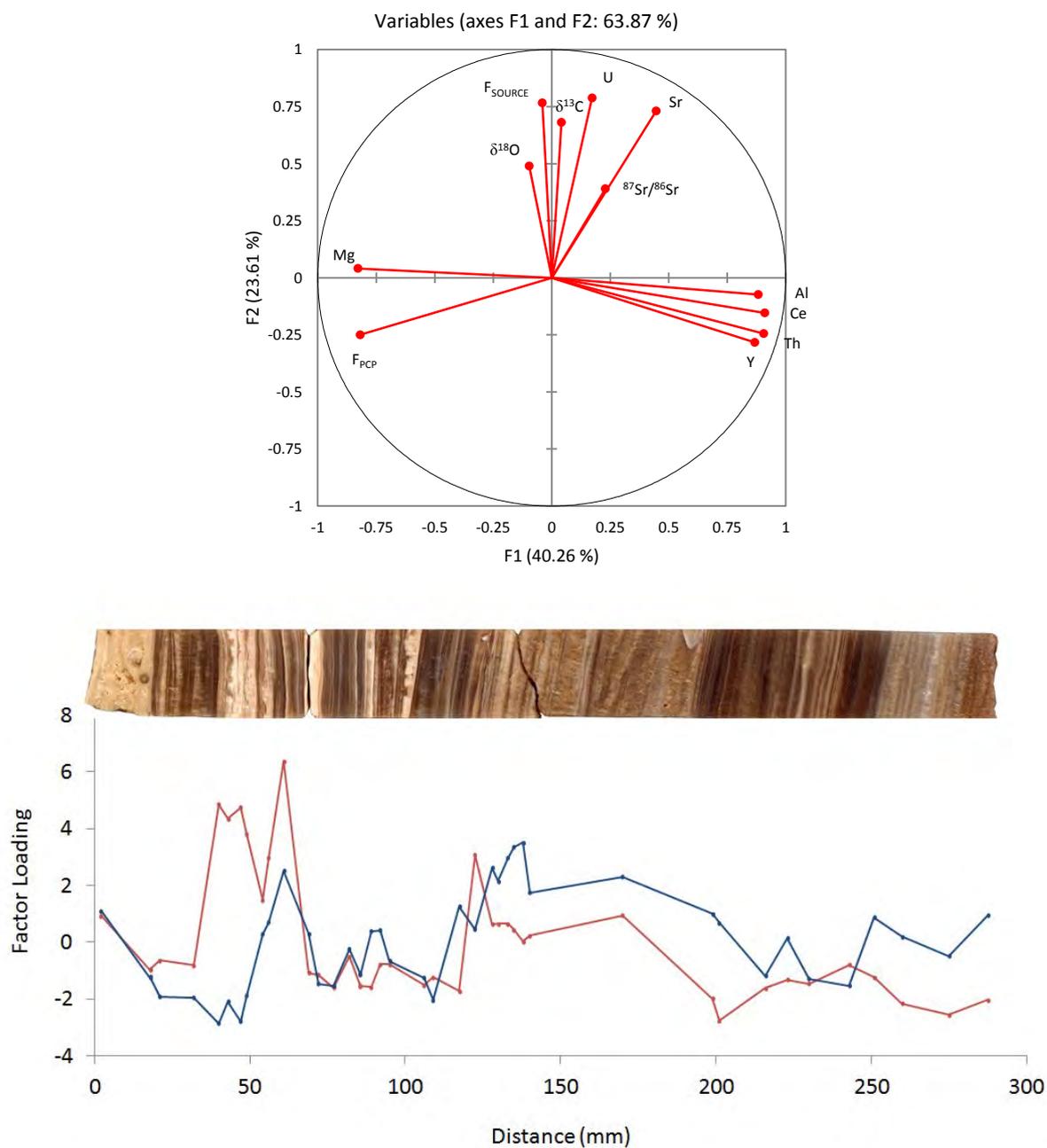
Figure 4.21: PCA (Factor 1 red, Factor 2 blue) analysis of $^{87}$Sr/$^{86}$Sr isotope results combined with stable isotope, trace element and F$_{PCP}$ and F$_{SOURCE}$ vector calculations. Sample resolution is at the intervals of $^{87}$Sr/$^{86}$Sr results.

Figure 4.21 which plots the low resolution data, including Sr, Ca and O isotopes, presents the clear relationship where groupings of elements are well separated. The strongest contribution

to flowstone trace element geochemistry is the opposing influence of colloidally derived elements and, Mg and $F_{PCP}$ as presented on factor 1. Changing discharge rates have been identified as the predominant driver in shifts between elemental groupings. Mg and $F_{PCP}$, and colloidal element groupings can therefore be considered as end members representing dry and wet conditions respectively. Therefore all proxies that fall in between these end members on factor 1 are representative of recording variability in discharge.

Gib08 $\delta^{18}O$ demonstrates long term shifts that relate to the timing of glacial cycles observed in the LR04 marine record (Figure 4.11) suggesting that long term environmental changes are observable over any local scale fractionation and flowstone precipitation effects. However, shorter term more regional sapropel events (Figure 4.18) are not recorded in the $\delta^{18}O$ record (Figure 4.11). The Gib08 flowstone sample records changing climate systems and hence $\delta^{18}O$, the flux of terrigenous dust and possibly even the flux of calcareous dust with high Sr content. As established in Section 4.4.4 $^{87}Sr/^{86}Sr$ is controlled by varying terrestrial dust fluxes to the speleothem. The weak relationship between $\delta^{18}O$ and $^{87}Sr/^{86}Sr$ can therefore be accounted for by changes in the atmospheric terrestrial dust budget occurring during glacial and interglacial periods, with glacial dust deposition at high latitudes being as much as a 25 times higher than during interglacial periods (Winckler *et al.,* 2008). $F_{SOURCE}$ and Sr fall into the same group as $^{87}Sr/^{86}Sr$ and stable isotopes indicating a relationship with climate conditions and rainfall.

## 4.5. Conclusions

### *4.5.1. Flowstone growth processes*

Modern drip water sampling demonstrates evidence for prior calcite precipitation (PCP) processes taking place. PCP results in increased Mg/Ca and Sr/Ca in the flowstone calcite and is considered in palaeoenvironmental interpretations throughout the study. Mg and Sr demonstrate influence and evolution from a mixed carbonate/dolomitic end member source.

Calculated drip water to precipitated calcite distribution coefficients $K_{Mg} = 0.019$ and $K_{Sr} = 0.062$ are appropriate and comparable to that found in the literature. Values show original solution compositions for comparison to modern drip water (Figure 4.14). Indices calculations of PCP evolution ($F_{PCP}$) and dissolution source chemistry ($F_{SOURCE}$) offer new measures offering insight into source type and the extent of PCP occurring throughout the flowstone (Gib08) growth period (explored in Section 4.4.2). Trace element geochemistry has demonstrated a record of changing wetness (Figure 4.17). Two end members have been identified with colloidal incorporation being representative of wetter periods and, dolomite dissolution and high PCP being indicative of dry periods. The relationship between the Gib08 and other palaeoenvironmental records are summarised in Section 4.5.5.

### *4.5.2. Aerosol contributions to flowstone geochemistry*

Al and Fe from aerosol deposition have been determined as the most influential elemental contribution to be preserved in the flowstone record. However, Al and Fe solution transport masks aerosol deposition and it is not often possible to distinguish between the two elemental source processes. Seawater aerosols and the Gibraltar carbonate bedrock were identified as

the two dominant contributing end members to flowstone (Gib08a) carbonate through $^{87}Sr/^{86}Sr$ and Sr/Ca analysis. Seawater aerosol influences have been identified to provide a significant elemental source to the flowstone system in the modern environment. Cl⁻ calculations demonstrate modern average contributions of variable significance e.g. 7% for Mg, 19% for Sr, 1% for Ca. Temporal $^{87}Sr/^{86}Sr$ changes are attributed to small changes of highly radiogenic dust inputs. Cl⁻ based seawater contribution calculations provide a lower bound estimate, only estimating contributions from surface deposition and drip water transport, and do not include direct intra-cave seawater aerosol deposition.

### *4.5.3. Flowstone growth variability*

U-series geochronology has enabled the identification of hiatus events and the comparison of well constrained fast growth sections. A notable finding is that trace element geochemistry identifies potential smaller duration hiatus events not recorded in the geochronology, offering an additional tool for growth analysis. Hiatus occurrence is likely controlled by local rather than climatic processes, with each hiatus marking a change in the flowstone growth system as presented in Figure 4.17. System resetting at each hiatus results in varying geochemistry for each growth section. Due to the nature of flowstone growth, samples are liable to complex stratigraphy and unpredictable geochemical systems. Periods of fast growth demonstrate some similarities, such as elevated concentrations of colloidally transported elements. Fast growth events correlate with the timing of Mediterranean sapropel events which represent periods of increased continental rainfall (Figure 4.18), summarised in section 4.5.5.

Karst hydrology has the potential to significantly alter drip water supply, independently of surface precipitation. Altering flow pathways and storage (as introduced in Chapter 1, section

1.2.1 'Flowstone formation') may result in flow diversions or cessations in drip water supply to the flowstone surface. Changing pathways or periods of upper karst drip water storage would result in hiatus events which do not represent the climate or amount of precipitation at the surface. In addition to hydrological processes, flowstone features such as terracing and lobe switching will have notable impacts on sample geochemistry and stratigraphy. Terracing may alter the layering of flowstone samples. Terracing and the pooling of drip water will influence stable isotopes by altering fractionation processes. For example, isotopic fractionation may increase at the point of dam overflow due to thinning and disruption of the water flow, altering the recorded flowstone isotopic signature. Trace element concentrations may also be influenced by terracing features. For example, pooling of water may also allow the sedimentation of colloids transported in drip waters, resulting in areas of increased colloidal flowstone content. Additionally, the movement of the active flow path due to uneven calcite precipitation will change the distribution of flowstone formation. Lobe switching of active flowstone precipitation may result in growth hiatuses at certain points on the flowstone surface, which may be recorded in the flowstone core.

### *4.5.4. Geochemical interpretation*

Figure 4.22 and Table 4.9 present a summary of inferred environmental change and key observations for each section of flowstone growth. PCA analysis of LA-ICP-MS, $F_{PCP}$, and $F_{SOURCE}$ indices results (presented in Figure 4.17) are utilised to present qualitative changes in precipitation and discharge from wetter to drier conditions. Table 4.8 presents a summary of trace element interpretations made in this investigation.

| Element | Process | Environmental interpretation |
|---|---|---|
| Mg | Mg has been interpreted to be controlled by PCP and host-rock dissolution type. Increased PCP results in increased Mg concentrations in the residual solution. Dolomite dissolution will result in increased Mg solution incorporation. | Both PCP and dolomite dissolution will occur during lower flow, drier periods. Therefore increased Mg concentrations indicates drier conditions. |
| Sr, U | Sr concentrations are controlled by PCP and host rock dissolution and oppose the geochemical signature of Mg. This is indicative of variable carbonate and dolomite dissolution. $F_{SOURCE}$ and $F_{PCP}$ indices assist in the separation of PCP and source dissolution processes. Sr presents a relationship with Sr isotopes and stable isotopes indicating an additional external environmental control. | Periods of correlating Sr and Mg are indicative of PCP, under dry conditions. Increased Sr concentration may also be indicative of increased Sr supply from bedrock dissolution under wet conditions. |
| $F_{SOURCE}$ | Variable calcite and dolomite dissolution. Increasing values of $F_{SOURCE}$ indicates greater influences from dolomite dissolution and low values suggest calcite dissolution. Low $F_{SOURCE}$ can also be attributed to influence from external factors resulting in increased Sr. | $F_{SOURCE}$ is a measure of bedrock dissolution. Increased $F_{SOURCE}$ indicates dolomite dissolution under drier conditions and reduced $F_{SOURCE}$ suggesting carbonate dissolution in wetter conditions. |
| $F_{PCP}$ | Increasing $F_{PCP}$ values indicate greater PCP influences. | $F_{PCP}$ has been interpreted to be a proxy for drip water supply rates. Increased $F_{PCP}$ represents lower flow dry conditions, and reduced $F_{PCP}$ wetter conditions. |

| | | |
|---|---|---|
| Al, Fe, Ce, Y, Th | This group of elements have been assigned to colloidally derived sources. The element group is opposed to Mg. However, Al and Fe have also been identified as an aerosol signature. Separation of aerosol and solution supply can only be established during known slow growth low flow scenarios such as hiatuses where aerosol supply will dominate. | Colloidally sourced elements suggests growth under high discharge, high flow conditions. |

Table 4.8: Summary of trace element interpretations.
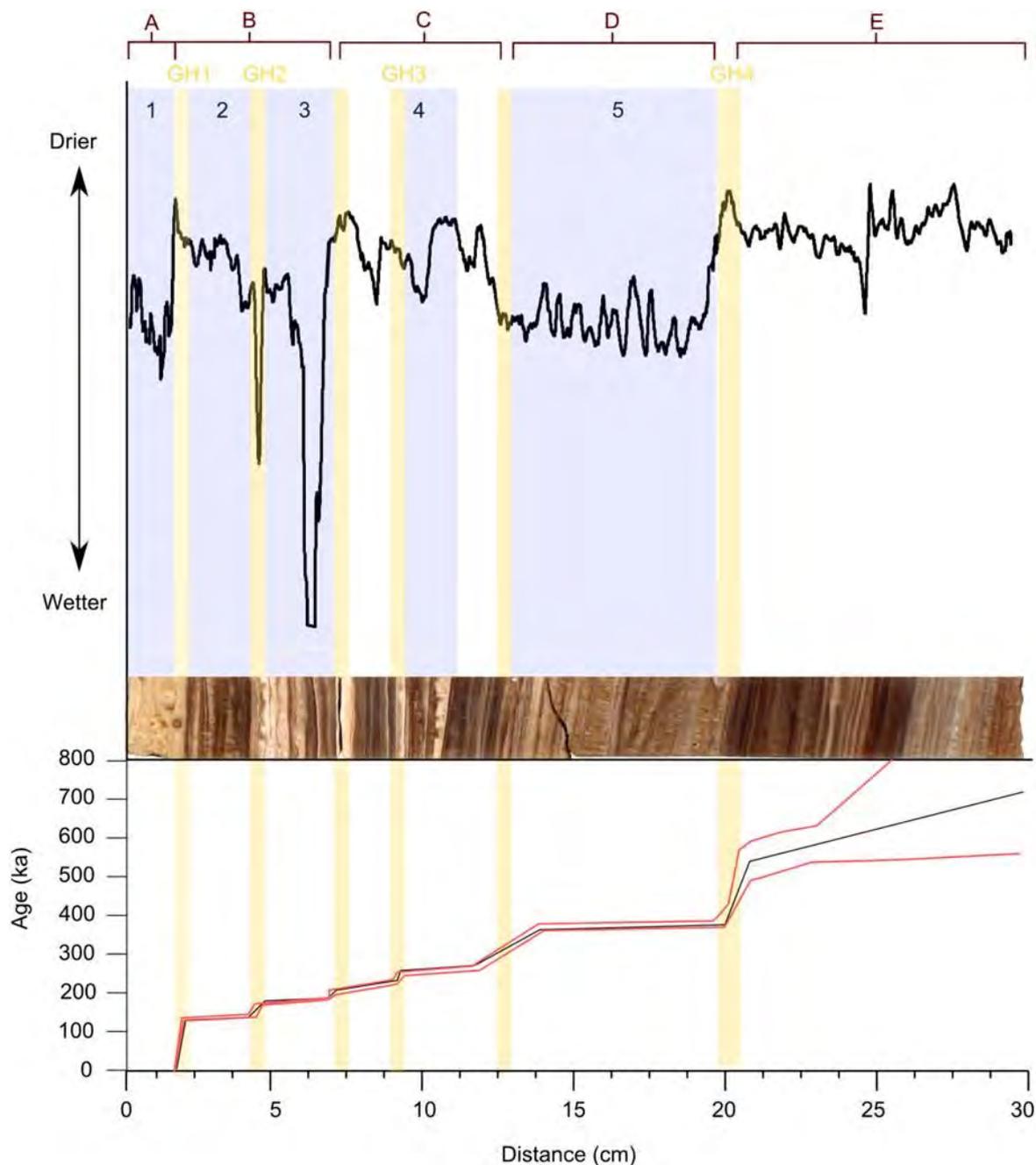
Figure 4.22: Factor 1 PCA analysis results (as in Figure 4.17) displayed with a 200 point running average line representing wetter and drier conditions, presented in the upper diagram. Flowstone image and sample geochronology presented in the lower diagram. Hiatus events are highlighted in yellow, fast growth events are highlighted in blue. Sections of notable characteristics at identified by A to E and are described in Table 4.9.

| Section | Characteristics | Interpretation |
|---|---|---|
| A | Characterised by porous growth of different coloration, geochemistry, growth rate and geochemistry to all other sections in the flowstone. | The observed contrast is indicative of a contrasting precipitation system resulting from differing local processes. The separation between this section and the rest of the core is marked by a 128ka hiatus. |
| B | Variable fabric and chemistry and interrupted by 2 hiatus events with 3 sections of fast growth identified | Cyclic periods of increasing wetness punctuated with hiatus events, each episode presents a system reset with a different geochemistry. One feature unites each section and that is the consistent influence of colloidally derived elements on speleothem geochemistry. |
| C | Variable growth punctuated by small hiatus events (micro-hiatuses) in some instances marked by microcrystalline precipitation | Each section presents system resetting. However, unlike section B each section returns to 'pre-hiatus' levels indicating some consistent baseline growth conditions throughout this period. |
| D | Geochemistry is dominated by variation in colloidally derived elements. Calcite fabric is composed of stable and constant development of large columnar crystals. | Both fabric and chemistry are suggestive of fast flow conditions. The stable growth throughout the period indicates relatively continuous and stable drip water supply. |
| E | Geochemistry presents greater variability than section D; however growth is defined by homogenous growth of fibrous calcite. An even distribution of layering is observed throughout. | The stable nature of formation suggests constant formation processes and that hydrological or environmental changes are driving geochemical variation. |

Table 4.9: Key characteristics and interpretations of growth sections A to E.
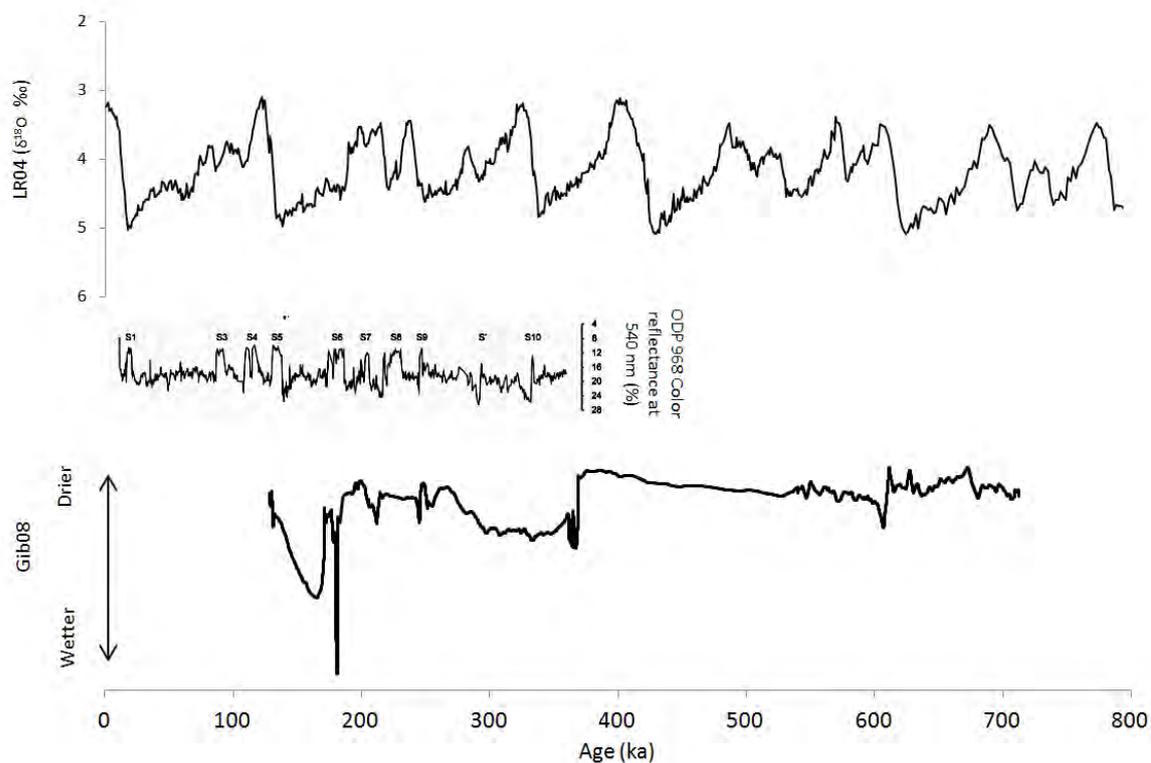
Figure 4.23: Gib08 Factor 1 PCA analysis results (as in Figure 4.17) displayed with a 200 point running average line representing wetter and drier conditions (lower graph) compared to the ODP Eastern Mediterranean marine sediment reflectance record – S1-10 mark sapropel layers (Ziegler et al., 2010) and LR04 $\delta^{18}$O deep sea record (Lisiecki & Raymo, 2005).

### *4.5.5. Palaeoclimatic interpretation*

Broad glacial-interglacial climatic shifts are recorded, indicating the strength of climatic processes over local processes such as PCP and bedrock dissolution processes during flowstone formation (Figure 4.11). Fast flow events occur during the timing of Mediterranean sapropel events (Figure 4.18) indicating a correlation with periods of increased terrestrial rainfall (as explored in section 4.4.3). Relationships between $^{87}Sr/^{86}Sr$ and $\delta^{18}O$ potentially represent glacial-interglacial shifts associated with changes in air circulation patterns and dust budgets as explored in Section 4.4.5. It has been demonstrated that the Gib08 flowstone sample records changing discharge and precipitation, the separation of these processes results in the broad relationships between local processes (PCP and bedrock dissolution) and those occurring externally (precipitation chemistry, dust fluxes).

# Black coloration of the Yarrangobilly flowstones: An investigation into forest fire aerosol and microbiological coloration processes



*Harrie Wood cave decorations with black coloration of horizontal surfaces.*

# Chapter 5: Black coloration of the Yarrangobilly flowstones: An investigation into forest fire aerosol and microbiological coloration processes

## 5.1. Introduction

Two Yarrangobilly cave sites, New South Wales (NSW), have been chosen for investigation stimulated by an existing working hypothesis of Australian scientists that black coloration of speleothem and cave surfaces there are the result of aerosol deposits from fires. The region is prone to fires and there is anecdotal evidence of the cave filling with smoke during modern fires. In 1985, fires burning for 3-4 weeks reaching within 15-20 km of Yarrangobilly caused the caves to fill with thick smoke. Yet, in 2003 fires burnt directly over Jersey Cave and, 24 hours after the event no smoke was seen in the cave with only a few tiny charcoal fragments within a few metres of the cave entrance (Andy Spate per. comm.). The black coloration only occurs on horizontal surfaces and this has been interpreted to be an indication of aerosol deposition, a feature which is displayed in the chapter cover page images (page 178).

This study aims to determine the extent of forest fire contributions to Yarrangobilly flowstones. Extensive excavations of flowstone were carried during the transformation of Yarrangobilly caves for public access. Consequently, a large resource of flowstone was available for analysis. Flowstone chemistry is investigated in an attempt to identify environmental processes which control coloration. Aerosol contributions to both organic and

inorganic chemistry are explored and their impact on flowstone geochemistry evaluated. This investigation seeks to find a unifying interpretation for flowstone coloration in Yarrangobilly caves and any potential links to cave aerosol deposition.

### *5.1.1. Yarrangobilly climate and fire history*

In modern Australia, arid climatic regimes characterise much of the continent and one-third of the landmass receives an annual rainfall of less than 250 mm (McLaren & Wallace, 2010), with approximately half of the land mass arid or semi-arid (Fitzsimmons *et al.*, 2013). However, the Snowy Mountains where Yarrangobilly caves are located have a more alpine/highland climate with cooler temperatures and winter snow. The warmest month is January with a mean minimum and maximum of 11.4 ℃ and 21.5 ℃ respectively. Coldest winter temperatures are in July of mean minimum -0.8 ℃ and mean maximum 3.9 ℃. Rainfall peaks in August producing 114.1 mm on average, with lowest rainfall occurring in January averaging 46.4 mm (MLA, 2014).

Millennial scale climate change in Australia broadly follows global climatic change and marine isotope stages (MIS), with shifts between wet and dry phases (Harle, 1997). Wet phases may have lagged 5-15 ka behind world temperature and sea level maxima, however there is some uncertainty surrounding the dating accuracy (Harle, 1997). Due to the nature of sedimentological records, few palaeoenvironmental reconstructions have been attempted beyond MIS 5 (Harle, 1997).

It is generally accepted that wettest conditions occurred during interglacial periods (Chappell, 1991). Modern vegetation type composition was established during the onset of the Holocene

(Chappell, 1991). The early and mid-Holocene were generally characterised by moderately humid conditions, demonstrated by lake level rise, source-bordering dune activity, and speleothem growth (Fitzsimmons *et al*., 2013). A weaker wet phase has been observed at 35-55 ka B.P (Bowler, 1986; Nanson *et al*., 1992). The timing of a later peak in fluvial aridity is debated to be 110 ka B.P. (Nanson *et al.,* 1992) at MIS 5e (Harle, 1997) or at the latter part of MIS 5 (Kershaw & Nanson, 1993).

Cold intervals of the late Pleistocene glacial cycles were arid in all parts of Australia (Hesse *et al*., 2004). Increasingly arid conditions developed into the late Holocene (Fitzsimmons *et al*., 2013) with driest conditions occurring at the Last Glacial Maximum (MIS 2) (Harle, 1997; Kershaw *et al,* 2007). Australian aridity is associated with dune building, a decrease in river and lake levels, and thinning vegetation in palaeoenvironments (Nanson *et al.,* 1992; Harle, 1997; Kershaw *et al*., 2007).

Fire events emit vast quantities of aerosol matter into the atmosphere, easily recognisable as smoke. A range of techniques are used to reconstruct past fire regimes often involving dendrochronology and sediment records (reviewed in Condera *et al*. 2009– techniques used in this investigation is outlined in Section 1.3). Australian forest fire frequency during the Quaternary varied temporally and regionally with glacial-interglacial cyclicity (Lynch *et al.,* 2007). Almost counter-intuitively, Australian forest fire burning was reduced in drier areas, but increased in relatively wetter areas where fuel levels were high (Lynch *et al*., 2007). However, sediment charcoal evidence suggests that fires were of greatest significance during the interstadial MIS 5c and the Last Glacial stage 2, with the latter possibly associated with anthropogenic activity (Harle, 1997). The incidence of fire over space and time is influenced

by complex interactions between climate, fuels, and ignition (Power *et al*., 2008), with each of these variable changing significantly throughout the Australia's history.

### 5.1.2. Flowstone coloration

Flowstone samples are utilised in this investigation because they are the primary resource displaying black calcite coloration and are readily available from previous cave management activities. Additionally, the variable growth rates and colloidal content often observed with flowstones are beneficial for determining changing environmental processes. However, the disadvantage of using these samples is it that their original cave locations are not known.

Speleothem colour can be caused by various impurities, pigments, and physical processes (White, 1997). Previous investigations have had problems determining the origin of coloration because a very small amount of a substance within or between the lattice of otherwise colourless calcite crystals may be sufficient to intensely colour a speleothem (Doerr *et al*., 2007). Suggestions for colouring agents include: host rock inorganic residue such as Mn, Fe or S compounds, organic traces such as organic acids, or airborne black carbon soot from wildfires (Doerr *et al*., 2007). White (1997) summarises the cause of speleothem coloration as: orange, tan and brown prodcued from humic and fulvic acids; blue, yellow and other colours due to metal ions; deep red from ferric oxides and hydroxides; and black from manganese oxides and carbon.

Red speleothem coloration is often attributed to, and associated with increased Fe concentrations. Black and red coloration are often observed in the same caves due to varying Mn and Fe contents respectively. Fe and Mn deposits were found to coat walls, floors and

ceilings forming over clay depositions and as part of flowstones in El Soplao Cave (Cantabria, Spain). Here, coloration is attributed to mobilisation of polymetallic sulphides in the host rock (Gázquez *et al.,* 2011). Black manganese oxide mineral coatings throughout a range of American caves were studied in White et al. (2009).

Black coloration has also been observed and attributed to the incorporation of aerosols from combustion from modern pollution (Jeong *et al.,* 2003; Chang *et al*., 2008) and human activity within caves (Steelmann *et al.,* 2002; Gradziński *et al.,* 2007). However, no records of natural forest fire influences have been presented in the literature. It should be noted at this point that, where combustion has been identified as the main cause of coloration, red coloration is not observed in association with black colour in the speleothem. The presence of red and black coloration together is therefore a preliminary indicator of Fe and Mn contributions.

Organic content of speleothems and coloration by bacteria and fungi is a developing sector of speleothem science, which is investigated further in section 4. However, an example of black coloration at Nullarbor caves, Western Australia, has been attributed to disseminated humic matter incorporated during speleothem growth (Blyth *et al.,* 2010). Goede et al. (1990) considered the coloration a cause of the small but significant amount of organic carbon found in the speleothem. An earlier study by Caldwell et al. (1982) determined that Fe, Mn, clay minerals and organic compounds are the pigments responsible for coloration.

### *5.1.3. Fire proxies*

Organic palaeofire proxies utilised in this study for speleothem investigation are introduced here.

Levoglucosan is a monosaccharide anhydride only produced during the combustion of woody material at temperatures of greater than 300 °C (Simoneit, 2002) and is therefore uniquely associated with higher-temperature forest fires. Methoxylated phenolic compounds (methoxyphenols) and levoglucosan (a sugar anhydride) have been suggested as a potential biomarker out of the hundred of compounds present in wood smoke (Simpson *et al.*, 2004). Levoglucosan is emitted at high concentrations during forest fires and is globally pervasive in its distribution (Simoneit *et al.* 1999; Kehrwald *et al.*, 2010).

Polycyclic aromatic hydrocarbons (PAHs) are ubiquitous pollutants sourced from the incomplete combustion biomass of fossil fuels (Kehrwald *et al.*, 2010). PAH are globally significant since they can be transported over global distances by wind systems (Gabrieli *et al.*, 2010); there is therefore a global PAH background signal with regional increases with proximity to the PAH source.

Charcoal analysis of lake sediments is often used as a tool for studying fire history (Whitlock & Larsen, 2001). Charcoal is a signature of biomass burning worldwide and its presence in the sedimentary record can shed light on the temporal and spatial characteristics of palaeofires (Buckman *et al.*, 2009). Charcoal particles are visually recognizable as opaque, angular and usually planar, black fragments which fracture into smaller angular fragments under pressure.

Charcoal can be detected through thin-section and image analysis, and separation by sieving or chemical extractions (Whitlock & Larsen, 2001).

The ability to utilise these proxies in speleothems will be highly dependent on the level of incorporation and preservation that occurs. Incorporation will be controlled by the transportation and deposition of the proxy to the speleothem. The level of preservation will be reliant on the robustness of the compound against alteration or removal processes which may prove low for aromatic organic compounds.

### *5.1.4. Location*

Yarrangobilly Caves are situated within Kosciusko National Park, which is located on the NSW Southern Tablelands, approximately 77 km SE of Tumut and 110 km NW of Cooma. The cave entrances are located in the Yarrangobilly river valley (Figure 5.1, Photograph D). The region is covered in vegetation, much of which was damaged in the 2003 forest fires, and damage in the region is still visible. The types of vegetation can be seen in most surface Photographs, with B, D and G providing an overview; Photograph H displays the Yarrangobilly River valley.

Photo A


Photo B


Photo C


Photo D



# Yarrangobilly Caves

Harrie Wood

Jillabenan Cave

Jersey Cave

Glory Hole

Yarrangobilly River

Shed

1094

1100

| Roads | Path |
|-------|------|
| Contours | Photo & direction |
| Water way | 250m |

QUEENSLAND — Brisbane

NEW SOUTH WALES

Yarrangobilly Caves — Sydney

VICTORIA — Canberra — Tasman Sea

Melbourne

200 miles / 200 km
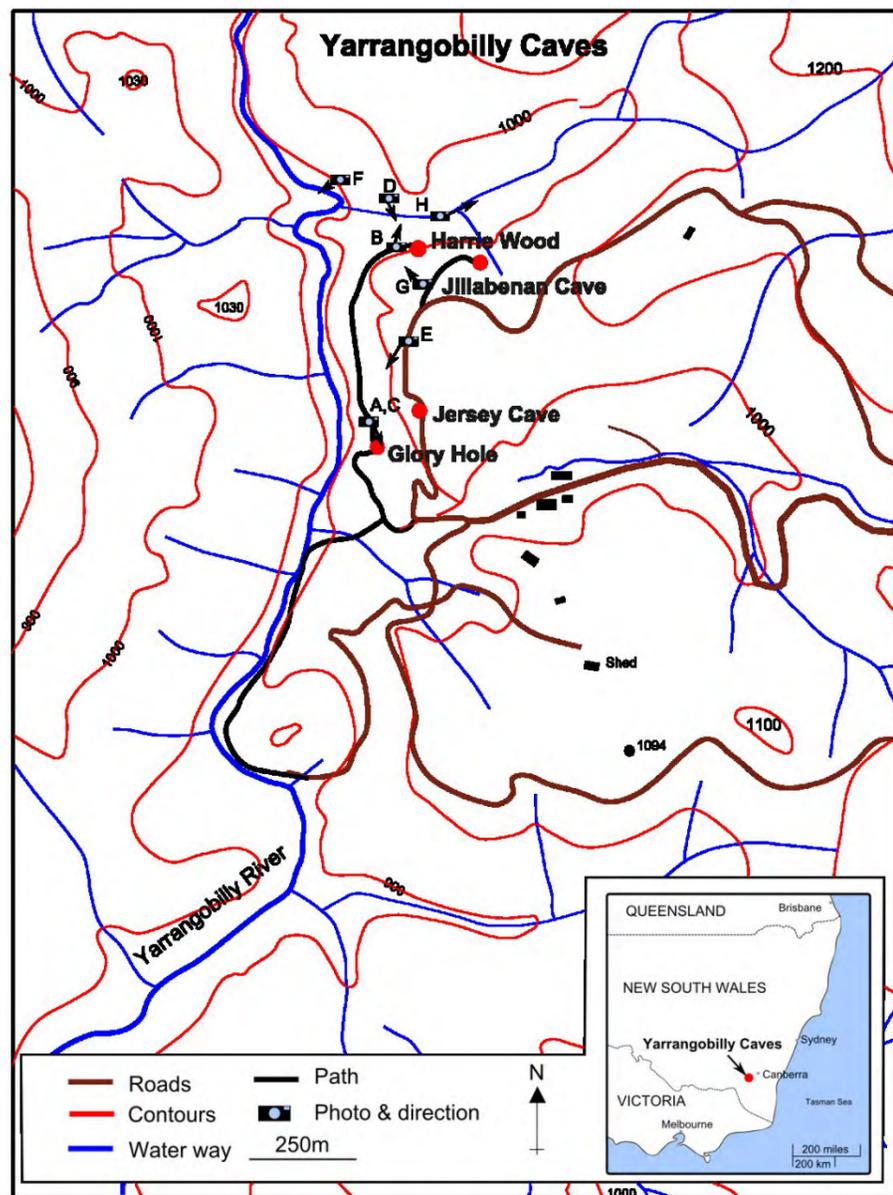
Figure 5.1: Yarrangobilly caves regional map with state map inset.


Photo E


Photo F


Photo G


Photo H
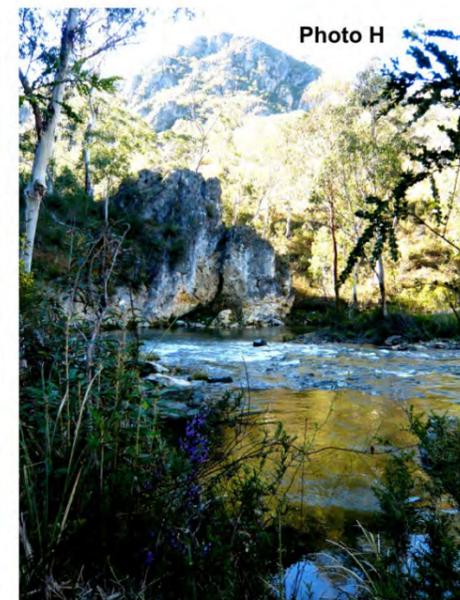
### *5.1.5. Geology*

The limestone at Yarrangobilly is of Late Silurian age and formed approximately 440 million years ago. The limestone occurs in a belt that is approximately 14 km long and 1.5 km wide (Rose, 1964) with steeply dipping, strike-controlled outcrops (Osborne & Branagan, 1988) and is overlain by slates, shales, sandstones and conglomerates of the Ravine Beds. Photograph F displays the Yarrangobilly limestone outcropping directly above Harrie Wood cave and Photograph C is the same limestone outcropping on the other side of the creek. The karst forms are impressive with large exposed sink holes (Photograph E) and long wide caves. Soils are predominantly categorised by loam to clay composition, red/dark orange in colour, with red Ferrosols overlying the Jersey cave location. Owing to the semi-arid climate the Yarrangobilly soil profile is thin, ranging in thickness from 0-30 cm. At the Jersey site location no O layer was observed, with soils showing a light clay A layer to a depth of 20 mm. A gradual transition to a light clay B horizon is presented at a depth of 50-100 mm. Overlying vegetation is characterised by dry sclerophyll forest vegetation made up of trees, lichens, shrubs, and tussock grasses (NSW Department of Environment and Climate Change, 2012).

### 5.1.6. Cave descriptions

*Harrie Wood Cave*

The location of Harrie Wood is shown in Figure 5.1 and its entrance is in a creek that feeds into the Yarrangobilly River valley. Photograph B shows the creek looking from the Yarrangobilly River towards the cave entrance. A cave map is presented in Figure 5.2, with sampling locations HW1 and HW2 marked on the map. The cave is approximately 70 m long and descends approximately 50 m from the entrance along its length. A stepped path has been carved through the cave and large excavations of flowstone have been carried out during the construction. The cave is well decorated in the open chambers as shown in Photographs J, K, L; the images clearly display the black coloration that has been thought to be from forest fires.

*Jersey Cave*

The location of Jersey cave is shown in Figure 5.1. Jersey cave is larger than Harrie Wood and has more speleothem decoration as shown in images Figure 5.3, Photographs N to Q. Unlike Harrie Wood cave, Jersey Cave has only a slight vertical change along its length as shown in the section map view in Figure 5.3. Photo O displays how modern calcite growth is forming without the black coloration; this can also be seen at Harrie Wood in Photo L. Photograph Q shows the contrast in coloration between horizontal and vertical surfaces, with only horizontal surfaces having the black coloration.
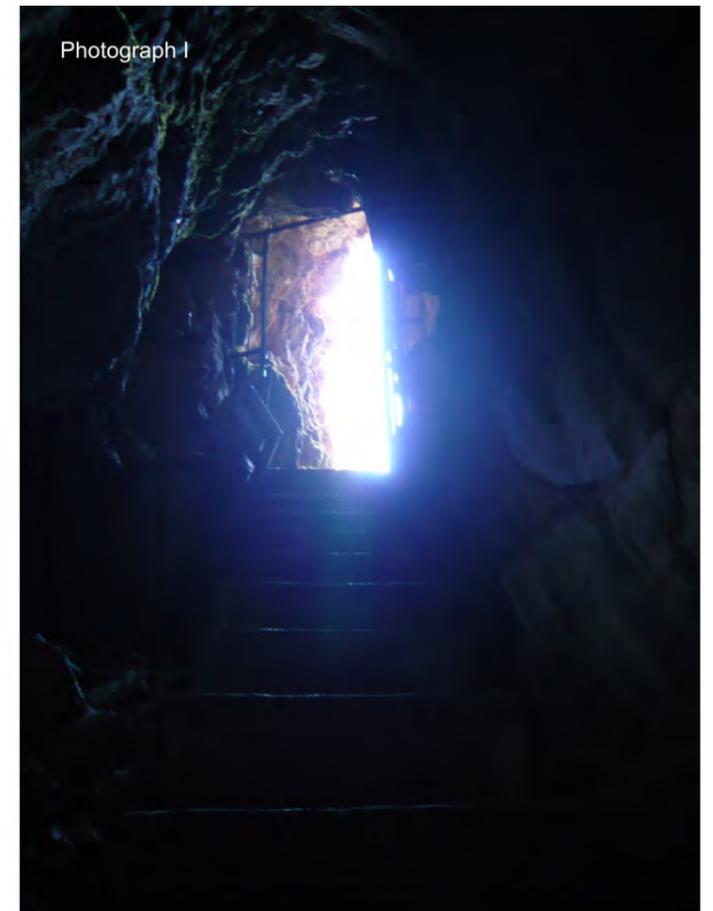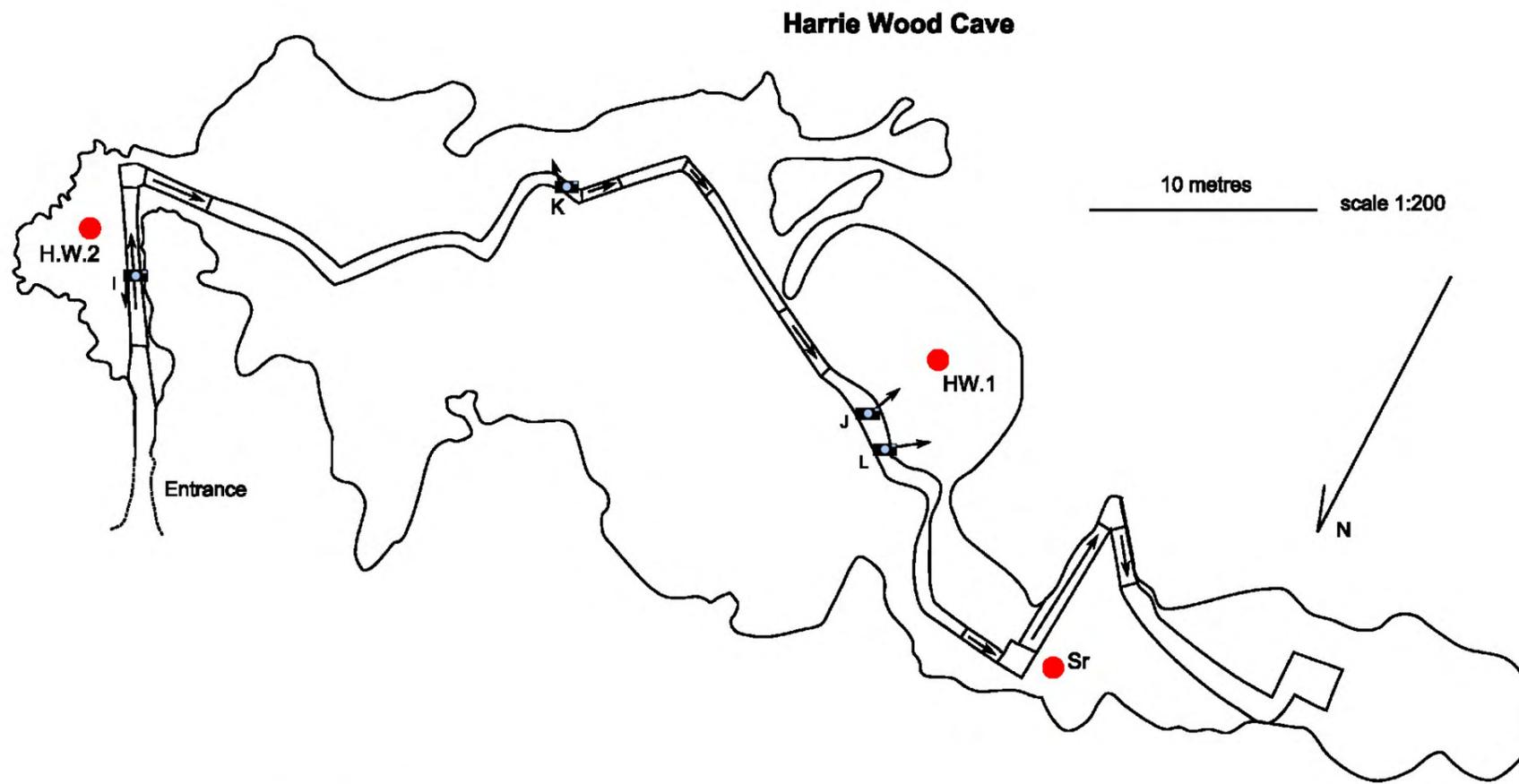
Figure 5.2: Cave map of Harrie Wood Cave. Sample locations marked by red circles. Photograph locations and view directions marked

201

# Jersey Cave

Plan

Entrance

AJ.2

O    Q    N    P

AJ.1

M

N

Section

Entrance

10 Metres
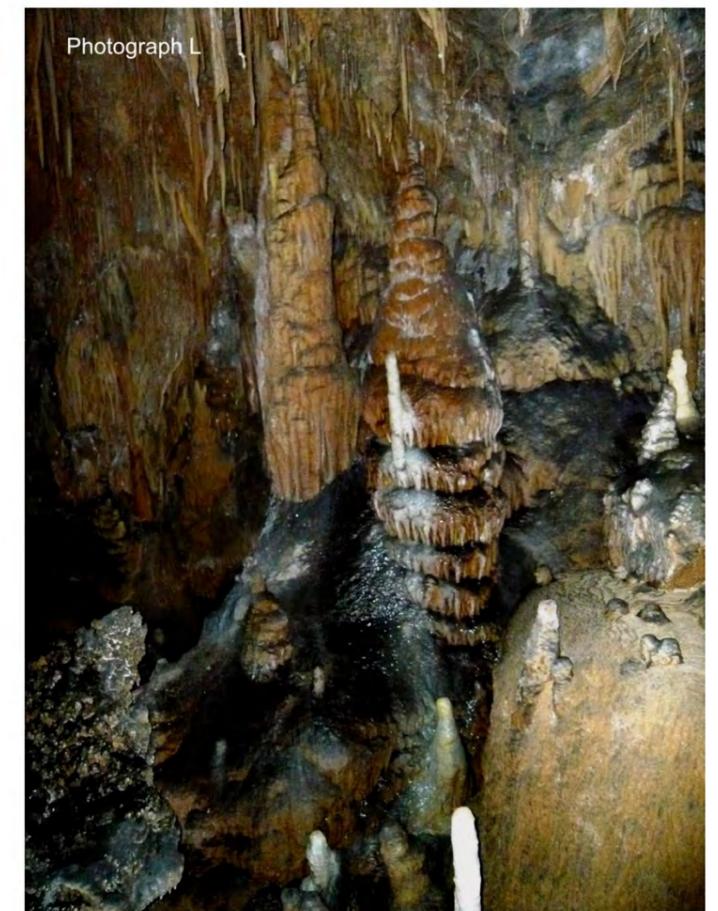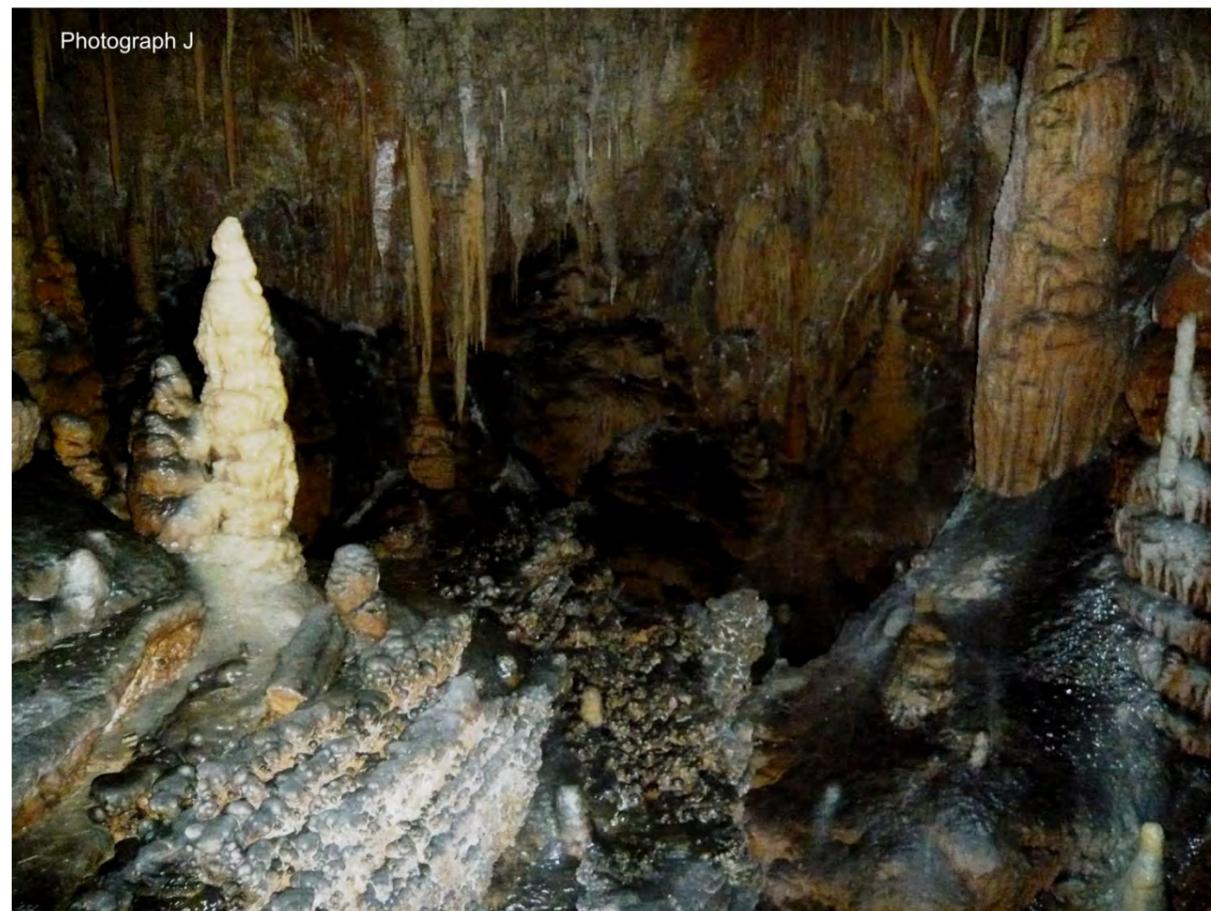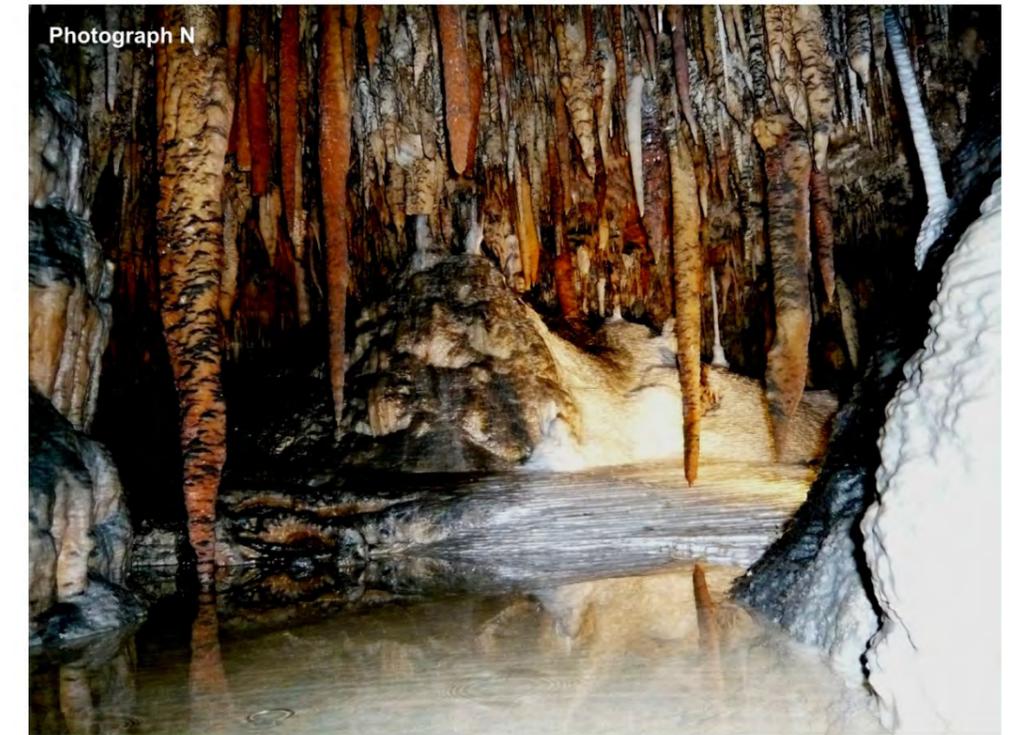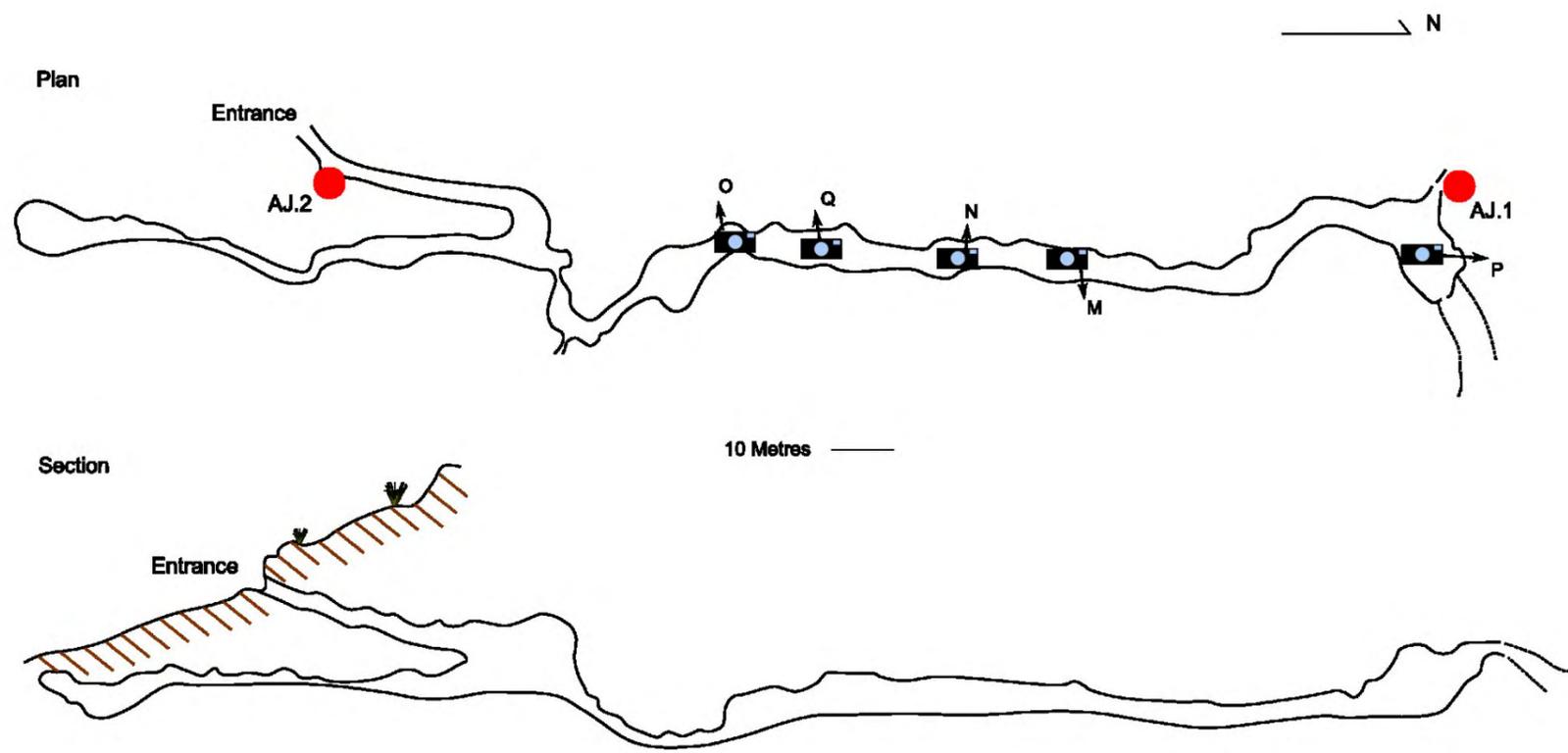
Figure 5.3: Jersey Cave map. Sample locations marked by red circles. Photograph locations and direction of view also marked.

Photograph M

Top

Photograph N

Photograph O

Photograph P

Photograph Q
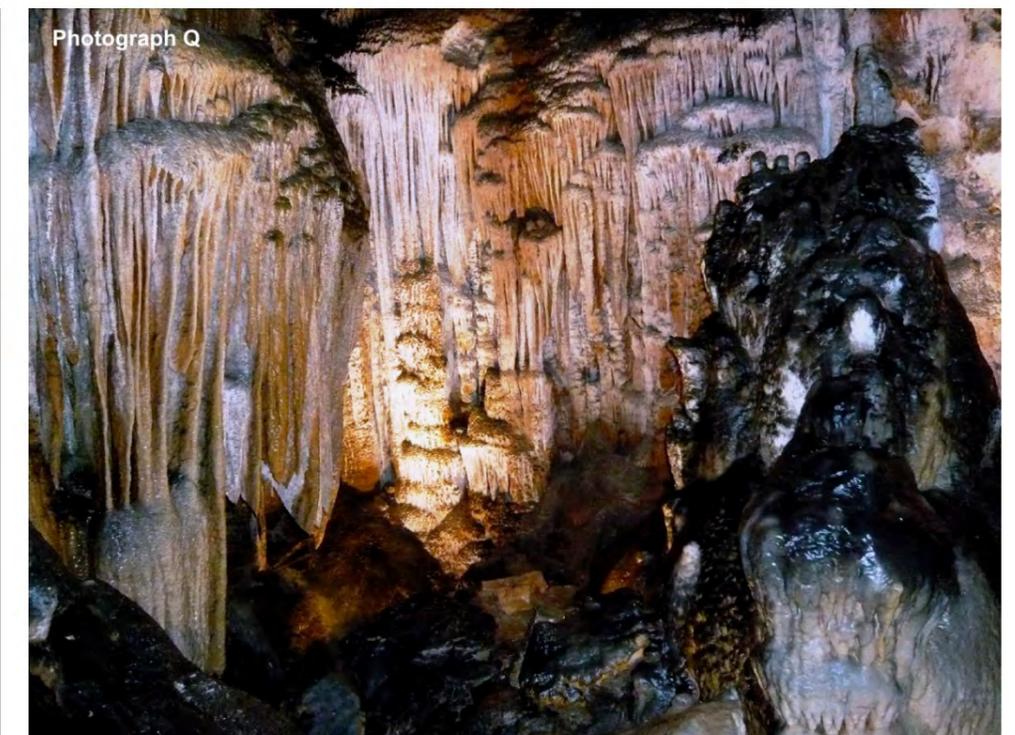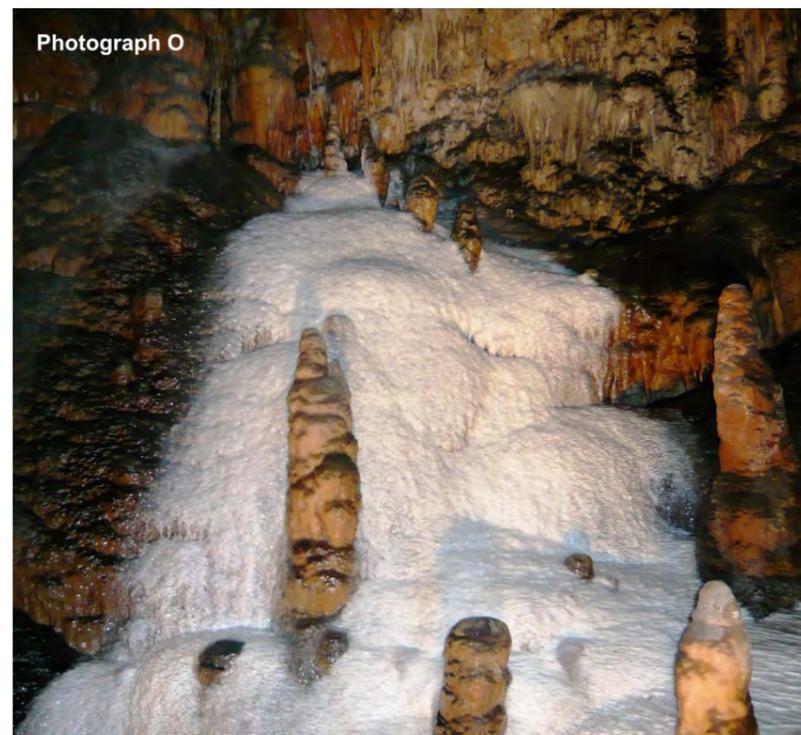
## 5.2. Methods

Further details of all methodologies employed in this investigation are described in the supplementary material sections S.1.- S.14.

### *5.2.1. Aerosol sampling*

*Inorganic surrogate surfaces*

Sampling apparatus were placed for both inorganic and organic components. Surrogate surface locations have been marked on the cave maps for both Harrie Wood and Jersey caves as shown in Figure 5.2 and 5.3 respectively. Petri dishes were used as surrogate collection surfaces. Glass petri dishes were cleaned in a 5% $HNO_3$ acid bath for a minimum of 24 hours, then triple-rinsed with double de-ionised water (DDIW). Surrogate surfaces were sealed before and after sampling to minimise external contamination. Further sampling details can be found in the supplementary material, section S.1.

*PAH surrogate surfaces*

PAH collection surface glass petri dishes and quartz filters were cleaned by heating at >450°C for a minimum of 5 hours (as of: Leister & Baker, 1994; Odabasi *et al* 1999; Vardar *et al*., 2002; Bozlaker *et al.,* 2008) to ash any potential organic contamination. Filters were placed in cleaned petri dishes and sealed as with inorganic aerosol methods, for transport.

*5.2.2. Inorganic analysis*

*Speleothem LA-ICP-MS*

Sections of samples were mounted in a single resin block and polished. Samples were ultrasonicated in DDIW for 5 min before loading into the ablation cell. The cell was then flushed through repeated cell evacuation and helium backfilling to create an oxygen free atmosphere and ensure the best outgassing of connate gases in sample pores. The analytical system used at the University of Melbourne comprises of a 193-nm ArF excimer laser, ablating in helium coupled to an Agilent 7700 quadrupole ICPMS. (Woodhead *et al*., 2005; Woodhead *et al*., 2012). Pre-ablation was performed to reduce sample surface contamination before data collection. In this case a larger aperture size than for the planned ablation for data collection was used, with a slit size of $400 \times 70$ µm, laser repetition rate oft 15 Hz, and stage translation speed of 0.12 mm/second.

Data collection was performed using a $23 \times 300$ µm slit size with a laser repition rate of 10 Hz and stage translation speed of 0.02 mm/second. The rectangular slit has the benefit of increasing the representative nature of each sample by sampling more calcite for each growth period. Elements were chosen for analysis based on an existing and established method framework with some modifications for speleothem analysis: Ca, Na, Mg, Al, P, Mn, Fe, Zn, As, Sr, Y, Nb, Sn, Sb, Ba, Ce, W, Tl, Pb, Th, U. Concentrations were calculated from a calibration using the NIST612 reference material (Further details on data calibration are displayed in the supplementary material, section S.13.). The element list used was a previously established method and different to those used for the Gibraltar sample (Chapter 4).

*ICP-MS analysis*

Both collected aerosol and solid carbonate were analysed by ICP-MS at Melbourne University School of Earth Sciences for the determination of trace element compositions. Aerosols were extracted from surrogate surfaces with multiple DDIW washes. Extraction solutions were then acidified to 2% with $HNO_3$ before analysis. YBJD1 flowstone samples were dissolved in $HNO_3$ and HF for ICP-MS analysis. Additionally, another large (60 g) section of YBJD1 flowstone sample of black calcite was dissolved for residue analysis (Full method detail are presented in the supplementary material, section S.12). HCl was progressively added to the flowstone sample until complete dissolution was achieved. The solution was then dried and rinsed by 5 DDIW washing and centrifuging cycles. The sample was split, with a sub-sample being used for SEM analysis. HCl was used for dissolution initially to preserve organic content for investigation. The remaining HCl dissolution was then subsequently dissolved in $HNO_3$ and rinsed (as above) to obtain the $HNO_3$ residue. Sample solutions were spiked with an internal standard (containing Rb, Re, Li, Sr, U) and diluted 3000-4000 times with 2% $HNO_3$ as in Eggins et al. (1997) and Zhou (2008). Analysis was carried out using an Agilent Technologies 7700 series Quadrupole Inductively Coupled Mass Spectrometer (Q-ICP-MS). Further details on extraction methods are displayed in the supplementary material, section S.10.

*U-disequilibrium dating*

Radiometric disequilibrium dating was conducted at the University of Melbourne, Australia. Samples were dissolved and chemically separated to elute non-analyte elements. Isotopic analysis (of $^{229}Th$, $^{230}Th$, $^{232}Th$, $^{233}U$, $^{234}U$, $^{235}U$, $^{236}U$) was carried out using a Nu Plasma multi-collector inductively coupled mass spectrometer (MC-ICP-MS). Harwell Uraninite

(HU-1) and Yarrangobilly flowstone stock (YB-1) were used for calibration and as secondary reference materials, respectively. Further details on the chemical separation method can be found in the supplementary material section S.11. and details of the analytical procedure can be found in Hellstrom (2003, 2006).

### 5.2.3. Organic analysis

*Sample preparation*

Flowstone samples of interest were sectioned and leached in high-purity $HNO_3$ to remove surface contamination. Sectioned samples were powdered and then placed in cleaned glass vials. All equipment, utensils, aluminium foil and glass vials were sequentially cleaned with DDIW water, HPLC grade methanol and GC grade Hexane. Samples were obtained representing both black and white calcite: 10 g was collected for carbohydrate analysis and 5 g samples were powdered for PAH analysis (×3).

*Speleothem PAH*

A solvent-extraction method was used for both surrogate surface and crushed carbonate samples. Carbonate or aerosol filter samples were covered in 10 mL of Dichloromethane (DCM) and internal standard added. Samples were capped and shaken for 2 hours to homogenise them. PAHs were analysed with GC-MS at the Environmental Health Sciences laboratories, University of Birmingham. PAH extraction methods are showed in more detail in the supplementary material, section S.4.

*Levoglucosan and methoxyphenols*

Analysis was carried out as in Zangrando et al. (2013). To avoid external sample contamination, preparation was performed under a clean air flow. Extraction was carried out using established Levoglucosan (Perrone *et al.,* 2012) and acrylamide (Zangrando *et al*., 2013) procedures. The acrylamide procedure was used for the determination of syringaldehyde and p-coumaric acids. Samples were extracted in methonal and spiked with 3 ng of vanillic acid $^{13}C_1$, 17 ng of vanillin $^{13}C_6$, and 2 ng of acrylamide $^{13}C$ as internal standards. The Levoglucosan protocol was used for the determination of levoglucosan, vanillic acid, homovanillic acid, syringic acid, ferulic acid, and coniferyl aldehyde. Samples were extracted in water and then spiked with 750 ng of levoglucosan $^{13}C_6$, 3 ng of vanillic acid $^{13}C_1$, and 17 ng of vanillin $^{13}C_6$ as internal standards. Analysis was carried out using Agilent 1100 Series HPLC system (Agilent, Waldbronn, Germany) with a binary pump, vacuum degasser, autosampler, and thermostatted column compartment. For the chromatographic analysis, 100 μL of the sample was injected into a Zorbax Extend C18 (150 mm × 4.6 mm, 3.5 μm, Agilent) column with an elution flow of 500 μL min$^{-1}$. Analysis was carried out by Roberta Zangrando at the Institute for the Dynamics of Environmental Processes-CNR (CNR-IDPA), Italy.

*Surface DGGE*

Denaturing gradient gel electrophoresis (DGGE) was used for surface microbiological DNA identification. Polymerase chain reaction (PCR) was used to amplify the 16S rRNA gene for bacterial identification. DGGE is used to separate out these copies based on the order of bases that they have (G, C, A and T). Separated DNA bands from the gel are sequenced using Sanger sequencing. Analysis was carried out by Rich Boden at the University of Plymouth.

**5.3. Results**

**YBJD 5**

53(+/-)2.5 ka
316(+/-)12ka
264(+/-)18ka
fail
fail
357(+/-)28ka
468(+/-)46ka

5cm

**YBJD 2**

45(+/-)3ka
106(+/-)1ka
152(+/-)44ka
208(+/-)7ka
245(+/-)7ka
fail
290(+/-)8ka
409(+/-)32ka

5cm

**YBJD 1**

-18(+/-)90ka
7.6(+/-)20ka
14(+/-)23ka
32(+/-)6ka
47(+/-)6ka
88(+/-)1.5ka
92(+/-)1.4ka
122(+/-)31ka
110(+/-)7ka

5cm

**YBJD 6**

420(+/-)45ka
Fail
334(+/-)23ka

5cm

**YBJD 7**

18(+/-)32ka
63(+/-)8ka
105(+/-)3ka
75(+/-)17ka

5cm

**YBJD 11**

276(+/-)672
632(+/-)223ka

5cm

**YBJD 10**

5cm

**YBJD 4**

437(+/-)46ka
516(+/-)101ka
Fail
518(+/-)103ka
815(+/-)657ka

5cm

**YBJD 3**

Fail
Fail
337(+/-)710ka
Beyond U-Th

5cm

**YBJD 9**

589(+/-)126ka
626(+/-)186ka
882(+/-)337ka
Beyond U-Th
Beyond U-Th

5cm

**YBJD 8**

53(+/-)1496ka
853(+/-)337ka
684(+/-)232ka
298(+/-)556 ka
766(+/-)1279ka
400(+/-)59ka
Fail

Figure 5.4: U-series dating results for Yarrangobilly flowstone samples.
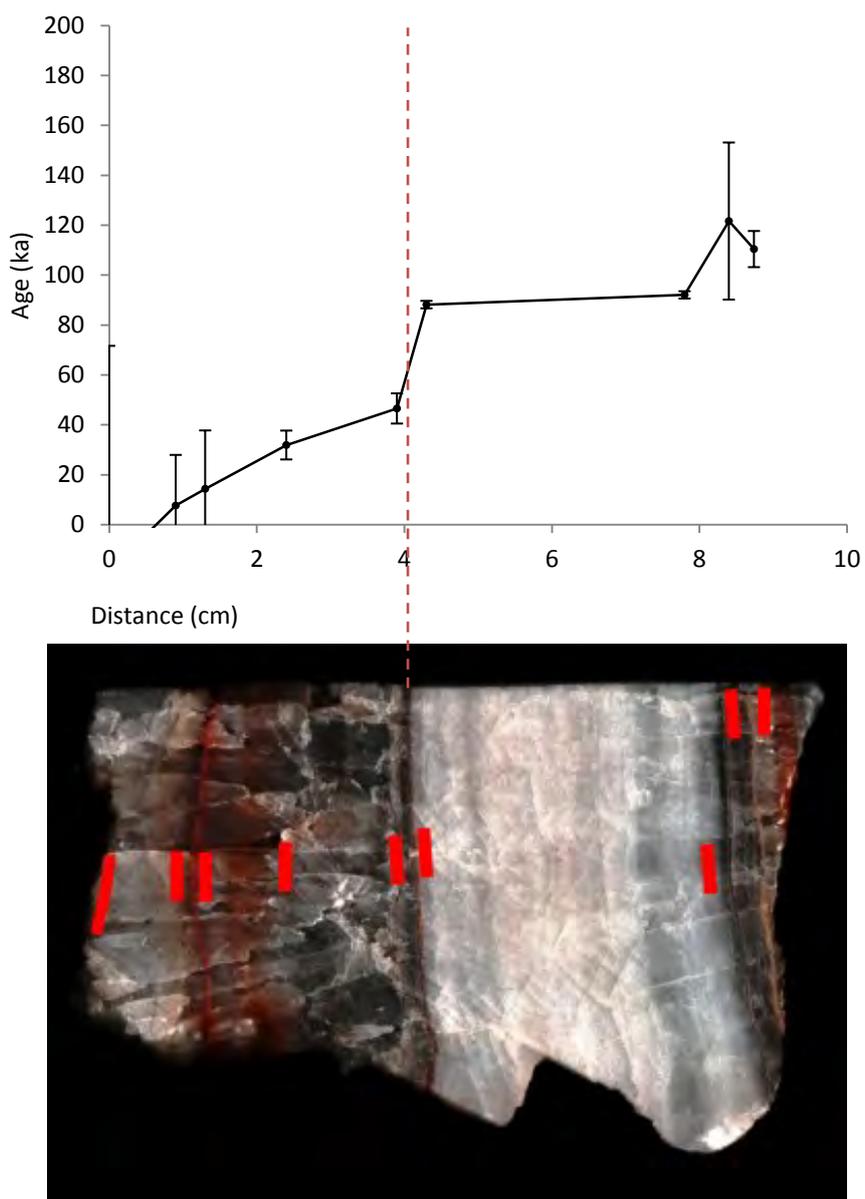
Figure 5.5: YBJD1 U-series disequilibrium geochronology age model. Sampling locations are marked on the flowstone scan in red. One potential hiatus location is marked by the red line.

There is a limited relationship between growth rate and flowstone colour as presented in Figure 5.5. One potential hiatus is identified corresponding with the transition from black to white calcite. Hiatus identification is limited by sample geochronological resolution with slow growth rates averaging 0.17 µm/year (maximum = 0.90 µm/year, minimum = 0.010 µm/year).

Consequently, further undetected hiatuses are likely to be occurring within the YBJD1 sample with faster growth rates than presented in Figure 5.5, punctuated by cessation in growth.
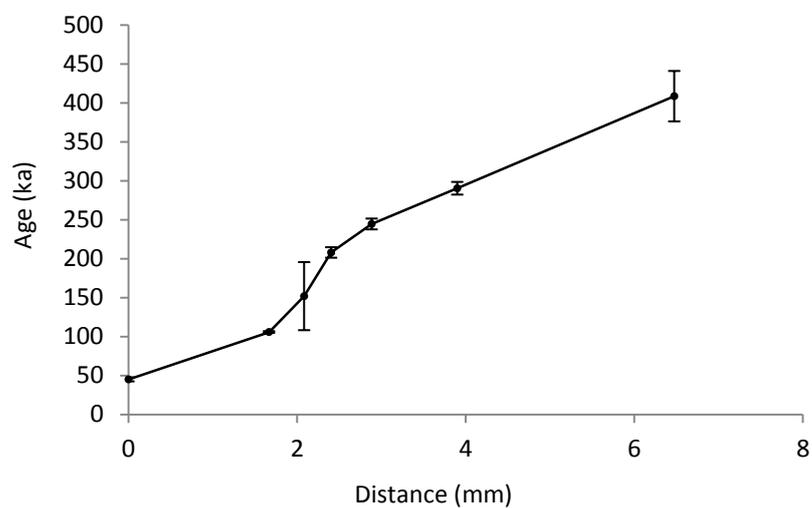


Figure 5.6: YBJD2 U-series disequilibrium geochronology age model. Sample locations are shown on the flowstone scan image.

YBJD2 presents relatively constant slower growth rates (Figure 5.6) when compared to YBJD1 (Figure 5.5) (average = 0.017 µm/year, minimum = 0.006 µm/year, maximum = 0.027 µm/year). As with YBJD1, growth rate variability and hiatus events may be occurring but remain undetectable at current dating resolution. Additionally, it is highly unlikely that such slow mean growth rates were sustained steadily over such long durations (~ 400 ka).

### 5.3.1. Drip water chemistry

| | HW1 | | HW2 | | HW3 | |
|---|---|---|---|---|---|---|
| | **Mean** | **± SD** | **Mean** | **± SD** | **Mean** | **± SD** |
| EC (mS cm$^{-1}$) | **317** | **17** | **277** | **30** | **277** | **30** |
| T (°C) | **11** | **0.48** | **11** | **0.45** | **11** | **0.42** |
| TDS | **212** | **10** | **182** | **22** | **184** | **20** |
| pH | **8.0** | **0.65** | **7.9** | **0.57** | **7.9** | **0.55** |
| Drips min$^{-1}$ | **0.89** | **0.27** | **0.86** | **0.72** | **1.4** | **0.80** |
| Ca (mg l$^{-1}$) | **66.6** | **5.8** | **56.2** | **8.2** | **62.0** | **7.0** |
| Mg (mg l$^{-1}$) | **0.57** | **0.056** | **0.57** | **0.047** | **0.57** | **0.050** |
| Sr (mg l$^{-1}$) | **1.8** | **0.25** | **1.8** | **0.23** | **1.8** | **0.24** |
| Cl (mg l$^{-1}$) | **1.6** | **0.4** | **1.7** | **0.4** | **1.6** | **0.4** |
| SO$_4$$^{2-}$ (mg l$^{-1}$) | **0.7** | **0.2** | **0.7** | **0.2** | **0.7** | **0.2** |
| NO$_3$$^{-}$ (mg l$^{-1}$) | **0.9** | **0.3** | **1.0** | **0.3** | **1.0** | **0.3** |

Table 5.1: Harrie Wood cave drip water chemistry at locations HW1, HW2 and HW3 (Tadros *et al*., 2014).

## 5.3.2. Aerosol monitoring

Cave aerosol deposition has been monitored in Jersey and Harrie Wood caves to provide an indication of the likely flux of aerosol deposition to Yarrangobilly flowstones. This section evaluates aerosol deposition levels and their associated spatial and temporal variance.
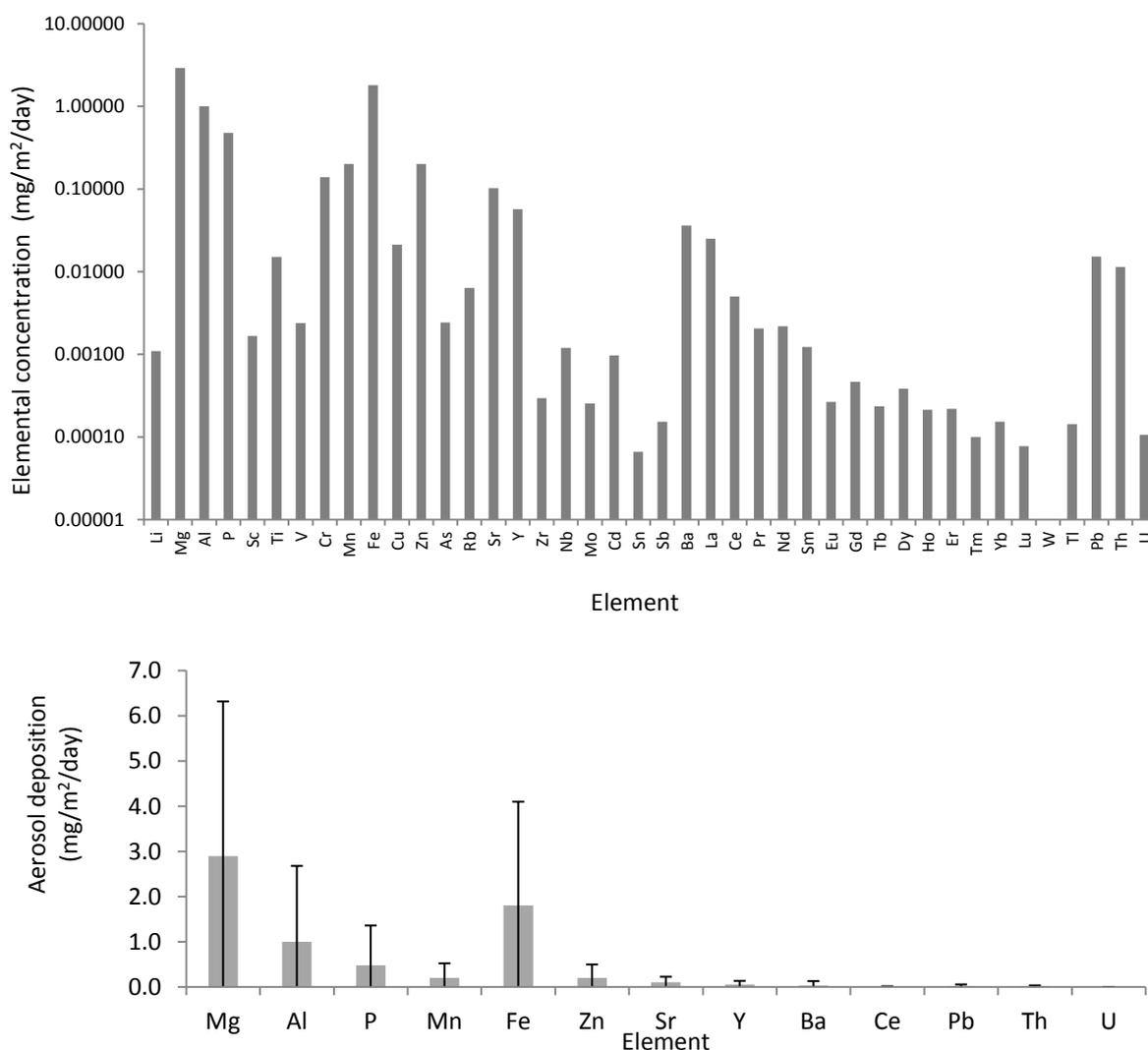


Figure 5.7: Average cave aerosol inorganic deposition from Harrie Wood and Jersey Caves. ICP-MS results are presented of $HNO_3$ solute from the surrogate surface DDIW wash. The entire ICP-MS suite of elements is presented in the upper graph, whereas a selection of elements commonly utilised in speleothem investigations is presented in the lower graph. Error bars presented represent standard deviation based on the elemental variance between all monitoring samples. Logarithmic upper y-axis, standard y-axis in the lower graph. Ca is excluded, presenting outlying high levels of deposition at 238 mg/m$^2$/day.

As presented in Figure 5.7 and Table 5.2 Mg, Al, P, Mn, Zn, Fe and Ca present the highest levels of depositional flux from the measured elements throughout the Yarrangobilly caves.

The comparison between entrance and cave interior aerosol depositional flux rates demonstrates elevated deposition for most elements at the cave entrance region in Harrie Wood cave (Figure 5.8 where HW2 is closer to the entrance of these respective caves). This observed spatial distribution is consistent with monitoring at different locations and from other studies (summarised in Chapter 2 - Dredge *et al*., 2013). However, Jersey cave displays the opposite distribution of aerosols. The aerosol levels in Jersey cave indicate a more complex ventilation regime with potential for an additional ventilation opening deeper within the cave.
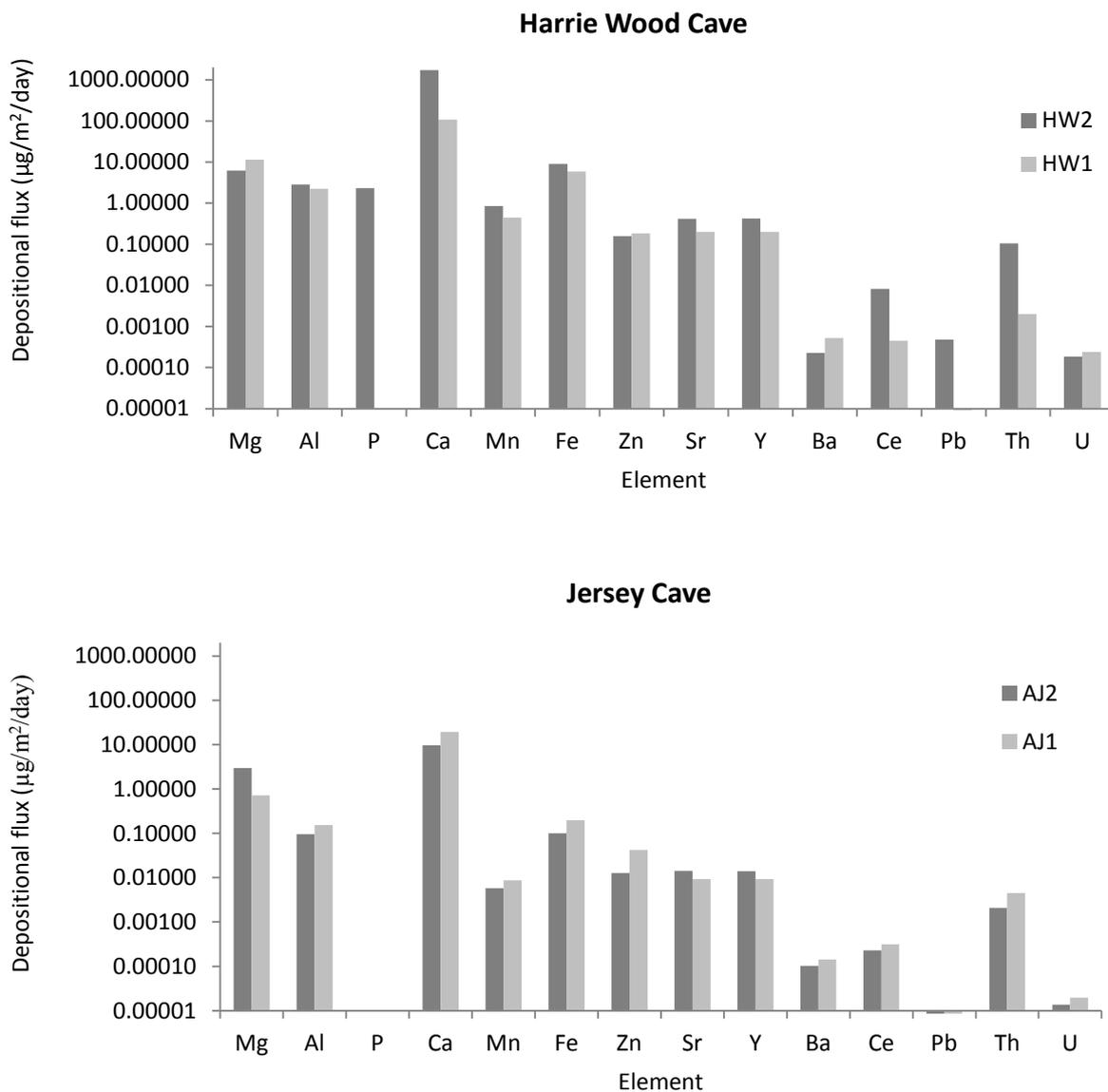
Figure 5.8: Comparison of deposition at locations AJ1 and AJ2, and HW1 and HW2 (during one collection period 13/12/11 and 25/05/12).

Harrie Wood presents much greater levels of aerosol deposition flux than Jersey cave for the majority of elements. However, the temporal and spatial variance in elemental deposition is often greater than total depositional values and should be considered with caution. Results indicate that temporal variability one standard deviation in deposition averages 114% of total depositional flux (Table 5.2). The average total variance for Harrie Wood and Jersey cave accounting for temporal and spatial change is 202% of the mean (Table 5.2). Another key contribution to monitoring variations can be attributed to sampling reproducibility, which has demonstrated 88% variance (elemental average one standard deviation, based on duplicate samples in one cave location). The aerosol deposition variability in Yarrangobilly caves is attributed to cave wall weathering which results in carbonate fragments falling into surrogate surface sampling equipment. Carbonate fragments were observed in some surrogate surface samples. Cave wall fragments significantly enrich the sample trace element geochemistry when compared to aerosol deposition alone. The uneven distribution of cave wall fragments will therefore result in sample variability. Samples with observed carbonate fragments were included in analysis, because fragments would also be included in forming flowstones and contribute to speleothem geochemistry.

| Element | Jersey Average | σ | σ% | Harrie Wood Average | σ | σ% | Average all |
|---|---|---|---|---|---|---|---|
| Mg | 0.58 | 0.84 | 143 | 5.2 | 6.0 | 116 | **2.9** |
| Al | 0.29 | 0.83 | 291 | 1.7 | 2.5 | 148 | **1.0** |
| P | 0.043 | 0.13 | 302 | 0.91 | 1.6 | 180 | **0.48** |
| Ca | 26 | 44 | 171 | 451 | 692 | 154 | **238** |
| Mn | 0.06 | 0.20 | 322 | 0.34 | 0.46 | 135 | **0.20** |
| Fe | 0.29 | 0.58 | 204 | 3.3 | 4.0 | 121 | **1.8** |
| Zn | 0.23 | 0.43 | 185 | 0.17 | 0.16 | 99 | 0.20 |
| Sr | 0.0094 | 0.009 | 97 | 0.20 | 0.25 | 127 | 0.10 |
| Y | 0.0061 | 0.007 | 108 | 0.11 | 0.16 | 145 | 0.057 |
| Ba | 0.0041 | 0.012 | 303 | 0.07 | 0.18 | 265 | 0.036 |
| Ce | 0.0021 | 0.007 | 335 | 0.008 | 0.017 | 218 | 0.0050 |
| Pb | 0.0093 | 0.031 | 334 | 0.021 | 0.056 | 265 | 0.015 |
| Th | 0.0050 | 0.012 | 235 | 0.018 | 0.038 | 214 | 0.011 |
| U | 0.000012 | 0.000034 | 277 | 0.00020 | 0.00034 | 169 | 0.00011 |
| Average | 1.95 | | 236 | 33 | | 168 | 18 |

Table 5.2: Aerosol monitoring results for each cave and averages ($\mu g\ m^{-2}\ day^{-1}$) based on several cave locations (HW1, HW2, AJ1 and AJ2) from the entrance to the interior and over a monitoring period from 12/10/2011 to 25/10/12 (in three batches 12/10/11 to 13/12/11, 13/12/11 to 25/05/12 and 25/05/12 to 25/10/12). Standard deviation ($\sigma$) and relative standard deviation ($\sigma$ %) compared cave deposition flux rates are displayed. Elements with the highest average deposition rates are highlighted in bold.

Vertical accretion rates calculated (as in Chapter 2, Section 2.4.2 'Cave ventilation and aerosol distribution') based on average deposition rates for both caves of 18 $\mu g\ m^{-2}\ day^{-1}$ (1.95 $\mu g\ m^{-2}\ day^{-1}$ for Jersey Cave, 33 $\mu g\ m^{-2}\ day^{-1}$ for Harrie Wood) equals 4 $\mu m$/year. This is much lower than the vertical accretion rates calculated for Gough's cave due to lower deposition fluxes.

| Element | Jersey σ | σ % | Harrie Wood σ | σ % |
|---------|----------|-----|---------------|-----|
| Mg | 0.17 | 40 | 4 | 82 |
| Al | 0.28 | 118 | 1.7 | 98 |
| P | 0.067 | 145 | 1.1 | 113 |
| Ca | 15 | 76 | 356 | 86 |
| Mn | 0.078 | 159 | 0.28 | 88 |
| Fe | 0.19 | 81 | 2.7 | 88 |
| Zn | 0.26 | 133 | 0.068 | 40 |
| Sr | 0.0030 | 41 | 0.16 | 87 |
| Y | 0.0030 | 64 | 0.13 | 155 |
| Ba | 0.0055 | 169 | 0.14 | 173 |
| Ce | 0.0027 | 162 | 0.013 | 144 |
| Pb | 0.013 | 173 | 0.042 | 173 |
| Th | 0.0058 | 141 | 0.020 | 136 |
| U | 0.0000091 | 92 | 0.00023 | 110 |
| Average | | 114 | 26 | 112 |

Table 5.3: Aerosol monitoring standard deviation results based on temporal variation between the three monitoring periods (12/10/11 to 13/12/11, 13/12/11 to 25/05/12 and 25/05/12 to 25/10/12) within Jersey and Harrie Wood caves. Standard deviation ($\sigma$), is based on the comparison of average cave deposition from each monitoring period at each cave. Standard deviations as a percentage of average deposition flux rates ($\sigma$ %) for each sampling period is displayed.
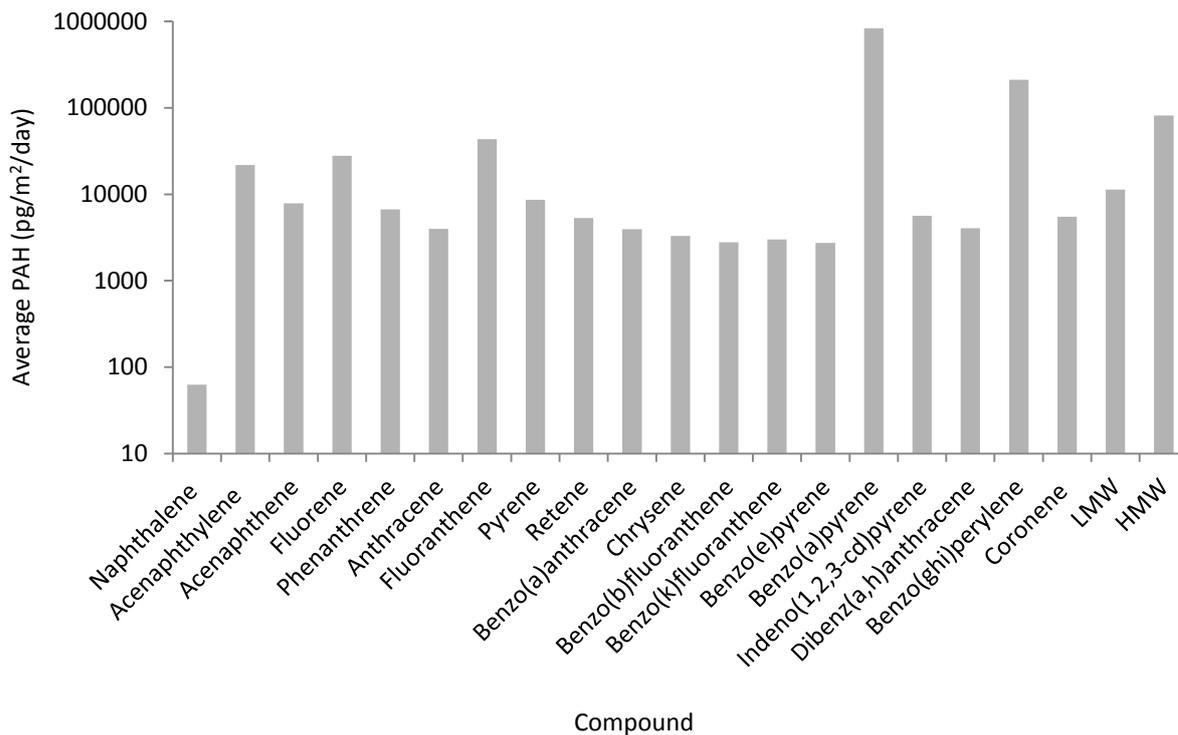
Figure 5.9: Average cave aerosol PAH deposition from surrogate surface monitoring throughout Harrie Wood and Jersey Caves. Compounds are ordered in terms of mass with napthalene being lightest and coronene being the heaviest compound. PAHs can be grouped into low molecular weight (LMW) and high molecular weight (HMW) classes representing napthalene to anthracene and fluoranthene to coronene representatively.

PAH concentrations present a more uniform distribution across compounds, unlike the elemental variability that is observed in the deposition of inorganic constituents. The majority of PAH compounds present similar deposition flux rates (with the exception of naphthalene, benzo(a)pyrene and benzo(ghi)perylene). Care was taken to place surrogate surface samplers away from active drips. However, it is possible that part of the measured aerosol signature may be sourced from drip water aerosols produced from 'splashing' processes (as outlined in Chapter 2, section 2.3.3. in the 'wet deposition' section and illustrated in Figure 2.5).

### 5.3.3. Palaeofire indicators

*Speleothem PAH*
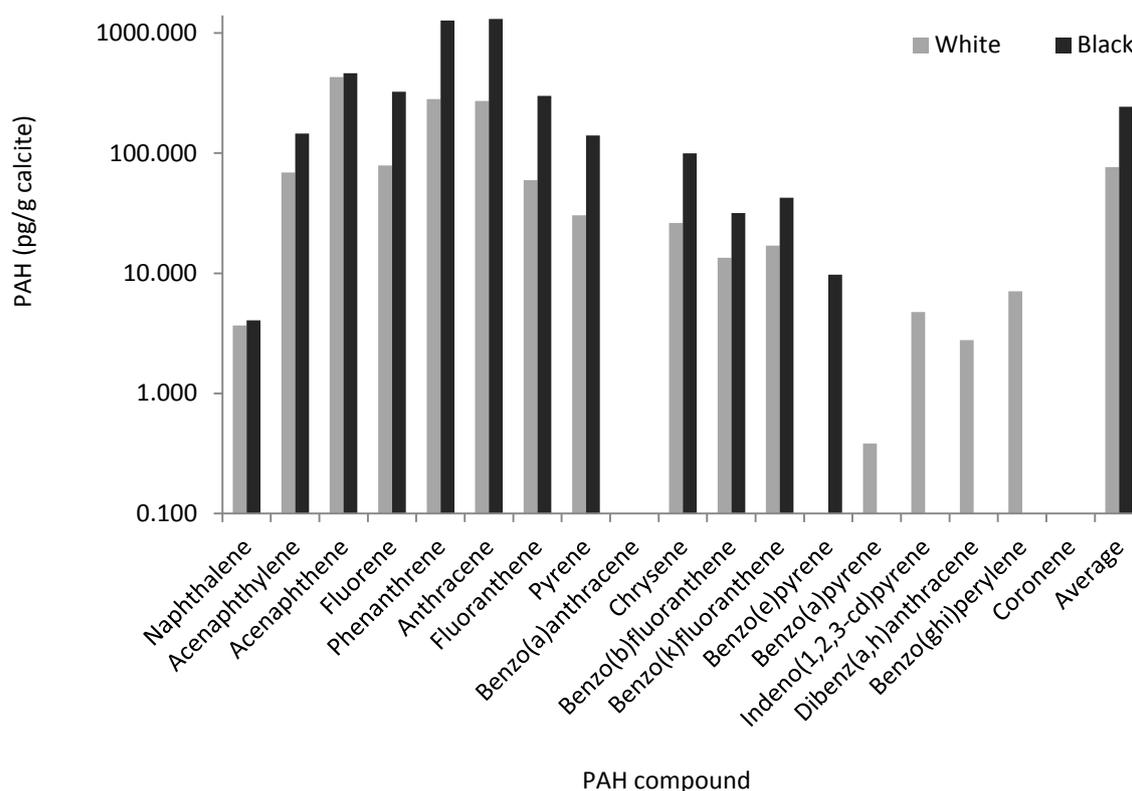


Figure 5.10: Comparison of white and black calcite PAH concentrations. PAHs not presented are below detection limits (0.017-0.25 pg/g calcite).

Average PAH contents are greater in the black calcite (as shown in Figure 5.10) for all PAH compounds in which they are detected. However, benzo(e)pyrene, indeno(1,2,3-cd)pyrene, dibenz(a,h)anthracene, benzo(ghi)perylene are only detected in the white calcite. Results indicate that during the precipitation of black calcite a smaller range of compounds with lower molecular weight are incorporated at higher concentrations relative to white calcite.

*Speleothem organic analysis*
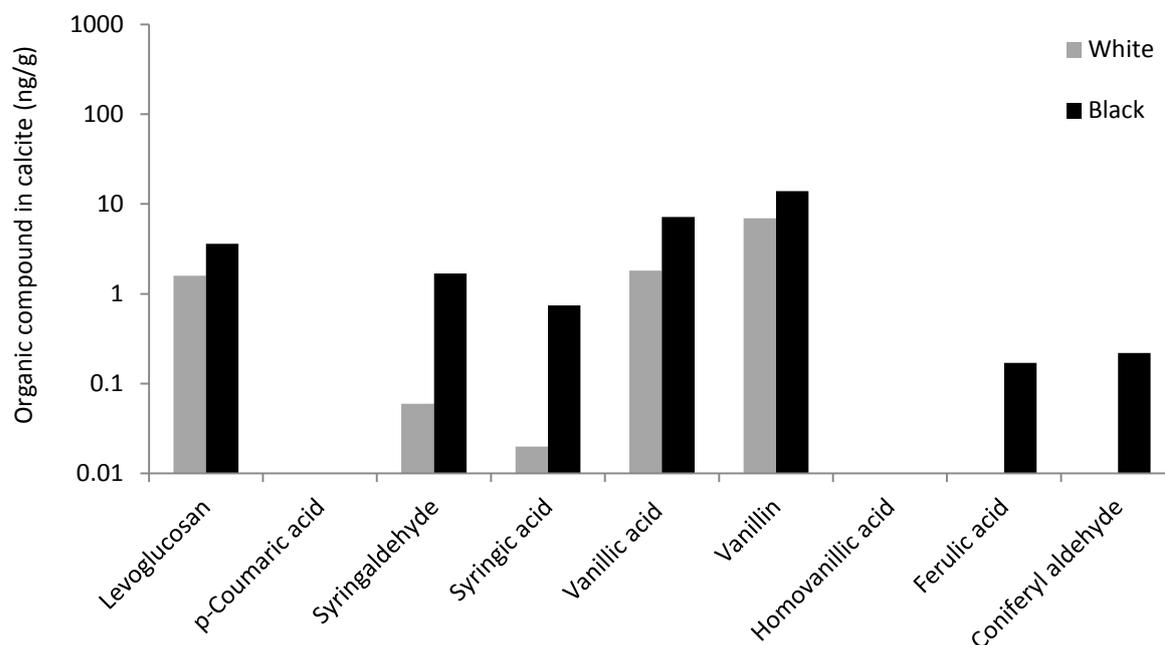


Figure 5.11: Levoglucosan and methoxyphenol calcite content of white and black calcite.

Previous studies have demonstrated the ability to utilise levoglucosan and methoxyphenols as proxies for forest fire occurrence (as outlined in Section 1). Figure 5.11 shows that greater concentrations of all forest fire proxies are observed in the black calcite. There is a clear association between PAH contents and other fire proxies in black calcite. The likely sources, mode of transport and level of incorporation of organic compounds will be explored in the discussion (Section 4).

## 5.3.4. Flowstone Geochemistry
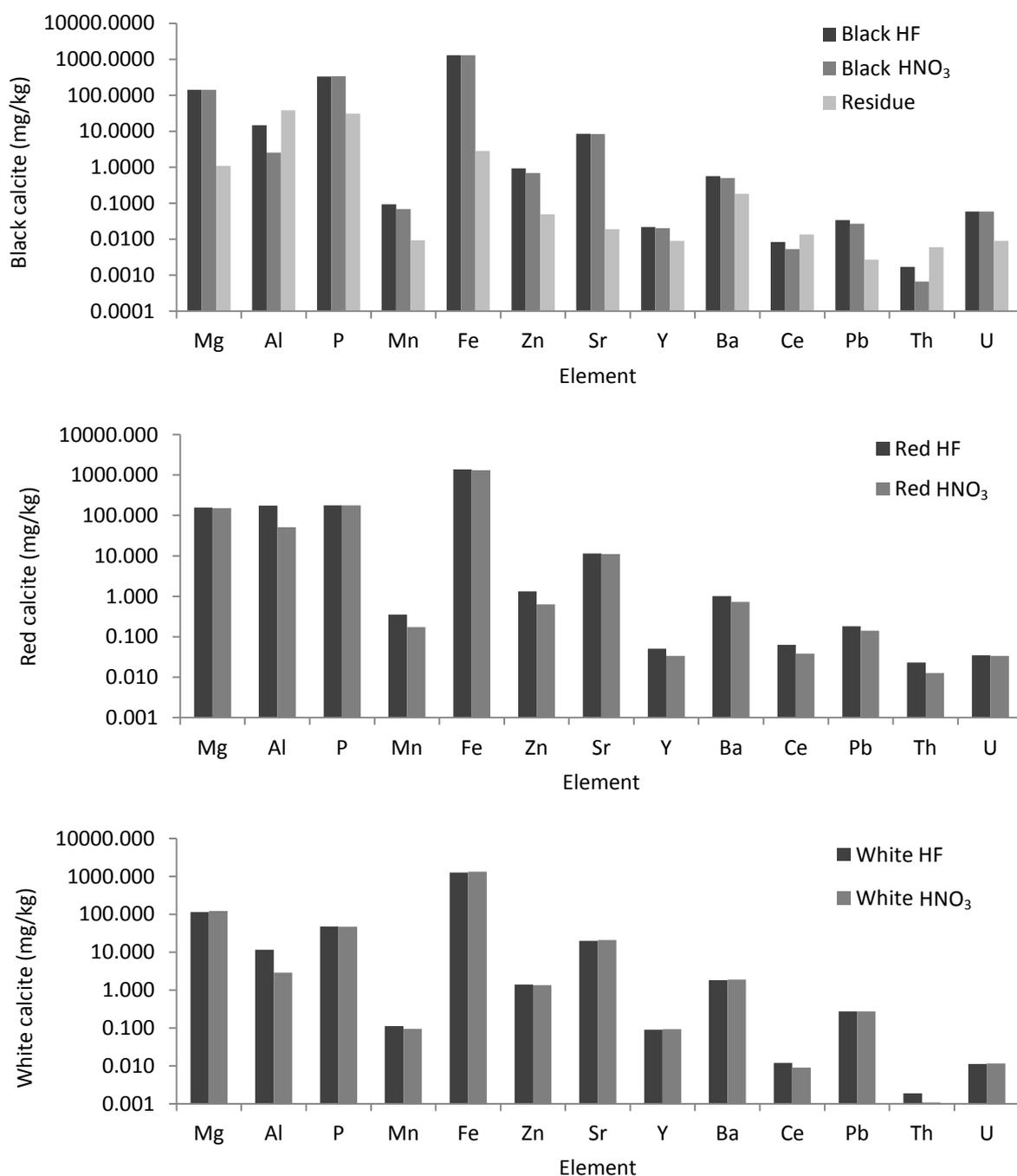


Figure 5.12: Black, red and white calcite solution analysis from YBJD1, of HF and HNO₃ calcite dissolutions, with HNO₃ residue analysis presented for black calcite only. HNO₃ residue results are converted to represent concentrations in original calcite for comparison to dissolution values. HNO₃ residue = Residue concentration (mg/kg) * (Residue mass (g))/(Calcite mass (g)).

| Element | B HF (mg/kg) | B HNO$_3$ (mg/kg) | B HNO$_3$ Residue (mg/kg) | HNO$_3$/HF (%) | HNO$_3$ Residue/HF (%) |
|---|---|---|---|---|---|
| Mg | 141 | 142 | 1.1 | 101 | 1 |
| Al | 15 | 2.5 | 38 | 17 | 257 |
| P | 333 | 340 | 31 | 102 | 9 |
| Ca | 403880 | 404738 | 69 | 100 | 0 |
| Mn | 0.093 | 0.069 | 0.009 | 74 | 10 |
| Fe | 1298 | 1285 | 2.9 | 99 | 0 |
| Zn | 0.93 | 0.69 | 0.049 | 74 | 5 |
| Sr | 8.5 | 8.4 | 0.019 | 99 | 0 |
| Y | 0.022 | 0.020 | 0.009 | 93 | 42 |
| Ba | 0.56 | 0.50 | 0.18 | 89 | 33 |
| Ce | 0.0084 | 0.0053 | 0.013 | 63 | 160 |
| Pb | 0.034 | 0.027 | 0.0027 | 79 | 8 |
| Th | 0.0017 | 0.00067 | 0.0061 | 39 | 351 |
| U | 0.059 | 0.059 | 0.0091 | 100 | 15 |

Table 5.4: Comparisons of HNO$_3$, HF dissolution and HNO$_3$ residue analysis results for black calcite for a selection of elements.

Results indicate that the residue accounts for a significant proportion of black flowstone geochemistry (averaging a contribution to the HF dissolution of 89% for all elements). Elements such as Al, Ti, V, Rb, Zr, Nb, Ce and Th present the highest concentrations in the residue. HNO$_3$ and HF dissolutions (Table 5.4) present similar elemental concentrations (with the exception of Al, Ce and Th) indicating that the majority of elemental release is occurring with a HNO$_3$ dissolution and is greatest for Mg, P, Ca, Fe, Sr and U.

In some cases, the relationship between HNO$_3$ dissolution and HNO$_3$ residue does not account for relative proportions in comparison to HF dissolution chemistry. These discrepancies suggest that residue remained after HF dissolution and so HF digestion does not necessarily represent total chemistry. However, by studying the relative concentrations as solutes from HNO$_3$ and HF dissolution an indication of relative residue components can be determined for different calcite colorations (Figure 5.9).
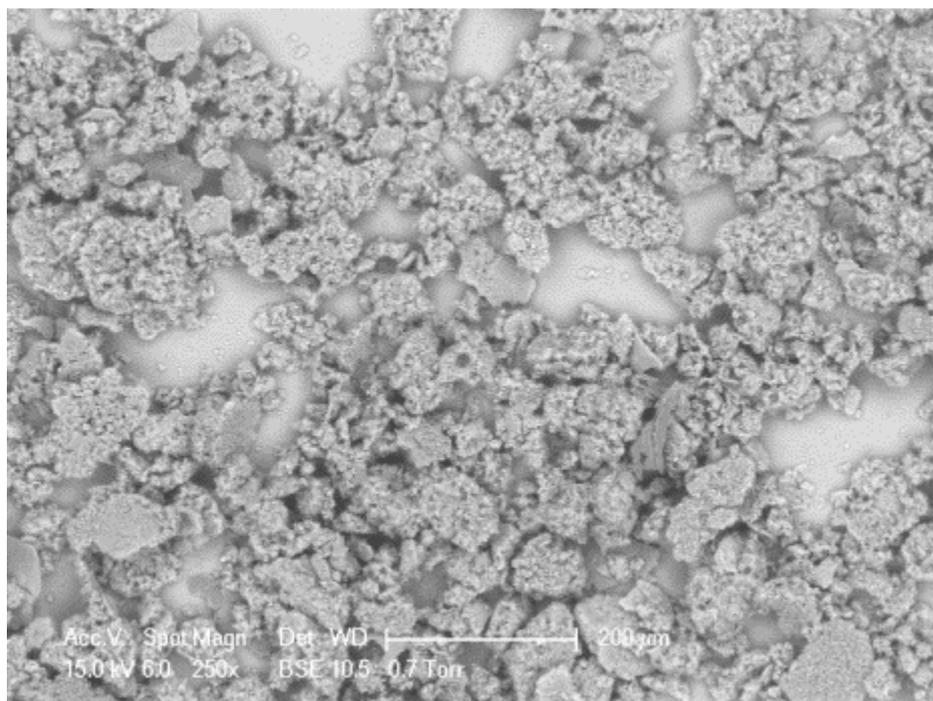
Figure 5.13: ESEM image of black calcite HCl residue at 250x magnification at 15 kV. HCl dissolution residue sampled from 60g black calcite section sampled from YBJD1.
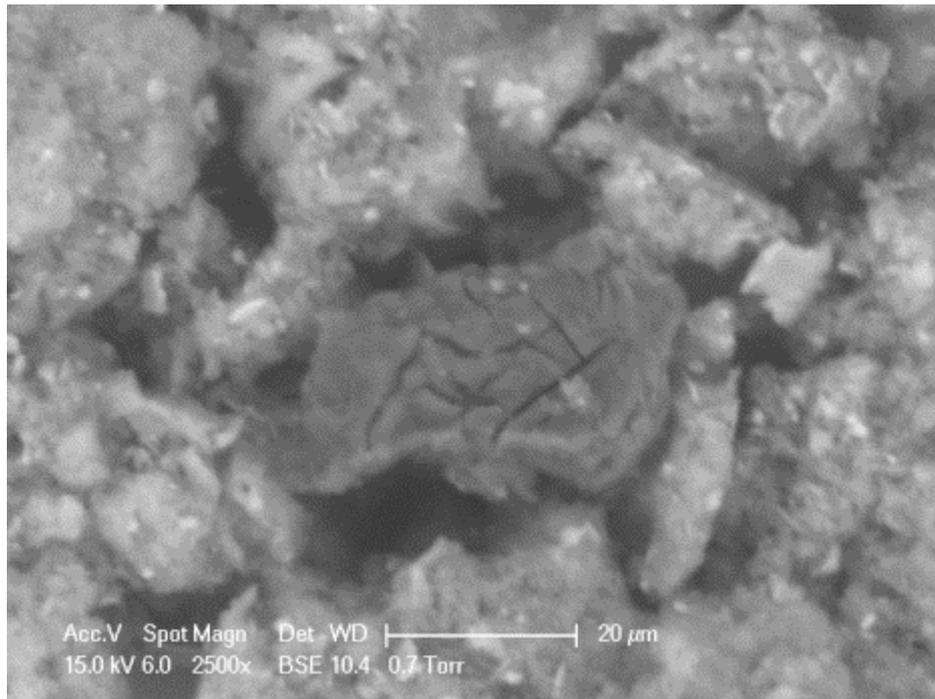
Figure 5.14: HCl residue ESEM image at 2500x magnification at 15 kV. Only one grain was present in the entire residue sample which displayed the optical properties that would indicate carbon (dark in colour – potentially displaying original organic features).
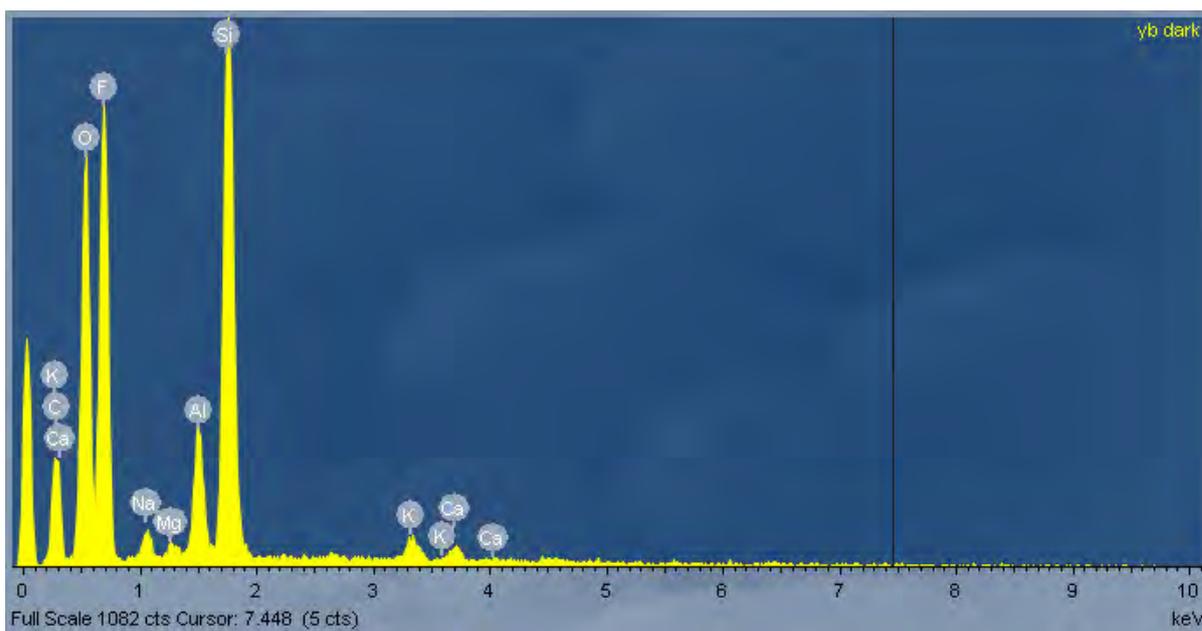
Figure 5.15: ESEM BSE analysis of black calcite HCl residue. Analysis was carried out of the entire residue sample.
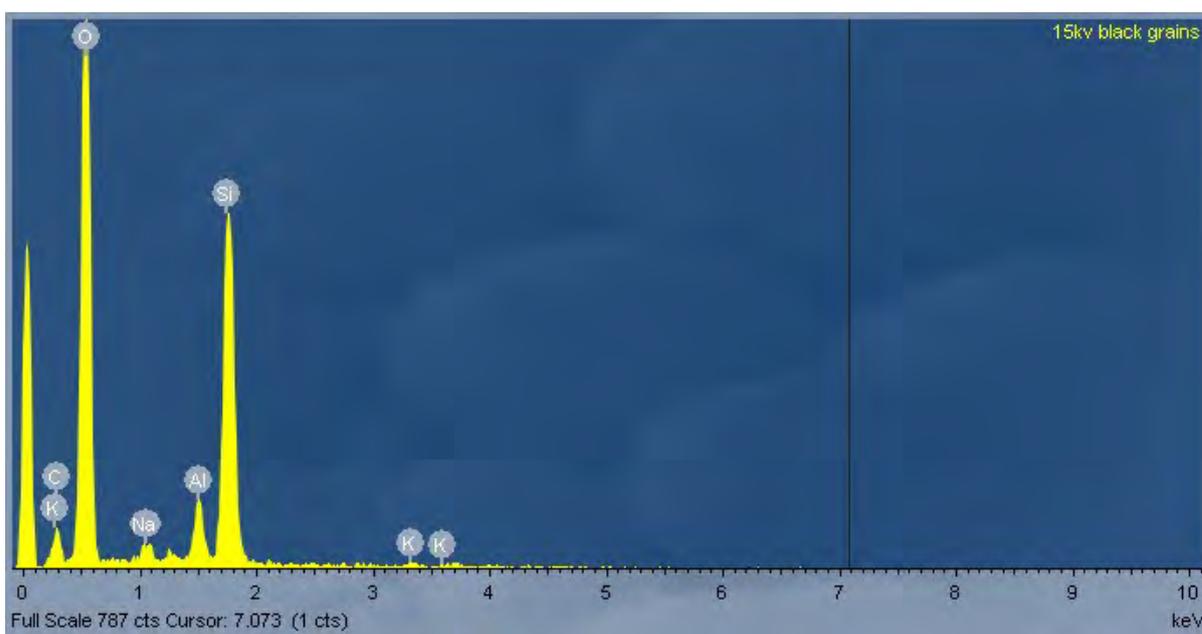


Figure 5.16: ESEM BSE analysis of black calcite HCl redisue. Analysis was carried out on a single black grain within the total sample (Total residue EDEM BSE analysis in Figure 5.15).

High Si contents and the presence of Al indicate the dominance of silicates in the HCl residue. Low levels of C suggest that limited or no carbonaceous material derived from forest fires is being observed in the calcite residue.

YBJD1 – Trace element chemistry
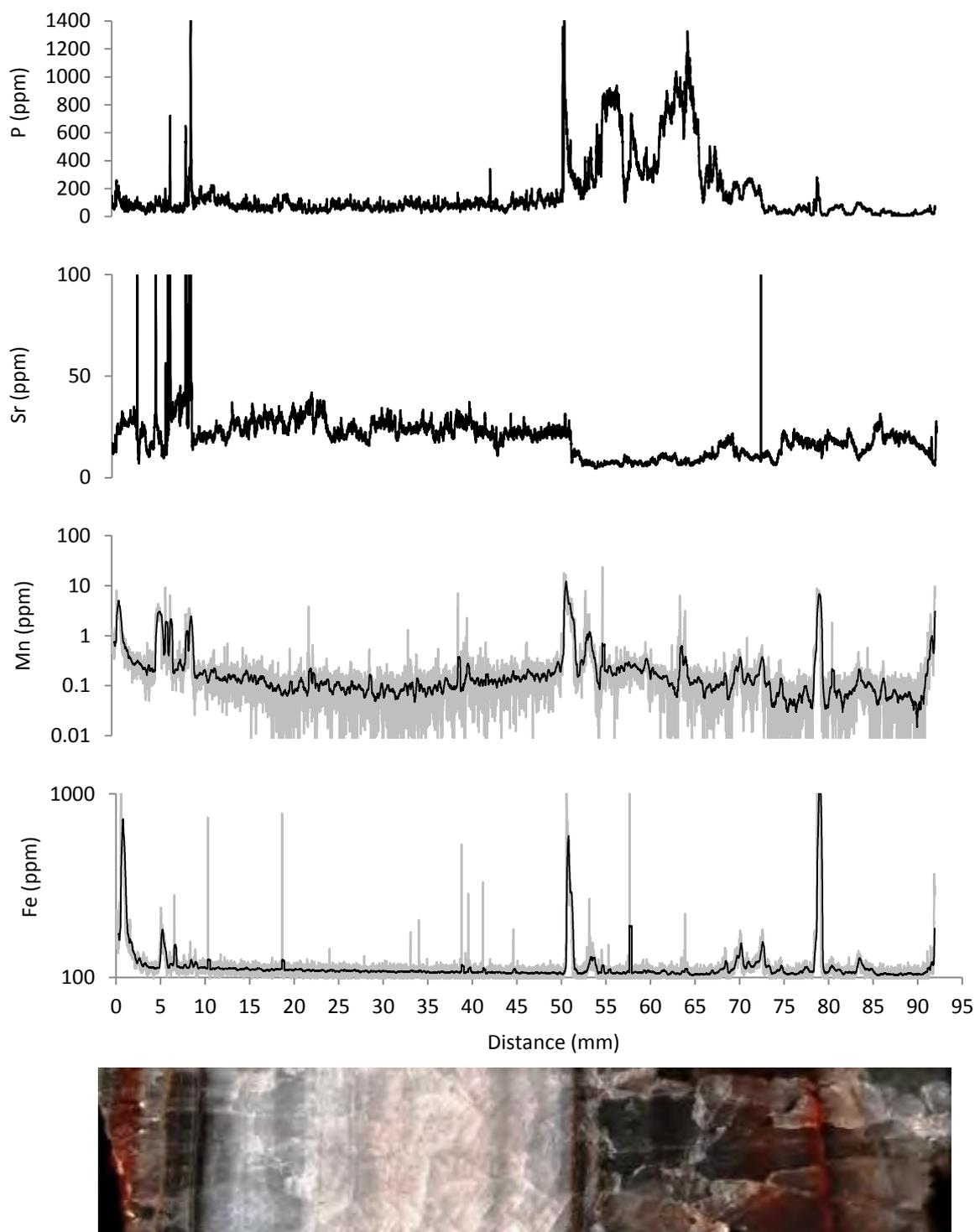


Figure 5.17: LAICPMS results for some key elements for the YBJD1 flowstone. Results are presented against distance along the flowstone section. Data is presented raw, except Mn and Fe where a 100-point moving average line (black) is displayed over the raw data (grey). An image of the flowstone core is shown above for reference. Full LA-ICP-MS results are presented in the supplementary material section S.17, Figure S.21.

P, Sr, Mn and Fe presented in Figure 5.17 are of importance for the later discussion, other LA-ICP-MS element results are presented in the supplementary material (Section S.17.). The most prominent feature in the YBJD1 geochemical record is a change in chemistry occurring across the hiatus surface (at 52 mm, Figure 5.17). Fe and Mn display a clear short lived concentration increase associated with the hiatus, with a positive correlation between both elements being observed throughout the sample. A long-term sustained shift in concentrations is shown by Sr. P shows significant variation and is higher in black calcite. Three peaks are observed within the main section of black calcite, with the final peak reducing abruptly at the timing of the hiatus. Other short lived concentration increases occur at 0-3, 5, 8-10 and 78-80 mm which are shown in Fe and Mn. Sr displays two cycles of decrease occurring after the timing of the 0-3 and 8-10 mm events, potentially indicating sample hiatuses. The 8-10 mm and 78-80 mm events are clearly presented in the P record, with the other older events not being recorded.

*YBJD1 PCA analysis*
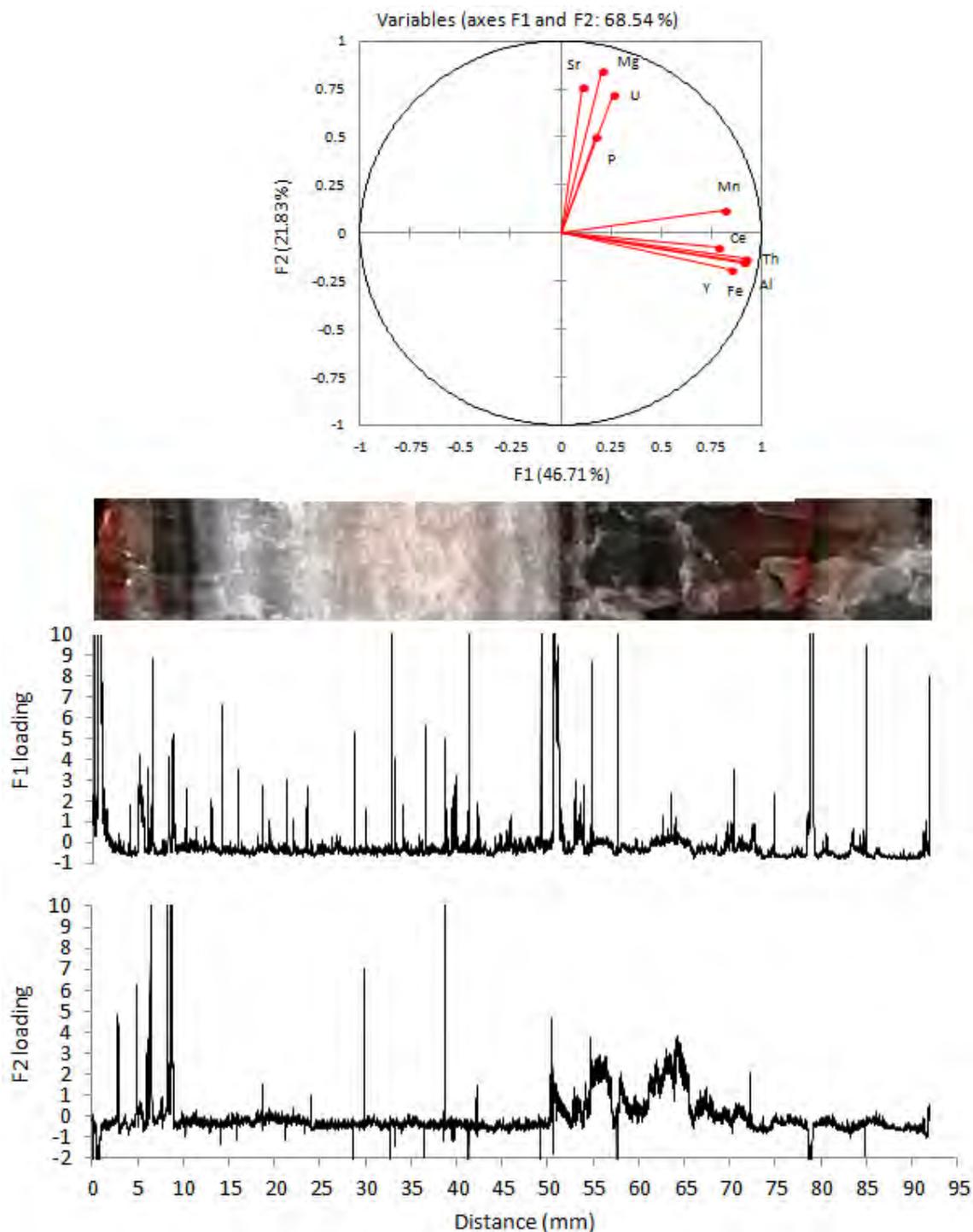


Figure 5.18: YBJD1 PCA analysis results for a selection of elements indicative of palaeoenvironmental situations (Sr, Mg, U, P, Mn, Ce, Th, Al, Fe, Y). Upper graph presents element factor loadings. Lower graphs present factor 1 and 2 PCA outputs against distance, with the sample image for reference.

PCA analysis (Figure 5.18) presents a clear distinction between Sr, Mg, U and P which load highly on factor two on the y-axis and Mn, Ce, Th, Al, Fe and Y which load on factor 1 on the x-axis, indicating two significant and separate geochemical controlling processes. Factor 1 elements include those found at other sites to be dominantly colloidally sourced (Fairchild & Treble, 2009) (Ce, Y, Al and Th) together with Mn and Fe. The influence of Mg, Sr and U on factor 2 suggests the influence of elements in the dissolved phase, sourced from changes in the bedrock dissolution processes. The correlation between Sr and Mg is indicative of prior calcite precipitation processes influencing flowstone geochemistry. P presents a weak influence on factor 1 and factor 2 indicating predominant influence by an additional separate process.

When observing the changing factor loadings with the flowstone core some dominant features are notable. Factor 1 presents a noisy signal with short lived large amplitude positive excursions. Factor 2 displays a smoother record with the most prominent feature being the change in chemistry associated with the hiatus event and sustained increased concentrations during the black flowstone coloration section.

*YBJD2 Trace element geochemistry*
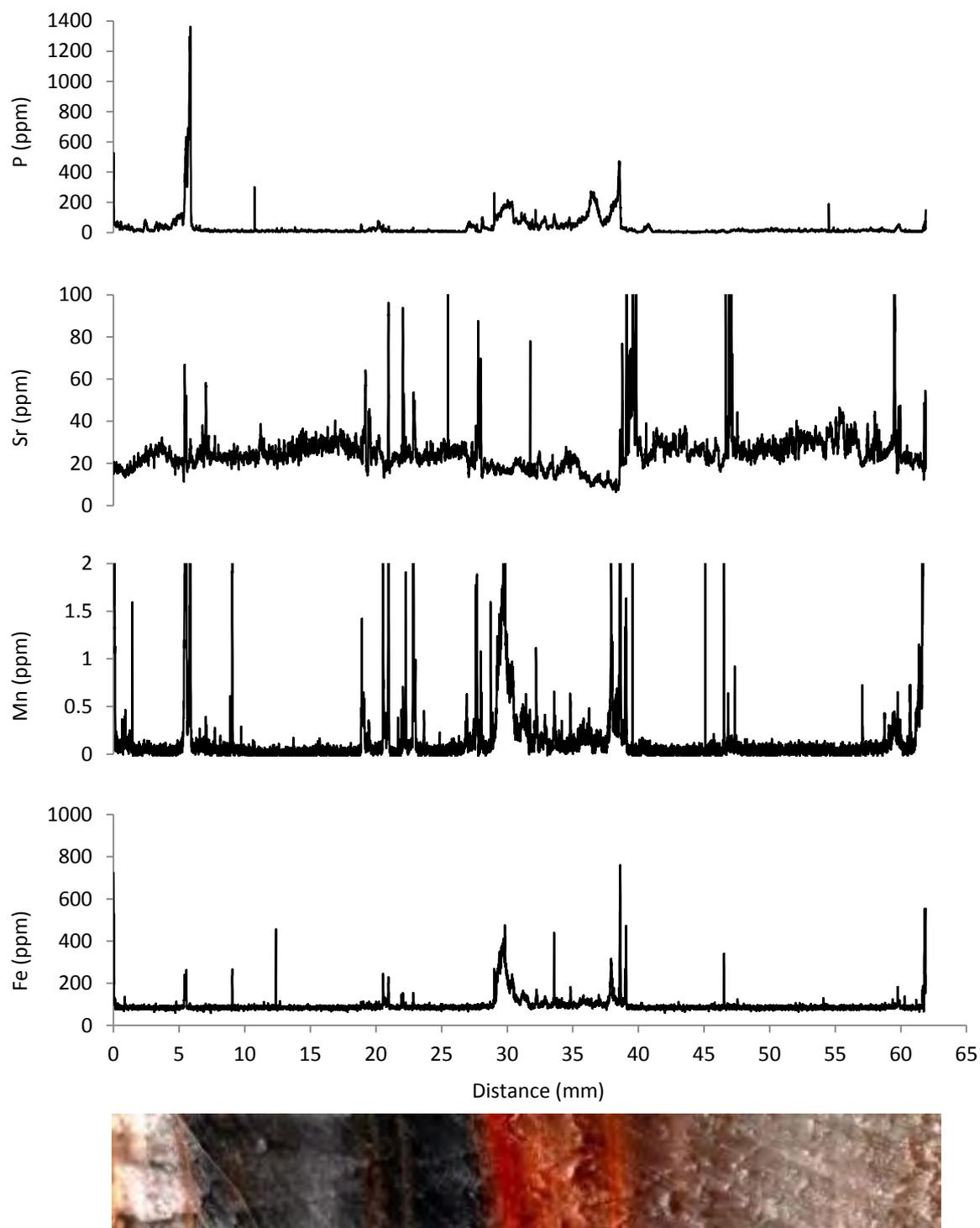


Figure 5.19: LA-ICP-MS results for the YBJD2 flowstone. Results are presented against distance along the flowstone section. An image of the flowstone core is shown above for reference. Full LA-ICP-MS results are presented in the supplementary material section S.17, Figure S.22.

YBJD2 presents several short lived events with large concentration increases and two longer duration periods of change associated with red coloration in the flowstone (Figure 5.19). Fe, Mn and P correlate positively with a period of elevated concentrations (28-40 mm) and two episode of further increase (29-32 and 38-40 mm). Sr presents a negative correlation with Fe, Mn and P at this point, with a sustained reduction relating to red coloration.

One short lived event is clearly shown in P, Sr, Fe and Mn at ~6 mm distance. A period of variability is observed from 19-25 mm in Sr Mn and Fe with large amplitude excursions, a small sustained increase is also observed in P. A similar relationship between elements is observed at 60 mm. However, Mn and Sr show a peak at 47 mm which is potentially correlated by a small spike in Fe but is not recorded in P. Abrupt increases in elemental concentrations which are observed for all elements may indicate hiatus events. Events at 5-6, 19-23 28, and 39 mm present increases across all elements which correlate with changes in fabric suggesting potential hiatus events.

*YBJD2 PCA Analysis*
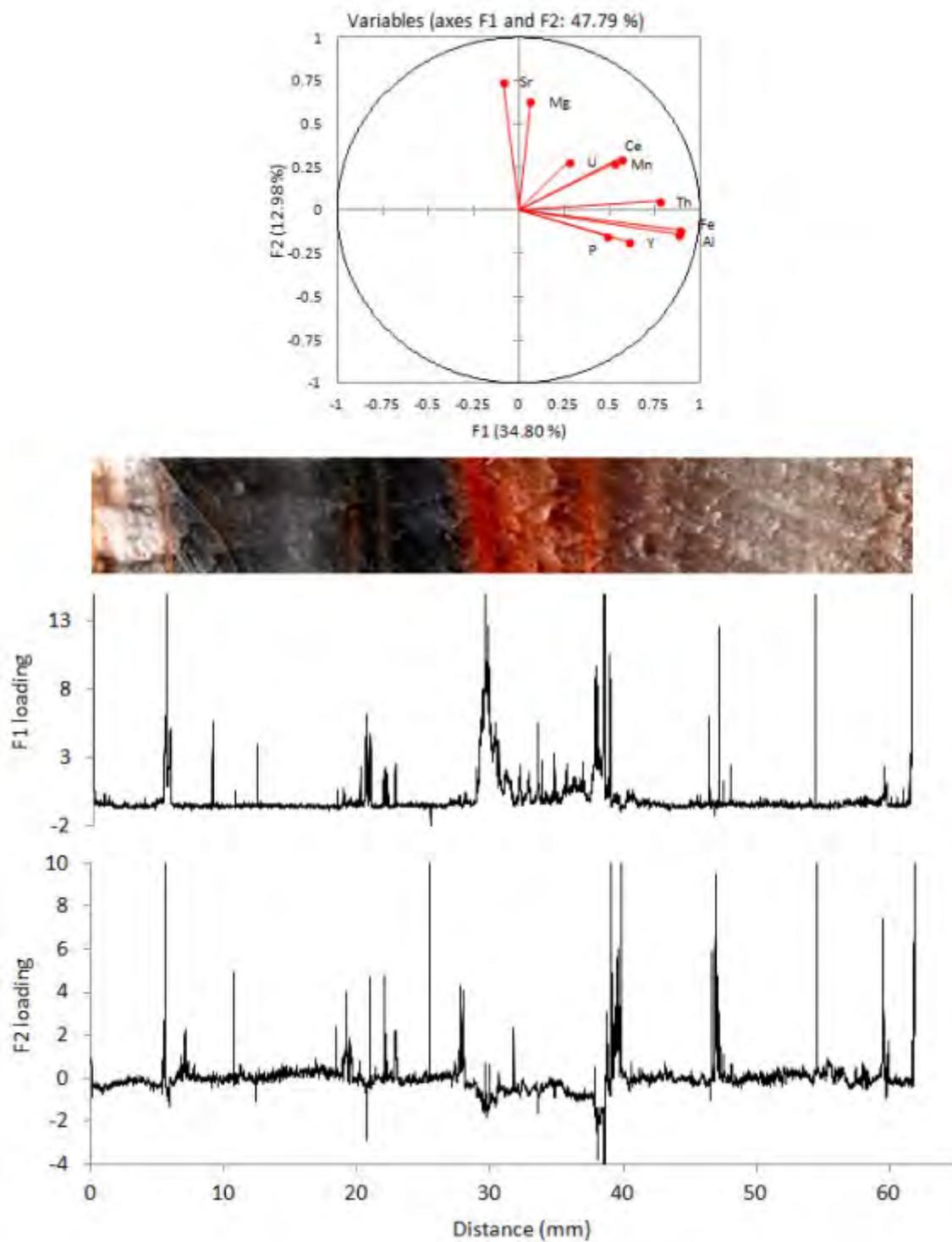


Figure 5.20: YBJD2 PCA analysis results for a selection of elements indicative of palaeoenvironmental situations.

YBJD2 PCA analysis results (Figure 5.20) presents a much greater elemental separation than that observed with YBJD1 (Figure 5.18). Three broad groupings are displayed: Sr and Mg; U, Ce and Mn; Th, Fe, Al, Y and P. Some similarities are observed between YBJD1 and YBJD2 in the grouping of elements. Sr and Mg display a correlation and influence on factor 2 as in YBJD1. The grouping of Th, Al, Y and influence on factor 1 is also similar to that observed for YBJD1 in Figure 5.18. Unlike YBJD1, Ce and Mn separated from the colloidally derived elements and group with U which in turn is separate from Mg and Sr.

Factor 1 presents a clear relationship with the central red section of growth, with the two main horizons being reflected in elevated loadings on factor 1. Factor 2 displays the opposite loading for the main red section of growth and switches between positive and negative correlation with factor 1 for several of the short lived events.

## 5.4. Discussion

### 5.4.1. Palaeofire record?

Firstly, the likelihood of forest fires causing the black coloration in the Yarrangobilly flowstone will be evaluated based on the range of analytical techniques.

Charcoal is often used as a palaeofire indicator in sedimentological studies (as outlined in Section 1.3) and is known to colour surfaces black and produce black aerosols during a fire event. Therefore, scanning electron microscopy was used to search for burnt material in HCl residues of black calcite. Characteristic charcoal microstructure was sought and elemental carbon content was measured in black Yarrangobilly flowstones to determine whether carbon was responsible for calcite coloration. Figure 5.13 shows an example of a typical SEM view presenting no evidence of charcoal fragments. Additionally, chemical analysis of multiple and single grains (Figures 5.15 and 5.16 respectively) did not present significant concentrations of carbon that would be indicative of input from forest fires. Therefore it is highly unlikely that flowstone coloration is occurring as a result of carbon aerosol deposits or from forest fire aerosol deposits as these would most likely also contain carbon particulates.

The comparison of PAH calcite concentrations for black and white calcite in Figure 5.10 shows that consistently greater PAH concentrations in the black calcite were detected. This is indicative of greater combustion and aerosol incorporation during the formation of the black calcite. However, PAHs are also present in the white calcite, indicating a supply of PAHs to the flowstone under both coloration formation conditions. Additionally, white calcite presents episodes of faster growth (YBJD1) which, assuming a constant PAH supply, would result in

the reduced PAH calcite concentrations. This is explored in Table 5.5, black calcite PAH concentrations (growth rate = 0.1 μm/year) are converted to represent PAH concentrations that would occur under white calcite growth rates (0.5 μm/year). Results show that PAH concentrations converted for growth rate are of similar levels, indicating growth rates as a predominant influence on Yarrangobilly speleothem flowstone PAH concentrations rather than changing supply. PAH supply could be taking place either through direct aerosol deposition to the flowstone surface, or via drip waters from deposition on the exterior ground surface. Speleothem PAH concentrations may be representing environmental background levels, with speleothem levels changing as a result of incorporation and transport processes separate from PAH production rates in the local region.

It is conceivable that solution PAH is sufficiently buffered by soil processes that PAH supply continues after forest fires have passed and provides baseline levels. The observed disparity in PAH concentrations between calcite colours would therefore be due to the direct deposition to cave surfaces during fire events or growth rate incorporation processes resulting in greater than baseline levels. However, this mechanism does not account for the lack of HMW PAHs in the black calcite. The impact of PAH molecular weight on solubility and transport is explored further in the discussion section 5.5.2 'Environment and soils'.

PAH aerosol monitoring has presented a supply across all PAH molecular weight compounds (Figure 5.9). Table 5.5 presents the results of aerosol contribution to speleothem calculations based on modern PAH deposition monitoring.

| Compound | White$_{CaCO3}$ (pg/g) | Black GR Conv | Black$_{CaCO3}$ (pg/g) | HW$_{Dep}$ (pg/mm/yr) | AJ$_{Dep}$ (pg/mm/yr) | Mean$_{Dep}$ | White Cont % | Black Cont % |
|---|---|---|---|---|---|---|---|---|
| Naphthalene | 3.7 | 0.7 | 4.1 | 0.1 | 0.0 | 0.0 | 1534 | 1385 |
| Acenaphthylene | 68 | 24 | 145.9 | 6.5 | 8.9 | 7.7 | 24262 | 11447 |
| Acenaphthene | 431 | 77 | 462.2 | 1.0 | 4.2 | 2.6 | 1320 | 1230 |
| Fluorene | 79 | 54 | 324.3 | 2.6 | 15.8 | 9.2 | 25152 | 6138 |
| Phenanthrene | 281 | 212 | 1273.1 | 1.0 | 3.5 | 2.3 | 1734 | 383 |
| Anthracene | 271.7 | 218 | 1307.8 | 0.6 | 2.1 | 1.3 | 1066 | 221 |
| Fluoranthene | 59.8 | 50 | 300.0 | 10.9 | 19.3 | 15.1 | 54834 | 10921 |
| Pyrene | 30.5 | 23 | 140.1 | 2.8 | 3.4 | 3.1 | 21945 | 4768 |
| Retene | - | | - | 2.3 | 1.6 | 2.0 | - | - |
| Benzo(a)anthracene | 0.0 | 0 | 0.0 | 1.2 | 1.6 | 1.4 | - | - |
| Chrysene | 26.3 | 17 | 99.5 | 1.2 | 1.2 | 1.2 | 9866 | 2606 |
| Benzo(b)fluoranthene | 13.5 | 5.3 | 31.7 | 1.1 | 0.9 | 1.0 | 16335 | 6926 |
| Benzo(k)fluoranthene | 17.0 | 7.1 | 42.6 | 1.0 | 1.1 | 1.1 | 13810 | 5506 |
| Benzo(e)pyrene | 0.0 | 1.6 | 9.7 | 0.5 | 1.4 | 0.9 | - | 20724 |
| Benzo(a)pyrene | 0.4 | 0 | 0.0 | 567 | 91 | 329 | 187072605 | - |
| Indeno(1,2,3-cd)pyrene | 4.8 | 0 | 0.0 | 1.3 | 2.6 | 2.0 | 89491 | - |
| Dibenz(a,h)anthracene | 2.8 | 0 | 0.0 | 0.8 | 2.0 | 1.4 | 108030 | - |
| Benzo(ghi)perylene | 7.1 | 0 | 0.0 | 65 | 84 | 75.1 | 2302179 | - |
| Coronene | 0.0 | 0 | 0.0 | 1.9 | 2.2 | 2.0 | - | - |

Table 5.5: White CaCO$_3$ and black CaCO$_3$ are the average of triplicate carbonate extraction analysis with results presented in pg g$^{-1}$ of calcite. Black GR conv, is the converted data from black calcite PAH concentrations adjusted by growth rate to represent concentrations that would occur at white calcite growth rates. HW$_{Dep}$ and J$_{Dep}$ are surrogate surface aerosol deposition results averaged over several monitoring periods (as in Table 5.2 and 5.3) and several locations throughout the cave network, Mean$_{Dep}$ is the average of HW and J caves. White and black contributions are calculated from the average deposition at HW and AJ. White and black % contributions = Dep$_{Mean}$/[Colour]$_{CaCO3}$.Calculations are based on the average growth rate of YBJD1 of 1.7 μm per year.

Results indicate that PAH aerosol supply in the modern environment (in the absence of fires at the time of monitoring) is orders of magnitude greater than that required to result in levels observed in both white and black flowstone concentrations. Modern PAH emission from anthropogenic activity will likely cause much higher atmospheric levels than pre-industrial levels and will most likely not be representative of historical PAH deposition levels.

However, this suggests that forest fire PAH supply is not required to produce the PAH concentrations in black calcite. High levels of oversupply suggests that losses are occurring subsequent to capture within flowstone calcite, that PAH aerosol incorporation is at low efficiencies, or a combination of these processes is taking place.
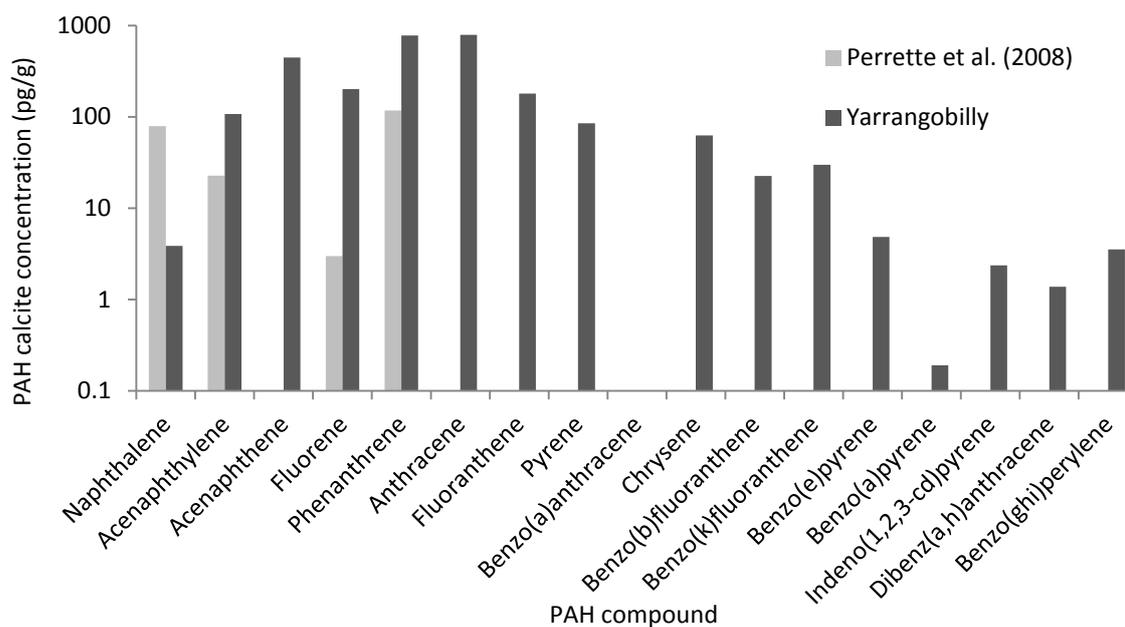


Figure 5.21: Comparison of average (black and white) Yarrangobilly calcite PAH concentrations to the results of Perrette et al. (2008).

Greater concentrations of PAHs are found in Yarrangobilly samples covering the entire PAH mass spectrum in comparison to the stalagmites analysed by Perrette et al. (2008). A similar mass distribution is observed in both samples, with greatest PAH levels being detected in the lower masses compounds. Although stated tentatively, Perrette et al. (2008) attributed the observed mass fractionation to the mode of transportation, with PAHs being transported in solution rather than sorbed on organic or mineral fragments. Consequently, PAH

incorporations may be affected by solution–calcite partitioning similar to that observed with trace elements in speleothem.

Levoglucosan and methoxyphenol have been effectively used as palaeofire proxies in previous investigations (as described in Section 1.3). Consistently higher concentrations of levoglucosan and methoxyphenol are observed in the black calcite (Figure 5.11). However, black calcite concentrations are not sufficiently greater than white calcite to be attributed to forest fires causing the black flowstone coloration. Levoglucosan and Methoxyphenol differences may be solely due to differing growth rates and incorporation as explored in Table 5.5.

In conclusion, there is no distinct evidence to suggest that the difference in PAH, levoglucosan and methoxyphenol concentrations is occurring as a direct result of forest fire aerosol deposition to the speleothem from activity in the area surrounding Yarrangobilly caves, resulting in the black coloration. Evidence suggests that solution supply, changing incorporation efficiencies, differing growth rates and preservation rates are resulting in the differences between black and white calcite rather than variations in the level of direct deposition to the flowstone surface.

*5.4.2. Drip water and aerosol contributions*

Aerosol monitoring results have demonstrated elemental (Figure 5.7), temporal (Table 5.3) and spatial variability (Figure 5.8). The distribution of black coloration throughout both caves is a line of evidence that had traditionally been used locally to suggest forest fire aerosols as the main cause of the coloration. Photograph K, Figure 5.2 displays evidence of preferential flowstone coloration on the entrance-facing surfaces. Additionally, black coloration is only observed on horizontal surfaces with normal coloration on vertical surfaces (Photographs J, K, L in Figure 5.2, and Photographs N and O, Figure 5.3). It has been established (Section 4.1.) that forest fires are not the likely cause of coloration events. However, the distribution of coloration still indicates a relationship with aerosol deposition from gravitational settling processes. This section explores the relationship of drip water and aerosol contributions to the Yarrangobilly flowstones.

Aerosol contributions to speleothem geochemistry are calculated as in Chapter 2. Annual aerosol deposition rates are compared to elemental masses accumulated through one year of speleothem precipitation. A summary of the results for these calculations are shown in Table 5.6.

| | Sr (%) | Mg (%) | P (%) | Al (%) | Zn (%) |
|---|---|---|---|---|---|
| **Harrie Wood** | | | | | |
| Max | 352 | 577 | 1315 | 24509 | 41481 |
| Min | 2 | 7 | 4 | 2 | 1 |
| STDEV | 56 | 70 | 143 | 1718 | 967 |
| Average | 100 | 255 | 122 | 1100 | 264 |
| | | | | | |
| **Jersey** | | | | | |
| Max | 17 | 65 | 62 | 4101 | 58333 |
| Min | 0 | 1 | 0 | 0 | 2 |
| STDEV | 3 | 8 | 7 | 287 | 1360 |
| Average | 5 | 29 | 6 | 184 | 371 |
| | | | | | |
| **Average** | | | | | |
| Max | 185 | 321 | 688 | 14305 | 49907 |
| Min | 1 | 4 | 2 | 1 | 1 |
| STDEV | 29 | 39 | 75 | 1003 | 1163 |
| Average | 52 | 142 | 64 | 642 | 318 |

Table 5.6: Aerosol contributions to speleothem geochemistry % results. Results display the aerosol contribution as a percentage of total speleothem elemental abundance. Results are based on speleothem growth of 1.7 μm year $^{-1}$ (averaged from YBJD1) and compared to YBJD1 speleothem geochemistry. Minimum, maximum and standard deviations apply to the range in results when a single deposition values was applied to the speleothem LA-ICP-MS data for the entire growth duration.

Table 5.6 presents average contributions for YBJD1; during hiatus events the relative contribution of aerosols would increase further. Additionally, YBJD2 presents slower growth rates which would result in further elevated aerosol contributions relative to speleothem geochemistry. Characteristic aerosol enrichments of environmental significance are observed in Mg, Al, P and Fe aerosol deposition flux (Figure 5.7). The relationship between supply and

flowstone geochemistry suggests that low aerosol incorporation efficiencies are taking place. Table 5.7 presents the levels of aerosol and drip water elemental supply. Limiting drip rates present the drip water discharge rates that would be required to reduce elemental supply to that of aerosol supply. However, modern monitoring may not accurately represent conditions during flowstone formation. Opening of the cave to visitors may have caused increased cave ventilation and aerosol transportation processes resulting in elevated aerosol deposition flux.

| Sample | Oversupply (%) | | Limiting drip rate (L/yr) |
|---|---|---|---|
| | Drip | Aerosol | |
| **YBJD1** | | | |
| Mg | 36400000 | 1200 | 0.0019 |
| Sr | 1030000000 | 382 | 0.000021 |
| **YBJD2** | | | |
| Mg | 30800000 | 942 | 0.0017 |
| Sr | 294000000 | 318 | 0.000061 |

Table 5.7: Drip water and aerosol oversupply (%) and limiting drip rates (L/yr) based on 56 L/yr discharge rate and 1.7 μm speleothem growth rates. Limiting drip rates are those at which drip water chemistry supply is equal to that of aerosol flux. Drip water oversupply (%) = 1/[ Mg of element per year calcite growth / Mg of drip water supply per year ×100] ×100. Aerosol flux oversupply (%) = 1/[Mg of element per year calcite growth / Mg of aerosol flux to speleothem surface per year) ×100] ×100.

Speleothem geochemistry will therefore be evaluated with the understanding that aerosol supply has the potential to substantially increase flowstone concentrations under suitable incorporation scenarios.

### 5.4.3. Flowstone Geochemistry

PCA analysis of the entire LA-ICP-MS results highlights the predominant geochemical groupings and allows deduction of the processes influencing flowstone geochemistry.

YBJD1 PCA results (Figure 5.18) display a clear and distinct separation of elements into two groups: 1) Sr, Mg, U, P and 2) Mn, Ce, Th, Al, Fe, Y. Results indicate a shift between the influence of hydrological processes and colloidal transport to the flowstone. Colloidal influences on YBJD1 (Factor 1 loading, Figure 5.15) present short lived high amplitude events. Increased colloidal element concentrations are observed at red horizons and the main sample hiatus event. High discharge events and hiatus events often result in elevated colloidal influence (Treble & Fairchild, 2009). The loading of Sr, Mg and U on factor 2 indicates a dominant hydrological control with increased concentrations indicating drier conditions. There is a clear relationship between hydrological influences and black calcite, with elevated influence occurring at each section (Figure 5.15 – factor 2 results).

YBJD2 PCA analysis (Figure 5.20) presents a similar grouping to YBJD1. Colloidally derived elements (Th, Fe, Al, Y) display a clear separation from hydrologically controlled Sr and Mg. However, the system presents more complexity than YBJD1 with U, Ce and Mn presenting a separate correlation to hydrological and colloidal influences. Additionally, P aligns with colloidally controlled elements which differ to YBJD1, where P presents a correlation with hydrological processes.

Average chemistries of different calcite sample colours are presented in Table 5.8. For the majority of elements, the greatest concentrations are observed in the red calcite, in both

samples. High elemental variability is observed across all elements and calcite coloration, as demonstrated by section standard deviations (σ). Relative standard deviations (Table 5.8) demonstrate a high level of variability within each section of growth. The highest levels of variability are observed with Ce and Th, and overall with the white calcite.

Microbial bioaccumulation processes may be occurring and influence the environmental signature observed in the Yarrangobilly flowstones. The evidence for bacterial colonisation and geochemical influencing processes are explored further in section 5.5.3.

| YBJD1 | | Mg | Al | P | Mn | Fe | Sr | Y | Ce | Th | U |
|---|---|---|---|---|---|---|---|---|---|---|---|
| **Total** | **Average** | 191 | 81 | 166 | 0.32 | 121 | 21 | 0.061 | 0.024 | 0.0078 | 0.0187 |
| | σ | 248 | 307 | 216 | 1.02 | 91 | 31 | 0.127 | 0.142 | 0.0462 | 0.0251 |
| **Black** | **Average** | 169 | 25 | **563** | 0.26 | 110 | 8 | 0.024 | 0.007 | 0.0017 | **0.0557** |
| | σ | 46 | 57 | 267 | 0.58 | 86 | 2 | 0.033 | 0.013 | 0.0048 | 0.0276 |
| **Red** | **Average** | **223** | **178** | 87 | **0.38** | **157** | 14 | 0.073 | **0.054** | **0.0246** | 0.0121 |
| | σ | 54 | 659 | 77 | 1.28 | 203 | 5 | 0.302 | 0.183 | 0.0909 | 0.0117 |
| **White** | **Average** | 143 | 60 | 77 | 0.11 | 108 | **24** | **0.078** | 0.007 | 0.0004 | 0.0087 |
| | σ | 26 | 174 | 24 | 0.15 | 10 | 4 | 0.052 | 0.168 | 0.0017 | 0.0193 |
| | | | | | | | | | | | |
| **YBJD2** | | | | | | | | | | | |
| **Total** | **Average** | 244 | 44 | 35 | 0.22 | 95 | 26 | 0.25 | 0.0352 | 0.0076 | 0.017 |
| | σ | 374 | 149 | 77 | 1.92 | 40 | 14 | 0.55 | 0.4206 | 0.0387 | 0.045 |
| **Black** | **Average** | **280** | 11 | 12 | 0.10 | 87 | 26 | 0.12 | 0.0075 | 0.0019 | 0.015 |
| | σ | 132 | 45 | 11 | 0.35 | 14 | 10 | 0.19 | 0.0287 | 0.0082 | 0.016 |
| **Red** | **Average** | 233 | **187** | **93** | **0.36** | **133** | 17 | **0.50** | **0.0864** | **0.0291** | **0.023** |
| | σ | 104 | 289 | 70 | 0.63 | 73 | 12 | 1.20 | 0.2129 | 0.0647 | 0.028 |
| **White** | **Average** | 224 | 14 | 12 | 0.26 | 87 | **30** | 0.30 | 0.0191 | 0.0029 | 0.016 |
| | σ | 596 | 64 | 9 | 3.07 | 21 | 18 | 0.22 | 0.3126 | 0.0314 | 0.068 |

Table 5.8: Average flowstone element concentrations (ppm) and standard deviation values of entire samples, black, red and white sections of growth for samples YBJD1 and YBJD2 from LA-ICP-MS results. Highest concentrations for each element are highlighted in bold.

Table 5.8 highlights elements of high concentration for different flowstone coloration. One feature of importance is the consistently high levels of Th in red calcite (to a lesser extent the black calcite). This is significant for the consideration of U/Th dating when considering samples of low detrital Th levels, where red calcite sections should be avoided. The following sections study each period of black and red calcite formation to identify characteristic features and processes which may be acting to cause coloration.

### 5.4.4. Flowstone coloration

*Coloration event timing*

Two main black coloration events have been identified from the dating of 8 flowstones presenting black calcite growth. Two broad horizons have been identified: interval one occurring within 20-80 ka and interval two 110-180 ka. A third potential episode is identified at 330 ka to 420 ka, but with little confidence since only being observed in one sample. Red coloration events are poorly constrained as dating focused on identifying the timing of black horizons. However, two main red coloration events are identified at 0-40 ka and 240-300 ka. Figure 5.22 summarises the start and finishing times of some of the most notable black coloration horizons.
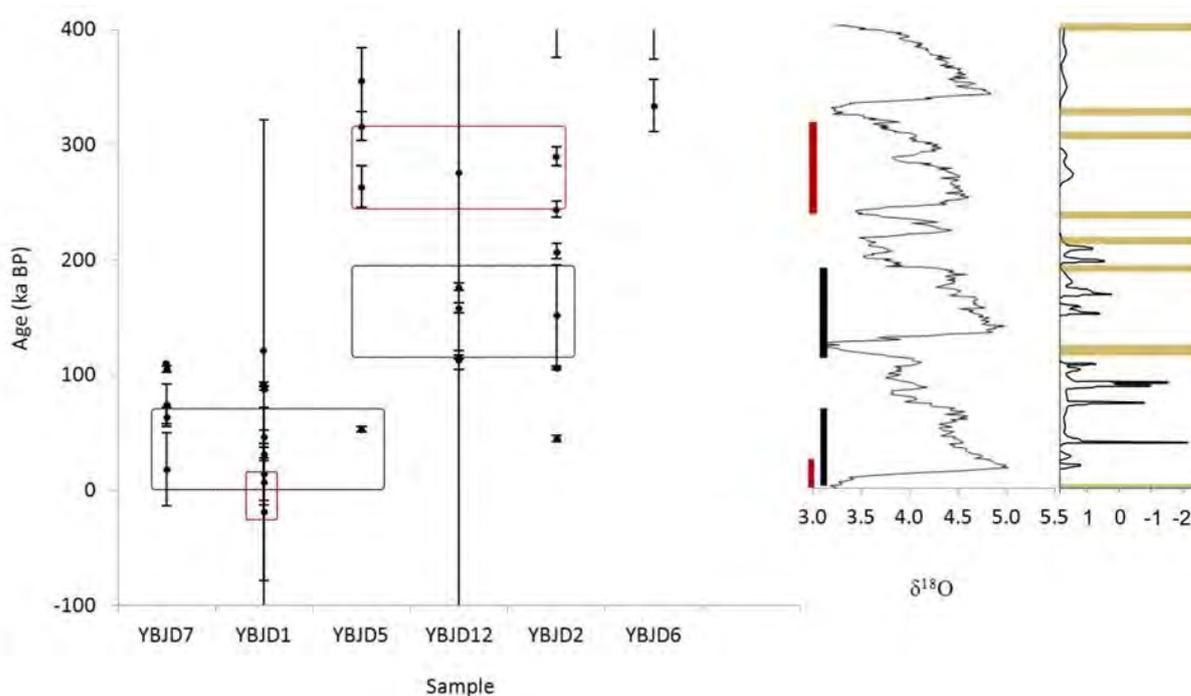


Figure 5.22: Timing of two black and two red horizon events in all samples. The timing of coloration events are compared to the global LR04 benthic $\delta^{18}O$ record (left of right panel) (Lisieki & Raymo, 2005) and Southern Australia Speleothem $\delta^{18}O$ with warm interstadials marked by yellow highlights (right graph of right panel) (Ayliffe *et al.,* 1998).

Due to the long duration of coloration events and uncertainty in the exact timing of event occurrence, palaeoclimate interpretations relating to coloration are tentative. However, results indicate that coloration events tend to begin during the transition to cooler global conditions and finish at the point of glacial termination. Therefore coloration occurs during the transition from wet vegetated periods to arid environments (Section 1.1). The dieback of vegetation occurring during the transition to glacial conditions may result in elevated organic acid release and transport from vegetation decay which could result in flowstone coloration. Specific surface and cave environmental conditions may be required for bacterial colonisation of cave surfaces, therefore colonisation may relate to environmental cycles. Surface bacterial growth may results in bioaccumulation processes or organic binding causing episodes of coloration, these concepts are explored further in section 5.5.3 and 5.5.4.

By considering sections of red and black calcite formation individually it is possible to identify reoccurring characteristics and features which separate each growth phase. The observations and comparisons underpin later process interpretations in Section 5.5.

*Red flowstone coloration*

Red sections of growth present a clear relationship with Fe and Mn when observing LA-ICP-MS results in Figures 5.17 and 5.19. Red calcite chemical composition presents a similar composition in both YBJD1 and YBJD2. PCA analysis results for sections of red calcite chemistry are presented in Figure 5.23 and 5.24, for YBJD1 and YBJD2 respectively. Both samples display a strong influence from colloidally derived elements Ce, Y, Al and Fe with loading on factor 1. Sr and P display opposing loading on factor two, potentially as a consequence of P blocking sites for Sr in calcite incorporation.

Differing acid dissolution strengths offer an insight into the amount of residue components in flowstone samples (Figure 5.12). Red calcite presents the highest levels of residue content for the majority of elements, which can be seen by the relative differences between elemental concentrations obtained via HF and $HNO_3$ dissolution.
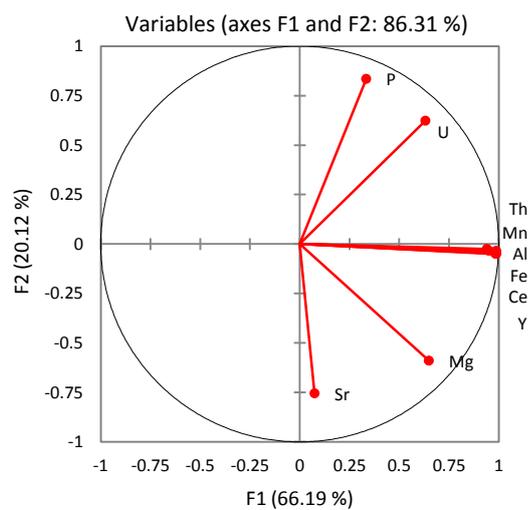
Figure 5.23: YBJD1 geochemistry PCA analysis of section of red calcite.
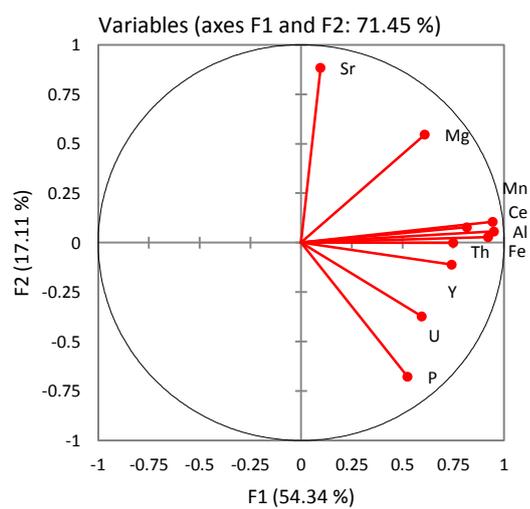


Figure 5.24: YBJD2 geochemistry PCA analysis of section of red calcite.

*Black flowstone coloration*

Black calcite offers less in terms of a definitive geochemical signature which is reproduced between samples. A study by Frisia et al. (2012) concluded that P concentrations are controlled by a diverse range of processes, which may not relate to seasonal infiltration. Additionally, it was observed that P peaks appear to not be related to an increase in colloidal transport from the soil in YBJD1, but to complex interactions between hydrological and microbial processes. P shows a clear relationship with the black section of growth in YBJD1 (Figure 5.17). However, P correlates with red coloration in YBJD2 and does not respond with the transition to black calcite (Figure 5.19). The relationship of P to other elements in the PCA analysis of YBJD1 and YBJD2 indicates that P is controlled by a different process to colloidal (YBJD1) and hydrological processes (YBJD2).

PCA analysis results highlight the different relationships between elements for YBJD1 and YBJD2, presented in Figures 5.25 and 5.26 respectively. The relationship between Sr and Mg differs between each sample, with YBJD1 presenting a strong correlation indicative of PCP processes and YBJD2 presenting a weak opposing influence of Sr and Mg. U and P present a strong correlation and influence on factor 1 loading in YBJD1. This relationship is not observed for YBJD2, with U and P presenting opposing influence on factor 2 and weak influence on factor 1. However, there are some overall consistencies in chemistry between samples. The most prominent constant feature is the correlation between colloidal element (Fe, Ce, Al and Th) influence. The extent of influence on the black calcite section chemistry is relatively limited in comparison to the factor 1 loadings observed in the red sections of growth. This indicates that colloidal element transport is occurring, but having a reduced

influence during periods of black calcite formation. Additionally, the opposition of P to Sr indicates element site competition for calcite inclusion as in the red sections of growth.
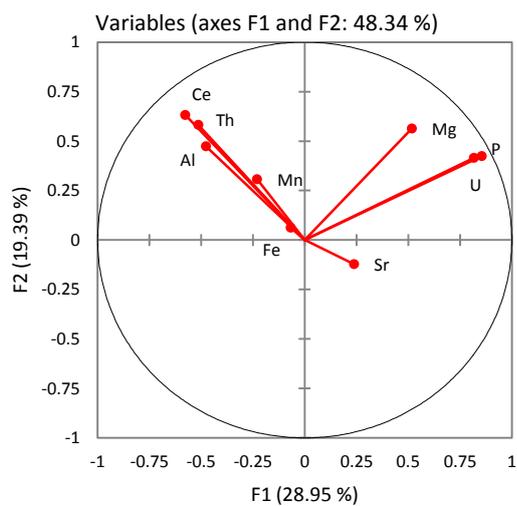
Figure 5.25: YBJD1 geochemistry PCA analysis of section of black calcite.
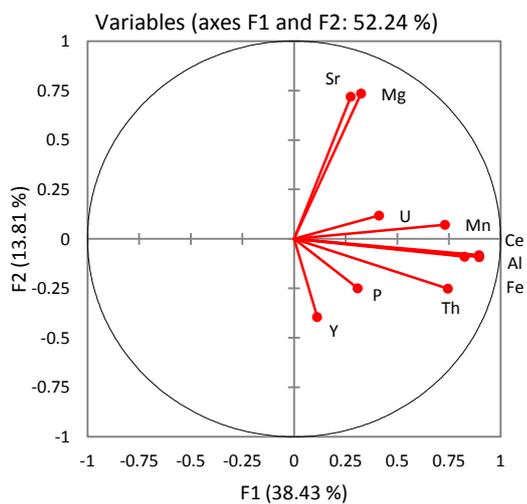


Figure 5.26: YBJD2 geochemistry PCA analysis of section of black calcite.

Bacterial analysis of modern surfaces showed that extensive colonisation is taking place on regions with black calcite, and no evidence for microbial life was observed on white coloured surfaces. A total of 8 DGGE bands were detected, falling into 6 operational taxonomic units present (OTUs, here defined as equivalent to "genus"). *Bacillus*, *Rhodococcus*, *Janibacter*, *Lechavalieria*, *Streptomyces* bacteria were detected in the black calcite sample. Additionally, luminescence analysis of black and white calcite on sample YBF1 presents a clear increase with black coloration suggesting greater organic content (Figure 5.27).
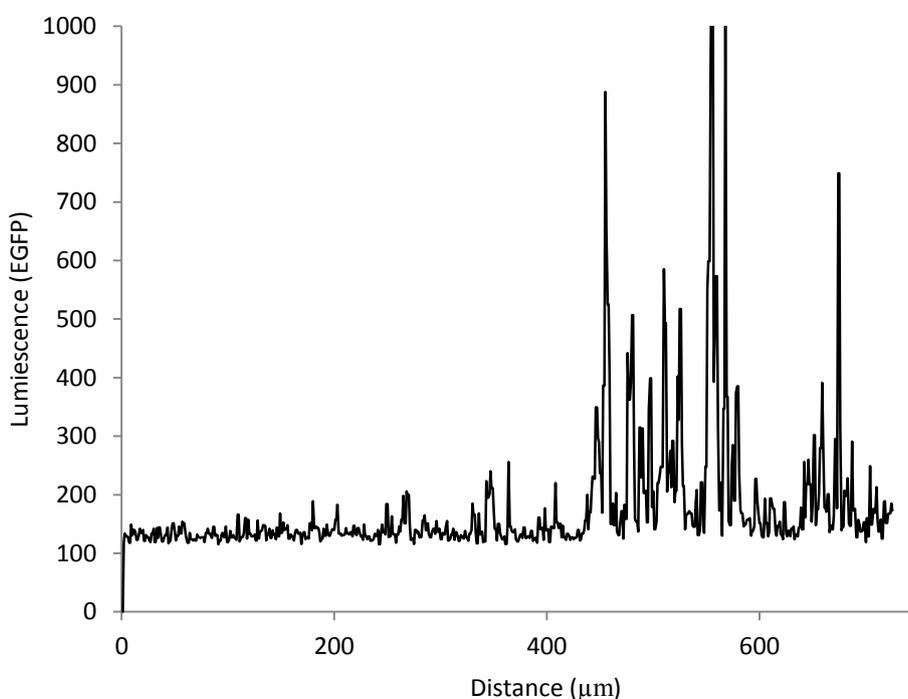


Figure 5.27: Enhanced Green Fluorescent Protein (EGFP) luminescence transitioning from white to black calcite (sample YBF1).

Black calcite sections do not present reproducibly characteristic chemical features. However, it is clear from levoglucosan, methoxyphenol, PAH and luminescence results that organic contents are higher in the black calcite. However, sufficient levels are also observed in the white calcite indicating that supply processes occur across all calcite formation types. The

pattern of coloration within the cave suggests that aerosol deposition is controlling the spatial distribution of the coloration process. It has been established from contribution calculations that the aerosol supply of inorganic (Table 5.7, Oversupply %) and PAH aerosols (Table 5.5, White Cont. % and Black Cont. %) is potentially sufficient to account for all speleothem geochemistry. However, this Chapter has highlighted the lack of representation of modern aerosol monitoring to pre-industrial flowstone growth (e.g. Section 5.4.1), and that future investigations should consider monitored aerosol levels and their potential contributions carefully.

## 5.5. Final interpretation theories and conclusions

In this section theories for calcite coloration based on evidence from this study are outlined and the conclusion presented.

### 5.5.1. Forest fires

Results presented in this study suggest that influences from regional forest fires are providing a constant signal to Yarrangobilly flowstones which is predominantly sourced through drip waters and significantly buffered by overlying soils (discussed in section 5.4.1). Increased levels of palaeofire proxies in black calcite have been predominantly attributed to reduced retention/increased incorporation due to climatic (Figure 5.22), soil and environmental processes (summarised in Section 5.5.2) and variable growth rates (Table 5.5) rather than a consequence of changing levels of supply.

### 5.5.2. Environment and soils

A weak relationship has been observed between the timing of coloration events and global climate (Figure 5.22). Coloration events initiate during the transition to arid conditions and finish at the point of glacial termination and the onset of wet conditions. Consequently, the coloration of Yarrangobilly speleothems may be caused by changing soil conditions, which in turn reflect changing environmental conditions.

Cave colouration as a result of metal oxidation has been observed in several cave locations (e.g. Lechuguilla Cave, Ochtin, Jaskinia Czarna) from ferromanganese deposits, occurring in a range of colours and chemistry with variable amounts of clay and Al-oxide minerals; all are

rich in Mn and Fe oxides (Spilde *et al*., 2005). Growth of red calcite is likely to occur during periods of oxygenated soils rich in Fe-oxide, with coloration simply being a representation of elemental transport from the overlying soils. When precipitation increases, soils begin to reduce and result in reduced oxide transport to the speleothem. The same process may be resulting in black coloration, with Mn oxides providing the source of colour.

P has shown a correlation with black coloration in YBJD1 (Figure 5.17) and red coloration in YBJD2 (Figure 5.19). P transfer processes to speleothems have been shown to vary between sites (Frisia *et al.,* 2012). However, P has generally been used to indicate mobilization during vegetation die-back and high infiltration situations (Fairchild & Treble, 2009). Additionally, the retention and release of trace elements from soil profiles through complexing with natural organic matter (NOM) is widely recognised (Hartland *et al.,* 2012). Elevated P may mark vegetative die-back events and correlate with the transition to drier more oxic soils with Fe and Mn transport through organic complexing.

An additional line of evidence for changing soil conditions is the organic supply to the flowstone sample. Assuming PAH supply to the speleothem is buffered to the extent where forest fire PAH emissions has no direct effect on speleothem concentrations, soil conditions may be the dominant control on supply. In a closed and less ventilated cave, the main source of PAH aerosols would be through the cave drip waters sourced from the overlying soils. Modern monitoring has demonstrated high levels of PAH supply across the entire mass range (Figure 5.6). Lower concentrations of PAHs would be supplied to the speleothem in high discharge scenarios due to dilution by drip water. Lower molecular weight (LMW) compounds are more easily degradable, more volatile and more water soluble than HMW

PAHs (Wilcke, 2000). During low discharge scenarios, increased solution concentrations of PAHs may occur, with soil organic binding processes having a greater influence. This would occur in the fractionation of PAHs through retention of HMW compounds, resulting in the distribution shown in Figure 5.10. Elevated levoglucosan and methoxyphenol concentrations (Figure 5.11) and increased luminescence (Figure 5.27) are also observed in the black calcite indicating a similar organic supply processes.

### 5.5.3. Microbial element fixation

Bacteria and fungi are capable of colonizing almost every niche (Bastian & Alabouvette, 2009) and a wide range of microbes are known to inhabit cave environments (reviewed in Northup & Lavoie (2001), and Barton & Northup (2007)). Bacteria are shown to be transported as an aerosol and distributed throughout cave networks in Chapter 2, Section 5.2.

Black coloration of geological material as a result of manganese staining occurs in a range of environmental settings including deserts and deep-sea deposits. Microorganisms may contribute to the formation of Mn and Fe oxide-rich deposits (Northrup *et al*., 2003) since bacteria are known to concentrate metals from their environment, most probably from water (Dorn & Oberlander, 1981). Bacteria have also been known to increase the rate of manganese oxidation by up to five orders of magnitude (Tebo *et al*., 1997). Therefore bacteria may be acting to increase element concentrations during flowstone formation resulting in coloration from Mn and Fe oxide contents. *Actinomycetes,* a bacterial strain detected in Jersey Cave have been found to produce iron and manganese oxides producing coloured deposits on cave surfaces in Guadalupe Caves (Northup *et al*. 2000; Northup *et al.,* 2003).

Clay minerals are of importance since the bacteria can adsorb on them and use nutrients that also adsorb on clay (Shahack-Gross *et al*, 1997). PCA analysis results (Figure 5.18 and 5.20) presents an association between colloidally derived elements and coloration. Greater solution bacterial supply may be occurring during periods of increased solution colloidal supply resulting in oxide bioaccumulation processes and coloration.

Frisia et al. (2012) found that microbial processes may have been involved in P incorporation in Nullarbor speleothems, and that the stromatolite-like layers mark periods of reduced drip rate and thus potentially indicative of dry phases. It is possible a similar process is taking place in Yarrangobilly, with drip water bacteria fixing P, Fe and Mn resulting in the correlation between coloration and P.

Bacterial colonisation during periods of increased colloidal supply to cave surfaces may result in bioaccumulation processes which provide a secondary feedback elevating Fe and Mn concentrations even further. However, coloration of surfaces which are not directly exposed to drip water processes requires further explanation and may be due to bacterial staining processes covered in the following section.

### *5.5.4. Bacteria and fungi melanin staining*

In addition to microbiological bioaccumulation and concentration processes, bacteria may be directly causing calcite coloration. Dark brown and black pigments are known to be produced by fungi and bacteria.

The bacterial strain s*treptomyces* in the *actinobacteria* tree, which was detected on black cave surfaces has been shown to produce melanin, creating a dark brown pigment (Vasanthabharathi *et al.,* 2011). *Streptomyces* has been also been described to cause a wide spectrum of discoloration of mural paintings in ancient Egyptian tombs (Abdel-Haliem *et al*., 2013). Groth et al. (1999) found that the majority of isolates from sampling in Altamira Cave could be assigned to *streptomyces,* with several *streptomycete* isolates producing pigments of different colour (reddish yellow, red, brown, black).

In addition to bacteria, fungi have been found to colour cave surfaces. Black stains were detected on the ceiling and banks of passages in Lascaux Cave, France. Melanised fungi were mostly responsible for these stains (Bastian & Alabouvette, 2009 Bastian *et* al., 2010). In a more recent study two new species of fungi have been identified and isolated from the black stains (Martin-Sanchez *et al.,* 2012). Fungal genera (*Cladosporium* and *Epicoccum*) detected in Altamira have the ability to form black stains and synthesize black phenolic polymers (Saiz-Jimenez *et al.,* 1995). Additionally, bacteria and fungi may interact together to produce colouring. Some bacterial species may serve as sources of substrates for melanisation of different fungi in the environment (Frases *et al*., 2006).

Aerobiology of caves is still in its infancy (Porca *et al*., 2011). However, cave ventilation is known to distribute and provide nutrient distribution throughout cave networks (Porca *et al*., 2011; Dredge *et al.,* 2013). Consequently, there will be a supply of bacteria to all cave surfaces with colonisation only occurring when optimal conditions are met. A sufficient nutrient supply is required for colonisation, it has been established that a high amount of aerosol flux to cave surfaces is taking place (Table 5.6). Bacterial colonisation as a consequence of aerosol deposition may explain the distribution of coloration observed in Yarrangobilly caves (distribution on horizontal surfaces Photographs J, L, O). Additionally, modern surface bacterial analysis demonstrated colonisation only on black coloured surfaces (described in 'Black Coloration', Section 5.4.4).

### 5.5.5. Overall conclusion

There is no evidence to suggest that flowstone coloration is occurring as a direct consequence of forest fire aerosol deposits from within the cave. Bacterial controlled processes are most likely resulting in speleothem coloration, either by melanisation processes on cave surfaces or by the bioaccumulation of Fe and Mn oxides. Melanisation by bacteria, staining cave surfaces accounts for the observed distribution of black coloration in Yarrangobilly caves on horizontal and windward surfaces. However, before the creation of artificial entrances when ventilation was lower, aerobiological fluxes to cave surfaces would have been lower and may not have caused the distribution of coloration occurring in the modern cave environment. Cave drip water and soil influences may have been of greater influence during times of reduced aerobiological and aerosol nutrient supply. During these phases coloration may have only occurred on actively forming flowstone surfaces. Figure 5.28 displays the processes that have been interpreted to cause Yarrangobilly flowstone coloration and characteristic features of the different calcite colours.
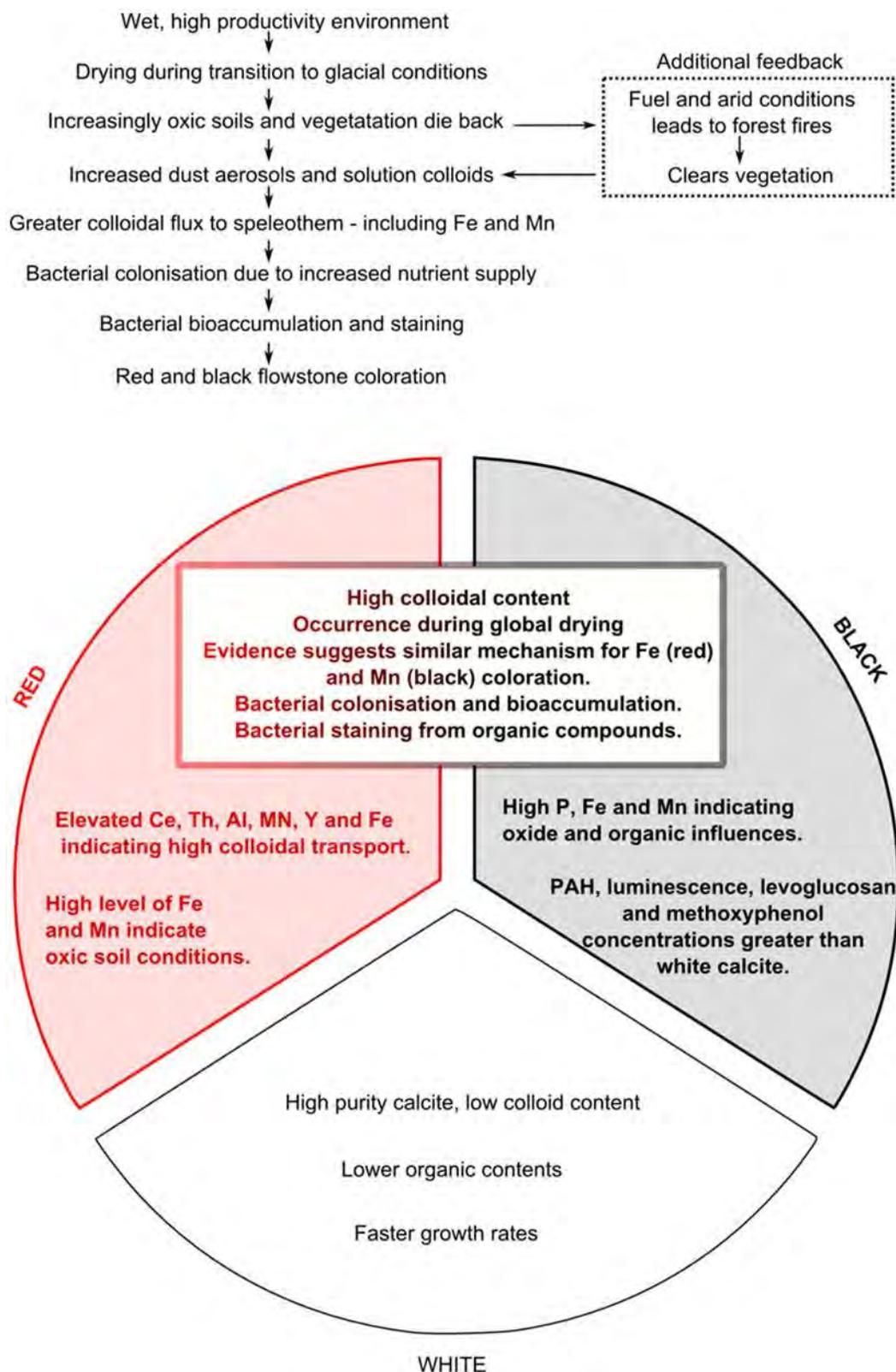
Figure 5.28: Environmental processes leading to coloration and the key chemical characteristics of red, black and white coloured flowstones. Similar features between red and black calcite are also outlined.

# Conclusions to aerosol contributions to speleothem geochemistry



*Cave field work in Gibraltar (Cave location used in Chapter 4).*

# Chapter 6: Conclusions

This project constitutes the first study of aerosol contributions to speleothem geochemistry. Issues surrounding cave aerosols and incorporation in speleothem have been explored and synthesized.

## 6.1. Aerosols

Aerosol introduction, distribution, deposition and incorporation are complex and variable processes dictated heavily by the specific cave situation (as explored in Chapter 1). Details on cave aerosol distribution and transport are described in Section 2.3.2. The type of speleothem formation and cave morphology (Chamber size, air flow rates and aerosol deposition, Figure 2.19) has been determined to control deposition through impaction/interception processes. Gravitational sedimentation (Progressive suspended load losses, Figure 2.19) and cave entrance zone aerosol deposition (Figure 2.13) have been identified as dominant processes involved with influencing cave aerosol distribution.

Surrogate surface (Chapters 2, 3, 4 and 5), active suspended aerosol sampling (Chapter 4) and particle counting methods (Chapter 2 and 3) were employed in this investigation. Methods were primarily chosen based on their ability to be transported to, and within cave networks, and operate without mains power. A summary of cave aerosol methods and analytical techniques are reviewed in Chapter 1, Section 2.2.

Cave aerosols are sensitive to environmental conditions (ventilation, drip water flow rates) and therefore will exhibit temporal and spatial variations. Chapter 2 shows that aerosol monitoring has the potential to be used in cave ventilation studies in place of existing $CO_2$ and temperature work. Suspended aerosol concentrations show a clear correlation with cave $pCO_2$ indicating a ventilation control (Figure 2.10, Figure 2.14 and Figure 3.5). Cave aerosols are sensitive to anthropogenic influences (Discussed in Section 2.4.1, Figure 2.6 and Figure 2.7) and also present relatively fast recovery rates to baseline levels (compared to $CO_2$ and T). Monitoring in Chapter 3 demonstrates that daily aerosol minima provide a unique indicator of natural seasonal ventilation processes, little perturbed by anthropogenic influences (Figure 3.5). A summary of cave aerosol production and removal processes are illustrated and in Figure 2.5.

Calculations in Chapter 2 have demonstrated that the ultimate aerosol contribution to speleothem geochemistry is predominantly dependent on growth rates, deposition flux, and aerosol incorporation factors (Relationship between aerosol deposition flux, speleothem growth rates and calcite concentrations presented in Figure 2.21). Results have shown that aerosol contributions to speleothem chemistry will commonly be of low significance (e.g. Obir Cave Austria Figure 2.22); but, in certain instances aerosols may provide considerable additions to geochemistry.

Situations where aerosol deposition may provide noteworthy contributions to speleothem have been summarised:

- Hiatus events (ceased/very slow speleothem growth) (explored in Chapter 2)

- Very high deposition flux rates as a result of a combination of efficient aerosol transport and large external suspended loads

- Secondary microbial feedback processes resulting in increased concentrations (further confirmed in Chapter 5)

In such instances aerosols, through speleothem incorporation, may provide a novel environmental indicator not yet constrained by existing proxies. Case studies of aerosol contributions to flowstones have shown location specific aerosol source additions of varying significance.

External aerosol emissions can occur from a range of sources (summarised in Figure 2.1). Terrestrial and marine external aerosol contributions through surface deposition and solution transport have been identified in Gibraltar (Chapter 4, Section 4.4.4). Marine aerosols are a significant contributor to Gibraltar flowstone geochemistry, accounting for 18.5% of modern drip water Sr content (based on calculations in Section 4.4.4, results in Table 4.7). Al and Fe from terrestrial aerosol source have been determined as the most influential elemental contribution to be preserved in the Gib08 flowstone record from New St Michaels Cave, Gibraltar. Additionally, temporal $^{87}Sr/^{86}Sr$ changes in the Gibraltar flowstone are attributed to small changes of highly radiogenic dust inputs associated with millennial scale global climate change (Sr isotope mixing presented in Figure 4.20).

Bacteria transported in the form of aerosols have shown to be distributed throughout Altamira cave, Spain (Chapter 2, Section 2.5.2, Figure 2.23). In Yarrangobilly caves (Chapter 5) *Actinomycetes* bacteria has been detected and may be acting to increase element

concentrations during flowstone formation resulting in coloration from Mn and Fe oxide contents. In addition to microbiological bioaccumulation and concentration processes, aerosol-sourced bacteria (*Streptomyces*) may be directly causing calcite coloration through melanisation staining processes (Summary of Yarrangobilly flowstone coloration process in Figure 5.28). Results from Chapters 2 and 5 have shown that there will be a supply of bacteria to all cave surfaces, and it is suggested that colonisation will only occur when optimal conditions are met. It has therefore been concluded that inorganic aerosol deposition to cave surfaces is an influential component on the distribution of aero-microbiological colonisation.

## 6.2. Flowstones

Flowstone geochemistry has been investigated in order to explore aerosol contributions to chemistry. Modern drip water sampling in Gibraltar (Chapter 4) demonstrates evidence for prior calcite precipitation (PCP) processes taking place (Figure 4.6). Calculated indices for PCP evolution ($F_{PCP}$) and dissolution source chemistry ($F_{SOURCE}$) offer new measures for source type and the extent of PCP occurring throughout the flowstone (Gib08) growth period (explored in Section 4.4.2, Figure 4.16 presents the Gib08 $F_{PCP}$ and $F_{SOURCE}$ record). Comparisons of trace element compositions of coloured sections in Yarrangobilly flowstone growth (Chapter 5) have revealed the changing environments and processes throughout sample growth periods.

U-series dating of flowstones have enabled the identification of hiatus events and comparison of well constrained fast growth sections in Chapter 4 and 5. A notable finding is that trace element geochemistry identifies potential smaller duration hiatus events not recorded in the geochronology, offering an additional tool for growth analysis. Hiatus occurrence has been established to be controlled by local rather than climatic processes, with each hiatus marking a change in the flowstone growth systems.

Yarrangobilly flowstone coloration has been established (through geochemical analysis) as an indicator of increased colloidal contents (section 5.4.3), and increased detrital Th. Therefore coloration may provide a useful tool in avoiding high detrital Th concentration samples in future studies of coloured speleothem samples.

## 6.3. Palaeoclimate interpretations

Based on the additional insights of aerosol contributions to flowstone geochemistry, palaeoclimate interpretations have been formed. Broad glacial-interglacial climatic shifts are observed in the Gibraltar flowstone core results, presented in Chapters 4. Fast growth events present a strong relationship with the timing of Mediterranean region sapropel events indicating a relationship with continental rainfall levels (Figure 4.18). Results have shown the strength of climatic processes over local processes such as PCP and bedrock dissolution during flowstone formation, further validating the use of flowstones in palaeoclimatic and aerosol investigations. Palaeoclimatic geochemical manifestations vary substantially between Gibraltar and Yarrangobilly.

Relationships between $^{87}Sr/^{86}Sr$ and $\delta^{18}O$ in the Gib08 flowstone record (Figure 4.21) potentially represent glacial-interglacial shifts associated with changes in air circulation patterns and dust budgets. Additionally, trace elements present a record of discharge and precipitation (Figure 4.17) resulting in the broad relationships between local processes (PCP and bedrock dissolution) and those occurring externally (precipitation chemistry, dust fluxes).

A connection has been observed between the timing of coloration events in Yarrangobilly flowstones and global climate in Chapter 5. Consequently, the coloration of Yarrangobilly speleothem may be indirectly caused by changing soil conditions, which in turn reflect changing environmental conditions. Additionally, microbial colonisation may occur as a result of changing soil colloid transport and result in coloration through bioaccumulation or melanisation processes.

Aerosol processes which significantly contribute to speleothem geochemistry have been identified and investigated at two flowstone locations. The work presented in this thesis has successfully met the original project aims and objectives (Chapter 1, Section 1.4.).

1. The transport, distribution and deposition of aerosols have been explored throughout several cave locations and successfully quantified (Chapters 2 and 3)

2. Contributions of inorganic, organic and bio-aerosols to speleothem geochemistry have been defined and effectively quantified through theoretical and empirical modelling based on monitoring at several locations (Chapters 2, 4 and 5)

3. Analysis of flowstone samples from Gibraltar (Chapter 4) and Yarrangobilly (Chapter 5) have explored aerosol contributions from a range of processes and identified significant aerosol contributions at each site

## 6.4. Project limitations, future work and wider implications.

This investigation has explored a range of topics associated with cave aerosols, but has also identified avenues for further investigation. This section will describe opportunities for further research regarding aerosol contributions to speleothem geochemistry. Additionally, the wider implications and application of the research conducted as part of this thesis and future work will be explored.

*Aerosol palaeoenvironmental proxies*

Aerosol chemical signatures must be identifiable in order to fully utilise aerosols as a palaeoenvironmental proxy. Therefore, one of the primary aspects of future work will involve recognising aerosols chemistry contributions from specific sources preserved in the

speleothem record. Aerosol source chemistries are well known (Harrison *et al.,* 2003), the greatest challenge is separating aerosol chemistry contributions from other sources. This can only be achieved in situations where a unique identifiable aerosol feature can be observed. It is possible that further information could be obtained through the combined investigation of speleothem and aerosol REE compositions. Therefore future research should focus on searching for specific markers of aerosol events which are not detected in speleothems as a consequence other environmental processes. For example, there is potential for processes such as PAH mass fractionation (as explored in Section 5.4.1) to separate drip water and aerosol supply processes effectively. Once aerosol signatures are effectively deciphered, records of currently undetectable environmental processes may be determined. Greater understanding of atmospheric processes has the potential to vastly improve our understanding of palaeoclimate processes. Aerosol science has had a recent increased research effort stemming from recognition of the impact that aerosols have on the climate system and the large uncertainties associated with the role of aerosols in the radiation budget (Engelstaedter *et al*., 2006). Speleothem have the potential to reveal the relationship between aerosols and climate, and most importantly, since much of current palaeoenvironmental data is sourced from marine or fluvial records, how this affects the terrestrial environment.

*Aerosols and speleothem stratigraphy*

This study has confirmed the importance of hiatuses when investigating aerosols in speleothem (section 2.5). If aerosols can be detected in speleothem effectively then hiatuses offer two perspectives of study. The accumulation of aerosols can be used to confirm the length of an already detected growth hiatus by through rates of vertical accretion (as conducted in sections 2.4.2 and 5.3.2). Alternatively, aerosol signatures can be utilised to

determine the presence of unknown hiatuses. Hiatuses in samples of complex stratigraphy may be numerous and short-lived, and undetectable by currently available dating resolution. Therefore aerosol accumulation identification would reveal the intricacies of sample stratigraphy, improving age models and palaeoclimatic interpretations. Further research could conduct specific analysis of hiatus event geochemistry to explore aerosol contributions. SEM imaging of hiatus horizons would potentially allow for identification of specific aerosols grains. Targeted chemical analysis could then be utilised to investigate specific aerosol accumulation events associated with growth hiatuses. Additionally, aerosol accumulation has the potential to provide palaeoenvironmental insights during hiatus periods, improving incomplete data sets. The focused (high resolution) investigation of hiatus events will most likely yield the greatest advances in the understanding of aerosol additions to speleothem in the future.

*Aerosols and cave ventilation/environments*

Aerosol monitoring in cave environments has demonstrated the relationship between the cave environment and suspended aerosol concentrations, especially with ventilation processes as explored in Chapter 3. This sector of cave aerosol science demonstrates promise in its ability to develop cave ventilation monitoring. The sensitivity of cave aerosols (explored in Chapter 2) allows for the determination of cave atmospheric recovery and the quantitative determination of ventilation rates. Furthermore, such calculations of natural ventilation processes can potentially be carried out in anthropogenically influenced environments through the separation of baseline natural ventilation and human activity. Future research could develop the ability to utilise aerosols as a ventilation proxy by monitoring in more cave locations. Due to the limitations of this investigation (and flooding) the combination of spatial

and temporal monitoring was not achieved. Monitoring in this investigation was limited to the summer-winter transition, due to time constraints. Therefore, monitoring suspended aerosols over long time durations (>2 seasons), in multiple cave sites, with multiple intra-cave locations would offer further insight into the potential of aerosol monitoring. Additionally, monitoring different aerosol size groups would provide further information on aerosol transport processes based on suspension velocities (Figure 2.3). Combining suspended aerosol monitoring, aerosol deposition monitoring and aerosol sample geochemical analysis would provide insight into the relationship between aerosol supply, distribution, ventilation and chemistry. A combined study could potentially reveal new discoveries regarding ventilation and speleothem chemistry further contributing to the value of aerosols as a palaeoenvironmental proxy.

*Aerosol imaging*

Further imaging of residue analysis (imaging results, section 5.3.4, Figure 5.13 and Figure 5.14) especially of hiatus sections may provide more details on speleothem aerosol contents, and the type and size of incorporated aerosols. Combining imaging (e.g. SEM analysis) of calcite residue, external aerosols and cave aerosol samples would allow for the identification of potentially consistent aerosol incorporations. Imaging would provide further evidence regarding aerosol accumulation and incorporation which could be applied when searching for aerosol contributions at hiatus events, and within speleothem formation.

*Bioaeorosls*

Chapter 5 (section 5.5.4) proposed the relationship between aerosol deposition, bioaerosol transport, microbial colonisation of cave surfaces and speleothem coloration in Yarrangobilly

Caves, Australia. The science of bioaerosols is in its infancy (Porca *et al.*, 2011), consequently there are many avenues for further investigation that build on the work of this thesis and the literature. However, studying the relationship between bioaerosol and inorganic aerosol deposition to cave surfaces and microbial colonisation would be a very useful addition to speleothem science. There is potential for microbial colonisation to significantly influence speleothem geochemistry and speleothem formation. Understanding the extent to which aerosol deposition contributes to colonisation processes, combined with a better understanding of speleothem aerosol contents could improve knowledge of how colonisation influences speleothem geochemistry. Ultimately, this sector of investigation could lead to the discovery of further environmental proxies.

# References

Abdel-Haliem., M.E.F. Sakr, A.A., Ali, M.F., Ghaly, M.F. & Sohlenkamp, C. 2013. Characterization of Streptomyces isolates causing colour changes of mural paintings in ancient Egyptian tombs, *Microbiological Research*, **168(7),** 428-437.

Alfödy, B., Török, S.Z., Hofmann, W. & Bergmann, R. 2000. Intrapulmonary particle deposition and retention. *Journal of Aerosol Science*, **31(Supp 1)**, S504-S505.

Alfödy, B., Török, Sz., Kocsonya, A., Szökefalvi-Nagy, Z. & Balla, Md.I. 2001. X-ray analysis of aerosol samples from a therapeutic cave. *Nuclear Instruments and Methods in Physics Research B*, **174**, 361-366.

Allen, A.G., Nemitz, E., Shi, J.P., Harrison, R.M. & Greenwood, J.C. 2001. Size distributions of trace metals in atmospheric aerosols in the United Kingdom. *Atmospheric Environment*, **35,** 4581–4591.

Andrews, J.E., Portman, C., Rowe, P.J., Leeder, M.R. & Kramers, J.D. 2007. Sub-orbital sea-level change in early MIS 5e: New evidence from the Gulf of Corinth, Greece. *Earth and Planetary Science Letters*, **259(3–4)**, 457-468.

Avigour, A., Magaritz, M., Issar, A. & Dodson, M.H. 1990. Sr isotope study of vein and cave calcites from southern Israel. *Chemical Geology*, **82**. 69-81.

Ayalon, A., Bar-Matthews, M. & Kaufman, A. 1999. Petrology, strontium, barium and uranium concentration, and strontium and uranium isotope ratios in speleothems as palaeoclimatic proxies: Soreq Cave, Israel. *The Holocene,* **9(6)**, 715-722.

Ayliffe, L.K., Marianelli, P.C., Moriaty, K.C., Wells, R.T., McCulloch, M.T., Mortimer, G.E., Hellstrom, J.C. 1998. 500ka precipitation record from southeastern Australia: Evidence for interglacial relative aridity. *Geology*, **26(2)**, 147-150.

Badino, G. 2004. Clouds in Caves. *Speleogenesis and Evolution of Karst Aquifers*, **2(2)**.

Bae, S. Y., Yi, S. M. & Kim, Y.P. 2002. Temporal and spatial variations of the particle size distribution of PAHs and their dry deposition fluxes in Korea. *Atmospheric Environment*, **36**, 5491-550.

Baker, A. & Smart, P.L. 1995. Recent flowstone growth rates: field measurements in comparison to theoretical predictions. *Chemical Geology*, **122**, 121–128.

Baker, A., Ito, W., Smart, P.L. & McEwan, R.F. 1997. Elevated and variable values of $^{13}$C in speleothems in a British cave system. *Chemical Geology*, **136**, 263–270.

Baldini, J.U.L., McDermott, F. & Fairchild, I.J. 2006. Spatial variability in cave drip water hydrochemistry: Implications for stalagmite paleoclimate records, *Chemical Geology*, **235(3–4)**, 390-404.

Baldini, J.U.L., McDermott, F., Hoffmann, D.L., Richards, D.A. & Clipson, N. 2008. Very high-frequency and seasonal cave atmosphere $PCO_2$ variability: Implications for stalagmite growth and oxygen isotope-based palaeoclimate records. *Earth and Planetary Science Letters,* **277**, 118-129.

Banner, J.L., Musgrove, M.-L., Asmerom, Y., Edwards, R.L. & Hoff, J.A. 1996. High-resolution temporal record of Holocene ground-water chemistry: tracing links between climate and hydrology. *Geology*, **24**, 1049–1053.

Banner, J.L., Guilfoyle, A., James, E.W., Stern, L.A. & Musgrove, M. 2007. Seasonal variations in modern speleothem calcite growth in Central Texas, USA. *Journal of Sedimentary Research*. **77**, 615–622.

Bar-Matthews, M., Ayalon, A., Matthews, A., Sass, E. & Halicz, L. 1996. Carbon and oxygen isotopic study of the active water-carbonate system in a karstic Mediterranean cave: implications for palaeoclimate research in semiarid regions. *Geochimica et Cosmochimica Acta*, **60**, 337–347.

Bar-Matthews, M., Ayalon, A. & Kaufman, A. 1997. Late Quaternary paleoclimate in the Eastern Mediterranean region from stable isotope analysis of speleothems at Soreq Cave, Israel. *Quaternary Research*, **47**, 155–168.

Bar-Matthews, M., Ayalon, A., Kaufman, A. & Wasserburg, G.J. 1999. The Eastern Mediterranean palaeoclimate as a reflection of regional events: Soreq cave, Israel. *Earth and Planetary Science Letters*, **166**, 85-95.

Bar-Matthews, M., Ayalon, A. & Kaufman, A. 2000. Timing and hydrological conditions of sapropel events in the eastern Mediterranean, as evident from speleothems, Soreq Cave, Israel. *Chemical Geology,* **169**, 145–156.

Baron, P. A. & Willeke, K. 1999. Gas and Particle Motion. Aerosol Measurement: Principles, Techniques and Applications, Eds: Klaus Willeke and Paul A. Baron. Van Nostrand Reinhold, New York.

Bartenev, O.S. & Veselova, N.V., 1987. On anthropogenic dust pollution in caves of the Cupp-Coutunn Cave System. Kiev, *Problemy Izucheniya, Ekologii i Okhrany Pescher,* **159**

Barton, H.A. & Northup, D.E. 2007. Geomicrobiology in cave environments: past, current and future perspectives. *Jounral of Cave and Karst Studies,* **69(1),** 163-178**.**

Bastian, F. & Alabouvette, C. 2009a. Light and shadows on the conservation of a rock art cave: The case of Lascaux cave. *International Journal of Speleology*, **38(1)**, 55-60.

Bastain, F., Alabouvette, C. & Saiz-Jimenez, C. 2009b. The impact of arthropods on fungal community structure in Lascaux Cave. *Journal of Applied Microbiology*, **106**, 1456–1462.

Bastain, F., Alabouvette, C., Saiz-Jimenez, C. 2009c. Bacteria and free-living amoeba in the Lascaux Cave. *Research in Microbiology*, **160**, 38-40.

Bastian, F., Jurado, V., Novákova, A., Alabouvette, C. & Saiz-Jimenez, C. 2010. The microbiology of Lascaux Cave. *Microbiology*, **156**, 644-652.

Bastin, B. 1978. L'analyse pollinique des stalagmites:Une nouvelle possibilite d'approche des fluctuations climatiques du quaternaire. *Annales de la Societé Geologique de Belgique*, TlOl, 13-19.

Blyth A.J., Watson, J.S., Woodhead, J. & Hellstrom, J. 2010. Organic compounds preserved in a three million year old stalagmite from the Nullarbor Plain, Australia. *Chemical Geology*, **279**, 101-105.

Borsato, A., Frisia, S., Fairchild, I.J., Somogyi, A. & Susini, J. 2007. Trace element distribution in annual stalagmite laminae mapped by micrometer-resolution X-ray

fluorescence: Implications for incorporation of environmentally significant species. *Geochemica et Cosmochimica Acta*, **71,** 1494-1512.

Boonyatumanond, R., Wattayakorn, G., Togo, A. & Takada, H. 2006. Distribution and origins of polycyclic aromatic hydrocarbons in (PAHs) in riverine, estuarine and marine sediments in Thailand. *Marrine Pollution Bulletin,* **52(8)**, 942-956.

Bowket, 2012. MSc thesis.

Bowler, J.M. 1986. Quaternary landform evolution. IN: Jeans, D.N. Australia – A Geography, Volume 1. The Natural Environment. *Sydney University Press.* 117-147.

Bozlaker, A., Muezzinoglu, A., Odabasi, M. 2008. Atmospheric concentrations, dry deposition and air-soil exchange of polycyclic aromatic hydrocarbons (PAHs) in an industrial region in Turkey. *Journal of Hazardous Materials*, **153**, 1093-1102.

Bridgman, H., 1994. Global Air Pollution: problems for the 1990s. Chichester: John Wiley and Sons.

Buckman, S., Brownlie, K.C., Bourman, R.P., Murray-Wallace, C.V., Morris, R.H., Lachlan, T.J., Roberts, R.G., Arnold, L.J. & Cann, J.H. 2009. Holocene palaeofire records in a high-level, proximal valley-fill (Wilson Bog), Mount Lofty Ranges, South Australia. *The Holocene*. **19**. 1017-1029.

Burney, D.A. & Burney, L. 1993. Modern pollen deposition in cave sites: Experimental results from New York State. *New Phytologist,* **124,** 523–535.

Burton, E.A. & Walter, L.M. 1991. The effects of $P_{CO2}$ and temperature on magnesium incorporation in calcite in seawater and $MgCl_2$-$CaCl_2$ solutions. *Geochimica et Cosmochimica Acta* **, 55,** 777–785.

Bytnerowicz, A., Miller, P. R. & Olszyk, D. M. 1987. Dry deposition of nitrate, ammonium and sulfate to a Ceanothus crassifolius canopy and surrogate surfaces. *Atmospheric Environment*, **21(8)**, 1749-1757.

Caldwell, J.R., Davey, A.G., Jennings, J.N. & Spate, A.P. 1982. Colour in some Nullarbor Plain Speleothems. *Helictite,* **20**, 3-10.

Caseldine, C.J. McGarry, S.F., Baker, A., Hawkesworth, C. & Smart, P.L. 2008. Late Quaternary speleothem pollen in the British Isles. *Journal of Quaternary Science*, **23(2)**, 193-200.

Chang, S.J., Jeong, G.Y. & Kim, S.J. 2008. The origin of black carbon on speleothems in tourist caves in South Korea: Chemical characterization and source discrimination by radiocarbon measurement. *Atmospheric Environment*, **42**, 1790-1800

Chappell , J. 1991. Late quaternary environmental change in eastern and central Australia, and their climatic interpretation. *Quaternary Science Reviews,* **10,** 377-390.

Cheng, H., Edwards, R.L., Broecker, W.S., Denton, G.H., Kong, X. et al. 2009a. Ice Age Terminations. *Science*. **326**, 248-252.

Cheng, H., Fleitmann, D., Edwards, R.L. et al. 2009b. Timing and structure of the 8.2 ka event inferred from $\delta^{18}O$ records of stalagmites from China, Oman and Brazil. *Geology*, **37**, 1007–1010.

Christoforou, C.S., Salmon, L.G. & Cass, G.R. 1994. Deposition of Atmospheric Particles within the Buddhist Cave Temples at Yungang, China. *Atmospheric Environment*, **28** (12), 2081 – 2091.

Christoforou, C.S., Salmon, L.G. & Cass, G.R. 1996a. Fate of Atmospheric Particles within the Buddhist Cave Temples at Yungang, China. *Environment of Science and Technology*, **30**, 3425-3434.

Christoforou, C.S., Salmon, L.G. & Cass, G.R. 1996b. Air exchange within the Buddist cave temples at Yungang, China. *Atmospheric Environment*, **30(23)**, 3995-4006.

Chu, C.C., Fang, G.C., Chen, J.C. & Yang, I.L. 2008. Dry deposition study by using dry deposition plate and water surface sampler in Shalu, central Taiwan. *Environmental Monitoring and Assessment* **146(1)**, 441-451.

Cigna, A. 1983. The Criterion of Visitors Capacity of Commercial Caves. *International Meeting on the Show Caves and their Problems.*

Cigna, A. 1993. Environmental Management of Tourist Caves. The Examples of Grotta di Castellana and Grotta Grande del Vento, Italy. *Environmental Geology*, **21,** 173-180.

Cigna, A. & Forti, P. 1989. The Environmental Impact Assessment of a Tourist Cave. *Cave Tourism: Proceedings International Symposium for the 170th Anniversary of Postojnska Jama, Postojna*, pp 29-38.

Cigna, A. & Hill, C.A. 1997. Aerosols: Are They a Mechanism of Speleothem Growth? In: Hill, C. & Forti, P. (eds) Cave Minerals of the World. National speleological Association, Huntsville, Alabama, 255– 258.

Coles, G.M., Gilbertson, D.D., Hunt, C.O., Jenkinson, R.D.S. 1989. Taphonomy and the palynology of Cave Deposits. *Cave Science*, **16**, 83–89.

Coles, G.M. & Gilbertson, D.D. 1994. The airfall-pollen budget of archaeologically important sites: Creswell Crags, England. *Journal of Archaeological Science,* **21**, 735–755.

Conedera, M., Tinner, W., Neff, C., Meurer, M., Dickens, A.F. & Krebs, P. 2009. Reconstructing past fire regimes: methods, applications, and relevance to fire management and conservation. *Quaternary Science Reviews*, **28**, 555-576.

Conn, H.W. 1966. Barometric wind in Wind and Jewel caves, South Dakota. *Bulletin of the National Speleological Society*, **28**, 55–69.

Cuezva, S., Sanchez-Moral, S., Saiz-Jimenez, C. & Cañaveras, J.C. 2009. Microbial Communities and Associated Mineral Fabrics in Altamira Cave, Spain. *International Journal of Speleology,* **38(1)**, 83-92.

Cuezva, S., Fernandez-Cortes, A., Benavente, D., Serrano-Ortiz, P., Kowalski, A.S. & Sanchez-Moral, S. 2011. Short-term $CO_2$(g) exchange between a shallow karstic cavity and the external atmosphere during summer: Role of the surface soil layer. *Atmospheric Environment*, **46**, 1418-1427

Cuezva, S., Fernandez-Cortes, A., Porca, E., Pašić, L., Jurado, V., Hernandez-Marine, M., Serrano-Ortiz, P., Hermosin, B., Cañaveras, J.C., Sanchez-Moral, S. & Saiz-Jimenez, C. 2012. The biogeochemical role of Actinobacteria in Altamira Cave, Spain. *FEMS Microbiology Ecology*, **81(1)**, 281-290.

Denniston, R.F., González, L.A., Asmerom, Y. et al. 1999. Evidence for increased cool season moisture during the middle Holocene. *Geology*, **27**, 815–818.

Doerr, S.H., Douglas, P., Webb, J.A., Yeong, E., Glover, F. & Ficken, K.J. 2007. Black colour of Australian speleothem: Origin and palaeoenvironmental implications. *IMOG*. P445-TH.

Domínguez-Villar, D., Fairchild, I.J., Baker, A., Carrasco, R.M. & Pedraza, J. 2013. Reconstruction of cave air temperature based on surface atmosphere temperature and vegetation changes: Implication for speleothem palaeoclimate records. *Earth and Planetary Science Letters.* **369–370**, 158–168

Dorale, J.A., Gonzalez, L.A., Reagan, M.K. et al. 1992. A high-Resolution Record of Holocene Climate Change in Speleothem Calcite from Cold Water Cave, Northeast Iowa, *Science*, **258**, 1626–1630.

Dorn, R. I. & Oberlander, T. M. 1981. Microbial origin of desert varnish. *Science,* **213,** 1245–1247.

Dredge, J., Fairchild, I.J., Harrison, R.M., Fernandez-Cortes, A., Sanchez-Moral, S. Jurado, V., Gunn, J., Smith, A., Spötl, C., Mattey, D., Wynn, P.M. & Grassineau, N. 2013. Cave aerosols: distribution and contribution to speleothem geochemistry. *Quaternary Science Reviews*, **63**, 23–41

Dredge, J., Fairchild, I.J., Harrison, R.M. & Gunn, J. 2014. Processes affecting aerosol concentrations in Gough's Cave, Cheddar Gorge, UK. *Cave and Karst Science*, **41(1)**.

Dreybrodt, W., Gabrovsek, F. & Perne, M. 2005. Condensation corrosion: a theoretical approach. *Acta Carsologica*, **34(2)**, 317-348.

Dublyansky, V.N. & Dublyansky, Y.V. 2000. The role of condensation in karst hydrogeology and speleogenesis. In Speleogenesis: Evolution of karst aquifers, A.

Dulinski, M. & Rozanski, K. 1990. Formation of $^{13}C/^{12}C$ isotope ratios in speleothems: a semi-dynamic model. *Radiocarbon*, **32**, 7–16.

Eggins, S.M., Woodhead, J.D., Kinsley, L.P.J., Mortimer, G.E., Sylvester, P., McCulloch, M.T., Hergt, J.M. & Handler, M.R. 1997. A simple method for the precise determination of $\geq$ 40 trace elements in geological samples by ICPMS using enriched isotope internal standardisation, *Chemical Geology*, **134 (4)**, 311-326.

Engelstaedter, S., Tegen, I. & Washington, R. 2006. North African dust emissions and transport. *Earth-Science Reviews*, **79**, 73–100.

Faimon, J., Štelcl, J. & Sas, D. 2006. Anthropogenic $CO_2$ – flux into cave atmosphere and its environmental impact: A case study in Císařská Cave (Moravian Karst, Czech Republic). *Science of the Total Environment*, **369**, 231-245.

Fairchild, I.J., Borsato, A., Tooth, A.F. et al. 2000. Controls on trace element (Sr-Mg) compositions of carbonate cave waters: implications for speleothem climatic records. *Chemical Geology*, **166**, 255–269.

Fairchild, I.J. & Treble, P. 2009. Trace elements in speleothems as recorders of environmental change. *Quaternary Science Reviews*, **28**, 449-468.

Fairchild, I.J., Spötl, C., Frisia, S., Borsato, A., Susini, J., Wynn, P.M., Cauzid, J. & EIMF. 2010. Petrology and geochemistry of annually laminated stalagmites from an Alpine cave (Obir, Austria): seasonal cave physiology. *Geological Society, London, Special Publications*, **336**, 295-321.

Fairchild, I.J. & Baker A. 2012. Speleothem Science. *Wiley-Blackwell, Chichester*.

Falguères, C., Lumley, H. & Bischoff, J.L. 1992. U-Series dates for stalagmitic flowstone E (Riss/Würm interglaciation) at Grotte du Lazaret, Nice, France, *Quaternary Research*, **38(2)**, 227-233.

Farrant, A.R., 2010. Gough's Cave – A Field Guide. British Cave research association cave science field meeting, *British Geological Survey Internal Report.*

Fernandez-Cortes, A., Calaforra, J.M. & Sanchez-Martos, F. 2006. Spatiotemporal analysis of air condition as a tool for the environmental management of a show cave (Cueva del Agua, Spain). *Atmospheric Environment*, **40**, 7378-7394.

Fernandez-Cortes, A., Sánchez-Moral, S., Cuezva, S., Cañaveras, JC. & Abella, R. 2009. Annual and transient signatures of gas exchange and transport in the Castañar de Íbor cave (Spain). *International Journal of Speleology*, **38(2)**, 153-162.

Fernandez-Cortes, A., Cuezva, S., Sanchez-Moral, S., Porca, E., Jurado, V., Martin-Sanchez, PM. & Saiz-Jimenez, C. 2011. Detection of human-induced environmental disturbances in a show cave. *Environmental Science and Pollution Research*, **18**, 1037–1045.

Fisher, E.C., Bar-Matthews, M., Jerardino, A. & Marean, C.W. 2010. Middle and Late Pleistocene paleoscape modelling along the southern coast of South Africa. *Quaternary Science Reviews*, **29**, 1382–1398.

Fitzsimmons, K.E., Cohen, T.J., Hesse, P.P., Jansen, J., Nanson, G.C., May, J-H., Barrows, T.T., Haberlan, D., Hilgers, A., Kelly, T., Lasen, J., Lomax, J. & Treble, P. 2013. Late Quaternary palaeoenvironmental change in the Australian drylands. *Quaternary Science Reviews,* **74**, 78-96.

Fleitmann, D., Burns, S.J., Neff, U. et al. 2003. Changing moisture sources over the last 330,000 years in Northern Oman from fluid-inclusion evidence in speleothems. *Quaternary Research*, **60**, 223–232.

Fleitmann, D., Burns, S.J., Neff, U. et al. 2004. Paleoclimate interpretation of high-resolution oxygen isotope profiles derived from annually laminated speleothems from Southern Oman. *Quaternary Science Reviews*, **23**, 935–945.

Frases S., Chaskes S., Dadachova E. & Casadevall A. 2006. Induction by Klebsiella aerogenes of a melanin like pigment in Cryptococcus neoformans. *Applied and Environmental Microbiology*, **72**, 1542–1550.

Frisia, S., Bini., A. & Quinif., Y. 1993. Morphologic, crystallographic and isotopic study of an ancient flowstone (Grotta di Cunturines, Dolomites)—implications for Paleoenvironmental reconstructions. *Speleochronos*, **5**, 3–18.

Frisia, S., Borsato, A., Fairchaild, I.J. & McDermott, F. 2000. Calcite Fabrics, Growth Mechanisms, and environments of formation in speleothems from the Italian alps and Southwestern Ireland. *Journal of Sedimentary Research*, **70(5)**, 1183–1196.

Frisia, S. & Borsato, A. 2010. Karst. In: Alonso-Zarza, A.M. & Tanner, L.H. (eds.) Carbonates in Continental Settings. Elsevier, Amsterdam, pp. 269–318.

Frisia, S., Fairchild, I. J., Fohlmeister, J., Miorandi, R., Spötl, C. & Borsato, A. 2011. Carbon mass-balance modelling and carbon isotope exchange processes in dynamic caves. *Geochimica et Cosmochimica Acta*, **75** (2), 380-400.

Frisia, S., Borsato, A., Drysdale, R.N., Paul, B., Greig, A., Cotte, M. 2012. A re-evaluation of the palaeoclimatic significance of phosphorus variability in speleothems revealed by high-resolution synchrotron micro XRF mapping. *Climate of the Past,* **8**, 2039-2051.

Frumkin, A. & Stein, M. 2004. The Sahara-East Mediterranean dust and climate connection revealed by strontium and uranium isotopes in a Jerusalem speleothem. *Earth and Planetary Science Letters*, **217**, 415-464.

Gabitov, R.I., Sadekov, A. & Leinweber, A. 2014. Crystal growth rate effect on Mg/Ca and Sr/Ca partitioning between calcite and fluid: An in situ approach, *Chemical Geology*, In press, accepted manuscript.

Gabitov, R.I. & Watson, E.B. 2006. Partitioning of strontium between calcite and fluid. *Geochemistry, Geophysics, Geosystems.* **7(11)**, Q11004.

Gabrieli, J., Vallelonga, P., Cozzi, G., Gabrielli, P., Gambaro A., Sigl, M., Decet, F., Schwikowski, M., Gggeler, H., Boutron, C., Cescon, P. & Barbante, C. 2010. Post 17th-Century Changes of European PAH Emissions Recorded in High-Altitude Alpine Snow and Ice. *Environmental Science and Technology*, **44**, 3260-3266.

Garcia-Anton, E., Cuezva, S., Fernandez-Cortes, A., Sanchez-Moral, S. & Canaveras, J.C. 2012. Multiparametric surveillance of conservation measures at subterranean rock-art site: case of Altamira cave. *Geophysical Research Abstracts*, **14 (EGU2012-831)**.

Gascoyne, M. 1983. Trace-element partition coefficients in the calcite-water system and their paleoclimatic significance in cave studies. *Journal of Hydrology*, **61**, 213–222.

Gázquez, F.F., Calforra, J.M. & Forti, P. 2011. Black Mn-Fe crusts as markers of abrupt palaeoenvironmental changes in El Soplao Cave (Cantabria, Spain). *International Journal of Speleology*. **40(2)**, 163-169.

Genty, D., Diot, M-F. & O'YL, W. 2001. Sources of pollen in stalactite drip water in two caves in southwest France. *Cave and Karst Science*, **28**, 59-66

Genty, D., Blamart, D, Ouahdi, R. et al. 2003. Precise dating of Dansgaard-Oeschger climate oscillations in western Europe from stalagmite data. *Nature*, **421**, 833–837.

Genty, D., Blamart, D., Ghaleb, B., Plagnes, V., Causs, Ch., Bakalowicz, M., Zouari, K., Chkir, N., Hellstrom, J., Wainer, K. & Bourges, F. 2006. Timing and dynamics of the last deglaciation from European and North African $\delta^{13}C$ stalagmite profiles - comparisons with Chinese and South Hemisphere stalagmites. *Quaternary Science Reviews*. **25**, 2118–2142.

Ghedini, N., Gobbi, G., Sabbioni, C. & Zappia, G. 2000. Determination of elemental and organic carbon on damaged stone monuments. *Atmospheric Environment*, **34**, 4383–439

Goede, A., McCulloch, M., McDermott, F. & Hawkesworth, C. 1998. Aeolian contribution to strontium and strontium isotope variations in a Tasmanian speleothem. *Chemical Geology*, **149(1-2)**, 37-50.

Goede, A., Harmon, R.S., Atkinson, T.C. & Rowe, P.J. 1990. Pleistocene climatic change in Southern Australia and its effect on speleothem deposition in some Nullarbor caves. *Journal of Quaternary Science,* **5(1)**, 29-38.

Gradziński, M., Hercman, H., Nowak, M. & Bella, P. 2007. Age of black coloured laminae within spleothems from Domica Cave and its significance for dating of prehistoric human settlement. *Geochronometria,* **28**, 39-45.

Groth, I., Vettermann, R., Schuetze, B., Schumann, P. & Saiz-Jimenez, C. 1999. Actinomycetes in Karstic caves of northern Spain (Altamira and Tito Bustillo), *Journal of Microbiological Methods*, **36(1-2)**, 115-122

Hajna, N.Z. 2003. Chemical Weathering of Limestones and Dolomites in a Cave Environment. *Speleogenesis and Evolution of Karst Aquifers*, **1 (3)**, 2-8.

Hammer, Ø., Dysthe, D.K. & Jamtveit, B. 2010. Travertine terracing: patterns and mechanisms. *Geological Society, London, Special Publications* 2010, **336,** 345-355.

Harle, 1997. Late Quaternary vegetation and climate change in southeastern Australia: palynological evidence from marine core E55-6. *Palaeogeography, Palaeoclimatology, Palaeoecology,* **131,** 465-483.

Harper, S.L., Walling, J.F., Holland, D.M. & Pranger, L.J. 1983. Simplex optimization of multi element  ultrasonic extraction of atmospheric particulates. *Analytical Chemistry*, **55**, 1553–1557.

Harrison, R. M., Delgado-Saborit, J. M., Baker, S. J., Aquilina, N., Meddings, C., Harrad, S., Matthews, I., Vardoulakis, S. & Anderson, H. R. 2009. Measurement and modelling of exposure to selected air toxics for health effects studies and verification by biomarkers. *Research report (Health Effects Institute),* **143**, 3.

Harrison, R.M., Tilling, R., Callien Romero, M.S., Harrad, S. & Jarvis, K. 2003. A study of trace metals and polycyclic aromatic hydrocarbons in the roadside environment. *Atmospheric Environment*, **37**, 2391–2402.

Hartland, A., Fairchild, I.J. Lead, J.R. et al. 2011. Size, speciation and lability of NOM-metal complexes in hyperalkaline cave dripwater. *Geochimica et Cosmochimica Acta*, **75**, 7533–7551.

Hartland, A., Fairchild, I.J., Lead, J.R., Borsato, A., Baker, A., Frisia, S. & Baalousha, M. 2012. From soil to cave: Transport of trace metals by natural organic matter in karst dripwaters, *Chemical Geology*, **304–305**, 68-82.

Hellstrom, J.C. & McCulloch, M.T. 2000. Multi-proxy constraints on the climatic significance of trace element records from a New Zealand speleothem. *Earth and Planetary Letters*, **179**, 287–297.

Hellstrom, J.C. Rapid and accurate U/Th dating using parallel ion-counting multi-collector ICP-MS. *Journal of Analytical Atomic Spectrometry*, **18**, 1346-1351.

Hellstrom, J.C. 2006. U–Th dating of speleothems with high initial $^{230}$Th using stratigraphical constraint. *Quaternary Geochronology*, **1(4)**, 289-295.

Hendy, C.H. & Wilson, A.T. 1968. Palaeoclimatic data from speleothem. *Nature*, **216**, 48–51.

Hendy, C.H. 1971. The isotopic geochemistry of speleothems- I. The calculation of the effects of different modes of formation on the isotopic composition of speleothems and their applicability as palaeoclimatic indicators. *Geochimica et Cosmochimica Acta*, **35**, 801–824.

Hesse, P.P., Magee, J.W. & Kaars, S. 2004. Late Quaternary climate of the Australian arid zone: a review. *Quaternary International*, **118-119**, 87-102.

Hinds, W. C. 1999. Aerosol technology: properties, behavior, and measurement of airborne particles. Second Edition, John Wiley & Sons.

Holsen, T. M. & Noll, K. E. 1992. Dry deposition of atmospheric particles: Application of current models to ambient data. *Environmental Science and Technology*, **26**, 1802–1814.

Hopley, P.J., Weedon, G.P., Marshall, J.D., Herries, A.I.R., Latham, A.G. & Kuykendall, K.L. 2007a. High- and low-latitude orbital forcing of early hominin habitats in South Africa. *Earth and Planetary Science Letters*, **256(3–4)**, 419-432.

Hopley, P.J., Marshall, J.D., Weedon, G.P., Latham, A.G., Herries, A.I.R. & Kuykendall, K.L. 2007b. Orbital forcing and the spread of C4 grasses in the late Neogene: stable isotope evidence from South African speleothems. *Journal of Human Evolution*, **53(5)**, 620-634.

Hori, M., Ishikawa, Tsuyoshi, Nagaishi, K, Lin, K., Wang, Bo-Shian., You, C-F., Shen, C-C. & Kano, A. 2013. Prior calcite precipitation and source mixing process influence Sr/Ca,

Ba/Ca and $^{87}Sr/^{86}Sr$ of a stalagmite developed in southwestern Japan during 18.0 4.0 ka. *Chemical Geology*, **347,** 190-198.

Hu, M., Peng, J., Sun, K., Yue, D., Guo, S., Wiedensohler, A., Zhijun, W. 2012. Estimation of size-resolved ambient particle density based on the measurement of aerosol number, mass and chemical size distributions in the winter of Beijing. *Environmental Science & Technology*, **46 (18)**, 9941–9947.

Huang, Y. & Fairchild, I.J. 2001. Partitioning of $Sr^{2+}$ and $Mg^{2+}$ into calcite under karst-analogue experimental conditions. *Geochim. Cosmochim. Acta,* **65**, 47–62.

Huang, Y., Fairchild, I.J., Borasato, A., Frisia, S., Cassidy, C.J., McDermott, F. & Hawkesworth, C.J., 2001. Seasonal variations in Sr, Mg, and P in modern speleothems, Grotta di Ernesto, Italy. *Chemical Geology*, **175**, 429–448.

Hurrell, J.W., Kushnir, Y., Ottersen, G. & Visbeck, M. 2003. The North Atlantic Oscillation: Climatic Significance and Environmental Impact. *Geophysical Monograph*, **134**.

Iskra, I., Kávási, N. & Vaupotič, J. 2010. Nano aerosols in the Postojna cave. *Acta Carsologica,* **39(3),** 523-528.

Janssen, N.A.H., Van Mansom, D.F.M., Van der Jagt, K., Harssema, H. & Hoek, G. 1997. Mass concentration and elemental composition of airborne particulate matter at street and background locations. *Atmospheric Environment*, **31 (8),** 1185–1193.

Jeong, G. Y., Kim, S. J. & Chang, S. J. 2003. Black carbon pollution of speleothems by fine urban aerosols in tourist caves. *American Mineralogist*, **88(11-12),** 1872-1878.

Jin, Z., You, C-F., Yu, J., Wu, L., Zhang, F. & Liu, H-C. 2011. Seasonal contributions of catchment weathering and eolian dust to river water chemistry, northeastern Tibetan Plateau: Chemical and Sr isotopic constraints. *Journal of Geophysical Research,* **116**, F04006.

Johnson, K.R., Hu, C., Belshaw, N.S. & Henderson, G.M. 2006. Seasonal trace-element and stable isotope variations in a Chinese speleothem: the potential for high resolution paleomonsoon reconstruction. *Earth and Planetary Science Letters*, **244**, 394–407.

Jones, A.M. & Harrison, R.M. 2004. The effects of meteorological factors on atmospheric bioaerosol concentrations – a review. *Science of the Total Environment,* **326**, 151-180.

Jones, A.M. & Harrison, R.M. 2005. Interpretation of particulate elemental and organic carbon concentrations at rural, urban and kerbside sites. *Atmospheric Environment,* **39**, 7114-7126.

Jones, B. 2009. Phosphatic precipitates associated with actinomycetes in speleothems from Grand Cayman, British West Indies. *Sedimentary Geology*, **219,** 302-317.

Jurado, V., Fernandez-Cortes, A., Cuezva, Soledad., Laiz, Leonila., Cañaveras, J.C., Sanchez-Moral, S. & Saiz-Jimenez, C. 2009. The fungal colonisation of rock-art caves: experimental evidence. *Naturwissenschaften,* **96**, 1027-1034.

Jurado, V., Porca, E., Cuezva, S., Fernandez-Cortes, A., Sanchez-Moral, S. & Saiz-Jimenez, C. 2010. Fungal outbreak in a show cave. *Science of the Total Environment,* **408**, 3632-3638.

Karmann, I., Cruz, F.W., Viana, O. & Burns, S.J. 2007. Climate influence on trace element geochemistry of waters from Santana–Pérolas cave system, Brazil. *Chemical Geology*, **244**, 232–247.

Kawamura, K., Suzuki, I., Fuji, Y., Watanabe, O. 1994. Ice records of polycyclic aromatic hydrocarbons over the past 400 years. *Naturwissenschaften,* **11**, 502-505.

Kehrwald, N., Zangrando, R., Gambaro, A., Cescon, P. & Barbante C. 2010a. Specific molecular markers in ice cores provide large-scale patterns in biomass burning. *PAGES news*, **18 (2)**, 59-61.

Kehrwald, N., Zangrando, R., Gambaro, A. & Barbante, C. 2010b. Fire and climate: Biomass burning recorded in ice and lake cores. *EPJ Web of Conferences*, **9**, 105-114.

Kershaw, A.P. & Nanson, G.C. 1993. The last full glacial cycle in the Australian region. *Global Planetary Change*, **7(1-3)**, 1-9.

Kershaw, A.P., McKenzie, G.M., Porch, N., Roberts, R.G., Brown, J., Heijnis, H., Orr, M.L., Jacobsen, G. & Newall, P.R. 2007. A high-resolution record of vegetation and climate

through the last glacial cycle from Caledonia Fen, southeastern highlands of Australia. *Journal of Quaternary Science,* **22(5),** 481-500.

Kertész, Zs., Borbély-Kiss, I. & Hunyadi, I. 1999. Study of aerosols collected in a speleotherapeutic cave situated below Budapest, Hungary. *Nuclear Instruments and Methods in Physics Research B*, 384-391.

Kertéz, Zs., Borbély-Kiss, I., Rajita, I., Uzonyi, I. & Kiss, Á.Z. 2000. Analysis of single aerosol particles collected in urban and cave environment by proton microprobe. *Nuclear Instruments and Methods in Physics Research B*, **161-163**, 808-813.

Kertéz, Zs., Balásházy, I., Borbély-Kiss, I., Hofmann, W., Hunyadi, I., Salma, I. & Winkler-Heil, R. 2002. Composition, size distribution and lung deposition distribution of aerosols collected in the atmosphere of a speleotherapeutic cave situated below Budapest, Hungary. *Nuclear Instruments and Methods in Physics Research B*, **189**, 221-226.

Kim, E., Kalman, D. & Larson, T. 2000. Dry deposition of large, airborne particles onto a surrogate surface. *Atmospheric Environment,* **34(15)**, 2387-2397.

King, A. D., Hocking, A. D. & Pitt, J. I. 1979. Dichloran-rose Bengal medium for enumeration and isolation of molds from foods. *Applied and Environmental Microbiology,* **37**, 959-964.

Klimchouk, A.B. 1994. Speleogenesis under confined conditions, with recharge from adjacent formations. Publ. Serv. Geol. Luxembourg, Comptes Rednus du Colloque International de Karstology a Luxembourg, **27**, 85-95.

Klimchouck, A.B., Nasedkin, V.M. & Cunningham, K.I. 1995. Speleothems of aerosol origin: Reply. *National Speleological Society Bulletin*, **57**, 31-42.

Kowalczk, A. J. & Froelich, P. N. 2010. Cave air ventilation and $CO_2$ outgassing by radon-222 modeling: How fast do caves breathe*? Earth and Planetary Science Letters*, **289(1–2)**, 209–219.

Kulkarni, P., Baron, P. A. & Willeke, K. 2011. Particle migration in external force fields. In: Aerosol Measurement - Principles, Techniques, and Applications (3rd Edition). John Wiley & Sons. pp. 23.

Lachniet, M. S. 2009. Climatic and environmental controls on speleothem oxygen-isotope values, *Quaternary Science Reviews*, **28 (5–6),** 412-432.

Laird, L.D. & Campbell, I.D. 2000. High resolution palaeofire signals from Christina Lake, Alberta: a comparison of the charcoal signals extracted by two different methods. *Palaeogeography, Palaeoclimatology, Palaeoecology*, **164**, 111-123.

Lambert, W.J. & Aharon, P. 2011. Controls on dissolved inorganic carbon and $\delta^{13}C$ in cave waters from DeSoto Caverns: implications for speleothem $\delta^{13}C$ assessments. *Geochimica et Cosmochimica Acta*, **75**, 753–768.

Lauritzen, S-E., Løvlie, R., Dagfinn, M., Østbyes, E. 1990. Palaeoclimate deduced from a multidisciplinary study of a half million year old stalagmite from Rana, northern Norway. *Quaternary Research,* **34**, 306-316.

Lauritzen, S.-E. & Lundberg, J. 1999. Calibration of the speleothem delta function: an absolute temperature record for the Holocene in northern Norway. *The Holocene*, **9**, 659–669.

Lawrence, C.R. & Neff, J.C. 2009. The contemporary physical and chemical flux of aeolian dust: A synthesis of direct measurements of dust deposition. *Chemical Geology*, **267**, 46–63.

Leister, D.L. & Baker, J.E. Atmospheric deposition of organic contaminants to the Chesapeake Bay. *Atmospheric Environment*, **28(8),** 1499-1520.

Li, H-C., Ku, T-L., You, C-F., Cheng, H., Edwards, L., Ma, Z-B., Tsai, W-S. & Li, M-D. 2005. $^{87}Sr/^{86}Sr$ and Sr/Ca in speleothems for paleoclimate reconstruction in Central China between 70 and 280 kyr ago. *Geochemica et Cosmochimica Acta*, **69**, 3933-3947.

Lim, J-H., Sabin, L.S., Schiff, K.C. & Stolzenbach, K.D. 2006. Concentration, size distribution, and dry deposition rate of particle-associated metals in the Los Angeles region. *Atmospheric Environment*, **40**, 7810-7823.

Loosmore, G.A. & Cederwall, R.T. 2004. Precipitaiton scavenging of atmospheric aerosols for emergency response applications: testing an updated model with new real-time data. *Atmospheric Environment,* **38**, 993-1003.

Lyman, S. N., Gustin, M.S., Prestbo, E. M. & Marsik, F. J. 2007. Estimation of dry deposition of mercury in Nevada by direct and indirect methods. *Environmental Science and Technology*, **41**, 1970–1976.

Lynch, A.H., Beringer, J., Kershaw, P., Marshall, A., Mooney, S., Tapper, N., Turner, C. & Van Der Kass, S. 2007. Using the Paleorecord to Evaluate Climate and Fire Interactions in Australia. *Annual Review of Earth and Planetary Sciences,* **35,** 215-239.

Lynch-Stieglitz, J., Adkins, J.F., Curry, W.B. et al. 2007. Atlantic Meridional Overturning Circulation During the Last Glacial Maximum. *Science,* **314**, 66-69.

Maas, R., Kamenetsky, M.B., Sobolev, A.V., Kamenetsky, V.S. & Sobolev, N.V. 2005. Sr, Nd, and Pb isotope evidence for a mantle origin of alkali chlorides and carbonates in the Udachnaya kimberlite, Siberia. *Geology*, **33(7)**, 549-552.

Maltsev, V. A. 1997. Speleothems of aerosol origin: Discussion. *Journal of Cave and Karst Studies*, **April**, 43-43.

Martin-Sanchez, P.M., Sanchez-Cortez, S., Lopez-Tobar, E., Jurado, V., Bastian, F., Alabouvette, C. & Saiz-Jimenez, C. 2011. The nature of black stains in Lascaux Cave, France, as revealed by surface-enhanced Raman spectroscopy. *Journal of Raman Spectroscopy*, **43**, 464–467.

Martin-Sanchez, P.M., Nováková, A., Bastian, F., Alabouvette, C. & Saiz-Jimenez, C. 2012. Two new species of the genus Ochroconis, O. lascauxensis and O. anomala isolated from black stains in Lascaux Cave, France, *Fungal Biology*, **116(5)**, 574-589.

Masson, O., Piga, D., Gurriaran, R. & D'Amico, D. 2010. Impact of an exceptiona Saharan dust outbreak in France: $PM_{10}$ and artificial radionuclides concentrations in air and in dust deposits. Atmospheric Environment, **44(20)**, 2478–2486.

Mattey, D., Lowey, D., Duffet, J., Fisher, R., Hodge, E. & Frisia, S. 2008. A 53 year seasonally resolved oxygen and carbon isotope record from a modern Gibraltar speleothem: Reconstructed drip water and relationship to local precipitation. *Earth and Planetary Science Letters*, **269 (1-2)**, 80-95.

Mattey, D., Fairchild, I.J., Atkinson, T.C., Latin, J-P, Ainsworth, M. & Durell, R. 2010. Seasonal microclimate control of calcite fabrics, stable isotopes and trace elements in modern speleothem from St. Michaels Cave, Gibraltar. IN: *Tufas and Speleothems: Unravelling the Microbial and Physical Controls, Geological Society of London Special Volume,* **336**, 323-344.

McDermott, F., Frisia, S., Huang, Y. et al. 1999. Holocene climate variability in Europe: evidence from $\delta^{18}$O, textural and extension-rate variations in three speleothems. *Quaternary Science Reviews*, **18,** 1021–1038.

McDermott, F. 2004. Palaeo-climate reconstruction from stable isotope variations in speleothems: a review. *Quaternary Science Reviews*, **23**, 901–918.

McDermott, F., Schwarcz, H. & Rowe, P.J. 2005. Isotopes in Speleothems. In: M.J. Leng (ed.). Isotopes in Palaeoenvironmental Research. *Springer*.

McDermott, F., Atkinson, T.C., Fairchild, I.J., Baldini, L.M. & Mattey, D.P. 2011. A first evaluation of the spatial gradients in $\delta^{18}$O recorded by European Holocene speleothems. *Global and Planetary Change*, **79(3–4),** 275-287.

McGarry, S.F. & Caseldine, C. 2004. Speleothem palynology: an undervalued tool in Quaternary studies. *Quaternary Science Reviews*, **23**, 2389-2404.

McLaren, S. & Wallace, M.W. 2010. Plio-Pleistocene climate change and the onset of aridity in southeastern Asutralia. *Global and Planetary Change*, **71**, 55-72.

McManus, J.F., Francois, R., Gheradi, J-M., Keigwin, L.D. & Brown-Leger, S. 2004. Collapse and rapid resumption of Atlantic meridional circulation linked to deglacial climate changes. *Nature*, **428**, 834-837.

McMillan, E.A., Fairchild, I.J., Frisia, S. et al. 2005. Annual trace element cycles in calcite-aragonite speleothems:evidence of drought in the western Mediterranean 1200–1100 yr BP. *Journal of Quaternary Science*, **20**, 423–433.

Meyer, M.C., Cliff, R.A., Spötl, C., Knipping, M. & Mangini, A. 2009. Speleothems from the earliest Quaternary: Snapshots of palaeoclimate and landscape evolution at the northern rim of the Alps. *Quaternary Science Reviews*, **28**, 1374-1391.

Meyer, M.C., Spötl, C., Mangini, A. & Tessadri, R. 2012. Speleothem deposition at the glaciation threshold — An attempt to constrain the age and paleoenvironmental significance of a detrital-rich flowstone sequence from Entrische Kirche Cave (Austria). *Palaeogeography, Palaeoclimatology, Palaeoecology*, **319–320**, 93-106.

Michie, N.A. 1997. The threat to caves of the human dust source. IN*: Proceedings of the 12th International Congress of Speleology*, International Union of Speleology/Swiss Speleological Society, **5**, 43 - 46.

Michie, N.A., 1999. An instrument and method for measurement of dust fall in caves. *National Cave and Karst Management Symposium, Chattanooga (Tennessee).* 123-128

Michie, N.A., 2003. Tourist Caves: Airbone Debris. In: Encyclopaedia of Cave and Karst Science. New York, USA: Routledge Taylor & Francis Group

MLA, 2014. Yarrangobilly Caves Climate. Meat and Livestock Australia.

Morse, J.W. & Bender, M.L. 1990. Partition coefficients in calcite: examination of factors influencing the validity of experimental results and their application to natural systems. *Chemical Geology*, **82**, 265–277.

Mucci,A. 1987. Influence of temperature on the composition of magnesian calcite overgrowths precipitated from seawater. *Geochimica et Cosmochimica Acta*, **51**, 1977-1984.

Mucci, A. & Morse, J.W. 1990. Chemistry of low-temperature abiotic calcites: Experimental studies on coprecipitation, stability and fractionation. *Reviews in Aquatic Science,* **3,** 217–254.

Mühlinghaus, C., Scholz, D. & Mangini, A. 2009. Modelling fractionation of stable isotopes in stalagmites. *Geochimica et Cosmochimica Acta*, **73**, 7275–7289.

Nanson, G.C., Price, D.M. & Short, S.A. 1992. Wetting and drying of Australia over the past 300 ka. *Geology,* **20**, 791-794.

NASA. 2014. SeaWiFS Project. NASA Goddard Space Flight Center. http://oceancolor.gsfc.nasa.gov/SeaWiFS/

Nava, S. Becherini, F., Bernardi, A., Bonazza, A., Chiari, M., García-Orellana, I., Lucarelli, F., Ludwig, N., Migliori, A., Sabbioni, C., Udisti, R., Valli, G. & Vecchi, R. 2010. An integrated approach to assess air pollution threats to cultural heritage in a semi-confined environment: The case study of Michelozzo's Courtyard in Florence (Italy). *Science of the Total Environment*, **408**, 1403-1413.

Navarro, C., Carrión, J.S., Munuera, M. & Prieto, A.R. 2001. Cave surface pollen and the palynological potential of karstic cave sediments in palaeoecology. *Review of Palaeobotany and Palynology*, **117**, 245-265.

Northup, D.E., Dahm, C.N., Melim, L.A., Spilde, M.N. Crossey, L.J., Lavoie, K.H., Mallory, L.M., Boston, P.J., Cunningham, K.I. & Barns, S.M. 2000. Evidence for geomicrobiological interactions in Guadalupe caves. *Journal of Cave and Karst Studies*. **62(2)**, 80-90.

Northup, D.E. & Lavoie, K.H. 2001. Geomicrobiology of Caves: A Review. *Geomicrobiology Journal*, **18**, 199-222.

Northup, D.E., Barns, S.M., Yu, K.E., Spilde, M.N., Schelble, R.T., Dano, K.E., Crossey, L.J, Connolly, C.A., Boston, P.J., Natvig, D.O. & Dahm, C.N. 2003. Diverse microbial communities inhabiting ferromanganese deposits in Lechuguilla and Spider Caves. *Environmental Microbiology,* **5(11)**, 1071-1086.

NSW Department of Environment and Climate Change. 2012. SALIS soil technical report, New South Wales Government, Environment and Heritage department.

Odabasi, M., Vardar, N., Sofouglu, A., Tasdemir, Y. & Holsen, T.M. 1999. Polycyclic aromatic hydrocarbons (PAHs) in Chicago air. *The Science of the Total Environment*, **227**, 57-67.

Ohms, M. 2003. Dust deposition along the Candlelight tour, Wind Cave National Park. *Inside Earth (Cave & Karst Program, Geologic Resources Division, U.S. National Park Service)*, **6(1)**, 1-3.

Oomori T., Kaneshima H. & Maezato Y. 1987. Distribution coefficient of $Mg^{2+}$ ions between calcite and solution at 10–50°C. *Marine Chemistry,* **20,** 327–336.

Orlić, M., Kuzmić, M. & Pasarić, Z. 1994. Response of the Adriatic Sea to the bora and sirocco forcing. *Continental Shelf Research,* **14(1),** 91-116.

Osborne, R.A.L. & Branagan, D.F. 1988 Karst landscapes of New South Wales, Australia. *Earth-Science Reviews*, **25**, 467-480.

Pashchenko, A., Dublyansky, Y. & Andreichuk, V. 1993. Aerosol study in the Kungur Ice Cave (Urals, Russia*). Proceedings of the XI International Congress of Speleology, Beijing*

Pashchenko, S.E. & Sabelfeld, K.K. 1992. Atmospheric and technogenic aerosol (kinetic, electronic-sounding, and numerical methods of investigation), pt. 2. Novosibirsk, SO RAN, pp 118.

Pashenko, S.E. & Dublyanksky, Y.V. 1997. Generation of cave aerosols by alpha particles: Critical evaluation of the hypothesis. *Journal of Cave and Karst Studies*, **59(3)**, 103-105.

Perrette, Y., Poulenard, J., Saber, A-I., Fanget, B., Guittonneau, S., Ghaleb, B. & Garaudee, S. 2008. Polycyclic aromatic mhydrocarbons in stalagmites: Occurrence and use for analyzing past environments. *Chemical Geology*, **251**, 67-76.

Perrone, M. G., Larsen, B. R., Ferrero, L., Sangiorgi, G., DeGennaro, G., Udisti, R., Zangrando, R., Gambaro, A. & Bolzacchini, E. 2012. Sources of high PM2.5 concentrations in Milan, Northern Italy: Molecular marker data and CMB modelling. *Science of the Total Environment*,**414**, 343−355.

Petroff, A., Mailliat, A., Amielh, M. & Anselmet, F. 2008. Aerosol dry deposition on vegetative canopies. Part I: Review of present knowledge. *Atmospheric Environment*, **42**, 3625-3653.

Pickering, R., Kramers, J.D., Hancox, P.J., Ruiter, D.J. & Woodhead, J.D. 2011. Contemporary flowstone development links early hominin bearing cave deposits in South Africa. *Earth and Planetary Science Letters*, **306(1–2)**, 23-32.

Pickering, R. 2012. U-Pb dating of flowstones: challenges, age models and success stories, *Quaternary International*, **279–280**, 380.

Porca, E., Jurado, V., Martin-Sanchez, P.M., Hermosin, B., Bastian, F., Alabouvette, C. & Saiz-Jimenez, C. 2011. Aerobiology: An ecological indicator for early detection and control of fungal outbreaks in caves. *Ecological Indicators*, **11,** 1594–1598.

Power, M.J., Marlon, J., Ortiz, N. et al. 2008: Changes in fire regimes since the Last Glacial Maximum: an assessment based on a global synthesis and analysis of charcoal data. *Climate Dynamics,* **30**, 887–907.

Qing, H., Bosence, D.W.J. & Rose, E.P.F. 2001. Dolomitization by penesaline sea water in Early Jurassic peritidal platform carbonates, Gibraltar, western Mediterranean. *Sedimentology,* **48,** 153-163.

Richards, D.A & Dorale, J.A. 2003. Uranium-series Chronology and Environmental Applications of Speleothems. *Reviews in Mineralogy and Geochemistry,* **52 (1)**, 407-460.

Rodríguez-Vidal, J., Finlayson,G., Finlayson, C., Negro,J.J., Cáceres, L.M., Fa, D.A. & Carrión, J.S. 2013. Undrowning a lost world — The Marine Isotope Stage 3 landscape of Gibraltar. *Geomorphology*, **203**, 105-114.

Rose, P.V. 1964. An introduction to the Yarrangobilly Caves, New South Wales, Australia, Part I. *Journal of the British Speleological Association*, **5(36)**, 203-216.

Saiz-Jimenez, C., Ortega-Calvo, J.J. & de Leeuw, J.W. 1995. The chemical structure of fungal melanins and their possible contribution to black stains in stone monuments. *Science of the Total Environment*. **167**, 305–314.

Saiz-Jimenez, C., Cuezva, S., Jurado, V., Fernandez-Cortes, A., Porca, E., Benavente, D., Cañaveras, J.C. & Sanchez-Moral, S. 2011. Paleolithic Art in Peril: Policy and Science Collide at Altamira Cave. *Science*, **334 (6052)**, 42-43.

Salmon, L., Christoforou, C. S. & Cass, G. R. 1994. Airborne Pollutants in the Buddhist Cave Temples at the Yungang Grottoes, China. *Environmental Science and Technology*, **28 (5)**, 805 − 811.

Salmon, L.G., Christoforou, C.S., Gerk, T.J., Cass, G.R., Cassucio, G.S., Cooke, G.A., Leger, M. & Olmez, I. 1995. Source Contributions to Airborne Particle Deposition at the Yungang Grottoes, China. *Science of the Total Environment*, **167(1)**, 33 − 47.

Sanchez-Moral, S., Soler, V., Cañaveras, J.C., Sanz-Rubio, E., Van Grieken, R. & Gysels, K. 1999. Inorganic deterioration affecting the Altamira Cave, N Spain: quantitative approach to wall-corrosion (solution etching) processes induced by visitors. *Science of the Total Environment,* **244**, 67-84.

Sanchez-Moral, S., Portillo, M.C., Janices, I., Cuezva, S., Fernandez-Cortes, A., Cañaveras, J.C. & Gonzalez, J.M. 2012. Participation of microorganisms in the formation of calcitic moonmilk deposits and speleothems in caves. *Geomorphology*, **139–140,** 285–29.

Scholz, D. & Hoffmann, D.L. 2011. StalAge − An algorithm designed for construction of speleothem age models. *Quaternary Geochronology,* **6,** 369-382.

Schwarcz, H. 2007. Carbonate Stable Isotopes: Speleothems. *Elsevier B.V.* 290.

Sehmel, G. A. & Hodgson, W.H. 1978. A model for predicting dry deposition of particles and gases to environmental surfaces. DOE Report PNL-SA-6721, Pacific Northwest Laboratories, Richland, WA.

Seinfeld, J. H. & Pandis, S. N. 1998. Atmospheric Chemistry and Physics. From Air Pollution to Climate Change. John Wiley & Sons.

Sharma, M & McBean, E.A. 2002. Atmospheric PAH deposition velocities and washout ratios. *Journal of Environmental Engineering,* **187.**

Shahack-Gross, R., Bar-Yosef, O. & Weiner, S. 1997. Black-coloured bones in Hayonim Cave, Israel: Differentiating between burning and oxide staining. *Journal of Archaeological Science,* **24,** 439-466.

Simoneit, B.R.T., Schauer, J.J., Nolte, C.G., Oros, D.R., Elias, V.O., Fraser, M.P., Rogge, W.F. & Cass, G.R. 1999. Levoglucosan, a tracer for cellulose in biomass burning and atmospheric particles. *Atmospheric Environment*, **33**, 173-182.

Simoneit, R.T. 2002. Biomass burning — a review of organic tracers for smoke from incomplete combustion. *Applied Geochemistry*, **17 (3)**, 129-162.

Simpson, C. D., Russel, L.D., Katz, B.S. & Kalman, D.A. 2004. Determination of levoglucosan in Atmospheric Fine Particulate Matter. *Air & Waste Management,* **54**, 689-694.

Smith, C.L., Fairchild, I.J., Spötl, C., Frisia, S., Borsato, A., Moreton, S.G. & Wynn, P.M. 2009. Chronology building using objective identification of annual signals in trace element profiles of stalagmites. *Quaternary Geochronology.* 11-21.

Smith, A. & Wynn, P. 2010. Aerosol logging data at Ingleborough Show Cave. MSc thesis unpublished.

Smith, A.C., Wynn, P.M. & Barker, P.A. 2013. Natural and anthropogenic factors which influence aerosol distribution in Ingleborough Show Cave, UK. *International Journal of Speleology*, **42**, 49-56.

Spilde, M.N., Northup, D.E., Boston, P.J., Schelble, R.T., Dano, K.E., Crossey, L.J. & Dahm, C.N. 2005. Geomicrobiology of cave ferromanganese deposits, a field and laboratory investigation. *Geomicrobiology Journal*, **22**, 99-116.

Spötl, C., Fairchild, I.J. & Tooth, A.F. 2005. Cave air control on dripwater geochemistry, Obir Caves (Austria): Implications for speleothem deposition in dynamically ventilated caves. *Geochimica et Cosmochimica Acta,* **69**(10), 2451-2468.

Stanton, W.I., 1953. The Survey of Cheddar Caves. *Annual Report of the Mendip Nature Research Committee*, **1951(2)**, 16-23.

Steelman, K.L., Rowe, M.W., Boutton, T.W., Southon, J.R., Merrell, C.L. & Hill, R.D. 2002. Stable Isotope and Radiocarbon Analyses of a Black Deposit Assocaited with Pictographs at Little Lost River Cave, Idaho. *Journal of Archaeological Science*, **29**, 1189-1198.

Stoeva, P., Stoev, A. & Kiskinova, N. 2006. Long-term changes in the cave atmosphere air temperature as a result of periodic heliophysical processes. *Physics and Chemistry of the Earth*, **31**, 123-128

Tadros, C.V., Treble, P., Baker, A. & Roach, R. 2014. Cave drip water hydrochemistry provides insight to palaeo-environmental records from Harrie Wood Caves, SE Australia. Unpublished manuscript.

Tebo, B.M., Ghiorse, W.C., Van Waasbergen, L.G., Siering, P.L. & Caspi, R. 1997. Bacterially mediated mineral formation: insights into manganese (II) oxidation from molecular genetic and biochemical studies. *Reviews in Mineralogy*, **35**, 225–266.

Terzi, E. & Samara, C. 2005. Dry deposition of polycyclic aromatic hydrocarbons in urban and rural sites of Western Greece. *Atmospheric Environment*, **39,** 6261–6270.

Thompson, P., Schwarcz, H.P. & Ford, D.C. 1974. Continental Pleistocene climatic variations from speleothem age and isotopic data. *Science*, **184**, 893–894.

Tooth, A.F. & Fairchild, I.J. 2003. Soil and karst aquifer hydrological controls on the geochemical evolution of speleothem-forming drip waters, Crag Cave, southwest Ireland. *Journal of Hydrology,* **273(1)**, 51-68.

Treble, P., Shelley, J.M.G. & Chappell, J. 2003. Comparison of high resolution sub-annual records of trace elements in a modern (1911-1992) speleothem with instrumental climate data from southwest Australia. *Earth and Planetary Science Letters,* **216**, 141-153.

Treble, P., Budd, W.F., Hope, P.K. & Rustomji, P.K. 2005. Synoptic-scale climate patterns associated with rainfall delta O-18 in southern Australia. *Journal of Hydrology,* **302**, 270–282.

Treble, P., Fairchild, I.J. & Fischer, M.J. 2008. Understanding climate proxies in southwest-Australian speleothems. *PAGES News*, **16**, 17–19.

Vaks, A., Bar-Matthews, M., Matthews, A., Ayalon, A., Frumkin, A. 2010. Middle-Late Quaternary palaeoclimate of northern margins of the Saharan-Arabian Desert; reconstruction from speleothems of Negev Desert, Israel. *Quaternary Science Reviews*, **29**, 2647-2662.

Vardar, N., Odabasi, M. & Holsen, T.M. 2002. Particulate dry deposition and overall deposition velocities of polycyclic aromatic hydrocarbons. *Journal of Environmental Engineering,* **128(3)**, 269-274.

Vasanthabharathi, V., Lakshminarayanan, R. & Jayalakshmi, S. 2011. Melanin production from marine Streptomyces. *African Journal of Biotechnology,* **10(54),** 11224-11234.

Vawda, Y., Harrison, R.M. & Nicholson, K.W. 1990. Use of surrogate surfaces for dry deposition measurements. *Journal of Aerosol Science,* **21(1)**, 201-204.

Verheyden, S., Keppens, E., Fairchild, I.J., McDermott, F. & Weis, D. 2000. Mg, Sr and Sr isotope geochemistry of a Belgian Holocene speleothem: implications for palaeoclimate reconstructions. *Chemical Geology*, **169**, 131-144.

Viana, M., Kuhlbusch, T. A. J., Querol, X. et al. 2008. Source apportionment of particulate matter in Europe: A review of methods and results. *Aerosol Science*, **39**, 827-849.

Vibeck, M.H., Hurrell, J.W., Polvani, L. & Cullen, H.M. 2001. The North Atlantic Oscillation: Past, present, and future. *PNAS*, **98(23)**, 12876-12877.

Wai, K. M., Leung, K.Y. & Tanner, P. A. 2010. Observational and modelling study of dry deposition on surrogate surfaces in a South China city: implication of removal of atmospheric crustal particles. *Environmental Monitoring and Assessment*, **164(1-4)**, 143-152.

Wainer, K., Genty, D., Blamart, D. et al. 2011. Speleothem record of the last 180 ka in Villars cave (SW France): investigation of a large $\delta^{18}O$ shift between MIS6 and MIS5. *Quaternary Science Review*, **30**, 130–146.

Wainer, K., Genty, D., Blamart, D., Bar-Matthews, M., Quinif, Y. & Plagnes, V. 2013. Millennial climatic instability during penultimate glacial period recorded in a south-western France speleothem, *Palaeogeography, Palaeoclimatology, Palaeoecology*, **376**, 122-131.

Wallace, J,M. & Hobb, P.V. 2006. Atmospheric science: an introductory survey. Second Edition. *Academic Press, San Diego.*

Wang, W., Ma, Y., Ma, X., Wu, F., Ma, X., An, L. & Feng, H. 2010. Seasonal variations of airborne bacteria in the Mogao Grottoes, Dunhuang, China. *International Biodeterioration & Biodegradation*, **64**, 309-315.

Wang, W., Ma, X., Ma, Y., Mao, L., Wu, F., Ma, X., An, L. & Feng, H. 2011. Molecular characterization of airborne fungi in caves of the Mogao Grottoes, Dunhuang, China. *International Biodeterioration & Biodegration,* **65**, 726-731.

Wang, X., Peng, P.A. & Ding, Z.L. 2005. Black carbon records in Chinese Loess Plateau over the last two glacial cycles and implications for palaeofire. *Palaeogeography, Palaeoclimatology, Palaeoecology*, **223**, 9-19.

Wang, Y.J., Cheng, H., Edwards, R.L., An, Z.S., Wu, J.Y., Shen, C.C. & Dorale, J.A. 2001. A high-resolution absolute-dated Late Pleistocene monsoon record from Hulu Cave, China. *Science*, **294**, 2345–2348.

Wang, Y., Cheng, H., Edwards, R.L. et al. 2008. Millenial- and orbital-scale changes in the East Asian monsoon over the past 224,000 years. *Nature*, **451**, 1090-1093.

Wedyan, M, A. 2008. Characteristics of Amino Acids in the Atmospheric and Marine Environment. *World Applied Sciences Journal*, **3 (3)**, 454-469.

Wesely, M.L. & Hicks, B.B. 2000. A review of the current status of knowledge on dry deposition. *Atmospheric Environment*, **32**, 2261-2282.

Whitby, K.T. & Cantrell, B.K. 1975. Atmospheric aerosols characteristics and measurements. Presented at the *International conference for environmental sensing and assessment*, Las Vegas, NV.

White, W.B. 1997. Color of Speleothems. IN: Cave Minerals of the World. National Speleological Society, 2nd edition.

White, W.B., Vito, C. & Scheetz, B.E. 2009. The mineralogy and trace element chemistry of black manganese oxide deposits from caves. *Journal of Cave and Karst Studies,* **71(2)**, 136-143.

Whitlock, C. & Larsen, C. 2001. Charcoal as a fire proxy. IN: J. P. Smol, H. J. B. Birks., W. M. Last (eds.). 2001. Tracking Environmental Change Using Lake Sediments. Volume 3: Terrestrial, Algal, and Siliceous Indicators. Kluwer Academic Publishers, Dordrecht, The Netherlands.

Wieprecht, W., Acker, K., Müller, K., Spindler, G., Brüggemann, E., Maenhaut, W., Chi, X., Hitzenberger, R., Bauer, H. & Brink, H. T. 2004. INTERCOMP2000: ionic constitution and comparison of filter and impactor. *Atmospheric Environment*, **38,** 6477–6486.

Wigley, T.M.L. & Brown, M.C. 1971. Geophysical applications of heat and mass transfer in turbulent pipe flow. *Boundary-Layer Meteorology*, **1**, 300-320

Wilcke, W. 2000. Polycyclic Aromatic Hydrocarbons (PAHs) in Soil – a Review. *Journal of Plant Nutrition and Soil Science*, **163**, 229-248.

Wilkening, M.H. & Watkins, D.E. 1976. Air exchange and $^{222}$Rn concentrations  in the Carlsbad Caverns. *Health Physics*, **31**, 139–145.

Willeke, K. & Whitby, K.T. 1975. Atmospheric Aerosols: Size Distribution Interpretation. *Journal of the Air Pollution Control Association*, **25(5)**, 529-534

Williams, P.W., King, D.N.T., Zhao, J.X. & Collerson, K.D. 2005. Late Pleistocene to Holocene composite speleothem O-18 and C-13 chronologies from South Island, New Zealand — did a global Younger Dryas really exist? *Earth Planetary Science Letters*. **230**, 301–317.

Winckler, G., Anderson., R.F., Fleisher, M.Q., McGee, D. & Mahowalk, N. 2008. Covariant Glacial-Interglacial Dust Fluxes in the Equatorial Pacific and Antarctica. *Science*, **320**, 93-96.

Woodhead, J., Hergt, J., Shelley, M., Eggins, S. & Kemp, R. 2005. Zircon Hf-isotope analysis with an excimer laser, depth profiling, ablation of complex geometries, and concomitant age estimation, *Chemical Geology*, **209 (1–2),** 121-13.

Woodhead, J., Hellstrom, J., Pickering, R., Drysdale, R., Paul, B. & Bajo, P. 2012. U and Pb variability in older speleothems and strategies for their chronology, *Quaternary Geochronology*, **14**, 105-113.

Yang, H., Tsaib, C., Chaoc, M., Sua, Y. & Chiena, S. 2006. Source identification and size distribution of atmospheric polycyclic aromatic hydrocarbons during rice straw burning period. Atmospheric Environment, **40**, 1266–1274.

Yang, J., Li, G., Rao, W. & Ji, J. 2009. Isotopic evidences for provenance of East Asian Dust. *Atmospheric Environment*, **43**, 4481-4490.

Zangrando, R., Barbaro, E., Zennaro, P., Rossi, S., Kehrwald, N.M., Gabrieli, J., Barbante, C. & Gambaro, A. 2013. Molecular Markers of Biomass Burning in Arctic Aerosols. *Environmental Science and Technology,* **47**, 8565-8574.

Zhang, P., Cheng, H., Edwards, R.L. et al. 2008a. A Test of Climate, Sun, and Culture Relationships from an 1810-Year Chinese Cave Record. *Science.* **322**, 940-942.

Zhang, S., Zhang, W., Shen, Y., Wang, K., Hu, L. & Wang, X. 2008b. Dry deposition of atmospheric polycyclic aromatic hydrocarbons (PAHs) in the southeast suburb of Beijing, China. *Atmospheric Research*, **89**, 138–148.

Zhang, L., Fang, G.C, Liu, C.K., Huang, Y.L., Huang, J.H. & Huang, C.S. 2011. Dry deposition fluxes and deposition velocities of seven trace metal species at five sites in Central Taiwan – a summary of surrogate surface measurements and a comparison with model estimation. *Atmospheric Chemistry and Physics,* **11,** 32847-32875.

Zhao, J.X., Yu, K. & Feng, Y. 2009. High-precision $^{238}$U–$^{234}$U–$^{230}$Th disequilibrium dating of the recent past: a review. *Quaternary Geochronology,* **4**, 423–433.

Zhou, B., Shen, C., Sun, W., Zheng, H., Yang, Y., Sun, Y. & An, Z. 2007. Elemental carbon record of palaeofire history on the Chinese Loess Plateau during the last 420ka and its response to environmental and climate change. *Palaeogeography, Palaeoclimatology, Palaeoecology*, **252**, 617-625.

Zhou H.Y., Wang Q., Zhao J. X., Zheng L. N., Guan H. Z., Feng Y. X. & Greig, A. 2008. Rare earth elements and yttrium in a stalagmite from Central China and potential paleoclimatic implications. *Palaeogeography Palaeoclimatology Palaeoecology*, **270**, 128–138.

Zhou, H., Feng, Y-X., Zhao, J-X., Shen, C-C., You, C-F. & Lin, Y. 2009. Deglacial variations of Sr and $^{87}$Sr/$^{86}$Sr ratio recorded by a stalagmite from Central China and their association with past climate and environment. *Chemical Geology*, **268**, 233-247.

Ziegler, M., Tuenter, E., Lourens, L.J. 2010. The precession phase of the boreal summer monsoon as viewed from the eastern Mediterranean (ODP Site 968). *Quaternary Science Reviews*, **29**, 1481-1490.

Zou, S., Li, R., Shucheng, X., Junying, Z., Xinjun, W. & Junhua, H. 2010. Paleofire indicated by polycyclic aromatic hydrocarbons in soil of Jinluojia archaeological site, Hubei, China. *Journal of Earth Science*, **21(3)**, 247-256.

Zufall, M. J., Davidson,  C. I., Caffrey, P.F. & Ondov, J.M. 1998. Airborne Concentrations and Dry Deposition Fluxes of Particulate Species to Surrogate Surfaces Deployed in Southern Lake Michigan. *Environmental Science & Technology,* **32(11)**, 1623-1628.

# Supplementary material

**S.1. Aerosol sampling methods**


*Surrogate surfaces*

There is no generally accepted method to directly measure or estimate dry deposition (Chu, 2008). However, it has been established that a smooth horizontal surrogate surface provides a lower bound estimate of the dry deposition flux onto a horizontal surface (Sehmel, 1978; Holsen *et al*. 1992). The utilisation of the surrogate surface method for sampling was selected to provide a sample of aerosols which will closest represent the quantity and type of aerosol that may become incorporated into speleothem growth. The use of surrogate surfaces also has the benefits of being easy to transport and do not require any power which is important considering the logistics of working in a cave environment. The specific method of using Petri dishes (displayed in Figure S.1.) was chosen to allow for sealing and therefore reduce the potential of contamination during transportation from the laboratory to the field site and back to laboratory once the sampling duration has completed.
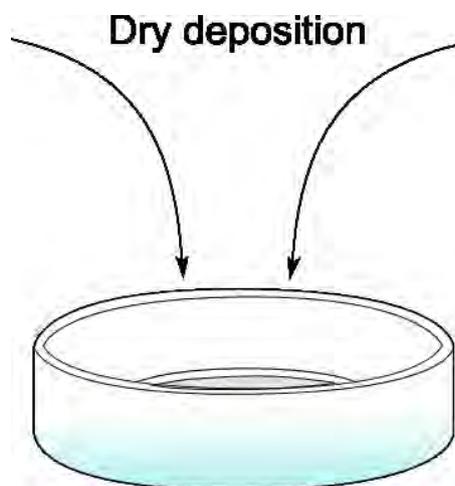


Figure S.1: Surrogate surface sampling apparatus, consisting of a Petri dish containing a collection surface.


The collection surface is selected, dependent on the aerosol species of interest, since certain properties are required for differing aerosol species collection. Specific preparation and extraction procedures are required for the collection and analysis of the different aerosol species. Quartz filters were used as a collection surface for samples where the aerosol

component under investigation was Polycyclic Aromatic Hydrocarbons (PAH). The quartz filter's properties allow it to be heated at very high temperatures without degradation of the filter medium, which is an important step in the surrogate surface preparation process. It was also necessary for the filter medium to withstand Dichloromethane (DCM), critical to the extraction procedure. Polytetrafluoroethylene (PTFE) filters were used as a surrogate surface collection medium in samples where the inorganic aerosol component was to be analysed. PTFE filters are resistant to strong acids, particularly nitric acid which is important for the cleaning and extraction processes. PTFE filters are cleaner (reduced blank levels) than other filters available reducing any potential inorganic sample contamination from the filter medium.

*Pumped samples*

Filters were prepared as described in '*preparation and cleaning*' and transported to the field site in the same manner as the surrogate surfaces. At the field site the pumps and in-line filter holders were prepared and put into position as displayed in Figure S.2. The filters were then removed and placed in the cleaned in-line filter holder, using tweezers to handle the filter (Teflon and metal tweezers were used for PTFE and quartz filters respectively). The pump start and finish times were noted as well the run time displayed on the pump in order to determine the volume of pumped air. The pumps were calibrated to 3 L min$^{-1}$ and this was verified in the field before the sampling period initiated to ensure that a quantitative calculation of suspended aerosol concentrations could be obtained.
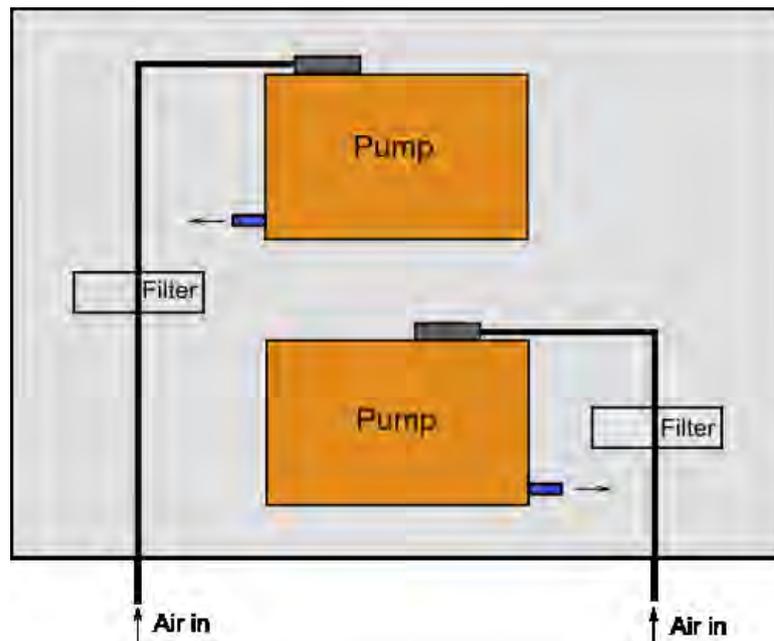
Figure S.2: Pump and inline filter apparatus setup.

Moisture has the ability to saturate filters and consequently reduce the permeability of the filter and even stop the flow of air completely. High humidity is typical of cave air and therefore a drier was produced to reduce the potential effect of high humidity on flow velocities. Figure S.3 displays the first design for an in-line silica crystal diffusion drier which was implemented during 24 hour active sampling during this field visit to test its necessity and effectiveness.
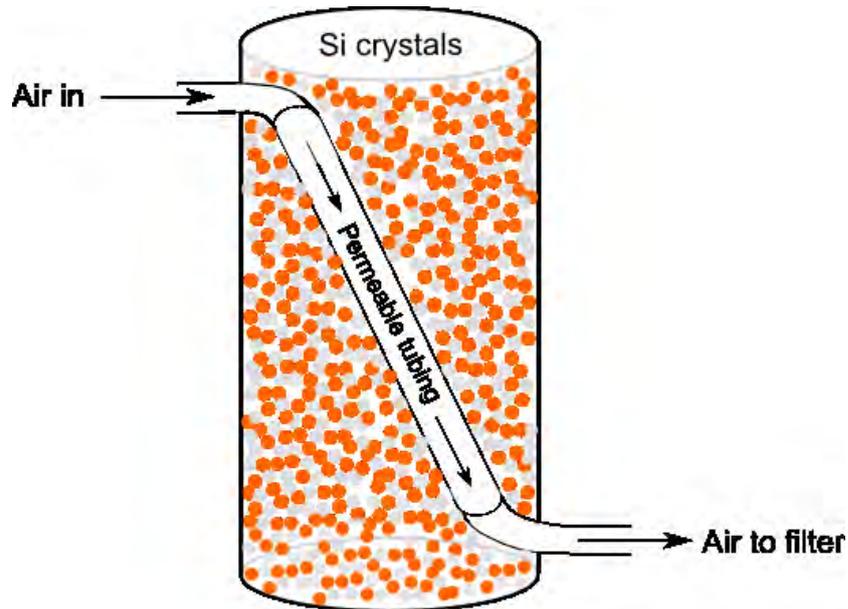
Figure S.3: Illustration of silica diffusion drier implemented during active sampling.

The silica diffusion driers were attached on the flow line to reduce the pumped air's moisture content before passing through the filter. Pump flow rates were unaffected by the connection of the silica driers and ran for the full 1440 minutes. The humidity did not to affect the flow rate of pumps it was therefore concluded that the potential added benefit of marginal drying was out weighted by possible sample contamination and the likely loss of aerosols due to impaction processes.

*Preparation and Cleaning*

Surrogate surfaces and filters were cleaned in the lab prior to deployment to reduce any contamination. This is of significant importance when collecting air samples from the cave environment since it was anticipated that the samples would be of low concentrations. The method of preparation differed dependent on the type of aerosol species under investigation. Surrogate surfaces with the intended use of PAH collection were prepared as follows: glass Petri dishes and quartz filters were heated at >450°C for a minimum of 5 hours to 24 hours (as of: Leister & Baker, 1994; Odabasi *et al* 1999; Vardar *et al*., 2002; Bozlaker *et al.,* 2008) to ash any potential organic contamination. Those being used for inorganic collection had a differing preparation method: glass Petri dishes and filters were placed in a 5% $HNO_3$ acid bath for a minimum of 24 hours. PTFE filters float, therefore a weight was added to the top of the PTFE filters to ensure they remained submerged for the entire cleaning duration. The Petri dishes were then triple-rinsed with double de-ionised water (DDIW) ensuring water quality was maintained at 18 MΩ (as with all stages of laboratory work). PTFE filters were placed in a DDIW water bath for 24 hours and rinsed again in clean DDIW. Upon completion the cleaned filters were placed in the clean Petri dishes, closed with their lids and sealed with cling wrap. Once cleaned all handling of filters was with cleaned Teflon tweezers for PTFE and metal tweezers cleaned with Dichloromethane (DCM) for quartz filters within a clean air hood (the hood provides a positive laminar flow of filtered clean air over the samples during handling). The sealed Petri dishes were then placed in a sealed clean container for transport.

*Surrogate surface deployment and collection*

Gloves were worn for handling sampling equipment during deployment and collection to minimise contamination. During deployment and collection of the surrogate surface samplers (Petri dishes) any likely sources of aerosol contamination and minimise these throughout the procedure e.g. not leaning over samplers.

Surrogate surface sample deployment:
1) At sample site the Petri dish was removed from the sealed container and cling wrap removed
2) Surrogate surfaces were placed in dry locations which are not directly influenced by drip waters. The Petri dish base and filter were placed on the most horizontal surface possible so samples did not move (or fall) during the sampling period. In show caves care was taken to place samples out of reach and away from direct influence by visitors. If in sight of a main tourist route a notice outlining the purpose and owner of the surrogate surfaces was placed
3) Lids were taken from the sealed box and used to seal the Petri dishes which were then secured with cling wrap
4) The date, sample number and location was noted

Surrogate surface sample collection:
1) Sample numbers and locations of Petri dishes being collected was recorded
2) Wearing gloves
3) The Petri dish lid was removed from the clean container at the sample location
4) The Petri dish lid was placed onto the Petri dish and totally sealed lid and base Petri dish containing the filter with cling wrap at sample location
5) The sealed Petri dish was placed into the sealed container for transport
6) Process repeated for each sample

*Sample storage*

Optimal sample storage conditions were met as close to the time of collection as possible (samples were always completely sealed from collection through storage), but due to the logistics of working in the cave environment and often overseas from the research institution samples were exposed to a period during transportation when optimal conditions could not be met. Ideal storage conditions are that samples are stored in refrigerated conditions below -4°C to minimise any loss of volatile compounds, that the sample seal was maintained and that there is minimal physical disturbance of the filter to reduce particles from becoming dislodged.

## S.2. Extraction for inorganic analysis

At completion of the sampling duration samples are sealed and transported as outlined in '*Surrogate surface deployment and collection'*.

All extraction was carried out in high density polypropylene vials with tightly fitting screw caps to avoid losses of volatile species during any heating steps. Filters were cut in half, in order to allow for separate extraction procedures for both ICP-AES and ion chromatography analysis. The filters were cut in half with a cleaned ceramic knife within a laminar flow clean air hood and immediately placed into extraction vial or returned to their corresponding collection Petri dishes.

*Ion Chromatography*

Extraction method:

1. Half of the filter was placed in 10 ml of DDIW and ultrasonicated for 120 mins (98% recovery (Chu, 2008)) for ion chromatography analysis. Extraction was carried out within 24 hours of anion analysis and the solutions refrigerated to maintain sample stability

2. Eluent removed and place in cleaned vials 0.5 ml cartridges and placed in the auto sampler ready for analysis

3. Initial inorganic samples were collected on quartz filters and filtration was required due to degradation of the filter during the extraction process between steps 1 and 2

*Inductively Coupled Plasma Atomic Emission Spectrometry (ICP-AES)*

Extraction method:

1. Half of the filter was placed in Aristar grade $HNO_3$ at 2% concentration

2. Samples shaken for 1 hour

3. A combination of ultrasonication and heat was used for extraction. Samples were heated to 80°C and ultrasonicated for 120 minutes. This method was chosen as an alteration of the often employed Harper method (Harper *et al.,*1983) which uses 60 mins of ultrasonication at 100°C. $HNO_3$ was chosen as opposed to Aqua Regia to better replicate any future carbonate analysis that may be carried out which uses a $HNO_3$ dissolution method

4. Sampled were left for 3 days at room temperature

5. Quartz filter samples filtered due to the degradation of the filter medium resulting in particulates in the solution

6. Vials were directly placed in the auto sampler

7. Analysed with ICP-AES

## S.3. Inorganic analysis calibration and data analysis

Procedural and field blanks were used to determine the presence of contamination throughout the sampling and preparation procedures for all analytical procedures.

*ICP-AES*

Sample concentrations are determined by calibrating an intensity from the analysis to an actual know concentration value. Both in house and international reference materials where used to produce standards for data calibration. The standards used are multi-element and are therefore for all the analytes of interest.

At Royal Holloway 0.2 g of standard was used to make up to 20.8ml, including the acid weight resulting in a 1:100 dilution. Analysis of external standards from Birmingham University determined this to actually be a 1:112 scaling. During the analysis an in-house monitor standard was run every 8 samples to determine analytical drift. Data was then corrected assuming a linear drift across the group of 8 samples. The ICP-AES remained stable and drift proved to be very small during the analysis and had little influence on sample values.

*Ion Chromatography*

Cation analysis was carried out using a Dionex DX500 ion chromatograph and anions were measured using a Dionex ICS2000 ion chromatograph. Both anion and cation analysis was carried out in the Environmental Health Science laboratories at the University of Birmingham. Single element standard solutions were produced. Standards were prepared for each analyte of interest and diluted to produce a range of concentrations (0.5, 1.0, 2.5, 5.0, 10, 15, 15, 50 ppm) in preparation for analysis. All standards were weighed and dilutions prepared in glassware acid washed for a minimum of 24 hours. The compounds used for each specific analyte of interest are listed below:

Cations:

- NaCl –Na
- $(NH_4)_2SO_4 – NH^+$
- KCl - K
- $MgCl_2$ - Mg
- $CaCl_2 – Ca$

Anions:

- NaCl - Cl
- $NaNO_3 – N$
- $Na_2SO_4$ - S
- $Na_2HPO_4$ - P

For both anions and cations a chromatograph is produced for each analyte which is intensity against time with each analyte having a specific retention time. Each chromatograph is integrated to determine an intensity value which is then calibrated against the standard intensity values of known solution concentration. Each of the standard to intensity values are plotted to determine a calibration line, of which a high $r^2$ value is required >97% to ensure an acceptable level of accuracy is reached.

*Data analysis*

ICP-AES data is produced in parts per million (ppm) concentration values as calculated from a linear calibration between intensity (counts) and standard concentrations. The ppm concentrations are those of the extraction solutions.

Solution concentrations need to be transformed into atmospheric concentrations which are expressed as mass per unit of volume over a period of time in this investigation this will usually be displayed using $\mu g\ m^{-3}$ for pumped samples and surrogate surfaces expressed as mass per area over a period of time $\mu g\ m^{-2}\ day^{-1}$.

A ppm concentration is calculated on the basis of this calibration. The concentration must then be converted into a mass per unit area per time value for samples collected with surrogate surfaces or a mass per volume of air per time period for those collected with pumps. The calculation for this is outlined below and applicable for both ICP-AES and Ion Chromatography since the same extraction volume was used of 5 ml.

Ppm concentrations are equal to $\mu g\ ml^{-1}$. 1 Each extraction was carried out in 5 ml of solution. Each sample is an extraction from half the filter and therefore represents half the total atmospheric abundance. Therefore each ppm concentration value must be multiplied by a factor of ten to obtain the mass value per filter.

*Pumped samples*

Each sample is the product of a time (minutes) period of pumping at a pumping rate 3 L min$^{-1}$. The total volume of air collected is a total of the period of sampling multiplied by the pumping rate, time in minutes multiplied by 3 L. To produce the data per metre, litres must be converted to m$^3$ where 1000 L equals 1 m$^3$. Therefore the volume of air in m$^3$ = time (minutes) $\times$ 3 / 1000. The final expression for conversion is displayed below:

$$\frac{(\text{Sample concentration (ppm)} \times 10)}{\left(\frac{\text{time (minutes)} \times 3}{1000}\right)} = \mu g \ m^{-3}$$

$$\frac{\text{Sample concentration (ppm)}}{\left(\frac{\text{time (minutes)} \times 3}{10000}\right)} = \mu g \ m^{-3}$$

*Surrogate Surfaces*

Surrogate surfaces sample dry deposition of aerosol over a time period. Data is expressed a mass per unit area over a period of time. Each filter has a diameter of 47 mm equating to an area of 1735 mm$^2$ or 0.0017 m$^2$. The final expression is shown below:

$$\frac{(\text{Sample concentration (ppm)} \times 10)}{(0.0017 \times \text{time (days)})} = \mu g \ m^{-2} \ day^{-1}$$

## S.4. PAH extraction method

| Step | Action | Reason |
|------|--------|--------|
| 1 | Sampling glassware and quartz filters heated at 500°C for a minimum of 5 hours | Ash any organics therefore removing contamination |
| 2 | All lab glassware cleaned with DCM (triple rinsed) before use | Lab glassware may need to be combusted to further reduce lab blank levels. |
| 3 | Sample filter placed in glass container | For extraction |
| 4 | 50µL of PAH internal standard added (PAH 15) | To check extraction efficiency in order to correct data output |
| 5 | 10ml of DCM added to cover the filter completely | Solvent extraction |
| 6 | Samples placed on shaker for 20mins | Homogenise sample |
| 7 | Filters constructed (1 per sample) in pipette with glass wool and sodium sulphate anhydrous | Remove particles and moisture respectively |
| 8 | Filter container rinsed to DCM and run through filter 3 times | Ensure complete sample collection |
| 9 | Filter then washed through with DCM | |
| 10 | Nitrogen blow down - Blow down to 2ml and transfer solution into analysis vial | Concentrate sample |
| 11 | Blow down to <0.5ml in analysis vial | |
| 12 | Transfer solution into vial inserts | |
| 13 | Blow down to base bead level | |
| 14 | Rinse container at each step and add to new container | Ensure complete sample transfer |
| 16 | Add 25µL of nonane for long time period storage of sample and place in freezer | To reduce and sample loss – predominantly light PAHs |
| 17 | Add 25µL of paraterphenyl | Added as a check of sample dilution to correct GCMS output data |

### S.5. GC-MS PAH analysis

*Data correction*

1. External standards A-E with varying concentrations are analysed to produce a calibration for each PAH. These consist of natural PAHs of concentrations A = 20µg/µL, B = 50, C = 200, D = 500, E = 1000, deuterated PAHs always at 1000 µg/µL and p-tephenyl at 1000 µg/µL.

2. This calibration is the response ratio (STD natural response against the corresponding deuterated STD response) against known concentration 20-1000 µg/µL.
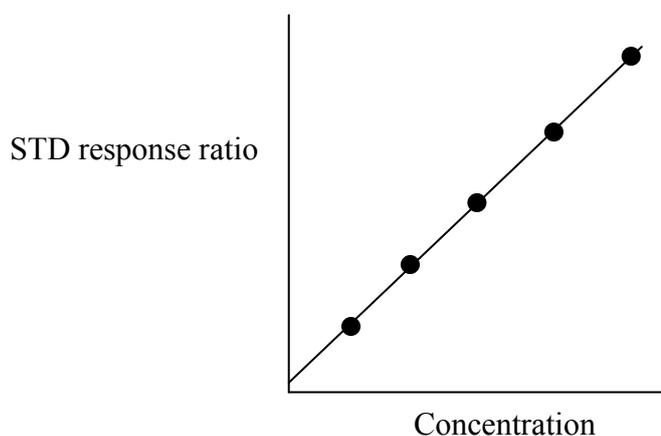


3. The PAH 15 internal STD is made up of the deuterated PAHs 1000 µg/µL.

4. Each sample analysis produces a response. This sample response is compared to its corresponding deuterated STD response in the PAH15 producing a response ratio. The response ratio is then checked against the calibration line for each PAH and a concentration determined.

Sample response ratio
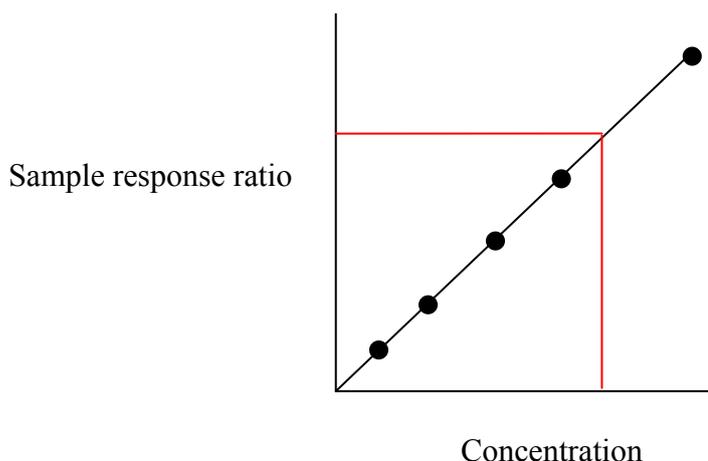
Concentration

5. This method takes into consideration any sample losses during the extraction procedure or any dilution/concentration effects since the STD solution as the initial step in the extraction. E.g. If 50% sample loses occur 50% of the STD PAH15 will also be lost, therefore the response ratio will not be affected. Therefore when compared to the calibration line constructed from STD solutions A-E the final concentration value will not be skewed as a result of any sample loss.

The software automatically corrects the data for any losses. In order to check the recovery efficiency p-terphenyl is added at the final step. The response of this p-terphenyl is compared to the p-terphenyl response of the STD providing a dilution ratio. The total sample recovery % is calculated as below and should be ~>80%.

(PTsample/PTstandard) = dilution ratio

(STD sample/STD calibration) = extraction efficiency

(p-terphenyl ratio/STD ratio) * 100 = total % sample recovery

To determine the total sample mass of PAH the concentration must be multiplied by 50 since there is a 50μL total sample volume and the GCMS analysis is undertaken on 1μL. Therefore the concentration in pg/μL is converted to a mass value in pg.

For pumped filter samples the atmospheric concentration is determined by dividing the mass of PAH by the total volume of air that passed through the filter during the sampling period. This produces an atmospheric concentration in mass/air volume e.g. $pg/m^3$.

## S.6. Surrogate surface method testing

A car park experiment was set up in order to test various different collection methods. At this time early in the investigation quartz filter media were used.
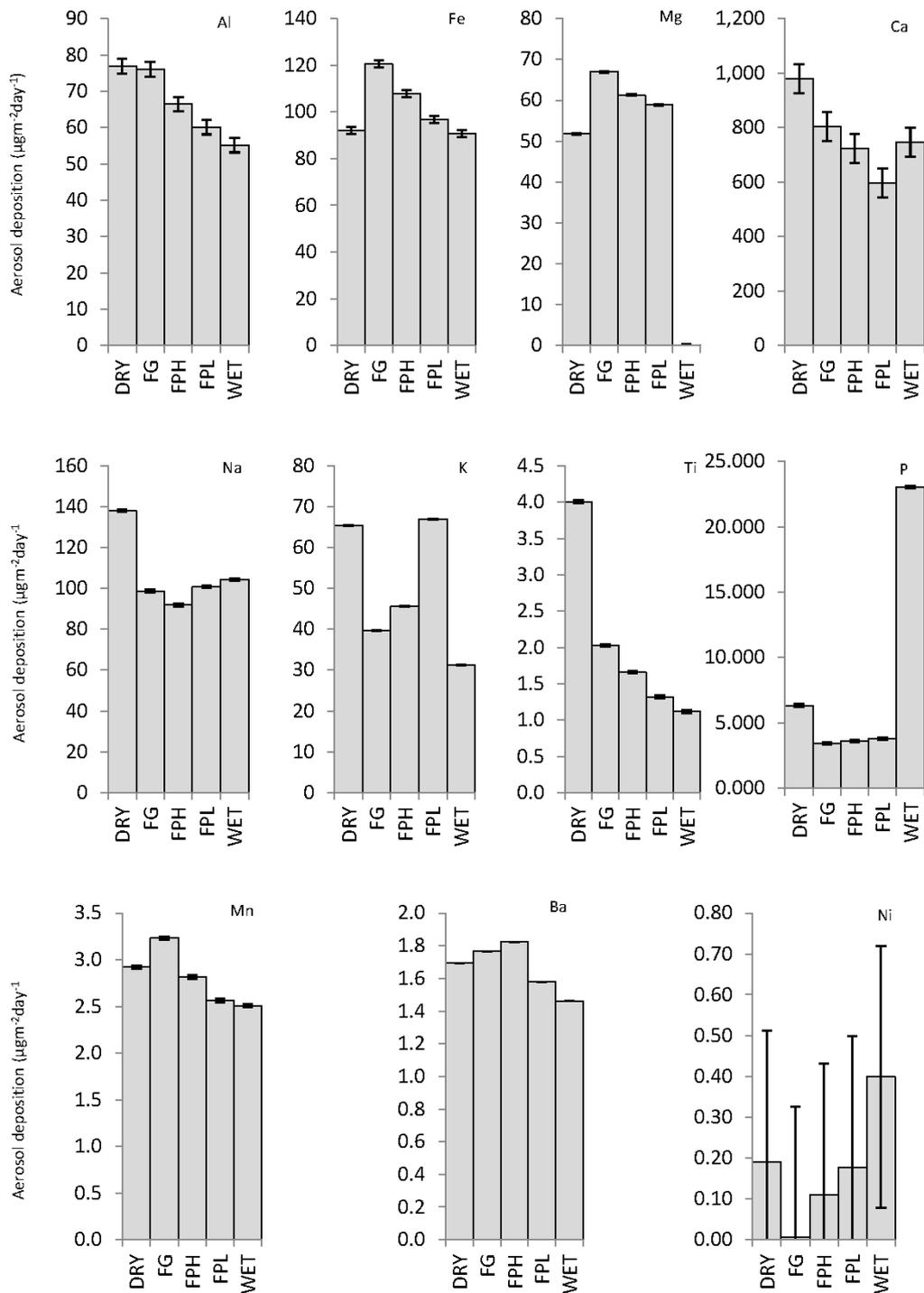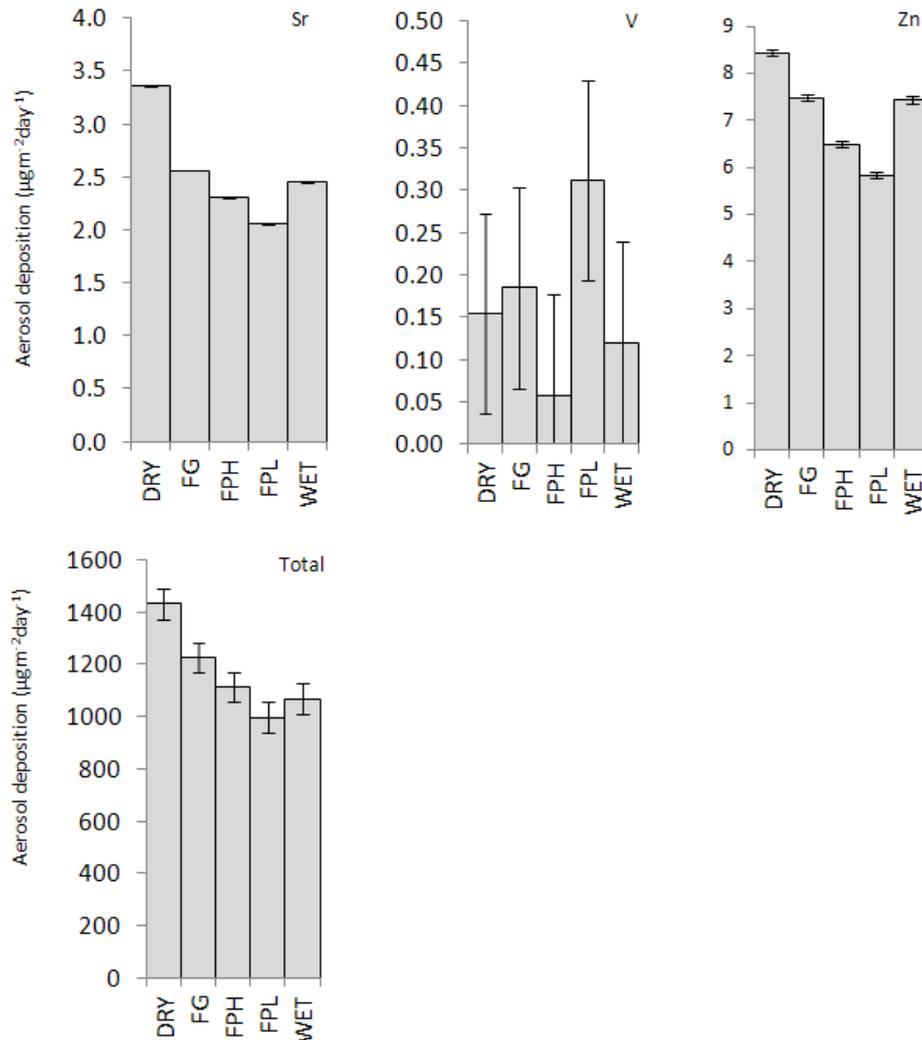
Figure S.4: ICP-AES elemental totals for Al, Fe, Mg, Ca, Na, K, Ti, P, Mn Ba, Ni, Sr, V and Zn. DRY = Empty dry glass petri dish, FG = Filter medium in a glass petri dish, FPH = Filter in a plastic petri dish with high sides, FPL = Filter in a plastic petri dish with low sides, WET = Glass petri dish containing water.

The dry Petri dish showed the highest collection (as shown in Figure S.4 sample named 'DRY') of dry deposition. For this sample 2% $HNO_3$ was used to wash out the Petri dish base and the solution then diluted to 5 ml volume. This process has much less potential for there to be aerosol remaining in the Petri dish. In the filter extraction method (as described in the extraction section) only the filter exposed to the extraction anything that is not retained by the filter medium will remain in the Petri dish and not be analysed. The 'DRY; method does not represent 100% of all dry deposition as there will be losses in both sampling and extraction procedures. Even though it is has been established that a general increase of downward flux

is observed with increasing collector surface roughness (Vawda *et al.,* 1990) the extraction method involved with using a filter medium results in more losses than the likely increase of collection as a result of the increased collection surface roughness. This could be easily avoided by washing out the Petri dish in order to collect any remaining aerosols that have become dislodged from the filter during handing and transportation. However this step is not possible when sample splitting is required for different extractions and analytical techniques.

The result displayed in Figure S.4 do not demonstrate the same as the finding of work by Wai *et al*. (2010) that demonstrated that in general water collects more materials (about or more than ten times of acidic and alkaline species), while glass collects similar or lesser amounts of various species than polystyrene. In this car park study the sample using water as a collection medium did not collect as much as the dry technique. Except from phosphorus, which collection was vastly improved by the wet collection technique.

Data suggests an 8% advantage for inorganic collection in having high Petri dish sides compared to low (percentage relative to maximum DRY collection total). The method that was chosen for inorganic analysis was use of a PTFE filter due to its low blanks and a glass Petri dish. Glass Petri dishes were chosen since they proved to be more robust which is important during sample transportation. Collection efficiency and the differences between the techniques will be compared to the DRY collection as this proved to collect the most aerosol deposition. The totals vary down to 70% of the DRY collection therefore there is a 30% variance in collection across all techniques. Of the samples with filters there is only a 15% variance and less than half the difference for the two plastic collection dishes at 8%. This demonstrates that deposition collection does vary, but the average difference in collection relative to the DRY collection is 23%. Although not ideal depending on the environmental situation it may be possible to detect environmental change even across sampling methods
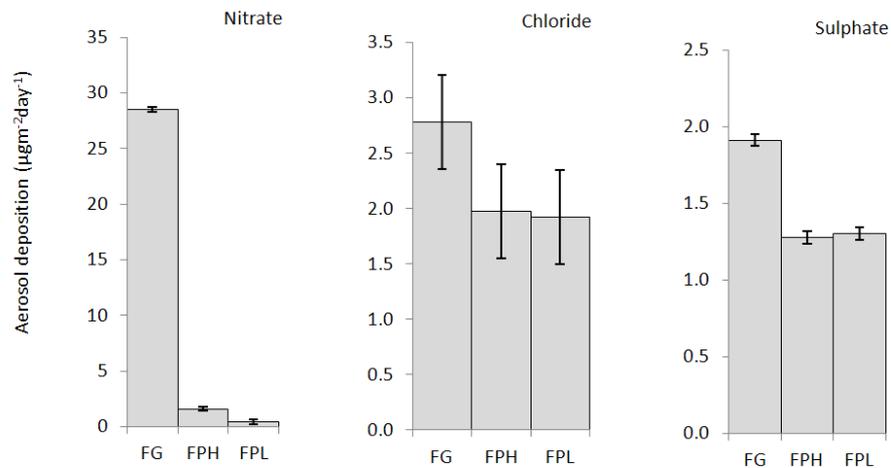
Figure S.5: Anion results from methods testing.

The anion results shown in Figure S.5 demonstrate that glass provides greater collection efficiency in comparison to the plastic for all the anions. Figure S.6 shows that superior collection is also obtained for the cations. This is complementary to the data obtained from the ICP-AES analysis and demonstrates that a glass collection device is superior.
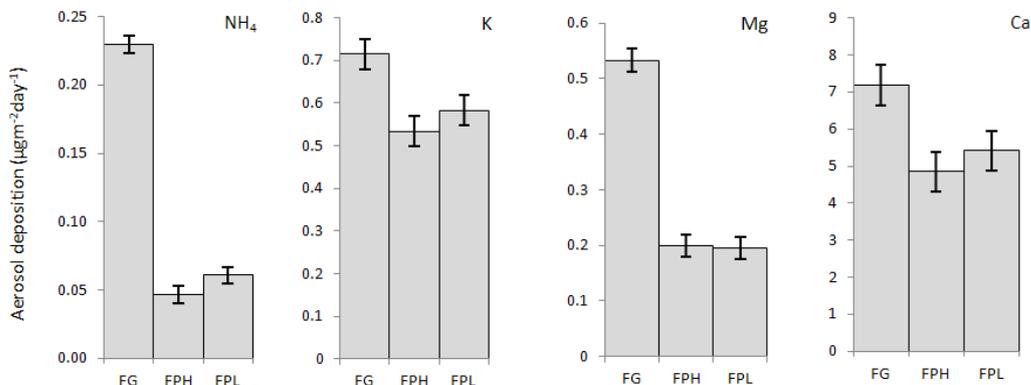


Figure S.6: Cation results from methods testing.

Less flexibility was available for the organic sampling since a filter medium and container that could withstand the high temperature ashing cleaning and strong solvents was required. Therefore glass Petri dishes and a quartz filter were required. It is possible to use a larger filter surface but this would have introduced new logistical issues since a Petri dish could no longer be used. But this was not deemed necessary since initial studies demonstrated that a

large enough signal was being obtained during the shortest deployment of one month at Cheddar Gorge, UK.

## S.7. Surrogate surface method reproducibility

To test the ability of surrogate surfaces to precisely record environmental aerosol deposition test duplicate samples were deployed. Figure S.7 displays 18 PAH compounds for two surrogate surface samples deployed in a controlled setting over the same time period.
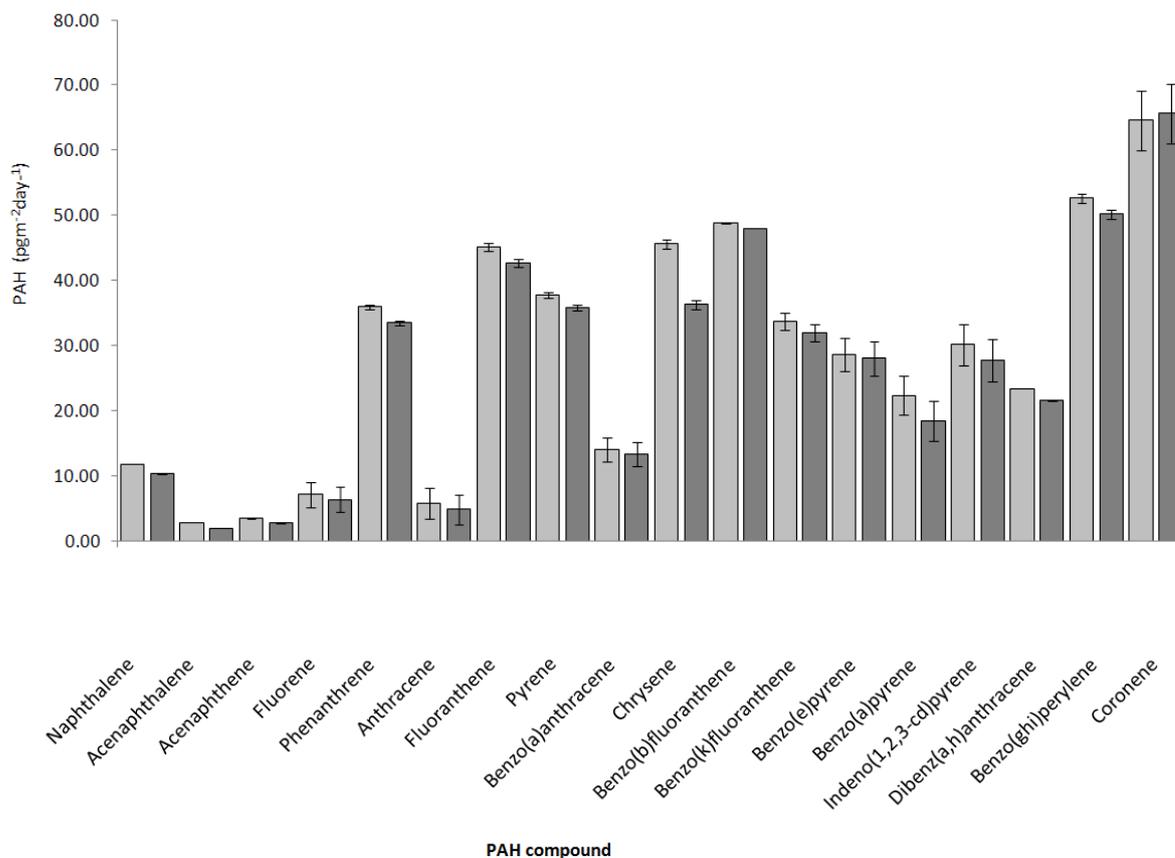


Figure S.7: PAH dry deposition for two replicate surrogate surfaces deployed in the same aerosol environment over the same time period.

The duplicate samples in Figure S.7 show that 8 out of the 18 compounds fall within error range of each other (limit of detection error displayed in Figure S.7 as calculated from blank analysis).

The ratios between the two samples are displayed in Figure S.8 and demonstrate a good level of precision with an average of 90% reproducibility ((1 - mean difference)*100)) between the samples, ranging from 69% to 99%. This indicates that a change over 10% can be considered of environmental change. A systematic bias is observed in this comparison with one sample presenting higher levels across all compounds with the exception of Coronene. Compounds should be viewed individually since there may be consistent procedural and analytical errors associated with specific PAH compounds. Further investigation into sample variability will also clarify this.
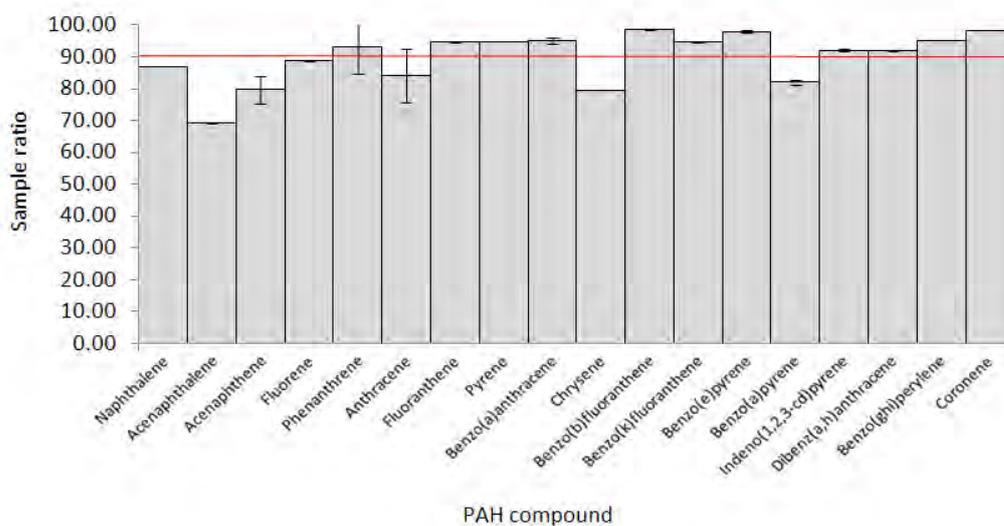


Figure S.8: Percentage compound reproducibility ((Sample A/ Sample B)*100) of replicate surrogate surface samples. Average reproducibility marked in red.

Errors displayed in Figure S.7 are element specific limit of detections (LOD) as determined from the standard deviation of the blanks. These are displayed in order to be comparable to the error used in the inorganic analysis. The LOD determined from integration of the inter peak baseline is lower for compounds where a blank value was detectable.  Figure S.9 displays a comparison of the two type of LOD. The baseline LOD provides an indication of purely analytical variance, the blank LOD also takes into consideration the procedural variability of contamination as is a better indication of the deviation associated with the complete extraction and analytical procedure.
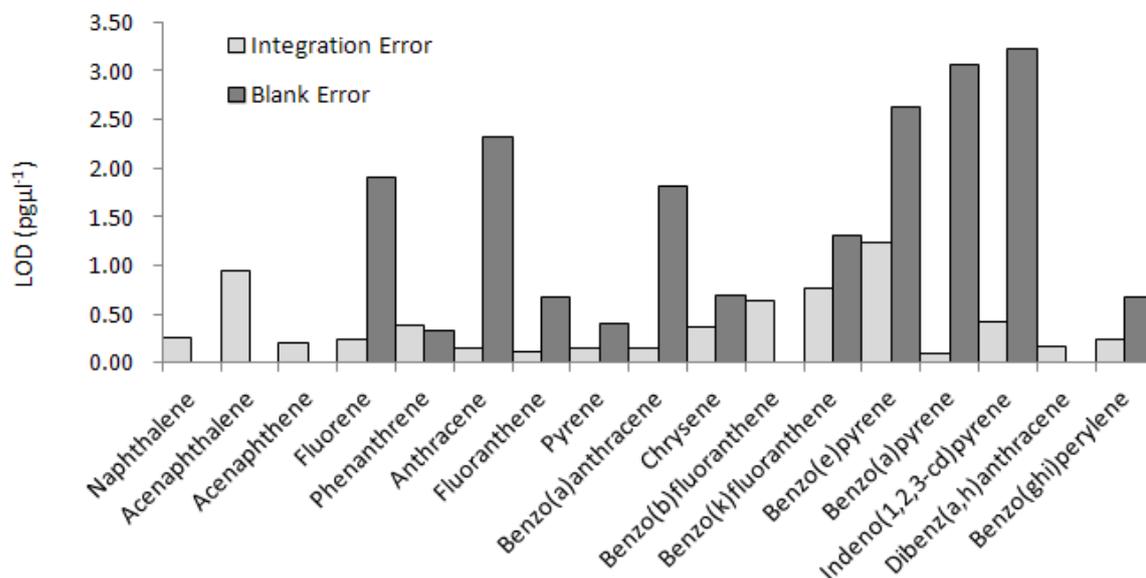
Figure S.9: Comparison of integrated LOD from baseline chromatograph fluctuations and LOD obtained from the deviation of blank analyses (instrumental variation only).

The lack of errors for the lower molecular weight compounds as determined from the blanks is likely due to volatile losses during the extraction process. Assuming the integration error for the lighter PAH compounds would bring the duplicates closer to being within analytical error of each other rather than random sampling error. However, blank error still provides a more accurate estimate for the error associated with both extraction and analysis.
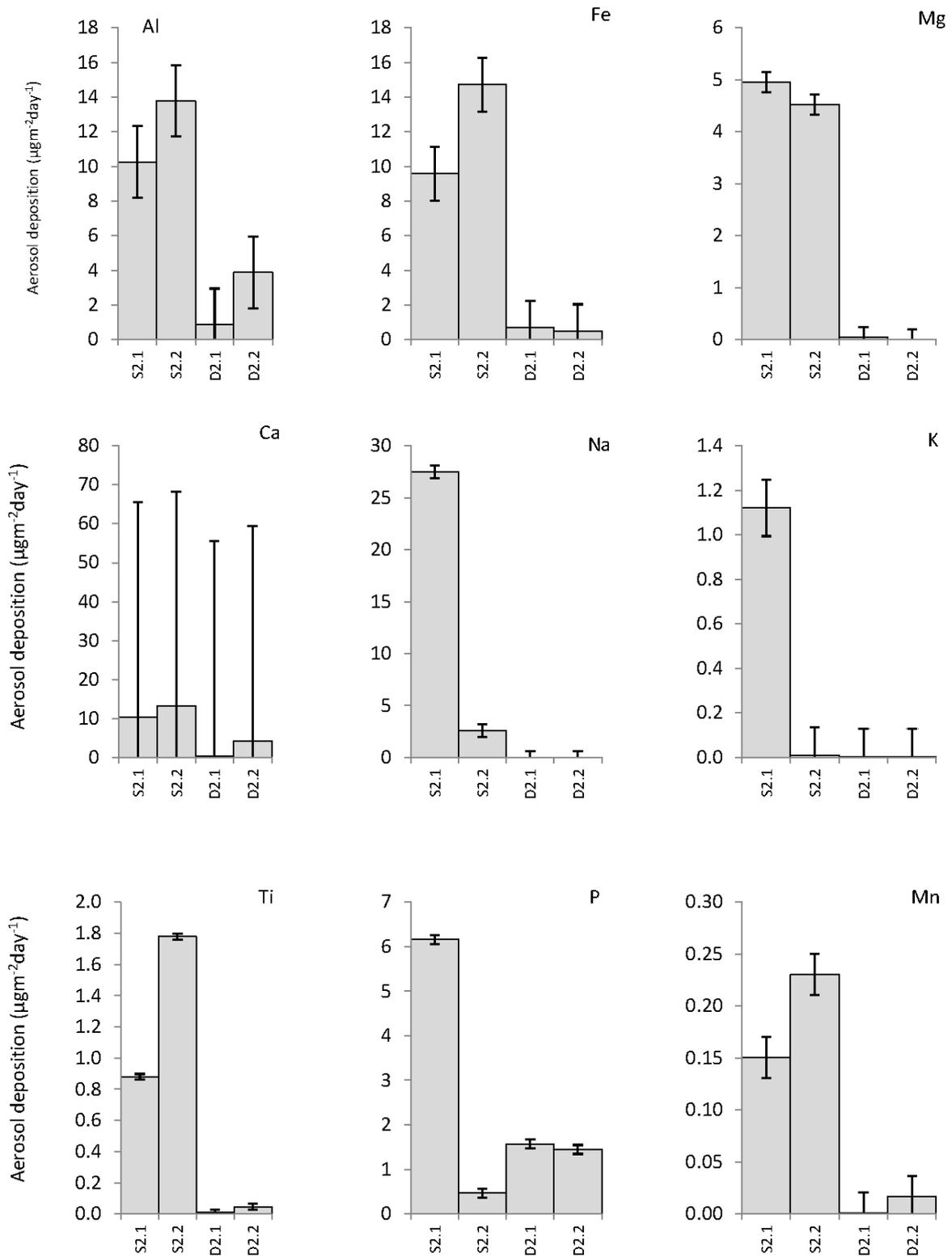
Figure caption on following page
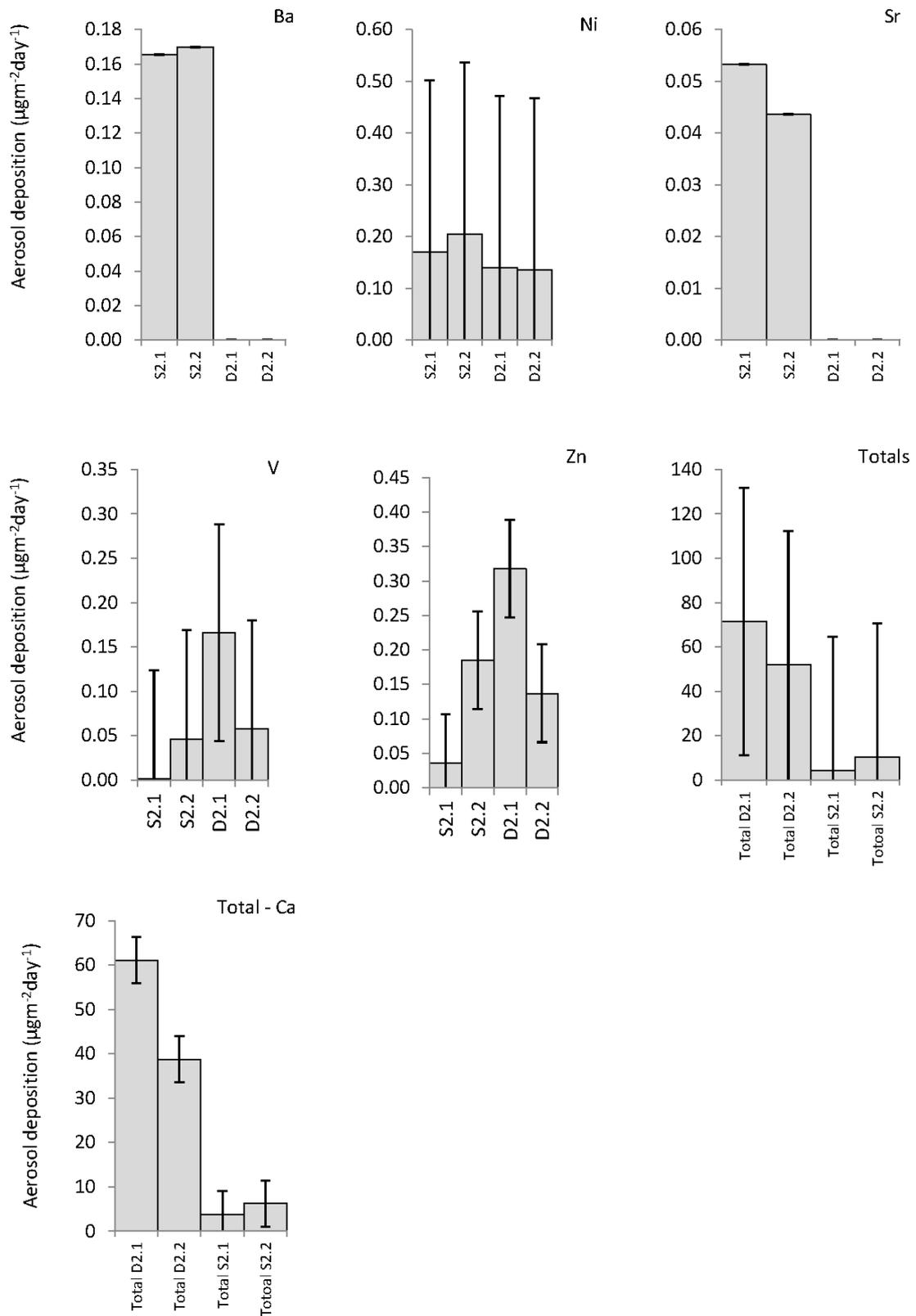
Figure S.10: ICP-AES results of cave surrogate surface samples. Final two graphs display

totals, with the penultimate displaying all elements and final displaying all elements except Ca. Ca was removed due to the large errors.

*Car Park duplicates*

Although not exact duplicates FPH and FPL both use plastic collection dishes and display an average difference across all elements of 8%. In subsequent studies often the environmental variation far exceeds 8% and therefore this level of repeatability would prove satisfactory for environmental interpretation of the data. One observation is that, with the exception of P, the only elements to show higher concentrations (beyond error) in FPL than FPH are Na and K since these group I elements are likely to enter as part of water soluble compounds.

*Ion Chromatography*

At Obir cave the environmental signal is greater than that of the combined analytical and sampling errors and can still be determined across the majority of elements. That may be a lack of sampling repeatability can also be interpreted as a true environmental signal. Local-scale depositional processes may result in large depositional differences over small distances. This would result in the large relative differences observed within the samples. In addition to this the same processes may also result in aerosols of different properties being deposited to each surrogate surface. As a consequence the observed disparity in elemental concentrations between replicate samples would occur which display high levels of reproducibility in with other elements. Reproducibility is poor for sampling and ion chromatography analysis for both anions and cations.

The car park location where the methods testing were carried out has much higher aerosol concentrations. Figure S.5 and S.6 displays a comparison of 3 collection techniques. FPH (filter paper high) and FPL (filter paper low) both use plastic Petri dishes as surrogate surface collection containers. All cation duplicates are within analytical error. Cation results do not demonstrate the same level of difference between high and low Petri dishes. At these high concentrations reproducibility is good; therefore it is a suitable technique for sampling. Anions also demonstrate reasonable repeatability with only nitrate not showing collection within analytical error, Chloride and sulphate are reproducible using this surrogate surface technique.

**S.8. Aerosol method conclusions**

Currently adopted methods are suitable for aerosol collections where the environment signal vary temporally or spatially in the order of between samples of 50% for low concentrations and 8% in high depositional environments. Obir samples for ICP-AES demonstrates the potential environmental variability, with location D averaging at 88% lower than location 3, well beyond the highest sampling error observed. Certain elements respond better to environmental change such as Sr, Ba and Mg. Sr also demonstrates this in other field sites; Spain shows a 99.78% difference between two locations. Therefore the environmental influence far exceeds any sampling variability that is observed.

## S.9. $^{87}$Sr/$^{86}$Sr chemical separation method

Strontium isotope analysis was carried out at the University of Melbourne Earth Sciences department using a Nu Plasma MC-ICP-MS instrument. Solution samples were run manually. The chemical separation methods are presented below.

Both waters and acid are processed through a two stage distillation process.

*Beaker preparation*

1) Using pre cleaned Teflon beakers (3-7 ml)
2) Reflux with concentrated $HNO_3$ for at least one hour (best overnight)
3) Once reflux complete discard acid and rinse with DDIW checking for 'sticky' spots. 'Sticky' spots will be residue from previous samples and therefore contaminate any future analyses

No solution splitting

1) Label beakers with sample names
2) Weight beaker
3) Place sample in beaker record combined weight
4) Cap beaker

Solution splitting

1) Beakers must be cool and dry
2) Label beakers
3) Weigh beaker and lid and record
4) Weigh beaker alone and record then tare
5) Place sample in the beaker and record weight
6) Cap beaker

*Sample cleaning*

If sample is in chips or crystals they may be leached in weak $HNO_3$ and rinsed with DDIW to reduce surface contamination. Powders cannot be cleaned.

Dissolution

1) Add 0.5 ml of DDIW to each sample
2) Add concentrated $HNO_3$ adding one drop at a time, only adding the next drop when the dissolution reaction has ceased (to a maximum of 3 drops)
3) Add 1 ml of 2M $HNO_3$ to each sample
4) If no sample splitting for ICPMS is required samples are now ready for Sr extraction

Solution splitting

1) Solutions can be split in order to analyse the sample for trace elements by ICP-MS
2) Weigh the entire beaker, lid and solution
3) Remove 0.15 ml (approximately 10%) of the solution and place into new cleaned beaker
4) Weight the original beaker again and record weight
5) The difference in the mass used for to determine masses from ICPMS analysis

*Sr Extraction*

Column preparation

1) Eichrom Sr resin is highly selective of Sr and Pb only providing good separation with small resin and reagent volumes

2) Columns are constructed of glass (4 mm stem and 6ml acid reservoir size). These are set up in column stands

3) Columns are pre cleaned with a few drop of concentrated $HNO_3$ followed by a DDIW rinse

4) Columns are then filled with a 3-5 mm bed of EICHROM prefilter resin and a 12-15mm bed of pre-cleaned Sr resin. Resin is pre cleaned with 6M HCL then 0.05M $HNO_3$ followed by 2M $HNO_3$

Clean resin

1) Resin cleaned using 5 ml 0.05M $HNO_3$ (takes 1hr to drip through)

2) Resin equilibrated with 1 ml 2M $HNO_3$

3) Loading samples with 1-2 ml 2M $HNO_3$

4) Elute Ca, Rb and REE etc with 3, 1 ml 2M $HNO_3$ reservoirs

5) Elute Ba with 3 ml of 7M $HNO_3$

6) Nitric is then washed through using 0.5 ml 2M $HNO_3$

Collect Sr

1) Cleaned beakers now placed under columns with samples name and noted at being the Sr fraction

2) Elute Sr with 0.5 ml of 0.05M $HNO_3$ followed by 1ml of 0.05M $HNO_3$

3) Dry down collected samples on a hotplate

Packing up

1) Remove resin from columns

2) Place column in dilute AR grade acid on a hotplate overnight

3) Rinse columns inside and out

4) Store columns in distilled HCL or $HNO_3$ in a 1L Savillex teflon jar

**S.10. Melbourne ICP-MS extraction methods**

Analysis was carried out using an Agilent Technologies 7700 series Quadrupole Inductively Coupled Mass Spectrometer (Q-ICP-MS) in the University of Melbourne Earth Sciences department.

*Surrogate surfaces*

All acid used are double distilled AR grade acids.

Filters:

1) Filter cut in half
2) Half filter placed in a test tube the other return to the surrogate surface and sealed for storage and later analysis by IC
3) 5 ml DDIW added to test tube
4) 100 μl of concentrated $HNO_3$ added to sample solution to acidify to ~2%
5) Samples ultrasonicated with heat for 120 mins

No filter:

1) 5ml DDIW added to Petri dish in stages
2) 1ml rinses were used with 0.5ml going to separate vials. This step is to ensure the best mix of the solution is separated between the sample used for ICPMS and IC analysis.
3) 2.5ml is stored for later IC analysis
4) 50μl of concentrated $HNO_3$ added to acidify 2.5 ml of sample solution to ~2% for ICPMS analysis.

*Calcite*

Analysis of three different calcite colours

1) Three sections of ~0.3 g (exact masses in appendix) calcite were sampled one of each of the Red, Black and white calcite
2) 1ml of DDIW was added to cover the sample
3) Concentrated 15M $HNO_3$ was added to the samples in 2 drop addition steps to ensure a controlled dissolution reaction

4) When the reaction was completed a further 10 drops were added to ensure complete calcite dissolution to a total of ~1 ml of 15M $HNO_3$

5) Sample were then diluted with 2% $HNO_3$ to 18 ml

6) Samples contained a residue which did not dissolve. The samples were left to settle overnight allowing the residue to sink to the base of the vial

7) 9ml of sample solution was removed from the upper water column within the vial without disturbing the settled residue. The $HNO_3$ sample solution aliquot was then centrifuged to ensure that no residue had been collected during the sampling. This was stored for ICPMS analysis.

8) The remaining solution was dried down

9) HF was then added

10) Samples were dried down again

11) Samples were dissolved in 2% $HNO_3$ ready for ICPMS analysis

*Spiking*

- Samples were then spiked with an internal standard.

- Samples were spiked to a target concentration of 2 ppb from the stock standard solution concentration of 50 ppb

Therefore the dilution factor required is:

*Calcite*

- DF= solution weight/sample weight

- Target DF = 4000

- Solution total is 10 ml

- Aliquot of sample required is =DF/4000*10 ml

*Aerosol samples*

Since the sample mass is unknown. Calculations were based on previous sample masses from ICP-AES data.

Solution weight×2 ppb/ (stock solution 50 ppb-target concentration 2 ppb)

## S.11. U-Th dating methods

All U-Th laboratory work is carried out in the University of Melbourne Earth Science clean laboratory. Protective/clean cover clothing, gloves and dedicated clean lab shoes are worn to protect the lab user and reduce outside contamination into the lab. The lab environment is temperature controlled and air is HEPA filtered (HEPA filter air must remove at least 99.97% of particulates of size less than 0.3µm).

*Method Summary*

Radiometric disequilibrium dating was conducted at the University of Melbourne, Australia. Samples were dissolved and chemically separated to elute non-analyte elements. Isotopic analysis ( of $^{229}$Th, $^{230}$Th, $^{232}$Th, $^{233}$U, $^{234}$U, $^{235}$U, $^{236}$U) was carried out using a Nu Plasma multi collector inductively couples mass spectrometer (MC-ICP-MS). Internal standards (Yarrangobilly flowstone stock, YB-1) and external standards (Harwell Uraninite, HU-1) were analysed to determine accuracy. Full details of the analytical procedure can be found in Hellstrom (2003) and Hellstrom (2006).

*Sample mass*

U-Th separation chemistry is prepared in groups of 24. Each group typically consists of two standard reference material samples, two lab blanks (one spiked, one unspiked).

A target sample mass can be calculated from the known or predicted sample Uranium (U) concentration. U concentrations can be determined from (LA) ICP-MS analysis of the sample or predicted from similar samples. In cases where very little is known about samples it is best to determine U concentrations in order to optimise sampling and the separation chemistry. The range of U is constrained by instrument sensitivity and the efficiency optimisation of separation chemistry. This will vary dependent on the instrument for analysis and the laboratory setups. The University of Melbourne instrument is setup to work best with between 10 and 20 ng of U. Therefore if a sample has a known U concentration of 0.2 ppm between 100 and 200 mg of samples will be required. Often U contents will vary throughout the formation period of the speleothem. Sample masses can be adjusted incorporate known changes in the U concentration between samples; where done this will be carried out in

groups for 5-10 samples. However, this is not critical due to the flexibility in the U-Th dating procedure, it only become necessary when variations in orders of magnitude are reached in U concentrations.

*Sampling*

Several sampling methods exist, but the most appropriate one is dependent on the laboratory setup and sample concentrations.

Hand drilling – Probably the quickest and cheapest method of sampling is a small hand held drill with a 1 mm diameter drill bit to produce powders for analysis. Where only small samples are required it is often difficult to obtain high spatial resolution (dependent on user's skill).

Automated drilling / milling – This method is far superior to hand drilling in terms of control and therefore spatial resolution. It is a slower sampling method and involves more sample preparation. Samples need to be completely flat in order to be mounted to the XYZ stage; this can be achieved by smoothing a sample or mounting the sample in resin. The sample is then clamped tightly to the XYZ stage (shown in Figure S.11). The drill is then brought to the sample and the stage moves beneath the drill. The stage is controlled via computer software and can be moved in extremely small increments drilling as shown in Figure S.12. The system used at Melbourne University is MPS 2000, this system does not have optics. Other systems incorporate optics into the software allowing for extremely accurate drill positioning and intricate drilling paths.
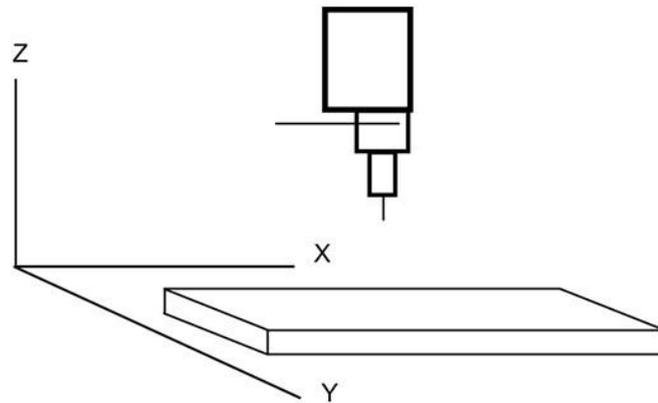
Figure S.11: XYZ drill setup.

In both hand drilling and automated drilling the powders must be collected manually. This is done in various ways, but all powder must be collected and then weighed to ensure that it falls within the sample mass range required. It is critical that the samples, all surfaces and tools are cleaned with ethanol, removing all powder. Any remaining powder could result in cross contamination of samples resulting in poor sample accuracy.



Figure S.12: Automated drilling of Yarrangobilly speleothem sample following growth laminations to maximise spatial resolution.

Figure S.13: Drilling stage setup and stage control interface.

*Solid sampling*

This method is used in situations where sample contamination is of concern. Samples of required mass are removed as a solid block. This reduced the surface area for contamination and allows for cleaning. Samples are generally cleaning by leaching the sample in weak acid to remove the out surface region that may have been exposed to contamination.

*U-Th separation chemistry*

1. Column stand preparation

   1) Waste containers and column holders are kept in weak acid for cleaning.

   2) Plastic ware is removed from acids and washed with DDIW

   3) Waste vials and number column holders are placed on wipes on a cleaned bench in numerical order

   4) Column sleeves are stored in DDIW, and washed with DDIW then placed in Column in the column stand

   5) U-Th dissolution tubes are removed from storing acid and rinsed with DDIW three times. They are then placed in the column sleeves as shown in Figure S.14
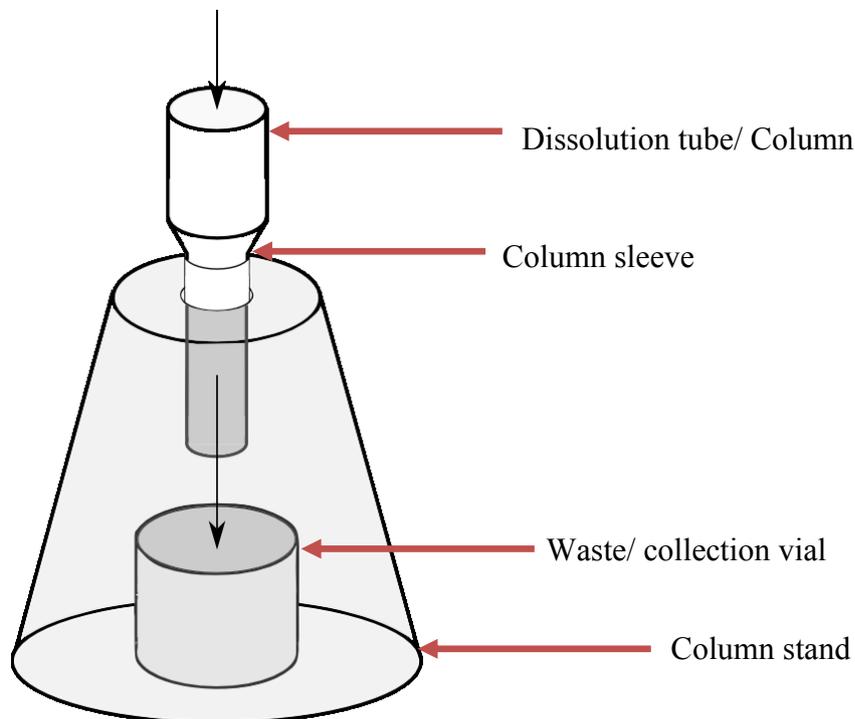


Figure S.14: Column stand with dissolution tube, column sleeve and collection vial in place.

   6) Cleaned 7ml beakers are placed in numerical order in front of column stands. The vial numbers and column stand numbers are noted to their corresponding sample numbers. All ordering is numerical to reduce the possibility of sample confusion

2. Weighing samples

1) Calibrate scales

2) Sample IDs and vials numbers are noted on running sheet

3) Vials are weighed without their lids, placed on scales and any static build-up is removed with a static gun

4) The vial mass is tared

5) Samples are then placed in their corresponding vials, the sample mass is then weighed and recorded

6) Standards are weighed out in this stage

3. Sample dissolution

1) Vials are placed under column stands and DDIW added to cover the sample through the dissolution tube

2) Two drops of concentrated $HNO_3$ is added to the samples

3) This is then repeated until the dissolution reaction stops. 10 more drops are then added to ensure complete dissolution

4) Vials are then filled to 60% of capacity with 1.5M $HNO_3$

4. Spiking samples

1) U-Th spike 4 is used

2) Spike amount calculation based on estimated sample uranium quantities as shown in Figure S.15
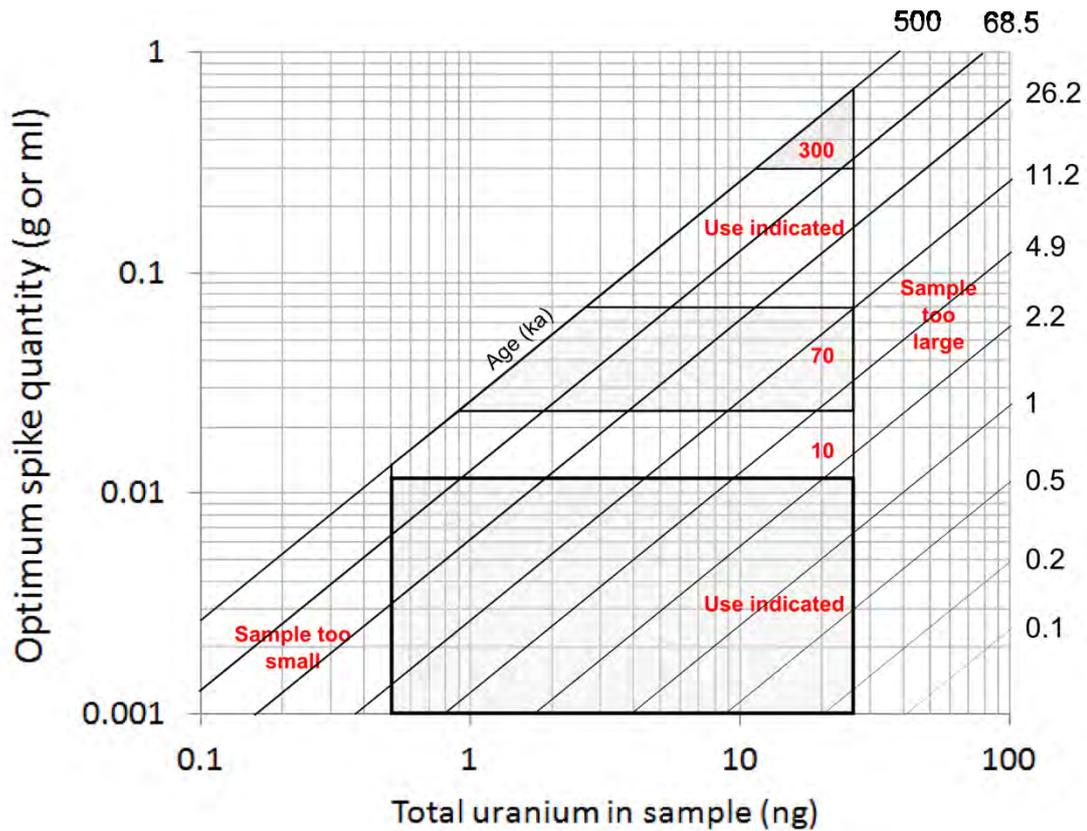
Figure S.15: U-Th spike 4 weight and spike calculator.

3) The stated volume is added to the samples using one pipette for each sample. The spike is added directly into the liquid to ensure complete addition.

4) Spiked samples are then caped and placed on a hot plate at over 100˚C overnight to homogenise.

5) Once completed dissolution tubes are removed and placed in Aqua Regia.

5. Column preparation

1) Columns are removed from acid storage and triple rinsed with DDIW.

2) Columns placed in column stand.

3) A full reservoir of DDIW is poured into columns to remove any bubbles

6. Applying resin

1) TRU spec/ Pre filter is mixed in DDIW

2) The resin slurry is pipette into the column to the base of the upper reservoir as shown in Figure S.16.
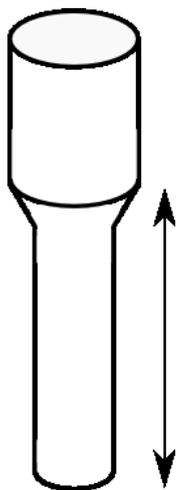
Figure S.16: Column with resin depth height displayed.

3) Once the target resin height has been achieved samples are left to stabilise for approximately 12 minutes. After which, if any air bubbles remain these are removed with a pipette.

7. Resin cleaning

The following steps are intended to thoroughly clean the resin and elute all elements. $HNO_3$ and HCL remove all elements except U and Th, and HF to remove U and Th.

1) A full reservoir of 1.5M $HNO_3$ is added
2) 2 times 0.5 ml of 1.5M $HNO_3$
3) 4 times 0.5 ml of 4M HCl
4) 4 times 0.5 ml of 0.1M HCl – 0.2M HF mix
5) 2 times 0.5 ml 1.5M $HNO_3$
6) Once the above cleaning steps have been completed the waste acids are disposed of

8. Sample addition and element elution to waste

1) Samples are removed from the hotplate and shaken to homogenise.
2) The sample is poured into the column and vials placed in beaker for cleaning (see vial cleaning).

3) All element except U and Th are now removed by the addition of $HNO_3$ and HCL.

4) 4 times 0.5 ml 1.5M $HNO_3$

5) 4 times 0.5 ml 4M HCl

9. Elute U-Th and collect

1) U-Th 3 ml sample beakers are placed in numerical order and beaker numbers are recorded with corresponding column stand and sample numbers

2) Five drops of concentrated $HNO_3$ are added to the U-Th beakers and then placed beneath columns

3) U and Th are eluted using the HCl-HF mix.

4) 4 times 0.5 ml 0.1HCl – 0.2M HF

5) The U-Th vials are then closed and placed on a cleaned hotplate with lids off at 80°C for 18 hours. Once completed samples are stored in a sealed box marked 'U-Th ready to run'

Clean up

1) Columns are cleaned and the resin removed with DDIW. They are then placed in a beaker with HCl/$HNO_3$ for cleaning

2) Column holders are grouped into six and placed in a beaker with DDIW and concentrated $HNO_3$

3) Bench is wiped down

Vial cleaning

4) Beakers are washed in detergent (Micro 90) for 2-3 days. Lids in one bottle vials in another

5) The beakers are then rinsed to remove all detergent

6) Reflux acid is placed at the base of the vial and closed vials are placed on a hot plate at over 100°C overnight

7) The acid is removed and the vial triple rinsed with DDIW. The vial is also checked for 'sticky spots', which are the result of residue from previous samples and if remain would result in sample contamination

Analysis

1. Prepared samples are re-dissolved in a 1ml 5% $HNO_3$ + 0.5 % Hf mix and placed on a hotplate to equilibrate for a minimum of 30mins

2. Sample introduction is carried out by a DeSolvation Nebulizer system (DSN-100) by an Argon gas stream (at 30-40 PSI pressure) creating an aspirated aerosol for analysis

3. Analysis is then carried out on a NU Plasma multiple collector inductively coupled mass spectrometer (MC-ICP-MS). Machine setup involves warm up and tuning, in which signal strength and peak is optimised and background noise minimised. Tuning is achieved by finding optimal conditions for the Ion beam by altering: nebuliser gas flows, plasma position, beam focus and beam position

4. Both internal standards (Yarrangobilly flowstone stock, YB-1) and external standards (Harwell Uraninite, HU-1) to determine accuracy

## S.12. Residue extraction method

Residue extraction was carried out by calcite dissolution in HCl. Early attempts produced a slurry formed of $CaCl_2$ which, once dried, would then absorb water from the atmosphere and return to a slurry. This early extraction when analysed using a PHILIPS (FEI) XL30 ESEM TMP. Consequently it was decided that a larger sample was required to obtain more residue, and that more cleaning was required.

*Sample dissolution*

1. In the later residue extraction a larger sample size was used of 61g of calcite. Progressive addition of concentrated HCl was used to dissolve the sample over two nights in a large beaker
2. The remaining solution was then dried down at 100˚C

*Washing*

The following steps were used to clean to sample of all chloride crystals that may have formed as a result of the dissolution in HCl.

1. Double de-ionised water (DDIW) was then added to the dried-down remains to produce 100 ml of solution for centrifuging
2. The solution was then shaken to homogenise and centrifuged for 30 minutes at 3000 revolutions per minute, until the solution was clear
3. The wash solution (containing dissolved chloride) was then removed and clean DDIW added. The sample was shaken to ensure cleaning of the entire residue. The mix was then centrifuged again for 2 mins (until clear) and the wash solution removed. This process was repeated 5 times
4. The final wash water was removed and a triple rinse with DDIW was used to transfer the residue from the centrifuge tube into a cleaned and pre weighed Teflon vial for drying dow
5. The vial was then placed on a hotplate at 100˚C overnight to dry down
6. The vial was then weighed to obtain the residue mass

*Residue dissolution*

The residue sample was then sub sampled for $HNO_3$ dissolution and half retained for reference.

1. Residue was covered in 2% $HNO_3$
2. This was left overnight and then dried down
3. The same washing procedure as described above in 'washing' was used again with 5 washes
4. The final residue was transferred to the vial and dried down
5. This residue was also weighed
6. All stages of the extraction method are displayed diagrammatically in Figure S.17

**Yarrangobilly calcite sample**

Sample cut to remove black calcite.

Sample was sectioned along this axis to retain some sample as reference.

**Sample dissolution**

HCL

Dissolution

HCL

Drying

**Sample washing**

Centrifuge

Remove wash

Clean DDIW

DDIW

DDIW

Residue

DDIW

Residue

DDIW

Residue

x5

DDIW

Drying

Weighing & splitting

**Residue leaching**

HNO₃

Drying followed by washing procedure
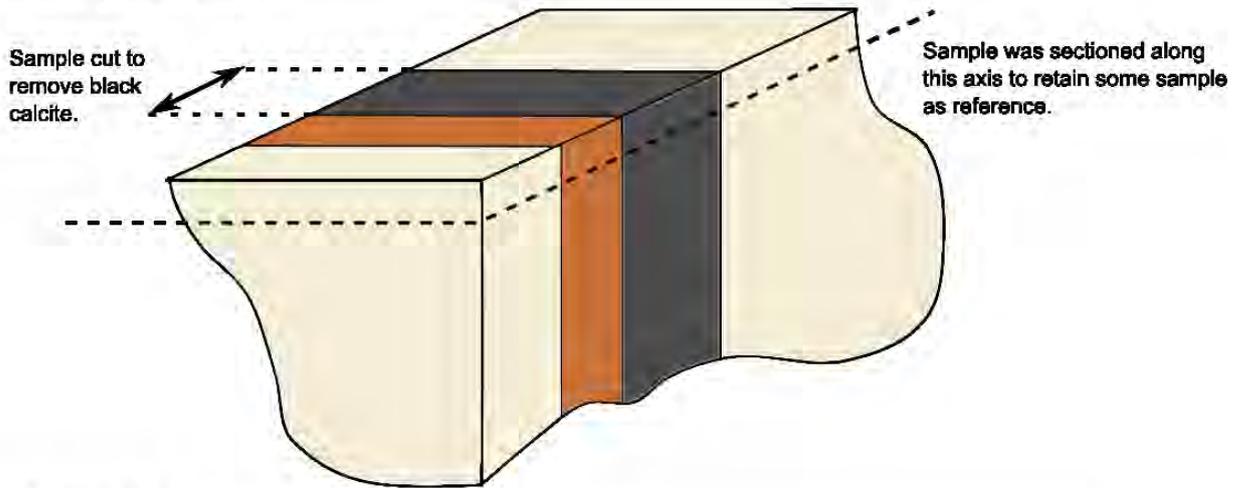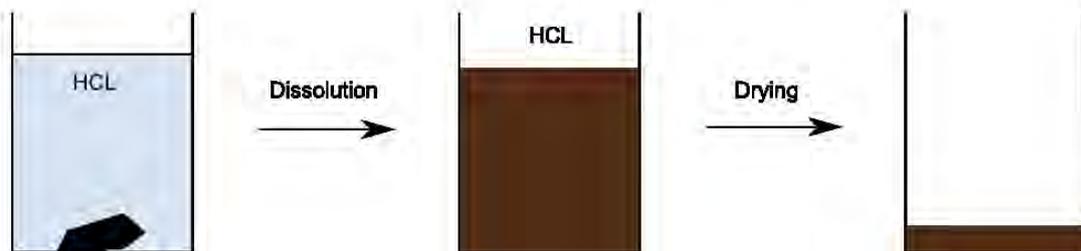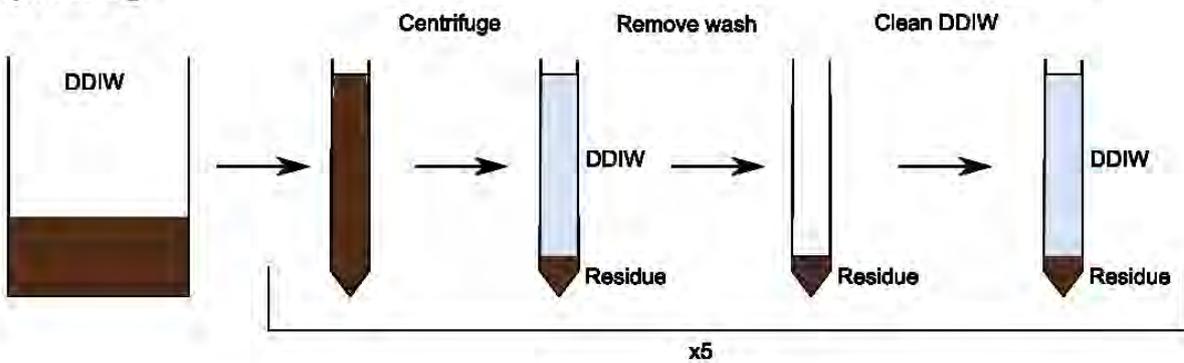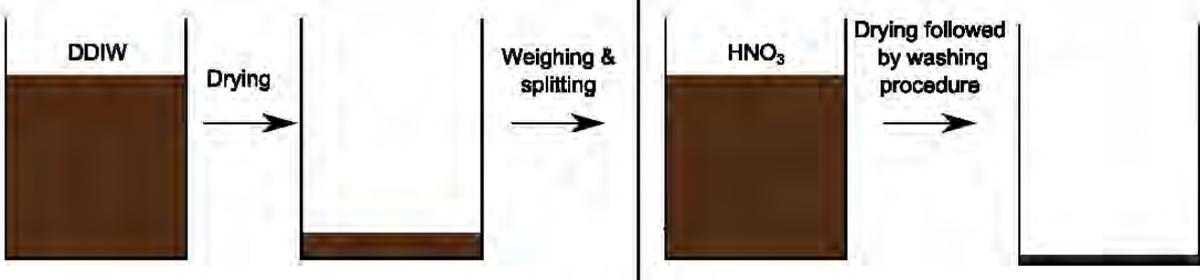
Figure S.17: Residue extraction methods

## S.13. LA-ICP-MS method

Laser ablation sample acquisition trace element analysis was performed on polished thick sections. Two separate systems were utilised during this investigation for Gibraltar and Yarrangobilly samples at Royal Holloway University of London and the University of Melbourne respectively. Gibraltar analysis by LA-ICP-MS was carried out as part of an MSc project in 2010.

*Sample preparation and loading*

Samples for analysis at RHUL were prepared in thick sections. Samples at Melbourne were combined into set blocks of resin and polished. Before analysis cleaning was carried out with ultrasonication in a water bath and cleaned with methanol. Delicate thin samples were not ultrasonicated.

Samples were placed into universal sample holders making sure that the polished surface of samples were level, and aligned with the reference material surface (NBS-19). Sample cells was sealed and purged with N gas and backfilled eight times to remove air and contaminantation. Sample holders were scanned and registered in the Resonetics laser ablation software in order to create ablation paths. Ablation path and ablation parameters were programmed to obtain the most data from each sample section at the most efficient resolution. Pre-ablation was used to remove the upper surface of the sample to reduce the risk of sample contamination. This was carried out at 25hz and 0.1mm/sec along the predetermined ablation path which runs the length of the sample growth axis.
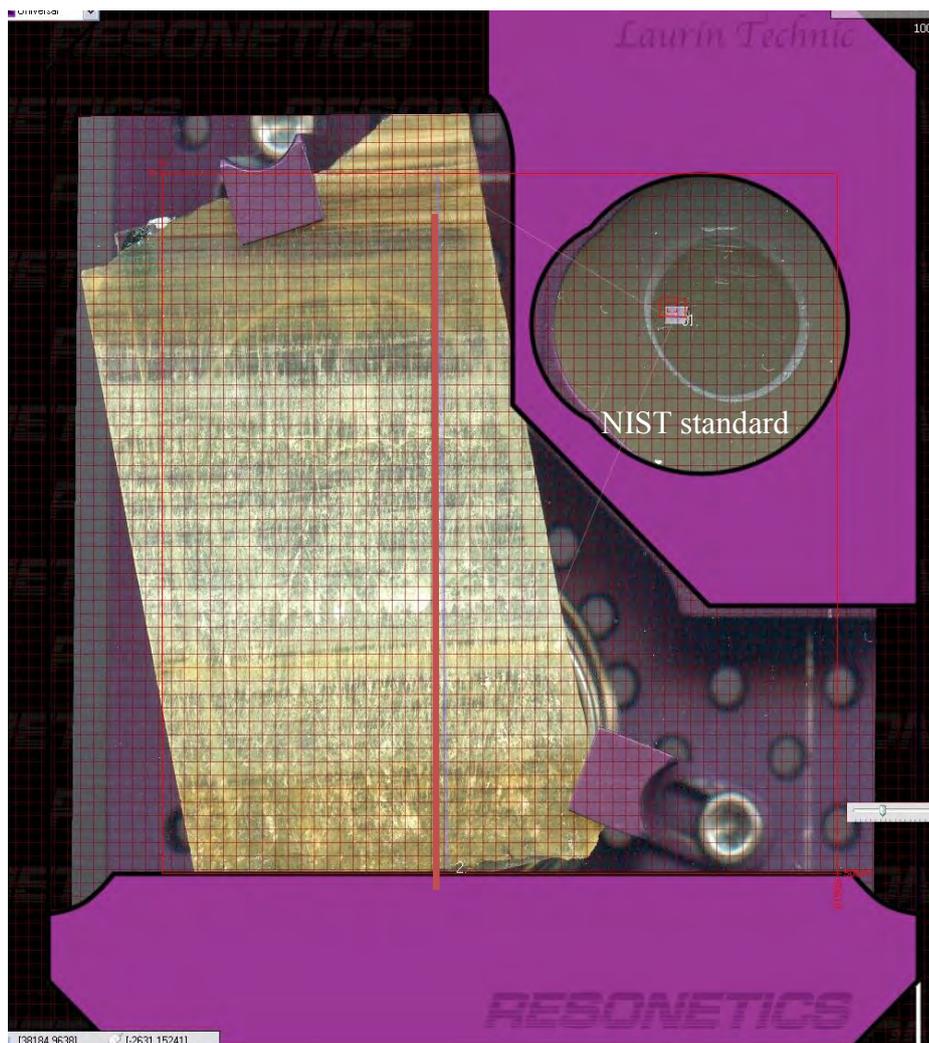
Figure S.18: Screenshot displaying ablation path (blue line), mounting of the sample in the Laurin Technic universal sample change and the Resonetics laser ablations control software.

The custom-built excimer laser-ablation system consistin of a two volume laser-ablation coupled to a quadrupole inductively coupled mass spectrometer (LA-ICP-MS) located at Royal Holloway, the same (but older) system was location at the University of Melbourne. The 2 volume laser ablation cell has the advantages of accommodating large samples in its universal sample holder whilst maintaining rapid (<1.5s for 99%) washout and a high sensitivity (Müller *et al.,* 2009).

*Data Analysis*

The National Institute of Standards and Technology (NIST) series standard is widely used in laser ablation calibration and is internationally certified for 5 elements. NIST synthetic glass contains 40 mg kg$^{-1}$for every element and was used in the calibration of data from intensity in counts per second (cps) to concentrations in part per million (ppm).

Data was calibrated with the NIST 612 standard from intensity values obtained by ICP-MS by using the equation expressed below (from Heinrich *et al.*, 2006):

$$C_i^{\text{SAMP}} = C_r^{\text{SAMP}} \cdot \frac{C_i^{\text{STD}}}{C_r^{\text{STD}}} \cdot \frac{I_i^{\text{SAMP}} \; I_r^{\text{STD}}}{I_r^{\text{SAMP}} \; I_i^{\text{STD}}}$$

Where:

*C refers to the concentration of the subscripted element*

*r is a reference element or internal standard*

*i is unknown elements*

*I refers to the corresponding background-corrected signal intensity in counts per second (counts/s)*

## S.14. Supplementary Method References

Bozlaker, A., Muezzinoglu, A.., Odabasi, M. 2008. Atmospheric concentration, dry deposition and air-soil exchange of polycyclic aromatic hydrocarbons (PAHs) in an industrial region in Turkey. *Journal of Hazardous Material,* **153**, 1093-1102.

Chu, C.C., Fang, G.C., Chen, J.C., Yang, I.L. 2008. Dry deposition study by using dry deposition plate and water surface sampler in Shalu, central Taiwan. *Environmental Monitoring and Assessment* **146(1)**, 441-451.

Harper, S.L., Walling, J.F., Holland, D.M. & Pranger, L.J. 1983. Simplex optimization of multi element ultrasonic extraction of atmospheric particulates. *Analytical Chemistry*, **55**, 1553–1557.

Heinrich, C.A., Petike, T., Halter, W.E., Aigner-Torres, M., Aud'etat, A., G'unther, D., Hattendorf, B., Bleiner, D., Gullong, M., Horn, I. 2006. Quantitative multi-element analysis of minerals, fluid and melt inclusions by laser-ablation inductively-coupled-plasma mass-spectrometry. *Geochimica et Cosmochimica Acta*, **67** (18), 3473–3496.

Hellstrom, J. 2003. Rapid and accurate U/Th dating using parallel ion-counting multicollector ICP-MS. *Journal of Analytical Atomic Spectrometry*, **18**, 1346–1351

Hellstrom, J. 2006. U–Th dating of speleothems with high initial $^{230}$Th using stratigraphical constraint. *Quaternary Geochronology*, **1**, 289–295.

Holsen, T. M., Noll, K. E. 1992. Dry deposition of atmospheric particles: Application of current models to ambient data. *Environmental Science and Technology*, **26**, 1802–1814.

Leister, D.L. & Baker, J.E. 1994. Atmospheric deposition of organic contaminants to the Chesapeake Bay. *Atmospheric Environment,* **28**, 1499-1520.

Müller, W., Shelley, M., Miller, P. & Broude, S. 2009. Initial performance metrics of a new custom-designed ArF excimer LA-ICPMS system coupled to a two-volume laser-ablation cell. *Journal of Analytical Atomic Spectrometry*, **24**, 209–214.

Odabasi, M., Vardar, N., Sofuoglu, A., Tasdemir, Y. & Holsen, T.M. 1999. Polycyclic aromatic hydrocarbons (PAHs) in Chicago air. *The Science of the Total Environment,* **227**, 57-67.

Pietrogrande, M. C., Mercuriali, M., Perrone, M.G., Ferrero, L., Sangiorgi, G., Bolzacchini, E. 2010. Distribution of *n*-alkanes in the Northern Italy aerosols: data handling of GC-MS signals for homologous series characterization. Environmenal Science & Technology, **44,** 4232-40.

Sehmel, G. A. & Hodgson, W.H. 1978. A model for predicting dry deposition of particles and gases to environmental surfaces. DOE Report PNL-SA-6721, Pacific Northwest Laboratories, Richland, WA.

Vardar, N., Odabasi, M. & Holsen, T.M. 2002. Particulate Dry Deposition and Overall Deposition Velocities of Polycyclic Aromatic Hydrocarbons. *Journal of Environmental Engineering*, **269.**

Vawda, Y., R. M. Harrison, *et al*. 1990. Use of surrogate surfaces for dry deposition measurements. *Journal of Aerosol Science,* **21** (Supplement 1), 201-204.

Wai, K. M., Leung, K.Y. & Tanner, P. A. 2010. Observational and modelling study of dry deposition on surrogate surfaces in a South China city: implication of removal of atmospheric crustal particles. *Environmental Monitoring and Assessment* **164(1-4)**, 143-152.

## S.15. Gibraltar LA-ICP-MS results
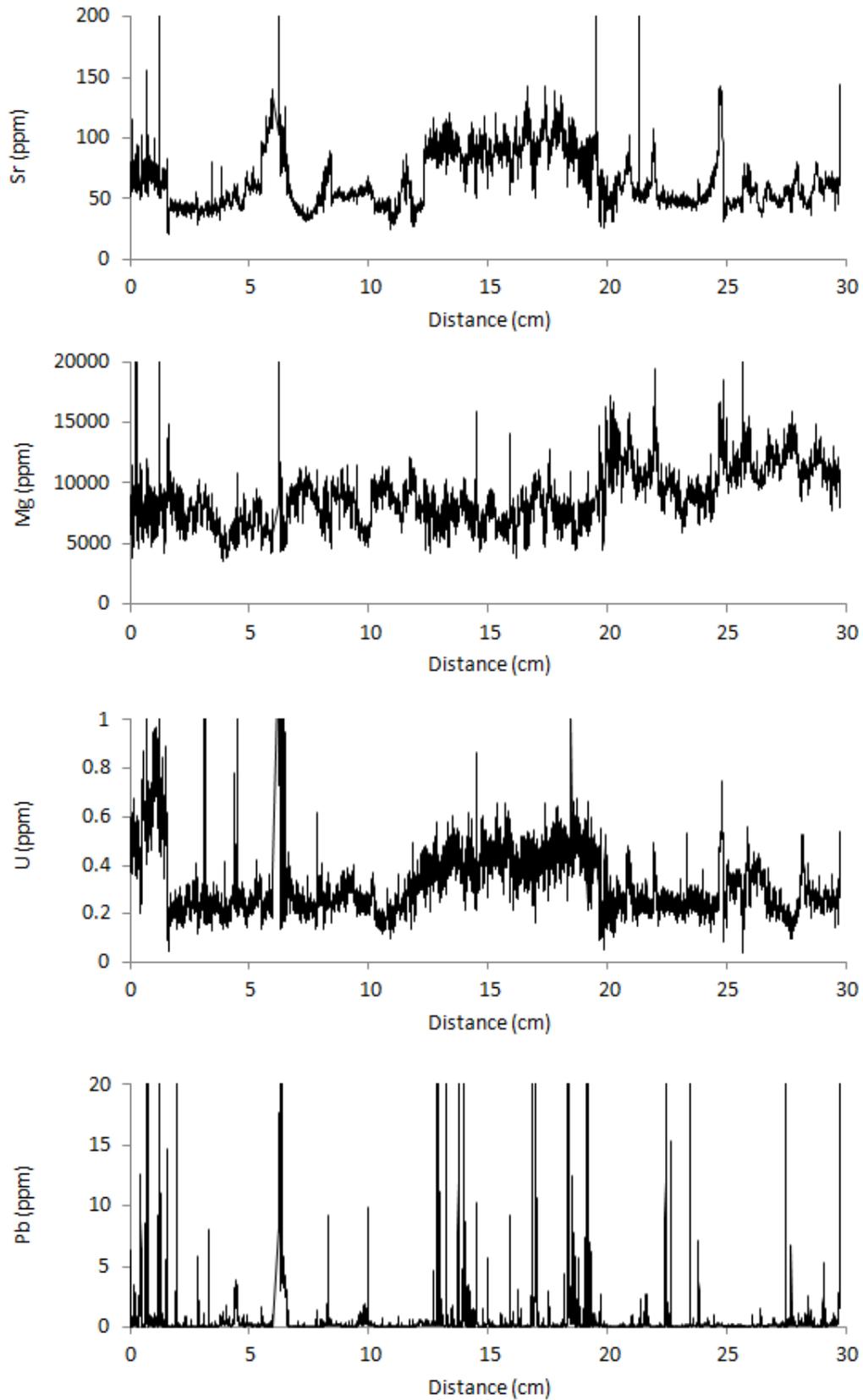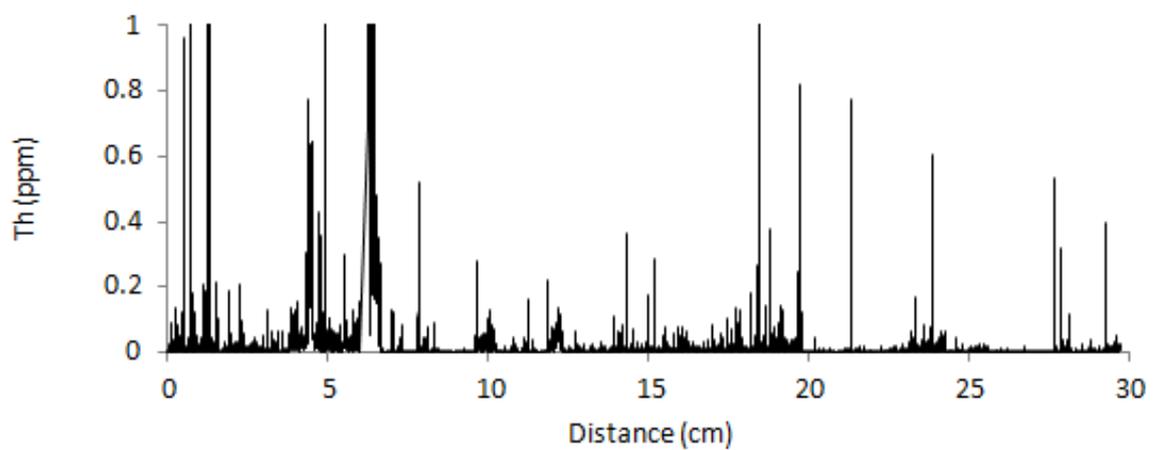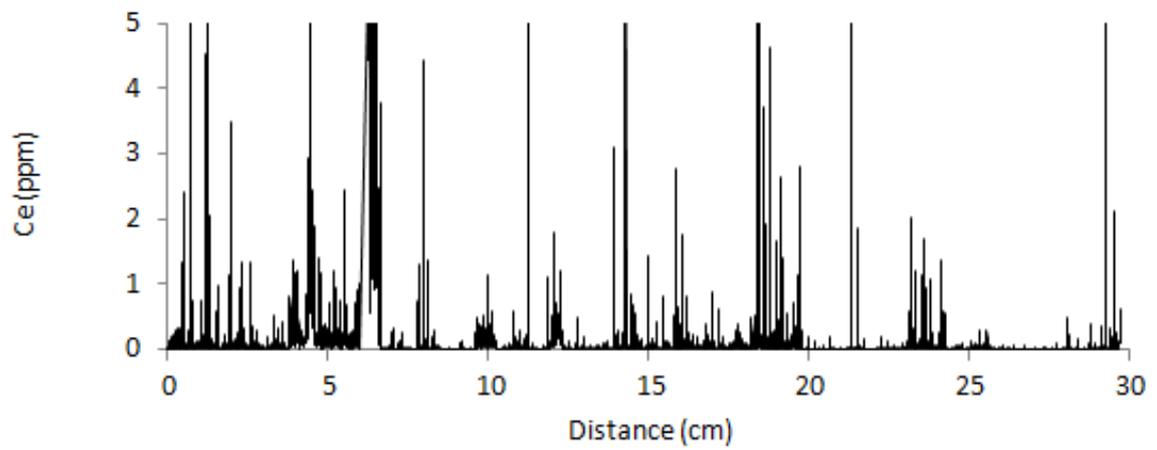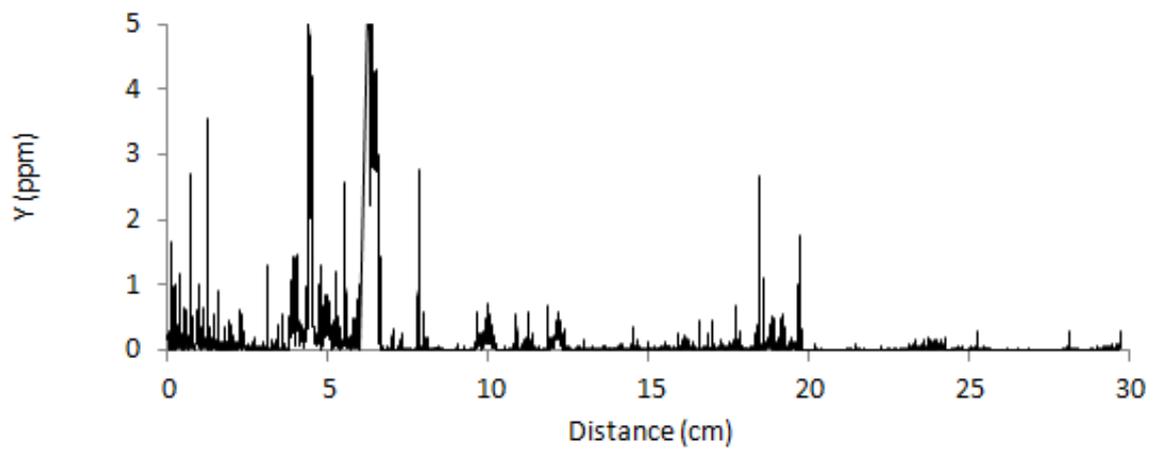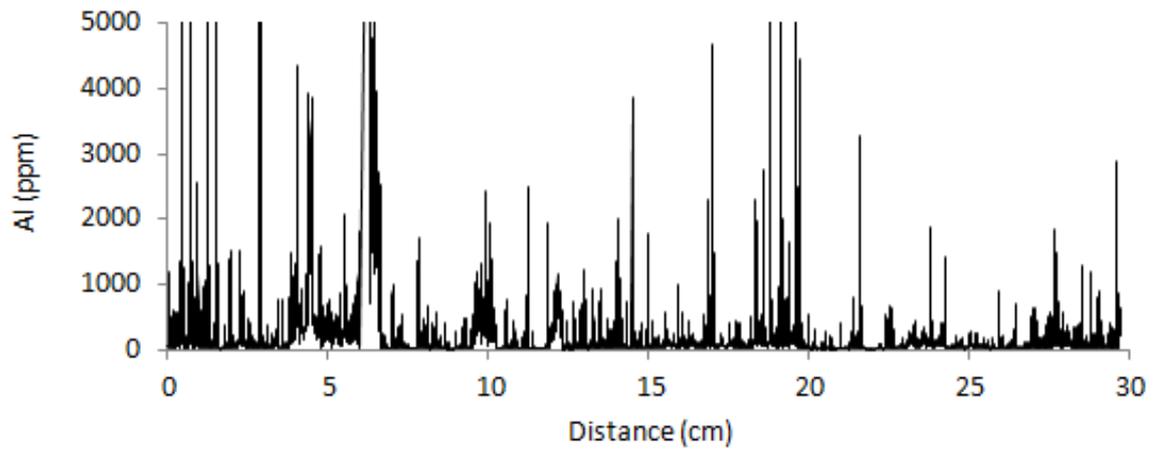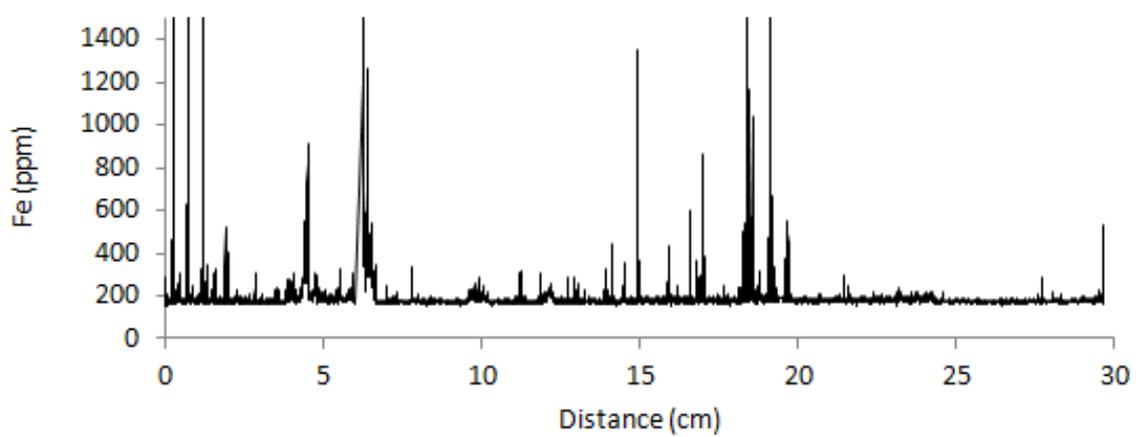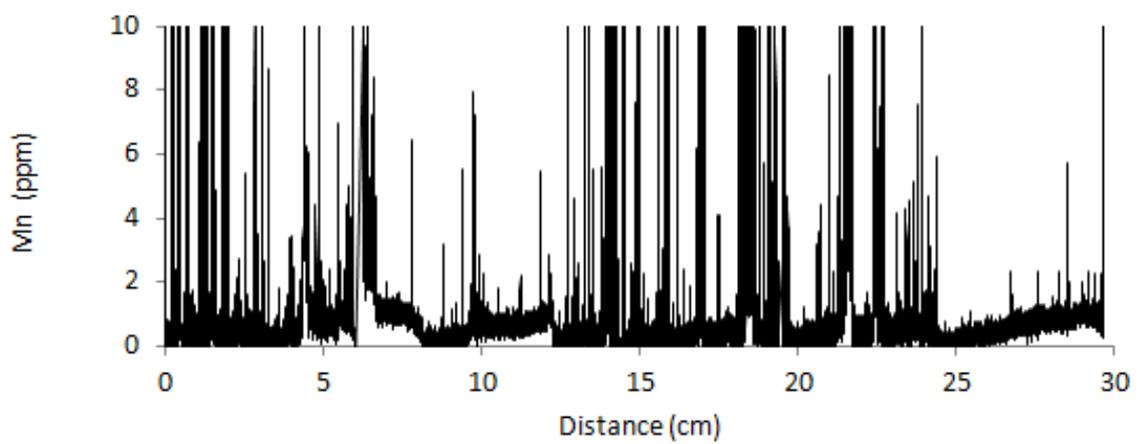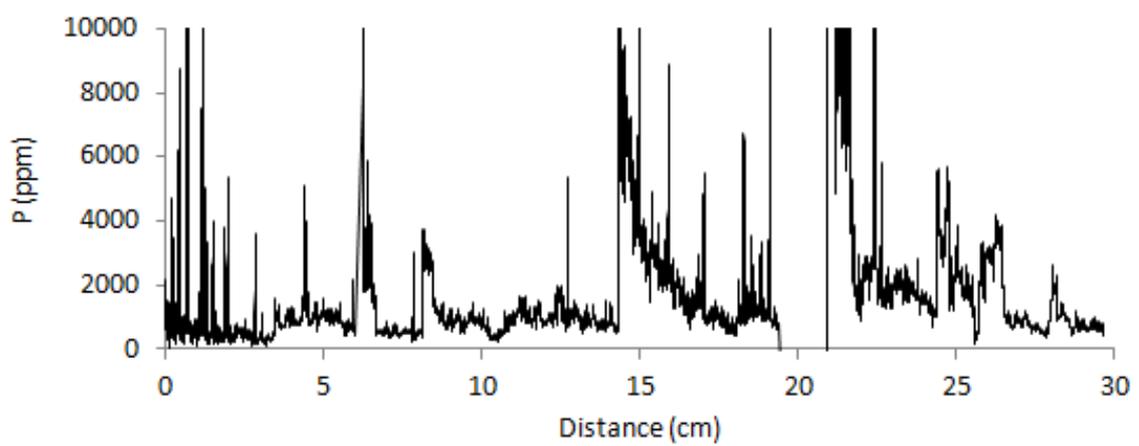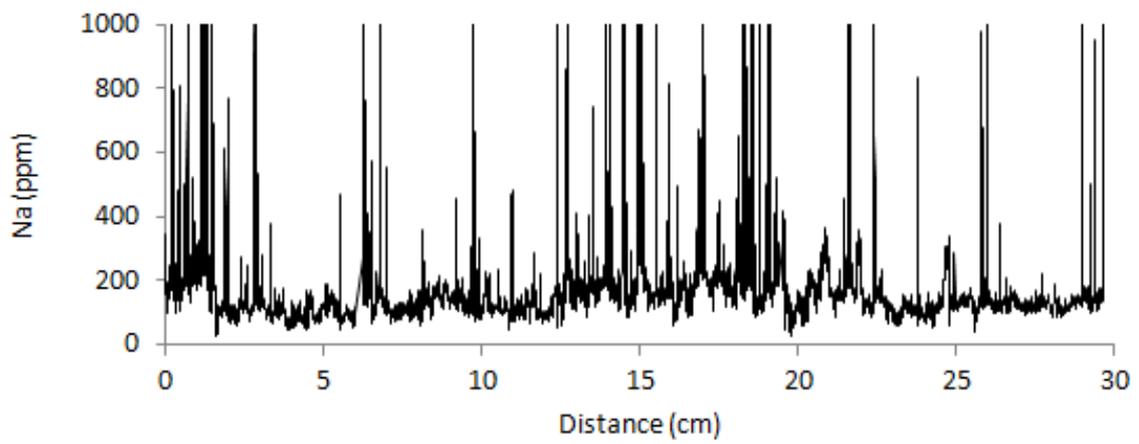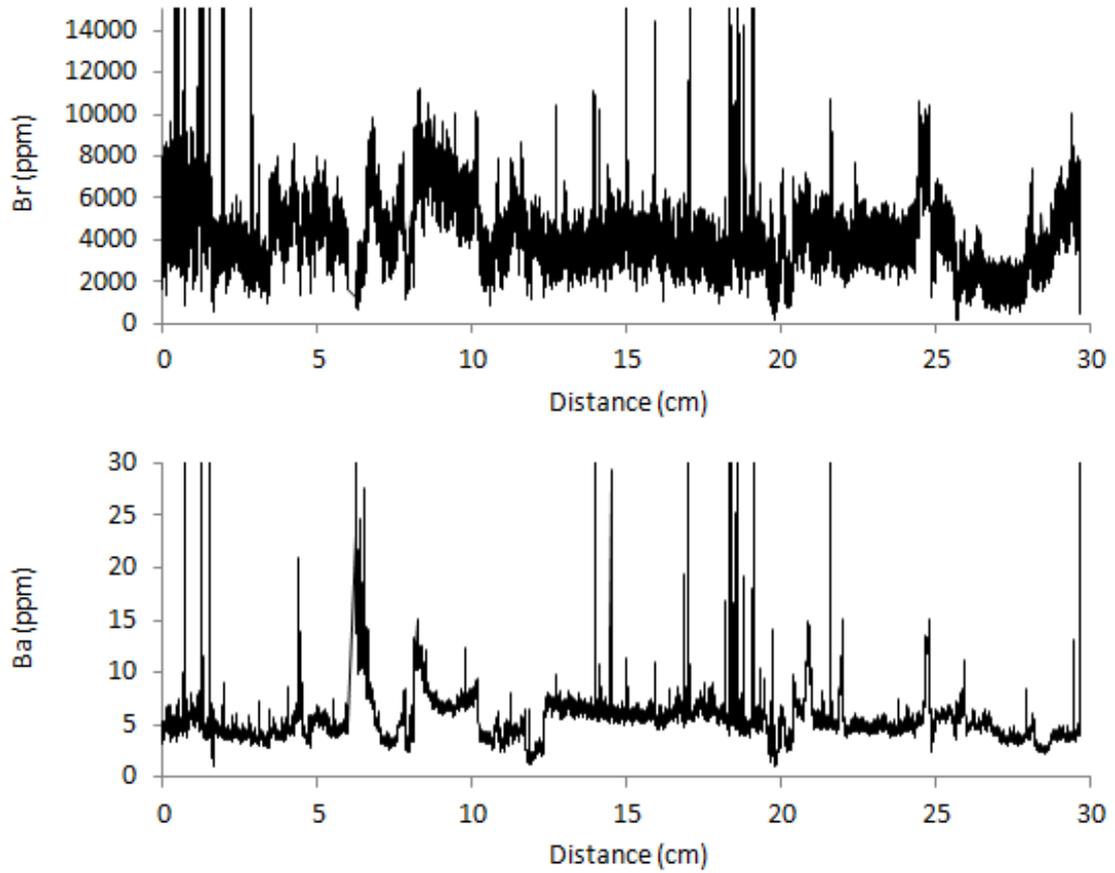
Figure S.19: Gibraltar LA-ICP-MS results.

## S.16. Gibraltar $F_{PCP}$ and $F_{SOURCE}$ line calculations (Chapter 5)

As displayed in Figures 5.14 and 5.15, the PCP vectors have a line equation of:

$(Sr/Ca)_S = 0.0023(Mg/Ca)_S + C$

*Where:*

*$(Tr/Ca)_S$ = Speleothem trace element values corrected to present original drip water values through the application of their respective $K_{Tr}$ values.*

*C = The original source Mg and Sr before the influence of PCP, which is represented by the intercept between the source line and sample PCP vector.*

As displayed in Figures 5.14 and 5.15, the Source line has line equation of:

$(Sr/Ca)_S = -0.0021(Mg/Ca)_S + 1.5632$

In order to determine the extent of progression along the PCP vector for each sample, the original source value must be determined for reference. This can be calculated by solving the source mixing line with the sample PCP evolution line at the point of intersection. Subsequently the initial Mg and Sr values can be obtained, this method can be described by:

$0.0023(Mg/Ca)_i + C = -0.0021(Mg/Ca)_i + 1.5632$

$(((Sr/Ca)_i - 1.5632)/(-0.0021)) = (((Sr/Ca)_i - C)/0.0023)$

*Where,*

*C = y intercept of the sample PCP vector.*

*$(Tr/Ca)i$ = Source line-PCP vector intersection point*

Each sample has its own PCP line and therefore y-intercept (C). This can be obtained for each PCP evolution line by:

$(Sr/Ca)_S = 0.0023*(Mg/Ca)_S + C$

$C = (Sr/Ca)_S - 0.0023*(Mg/Ca)_S$

By rearranging for $(Mg/Ca)_i$ and $(Sr/Ca)_i$ gives and using the above formula for C the PCP evolution-Source intercept can be expressed by:

$(Mg/Ca)_i = ((1.56 - ((Sr/Ca)_S - 0.0023*(Mg/Ca)_S))/0.0044$

$(Sr/Ca)_i = (0.48*((Sr/Ca)_S - 0.0023*(Mg/Ca)_S)) + 0.8171$

With the original source point determined and the final PCP influenced sample value known, the extent of PCP influence can be determined. This requires calculating the distance of progression along the PCP vector line, which can be expressed by:

$F_{PCP} = \sqrt{(\Delta(Mg/Ca)^2 + \Delta(Sr/Ca)^2)}$

*Where,*

$\Delta(Mg/Ca) = (Mg/Ca)_S - (Mg/Ca)_i$

$\Delta(Sr/Ca) = (Sr/Ca)_S - (Sr/Ca)_i$

$F_{PCP} = $ *The extent of PCP influence index.*

Similarly, the type of source can be quantified by determining each samples origin along the source line. This can be determined by comparing the PCP evolution-source intercept for each sample with the source line y-intercept, as expressed by:

$F_{source} = \sqrt{(((Mg/Ca)_C - (Mg/Ca)_i)^2 + ((Sr/Ca)_C - (Sr/Ca)_i)^2)}$

*Where,*

$(Tr/Ca)_C = $ *the y-intercept value of the source line.*

$F_{source} = $ *Type of source geochemistry index*

Since, $(Mg/Ca)_C = 0$

$F_{source} = \sqrt{((Mg/Ca)_i^2 + ((Sr/Ca)_C - (Sr/Ca)_i)^2)}$

## S.17. Yarrangobilly LA-ICP-MS Results
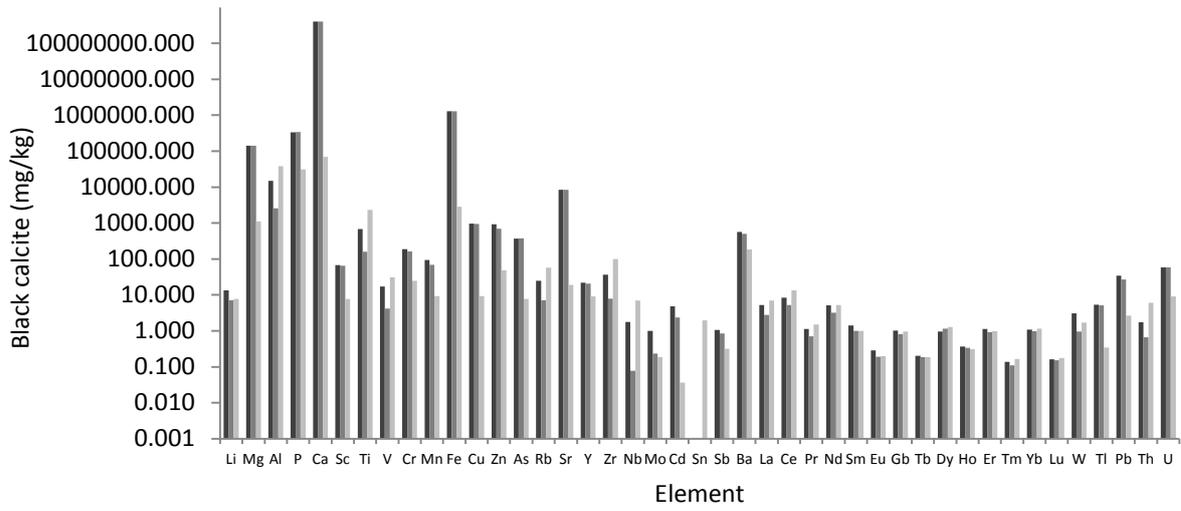


Figure S.20: Solution ICP-MS analysis comparison of HF, $HNO_3$ dissolution and residue analysis.
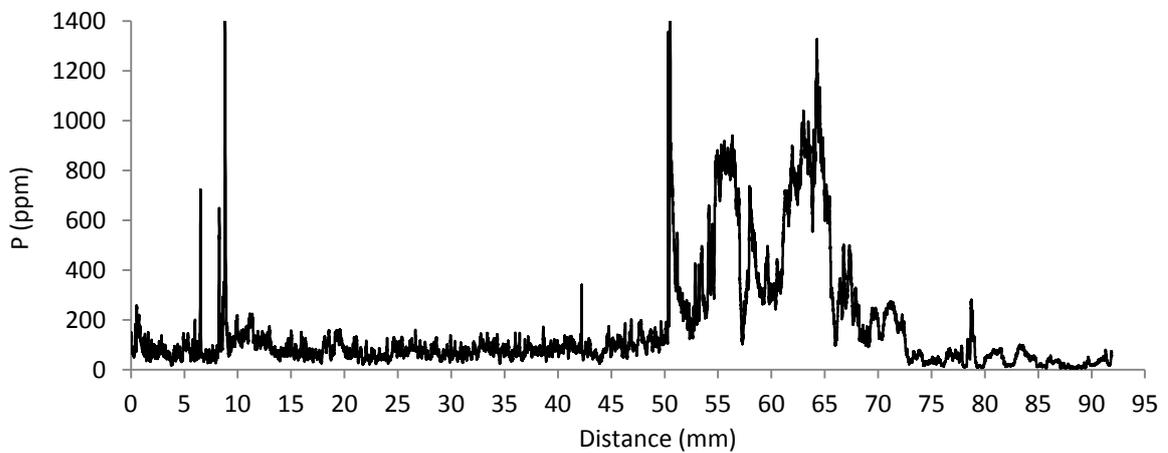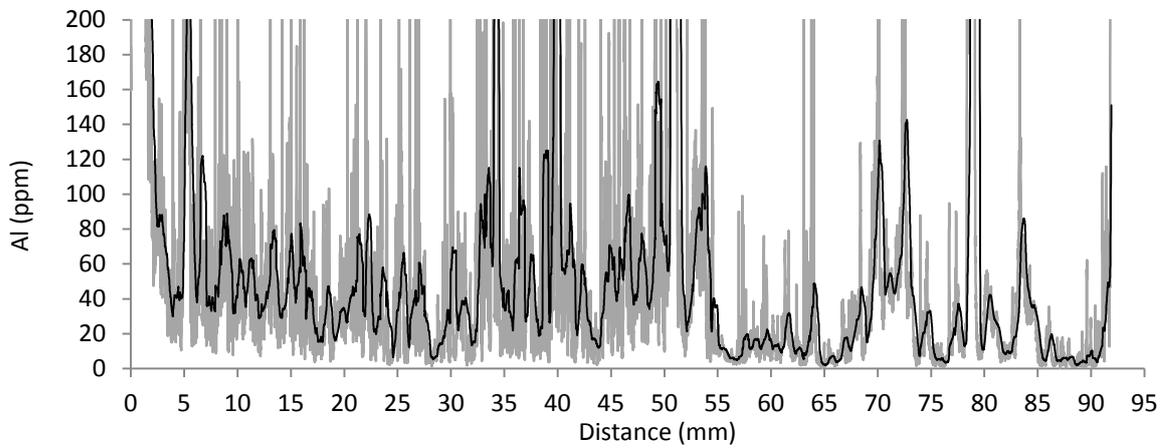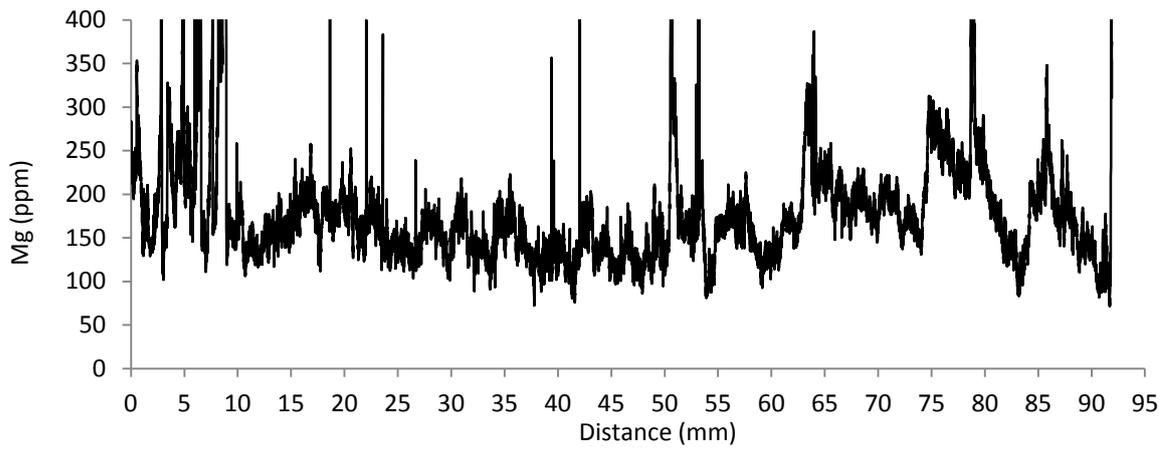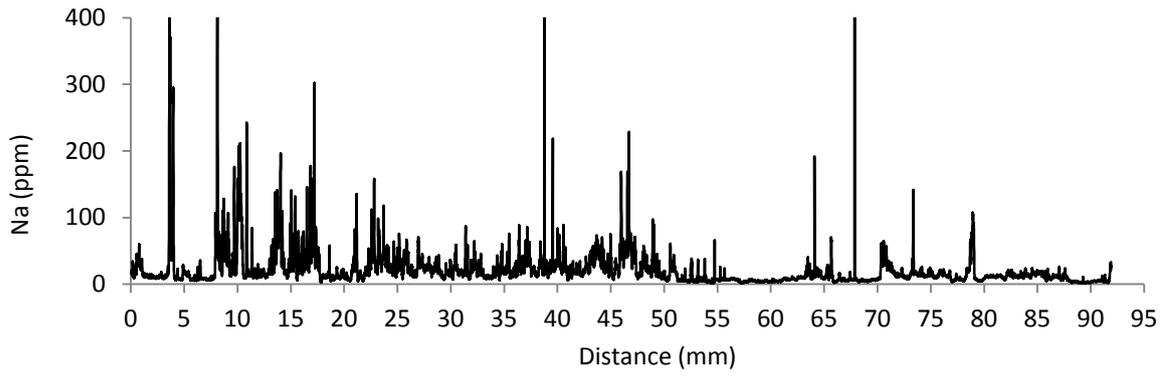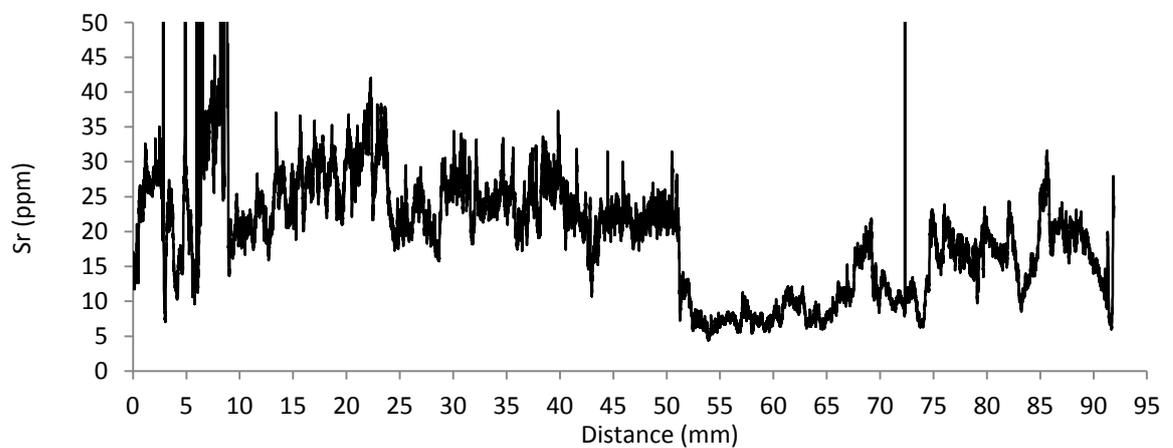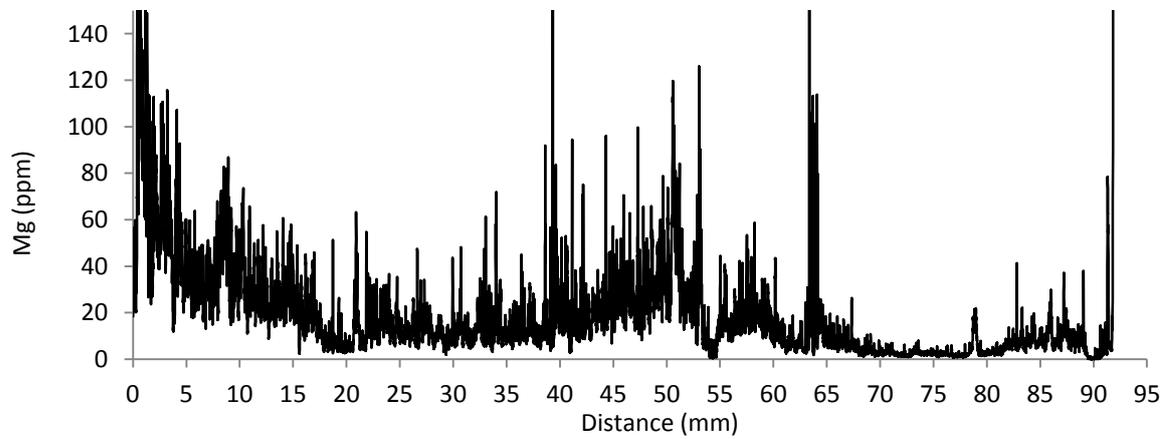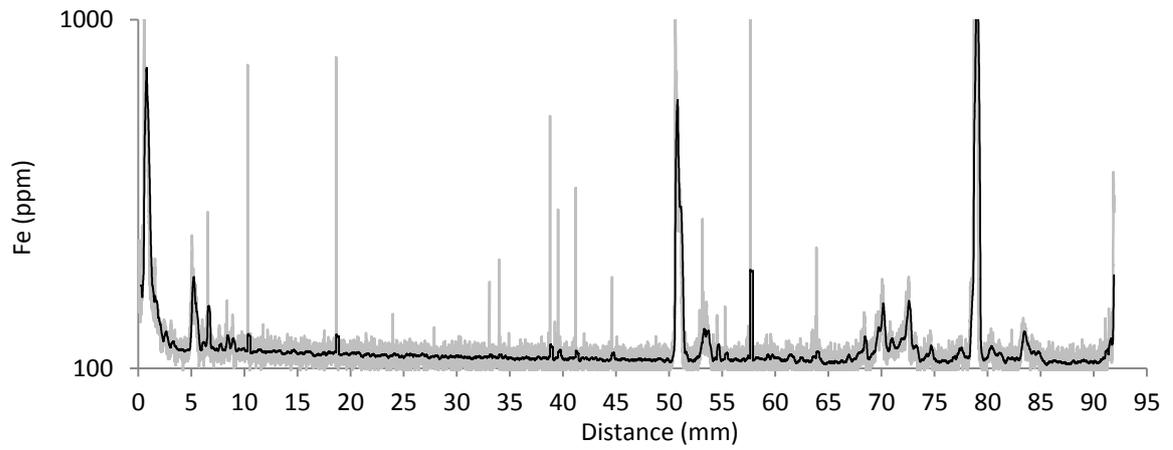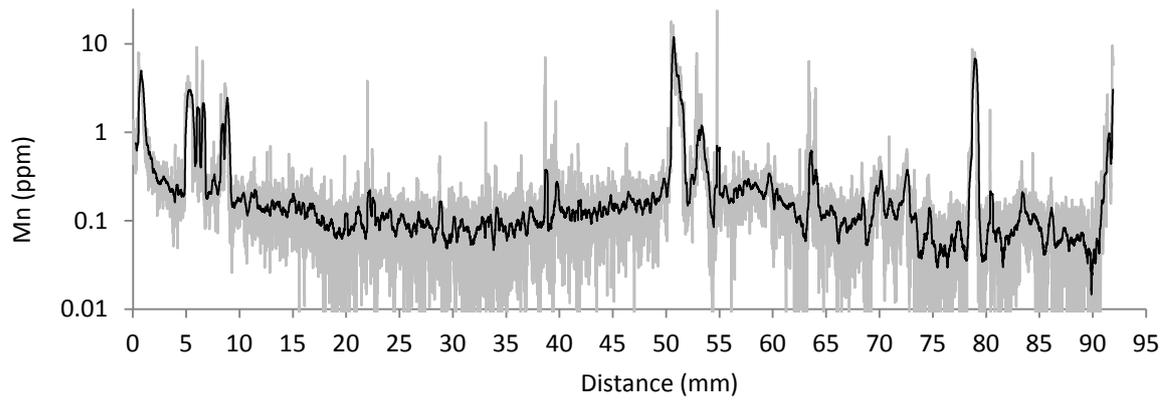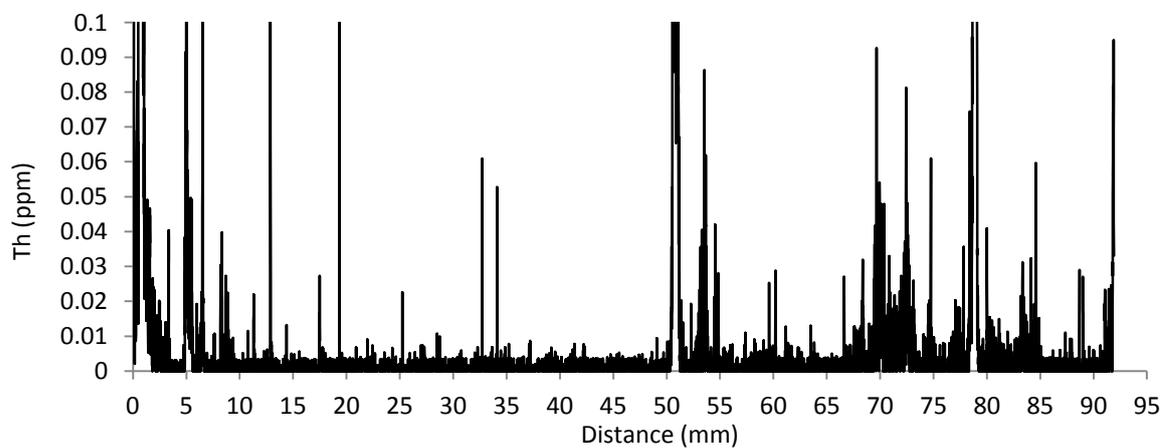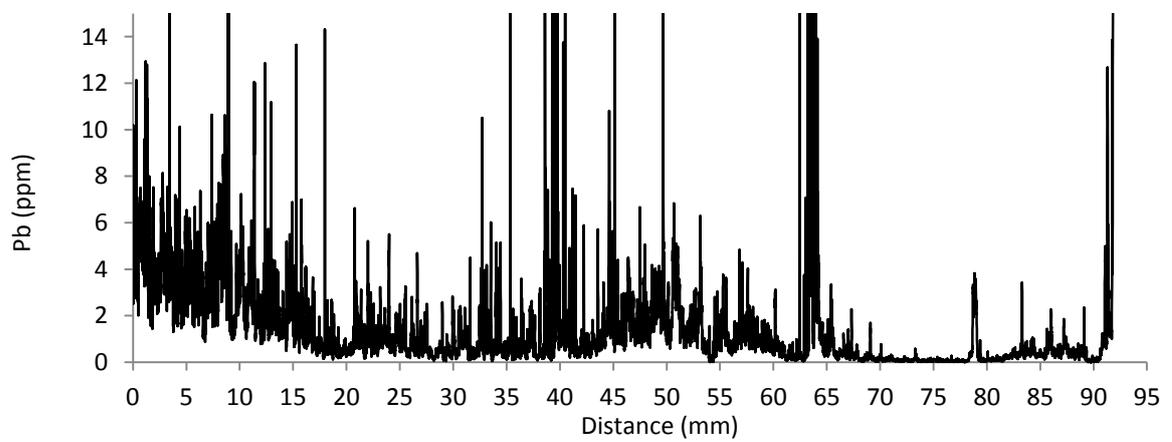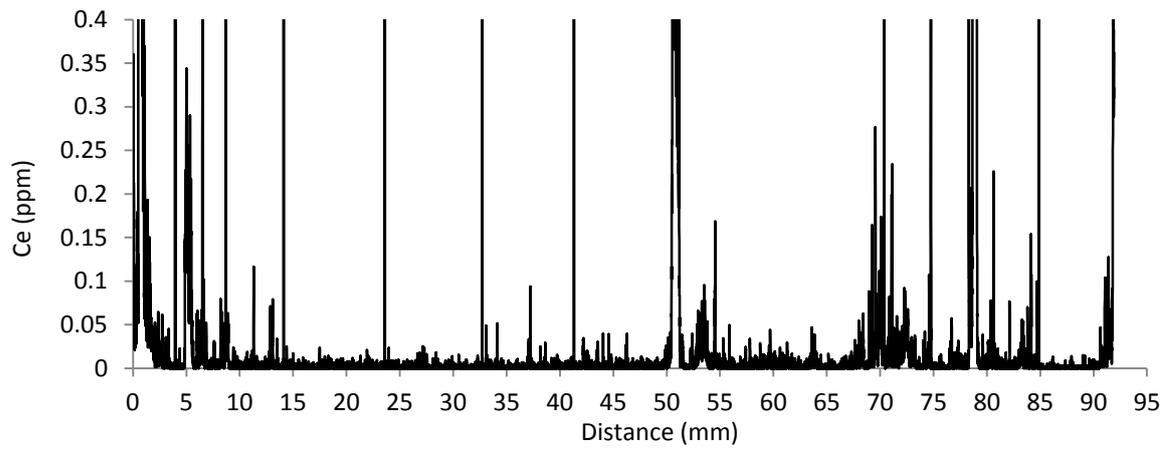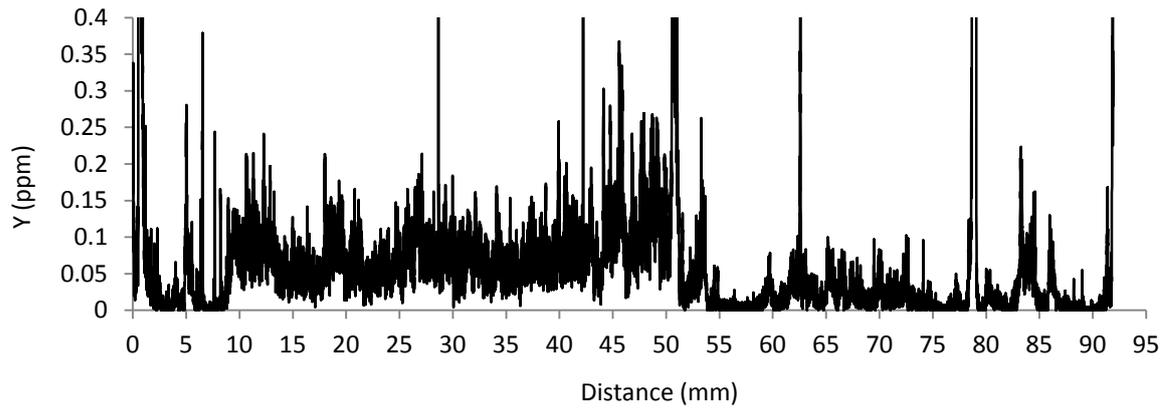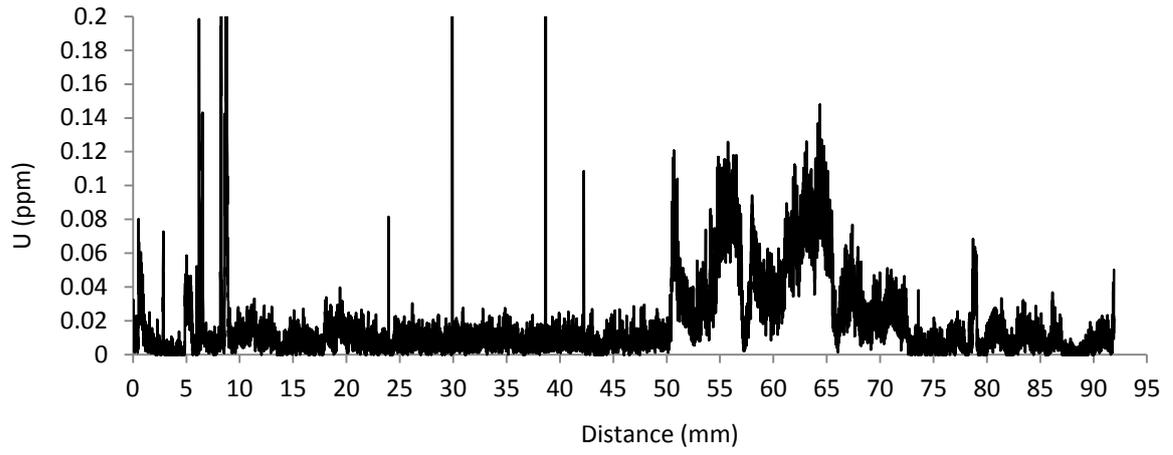
Figure S.21: Yarrangobilly flowstone YBJD1 LA-ICP-MS results.
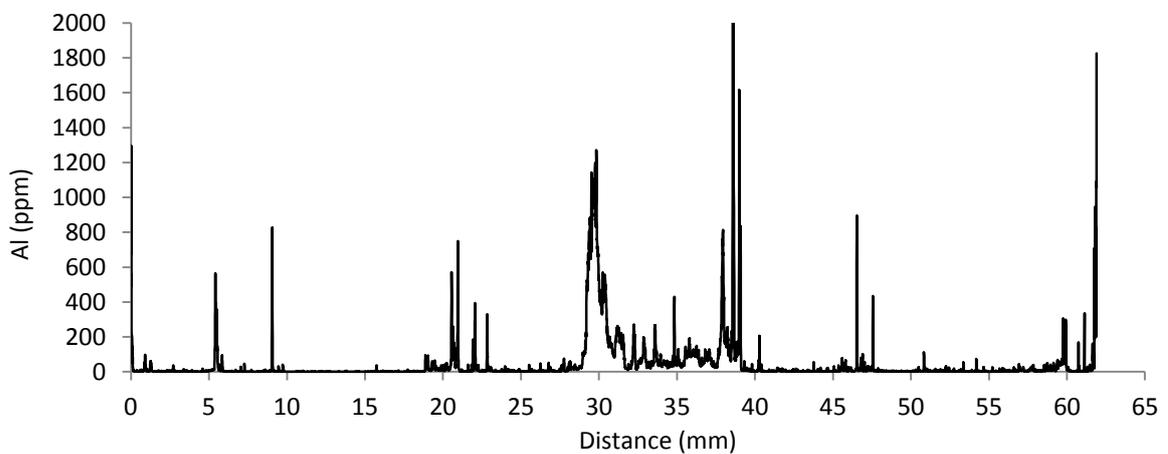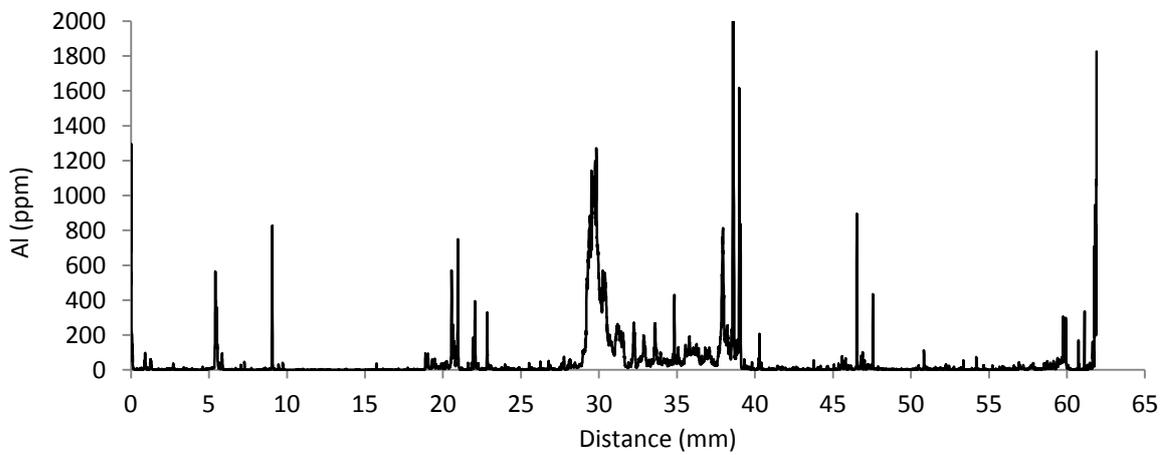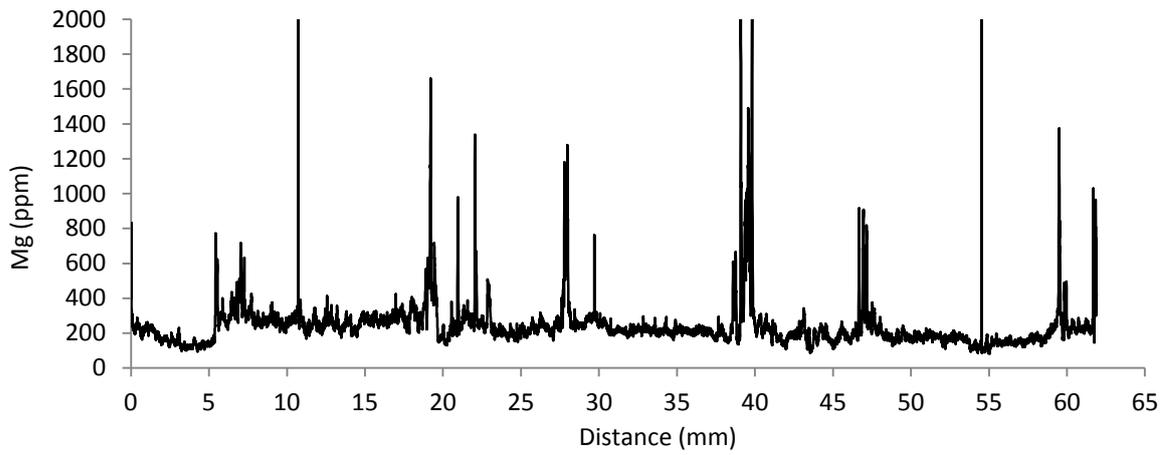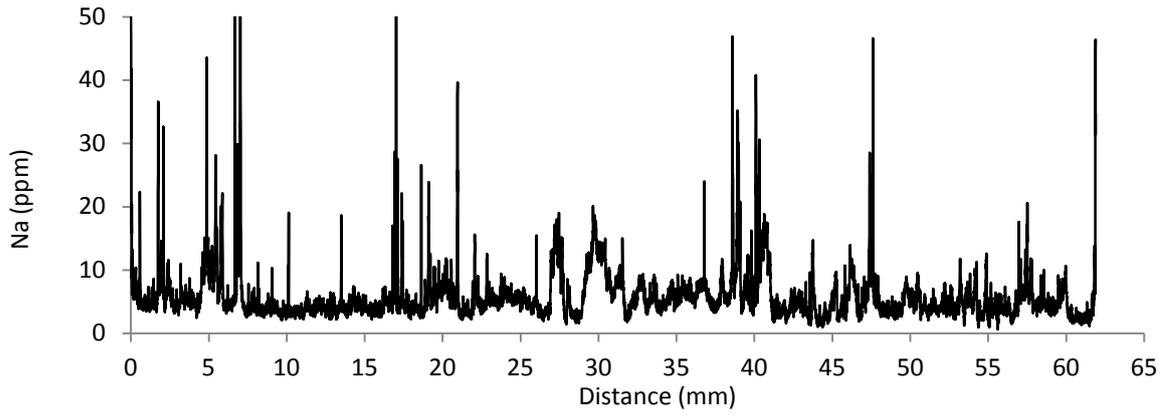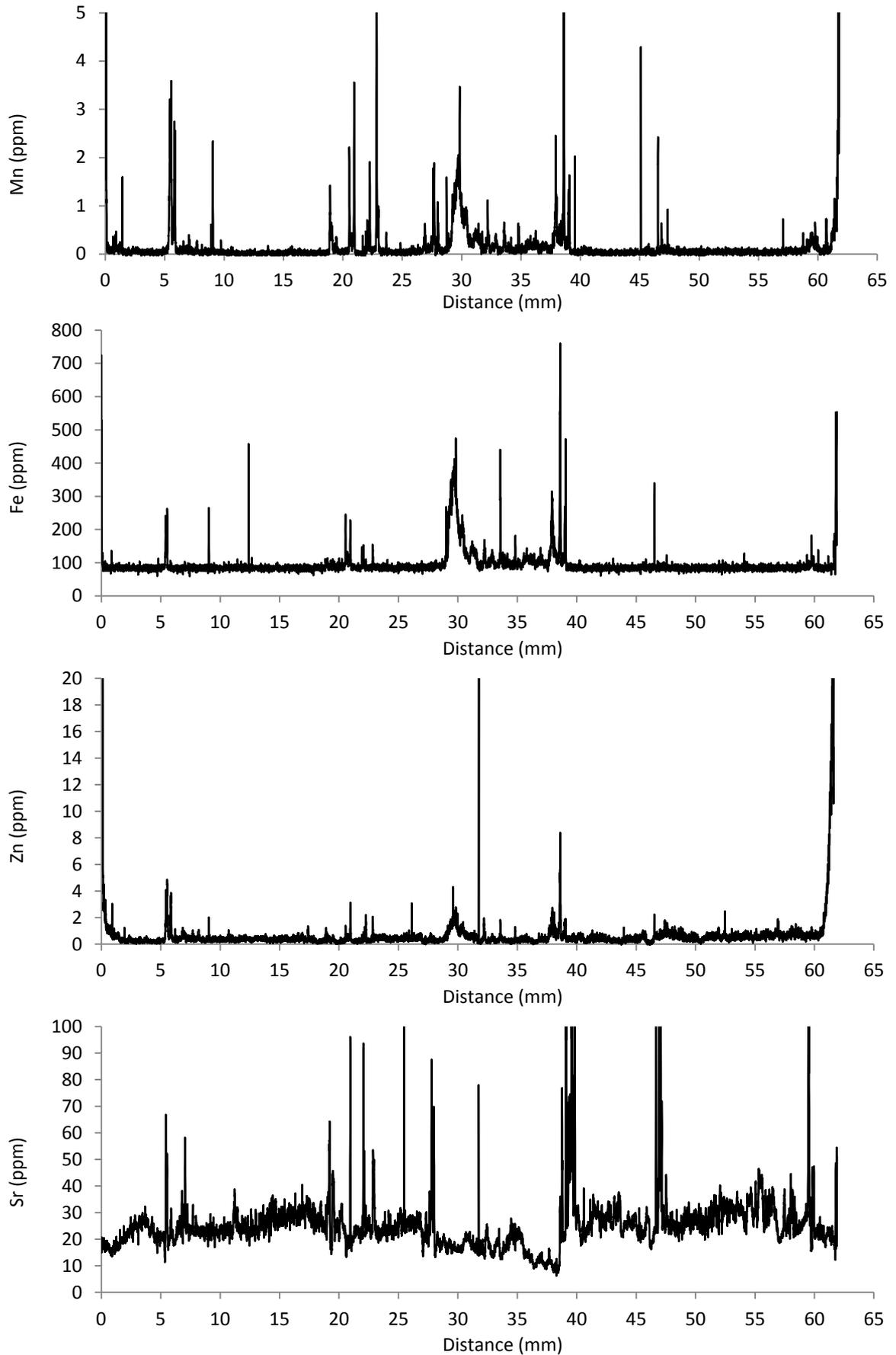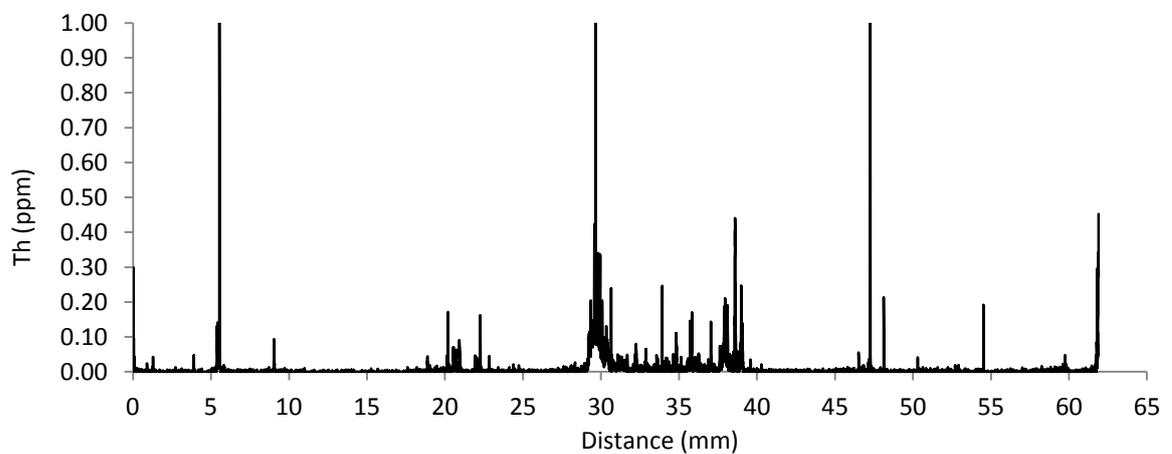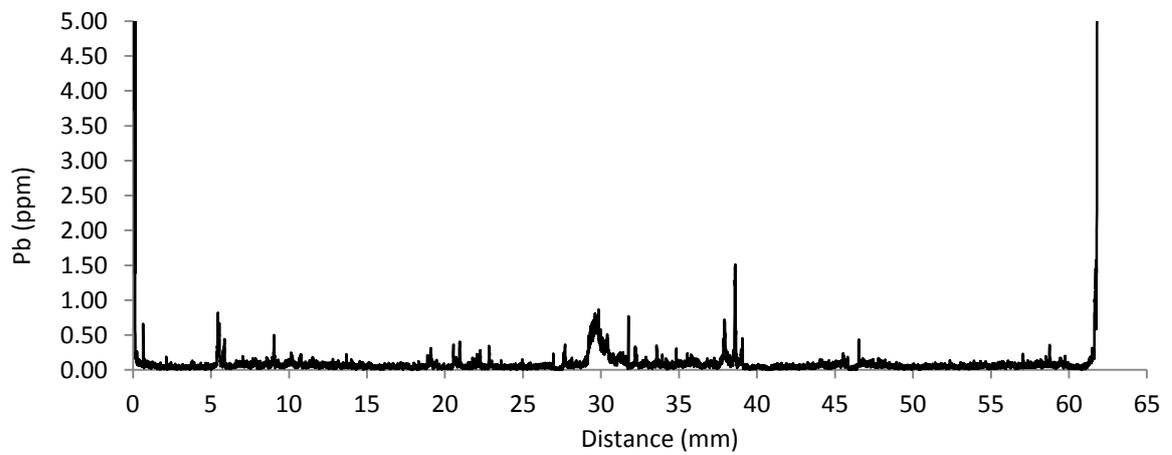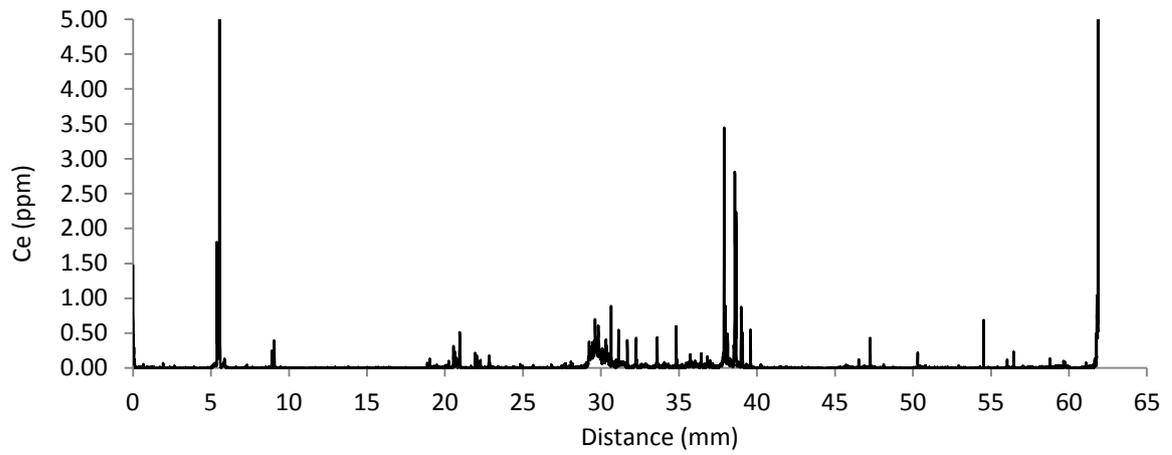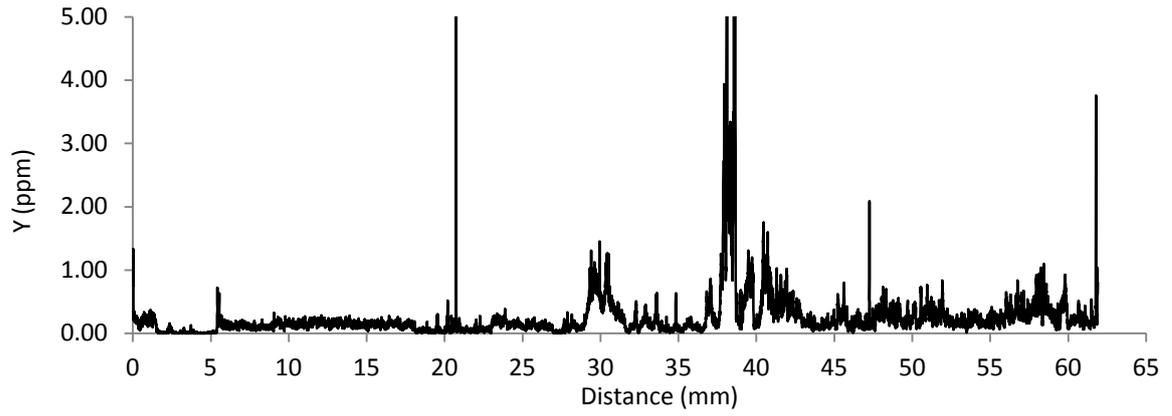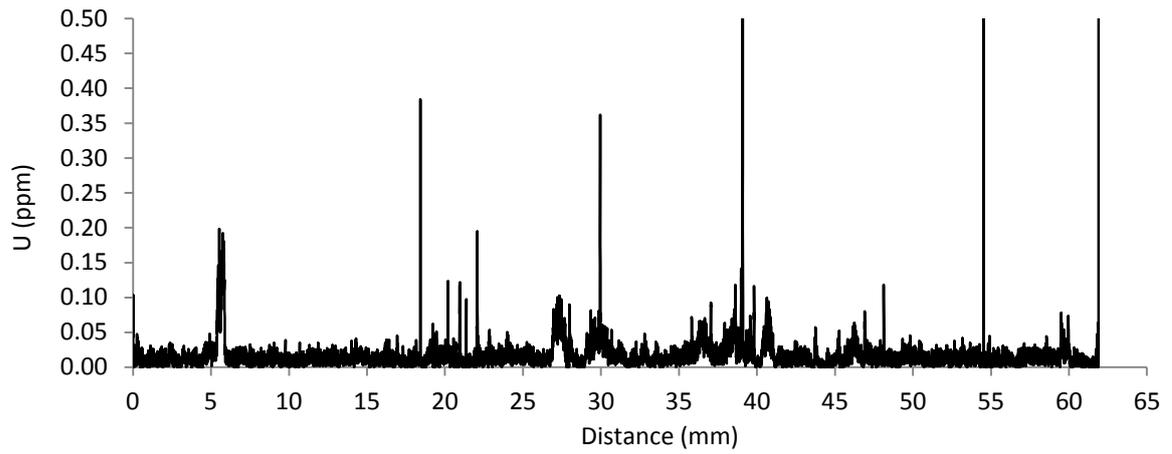
Figure S.22: Yarrangobilly flowstone YBJD2 LA-ICP-MS results.

**S.18. Publications**

Invited review

# Cave aerosols: distribution and contribution to speleothem geochemistry

Jonathan Dredge [a,*], Ian J. Fairchild [a], Roy M. Harrison [a,b], Angel Fernandez-Cortes [c], Sergio Sanchez-Moral [c], Valme Jurado [d], John Gunn [a], Andrew Smith [e], Christoph Spötl [f], Dave Mattey [g], Peter M. Wynn [e], Nathalie Grassineau [g]

[a] School of Geography, Earth and Environmental Sciences, University of Birmingham, Edgbaston, Birmingham B15 2TT, UK
[b] Department of Environmental Sciences, Center of Excellence in Environmental Studies, King Abdulaziz University, PO Box 80203, Jeddah 21589, Saudi Arabia
[c] Departamento de Geología, Museo Nacional Ciencias Naturales (MNCN-CSIC), José Gutiérrez Abascal, 2, E-28006 Madrid, Spain
[d] Instituto de Recursos Naturales y Agrobiología, IRNASE-CSIC, Apartado 1052, 41080 Sevilla, Spain
[e] Lancaster Environment Centre, Lancaster University, Lancaster LA1 4YQ, UK
[f] Institut für Geologie und Paläontologie, Leopold-Franzens-Universität Innsbruck, Innrain 52, 6020 Innsbruck, Austria
[g] Department of Earth Sciences, Royal Holloway University of London, Egham Hill, Egham, Surrey TW20 0EX, UK

## ABSTRACT

There is developing interest in cave aerosols due to the increasing awareness of their impacts on the cave environment and speleothem; this paper provides the first attempt to synthesize the issues. Processes of cave aerosol introduction, transport, deposition, distribution and incorporation are explored, and reviewed from existing literature. Key issues of specific aerosol processes of distribution and production as well as cave location and morphology effects are highlighted through the presentation of preliminary monitoring data. This study identifies the strong relationship between cave ventilation, cave aerosols and their consequent spatial distribution.

The contribution of cave aerosol deposition to speleothem geochemistry is modelled and evaluated using a mass balance framework. As an example, speleothem trace element data from Obir Cave (Austria) are compared with aerosol inputs to evaluate their significance. The mass balance study demonstrates that generally, under normal continuous growth and environmental conditions aerosol deposition will be of only minor importance. However, it highlights specific scenarios in which aerosol contributions will be significant: speleothem hiatuses (or slow growth), high aerosol deposition, and secondary microbiological feedback.

© 2012 Elsevier Ltd. All rights reserved.

## 1. Introduction

A new sector of interest is developing within cave science regarding the influence of aerosols on the cave environment and the potential palaeoenvironmental record which may be preserved within cave precipitates as a result of aerosol incorporation.

The potential degradation of the cave environment resulting from cave aerosol deposition and associated mitigation practices are growing issues among cave management organisations especially for show caves. Degradation can occur from external pollutants or from visitor disturbances to the natural cave environment.

The effects of anthropogenic dust on caves may be subtle, but threaten the long-term preservation of cave environments.

Soiling of the cave environment has occurred as a result of coal industry pollutants (Christoforou et al., 1994; Salmon et al., 1994, 1995) and airborne dust from regional dust storms (Christoforou et al., 1994). Black deposits causing degradation in other caves have been attributed to deposits from vehicle exhaust (Jeong et al., 2003; Chang et al., 2008) and biomass burning emissions (Chang et al., 2008). Michie (1999) partially attributed the slow degradation of cave aesthetic values to cave visitors transporting, releasing and causing re-suspension of aerosols within the cave. In caves where candlelight or carbide lamps tours are operated (e.g. Ohms, 2003) the introduction of aerosols as a result of combustion will likely result in the degradation of cave surfaces in addition those stated by Michie (1999). In some cases aerosol

* Corresponding author.
  E-mail address: Jad099@bham.ac.uk (J. Dredge).

issues are remediated through improved cave conservation practices. For instance, Altamira Cave (Spain) was closed to visitors due to anthropogenic fine particle resuspension from cave floor sediments, provoking microparticle detachment (releasing bacterial and fungal spores), among other factors. Installation of a thermally insulated access door reduced the entry of airborne particles, the condensation rate in the entrance area, and the metabolic activity of the main visible microbial colonies (Saiz-Jimenez et al., 2011).

Aerosols are generally defined as the suspension of fine solid or liquid particles within a gaseous medium (often being the Earth's atmosphere). Aerosols become suspended into the Earth's atmosphere via many processes, both natural (e.g. volcanic eruptions, windblown sands, forest fires) and anthropogenic (e.g. biomass burning, vehicle emissions, constructions); examples of emissions to the external atmosphere are displayed in Fig. 1. Aerosols can be grouped and identified based on a range of properties, both physical (e.g. colour, morphology, size) and chemical (e.g. inorganic, organic, isotopic).

Atmospheric aerosols enter cave networks due to external transportation processes, travel within caves as a result of cave ventilation, and are either deposited, or transported with cave air and eventually removed from the cave system. The removal of aerosols from air occurs as a result of either wet or dry deposition. Dry deposition is the process by which atmospheric trace constituents are transferred by air motions to the surface of the Earth (Wesely and Hicks, 2000). The main processes by which dry deposition occurs are outlined below (Petroff et al., 2008):

- Brownian diffusion – The random movement and collision of particles can cause deposition; this process affects very fine particles typically smaller than 0.1 μm.
- Interception – Particles entrained in a stream flow are retained by an obstacle when their path passes within one particle radius of the object.

- Impaction – An aerosol with significant inertia transported by the flow towards an obstacle cannot follow the flow deviation in the vicinity of the obstacle causing particle collision with the obstacle and remaining on the surface.
- Sedimentation – particle fall-out due to gravitation.

Wet deposition is the removal of material from the atmosphere by hydrometeors as a result of condensation and precipitation. Wet deposition can also be referred to as precipitation scavenging, rainout (typically used for in-cloud processes), and washout (typically used for below-cloud processes) (Loosmore and Cederwall, 2004).

The dry depositional efficiency is expressed as a deposition velocity, $v_d$, where

$$v_d = F/C$$

where F is the particle flux to the surface, and C the airborne concentration at a reference height. Because deposition involves several mechanisms, as outlined above, $v_d$ is a complex function of particle size, with the highest values for very small (<0.1 μm diameter) and large (>1 μm) particles. In the range 0.1–1 μm where much of the mass of atmospheric aerosol resides, values of $v_d$ are very small. For very large particles, typically >10 μm diameter, $v_d$ becomes almost equal to the gravitational settling velocity, but for smaller particles (<10 μm) it is substantially greater (Seinfeld and Pandis, 1998).

Aerosols, once suspended into the atmosphere through emission processes, will be carried with parcels of air and mixed with other aerosol types which may have properties characteristic of their emission and geographical source. Hence it may be possible to determine palaeoenvironmental conditions through the incorporation of aerosols within speleothem. Sr isotope studies have demonstrated the ability to utilise aerosols to identify the geological source region of terrestrial dust by comparing to the Sr isotopic ratio
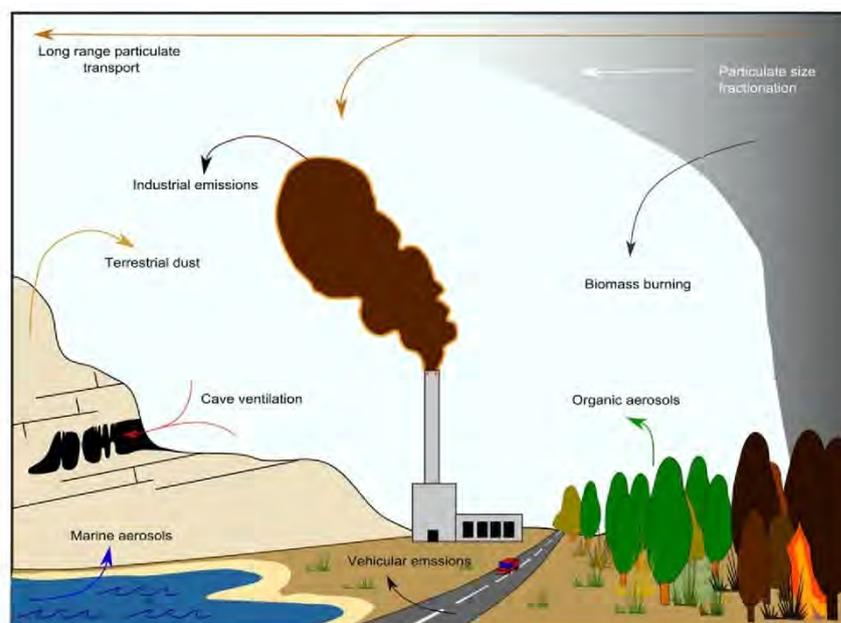


Fig. 1. Illustration of tropospheric aerosols which are likely to be emitted in large enough quantities to be incorporated and detectable within speleothems. Aerosols produced within the cave environment also have the potential to become incorporated in detectable quantities.

of dust surface deposits (Li et al., 2005; Yang et al., 2009; Masson et al., 2010), of waters (Jin et al., 2011) and in speleothem (Goede et al., 1998; Verheyden et al., 2000; Frumkin and Stein, 2004; Zhou et al., 2009) although the mode of transmission of the chemical signal is normally proposed to be via dripwater. Fire events and source regions have been successfully identified through constraining region-specific vegetation burning events in ice and sediments (Laird and Campbell, 2000; Wang et al., 2005; Zhou et al., 2007; Kehrwald et al., 2010a; 2010b; Wang et al., 2010) using a range of organic proxies (reviewed in Simoneit, 2002). Different types of vegetation have known associated organic components which are released during burning events; the region of burning and therefore the direction of transport can then be deciphered. Similar fire-proxy work may be applicable to speleothems.

For modern studies, air mass travel paths can be tracked and modelled. Atmospheric transport and dispersion modelling using HYSPLIT and other programs allows air mass trajectory estimation of past air movements, or projections to produce forecast trajectories (http://ready.arl.noaa.gov/HYSPLIT.php). These simulations are based on recorded or predicted meteorological conditions for past and future modelling respectively. Air mass trajectories provide an insight into the likely long-range aerosol source locations and thus aid in the identification of aerosol emission processes.

The presence of cave aerosols is controlled by a combination of internal aerosol production and the incorporation of transported externally sourced aerosols. Cave ventilation and morphology will strongly influence how aerosols are transported and deposited within the cave environment. The quantity and effect of cave aerosols on speleothem geochemistry has rarely been explicitly considered so far. By investigating and gaining an improved understanding of how aerosols are transported, distributed, deposited and ultimately incorporated into forming speleothem we will potentially be able to identify aerosol signatures within the speleothem palaeoenvironmental record. This paper provides the first attempt to synthesise the issues concerning cave aerosols, with particular focus on the situations in which aerosols will provide a significant contribution to speleothem chemistry. Specific processes affecting the transport and deposition of cave aerosols will be highlighted through the presentation of monitoring data at several sites. We demonstrate that although aerosols are expected to be of minor influence during normal speleothem growth, they can provide a major contribution to bulk chemistry at hiatuses.

The review will be structured as follows: previous aerosol investigations, associated methods and the methods (sampling, extraction and analytical) utilised for monitoring work presented in this paper will be discussed. Next, aerosol sources, processes, distribution and deposition mechanisms are explored. In the results section, specific aerosol processes will be highlighted with preliminary data from cave monitoring. Finally, aerosol contributions to speleothem geochemistry will be evaluated through the comparison of known deposition fluxes to dripwater and speleothem geochemistry in Obir cave, Austria, a site where distinct aerosol contributions to speleothem chemistry have been proposed (Fairchild et al., 2010).

## 2. Methods

A plethora of aerosol properties can be analysed to investigate specific processes. Some of the key properties and associated processes are summarised in Table 1.

An extensive range of methods exist for the sampling, monitoring and analysis of cave aerosols, each specific to the information required and depending on the application. Due to the logistics of working in the cave environment cave aerosol investigations will often require passive or self-powered portable equipment for aerosol sampling and in-situ analysis.

**Table 1**
Aerosol properties and the processes which can be explored as a result of their investigation.

| Cave aerosol property | Reason for investigation |
|---|---|
| Suspended concentration | Aerosol transport and distribution |
| Deposition flux | Aerosol distribution (especially to speleothem surface) |
| Inorganic chemistry | Source identification, potential chemical addition to speleothem, transport. |
| Organic chemistry and/or associated microorganisms | Source identification (especially processes associated with biomass burning), transport, airborne bacteria and fungi identification |
| Aerosol size | Transport, distribution |
| Aerosol morphology | Transport, source identification (lesser extent than chemistry) |

### 2.1. Sampling

#### 2.1.1. Dry deposition sampling

There is no generally accepted method to directly measure or estimate dry deposition (Chu et al., 2008). However, it has been established that a smooth horizontal surrogate surface provides a lower bound estimate of the dry deposition flux onto a horizontal surface (Sehmel and Hodgson, 1978; Holsen and Noll, 1992). Dry deposition is determined through the capture of aerosol deposition to a known surface area. Surrogate surface sampling does not require power and designs can be portable, making this method highly suitable for cave monitoring studies.

There is a range of apparatus currently being used for surrogate surface sampling. The most basic and generally used being a smooth horizontal plate surface to collect deposition. Smooth surfaces provide an interface which can be cleaned making it ideal for elemental chemistry analysis: polyvinyl chloride (Lim et al., 2006; Chu et al., 2008; Zhang et al., 2011) and glass slides (Salmon et al., 1995) have been used.

The positioning of surrogate surfaces within the cave network appears to be relatively robust in its sensitivity and exposure of the surrogate surface relatively unimportant: Michie (1997) found that even when sheltered by a covered surface (28 mm above) dust deposition is only reduced by 50%. In the external environment, retention has been shown to be influenced by atmospheric precipitation (Lyman et al., 2007). Therefore, in the cave environment care should be taken about the placement of surrogate surfaces in relation to active drip sites.

Petri dishes (see supplementary material section S.3 Figure S.1) provide a convenient means as the collection surface can be readily capped and then sealed with Parafilm™ reducing the potential of contamination during transportation once cleaned, and after sampling. Specific preparation and extraction procedures are required for the collection and analysis of the different aerosol species. In this study Polytetrafluoroethylene (PTFE) filters were used as a surrogate surface collection medium in samples where the inorganic aerosol component was to be analysed. PTFE filters provide reduced blank levels in comparison to other filter media available, and provide a rough collection surface. Further details on surrogate surface types and sampling methods can be found in the supplementary material section S.1.2.

#### 2.1.2. Suspended aerosol sampling

Where access to cave networks and time is available, active sampling provides an alternative to surrogate surfaces. Active sampling is conducted by pumping a known volume of air through a filter medium. The use of active sampling is advantageous over surrogate surfaces due to its ability to produce quantitative aerosol concentration levels at higher temporal resolution. Total atmospheric aerosol concentrations or specific aerosol species

26                                    *J. Dredge et al. / Quaternary Science Reviews 63 (2013) 23–41*

concentrations can be determined. This method is versatile since post-capture, aerosols can be weighed, observed and analysed dependent on the investigation type.

Increased pumping rates provide better aerosol collection and shorter durations offer improved temporal resolution, but generally pumped samples are run for 24–48 h at 1 to 30 L min$^{-1}$ in the cave environment (Sanchez-Moral et al., 1999; Alfödy et al., 2000; 2001; Yang et al., 2006; Faimon et al., 2006) as well as in confined situations (Nava et al., 2010) and often in the external environment too (e.g. Allen et al., 2001; Harrison et al., 2003). For this study pumps were run at 3 L min$^{-1}$ for 24 h duration. A dual pump setup (see supplementary material section S.3, Figure S.2) was chosen for simultaneous sampling onto two filter media for the collection of both inorganic and organic aerosols.

Suspended aerosol particle counters offer essentially instantaneous aerosol concentration values. Particle counters measure directly providing high resolution temporal data. A range of portable battery-powered particle counters exist which can be used for temporal monitoring of aerosol concentrations in cave systems and are suitable for detailed spatial monitoring. This has been successful both in the cave environment (Michie, 1999; Sanchez-Moral et al., 1999; Kertéz et al., 2000; 2002; Iskra et al., 2010) and in the external atmosphere (Allen et al., 2001; Jones and Harrison, 2005). Particle sizes reflect how aerosols become entrained and transported in the atmosphere; they are therefore a useful tool for the investigation of aerosol transport within the cave environment. Fig. 2 displays the size ranges for the aerosols types used in this investigation.

A TSI SidePak AM510 particle counter for 0.1–10 μm diameter particles was used in this investigation to determine suspended aerosol particle mass. Additionally, a TSI Aerotrak™ Model 9306 airborne particle counter was specifically used in the aerosol monitoring carried out at Altamira Cave (Spain). This device has a 0.1 CFM (2.83 L/min) flow rate and counts up to bin sizes from 0.3 to 25 μm, logging up to 6 particle sizes simultaneously.

Filter preparation in this study was the same for both pumped and surrogate surface sampling. PTFE filters and glass Petri dishes were cleaned for a minimum of 24 h in 2% HNO$_3$ then triple-rinsed with DDIW. The surrogate surface equipment was prepared in a clean laboratory environment to minimise blank values.

## 2.2. Extraction and analysis

Protocols for material extraction from filters and chemical analysis of deposited aerosols vary greatly, and are dependent on elements under investigation and sampling methods, but all techniques are constructed with the intention of reduced sample contamination throughout the procedure. Extraction methods will only be summarised and the methods chosen for this investigation justified. Detailed methods of extraction and analysis are presented in the supplementary material, section S.1.
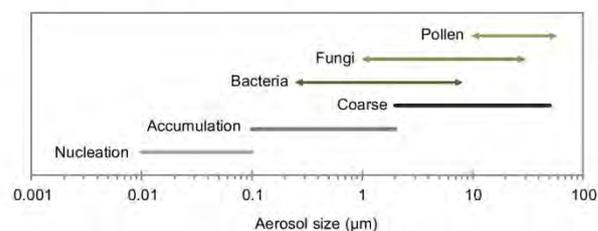


**Fig. 2.** Aerosol size distributions, both inorganic (Seinfeld and Pandis, 1998) and organic (Jones and Harrison, 2004) compared with size classes of Whitby and Cantrell (1975).

### 2.2.1. Inorganic

One of the most established and widely used methods (Janssen et al., 1997; Harrison et al., 2003) of air sample extraction from a filter medium is the reverse aqua regia digestion method developed in Harper et al. (1983). Various method combinations exist, but the majority involve ultrasonication and acid extraction with nitric acid (or DDIW for ionic species) as key components (Allen et al., 2001; Lim et al., 2006; Chu et al., 2008; Wai et al., 2010). More intensive digestion can also be used with a combination of HNO$_3$, HF and HClO$_4$ (e.g. Chang et al. 2008). In order to replicate a similar extraction to speleothem analysis a 2% HNO$_3$ and 120 min ultrasonication with heat was the chosen extraction method for this investigation. DDIW and 120 min ultrasonication was used for major ion species extraction (since 98% of sulphate, nitrate, and ammonium can be extracted with 120 min of ultrasonication (Chu et al., 2008)).

Inorganic aerosol chemistry in this investigation was obtained through ICP-AES analysis at Royal Holloway University of London. A suite of elements were analysed, total deposition in this paper refers to a total deposition of elements: Al, Fe, Mg, Na, K, Ti, P, Mn, Ba, Ni, Sr, V and Zn. Elements that demonstrate key processes will be displayed, as well as elements of importance to speleothems such as Mg and Sr.

### 2.2.2. Carbon

Carbon deposits have been established as a significant contributor to cave degradation and therefore the identification of carbon and its types are of increasing importance. Optical and thermal analytical techniques are most frequently used to measure carbon in atmospheric investigations (Ghedini et al., 2000). Studies often aim to investigate carbon types, total carbon (Nava et al., 2010) and differentiate between elemental and organic carbon (Jones and Harrison, 2005). Carbon isotopic composition offers an insight into the carbon mass fraction allowing for improved source identification. Characterization of radiocarbon as well as $^{13}$C/$^{12}$C has been utilised by Chang et al. (2008) to distinguish cave carbon deposits and emission sources.

### 2.2.3. Organic – bioaerosols

Atmospheric organic aerosol investigations typically involve the emission products of combustion for human health and environment studies. Emission products can be utilised as a tracer for aerosol transportation in suitable case locations, and organic aerosols in speleothem have the potential to be used as a proxy for emission events. PAHs (Polycyclic aromatic hydrocarbons) are widely investigated as a proxy for hydrocarbon combustion and emission. PAHs have been extracted from soils, sediments and speleothem samples, but extraction methods are refined dependent on the species under investigation. Perrette et al. (2008) used dichloromethane in both Soxhlet and ultrasonication extraction for the extraction of organic species from stalagmites and sediments. PAH analysis is often carried out by Gas chromatography–mass spectrometry (GC–MS) and High performance liquid chromatography (HPLC) techniques.

Microbial air sampling was conducted in this investigation to quantify the level of airborne bacteria and fungal spores in the aerosol monitoring survey carried out at Altamira Cave (Spain). A Duo SAS 360 sampler (International PBI, Milan, Italy) containing Petri dishes with Dichloran Rose Bengal Agar was used for the sampling of fungi. For bacteria, the medium Tryptone-Soya Agar (TSA) was used. Duplicate samples of 100 L in air volume were selected as the most appropriate method for easy counting in this cave. Some specific applications of these aerobiological techniques in subterranean environments, including this cave, are described by Fernandez-Cortes et al. (2011) and Porca et al. (2011). Further details can be found in the supplementary material section S.3.

## 3. Cave aerosol processes

In this section, aerosol transport, distribution and deposition mechanisms will be highlighted with preliminary data from cave monitoring. Cave locations were chosen to isolate and investigate specific aerosol emitting processes. Data from a range of cave sites throughout Europe will be used to demonstrate the relationship between aerosol deposition flux rates and speleothem growth rates.

### 3.1. Cave aerosol sources

#### 3.1.1. Externally sourced cave aerosols

Source areas and long-range transport of external aerosols can be determined to a degree through the utilisation of air mass trajectories since a body of air will incorporate aerosols released into the atmosphere which will then be transported as the air mass moves. Aerosols are then incorporated into the cave atmosphere through specific transport processes which are explored in Section 3.2.1.

#### 3.1.2. Internally produced cave aerosols

In addition to the transport of aerosols from external sources there is the possibility for the addition of suspended aerosols to the cave atmosphere from internal sources. In some cases the contribution of aerosols from within the cave network will be orders of magnitude greater than that of externally sourced and transported aerosols.

*3.1.2.1. Anthropogenic (cave visitor) production.* Degradation of the cave environment as a result of aerosol deposits from human or animal visitors is known (Cigna, 1983, 1989, 1993). Particulate matter can be present as an existing aerosol deposit and therefore the visitor disruption simply results in the re-suspension of particulates from an aerosol source or suspension of particulates from subaqueous deposition within the cave. Cave visitors can also act as a carrier of externally sourced aerosol and release them inside the cave (e.g. lint, mud on shoes).

Measurements have shown a constant rate of deposition of airborne particulate material from show cave visitors of approximately one microgram per person per second (Michie, 1999). Bartenev and Veselova (1987) carried out measurements of dust sedimentation from aerosols in the Cupp-Coutunn Cave System (Turkmenistan) noting that the rate of sedimentation raises more than 10 times within 20 m surrounding the main tourist passages, indicating the significant aerosol production from cave visitors.

*3.1.2.2. Hydrological production.* Aerosols can be generated from water drops falling from a cave ceiling or generated by rapids and waterfalls in cave streams (Maltsev, 1997). Turbulent water can produce aerosols by a similar mechanism to that which occurs in the production of sea spray, with gas scavenging resulting in bubbles which rise to the surface and burst producing hydro-aerosols. 'Splash' aerosols can also be produced as falling drip-waters impacting on cave surfaces resulting in small enough liquid aerosols to be transported in suspension. Aerosol deposition to water bodies causes suspension of liquid aerosols in the form of film and jet drops (Bridgman, 1994).

*3.1.2.3. Bedrock production.* Klimchouk (1994) and Klimchouck et al. (1995) proposed that cave aerosols can be generated as a result of radioactivity in the cave environment. It was proposed that alpha decay dislodges bedrock to form aerosols. This was further investigated by Pashenko and Dublyansky (1997) who suggested that the process of alpha decay dislodging bedrock is

a physically plausible but not essential role in the production of cave aerosols, since bedrock particles are produced during normal erosional processes of cave ceiling (Pashchenko and Sabelfeld, 1992) and walls. Cave wall aerosol generation can be augmented through host-rock alteration and corrosion as a consequence of condensation weathering processes. During further weathering the surface becomes increasingly fragile, from which fine carbonate particles can be derived (Zupan Hajna, 2003). Condensation weathering will be controlled by cave humidity and condensation processes as described in Section 3.2.2.4.

### 3.2. Distribution

The mechanisms of aerosol removal will be specific to each cave system, will vary within a cave, and may vary seasonally as the cave environment changes. Cave aerosol distribution processes will be explored in this section.

#### 3.2.1. Aerosol transport

In order to be incorporated into a speleothem once the aerosols reach the troposphere region surrounding the cave entrance they must be transmitted into the cave air which occurs via two main routes; direct transport into the cave through air exchange (Pashchenko et al., 1993) and dust carried in by visitors (Michie, 1999; Jeong et al., 2003) and animals.
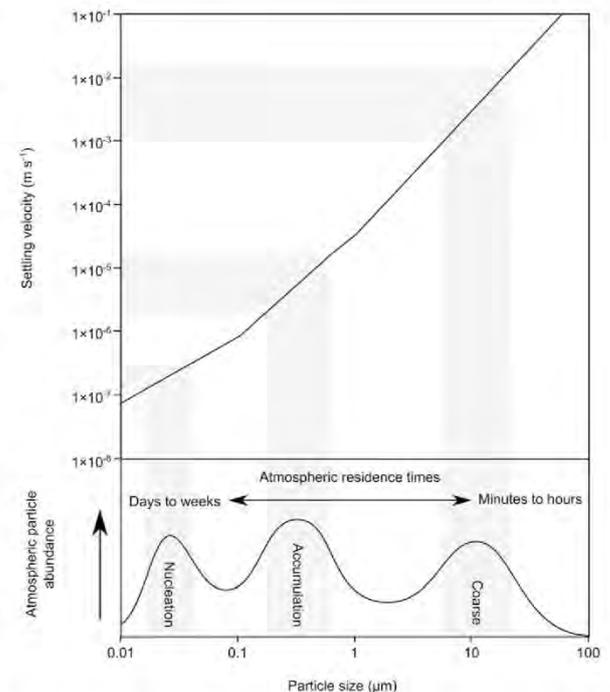


**Fig. 3.** Relationship between particle size and settling velocities. Relative atmospheric abundance of aerosols by particle size (Whitby and Cantrell, 1975) and particle size settling velocities (Kulkarni et al., 2011). Three dominant aerosol size groups (modes) present in the atmosphere: coarse (D1), accumulation (D2) and nucleation (D3) (Whitby and Cantrell, 1975). Each particle size mode is removed from the atmosphere at its associated deposition velocity. The aerosol contribution to speleothem chemistry will occur as a result of the total deposition to the speleothem surface from all aerosol types and sizes. Therefore the range and distribution of aerosol particle sizes must be considered when investigating chemistry.

Cave ventilation occurs as a result of several phenomena: cave breathing, wind-induced flow, chimney circulation or stack effect, convection and water-induced flow (Fairchild and Baker, 2012) and sometimes with short-term local turbulence as a result of anthropogenic influences (Fernandez-Cortes et al., 2009). The vigour of the air circulation affects the removal of internally generated gases such as carbon dioxide, radon (and its particulate daughters) and the introduction of aerosols (Fairchild and Baker, 2012). Christoforou et al. (1996a) determined that cave ventilation and its air flow patterns act as the primary mode of transport for pollutant particles into caves from the outdoors. However, the relative influence of cave visitors and natural cave ventilation will be dependent on the cave under investigation and the relative influence of its visitor footfall numbers and ventilation strength on aerosol production. Aerosols in the cave environment can essentially be thought of as a smaller version of the Earth's atmospheric system. The cave suspended aerosol load is a product of externally introduced aerosols which are analogous to long-range transported aerosols and internally produced aerosols resembling locally sourced aerosols.

*3.2.1.1. Transport source identification.* Pollen is perhaps the most intensively studied single cave aerosol type due to its significance in speleothem palaeoenvironmental archives as a recorder of terrestrial vegetation. A range of studies exploring the distribution of pollen through caves has been presented in the literature. A comprehensive review of literature regarding their mode of transport and distribution can be found in Caseldine et al. (2008).

Coles et al. (1989) proposed three transport mechanisms for pollen: airborne, waterborne and insect-borne. Similarly Lauritzen et al. (1990) emphasized percolating water, floodwaters that submerge speleothems, or airborne transport by cave

draughts as predominant mechanisms. They noted the importance of understanding transport mechanisms for interpreting pollen assemblages in speleothems. Although a method is yet to be established for the source discrimination of pollen, the airborne pollen influx into caves and modern surface pollen deposition has been reported to be similar in several investigations (Burney and Burney, 1993; McGarry and Caseldine, 2004). It is critical for internal cave aerosol composition to be representative of external aerosols for palaeoenvironmental studies. It may be assumed that the behaviour of pollen can be extrapolated to other aerosols of similar size which are controlled by the same transportation processes.

Source separation can be achieved through cave monitoring of aerosol deposition and using aerosol chemistry as a tool for identification. Where aerosol deposits are of contrasting composition to that of speleothem growth chemistry it may be possible to identify periods of significant aerosol deposition. The significance and ability to recognise aerosols in speleothem is discussed later in Section 5.

*3.2.2. Aerosol deposition*
*3.2.2.1. Gravitational sedimentation.* Gravitational sedimentation as a result of reduced air flow rates is thought to be the main mechanism behind aerosol deposition of coarse aerosols in cave networks. Michie (1997) determined the main processes which control the deposition of particles within the cave network: Brownian diffusion and collision for the smaller particles, and gravitation for the larger particles. It should be noted that gravitational sedimentation processes will not be of importance for stalactite samples which consequently may receive significantly lower aerosol fluxes than stalagmite surfaces.
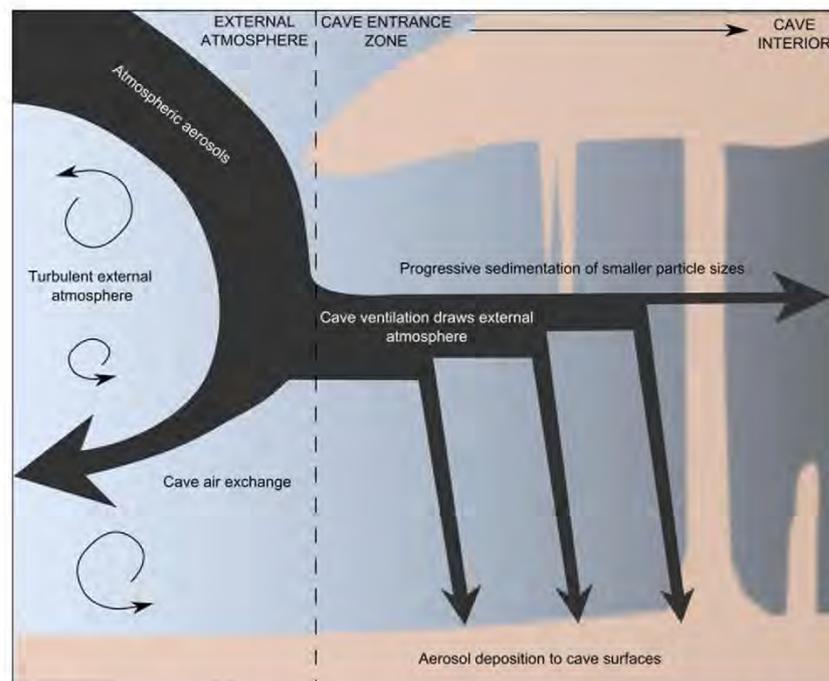


**Fig. 4.** Schematic of introduction and gravitational sedimentation of cave aerosols within the cave environment. A body of atmospheric air (of average composition) with air velocity greater than or equal to 0.1 m s$^{-1}$ will be have a suspended load (Ls) produced from a combination of groups D1, D2 and D3, therefore Ls = $\sum$(D1,D2,D3). Taking the simplified example of a horizontal cave with a singular entrance in which air exchange becomes progressively less influential with distance from the entrance (A), air velocity (V) will decrease with distance from the entrance to the back of the cave (A'). At 'A' Ls will be equal to $\sum$(D1,D2,D3), as the air progresses towards A' and loses velocity, particle modes D1, D2 and D3 will be progressively depleted by deposition.
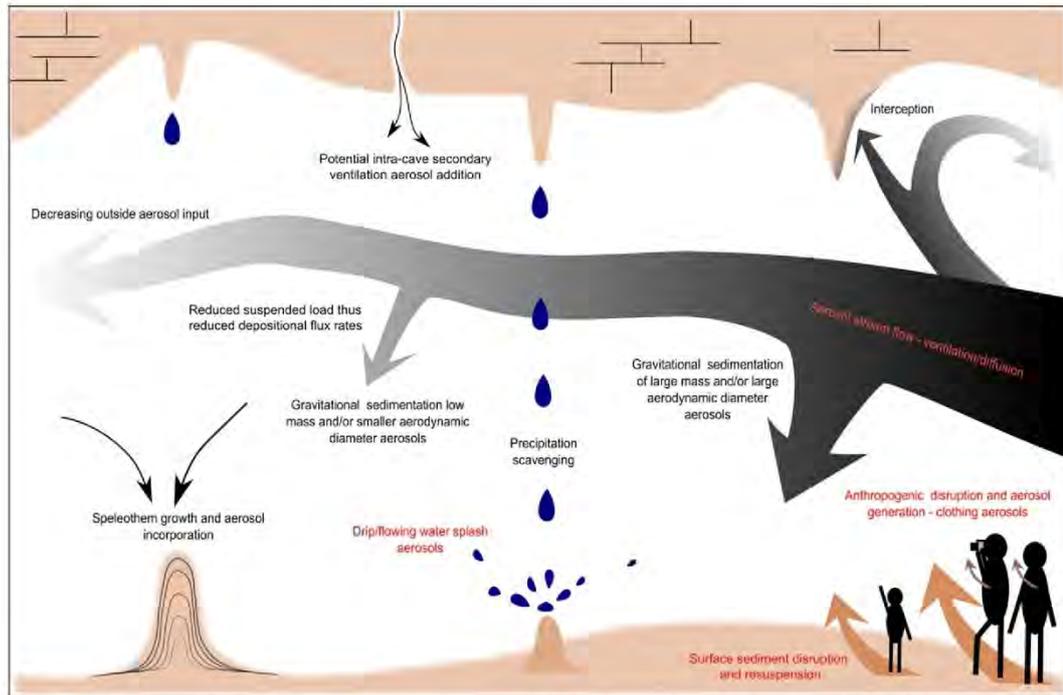
**Fig. 5.** An illustration summary of cave processes: aerosol creation (red), and aerosol removal processes (black).

Pollen grains which are known to be aerially transported are detected close to the entrance of cave systems (McGarry & Caseldine, 2004; Caseldine et al., 2008) with a reduction towards the cave interior (Burney and Burney, 1993; Coles and Gilbertson, 1994; Navarro et al., 2001). This distribution is expected since pollen as a coarse aerosol requires relatively high energy levels for particle transportation above that which can be sustained by cave ventilation flow (as displayed in Fig. 3).

The pattern of distribution presented by various investigations into pollen, although generally representative, can only be assumed if there is a single known cave entrance. It is also necessary to know that cave air flow rates are high enough to transport coarse aerosols whilst meeting threshold terminal velocity speeds to allow for total gravitational sedimentation of suspended aerosol particulates within the cave. Fig. 3 displays the relationship between particle size, deposition and air flow rates. Each cave should be monitored (as with other environmental variables) on a case study basis to ensure that an accurate understanding of cave aerosol transportation dynamics has been gained before interpretations are made. It is necessary to understand air flow rates and the factors controlling air flow in order to fully understand aerosol deposition (Christoforou et al., 1996b).

Air flow rates in cave locations will vary greatly and are generally too low for the transportation of coarser aerosols (cf. settling velocities shown in Fig. 3). However it is known in some instances that flow rates are sufficient for the transportation of even very coarse particulates. Flow velocities of $0.5 \text{ m s}^{-1}$ have been reached during winter ventilation in the interior of Obir cave (Fairchild et al., 2010) and exceptionally high velocities ($>10 \text{ m s}^{-1}$) are known to be reached in some cave sites (Conn, 1966). During periods of higher ventilation speeds larger suspended aerosol loads and large particles may be transported and deposited within the cave increasing the potential for aerosol contributions to speleothem geochemistry.

An aerosol deposition gradient was noted by Christoforou et al. (1994) with a loss in deposition rates over the entrance region, from $13.4 \text{ μg m}^{-2} \text{ s}^{-1}$ outdoors to $5.2 \text{ μg m}^{-2} \text{ s}^{-1}$ inside (over 1 year of monitoring). This indicates either low external aerosol transportation into the cave or significant suspended aerosol loss over the entrance zone. This progressive loss in suspended load is displayed schematically in Fig. 4. The flux of aerosols throughout the cave will be a product of the air velocity (driven by ventilation strength), cave cross-section A to A′, and cave morphology. Cave ventilation is known to be highly variable displaying strong diurnal and seasonal variations; consequently aerosol transport may display temporal variations. Cave cross-section and morphology
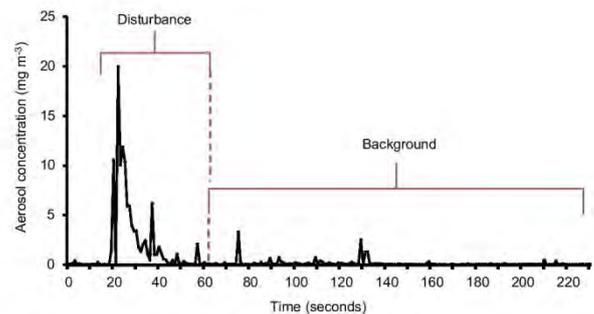


**Fig. 6.** Short term anthropogenic cave aerosol production in Gough's cave, Cheddar Gorge Show Cave, UK. Suspended aerosols monitored as a cave visitor passes by with TSI instruments SidePak AM510. The effect of the disturbance clearly dominates the background levels of aerosols. However, the impact of the disturbance on suspended aerosol loads is short-lived and is dependent on the cave situation and cave surface dusts.

*J. Dredge et al. / Quaternary Science Reviews 63 (2013) 23–41*

will also be highly variable depending on the cave under investigation, altering the distribution of deposition of the particle modes (discussed later in Section 3.2.2.2).

*3.2.2.2. Cave morphology effects on deposition processes.* Cave morphology has been postulated as a control on the distribution of pollen in cave sediments (Burney and Burney, 1993; Navarro et al., 2001). Cave morphology will strongly influence the transportation and deposition of aerosols throughout the cave network. Surface irregularity will result in turbulence within the air column causing increased particle collisions with the walls and consequently greater deposition. Cave morphology will also control ventilation-forced air flow rates and therefore gravitational sedimentation distribution. As a result increased gravitational aerosol depositional flux may be observed in open chambers, with interception and impaction (Section 3.2.2.3) processes being dominant in high flow constriction areas of a cave system. Changes in cave profile (floor elevation) may also induce gravitational processes. A package of cave air that reaches a rise in elevation may stagnate enough to fall below threshold deposition velocities, resulting in zones of increased deposition.

Interception of the streamline by irregularities will also result in impaction onto cave surfaces (as described in Section 3.2.2.3). Aerosols of greater inertia will be removed from the cave ventilation air flow stream. Therefore the 'windward' side of cave features (i.e. stalagmites) will have a greater aerosol impaction flux to the surface.

*3.2.2.3. Interception and impaction.* Interception and impaction are both the result an obstacle interrupting the air flow; in the cave environment this is likely to be speleothem formations. In addition to increased interception/impaction processes, the wet

surfaces of actively growing speleothems may retain more particles than dry cave surfaces as a consequence of hydraulic retention processes. As a result speleothem surfaces will potentially have higher depositional flux and aerosol retention rates than other surrounding cave surfaces. This proposed pattern of distribution was noted by Chang et al. (2008) who observed concentrated aerosol deposition to speleothem surfaces throughout Gosu, Ondal, and Sungryu caves in South Korea of 0.1 to several millimetres in thickness.

*3.2.2.4. Wet deposition.* Wet deposition can occur as a result of three main processes. Wet deposition can occur as dripwater falls through the cave atmosphere. However this contribution is likely to be negligible.

Badino (2004) considered the processes that could potentially result in the formation of clouds in caves. A key factor in cloud formation is the presence of aerosols which act as nucleation points for vapour condensation. The presence of a stable aerosol forming haze in a cave atmosphere is direct evidence of a supersaturation of moist air (water vapour pressure is above equilibrium), and it leads to thermal imbalances between the aerosols and the air (i.e. clouds are usually found near the cave ceiling and in the highest galleries because a humid air parcel is less dense than the drier air parcel). Aerosols may facilitate the formation of clouds through providing a surface for atmospheric condensate aerosol formation from high humidity cave air.

Condensation from atmospheric humidity can have an important speleogenetic role (Dublyansky and Dublyansky, 2000; Dreybrodt et al., 2005). Condensates from cave air will scavenge and deposit aerosol through wet deposition and in specific scenarios may influence speleothem geochemistry. In addition to influencing already precipitating speleothems, aerosols can
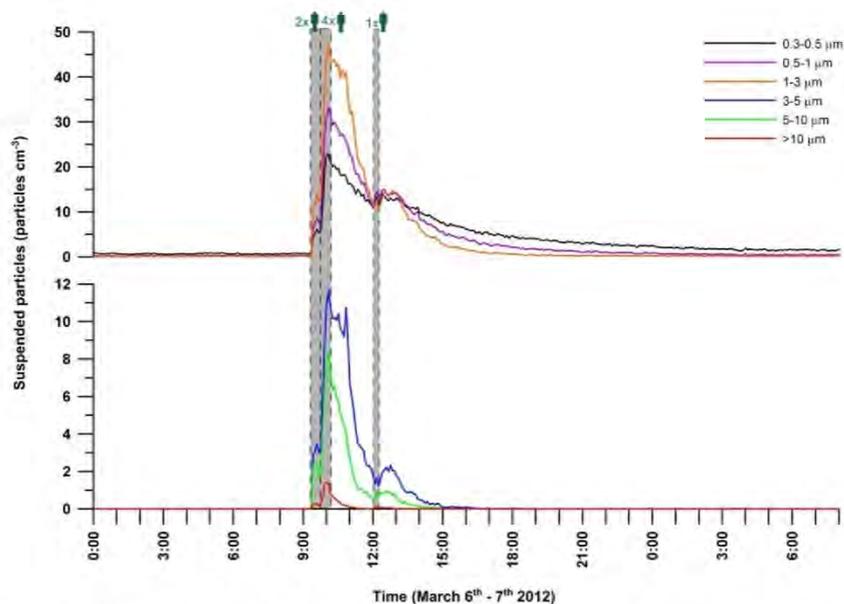


**Fig. 7.** Example of aerosol contributions and particle resuspension from ground sediments by short visits to Altamira Cave, Spain (1–4 people during less than 30 min) during maintenance operations of microclimatic monitoring equipments. The size distribution of particles was monitored every 5 min during a day cycle (6th March, 2012) by using an airborne particle counter (TSI Aerotrak™ Model 9306). The coarsest particles (>10 μm) were only detected once the visitors went into cave, provoking the microparticle detachment from soil and their own clothes. Levels of airborne particles rose to more than a thousand times the previous background levels (as in Goughs Cave). Particle detachment affected particles of 0.5–3 μm in size more than the finest particles of 0.3–0.5 μm diameter. Coarsest particles (>10 μm) were removed from suspension 3 h after the visit and particles ranging from 3 to 10 μm in size took approximately 9 h for removal. The finest particles (<3 μm) remained suspended for longer periods (roughly up to 24 h).

385

produce a mineral deposit when it reaches a cave wall, or directly from the vapour state (in the same mechanism of sublimation of ice from water vapour) (Cigna and Hill, 1997).

An illustration providing a summary of aerosol processes is displayed in Fig. 5.

## 4. Results

Through cave monitoring, results from this investigation will be displayed to demonstrate some of the key issues discussed above.

### 4.1. Internally sourced aerosols

#### 4.1.1. Anthropogenic disruption

Internal production of aerosols in some cave locations is likely to be dominated by anthropogenic processes. The magnitude of potential aerosol production relative to show cave background levels is displayed in Fig. 6.

Fig. 6 displays an example of short term aerosol impacts from a single disruption event by one cave visitor. The data presented in Fig. 7 displays a greater duration of cave atmosphere aerosol impact by longer, multiple visitor disturbances.

Monitoring work demonstrates the range of impacts and duration of anthropogenic aerosol production events. Such observations are critically important for evaluating risk to cave environments from visitor disruption.

#### 4.1.2. Hydrological aerosol production

The production of water aerosols may prove a significant source to the total aerosol budget for specific regions in some cave locations. The impact of hydrologically produced aerosol will only be of notable levels in caves with significant waters flows, which may be seasonally controlled. Fig. 8 displays an example of hydraulic internal aerosol production.

The peak in suspended aerosol concentrations at the Abyss/ Waterfall locations which has been attributed to the internal cave production of liquid aerosols, forming as a result of turbulent water from a flowing stream (Smith et al., 2013). The production of aerosols in this specific location is localised but substantial and has the potential to notably alter the geochemistry of proximal speleothem formations.

### 4.2. Cave ventilation and aerosol distribution

Cave air $CO_2$ is used as an indicator of cave ventilation, as the concentration of $CO_2$ in a cave passage is a function both of production and ventilation processes (Fairchild and Baker, 2012) with increased $CO_2$ concentrations being indicative of reduced air-
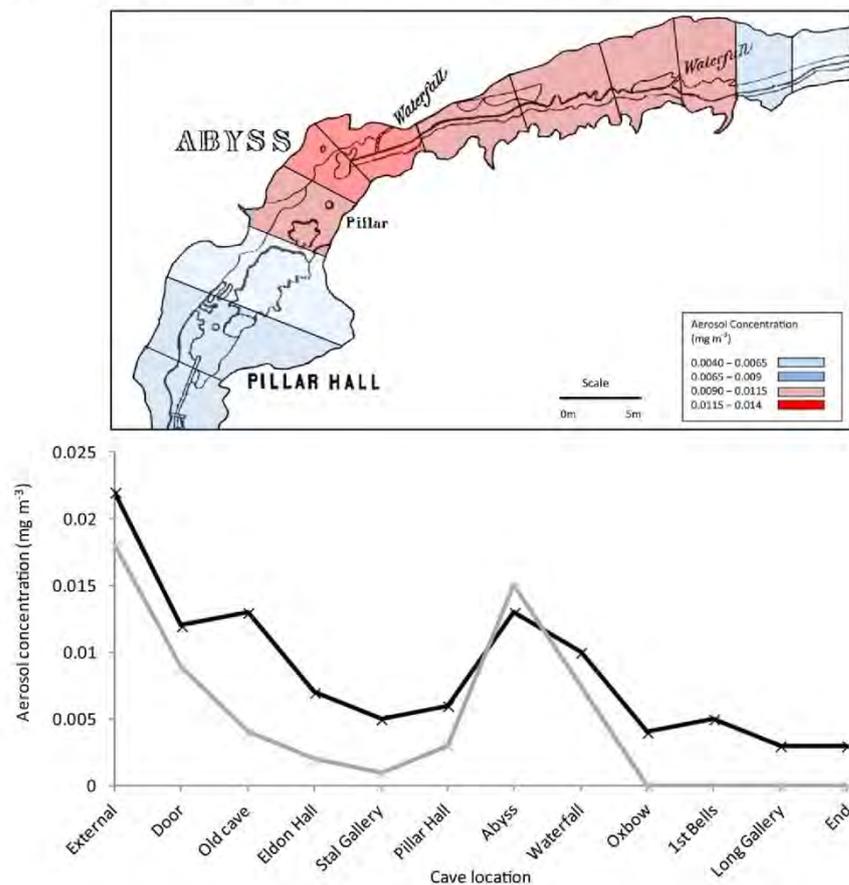


**Fig. 8.** Spatial distribution of suspended aerosols from Ingleborough show cave, UK. External site to 'End' is a distance of approximately 500 m, the 'End' location marks the end of the show cave not the entire system which continues for >1 km further. Data collection using TSI AM510 optical aerosol counter during winter (black) on the 28th Feb 2011 and summer sampling (grey) on the 14th July 2009. The insert displays waterfall zone aerosol concentrations (Smith et al., 2013). Hydro-aerosol production remains an apparent feature in both summer and winter monitoring.

*J. Dredge et al. / Quaternary Science Reviews 63 (2013) 23–41*

exchange with the low $CO_2$ concentration of external atmospheric air. Fig. 10 displays data from spot monitoring of Goughs Cave, Cheddar Gorge (UK) (sampling locations shown in Fig. 9).

Monitoring shows $CO_2$ rises towards the cave interior which can be interpreted as reducing air exchange and therefore reduced air velocity. Suspended aerosol concentrations demonstrate the opposite of $CO_2$, decreasing towards the cave interior. Temperature demonstrates a similar trend to aerosols. However, cave interior temperatures reached closer to the cave entrance (before location 2) and are then remain relatively constant throughout the cave.

The zone of significant change for $CO_2$ and suspended aerosol concentrations occurs between locations 3 and 5. The increase in $CO_2$ and associated reduction in suspended aerosol concentration indicates reduced air exchange. Reduced air exchange will be associated with lower air flow rates allowing for increased settling deposition processes. This is confirmed by an increased aerosol deposition flux being observed between locations 3–5 as shown in Fig. 11. A rise in cave floor elevation can be observed in Fig. 9 (in section) between location 2 and 3. This may account for the reduction in air exchange, as discussed in Section 3.2.2.2, increased elevation may result in the stagnation of air flow rates resulting in increased aerosol deposition.

The correlation of suspended aerosols, aerosol deposition flux and $CO_2$ demonstrates the relationship between deposition processes and cave ventilation. Cave ventilation has been confirmed as the one of the key processes controlling cave aerosol introduction, transport and deposition.

### 4.3. Entrance zone deposition

In addition to gravitational sedimentation there is also the potential for hygroscopic effects due to the high humidity compared to the external atmospheric humidity. Dry aerosols entering the cave environment may absorb water, increase in size, and fall out of the air stream flow. An example of substantial suspended load loss (and therefore deposition) occurring within the entrance zone is displayed in Fig. 13 presenting aerosol deposition monitoring data from Altamira Cave, Spain.

A detailed survey of suspended aerosol, airborne microorganisms and microclimatic monitoring was carried out at Altamira Cave (Spain), a World Heritage UNESCO site, world famous for a collection of Palaeolithic rock paintings and engravings that are mainly located in Polychromes Hall (Fig. 12). The preservation of these paintings is as a result of the cave being characterized by low rates of water infiltration, precipitation of mineral deposits and exchange with the external atmosphere; and the maintenance of very stable microenvironmental conditions because of limited air flow in the chamber. However, the opening to the public during previous decades provoked air warming and turbulence caused by visitors, resulting in increased air exchange between Polychromes Hall and areas closest to the entrance, where there are microbial colonization on walls and ceilings (Cuezva et al., 2009). The corrective measures implemented in recent years (since it last closed in 2002) have reduced the exchange between the cave atmosphere and exterior, decreasing the entry of airborne particles,
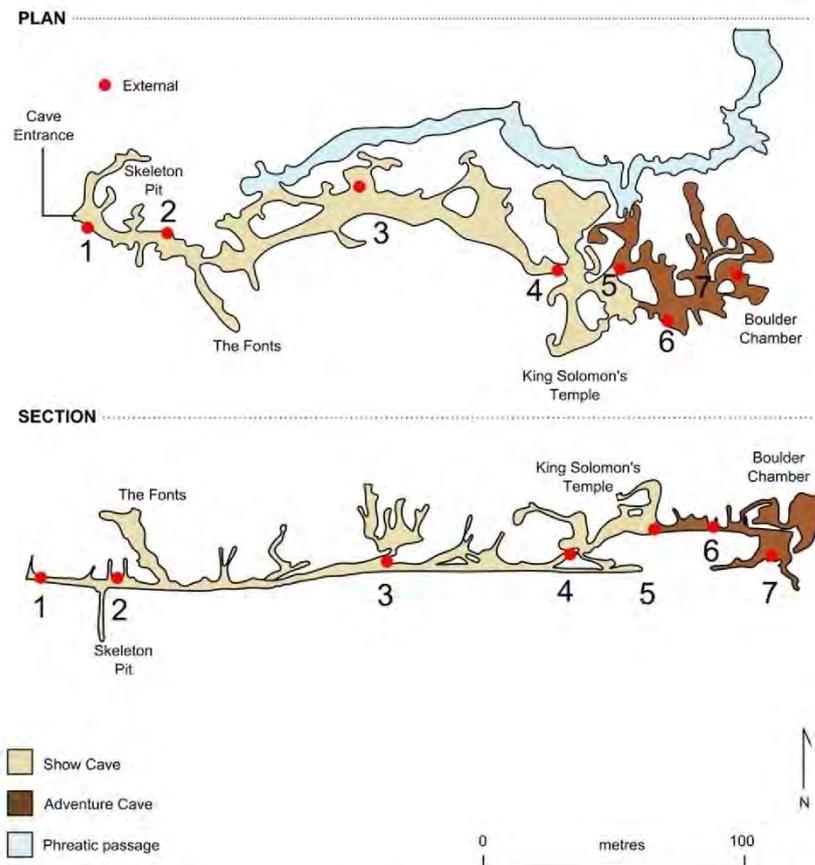


**Fig. 9.** Map of Goughs Cave, Cheddar Gorge with aerosol sampling locations. After Farrant (2010), based on survey data by Stanton (1953).
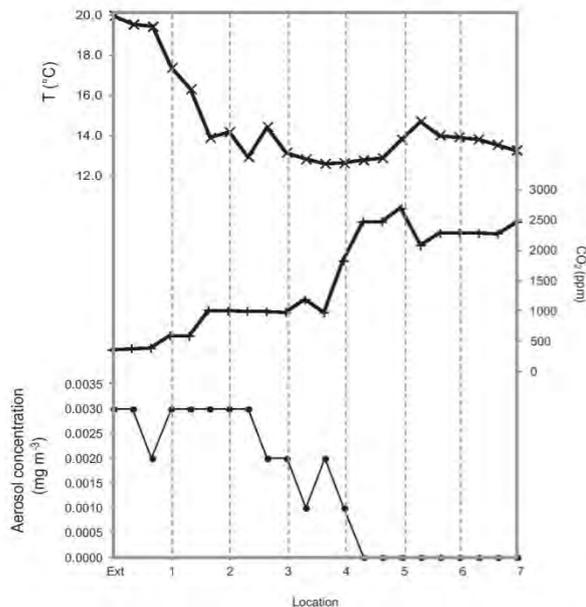
**Fig. 10.** Cave air $CO_2$ and suspended aerosol concentrations from spot monitoring throughout the Gough's Cave network on 19th and 20th July 2011. $CO_2$ recorded with a Sperian PHD6 instrument. Aerosol concentrations measured with TSI SidePak AM510 optical counter (data presented are counting duration minima during the 5 min sampling duration, in order to best achieve background levels). Five minute averages of temperature are displayed, measured with a Tinytag temperature logger. Samples were spread over ~275 m from the cave entrance to deepest interior.

the condensation rate in the entrance area, and the metabolic activity of the main visible microbial colonies (Saiz-Jimenez et al., 2011).

The transportation of aerosols throughout Altamira cave will also be hampered by the effect of a double-access door equipped with a thermal insulation system that reduces the entry of airborne particles (Saiz-Jimenez et al., 2011; Garcia-Anton et al., 2012).

The same relationship between suspended aerosols, $CO_2$ and temperature as observed in Gough's Cave (Fig. 10) is apparent in Altamira Cave as shown in Fig. 14. The loss in suspended aerosols
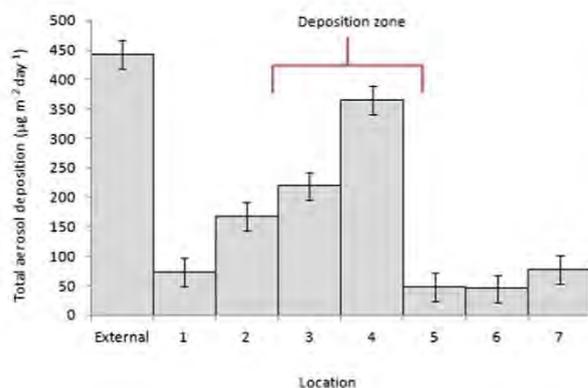


**Fig. 11.** Goughs Cave, Cheddar Gorge: the spatial distribution of depositional flux rates based on one month of surrogate surface monitoring over July. Total elemental deposition displayed as described in Section 2.2.1. Samples collected on the 20th of July. Limit of detection ($3\sigma$) displayed with error bars.

from optical particle counting methods confirms the results displayed in Fig. 13 from pumped sampling and ICP-AES analysis. Smaller particles of less than 1 μm demonstrate the strongest relationship with $CO_2$ and the highest variance (Fig. 15). This is consistent with the idea of entrance zone coarse aerosol deposition and the concept of progressive gravitational sedimentation throughout caves.

### 4.4. Progressive gravitational sedimentation

Under a simplified cave model where gravitational sedimentation is the key process of aerosol deposition, progressive deposition will be observed. Fig. 17 displays a pattern of aerosol distribution that may represent progressive gravitational deposition in St Michaels Cave, Gibraltar (Fig. 16) (Mattey et al., 2008, 2010).

Often the relationship between cave ventilation and aerosol processes will be significantly influenced by cave morphology, with caves often having an intricate morphology associated with an extensive network of interconnecting fissures resulting in a complex distribution of aerosol deposition. Additional processes to gravitational sedimentation may overprint any trends, making deciphering such processes difficult.

### 4.5. Cave morphology and aerosol deposition

An example of the control of cave morphology on aerosol deposition rates has been observed at Obir cave, Austria. Surrogate surfaces were deployed in two locations (shown in Fig. 18) within the cave to determine the deposition rates close to the position of speleothems previously studied by Fairchild et al. (2010). One sample was situated at in Säulenhalle (S), an open chamber with active speleothem formation and a terminal pool (Silbersee) and the other at Düse (D), a nearby constricted passage with sensible air flow.

Fig. 19 displays a comparison of depositional flux rates at locations S and D, with location S recording greater levels of total aerosol deposition flux. This can be accounted for simply by gravitational processes. Aerosols remain in suspension as they travel through the constriction due to the higher flow rates, upon entering the larger Säulenhalle chamber where air flow velocities are reduced. Increased deposition will likely occur near Silbersee pool regardless of the suspended load and ventilation direction simply as a result of the proposed morphologically controlled reduction in ventilation air flow rates.

With knowledge of the potential processes affecting aerosol deposition fluxes to speleothem surfaces it is possible to evaluate the contribution of aerosol deposition to speleothem geochemistry.

### 5. Aerosol contributions to speleothem geochemistry

The mode of transport and deposition is expected to have a relationship with the chemistry of aerosol being deposited. For instance, in the case of gravitational sedimentation, the larger and denser particulates will be removed from suspension first and will often be associated with specific sources and chemical composition. In a study by Faimon et al. (2006) aerosol compositions were determined to be highly variable with space and time but were broadly composed of Si, Ca, Al and Fe with fine particles formed of S, P, K and Cl. This relationship was not observed with the preliminary spatial deposition monitoring pattern and the chemical composition of aerosol deposition in Obir cave. The lack of a relationship between location and chemistry is likely due to the range of processes effecting the transport and deposition of aerosols, combined with the changing environmental conditions inside the cave and externally.

**Fig. 12.** Locations at Altamira Cave during the aerosols survey utilising a double pump and in-line filter equipment, running at 3 L min⁻¹ for 24 h duration, airborne particle counter (TSI Aerotrak™ Model 9306), microbial air sampler (Duo SAS 360, International PBI) and microclimatic records.

The comparison of aerosol deposition data from Obir cave demonstrates that elemental deposition flux rates differ between elements and some display trends unlike the overall total depositional flux rate distribution. Internally produced aerosols would be expected to be observed at greater concentrations in the cave interior in comparison to the entrance region, but no clear distinction was identifiable.

Based on monitoring data at Obir, it is possible to calculate the aerosol addition to speleothem geochemistry. The following calculations are based on deposition per 1 mm² of speleothem surface over a period of one year, assuming constant growth (as shown in Fig. 20).

In order to determine the impact of aerosol deposition upon speleothem composition the rate of deposition and the calcite supply must be known. The potential (maximum) aerosol concentration in calcite (P) is a function of aerosol depositional flux and speleothem growth rate and is related to aerosol deposition and speleothem growth as follows:

$$P = F/(R \times \rho)$$

where P = Potential aerosol concentration in calcite ($\mu g\ g^{-1}$)

    F = aerosol depositional flux ($\mu g\ mm^{-2}\ year^{-1}$)
    R = speleothem growth rate ($mm\ year^{-1}$)
    $\rho$ = 0.00271 = calcite density ($g\ mm^{-3}$)
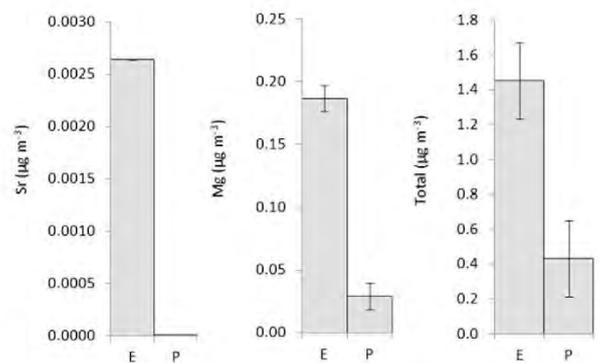


**Fig. 13.** Comparison of suspended aerosol concentrations from the cave entrance zone and Polychromes hall, Altamira Cave within the cave interior. Pumped collection of suspended aerosols at 3 L min⁻¹ over 24 h. Limit of detection (3σ) are displayed for each element with error bars. A significant reduction in suspended aerosol concentrations from the entrance zone (E) to the Polychromes Hall (P) within the cave interior can be observed. This is consistent with the patterns of distribution observed in previous studies involving the transportation of coarse aerosols. However, Location P is a side chamber which may experience reduced ventilation and the lower detected aerosol concentrations can also be attributed to the chamber's location relative to active ventilation stream flow (a bidirectional flux between cave entrance and deeper areas).
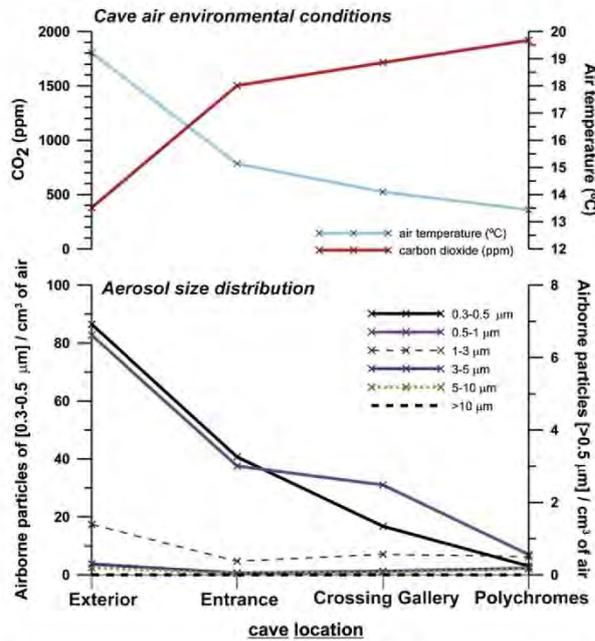
**Fig. 14.** Aerosol size distribution: Suspended particle counts of particle size ranges 0.3–0.5 μm (secondary axis), 0.5–1, 1–3, 3–5, 5–10 and >10 μm. Cave air environmental conditions: $CO_2$ (ppm) and temperature (°C). Data displayed is averaged from four cave visits on the same day 7:18–7:57am, 9:29–10:05 am, 11:49 am–12:17 pm and 2:57–3:27 pm. During this time monitoring was only exposed to the influence of the operator.

The relationship between speleothem calcite concentration and aerosol deposition flux as a function of growth rate is displayed graphically in Fig. 21.

By adding known deposition flux rates into the equation the potential aerosol contribution in calcite can be calculated. Here, data from Obir cave monitoring (Fairchild et al., 2010) are presented to demonstrate the maximum possible extent of aerosol contribution to speleothem chemistry. An approximation of aerosol contributions to calcite trace element concentrations is shown in Fig. 22 based on maximum aerosol deposition flux rates.

Aerosol contributions can be expressed as a percentage of the speleothem concentration of individual elements:

$$A(\text{aerosol contribution}, \%) = (P/C) \times 100$$

where:

C = elemental calcite concentration

The maximum theoretical contribution of aerosols to speleothem chemistry has been shown to vary significantly between different elements as shown in Table 2. Values range from 0.002% to 71.8% dependent on the element and speleothem under investigation. Fairchild et al. 2006 introduced three different types of control on trace element incorporation efficiencies: 1) Crystal dominated, where crystallographic factors control variability. 2) Temperature, where incorporation efficiencies are temperature dependent such as for Mg. 3) Fluid-dominated pattern where changes in elemental composition of the fluid trace element source drives comparable variations in calcite. Fluid dominated situations are typical when large variations of trace element composition occur over time and this is the case here.
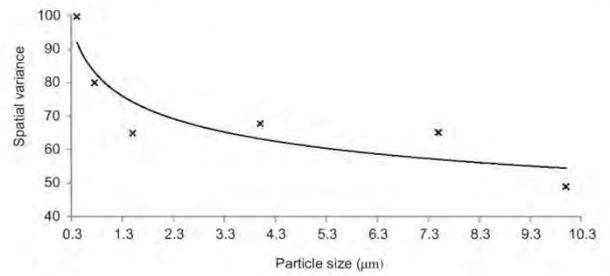


**Fig. 15.** Relationship between spatial variance of aerosols and particle size. Spatial variance = [STDEV(aerosol counts)/aerosol counts] × 100.

The comparison of drip water supply and aerosol flux supply to modern calcite concentrations (Table 3) has shown that at current drip water flow rates the drip water chemistry supply is orders of magnitude greater than that offered by aerosol flux. Limiting drip rates demonstrate that for all elements compared a >99.9% reduction in flow rates is required to reduce the drip water supply to quantities equal to the aerosol supply.

The data and calculations presented here so far are based on several assumptions. The first is that the surrogate surface aerosol deposition provides a suitable replication of the type of aerosol flux that would occur to the speleothem surface. Secondly and likely to be of greater impact is that the above calculations are based on complete incorporation (i.e. 100% efficiency). There are however several processes that will occur that would result in less than total incorporation of aerosol deposition within growing speleothem.



**Fig. 16.** Lower New St Michaels Cave network map with cave aerosol sampling locations (after Mattey et al., 2008).
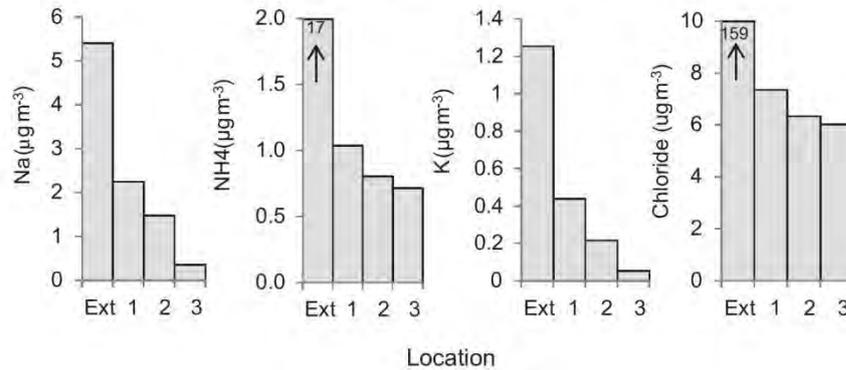
**Fig. 17.** Examples of potential evidence for progressive gravitational sedimentation. Suspended aerosol distribution in St Michaels Cave, Gibraltar. Samples spread over approximately 100 m distance from the cave entrance (Ext = Exterior) to interior.

### 5.1. Potential aerosol calcite contribution – incorporation

The aerosol contribution to speleothem geochemistry (P) is in practice a maximum since aerosol preservation will be highly dependent on drip water flow rates and the mechanism of deposition. Aerosols deposited to the surface of an actively growing speleothem may be washed away by drip water flowing over the speleothem surface. Conversely, deposition to the surface of a dry speleothem (during a speleothem growth hiatus) could result in the formation of a deposit predominantly composed of aerosol deposits and the incorporation mechanisms

of trace elements within the solid deposit may differ from that operative during partitioning into calcite during normal growth. Any aerosol deposits during a hiatus period would be affected by the possible drip water removal processes upon resumption of drip water flow over the speleothem surface. However, if binding of aerosol deposits occur to produce a consolidated horizon of calcareous or non-calcareous composition it would be resistant to drip water flow. Since calcite concentration will be a function of growth rates, it is during hiatus events where aerosol deposition will have the greatest influence on speleothem chemistry.
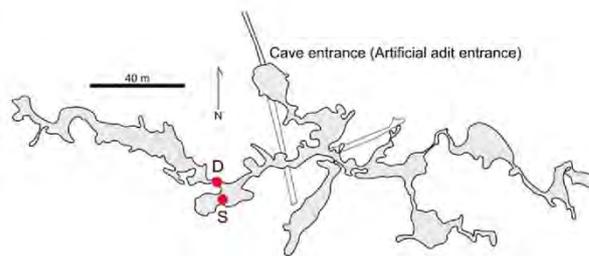


**Fig. 18.** Obir Cave map and surrogate surface locations (after Spötl et al., 2005).
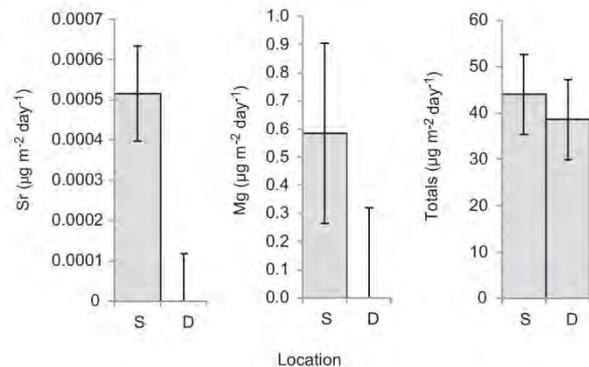


**Fig. 19.** Depositional flux rates at two locations: near Silbersee pool (S) and at Düse (D). Results from surrogate surface monitoring from 15th April to 11th July 2012 in Obir Cave, Austria. Error bars display elemental limit of detection (3σ) as errors.
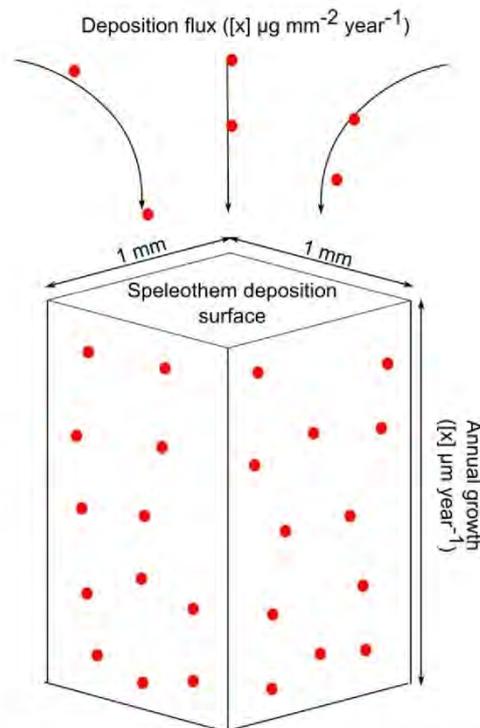


**Fig. 20.** Calculation variables: deposition flux and growth rate. Calculations are based on 1 mm² calcite surface area for one year of speleothem growth.
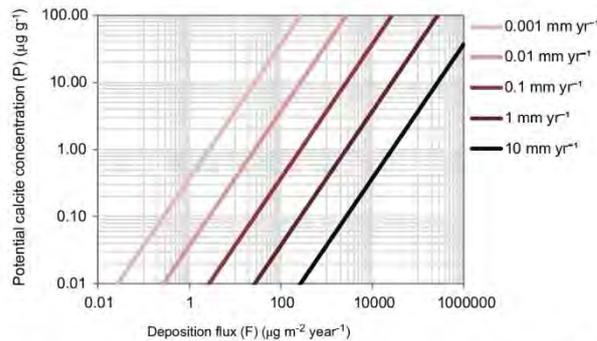
**Fig. 21.** Relationship between aerosol deposition flux (F) of a trace species and its potential concentration in calcite (P) as a function of varying growth rates from 0.001 mm yr$^{-1}$ to 10 mm yr$^{-1}$.
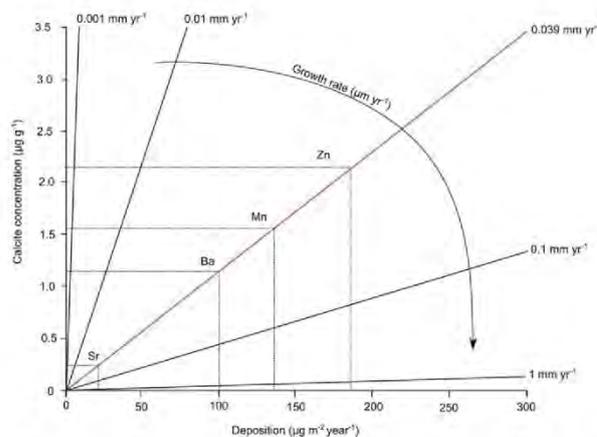


**Fig. 22.** The relationship between aerosol deposition flux (F), growth rate (R) and potential concentration in calcite (P) for speleothem OBI12 with a recorded growth rate of 0.039 mm yr$^{-1}$. Maximum Sr, Ba, Mn and Zn deposition flux rates are plotted to give their corresponding potential concentration in calcite contribution values based on this annual growth rate.

### 5.1.1. Incorporation type

Deposited aerosols remaining on the surface retain the potential to become incorporated into the speleothem. However, this process will not be 100% efficient in capturing the entire aerosol signature. Solutes will be coprecipitated, providing an addition to drip water chemistry. Particulates are likely to become incorporated through intercrystalline capture.

In evaporative scenarios with low to zero drip rates it may be possible for liquid aerosols to create a defined horizon through precipitation. Aerosols which become incorporated into the crystal lattice will be subjected to incorporation factors dependent on the chemistry and type of aerosol deposited. Notably, a number of trace elements are preferentially incorporated in the solid phase as a result of adsorption and complexing processes described in

**Table 3**
Comparison of drip water (at 287 L year$^{-1}$ flow rate) and aerosol flux contributions to speleothem geochemistry. Limiting drip rates are those at which drip water chemistry supply is equal to that of aerosol flux. Drip water oversupply (%) = 1/[mg of element per year calcite growth/mg of drip water supply per year × 100] × 100. Aerosol flux oversupply (%) = 1/[(mg of element per year calcite growth/mg of aerosol flux to speleothem surface per year) × 100] × 100.

| Element | Oversupply (%) | | Limiting drip rate (L yr$^{-1}$) |
|---|---|---|---|
| | Drip water | Aerosol flux | |
| Zn | 18 | 0.00014 | 0.0022 |
| Mg | 9583 | 0.00073 | 0.000022 |
| P | 99 | 0.012 | 0.036 |

Fairchild and Baker (2012, chapter 8). Here we modelled potential contributions from aerosols assuming 100% efficiency of incorporation into the solid phase. Whereas ions are removed from dripwater at quite low efficiencies (and this is specifically the case as Obir cave, Fairchild et al., 2010), at minimal drip rates, solid phase accretion processes will tend to be less discriminatory between elements. Aerosol preservation will therefore be a function of: drip water flow rates, speleothem growth rates (also a function of flow rates), aerosol deposition type (wet or dry deposition) and aerosol type.

### 5.2. Cave aerosol, aerobiology and microbial communities

Microbial material is known to be distributed throughout cave networks (Jurado et al., 2009, 2010; Cuezva et al., 2009; Bastain and Alabouvette, 2009, Bastian et al., 2009a, 2009b, 2010). The distribution of microorganisms may be influenced by transportation as aerosols. In addition to, or as a separate process, microbiological activity throughout caves is known to occur as a consequence of anthropogenic transportation and is often an issue for cave management practices. Aerosols of fungi (Wang et al., 2011) and bacteria (Wang et al., 2010; Martin-Sanchez et al., 2011) have been shown to be distributed throughout cave networks with visitors having a significant influence of the type and concentration of the biological aerosols. Visitors carry spores, seeds and bacteria on clothing and deposit them within the cave network. In addition to providing an introduction mechanism visitors result in increased disturbance and aerosol production.

Regarding the contribution of aerosol deposition to speleothem, microbiological processes may provide an additional feedback. Aerosol deposition contributions to speleothem surfaces may not be sufficient to influence speleothem chemistry directly to a significant degree. However, the presence of deposits may facilitate and sustain microbial communities which subsequently, through bioaccumulative processes, result in inorganic concentration horizons of notable levels. Some bacteria are known to be capable of concentrating metals from their environment (Dorn and Oberlander, 1981) and have been known to increase the rate of manganese oxidation by up to five orders of magnitude (Tebo et al., 1997). Microorganisms may contribute to the formation of manganese and iron oxide-rich deposits (Northup et al., 2003). In addition to metals cave biota have been also shown to accumulate and precipitate calcium phosphate in significant quantities (Jones, 2009). In the particular case study of Altamira Cave, the

**Table 2**
Values of maximum theoretical aerosol contributions (A, %) to concentrations of individual elements for samples taken across the growth range of the Obir speleothems, based on depositional flux at location S. Uncertainties are one standard deviation. Extended statistical results of OBI12 and OBI84 for location S are displayed in the supplementary material S.4, Table S.1.

| | Mg | P | Mn | Zn | Sr | Ba |
|---|---|---|---|---|---|---|
| OBI12 | 1.1 ± 0.31 | 14 ± 5.4 | 72 ± 34 | 0.0068 ± 0.0027 | 0.45 ± 0.11 | 0.20 ± 0.043 |
| OBI84 | 0.43 ± 0.34 | 5.0 ± 4.0 | 30 ± 32 | 0.0024 ± 0.0015 | 0.13 ± 0.18 | 0.079 ± 0.066 |
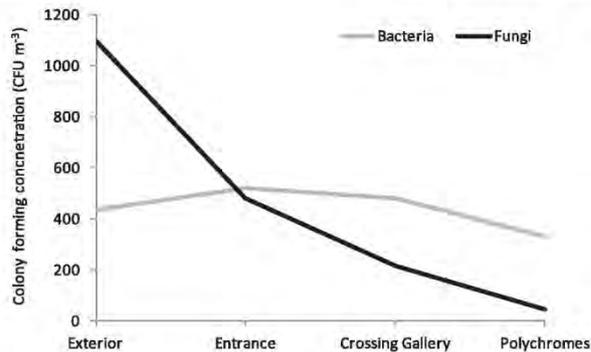
**Fig. 23.** Airborne bacteria and fungi aerosol concentrations expressed as colony forming units per $m^3$ of air in Altamira Cave, Spain. Data displayed is averaged from four cave visits on the same day 7:18–7:57 am, 9:29–10:05 am, 11:49 am–12:17 pm and 2:57–3:27 pm. During this time monitoring was only exposed to the influence of the operator.

Actinobacteria, forming grey spots in the cave surface near the entrance, can use the captured $CO_2$ to dissolve the rock and subsequently generate crystals of $CaCO_3$ in periods of lower humidity and/or $CO_2$ (Cuezva et al., 2012). Likewise, bacteria are also involved in the formation of calcitic moonmilk deposits in this cave (Sanchez-Moral et al., 2012). In some instances the aerosol contribution to speleothem could be significantly increased as a result of secondary feedback concentrating processes and provide a proxy for emissions events which would not be detectable otherwise.

Monitoring of suspended fungi and bacteria was undertaken in Altamira Cave to determine the spatial distribution of microbial aerosols throughout the cave network, the results of which are displayed in Fig. 23. Fungi demonstrate the same distribution observed in the suspended aerosol counts carried out during the same fieldwork period indicating the same ventilation driven distribution mechanism as other aerosols. It should be noted that fungi may associate with larger particles which were not detected by the particle counter. However, bacteria demonstrate a pervasive but spatially independent distribution. This is coherent with the distribution of intermediate to coarser aerosols observed from suspended aerosol monitoring, as bacterial aerosols are typically of 0.3–10 µm in size (as shown in Fig. 2). The aerial distribution of suspended bacteria differs to the observations of bacterial colonisation, which is dominant nearest the cave entrance. It is plausible that the relationship between bioaerosols and cave surface colonisation is controlled by the distribution of inorganic aerosols which provide a nutrient flux creating conditions suitable for sustaining microbial production. Therefore colonisation differences occur as a consequence of relatively high nutrient fluxes to cave surfaces rather the direct deposition of bacteria.

## 6. Conclusions

A range of cave aerosol issues have been explored in this review providing the first synthesis of cave aerosol literature combined with the presentation of cave aerosol monitoring data highlighting topics of key importance.

Methodologies have been outlined for the analysis and identification of aerosols. Surrogate surface and particle counting methods have been shown to offer the most suitable methods for cave dry deposition and suspended aerosol sampling respectively. Subsequent to aerosol capture a wealth of geochemical, morphological and quantitative information can be obtained through both inorganic and organic analytical techniques such as ICP-MS, SEM and GC–MS respectively.

Data has shown that cave aerosols are internally and externally sourced from both natural and anthropogenic processes. Monitoring data demonstrates that cave visitor disruptions release aerosols to levels orders of magnitude greater than that of the natural background. Cave environment degradation from combustion emissions and cave visitors is becoming increasingly common and is developing as a cave management problem. Cave preservation practices involving ventilation control and visitor number restrictions have been shown to reduce the introduction of cave aerosols and their detrimental impacts.

Cave aerosols are sensitive to environmental conditions and will therefore exhibit temporal and spatial variations. A range of cave processes can be investigated by measurement of suspended aerosol loads, aerosol deposition and aerosol type. Data has shown that cave atmosphere aerosol transport is predominantly controlled by cave ventilation and anthropogenic disturbances. As aerosol monitoring instruments become more widely available, aerosols may become a preferable environmental monitoring indicator providing greater sensitivity over more commonly used indicators such as cave air $CO_2$ and temperature.

Aerosol introduction, distribution, deposition and incorporation are complex and variable processes dictated heavily by the specific cave situation. Cave morphology has been shown to influence cave aerosol deposition to speleothem through the control of ventilation forced air flow rates and creation of turbulence. Monitoring data displays evidence of progressive aerosol deposition with significant fallout within the entrance region of caves. Hydrological aerosol production has been shown to be of significance and may provide notable additions to speleothem geochemistry in proximity to active water flows. The distribution of aerosol deposition as a consequence of cave morphological effects, internal aerosol production and subsequent variable potential contribution to speleothem geochemistry throughout caves demonstrates the need in some cases to consider aerosol deposition distributions when choosing speleothem for palaeoenvironmental investigations.

Calculations have demonstrated that the ultimate contribution of aerosols to speleothem geochemistry is predominantly dependent on growth rates, deposition flux, and aerosol incorporation factors. Results have shown that aerosol contributions to speleothem chemistry will commonly be of low significance; but, in certain instances aerosols may provide considerable additions. Comparisons of dry deposition flux rates to speleothem geochemistry have demonstrated that in the case of Obir Cave (Austria) a >99.9% reduction in drip water flow rates is required to reduce trace element supply quantities to equal that of aerosol supply. In some scenarios aerosol contributions may contaminate samples for some geochemical analytical techniques, such as radiogenic isotope studies, or skew drip water environmental signatures. Conversely, with greater understanding, aerosols through speleothem incorporation may provide a novel environmental indicator not yet constrained by existing proxies especially in the identification and interpretation of speleothem growth hiatus events.

Aerosol deposition contributions to speleothem surfaces may not be sufficient to influence speleothem chemistry directly to a significant degree. However, microbiological processes may provide a positive feedback to aerosol deposition. The presence of deposits may facilitate and sustain microbial communities which subsequently, through bio-accumulative processes, result in inorganic concentration horizons of notable levels.

To summarise, the key situations where aerosol deposition may provide noteworthy contributions to speleothem are:

- Hiatus events (ceased/very slow speleothem growth).
- Very high deposition flux rates as a result of a combination of efficient aerosol transport and large external suspended loads.

- Secondary microbial feedback processes resulting in increased concentrations.

## Acknowledgements

## Appendix A. Supplementary data

Supplementary data related to this article can be found at http://dx.doi.org/10.1016/j.quascirev.2012.11.016.

## References

Alfödy, B., Török, S.Z., Hofmann, W., Bergmann, R., 2000. Intrapulmonary particle deposition and retention. Journal of Aerosol Science 31 (Supp. 1), S504–S505.

Alfödy, B., Török, Sz., Kocsonya, A., Szökefalvi-Nagy, Z., Balla, Md.I., 2001. X-ray analysis of aerosol samples from a therapeutic cave. Nuclear Instruments and Methods in Physics Research B 174, 361–366.

Allen, A.G., Nemitz, E., Shi, J.P., Harrison, R.M., Greenwood, J.C., 2001. Size distributions of trace metals in atmospheric aerosols in the United Kingdom. Atmospheric Environment 35, 4581–4591.

Badino, G., 2004. Clouds in Caves. Speleogenesis and Evolution of Karst Aquifers 2 (2).

Bartenev, O.S., Veselova, N.V., 1987. On Anthropogenic Dust Pollution in Caves of the Cupp-Coutunn Cave System. Problemy Izucheniya, Ekologii i Okhrany Pescher, Kiev, p. 159.

Bastain, F., Alabouvette, C., Saiz-Jimenez, C., 2009a. The impact of arthropods on fungal community structure in Lascaux Cave. Journal of Applied Microbiology 106, 1456–1462.

Bastain, F., Alabouvette, C., Saiz-Jimenez, C., 2009b. Bacteria and free-living amoeba in the Lascaux Cave. Research in Microbiology 160, 38–40.

Bastain, F., Alabouvette, C., 2009. Light and shadows on the conservation of a rock art cave: the case of Lascaux cave. International Journal of Speleology 38 (1), 55–60.

Bastian, F., Jurado, V., Nováková, A., Alabouvette, C., Saiz-Jimenez, C., 2010. The microbiology of Lascaux Cave. Microbiology 156, 644–652.

Bridgman, H., 1994. Global Air Pollution: Problems for the 1990s. John Wiley and Sons, Chichester.

Burney, D.A., Burney, L., 1993. Modern pollen deposition in cave sites: experimental results from New York State. New Phytologist 124, 523–535.

Caseldine, C.J., McGarry, S.F., Baker, A., Hawkesworth, C., Smart, P.L., 2008. Late Quaternary speleothem pollen in the British Isles. Journal of Quaternary Science 23 (2), 193–200.

Chang, S.J., Jeong, G.Y., Kim, S.J., 2008. The origin of black carbon on speleothems in tourist caves in South Korea: chemical characterization and source discrimination by radiocarbon measurement. Atmospheric Environment 42, 1790–1800.

Christoforou, C.S., Salmon, L.G., Cass, G.R., 1994. Deposition of atmospheric particles within the Buddhist Cave Temples at Yungang, China. Atmospheric Environment 28 (12), 2081–2091.

Christoforou, C.S., Salmon, L.G., Cass, G.R., 1996a. Fate of atmospheric particles within the Buddhist Cave Temples at Yungang, China. Environment of Science and Technology 30, 3425–3434.

Christoforou, C.S., Salmon, L.G., Cass, G.R., 1996b. Air exchange within the Buddhist cave temples at Yungang, China. Atmospheric Environment 30 (23), 3995–4006.

Chu, C.C., Fang, G.C., Chen, J.C., Yang, I.L., 2008. Dry deposition study by using dry deposition plate and water surface sampler in Shalu, central Taiwan. Environmental Monitoring and Assessment 146 (1), 441–451.

Cigna, A., 1983. The Criterion of Visitors Capacity of Commercial Caves. International Meeting on the Show Caves and their Problems. Hellenic Speleological Society, p. 124.

Cigna, A., 1993. Environmental management of tourist caves. The examples of Grotta di Castellana and Grotta Grande del Vento, Italy. Environmental Geology 21, 173–180.

Cigna, A., Forti, P., 1989. The environmental impact assessment of a tourist cave. In: Cave Tourism: Proceedings International Symposium for the 170th Anniversary of Postojnska Jama, Postojna, pp. 29–38.

Cigna, A., Hill, C.A., 1997. Aerosols: are they a mechanism of speleothem growth? In: Hill, C., Forti, P. (Eds.), Cave Minerals of the World. National Speleological Association, Huntsville, Alabama, pp. 255–258.

Coles, G.M., Gilbertson, D.D., 1994. The airfall-pollen budget of archaeologically important sites: creswell crags, England. Journal of Archaeological Science 21, 735–755.

Coles, G.M., Gilbertson, D.D., Hunt, C.O., Jenkinson, R.D.S., 1989. Taphonomy and the palynology of cave deposits. Cave Science 16, 83–89.

Conn, H.W., 1966. Barometric wind in wind and jewel caves, South Dakota. Bulletin of the National Speleological Society 28, 55–69.

Cuezva, S., Sanchez-Moral, S., Saiz-Jimenez, C., Cañaveras, J.C., 2009. Microbial communities and associated mineral fabrics in Altamira Cave, Spain. International Journal of Speleology 38 (1), 83–92.

Cuezva, S., Fernandez-Cortes, A., Porca, E., Pašić, L., Jurado, V., Hernandez-Marine, M., Serrano-Ortiz, P., Hermosin, B., Cañaveras, J.C., Sanchez-Moral, S., Saiz-Jimenez, C., 2012. The biogeochemical role of Actinobacteria in Altamira Cave, Spain. FEMS Microbiology Ecology 81, 281–290.

Dorn, R.I., Oberlander, T.M., 1981. Microbial origin of desert varnish. Science 213, 1245–1247.

Dreybrodt, W., Gabrovsek, F., Perne, M., 2005. Condensation corrosion: a theoretical approach. Acta Carsologica 34 (2), 317–348.

Dublyansky, V.N., Dublyansky, Y.V., 2000. The role of condensation in karst hydrogeology and speleogenesis. In: Speleogenesis: Evolution of Karst Aquifers, A.

Faimon, J., Štelcl, J., Sas, D., 2006. Anthropogenic $CO_2$ – flux into cave atmosphere and its environmental impact: a case study in Císařská Cave (Moravian Karst, Czech Republic). Science of the Total Environment 369, 231–245.

Fairchild, I.J., Baker, A., 2012. Speleothem Science. Wiley-Blackwell, Chichester.

Fairchild, I.J., Smith, C.L., Baker, A., Fuller, L., Spötl, C., Mattey, D., McDermott, F., EIMF, 2006. Modification and preservation of environmental signals in speleothems. Earth Science Reviews 75, 105–153.

Fairchild, I.J., Spötl, C., Frisia, S., Borsato, A., Susini, J., Wynn, P.M., Cauzid, J., EIMF, 2010. Petrology and geochemistry of annually laminated stalagmites from an Alpine Cave (Obir, Austria): seasonal cave physiology. In: Geological Society, London, Special Publications, vol. 336, pp. 295–321.

Farrant, A.R., 2010. Gough's Cave – a Field Guide. British Cave Research Association Cave Science Field meeting, British Geological Survey Internal Report.

Fernandez-Cortes, A., Sánchez-Moral, S., Cuezva, S., Cañaveras, J.C., Abella, R., 2009. Annual and transient signatures of gas exchange and transport in the Castañar de Íbor cave (Spain). International Journal of Speleology 38 (2), 153–162.

Fernandez-Cortes, A., Cuezva, S., Sanchez-Moral, S., Porca, E., Jurado, V., Martin-Sanchez, P.M., Saiz-Jimenez, C., 2011. Detection of human-induced environmental disturbances in a show cave. Environmental Science and Pollution Research 18, 1037–1045.

Frumkin, A., Stein, M., 2004. The Sahara-East Mediterranean dust and climate connection revealed by strontium and uranium isotopes in a Jerusalem speleothem. Earth and Planetary Science Letters 217, 415–464.

Garcia-Anton, E., Cuezva, S., Fernandez-Cortes, A., Sanchez-Moral, S., Canaveras, J.C., 2012. Multiparametric surveillance of conservation measures at subterranean rock-art site: case of Altamira cave. Geophysical Research Abstracts 14. EGU2012–831.

Ghedini, N., Gobbi, G., Sabbioni, C., Zappia, G., 2000. Determination of elemental and organic carbon on damaged stone monuments. Atmospheric Environment 34, 4383–4391.

Goede, A., McCulloch, M., McDermott, F., Hawkesworth, C., 1998. Aeolian contribution to strontium and strontium isotope variations in a Tasmanian speleothem. Chemical Geology 149 (1–2), 37–50.

Harper, S.L., Walling, J.F., Holland, D.M., Pranger, L.J., 1983. Simplex optimization of multi element ultrasonic extraction of atmospheric particulates. Analytical Chemistry 55, 1553–1557.

Harrison, R.M., Tilling, R., Callien Romero, M.S., Harrad, S., Jarvis, K., 2003. A study of trace metals and polycyclic aromatic hydrocarbons in the roadside environment. Atmospheric Environment 37, 2391–2402.

Holsen, T.M., Noll, K.E., 1992. Dry deposition of atmospheric particles: application of current models to ambient data. Environmental Science and Technology 26, 1802–1814.

Iskra, I., Kávási, N., Vaupotič, J., 2010. Nano aerosols in the Postojna cave. Acta Carsologica 39 (3), 523–528.

Janssen, N.A.H., Van Mansom, D.F.M., Van der Jagt, K., Harssema, H., Hoek, G., 1997. Mass concentration and elemental composition of airborne particulate matter at street and background locations. Atmospheric Environment 31 (8), 1185–1193.

Jeong, G.Y., Kim, S.J., Chang, S.J., 2003. Black carbon pollution of speleothems by fine urban aerosols in tourist caves. American Mineralogist 88, 1872–1878.

Jin, Z., You, C.-F., Yu, J., Wu, L., Zhang, F., Liu, H.-C., 2011. Seasonal contributions of catchment weathering and eolian dust to river water chemistry, northeastern Tibetan Plateau: chemical and Sr isotopic constraints. Journal of Geophysical Research 116, F04006. http://dx.doi.org/10.1029/2011JF002002.

Jones, B., 2009. Phosphatic precipitates associated with actinomycetes in speleothems from Grand Cayman, British West Indies. Sedimentary Geology 219, 302–317.

Jones, A.M., Harrison, R.M., 2004. The effects of meteorological factors on atmospheric bioaerosol concentrations – a review. Science of the Total Environment 326, 151–180.

Jones, A.M., Harrison, R.M., 2005. Interpretation of particulate elemental and organic carbon concentrations at rural, urban and kerbside sites. Atmospheric Environment 39, 7114–7126.

Jurado, V., Fernandez-Cortes, A., Cuezva, Soledad, Laiz, Leonila, Cañaveras, J.C., Sanchez-Moral, S., Saiz-Jimenez, 2009. The fungal colonisation of rock-art caves: experimental evidence. Naturwissenschaften 96, 1027–1034.

Jurado, V., Porca, E., Cuezva, S., Fernandez-Cortes, A., Sanchez-Moral, S., Saiz-Jimenez, C., 2010. Fungal outbreak in a show cave. Science of the Total Environment 408, 3632–3638.

Kehrwald, N., Zangrando, R., Gambaro, A., Cescon, P., Barbante, C., 2010a. Specific molecular markers in ice cores provide large-scale patterns in biomass burning. PAGES News 18 (2), 59–61.

Kehrwald, N., Zangrando, R., Gambaro, A., Barbante, C., 2010b. Fire and climate: biomass burning recorded in ice and lake cores. EPJ Web of Conferences 9, 105–114.

Kertéz, Zs., Borbély-Kiss, I., Rajita, I., Uzonyi, I., Kiss, Á.Z., 2000. Analysis of single aerosol particles collected in urban and cave environment by proton microprobe. Nuclear Instruments and Methods in Physics Research B 161–163, 808–813.

Kertéz, Zs., Balásházy, I., Borbély-Kiss, I., Hofmann, W., Hunyadi, I., Salma, I., Winkler-Heil, R., 2002. Composition, size distribution and lung deposition distribution of aerosols collected in the atmosphere of a speleotherapeutic cave situated below Budapest, Hungary. Nuclear Instruments and Methods in Physics Research B 189, 221–226.

Klimchouck, A.B., Nasedkin, V.M., Cunningham, K.I., 1995. Speleothems of aerosol origin: reply. National Speleological Society Bulletin 57, 31–42.

Klimchouk, A.B., 1994. Speleogenesis under confined conditions, with recharge from adjacent formations. Publ. Serv. Geol 27, 85–95. Luxembourg, Comptes Rednus du Colloque International de Karstology a Luxembourg.

Kulkarni, P., Baron, P.A., Willeke, K., 2011. Particle migration in external force fields. In: Aerosol Measurement - Principles, Techniques, and Applications, third ed. John Wiley & Sons, p. 23.

Laird, L.D., Campbell, I.D., 2000. High resolution palaeofire signals from Christina Lake, Alberta: a comparison of the charcoal signals extracted by two different methods. Palaeogeography, Palaeoclimatology, Palaeoecology 164, 111–123.

Lauritzen, S.E., Lovlie, R., Moe, D., Østbye, E., 1990. Palaeoclimate deduced from a multidisciplinary study of a half-million year old stalagmite from Rana, Northern Norway. Quaternary Research 34, 306–316.

Li, H.-C., Ku, T.-L., You, C.-F., Cheng, H., Edwards, L., Ma, Z.-B., Tsai, W.-S., Li, M.-D., 2005. $^{87}$Sr/$^{86}$Sr and Sr/Ca in speleothems for paleoclimate reconstruction in Central China between 70 and 280 kyr ago. Geochimica et Cosmochimica Acta 69, 3933–3947.

Lim, J.-H., Sabin, L.S., Schiff, K.C., Stolzenbach, K.D., 2006. Concentration, size distribution, and dry deposition rate of particle-associated metals in the Los Angeles region. Atmospheric Environment 40, 7810–7823.

Loosmore, G.A., Cederwall, R.T., 2004. Precipitation scavenging of atmospheric aerosols for emergency response applications: testing an updated model with new real-time data. Atmospheric Environment 38, 993–1003.

Lyman, S.N., Gustin, M.S., Prestbo, E.M., Marsik, F.J., 2007. Estimation of dry deposition of mercury in Nevada by direct and indirect methods. Environmental Science & Technology 41, 1970–1976.

Maltsev, V.A., 1997. Speleothems of aerosol origin: discussion. Journal of Cave and Karst Studies 59. 43–43.

Martin-Sanchez, P.M., Sanchez-Cortez, S., Lopez-Tobar, E., Jurado, V., Bastian, F., Alabouvette, C., Saiz-Jimenez, C., 2011. The nature of black stains in Lascaux Cave, France, as revealed by surface-enhanced Raman spectroscopy. Journal of Raman Spectroscopy 43, 464–467.

Masson, O., Piga, D., Gurriaran, R., D'Amico, D., 2010. Impact of an exception a Saharan dust outbreak in France: PM$_{10}$ and artificial radionuclides concentrations in air and in dust deposits. Atmospheric Environment 44 (20), 2478–2486.

Mattey, D., Lowey, D., Duffet, J., Fisher, R., Hodge, E., Frisia, S., 2008. A 53 year seasonally resolved oxygen and carbon isotope record from a modern Gibraltar speleothem: reconstructed drip water and relationship to local precipitation. Earth and Planetary Science Letters 269 (1–2), 80–95.

Mattey, D., Fairchild, I.J., Atkinson, T.C., Latin, J.-P., Ainsworth, M., Durell, R., 2010. Seasonal microclimate control of calcite fabrics and trace elements in modern speleothem from St. Michaels Cave, Gibraltar. In: Pedley, H.M., Rogerson, M. (Eds.), Tufas and Speleothems: Unravelling the Microbial and Physical Controls. Geological Society of London Special Volume, vol. 336, pp. 323–344.

McGarry, S.F., Caseldine, C., 2004. Speleothem palynology: an undervalued tool in Quaternary studies. Quaternary Science Reviews 23, 2389–2404.

Michie, N.A., 1997. The threat to caves of the human dust source. In: Proceedings of the 12th International Congress of Speleology. International Union of Speleology/Swiss Speleological Society 5, pp. 43–46.

Michie, N.A., 1999. An instrument and method for measurement of dust fall in caves. National Cave and Karst Management Symposium, Chattanooga (Tennessee). 123–128.

Nava, S., Becherini, F., Bernardi, A., Bonazza, A., Chiari, M., García-Orellana, I., Lucarelli, F., Ludwig, N., Migliori, A., Sabbioni, C., Udisti, R., Valli, G., Vecchi, R., 2010. An integrated approach to assess air pollution threats to cultural heritage in a semi-confined environment: the case study of Michelozzo's Courtyard in Florence (Italy). Science of the Total Environment 408, 1403–1413.

Navarro, C., Carrión, J.S., Munuera, M., Prieto, A.R., 2001. Cave surface pollen and the palynological potential of Karstic cave sediments in palaeoecology. Review of Palaeobotany and Palynology 117, 245–265.

Northup, D.E., Barns, S.M., Yu, L.E., Spilde, M.N., Schelble, R.T., Dano, K.E., Crossey, L.J., Connolly, C.A., Boston, P.J., Natvig, D.O., Dahm, C.N., 2003. Diverse microbial communities inhabiting ferromanganese deposits in Lechuguilla and Spider Caves. Environmental Microbiology 5, 1071–1086.

Ohms, M., 2003. Dust Deposition along the Candlelight Tour, Wind Cave National Park. In: Inside Earth (Cave & Karst Program, Geologic Resources Division, U.S. National Park Service), vol. 6(1), pp. 1–3.

Pashchenko, S.E., Sabelfeld, K.K., 1992. Atmospheric and Technogenic Aerosol (Kinetic, Electronic-sounding, and Numerical Methods of Investigation). SO RAN, Novosibirsk. 118.

Pashchenko, A., Dublyansky, Y., Andreichuk, V., 1993. Aerosol study in the Kungur Ice Cave (Urals, Russia). In: Proceedings of the XI International Congress of Speleology, Beijing.

Pashenko, S.E., Dublyankskky, Y.V., 1997. Generation of cave aerosols by alpha particles: critical evaluation of the hypothesis. Journal of Cave and Karst Studies 59 (3), 103–105.

Perrette, Y., Poulenard, J., Saber, A.-I., Fanget, B., Guittonneau, S., Ghaleb, B., Garaudee, S., 2008. Polycyclic aromatic hydrocarbons in stalagmites: occurrence and use for analyzing past environments. Chemical Geology 251, 67–76.

Petroff, A., Mailliat, A., Amielh, M., Anselmet, F., 2008. Aerosol dry deposition on vegetative canopies. Part I: review of present knowledge. Atmospheric Environment 42, 3625–3653.

Porca, E., Jurado, V., Martin-Sanchez, P.M., Hermosin, B., Bastian, F., Alabouvette, C., Saiz-Jimenez, C., 2011. Aerobiology: an ecological indicator for early detection and control of fungal outbreaks in caves. Ecological Indicators 11, 1594–1598.

Saiz-Jimenez, C., Cuezva, S., Jurado, V., Fernandez-Cortes, A., Porca, E., Benavente, D., Cañaveras, J.C., Sanchez-Moral, S., 2011. Paleolithic art in peril: policy and science collide at Altamira Cave. Science 334 (6052), 42–43.

Salmon, L., Christoforou, C.S., Cass, G.R., 1994. Airborne pollutants in the Buddhist Cave Temples at the Yungang Grottoes, China. Environmental Science and Technology 28 (5), 805–811.

Salmon, L.G., Christoforou, C.S., Gerk, T.J., Cass, G.R., Cassucio, G.S., Cooke, G.A., Leger, M., Olmez, I., 1995. Source contributions to airborne particle deposition at the Yungang Grottoes, China. Science of the Total Environment 167 (1), 33–47.

Sanchez-Moral, S., Soler, V., Cañaveras, J.C., Sanz-Rubio, E., Van Grieken, R., Gysels, K., 1999. Inorganic deterioration affecting the Altamira Cave, N Spain: quantitative approach to wall-corrosion (solution etching) processes induced by visitors. Science of the Total Environment 244, 67–84.

Sanchez-Moral, S., Portillo, M.C., Janices, I., Cuezva, S., Fernandez-Cortes, A., Cañaveras, J.C., Gonzalez, J.M., 2012. The role of microorganisms in the formation of calcitic moonmilk deposits and speleothems in Altamira Cave. Geomorphology 139–140, 285–329.

Sehmel, G.A., Hodgson, W.H., 1978. A Model for Predicting Dry Deposition of Particles and Gases to Environmental Surfaces. DOE Report PNL-SA-6721. Pacific Northwest Laboratories, Richland, WA.

Seinfeld, J.H., Pandis, S.N., 1998. Atmospheric Chemistry and Physics. From Air Pollution to Climate Change. John Wiley & Sons.

Simoneit, R.T., 2002. Biomass burning – a review of organic tracers for smoke from incomplete combustion. Applied Geochemistry 17 (3), 129–162.

Smith, A.C., Wynn, P.M., Barker, P.A., 2013. Natural and anthropogenic factors which influence aerosol distribution in Ingleborough Show Cave, UK. International Journal of Speleology 42 (1), 49–56.

Spötl, C., Fairchild, I.J., Tooth, A.F., 2005. Cave air control on dripwater geochemistry, Obir Caves (Austria): Implications for speleothem deposition in dynamically ventilated caves. Geochimica et Cosmochimica Acta 69 (10), 2451–2468.

Stanton, W.I., 1953. The Survey of Cheddar Caves, Annual Report of the Mendip Nature Research Committee, 1951/2, pp. 16–23.

Tebo, B.M., Ghiorse, W.C., Van Waasbergen, L.G., Siering, P.L., Caspi, R., 1997. Bacterially mediated mineral formation: insights into manganese (II) oxidation from molecular genetic and biochemical studies. Reviews in Mineralogy 35, 225–266.

Verheyden, S., Keppens, E., Fairchild, I.J., McDermott, F., Weis, D., 2000. Mg, Sr and Sr isotope geochemistry of a Belgian Holocene speleothem: implications for palaeoclimate reconstructions. Chemical Geology 169, 131–144.

Wai, K.M., Leung, K.Y., Tanner, P.A., 2010. Observational and modelling study of dry deposition on surrogate surfaces in a South China city: implication of removal of atmospheric crustal particles. Environmental Monitoring and Assessment 164 (1–4), 143–152.

Wang, X., Peng, P.A., Ding, Z.L., 2005. Black carbon records in Chinese Loess Plateau over the last two glacial cycles and implications for palaeofire. Palaeogeography, Palaeoclimatology, Palaeoecology 223, 9–19.

Wang, W., Ma, Y., Ma, X., Wu, F., Ma, X., An, L., Feng, H., 2010. Seasonal variations of airborne bacteria in the Mogao Grottoes, Dunhuang, China. International Biodeterioration & Biodegradation 64, 309–315.

Wang, W., Ma, X., Ma, Y., Mao, L., Wu, F., Ma, X., An, L., Feng, H., 2011. Molecular characterization of airborne fungi in caves of the Mogao Grottoes, Dunhuang, China. International Biodeterioration & Biodegration 65, 726–731.

Wesely, M.L., Hicks, B.B., 2000. A review of the current status of knowledge on dry deposition. Atmospheric Environment 32, 2261–2282.

Whitby, K.T., Cantrell, B.K., 1975. Atmospheric aerosols characteristics and measurements. In: International conference on environmental sensing and assessment, Las Vegas, NV.

Yang, H., Tsaib, C., Chaoc, M., Sua, Y., Chiena, S., 2006. Source identification and size distribution of atmospheric polycyclic aromatic hydrocarbons during rice straw burning period. Atmospheric Environment 40, 1266–1274.

Yang, J., Li, G., Rao, W., Ji, J., 2009. Isotopic evidences for provenance of East Asian Dust. Atmospheric Environment 43, 4481–4490.

Zhang, L., Fang, G.C., Liu, C.K., Huang, Y.L., Huang, J.H., Huang, C.S., 2011. Dry deposition fluxes and deposition velocities of seven trace metal species at five sites in Central Taiwan – a summary of surrogate surface measurements and a comparison with model estimation. Atmospheric Chemistry and Physics 11, 32847–32875.

Zhou, B., Shen, C., Sun, W., Zheng, H., Yang, Y., Sun, Y., An, Z., 2007. Elemental carbon record of palaeofire history on the Chinese Loess Plateau during the last 420 ka and its response to environmental and climate change. Palaeogeography, Palaeoclimatology, Palaeoecology 252, 617–625.

Zhou, H., Feng, Zhao, J.-X., Shen, C.-C., You, C.-F., Lin, Y., 2009. Deglacial variations of Sr and $^{87}$Sr/$^{86}$Sr ratio recorded by a stalagmite from Central China and their association with past climate and environment. Chemical Geology 268, 233–247.

Zupan Hajna, N.Z., 2003. Chemical weathering of limestones and dolomites in a cave environment. Speleogenesis and Evolution of Karst Aquifers 1 (3), 2–8.

## Further reading

Bae, S.Y., Yi, S.M., Kim, Y.P., 2002. Temporal and spatial variations of the particle size distribution of PAHs and their dry deposition fluxes in Korea. Atmospheric Environment 36, 5491–5550.

Bytnerowicz, A., Miller, P.R., Olszyk, D.M., 1987. Dry deposition of nitrate, ammonium and sulfate to a Ceanothus crassifolius canopy and surrogate surfaces. Atmospheric Environment 21 (8), 1749–1757.

Kim, E., Kalman, D., Larson, T., 2000. Dry deposition of large, airborne particles onto a surrogate surface. Atmospheric Environment 34 (15), 2387–2397.

King, A.D., Hocking, A.D., Pitt, J.I., 1979. Dichloran-rose Bengal medium for enumeration and isolation of molds from foods. Applied and Environmental Microbiology 37, 959–964.

Terzi, E., Samara, C., 2005. Dry deposition of polycyclic aromatic hydrocarbons in urban and rural sites of Western Greece. Atmospheric Environment 39, 6261–6270.

Vawda, Y., Harrison, R.M., et al., 1990. Use of surrogate surfaces for dry deposition measurements. Journal of Aerosol Science 21 (1), 201–204.

Wieprecht, W., Acker, K., Müller, K., Spindler, G., Brüggemann, E., Maenhaut, W., Chi, X., Hitzenberger, R., Bauer, H., Brink, H.T., 2004. INTERCOMP2000: ionic constitution and comparison of filter and impactor. Atmospheric Environment 38, 6477–6486.

Zhang, S., Zhang, W., Shen, Y., Wang, K., Hu, L., Wang, X., 2008. Dry deposition of atmospheric polycyclic aromatic hydrocarbons (PAHs) in the southeast suburb of Beijing, China. Atmospheric Research 89, 138–148.

Zufall, M.J., Davidson, C.I., Caffrey, P.F., Ondov, J.M., 1998. Airborne concentrations and dry deposition fluxes of particulate species to surrogate surfaces deployed in southern Lake Michigan. Environmental Science & Technology 32 (11), 1623–1628.

398

399